frontiers | Research Topics

The state of knowledge from operational ice service perspectives: previous and future mandates

Edited by
John Falkingham, Wolfgang Dierking, Andrew Fleming, Penelope Wagner, Ed Blockley, Nick Hughes and Ludovic Brucker

Published in
Frontiers in Marine Science

ISSN 1664-8714
ISBN 978-2-8325-7449-2
DOI 10.3389/978-2-8325-7449-2

Generative AI statement
Any alternative text (Alt text) provided alongside figures in the articles in this ebook has been generated by Frontiers with the support of artificial intelligence and reasonable efforts have been made to ensure accuracy, including review by the authors wherever possible. If you identify any issues, please contact us.

About Frontiers

Frontiers is more than just an open access publisher of scholarly articles: it is a pioneering approach to the world of academia, radically improving the way scholarly research is managed. The grand vision of Frontiers is a world where all people have an equal opportunity to seek, share and generate knowledge. Frontiers provides immediate and permanent online open access to all its publications, but this alone is not enough to realize our grand goals.

Frontiers journal series

The Frontiers journal series is a multi-tier and interdisciplinary set of open-access, online journals, promising a paradigm shift from the current review, selection and dissemination processes in academic publishing. All Frontiers journals are driven by researchers for researchers; therefore, they constitute a service to the scholarly community. At the same time, the *Frontiers journal series* operates on a revolutionary invention, the tiered publishing system, initially addressing specific communities of scholars, and gradually climbing up to broader public understanding, thus serving the interests of the lay society, too.

Dedication to quality

Each Frontiers article is a landmark of the highest quality, thanks to genuinely collaborative interactions between authors and review editors, who include some of the world's best academicians. Research must be certified by peers before entering a stream of knowledge that may eventually reach the public - and shape society; therefore, Frontiers only applies the most rigorous and unbiased reviews. Frontiers revolutionizes research publishing by freely delivering the most outstanding research, evaluated with no bias from both the academic and social point of view. By applying the most advanced information technologies, Frontiers is catapulting scholarly publishing into a new generation.

What are Frontiers Research Topics?

Frontiers Research Topics are very popular trademarks of the *Frontiers journals series*: they are collections of at least ten articles, all centered on a particular subject. With their unique mix of varied contributions from Original Research to Review Articles, Frontiers Research Topics unify the most influential researchers, the latest key findings and historical advances in a hot research area.

Find out more on how to host your own Frontiers Research Topic or contribute to one as an author by contacting the Frontiers editorial office: frontiersin.org/about/contact

The state of knowledge from operational ice service perspectives: previous and future mandates

Topic editors

John Falkingham — International Ice Charting Working Group, Canada
Wolfgang Dierking — Alfred Wegener Institute Helmholtz Centre for Polar and Marine Research (AWI), Germany
Andrew Fleming — British Antarctic Survey (BAS), United Kingdom
Penelope Wagner — Norwegian Meteorological Institute, Norway
Ed Blockley — Met Office, United Kingdom
Nick Hughes — Norwegian Meteorological Institute, Norway
Ludovic Brucker — NOAA NESDIS Center for Satellite Applications and Research & U.S. National Ice Center, United States

Citation

Falkingham, J., Dierking, W., Fleming, A., Wagner, P., Blockley, E., Hughes, N., Brucker, L., eds. (2026). *The state of knowledge from operational ice service perspectives: previous and future mandates*. Lausanne: Frontiers Media SA.
doi: 10.3389/978-2-8325-7449-2

Table of contents

frontiers | Frontiers in Marine Science

TYPE Editorial
PUBLISHED 19 January 2026
DOI 10.3389/fmars.2025.1764046

OPEN ACCESS

EDITED AND REVIEWED BY
Johannes Karstensen,
Helmholtz Association of German Research Centres (HZ), Germany

*CORRESPONDENCE
Penelope Wagner
penelopew@met.no

RECEIVED 09 December 2025
ACCEPTED 12 December 2025
PUBLISHED 19 January 2026

CITATION
Wagner P, Blockley E, Brucker L, Dierking W, Falkingham J, Fleming A and Hughes N (2026) Editorial: The state of knowledge from operational ice service perspectives: previous and future mandates.
Front. Mar. Sci. 12:1764046.
doi: 10.3389/fmars.2025.1764046

Editorial: The state of knowledge from operational ice service perspectives: previous and future mandates

Penelope Wagner[1]*, Ed Blockley[2], Ludovic Brucker[3], Wolfgang Dierking[4,5], John Falkingham[6], Andrew Fleming[7] and Nick Hughes[1]

[1]Sea Ice Operational Service, Forecasting Division for Northern Norway, Norwegian Meteorological Institute, Tromsø, Norway, [2]Polar Climate Group, Met Office, Exeter, United Kingdom, [3]NOAA Center for Satellite Applications and Research, College Park, MD, United States, [4]Alfred-Wegener-Institut Helmholtz-Zentrum fur Polar- und Meeresforschung, Bremerhaven, Germany, [5]UiT Norges arktiske universitet, Tromsø, Norway, [6]International Ice Charting Working Group Ex-officio, Ottawa, ON, Canada, [7]The Mapping and Geographic Information Centre (MAGIC), British Antarctic Survey, Cambridge, United Kingdom

KEYWORDS

Antarctic sea ice, Arctic sea ice, ice chart, iceberg, sea ice automation, sea ice classification, sea ice forecasting, sea ice service

Editorial on the Research Topic
The state of knowledge from operational ice service perspectives: previous and future mandates

Sea ice and iceberg services hold a unique and critical position at the interface of maritime activity, science, and policy in ice encumbered areas all around the world. They are the authoritative sources of sea ice and iceberg information and their role requires the use of non-traditional observations, satellite sensors, and local knowledge to translate complex cryospheric observations into practical information so those operating in these areas can make informed decisions using the most representative and relevant environmental information.

Polar and sub-polar regions have been experiencing rapid changes, shifting from stable ice regimes to more dynamic seasonal ice conditions. At the same time, satellite coverage has improved significantly over the past decade, and we expect the satellite coverage to increase with faster processing capabilities in the future. It is therefore essential for sea ice services, the research community, and third-party product providers to strengthen their collaboration to help meet current and future sea ice monitoring challenges and fully exploit emerging technologies.

The Research Topic The State of Knowledge from Operational Ice Service Perspectives: Previous and Future Mandates brings together thirteen diverse contributions from national ice services and innovative research focused on developing fit-for-purpose products for operational use. The papers also examine how national ice services and their products must evolve to meet emerging societal and environmental challenges.

The intent of the Research Topic is twofold: first, to document existing ice service practices and mandates, including future plans, across national services; and second, to

explore how recent scientific advances in remote sensing, modelling, forecasting, and data integration may support and complement these services. As human activity, including shipping, fisheries, tourism, offshore resource exploration, and research operations, increases across the Arctic, Antarctic, and seasonally ice-encumbered areas, the demands on sea ice services have expanded well beyond their historical roots in basic ice charting. The articles in this Research Topic provide an overview of these shifting responsibilities and technologies.

Several contributions examine the evolution and historical foundations of operational services. The long-term institutional perspective is presented in the paper, *The International Ice Charting Working Group: the first twenty-five years* by Falkingham, which chronicles the development of international coordination, standards, and shared practices since the IICWG's founding in 1999. This highlights how collaboration across nations has strengthened operational reliability and user confidence. At a national scale, *The MET Norway Ice Service: a comprehensive review of the historical and future evolution, ice chart creation, and end user interaction within METAREA XIX* by Copeland et al., provides an overview of the Norwegian ice operations servicing a wide range of users in Arctic waters, including tourism operators, research vessels, fisheries, and search-and-rescue services. In the Baltic, *Information on operational sea ice products and current and future activities of the German ice service* by Aldenhoff and Holfort, presents how operational workflows integrate satellite data, observations, and archive digitization to maintain consistent and timely products. *The Finnish Ice Service, its sea-ice monitoring of the Baltic Sea and operational concept* by Eriksson et al., describes the parallel evolution of the Baltic and European services, each shaped by specific regional environmental regimes and mandates, navigational demands, and long traditions of shipping support for operators working in and around sea ice.

Antarctic operational needs are presented in *Southern Ocean ice charts at the Argentine Naval Hydrographic Service*, by Scardelli et al. that highlights the importance of accurate charting for navigational safety in Antarctic waters. A complement to the Argentine operations is the *Multi-band SAR intercomparison study in the Antarctic Peninsula* by Salvo et al., which demonstrates how multi-frequency radar datasets are necessary to detect icebergs and complex sea-ice features under challenging conditions, emphasizing the importance of a system-of-sensors for regional monitoring.

A common thread through these reviews is that institutional experience built over many years, together with expert analysis and local knowledge, remains essential. Satellite and sensor data frequently contain ambiguities that require skilled interpretation, and ice services increasingly rely on analysts to ensure that information produced for operations remain accurate and representative. As national services integrate more advanced processing pipelines and adopt new sensors, there is a growing interest in semi-automated production methods, while balancing consistent quality and preserving the integrity of long-term ice chart records, particularly where ground-truth data are limited.

Several research contributions explore emerging capabilities that support sea ice automation and forecasting. Higher resolution satellite data are enabling more refined classification methods, while machine learning techniques show promise for operational automation. *Sea ice recognition for CFOSAT SWIM* by Liu et al. evaluates small-incidence-angle CFOSAT waveforms and demonstrates effective machine-learning approaches for distinguishing sea ice from open water. For sea ice concentration, *Multisensor data fusion of operational sea ice observations* by Wang et al. presents a framework that integrates synthetic aperture radar (SAR), optical, and *in situ* datasets to improve the consistency and reliability of operational products, illustrating how diverse sensors can be combined within one workflow.

Forecasting capabilities in this Research Topic present advancements. The paper *Greenlandic sea ice products with a focus on an updated operational forecast system* by Ponsoni et al. demonstrates how modern coupled ocean–sea-ice modelling and data assimilation approaches are becoming increasingly relevant for ice operations. The Wang et al. paper, *Improving short-term forecasts of sea-ice edge and MIZ around Svalbard*, describes the development and tests of a method to improve short-term forecasting of the sea-ice edge and marginal ice zone around Svalbard, demonstrating clear operational benefits for real-time decision support. For the Antarctic, *SIPN South: six years of coordinated seasonal Antarctic sea ice forecasting* by Massonet et al. summarizes a coordinated multi-model forecasting effort, highlighting both advances and challenges in seasonal prediction. Together, these works capture the accelerating push toward tactical and short-term forecasting and the integration of predictive tools into operational workflows. They also show how improvements in multi-sensor products, along with the use of non-traditional observations for sea-ice classification and forecasting, are helping to shape how future services can be supported.

Human activities in ice encumbered waters are further explored across two papers, reflecting the growing importance of operational guidance for vessel design and route planning support. Studies on polar class shipping accessibility, from the papers Vlietstra et al. analyzes *A decade of sea-ice variability to assess changes in polar-class vessel accessibility north of the Bering Strait* and Liu et al. reviews *Ship-performance models and ice-routing algorithms for Arctic navigation, emphasizing the influence of sea-ice conditions*, present how thinning ice, shifting ice edges, and more variable seasonal patterns influence routing strategies, operational risk, and user expectations for more specialized and tailored ice information.

The thirteen contributions in this Research Topic present a small subset of work being done in a field that is undergoing a significant transition, driven by changing user requirements, advances in automation, expanded observational capabilities, and new forecasting tools. While national sea ice services are adopting semi-automated workflows to meet evolving user needs, they, and the research community working on developments to support these services, reaffirm the importance of expert interpretation and regional knowledge that remain critical for services providing information for safe navigation. Future mandates of national ice services will extend beyond routine ice charting to include more parameters in ice charts, risk-informed decision-making, probabilistic forecasting, and may include the integration of autonomous systems for *in situ* data

collection. As climate change reshapes global sea ice regimes, deeper collaboration across scientific, operational, and policy communities is essential. By combining long-standing operational experience with emerging methodological advances, this Research Topic provides a timely basis for guiding the future development of sea ice services.

Author contributions

PW: Writing – original draft, Writing – review & editing. EB: Writing – review & editing. LB: Writing – review & editing. WD: Writing – review & editing. JF: Writing – review & editing. AF: Writing – review & editing. NH: Writing – review & editing.

Conflict of interest

The authors declared that this work was conducted in the absence of any commercial or financial relationships that could be construed as a potential conflict of interest.

Generative AI statement

The author(s) declared that generative AI was not used in the creation of this manuscript.

Any alternative text (alt text) provided alongside figures in this article has been generated by Frontiers with the support of artificial intelligence and reasonable efforts have been made to ensure accuracy, including review by the authors wherever possible. If you identify any issues, please contact us.

Publisher's note

frontiers | Frontiers in Marine Science

TYPE Original Research
PUBLISHED 13 September 2022
DOI 10.3389/fmars.2022.986228

OPEN ACCESS

EDITED BY
John Falkingham,
International Ice Charting Working Group, Canada

REVIEWED BY
Xiaoyi Shen,
Nanjing University, China
Yanmin Zhang,
Ocean University of China, China

*CORRESPONDENCE
Xi Zhang
xi.zhang@fio.org.cn

SPECIALTY SECTION
This article was submitted to Ocean Observation, a section of the journal Frontiers in Marine Science

RECEIVED 04 July 2022
ACCEPTED 24 August 2022
PUBLISHED 13 September 2022

CITATION
Liu M, Yan R, Zhang X, Xu Y, Chen P, Zhao Y, Guo Y, Chen Y, Zhang X and Li S (2022) Sea ice recognition for CFOSAT SWIM at multiple small incidence angles in the Arctic. *Front. Mar. Sci.* 9:986228. doi: 10.3389/fmars.2022.986228

Sea ice recognition for CFOSAT SWIM at multiple small incidence angles in the Arctic

Meijie Liu[1], Ran Yan[1], Xi Zhang[2*], Ying Xu[3], Ping Chen[4], Yongsen Zhao[1], Yuexiang Guo[1], Yangeng Chen[1], Xiaohan Zhang[1] and Shengxu Li[1]

[1]College of Physics, Qingdao University, Qingdao, China, [2]First Institute of Oceanography, Ministry of Natural Resources, Qingdao, China, [3]National Satellite Ocean Application Service, Beijing, China, [4]School of Electronic Information and Communications, Huazhong University of Science and Technology, Wuhan, China

Sea ice recognition is one of the main tasks for sea ice monitoring in the Arctic and is also applied for the detection of other ocean phenomena. The Surface Wave Investigation and Monitoring (SWIM) instrument, as an innovative remote sensor that operates at multiple small incidence angles, is different from existing sensors with moderate and normal incidence modes for sea ice monitoring. Sea ice recognition at small incidence angles has rarely been studied. Moreover, SWIM uses a discrimination flag of sea ice and sea water to remove sea ice from sea wave products. Therefore, this research focuses on sea ice recognition in the Arctic based on SWIM data from October 2020 to April 2021. Eleven features are first extracted, and applied for the analysis of the waveform characteristics using the cumulative probability distribution (CPD) and mutual information measurement (MIM). Then, random forest (RF), k-nearest neighbor (KNN) and support vector machine (SVM) classifiers are built, and their abilities of sea ice recognition are assessed. The optimal classifier is the KNN method with Euclidean distance and k equal to 11. Feature combinations are also used to separate sea ice and sea water based on the KNN method to select the optimal combination. Thus, the optimal classifier-feature assembly at each small incidence angle is established, and the highest overall accuracy reaches 97.1%. Moreover, the application of the optimal classifier–feature assemblies is studied, and its performance is fairly good. These assemblies yield high accuracies in the short- and long-term periods of sea ice recognition, and the overall accuracies are greater than 93.1%. So, the proposed method satisfies the SWIM requirement of removing the sea ice effect. Moreover, sea ice extents and edges can be extracted from SWIM sea ice recognition results at a high level of precision greater than 94.8%. As a result, the optimal classifier–feature assemblies based on SWIM data express the effectiveness of the SWIM approach in sea ice recognition. Our work not only highlights the new sea ice monitoring technology of remote sensing at small incidence angles, but also studies the application of SWIM data in sea ice services.

KEYWORDS

sea ice, Surface Wave Investigation and Monitoring (SWIM), Arctic, small incidence angles, waveform features, k-nearest neighbor method

1 Introduction

Sea ice plays an important role in global climate change, shipping, navigation and the extraction of natural resources (Komarov and Buehner, 2021), and influences the detection of other ocean phenomena; for example, sea wave retrieval requires the removal of sea ice 'pollution' (Ren et al., 2021; Wang J.K., et al., 2021). Thus, sea ice recognition has become a main task performed to meet the scientific and operational requirements of national and commercial ice services, which provides sea ice edge, extent, and concentration products (Cheng et al., 2020; de Gélis et al., 2021). Microwave remote sensors, including synthetic aperture radar (SAR), scatterometers, and altimeters, have become the main tools used for sea ice monitoring in the Arctic. These sensors operate at incidence angles of 0° or 20–60°. SAR is an imaging radar with multiple bands including L, C and X bands and a high spatial resolution of less than 1 m at 20–60°. Based on the available microwave backscattering information and image characteristics, SAR provides data mainly used to the regional distribution and change of the sea ice. Karvonen et al. (2005) proposed a segmentation technique based on intensity autocorrelation using C-band RADARSAT-1 SAR images; the accuracy of sea water recognition was 90%, and no results were reported for sea ice. Berg and Eriksson (2012) utilized a neural network to separate sea ice and sea water based on C-band ENVISAT and RADARSAT-2 SAR images, and the accuracies of sea ice and sea water identification were 87% and 94%, respectively. Asadi et al. (2021) proposed a multilayer perceptron (MLP) neural network for sea ice and sea water distinguishing based on RADARSAT-2 images, and the overall accuracy reached 82%. Komarov and Buehner (2021) presented a new method that could be applied at multiple spatial scales for automatic distinction between sea ice and sea water using RADARSAT-2 images, and the maximum overall accuracy reached 99%. At present, SAR has been used to obtain sea ice products for the Arctic region. Scatterometers can detect sea ice across the Arctic region at a coarse spatial resolution (several to tens of kilometers) and at two major frequencies: the C band (e.g., ASCAT and ERS-1/2) and the Ku-band (e.g., QuickSCAT and OSCAT). Sea ice recognition depends on the microwave backscattering powers of the horizontal and vertical polarizations, as well as the image reconstruction method (Gohin and Cavanie, 1994; Remund and Long, 1999; Rivas and Stoffelen, 2011; Otosaka et al., 2018). Haarpaintner and Spreen (2007) refined the detection method of low sea ice concentration using QuikSCAT data and improved the extraction accuracies of sea ice edges. Presently, operational sea ice edge, extent and concentration products in the Arctic have been generated for a long time, and sea ice recognition accuracies have reached 90% (Cavalieri et al., 1996; Breivik et al., 2012; Rivas et al., 2012; Remund and Long, 2014; Bi et al., 2018). Altimeters are mainly used for sea ice thickness retrieval based on large-scale and coarse spatial resolution observations similar to those of scatterometers; however, extracted sea ice and sea water information is needed to improve retrieval accuracies (Zhang et al., 2021). Some classifiers, such as the random forest (RF), k-nearest neighbor (KNN), and support vector machine (SVM) classifiers, are used for sea ice recognition based on the waveform features of echo signals which include the backscattering coefficient (σ_0), maximum power (MAX), pulse peakiness (PP), inverse mean power (IMP), leading edge width (LEW), and trailing edge slope (TES). The waveform features of airborne Ku-band radar altimeters were first used to discriminate the rough and smooth surfaces of sea ice, and a higher waveform peak and steeper trailing edge were associated with smooth surfaces (Drinkwater and Carsey, 1991). Laxon (1994) mapped sea ice extents based on PP and standard deviation of surface height extracted from ERS-1 radar altimeter data, which suggested clear operational applications in polar sea ice detection. Currently, the accuracies of sea ice and sea water recognition have reached 92% and 95%, respectively (Zygmuntowska et al., 2013; Rinne and Similä, 2016; Müller et al., 2017; Shen et al., 2017a; Shen et al., 2017b; Shu et al., 2019). However, the surface characteristics, snow coverage, and other factors certainly affect the stability of sea ice recognition accuracies, which needs further exploration. And these methods should be verified by more data in different study regions and long periods. Therefore, sea ice recognition using altimeters is still under study.

The Surface Wave Investigation and Monitoring (SWIM) instrument adopts a new observation mode with multiple small incidence angles (0° to 10°) for the detection of sea surface waves (Hauser et al., 2016; Hauser et al., 2017; Wang et al., 2019; Xu et al., 2019; Hauser et al., 2020). SWIM with a maximum latitude of 83°N can cover sea ice regions in the Arctic and be used for sea ice recognition. Moreover, SWIM sea wave products are influenced by the sea ice, resulting in that SWIM data should be labeled by the discrimination flag of sea ice and sea water. Thus, SWIM data with the new observation mode can be used for sea ice recognition and contribute to sea ice monitoring methods and operational techniques. Our previous study focused on sea ice type classification (Liu et al., 2021; Liu et al., 2022), and a method to distinguish between sea ice and sea water was not fully established. In addition, two new features (Inverse mean power, IMP; Trailing edge slope, TES) were introduced for first-year ice (FYI) and multiyear ice (MYI) separation, but these features were not used for sea water recognition. Therefore, based on our previous study, several key problems are explored in this study:

- New feature introduction and waveform analysis at small incidence angles to assess the use of different waveform features for separating sea ice and sea water;
- Classifier selection and assessment of the abilities for different classifiers with different settings;

- Establishment of the optimal classifier–feature assembly at each incidence angle; the assembly is established by combining the selected classifier and feature combinations. It can achieve sea ice recognition with high accuracy based on SWIM data obtained in the new detection mode;
- Application analysis of the optimal classifier–feature assemblies at small incidence angles, that is, whether these assemblies can be applied to remove sea ice from SWIM sea wave products and extract sea ice extents and edges for sea ice operational services.

Section 2 introduces the SWIM, SAR and sea ice chart data from the Arctic obtained between October 2020 and April 2021. Moreover, the waveform features of SWIM data are extracted, and classifiers for sea ice recognition are identified. Section 3 reveals the waveform analysis, and the overall accuracies of different classifiers and feature combinations, then, the optimal classifier-feature assembly for the SWIM data is established at each small incidence angle. Furthermore, the application of the optimal classifier-feature assemblies is also analyzed. Section 4 discusses the results in this study. Section 5 presents the conclusions and future work.

2 Data and methods

2.1 Data

There are three data sets used in this paper: SWIM, Sentinel-1 and sea ice chart data.

2.1.1 SWIM

The SWIM is loaded on the Chinese-French Oceanic Satellite (CFOSAT), which was successfully launched on October 29, 2018 (Wang et al., 2019; Xu et al., 2019). SWIM is the first spaceborne real aperture radar system that can operate at six small incidence angles (0° to 10°), the entire azimuth angle range (0–360°) and 13.575 GHz (Hauser et al., 2016; Hauser et al., 2017; Hauser et al., 2020). The main objective of SWIM is to provide wave spectra for the sea surface. SWIM spans nearly 90 km from 0° to 10° on the ground, and its footprint at 10° is approximately 18 km, as shown in Figure 1. SWIM can reach the northern and southern latitudes up to 83°. SWIM's orbit assures a complete Earth coverage at the end of the cycle (13 days) except for small holes around the equator. The mid- and high-latitudes are very well covered as required by the mission. Level 1A SWIM data, which can be used to extract waveform features to recognize sea ice and sea water, are used in this study.

2.1.2 Sentinel-1

Sentinel-1 was the first of five missions launched as part of the Copernicus Initiative of the European Commission (EC) and the European Space Agency (ESA). Sentinel-1 is in a near-polar, sun-synchronous orbit with a 12-day repeat cycle and 175 orbits per cycle for a single satellite. Sentinel-1A/B SAR can obtain all-weather, all-day images in the C-band in single-polarization (HH or VV) and dual-polarization (HH+HV or VV+VH) modes. Sentinel-1 SAR operates in four exclusive modes: stripmap (SM) mode, interferometric wide swath (IW) mode, extrawide swath (EW) mode and wave (WV) mode. Additionally, four products are provided: Level-0, Level-1 Single Look Complex (SLC), Level-1 Ground Range Detected (GRD) and Level-2 Ocean (OCN) data.

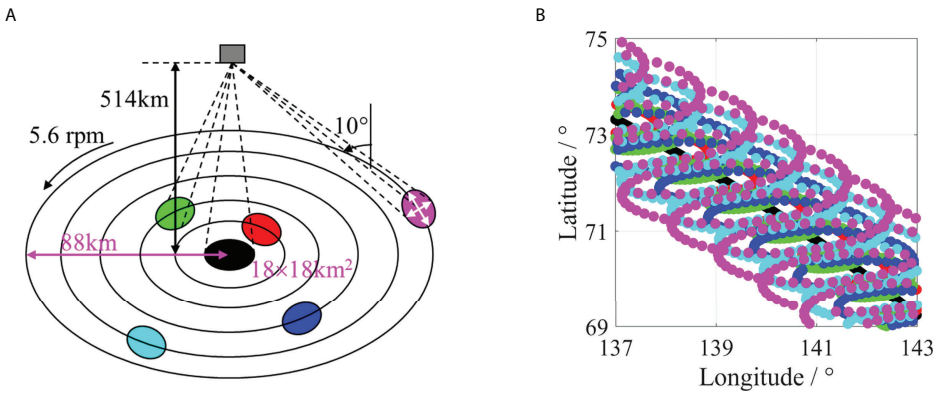

FIGURE 1
SWIM detection schematics for six incidence beams. **(A)** The projection geometries of the six beams in one macrocycle. One macrocycle represents six successive beams transmitting at small incidence angles with a discontinuous azimuth. **(B)** Samples of several macrocycles over the Earth's surface (antenna aperture: 2°×2°).

Sentinel-1A/B can support effective ice services, for example, the monitoring of sea ice extent, concentration and types in the Arctic (de Gélis et al., 2021, Li et al., 2021; Scharien and Nasonova, 2022). In this study, Sentinal-1 SAR images are used to evaluate sea ice recognition results of SWIM data. Considering the 18 km spatial resolution of SWIM products, we use the wide swath (about 400 km) and low resolution (about 90 m) SAR images of Lever-1 GRD products.

2.1.3 Sea ice charts

The sea ice charts used in this study are from the Arctic and Antarctic Research Institute (AARI) (AARI, 2022), and the National Snow and Ice Data Center (NSIDC) (Cavalieri et al., 1996; NSIDC, 2022).

(1) AARI

The AARI usually releases sea ice charts on Thursday. One sea ice chart covers three days from Sunday to Tuesday, including sea water and sea ice types (nilas, young ice, first-year ice and multiyear ice) in one Arctic ice year from October to April (AARI, 2022). In this study, only sea ice and sea water are separated in the Arctic from October 2020 to April 2021, and sea ice regions of different types are merged. During this period, thirty charts were issued, including 90 days. In general, multiyear ice (MYI) and sea water are the primary categories in the Arctic in October, and nilas (NI) and young ice (YI) only appear in small regions. Then, the sea ice rapidly develops from November to December. The sea ice distribution is stable from January to March and varies slowly in April. The characteristics of the sea ice distribution in April are similar to those from January to March. According to the characteristics of the sea ice distribution in the Arctic, sea ice development in one Arctic ice year can be divided into three stages: the first is October (Stage 1), the second is November to December (Stage 2), and the third is January to April (Stage 3).

(2) NSIDC

The NSIDC provides a sea ice concentration data set generated from the brightness temperature extracted from radiometer data, and one cell size is 25 ×25 km in the polar stereographic projection (Cavalieri et al., 1996; NSIDC, 2022). Notably, sea ice concentration products are generated daily. One cell where sea ice concentration is not lower than 15 percent is classified as sea ice, and the others are classified as sea water. Thus, the sea ice extents and edges are extracted and can be used to evaluate SWIM results.

2.1.4 Data matching and filtering

In this research, SWIM waveforms are matched and filtered for sea ice and sea water distinguishing in the Arctic based on the following criteria:

(1) SWIM data in the Arctic ice year from October 2020 to April 2021 are selected.

(2) The SWIM data in the coverage region of AARI sea ice charts are chosen. Then, these data are also matched to the observation time of each AARI sea ice chart in a three-day period from every Sunday to Tuesday mentioned in the Section 2.1.3.

(3) The waveforms of SWIM are labeled as sea ice or sea water based on matching with the AARI sea ice charts from the same dates. The sea ice distribution changes very slowly in the Arctic over three days in winter, especially when data with a coarse spatial resolution (tens of kilometers) are used. And, remote sensors with similar spatial resolution also do this method to obtain the information of the categories (Shen et al., 2017a; Shen et al., 2017b; Shu et al., 2019).

(4) If the powers of gates in one waveform are negative or higher than the maximum threshold value, the waveform is removed.

2.1.5 SWIM features

According to our previous work and other researches, eleven waveform features are extracted to assess the echo characteristics of SWIM at six small incidence angles (Laxon, 1994; Zygmuntowska et al., 2013; Rinne and Similä, 2016; Shen et al., 2017b; Shu et al., 2019; Liu et al., 2022). These features reflect the different waveform characteristics, for example, the power, structure, and overall characteristics of echo waveforms.

(1) Maximum power (MAX)

MAX is the maximum power of the echo in one footprint, which can reflect the surface properties of observed objects (Zakharova et al., 2015). MAX is defined by the following formula:

$$\mathrm{MAX}_{\theta} = \max\left(P_{i_\theta}\right),\ i_\theta = 1,\ 2,\ 3,\ \ldots, n_\theta\ ,\ \theta = 0°,\ 2°,\ 4°,\ 6°,\ 8°,\ 10°,\ \mathrm{n}\theta = 256,\ 765,\ 933,\ 2771,\ 2639,\ 3215 \quad (1)$$

where P_{i_θ} is the power in the i-th range gate and n_θ is the maximum range gate in one footprint at the incidence angle θ.

(2) Medium power (MED)

MED, as the medium power of all gates in one footprint, is a new feature of echo waveforms. This variable reflects the distribution of echo powers. MED is expressed as:

$$\mathrm{MED}_{\theta} = \mathrm{medium}\left(P_{i_\theta}\right),\ i_\theta = 1,\ 2,\ 3,\ \ldots, n_\theta \quad (2)$$

The backscattering coefficient (σ_0) was the main parameter used for sea ice and sea water distinction in previous studies. σ_0 is expressed by the radar frequency, polarization and incidence angle and depends on the surface properties of the observed objects, such as their roughness, geometry and dielectric characteristics. For altimeters at 0°, many methods are used to calculate the σ_0 values of a footprint, and the offset center of gravity (OCOG) approach is popular. Incidence angles of 2–10° in SWIM can support new

modes of sea ice detection, and these angles approximate 0°. Thus, OCOG and the mean value of one waveform are used to calculate σ_0 at 2–10° in this paper. Moreover, the mean value is an important feature for sea ice and sea water identification at 0°.

(3) Mean power (MEA)

MEA is the mean power of all gates in one footprint.

$$\mathrm{MEA}_\theta = \frac{\sum_{i_\theta=1}^{n_\theta} \mathrm{P}_{i_\theta}}{n_\theta} \tag{3}$$

(4) Offset center of gravity (OCOG)

OCOG is defined by:

$$\mathrm{OCOG}_\theta = \sqrt{\frac{\sum_{i_\theta=1}^{n_\theta} \mathrm{P}_{i_\theta}^4}{\sum_{i_\theta=1}^{n_\theta} \mathrm{P}_{i_\theta}^2}} \tag{4}$$

(5) Pulse peakiness (PP)

PP is related to the specular return of echo signals and is defined by the ratio of MAX to the accumulated echo power:

$$PP_\theta = \frac{\mathrm{P}_{\max_\theta}}{\sum_{i_\theta=1}^{n_\theta} \mathrm{P}_{i_\theta}} \times n_\theta \tag{5}$$

PP increases as the surface becomes smoother at 0° (Zygmuntowska et al., 2013).

(6) Stack standard deviation (SSD)

SSD is the standard deviation of the waveform and reflects the dispersion and stability of the waveform. Additionally, this variable depends on the surface roughness at 0°.

$$SSD_\theta = \sqrt{\frac{\sum_{i_\theta=1}^{n_\theta} \left(\mathrm{P}_{i_\theta} - \mathrm{MEA}_\theta\right)^2}{\mathrm{n}_\theta}} \tag{6}$$

In the discussion of our previous study, the inverse mean power (IMP) was useful to discriminate FYI and MYI (Liu et al., 2022). In this study, IMP is also introduced for sea ice and sea water separation.

(7) Inverse mean power (IMP)

IMP is the ratio of the maximum range gate to the total power in one footprint and is scaled by 2×10^{-13}; it increases as the surface becomes rougher at 0° (Aldenhoff et al., 2019).

$$\mathrm{IMP} = \frac{\mathrm{n}_\theta}{\sum_{i_\theta=1}^{n_\theta} \mathrm{P}_{i_\theta}} \cdot 2 \cdot 10^{-13} \tag{7}$$

IMP can improve the contrast of signals when waveforms do not exhibit obvious peaks.

(8) Leading edge width (LEW)

LEW represents the gate range at the leading edge, and the two gates are chosen at 5% and 95% of the maximum echo power; which can filter the effect of the thermal noise of the leading edge.

$$\begin{aligned} \mathrm{A}_{1\theta} &= \mathrm{MAX}_\theta \cdot 0.95,\ \mathrm{A}_{2\theta} = \mathrm{MAX}_\theta \cdot 0.95,\ \mathrm{LEW}_\theta \\ &= \mathrm{G}(\mathrm{A}_{1\theta}) - \mathrm{G}(\mathrm{A}_{2\theta}) \end{aligned} \tag{8}$$

where $\mathrm{G}(\mathrm{A}_{1\theta})$ and $\mathrm{G}(\mathrm{A}_{2\theta})$ represent the gates at 5% and 95% of the maximum echo power at the incidence angle θ, respectively.

(9) Trailing edge width (TEW)

TEW represents the gate range at the trailing edge, and the two gates are chosen at 5% and 95% of the maximum echo power. TEW increases as the diffuse reflection of rough surfaces increases at 0°.

$$\begin{aligned} \mathrm{A}_{1\theta} &= \mathrm{MAX}_\theta \cdot 0.95,\ \mathrm{A}_{2\theta} = \mathrm{MAX}_\theta \cdot 0.05,\ \mathrm{TEW}_\theta \\ &= \mathrm{G}(\mathrm{A}_{2\theta}) - \mathrm{G}(\mathrm{A}_{1\theta}) \end{aligned} \tag{9}$$

Our previous study indicated that LEW and TEW did not yield satisfactory results, and the echo power (MAX) and waveform shape (TEW) could be combined to improve the effects on distinguishing between FYI and MYI (Liu et al., 2022). In this study, we expand this method to separate sea ice and sea water.

(10) Leading edge slope (LES)

LES is MAX divided by LEW and expresses the rate of rise at the leading edge of the waveform.

$$\mathrm{LES}_\theta = \frac{\mathrm{MAX}_\theta}{\mathrm{LEW}_\theta}. \tag{10}$$

(11) Trailing edge slope (TES)

TES is MAX divided by TEW and expresses the rate of decline at the trailing edge of the waveform.

$$\mathrm{TES}_\theta = \frac{\mathrm{MAX}_\theta}{\mathrm{TEW}_\theta} \tag{11}$$

LES and TES consider the power and structure of an echo waveform, similar to PP, SSD and IMP, can reflect the overall properties of the waveform.

The above features can be used to construct 2047 feature combinations including 11 single features and multifeature combinations at each incidence angle. The feature combinations are represented by the ID Numbers, and are listed in the 'Supplementary Material' file. For single features, MAX, MED, MEA, OCOG, PP, SSD, IMP, LEW, TEW, LES, and TES are represented by the ID Numbers of F1–F11, respectively. For multifeature combinations, for example, the ID Number of F67 represents the feature combination (F{1,2,3}) including F1, F2 and F3 that are MAX, MED and MEA.

2.1.6 Waveform analysis

The cumulative probability distribution (CPD) and mutual information measurement (MIM) are applied to analyze SWIM waveforms using the eleven features at six small incidence angles.

(1) CPD

The CPD of a discrete random variable with a real value is defined as follows:

$$F_X(x) = \mathbf{Pr}(X \le x) \quad (12)$$

CPD represents the sum of the occurrence probabilities of the variable X that are less than and equal to a certain value x. X represents one of the waveform features.

(2) MIM

Mutual information measures the mutual dependence of two discrete random variables. The MIM of discrete random variables X and Y is defined by the following formula:

$$\mathrm{I(X, Y)} = \mathrm{H(X)} - \mathrm{H(Y|X)} \quad (13)$$

where $H(X)$ is the information entropy of X and $H(Y|X)$ represents the conditional entropy of Y if X is known. The variables X and Y represent two waveform features of one footprint.

2.2 Methods

The overall accuracy (OA) and F1 score (F1s) that are defined as seen in 'Supplementary Material' file are used to evaluate the abilities of classifiers for sea ice recognition. The introduction of classifiers is in terms of our previous work and other researches (Liu et al., 2015; Rinne and Similä, 2016; Shen et al., 2017a; Shen et al., 2017b; Jiang et al., 2019; Liu et al., 2022), so three classifiers are chosen for sea ice and sea water separation in this study, including the random forest (RF), k-nearest neighbors (KNN) and support vector machine (SVM). Then, the optimal classifier is chosen from the three ones, which is used to obtain the best feature combination. Thus, the optimal classifier-feature assembly is developed. We conduct random selection of 10 percent of all samples for training purposes and the rest samples for validation. So, the testing data are independent of the training dataset.

2.2.1 Optimal classifier selection

(1) RF

The RF method is a flexible approach based on ensemble learning techniques and regression decision trees. An RF can have many trees. In each tree, its training data are bootstrap sampled from all training data (Chan and Paelinckx, 2008; Hoekstra et al., 2020), and the features are selected randomly. Classification decisions are made by each individual decision tree. An RF can classify a large number of data sets in high-dimensional feature spaces (Shen et al., 2017a; Shen et al., 2017b). The RF method in this study includes 10–100 trees, with a step of 10.

(2) KNN

The KNN method is one of the most popular approaches for distinguishing between sea ice and sea water based on altimeter data (Rinne and Similä, 2016; Shen et al., 2017a; Shen et al., 2017b; Jiang et al., 2019). To assign the category of a sample in the validation space, a KNN needs to search for k points in the training space that are the closest neighbors around the sample. The KNN method is mainly based on two variables: the number of nearest neighbors (k) and the distance function which includes the Euclidean distance, Manhattan distance, or Mahalanobis distance.

(3) SVM

The SVM method, as a classic supervised machine learning technique, is also a popular and efficient approach for sea ice and sea water distinguishing based on altimeter data (Liu et al., 2015; Jiang et al., 2019); it produces appropriate nonlinear boundaries for discriminating categories based on kernel functions. There are three kernel functions applied in this paper: a Gaussian kernel, a linear kernel, and a polynomial kernel. The polynomial kernel includes the order q, and q is set to 2 and 3 in this study.

2.2.2 Optimal classifier-feature assembly establishment

After the classifier is selected from the abovementioned options, feature combinations derived from 11 waveform features are input into the selected classifier to obtain the subsequent overall accuracies and F1 scores. The feature combination and classifier that yield the highest accuracy are selected to establish the optimal classifier–feature assembly. Then, the application of the optimal classifier–feature assembly is analyzed.

3 Results

3.1 Waveform analysis

3.1.1 CPD

CPD illustrates the distribution ranges and probabilities of feature values for sea ice and sea water at six incidence angles, as shown in Figure 2. The eleven features are normalized in the range of [−1, 1]. The CPDs reveal that the distributions of the features at 0–10° for sea ice and sea water are different. Thus, the incidence angles can be separated into three sets: 0–2°, 4–6°, and 8–10°. The CPDs of most features of sea ice and sea water cover small ranges. Only TEW values for both sea ice and sea water distinctly cover large ranges, and they are relatively uniformly distributed. The features of which the CPDs are obviously different for sea ice and sea water at six small incidence angles are shown in Table 1. At 0–2°, the widths of the PP and LEW distributions for sea ice and sea water exhibit evident differences, suggesting that the two features may be useful for sea ice recognition; the TEW for both sea ice and sea water covers wide ranges but exhibits small difference, and LES displays a slightly larger width range. However, the remaining seven features span small ranges. At 4–6°, MED and MEA exhibit obvious discrepancies in terms of their distributions for sea ice and sea water. Additionally, MED and MEA exhibit obvious differences at 8°. The CPDs of single features do not

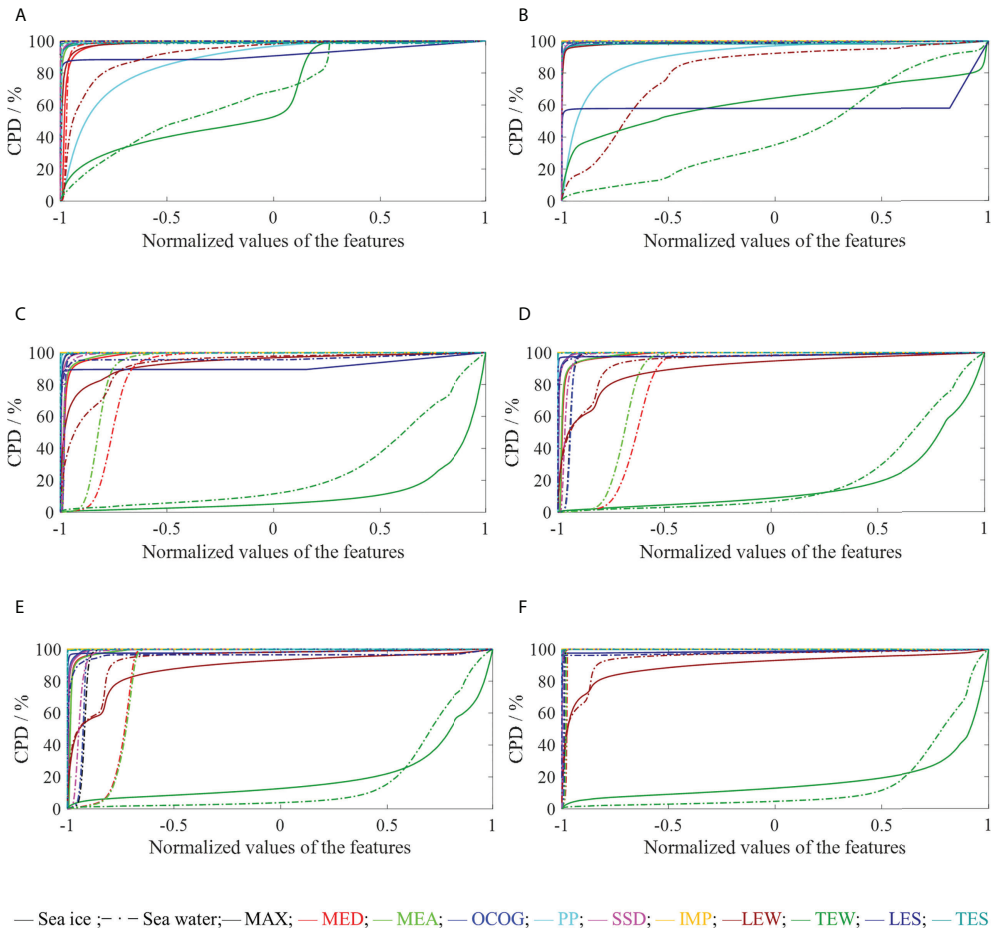

FIGURE 2
CPDs of eleven features at small incidence angles. **(A)** 0°; **(B)** 2°; **(C)** 4°; **(D)** 6°; **(E)** 8°; **(F)** 10°.

exhibit distinct differences at 10°, and by comparison, the most obvious features are MED and MEA, as listed in Table 1. The CPDs indicate that the properties at 4–6° are more similar to those at 8–10° than at 0–2°. Therefore, the CPD of one feature implies the separation ability of sea ice and sea water.

3.1.2 MIM

Eleven features can be used to establish 66 feature pairs, and the corresponding MIMs at six small incidence angles are shown in Figure 3. Larger MIMs of feature pairs imply higher redundancy or relevance, and MIMs larger than 0.65 indicate strong correlations (Zhang et al., 2021), as shown in Table 2. At 0–2°, three feature pairs, {OCOG–MAX}, {SSD–MAX} and {SSD–OCOG}, display high redundancy. At 4–6°, {OCOG–MAX} and {MEA–MED} pairs are most strongly correlated. At 8–10°, only the {MEA–MED} pair displays high relevancy. Thus, features at 4–6° may display the characteristics of features at both the 0–2° and 8–10°. More features with less redundancy at 8 – 10° may imply the independence of these features. The MIMs exhibit some consistency with the CPDs; for example, MEA and MED have high relevance and display similar CPD distributions at 4–10°. Consequently, a high MIM value indicates the high repeatability and redundancy of the two features in sea ice and sea water separation.

TABLE 1 The features of which the CPDs obviously differ for sea ice and sea water at six small incidence angles.

Angle	0°	2°	4°	6°	8°	10°
Feature	PP	PP	MED	MED	MED	MED
	LEW	LEW	MEA	MEA	MEA	MEA

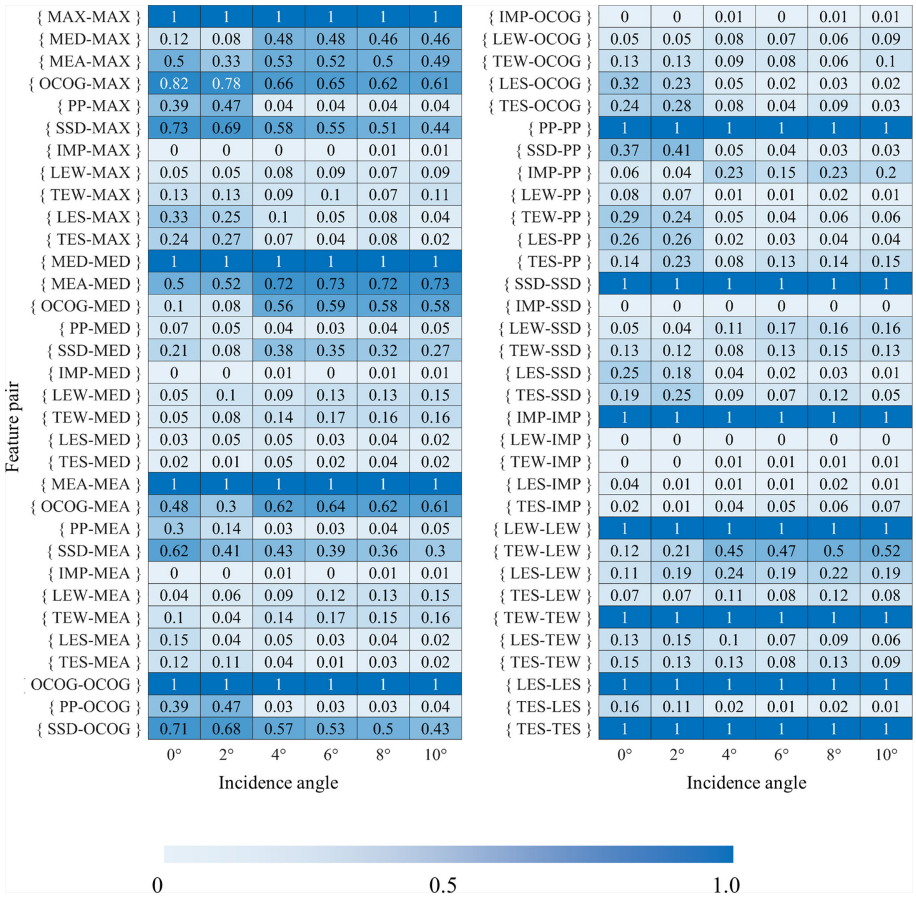

FIGURE 3
MIMs of 66 feature pairs at small incidence angles.

Considering that no one feature pair appears at all incidence angles, all features are considered in subsequent research.

3.2 Three classifiers

All features are used in the KNN, SVM and RF methods, and the model parameterization results are compared to the above feature analysis results.

3.2.1 RF

The number of decision trees in the RF method is varied from 10–100 with a step of 10, and the overall accuracies of sea ice and sea water are shown in Figure 4A. This subfigure shows that the accuracies are very steady under different conditions of decision trees, features and incidence angles, and the lines of maximum values are often very close to the lines of minimum values. The accuracies decrease very slowly as the number of trees increases, and the maximum change in the accuracies is approximately 1.2%. As a result, more trees do not produce higher accuracy for all features at six small incidence angles, but the run time does notably increase. Thus, the classification results of 10 decision trees (Tree 10) in the RF are compared with the KNN and SVM results.

TABLE 2 The feature pairs of which the MIMs are larger than 0.65 at six small incidence angles.

Angle	0°	2°	4°	6°	8°	10°
Feature pair	{OCOG–MAX} {SSD–MAX} {SSD–OCOG}	{OCOG–MAX} {SSD–MAX} {SSD–OCOG}	{OCOG–MAX} {MEA–MED}	{OCOG–MAX} {MEA–MED}	{MEA–MED}	{MEA–MED}

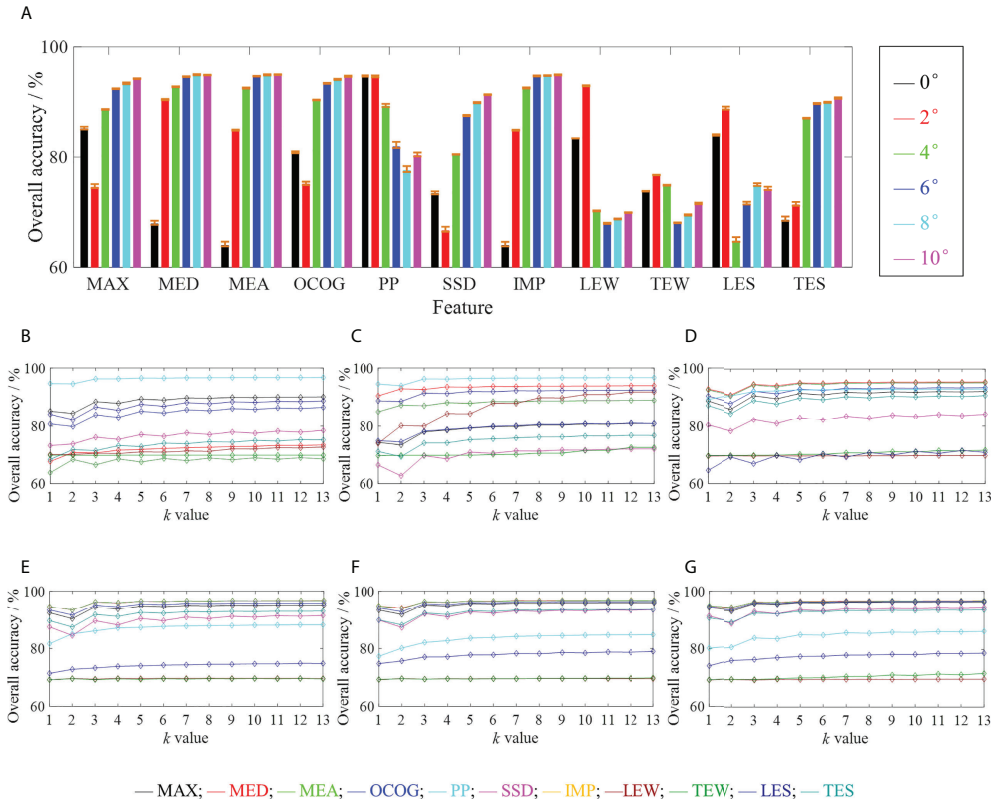

FIGURE 4
Overall accuracies of the RF method for different tree numbers and the KNN method for different *k* values at small incidence angles: **(A)** Different numbers of RF trees: Mean values of the overall accuracies are expressed by the bars; The maximum value and minimum value of the overall accuracies are indicated by two orange short lines on the bar, respectively; The upper line represents the maximum value, and the lower line is the minimum value; **(B)** Different *k* values at 0°; **(C)** Different *k* values at 2°; **(D)** Different *k* values at 4°; **(E)** Different *k* values at 6°; **(F)** Different *k* values at 8°; **(G)** Different *k* values at 10°.

3.2.2 KNN

Two parameters in the KNN method are tested: the *k* value and distance. The value range of *k* is set to 1 to 13, and the accuracy of the corresponding results is shown in Figures 4B–G. At all incidence angles, the change in accuracy can reach 17% before $k = 5$; then, the accuracy change remains at approximately 1.7% (only LEW of 2° is about 6.7%) for *k* values from 5 to 11, and 1.0% for *k* values larger than 11. Thus, *k* is set to 11 in the KNN model.

The three distances (Euclidean distance, Manhattan distance, and Mahalanobis distance) are analyzed, and the results are compared with those of the RF and SVM, as shown in Figure 5. The run time of the model with Euclidean distance is slightly shorter than that of the model based on the Manhattan distance and much shorter than that of the model with the Mahalanobis distance.

3.2.3 SVM

The SVM run times with different kernels are as follows in ascending order: linear kernel, Gaussian kernel, polynomial kernel with *q* equal to 2 (Polynomial 2), and polynomial kernel with *q* equal to 3 (Polynomial 3). The accuracy results are compared for eight cases, namely, 'Tree 10' for the RF with 10 trees, the KNN with $k = 11$ and three different distance measures, and the SVM with three different kernels, as shown in Figure 5.

The overall accuracy results illustrate that the KNN model with Euclidean distance yields better results than the other cases, except for IMP at 0°, LEW and TEW from 0–4°, and LES at 4°. Thus, the optimal classifier is the KNN method with Euclidean distance and *k* equal to 11. The overall accuracies for single features are shown in Table 3. The top-three features with the highest accuracies at small incidence angles are marked in red.

At 0–2°, PP and LES are common top features, and PP is also noted as a top feature in the CPDs (Section 3.1.1). At 4–6°, the results are similar to those at 8–10°, which is consistent with the CPD results. At 8–10°, higher accuracies are observed than those at other incidence angles. Moreover, at 4–6° and 8–10°, the two incidence sets have the same top-three features (MED, MEA, and IMP); both MED and MEA are effective for sea ice and sea

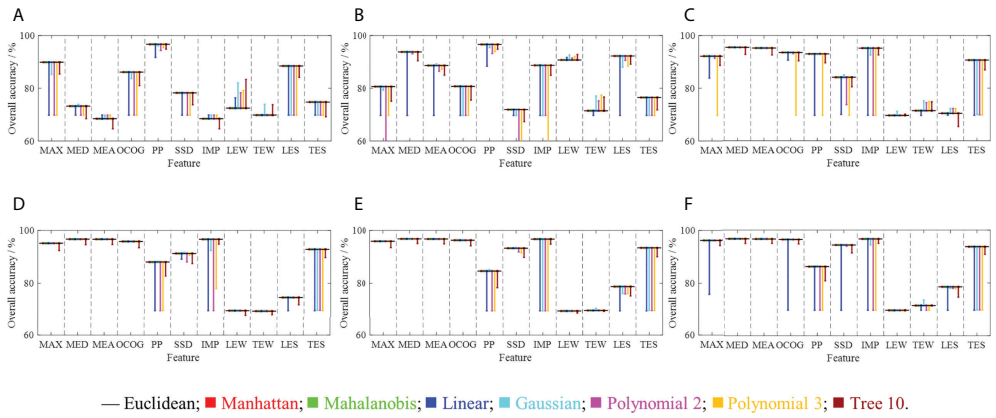

FIGURE 5
Overall accuracies of the individual RF, KNN and SVM models with different settings: **(A)** 0°; **(B)** 2°; **(C)** 4°; **(D)** 6°; **(E)** 8°; **(F)** 10°. The result of the Euclidean distance is expressed as the solid black line, and the other kernels, distances and Tree 10 are shown as bars based on the Euclidean distance. Upward bars express their accuracies higher than the overall accuracies of the Euclidean distance, and the downward bars express their accuracies less than the overall accuracies of the Euclidean distance.

water separation in agreement with their CPDs and MIMs in Section 3.1.

3.3 Optimal classifier-feature assembly

The eleven features can be used to construct 2047 feature combinations at each incidence angle. These feature combinations are input into the optimal classifier, that is, the KNN classifier with Euclidean distance and $k = 11$; the resulting F1 scores and overall accuracies are shown in Figure 6.

The optimal feature combination that yields the highest accuracy at each incidence angle is shown in Table 4. The highest overall accuracy reaches 97.1%. There are few identical features in the optimal combinations of each incidence set because of the large number of feature combinations. For different feature combinations, the numbers of overall accuracies better than 96% are 970, 948, 994, 1769, 1879, and 1430 at each incidence angles, respectively. As a result, we focus on not only the optimal feature combinations but also the feature combinations that score in the top-5 percent in terms of overall accuracy. The occurrence probabilities of single features in these top combinations are analyzed, as shown in Figure 6D. The results for 6–10° are better than those at other incidence angles.

At 0–2°, the optimal/top combinations mainly include MED, MEA, OCOG, PP, SSD, LES and TES (F{2,3,4,5,6,10,11}). PP (F5), as an important feature in altimeter-based sea ice recognition, is common in the top combinations and is high ranking in the above CPDs (Section 3.1.1) and single feature classification results (Section 3.2). OCOG and SSD (F4, F6) are relevant in MIMs, but are still functional in the optimal

TABLE 3 Overall accuracies of single features at small incidence angles using the optimal classifier (the KNN method with Euclidean distance and *k* equal to 11).

ID Number	Feature	0°	2°	4°	6°	8°	10°
F1	MAX	89.9%	80.6%	92.2%	95.1%	95.9%	96.2%
F2	MED	73.2%	93.8%	95.5%	96.7%	96.8%	96.7%
F3	MEA	68.5%	88.6%	95.3%	96.7%	96.8%	96.6%
F4	OCOG	86.1%	80.7%	93.6%	95.8%	96.3%	96.5%
F5	PP	96.7%	96.6%	93.0%	88.1%	84.7%	86.2%
F6	SSD	78.3%	71.9%	84.2%	91.3%	93.3%	94.4%
F7	IMP	68.5%	88.7%	95.2%	96.7%	96.7%	96.7%
F8	LEW	72.5%	90.8%	69.7%	69.7%	69.5%	69.6%
F9	TEW	69.8%	71.5%	71.5%	69.5%	69.7%	71.4%
F10	LES	88.5%	92.2%	70.5%	74.7%	78.8%	78.5%
F11	TES	74.8%	76.5%	90.7%	92.8%	93.4%	93.7%

10.3389/fmars.2022.986228

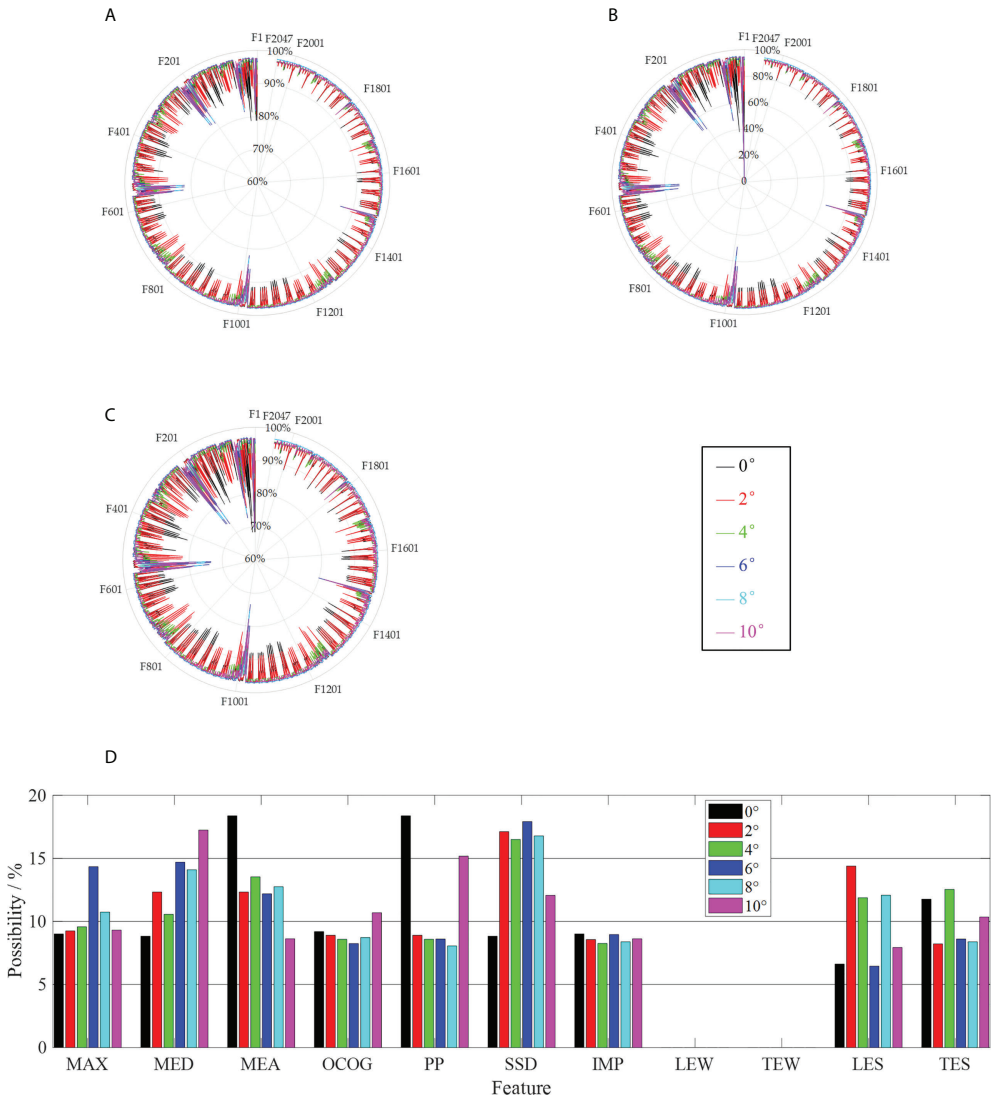

FIGURE 6
F1 scores and overall accuracies of 2047 feature combinations for sea ice and sea water discrimination at six small incidence angles. **(A)** F1 scores of sea ice; **(B)** F1 scores of sea water; **(C)** Overall accuracies; **(D)** Occurrence possibilities of single features in the top 5% feature combinations. The numbers in **(A)** – **(C)** represent the ID Numbers of the feature combinations, seen in the 'Supplementary Material' file.

TABLE 4 Overall accuracy of the optimal feature combination at each small incidence angle using the optimal classifier (the KNN method with Euclidean distance and *k* equal to 11).

ID Number	Combinations	OA/%	ID Number	Combinations	OA/%
0°				2°	
F441	F{3,4,5,11}	96.9%	F1033	F{1,2,3,4,6,10}	96.9%
4°				6°	
F1194	F{1,3,5,6,10,11}	96.7%	F247	F{1,2,5,6}	97.1%
8°				10°	
F578	F{1,2,3,6,10}	97.0%	F797	F{2,3,5,6,11}	96.9%

combination of F1033 at 2°, which implies that the two features can play their own roles for sea ice recognition. At 4–6°, the optimal/top combinations mainly include MAX, MED, MEA, PP, SSD, LES and TES (F{1,2,3,5,6,10,11}). MED and MEA (F2, F3) can also be effectively used to distinguish between sea ice and sea water suggested by CPDs and single feature classification. The two features have high relevance in MIMs, and they are the important features in optimal combinations of F1194 at 4° and F247 at 6°, respectively. At 8–10°, the optimal/top combinations mainly include MAX, MED, MEA, PP, SSD, LES and TES (F {1,2,3,5,6,10,11}). MED and MEA (F2, F3) are very useful to discriminate sea ice and sea water indicated by CPDs and single feature classification. MED and MEA are redundant in MIMs and provide respective contributions in the optimal combinations of F578 at 8° and F797 at 10°. MEA performs better than OCOG for 4° to 10°, which indicates that MEA may be more suitable to express σ_0 for 4° to 10°. The results at 4–6° are similar to those at 8–10°, as observed in the CPDs and single feature classification.

According to the above results, angles from 6° to 10° are best for distinguishing between sea ice and sea water. The top feature combinations display obvious consistency with the relevant CPD results and single feature classification results. Moreover, these results are in partial agreement with MIM analysis results. Nevertheless, some features in redundant or relevant feature pairs can play their own functions for sea ice and sea water discrimination in the optimal combination. Therefore, optimal classifier–feature assembly at each incidence angle can be used for sea ice recognition based on SWIM data.

3.4 Application analysis of optimal classer-feature assembly

3.4.1 Sea ice recognition accuracies in three stages of sea ice development

The three stages of sea ice development in the Arctic ice year of 2020/2021 are expressed specifically by combining the AARI and NSIDC sea ice charts as follows. The first stage is from 4th to 27th October, 2020 (Stage 1), when the sea ice changed clearly. The second stage is from 1st November to 29th December, 2020 (Stage 2), when the sea ice grew rapidly. The third stage is from 3rd January to 27th April, 2021 (Stage 3), when the sea ice distribution was stable. Several regions where sea ice and sea water do not vary throughout each stage are selected according to sea ice charts in the three stages. The selected invariant regions of the categories for Stages 1–3 are as large as possible, as shown in Figure 7.

For each stage, five time intervals of one day (T1), three days (T2), one week (T3), one month (T4) and one stage (T5) are selected, and T4 and T5 are the same in Stage 1. The overall accuracies are shown in Table 5.

In the three stages, the overall accuracies of the optimal assemblies at small incidence angles in T1–T5 are higher than 90%. In addition, the accuracy generally increases as sea ice development stabilizes. Moreover, the excellent accuracies may be partly due to homogeneous characteristics in these areas where boundary regions of sea ice and sea water are not included. Therefore, optimal classifier–feature assemblies can be effectively used for sea ice and sea water separation at all incidence angles in short- and long-term periods.

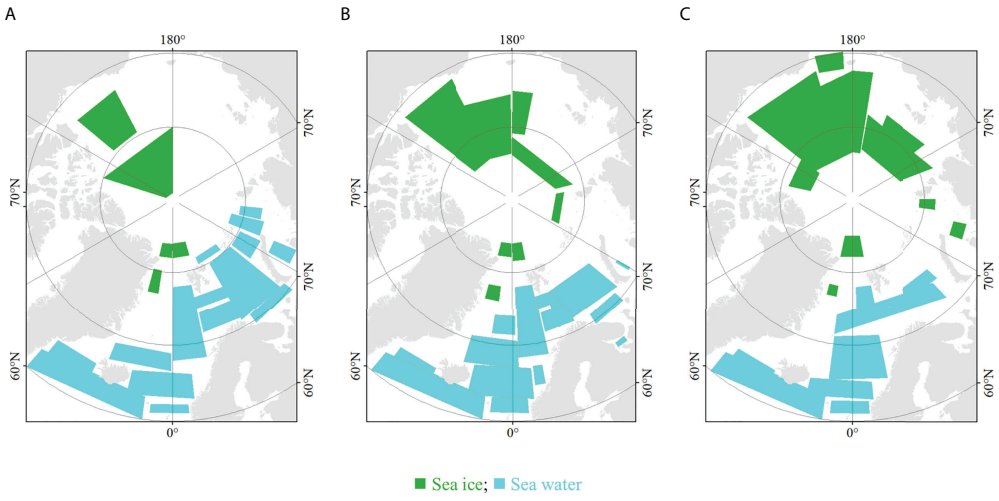

FIGURE 7
Invariant regions of the sea ice distribution at each stage: **(A)** Stage 1; **(B)** Stage 2; **(C)** Stage 3.

TABLE 5 The overall accuracies for Stages 1–3 using the optimal classifier–feature assembly at each small incidence angle.

Angle	Stage 1					Stage 2					Stage 3				
	T1	T2	T3	T4	T5	T1	T2	T3	T4	T5	T1	T2	T3	T4	T5
0°	94.8%	96.8%	96.9%	97.7%	97.7%	97.4%	98.4%	98.9%	99.2%	99.4%	99.8%	99.8%	99.8%	99.7%	99.7%
2°	98.9%	99.2%	99.4%	99.5%	99.5%	98.5%	99.2%	99.5%	99.8%	99.8%	99.9%	99.9%	99.9%	99.9%	99.9%
4°	98.5%	98.6%	98.9%	99.0%	99.0%	97.3%	98.1%	98.7%	99.2%	99.4%	99.9%	99.9%	99.9%	99.9%	99.9%
6°	97.2%	98.3%	98.5%	99.2%	99.2%	98.3%	98.9%	99.3%	99.6%	99.8%	99.7%	99.9%	99.9%	99.9%	99.9%
8°	95.2%	97.3%	97.2%	98.3%	98.3%	98.1%	98.8%	99.2%	99.5%	99.7%	99.3%	99.8%	99.8%	99.8%	99.8%
10°	93.1%	96.1%	95.9%	97.6%	97.6%	98.1%	98.7%	99.1%	99.4%	99.6%	99.1%	99.7%	99.7%	99.7%	99.7%

3.4.2 Sea ice extent and edge extraction

The sea ice recognition results based on SWIM data can be applied to detect sea ice extents and edges. According to the SWIM coverage, seven-day data are merged to build a grid image with a resolution of 25 km × 25 km in the polar stereographic projection, consistent with NSIDC sea ice products for the Arctic. In one grid, the sea ice proportion can be calculated based on the number of sea ice footprints divided by the total numbers of sea ice and sea water footprints. The grids where the sea ice proportion is not lower than 15% are set to sea ice regions, and others are sea water regions; then, sea ice extents and edges can be identified. Three SWIM results of sea ice extents and edges, combining synchronous Sentinel-1 SAR images from the ice year of 2020/2021, are used as examples to assess the proposed approach during November 11th – 17th, 2020, February 11th – 17th, 2021, and March 11th – 17th, 2021. Additionally, these results are also compared with the NSIDC sea ice products. The time difference between the acquisitions of the Sentinel-1 SAR images and the release of the AARI sea ice charts or the NSIDC products is less than 1 day. And, when SWIM results are evaluated by a SAR image, these results should be obtained on one day (SR-1). Then, the time difference between the acquisitions of the SAR image and SWIM data is less than 1 day. Comparison of sea ice extents and edges between SWIM and NSIDC are shown in Figure 8. For each grid, the type of SWIM (in seven days, SR-7) and NSIDC (in one day, NR-1) are compared, then the percentage of the grids with the same type (sea ice or water) is found to be 94.8% (SR-7 from November 11th – 17th, and SAR and NR-1 on November 11th), 97.7% (SR-7 from February 11th – 17th, and SAR and NR-1 on February 17th), and 98.2% (SR-7 from March 11th – 17th, and SAR and NR-1 on March 17th), respectively. These results reveal that SWIM sea ice extents are consistent with those of NSIDC.

The obvious differences of sea ice extents between SWIM and NSIDC mainly occur in coastal areas and sea ice edges. In the coastal areas, the land information can influence the results of sea ice recognition, and in sea ice edges, the confusion of sea ice and sea water may also affect the results. The differences in the sea ice edges are studied combining synchronous Sentinel-1 SAR images. And in order to clearly reveal these differences, only the sea ice edges of overlapping regions of NR-1 and SR-7 or SR-1 are shown in Figure 9.

From November 11th – 17th, the SWIM sea ice edges are matched with the Sentinel-1 SAR image obtained on November 11th. A comparison of the sea ice edges in the SWIM and NSIDC products with the Sentinel-1 image indicates that the sea ice distribution is overestimated in SR-7 and NR-1 products, and the result of SR-7 is worse than that of NR-1, as shown by the blue line and purple line in Figure 9H. Considering that sea ice developed rapidly in November, SR-1 on November 11th is chosen to build grids (Figure 9F–G), and many blank grids (no data) appear; then, only regions with data are analyzed. The sea ice edge of SR-1 product agrees with the Sentinel-1 image, which is more accurate than NR-1 results. However, there is still one grid incorrectly labeled as sea ice in SR-1 result. From February 11th – 17th, sea ice edges of SR-1 are matched with the Sentinel-1 SAR image obtained on February 17th. Sea ice regions are overestimated in the NR-1 product, and slightly underestimated in the SR-1 product. The sea ice edge result of SR-1 is a bit better than that of NR-1. From March 11th – 17th, the SWIM sea ice edges are matched with the Sentinel-1 SAR image obtained on March 17th. The lead in the top left corner of the Sentinel-1 image is marked with a red line. In this area, the sea ice edges in the NR-1 product are more accurate than those in the SR-1 product, and occur a little underestimated. The misjudged regions in the SR-1 product are approximately the width of 2–3 grids and may be due to multiple categories in one footprint. Below the lead, compared with SR-1 results, the sea ice edges in the NR-1 product are misjudged in some grids. Therefore, for sea ice extents, the SWIM results are more consistent with the NSIDC results in the stable sea ice stage. Moreover, the sea ice edges in the SR-1 product are precise. SWIM can be a new data source to generate practical sea ice products.

4 Discussion

Our study mainly focuses on two objectives: the development of a sea ice recognition method for the new

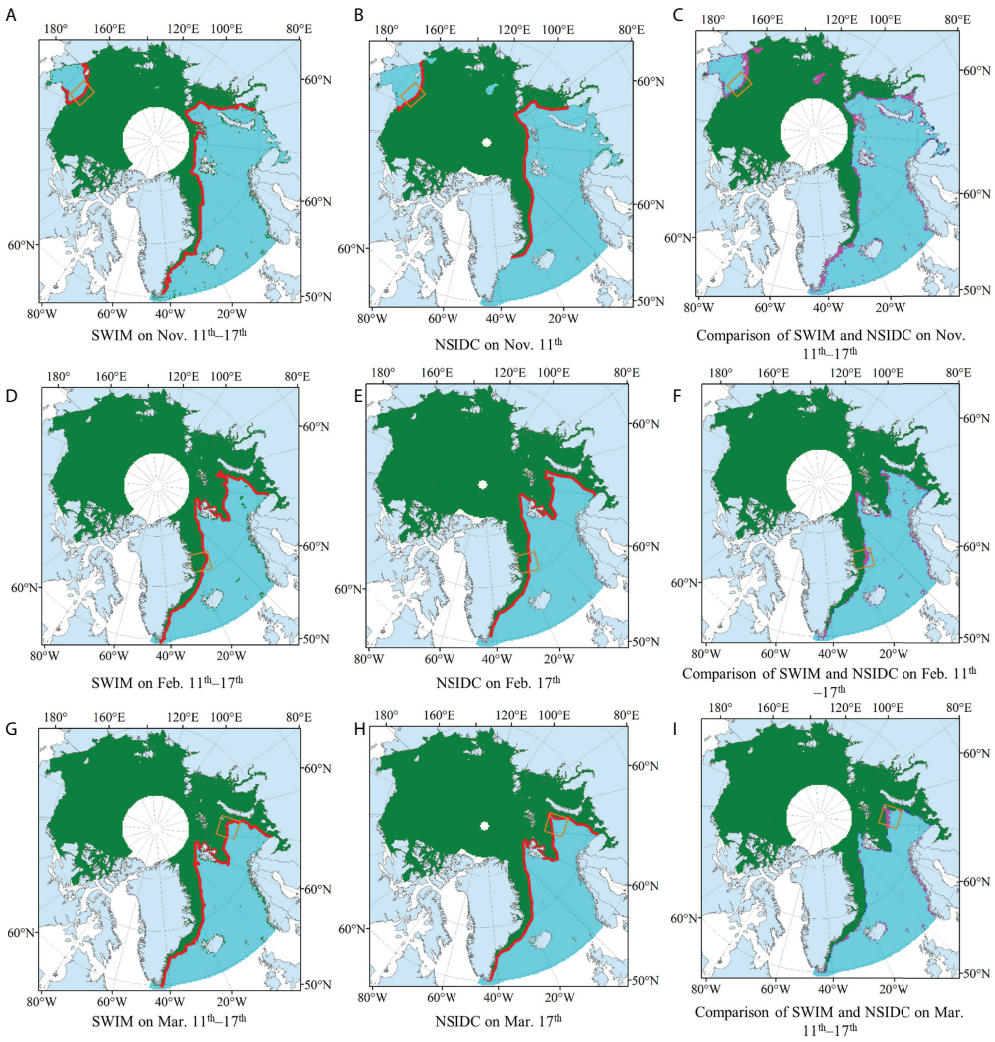

FIGURE 8
Comparison of sea ice extents and edges between SWIM and NSIDC. **(A)** SWIM on Nov. 11th – 17th; **(B)** NSIDC on Nov. 11th; **(C)** Comparison of SWIM and NSIDC on Nov. 11th – 17th; **(D)** SWIM on Feb. 11th – 17th; **(E)** NSIDC on Feb. 17th; **(F)** Comparison of SWIM and NSIDC on Feb. 11th – 17th; **(G)** SWIM on Mar. 11th – 17th; **(H)** NSIDC on Mar. 17th; **(I)** Comparison of SWIM and NSIDC on Mar. 11th – 17th.

SWIM observation mode and the application of SWIM data using optimal classifier–feature assemblies.

4.1 Development of sea ice recognition method

The six small incidence angles are divided into three sets according to the analysis of CPDs and MIMs, and these incidence sets exhibit distinct characteristics for sea ice recognition. The results at 4–6° encompass characteristics of those at 0–2° and 8–10° and coincide better with the results at 8–10°. For single feature classification, IMP and TES in our previous work were only used to separate FYI and MYI; whereas, in this study, they are adopted for sea ice and sea water separation, and the related feature LES is also used. In the previous work, the OCOG was used for 0° and MEA for 2–10°; whereas, in this study, both of them are used for all incidence angles. MED is a new feature, and is rarely introduced in other studies. At 0–2°, PP is the best feature, as previously reported for altimeter-based methods (Rinne and Similä, 2016; Paul et al., 2018; Jiang et al., 2019; Aldenhoff et al., 2019). From 4–10°, MEA, which reflects the properties of σ_0, highly enhances sea ice and water separation in conjunction with scatterometer and SAR

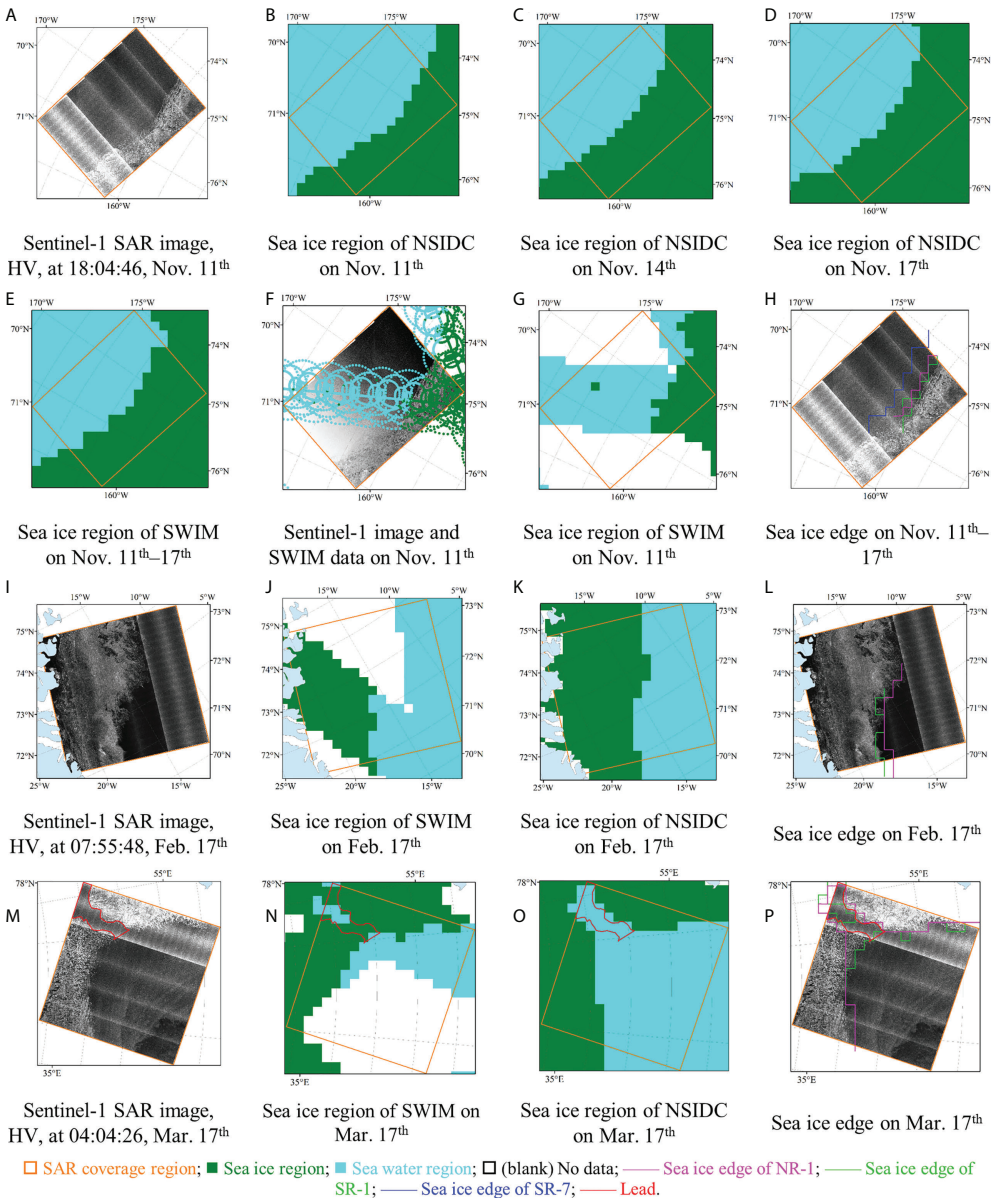

FIGURE 9
Sea ice edges based on SWIM and NSIDC data with synchronous Sentinel-1 SAR images. **(A)** Sentinel-1 SAR image, HV, at 18:04:46, Nov. 11th; **(B)** Sea ice region of NSIDC on Nov. 11th; **(C)** Sea ice region of NSIDC on Nov. 14th; **(D)** Sea ice region of NSIDC on Nov. 17th; **(E)** Sea ice region of SWIM on Nov. 11th – 17th; **(F)** Sentinel-1 image and SWIM data on Nov. 11th; **(G)** Sea ice region of SWIM on Nov. 11th; **(H)** Sea ice edge on Nov. 11th – 17th; **(I)** Sentinel-1 SAR image, HV, at 07:55:48, Feb. 17th; **(J)** Sea ice region of SWIM on Feb. 17th; **(K)** Sea ice region of NSIDC on Feb. 17th; **(L)** Sea ice edge on Feb. 17th; **(M)** Sentinel-1 SAR image, HV, at 04:04:26, Mar. 17th; **(N)** Sea ice region of SWIM on Mar. 17th; **(O)** Sea ice region of NSIDC on Mar. 17th; **(P)** Sea ice edge on Mar. 17th.

data (Otosaka et al., 2018; Zhang et al., 2019). Because LES and TES combine the properties of LEW and TEW with MAX, they yield higher accuracies than LEW and TEW in sea ice separation in agreement with our previous work (Liu et al., 2022). Although IMP is used in altimeter-based methods at 0° (Aldenhoff et al., 2019), it is also important from 4–10°. MED, not only reveals some of the characteristics of MAX but also describes the distribution properties of echo waveforms, and it yields excellent results from 2–10°. In general, the newly introduced MED, LES and TES features are valuable for sea ice recognition.

The main features in the optimal/top feature combinations at 0–2° are MED, MEA, OCOG, PP, SSD, LES and TES, agreeing with the results of previous studies. Drinkwater (1991) suggested that altimeters were sensitive to sea ice and that sea ice could be

detected based on waveform features such as pulse width (similar to LEW plus TEW), PP and σ_0 based on studies with a Ku-band airborne radar altimeter. Rinne and Similä (2016) reported classification accuracies of 87–92% for sea water and 31–97% for sea ice in three periods using the KNN method with PP, SSD, LEW, and LES based on Cryosat-2. Shen et al. 2017a; Shen et al., 2017b;) obtained a maximum accuracy of 96.6% for sea ice and 95.1% for sea water with an RF classifier using σ_0, MAX, PP, SSD, LEW, and TEW. Shu et al. (2019) distinguished between sea ice and sea water using an RF classifier with PP, LEW, TEW, SSD, MAX, and σ_0 and obtained accuracies above 95%. Müller et al. (2017) investigated Arctic areas using KNN and K-medoids classifiers with waveform features such as MAX and achieved accuracies up to 94%. Jiang et al. (2019) separated sea ice and sea water using KNN and SVM classifiers with wave features such as the PP of Haiyang-2 A/B, and their accuracies were approximately 80%. Thus, the classification accuracies in this study are better than those previously reported, which may be due to the using of more waveform features and the new feature (MED) at multiple small incidence angles in this paper.

The analysis of optimal/top feature combinations is consistent with that of the CPDs and it is partly consistent with that of the MIMs. Moreover, some feature pairs display high redundancy or relevance but play important roles in the optimal combination. The redundancy or relevance of features does not largely affect the performance of sea ice recognition using feature combinations. Therefore, sea ice and sea water recognition can be performed with high accuracy using the proposed optimal classifier–feature assemblies at small incidence angles. Moreover, our results are consistent with those of previous studies and indicate better effects.

4.2 Application of the optimal classifier–feature assemblies

The overall accuracies of sea ice recognition using the optimal classifier–feature assemblies in Stages 1–3 are higher than 90 percent. Sea ice development obviously affects the accuracy of the proposed approach. The invariant distribution of sea ice contributes to high overall accuracy. As a result, the optimal classifier–feature assembly can be used to provide sea ice recognition results with high accuracy, and sea ice can then be removed from SWIM sea wave products. Moreover, SWIM can be a valid data source for operational sea ice monitoring.

According to the sea ice recognition results based on SWIM data, sea ice extents and edges can be extracted and compared with Sentinel-1 SAR images and NSIDC sea ice products. SWIM sea ice extents are consistent with those of NSIDC at a high level of precision. And, SWIM provides a good one-day product of sea ice edges. In this study, the threshold of the sea ice proportion is 15 percent, following the common threshold used for sea ice recognition. However, one SWIM footprint may consist of both sea ice and sea water. In addition, areas with sea ice–water mixing can generate complex waveform signals (March 17th, 2021, Figure 9P), and a fixed proportional threshold of sea ice and sea water is not appropriate. As a result, the threshold for SWIM data should be further studied. The sea ice edges on March 17th are used as examples to analyze the threshold, and the thresholds are set as 40%, 50%, and 60%, as shown in Figure 10. Sea ice regions evidently decrease with increasing threshold, and the threshold of 50% is most suitable for sea ice edge extraction on March 17th, especially for the lead. Thus, the threshold of 15% is not appropriate for all situations. In future work, the threshold selection should be studied; for example, the sea ice distribution and its development stage should be considered. In addition, the probability that one SWIM footprint is classified to sea ice or sea water using the optimal classifier–feature assembly is extracted. As a result, one footprint is not simply judged to sea ice or sea water. The probability is used to calculate the sea ice proportion of one grid, which may improve its accuracies.

The results of sea ice recognition in this study are compared to those of sea ice classification in our previous study, and the optimal classifier–feature assemblies at all incidence angles proposed here yield better results. Therefore, sea ice recognition can be accurately performed with the optimal classifier–feature assemblies at small incidence angles in the short- and long-term periods. And, the optimal classifier–feature assemblies can satisfy the sea ice removal requirements for SWIM products, and improve sea ice extent and edge products. In order to further verify the optimal classifier–feature assemblies, more sea ice charts should be introduced, for example, sea ice products of Canadian Ice Service and the University of Bremen (Shi et al., 2020; Komarov and Buehner, 2021). Moreover, new validation methods are also considered for multiple sea ice charts (Wang J. et al., 2021). Our work can fill the gap of sea ice recognition at the multiple small incidence angles, then, achieve the sea ice recognition at normal-, small- and mid-incidence angles.

5 Conclusion

SWIM, as a new type of microwave remote sensor at multiple incidence angles, has been rarely used for sea ice recognition. The main objectives of this study are to develop a sea ice recognition method based on SWIM data with a new observation mode and assess the application of the proposal method, including waveform feature analysis, optimal classifier–feature assembly construction (classifier selection and parameter setting, and feature combination selection), and the assembly application.

(1) Waveform feature analysis

Eleven waveform features of SWIM data in the Arctic from October 2020 to April 2021 are extracted. CPDs and MIMs are

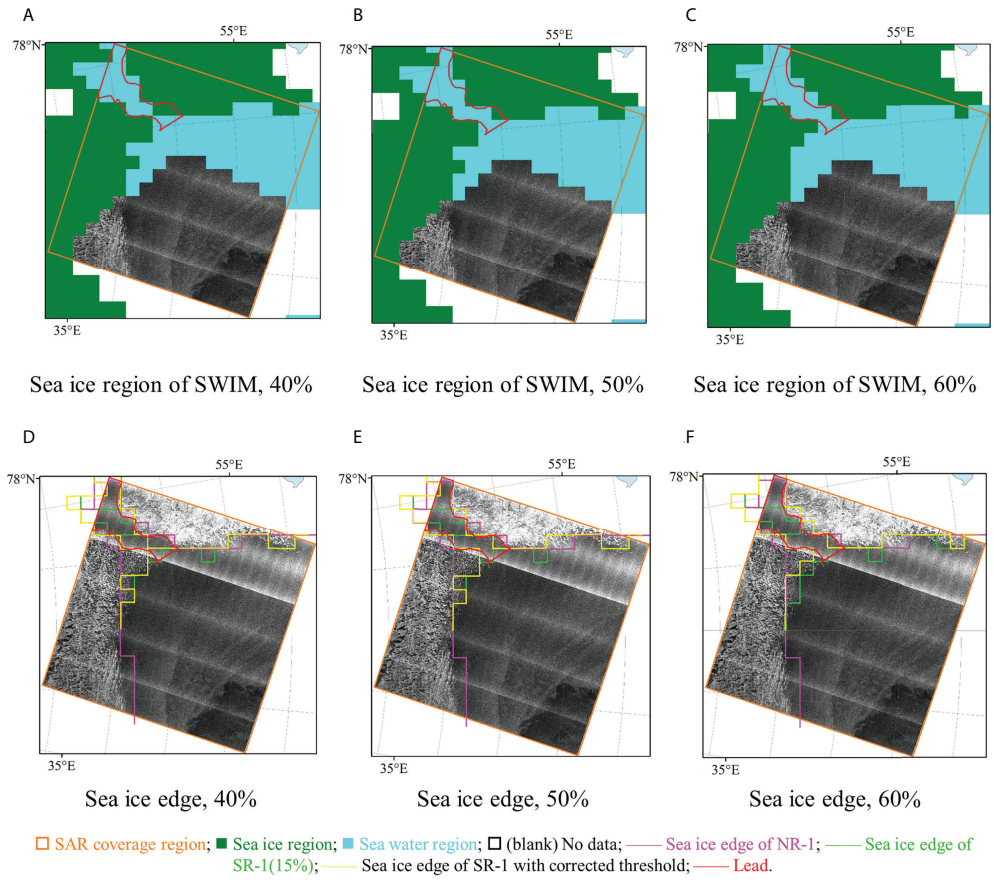

FIGURE 10
Sea ice edges based on SWIM data with different thresholds of the sea ice proportion. **(A)** Sea ice region of SWIM, 40%; **(B)** Sea ice region of SWIM, 50%; **(C)** Sea ice region of SWIM, 60%; **(D)** Sea ice edges, 40%; **(E)** Sea ice edges, 50%; **(F)** Sea ice edges, 60%.

used to analyze the characteristics of these waveform features. The results reveal that incidence angles can be divided into three sets at 0–2°, 4–6° and 8–10°. These incidence sets display unique distribution ranges and probabilities for each feature, and the redundancy or relevance of each feature pair is evaluated.

(2) Optimal classifier–feature assembly construction

The RF, KNN and SVM classifiers are explored, and their parameters are set according to the overall accuracies obtained for single features. The KNN classifier with Euclidean distance and k equal to 11 yields the optimal result. Then, feature combinations with the KNN method are used to separate sea ice and sea water and build the optimal classifier-feature assembly for each small incidence angle. The results illustrate that the highest overall accuracy at each incidence angle is greater than 96% and can reach 97.1%. The newly introduced features in this study, such as MED, perform very well.

(3) Optimal classifier–feature assembly application

The application of the optimal classifier–feature assemblies is analyzed. On the one hand, the optimal assemblies are used to distinguish between the sea ice and sea water in different growing stages, and the accuracies are higher than 93.1%, and can reach 99.9%. Then, the results can meet the requirements for SWIM-based sea wave retrieval. On the other hand, sea ice extents can be extracted from these SWIM results with high accuracies that are higher than 94.8% and up to 98.2%, and SWIM provides a better one-day product of sea ice edges than the NSIDC product. The results indicate that SWIM can provide new data for operational sea ice monitoring. Our results are also compared with those of other studies and indicate better effects and consistency.

In conclusion, in this study, a sea ice recognition method using optimal classifier–feature assemblies is proposed, and it can not only perform sea ice recognition with high accuracy using new-mode SWIM data but also provide discrimination flags of sea ice in SWIM products. Moreover, our research on the application of the proposal method can reliably provide sea ice extent and edge products, then SWIM data can be used as a new data source for operational sea ice monitoring.

In future work, more SWIM data from different ice years will be used to verify the validity and robustness of the classifier–feature assemblies. And, other classifiers, such as Bayesian, convolutional

neural network and propagation neural network classifiers, will be studied to potentially improve sea ice recognition. Moreover, more sea ice products such as the sea ice concentration and types will be further studied in conjunction with SWIM data.

Data availability statement

The original contributions presented in the study are included in the article/Supplementary Material. Further inquiries can be directed to the corresponding author.

Author contributions

ML made most of analysis and wrote the main manuscript. RY and XZi made interpretation and discussion of the results. PC and YX reviewed the manuscript. YZ, YG, YC, XZia, SL undertook the data processing. All authors made important contributions to the contents of the paper. All authors have revised and approved the manuscript.

Funding

This research was funded in part by the Shandong Provincial Natural Science Foundation, China under grant ZR2019MD016; the National Natural Science Foundation of China under grant 41976173, 61971455, and 41976168; the Shandong Provincial Natural Science Foundation, China under grant ZR2020MD095, ZR201910290171; the Shandong joint fund of National Natural Science Foundation of China under grant U2006207; and the Ministry of Science and Technology of China and the European Space Agency through the Dragon-5 Program under grant 57889.

Acknowledgments

Sea ice recognition was based on the SWIM. SWIM data of CFOSAT were obtained from https://osdds.nsoas.org.cn. The authors would like to thank NSOAS for providing the data free of charge. Sea ice charts were provided by the AARI and NSIDC. The accuracy evaluation of sea ice recognition was supported partly by Sentinel-1 SAR data. The publication is supported by the University-Industry Joint Center for Ocean Observation and Broadband Communication.

Conflict of interest

The authors declare that the research was conducted in the absence of any commercial or financial relationships that could be construed as a potential conflict of interest.

Publisher's note

All claims expressed in this article are solely those of the authors and do not necessarily represent those of their affiliated organizations, or those of the publisher, the editors and the reviewers. Any product that may be evaluated in this article, or claim that may be made by its manufacturer, is not guaranteed or endorsed by the publisher.

Supplementary material

The Supplementary Material for this article can be found online at: https://www.frontiersin.org/articles/10.3389/fmars.2022.986228/full#supplementary-material

References

Aldenhoff, W., Heuzé, C., and Eriksson, L. E. B. (2019). Sensitivity of radar altimeter waveform to changes in Sea ice type at resolution of synthetic aperture radar. *Remote Sens.* 11, 2602. doi: 10.3390/rs11222602

Arctic and Antarctic Research Institute (2022) *AARI*. Available at: http://www.aari.ru/ (Accessed 2022).

Asadi, N., Scott, K. A., Komarov, A. S., Buehner, M., and Clausi, D. A. (2021). Evaluation of a neural network with uncertainty for detection of ice and water in SAR imagery. *IEEE Trans. Geosci. Remote Sensing.* 59, 247–259. doi: 10.1109/TGRS.2020.2992454

Berg, A., and Eriksson, L. E. (2012). SAR algorithm for sea ice concentration–evaluation for the Baltic Sea. *IEEE Geosci. Remote Sens. Lett.* 9 (5), 938–942. doi: 10.1109/LGRS.2012.2186280

Bi, H., Zhang, J., Wang, Y., Zhang, Z., Zhang, Y., Fu, M., et al. (2018). Arctic Sea Ice volume changes in terms of age as revealed from satellite observations. *IEEE J. Sel. Top. Appl. Earth Obs. Remote Sens.* 11, 1–15. doi: 10.1109/JSTARS.2018.2823735

Breivik, L. A., Eastwood, S., and Lavergne, T. (2012). Use of c-band scatterometer for Sea ice edge identification. *IEEE Trans. Geosci. Remote Sens.* 50, 2669–2677. doi: 10.1109/TGRS.2012.2188898

Cavalieri, D. J., Parkinson, C., Gloersen, P., Zwally, H., Meier, W., Fetterer, F., et al. (1996). *Data from: Sea ice concentrations from nimbus-7 SMMR and DMSP SSM/I-SSMIS passive microwave data, version 1* (University of Colorado Boulder: NSIDC). Available at: https://nsidc.org/data/NSIDC-0051/versions/1.

Chan, C. W., and Paelinckx, D. (2008). Evaluation of random forest and adaboost tree-based ensemble classification and spectral band selection for ecotope mapping using airborne hyperspectral imagery. *Remote Sens. Environment.* 112, 2999–3011. doi: 10.1016/j.rse.2008.02.011

Cheng, A., Casati, B., Tivy, A., Zagon, T., Lemieux, J. F., and Tremblay, L. B. (2020). Accuracy and inter-analyst agreement of visually estimated sea ice concentrations in Canadian ice service ice charts using single-polarization RADARSAT-2. *Cryosphere.* 14, 1289–1310. doi: 10.5194/tc-14-1289-2020

de Gélis, I., Colin, A., and Longepe, N. (2021). Prediction of categorized sea ice concentration from sentinel-1 SAR images based on a fully convolutional network. *IEEE J. Selected Topics Appl. Earth Observat. Remote Sens.* 14, 5831–5841. doi: 10.1109/JSTARS.2021.3074068

Drinkwater, M. R. (1991). Kuband airborne radar altimeter observations of marginal sea ice during the 1984 marginal ice zone experiment. *J. Geophys. Res.* 96, 4555. doi: 10.1029/90jc01954

Drinkwater, M. R., and Carsey, F. D. (1991). Observations of the late-summer to fall sea ice transition with the 14.6 GHz seasat scat-terometer. *IEEE* 3, 1597–1600. doi: 10.1109/IGARSS.1991.579499

Gohin, F., and Cavanie, A. (1994). A first try at identification of sea ice using the three beam scatterometer of ERS-1. *Int. J. Remote Sensing.* 15, 1221–1228. doi: 10.1080/01431169408954156

Haarpaintner, J., and Spreen, G. (2007). Use of enhanced-resolution QuikSCAT/SeaWinds data for operational ice services and climate research: Sea ice edge, type, concentration, and drift. *IEEE Trans. Geosci. Remote Sens.* 45 (10), 3131–3137. doi: 10.1109/TGRS.2007.895419

Hauser, D., Tison, C., Amiot, T., Delaye, L., Corcoral, N., and Castillan, P. (2017). Swim: The first spaceborne wave scatterometer. *IEEE Trans. Geosci. Remote Sens.* 55, 3000–3014. doi: 10.1109/TGRS.2017.2658672

Hauser, D., Tison, C., Amiot, T., Delaye, L., Mouche, A., Guitton, G., et al. (2016). "CFOSAT: A new Chinese-French satellite for joint observations of ocean wind vector and directional spectra of ocean waves," in *Remote Sens. Ocean. Inland Wa-ters Tech. Appl. Chall.* . (New Delhi, India: SPIE Asia-Pacific Remote Sensing) 9878, 1–20. doi: 10.1117/12.2225619

Hauser, D., Tourain, C., Hermozo, L., Alraddawi, D., and Tran, N. T. (2020). New observations from the swim radar on-board cfosat: Instrument validation and ocean wave measurement assessment. *IEEE Trans. Geosci. Remote Sens.* 59, 5–26. doi: 10.1109/TGRS.2020.2994372

Hoekstra, M., Jiang, M., Clausi, D. A., and Duguay, C. (2020). Lake ice-water classification of RADARSAT-2 images by integrating IRGS segmentation with pixel-based random forest labeling. *Remote Sensing.* 12, 1425. doi: 10.3390/rs12091425

Jiang, C., Lin, M., and Wei, H. (2019). A study of the technology used to distinguish Sea ice and seawater on the haiyang-2A/B (HY-2A/B) altimeter data. *Remote Sens.* 11, 1490. doi: 10.3390/rs11121490

Karvonen, J., Simila, M., and Makynen, M. J. I. G. (2005). Open water detection from Baltic Sea ice radarsat-1 SAR imagery. *IEEE Geosci. Remote Sens. Lett.* 2, 275–279. doi: 10.1109/LGRS.2005.847930

Komarov, A. S., and Buehner, M. (2021). Ice concentration from dual-polarization SAR images using ice and water retrievals at multiple spatial scales. *IEEE Trans. Geosci. Remote Sens.* 59 (2), 950–961. doi: 10.1109/TGRS.2020.3000672

Laxon, S. (1994). Sea Ice extent mapping using the ERS-1 radar altimeter. *EARSeL Adv. Remote Sens* 3, 112–116.

Li, X. M., Sun, Y., and Zhang, Q. (2021). Extraction of sea ice cover by sentinel-1 SAR based on support vector machine with unsupervised generation of training data. *IEEE Trans. Geosci. Remote Sens.* 59 (4), 3040–3053. doi: 10.1109/TGRS.2020.3007789

Liu, H., Guo, H., and Zhang, L. (2015). SVM-based sea ice classification using textural features and concentration from RADARSAT-2 dual-pol ScanSAR data. *IEEE J. Selected Topics Appl. Earth Observat. Remote Sensing.* 8 (4), 1601–1613. doi: 10.1109/JSTARS.2014.2365215

Liu, M., Yan, R., Zhang, J., Xu, Y., Chen, P., Shi, L., et al. (2022). Arctic Sea Ice classification based on CFOSAT SWIM data at multiple small incidence angles. *Remote Sensing.* 14 (1), 91. doi: 10.3390/rs14010091

Liu, M., Zhang, X., Chen, P., Wang, J., and Zhong, S. (2021). "Arctic Sea-Ice type recognition based on the surface wave investigation and monitoring instrument of the China-French ocean satellite," in *In 2021 Photonics & Electromagnetics Research Symposium (PIERS)*. (Hangzhou, China: IEEE). 2362–2369. doi: 10.1109/PIERS53385.2021.9695052

Müller, F. L., Dettmering, D., Bosch, W., and Seitz, F. (2017). Monitoring the Arctic seas: How satellite altimetry can be used to detect open water in Sea-ice regions. *Remote Sens.* 9, 551. doi: 10.3390/rs9060551

National Snow and Ice Data Center (2022) *NSIDC*. Available at: https://nsidc.org/data/NSIDC-0051/versions/1.

Otosaka, I., Rivas, M. B., and Stoffelen, A. (2018). Bayesian Sea Ice detection with the ERS scatterometer and sea ice backscatter model at c-band. *IEEE Trans. Geosci. Remote Sensing.* 56, 2248–2254. doi: 10.1109/TGRS.2017.2777670

Paul, S., Hendricks, S., Ricker, R., Kern, S., and Rinne, E. (2018). Empirical parametrization of envisat freeboard retrieval of Arctic and Antarctic sea ice based on CryoSat-2: Progress in the ESA climate change initiative. *Cryosphere.* 12 (7), 2437–2460. doi: 10.5194/tc-12-2437-2018

Remund, Q. P., and Long, D. G. (1999). Sea-Ice extent mapping using Ku-band scatterometer data. *J. Geophys. Res. Ocean.* 104, 11515–11527. doi: 10.1029/98JC02373

Remund, Q. P., and Long, D. G. (2014). A decade of QuikSCAT scatterometer Sea ice extent data. *IEEE Trans. Geosci. Remote Sens.* 52, 4281–4290. doi: 10.1109/TGRS.2013.2281056

Ren, L., Yang, J., Xu, Y., Zhang, Y., Zheng, G., Wang, J., et al. (2021). Ocean surface wind speed dependence and retrieval from off-nadir CFOSAT SWIM data. *Earth Space Sci.* 8 (6), e2020EA001505. doi: 10.1029/2020EA001505

Rinne, E., and Similä, M. (2016). Utilisation of CryoSat-2 SAR altimeter in operational ice charting. *Cryosphere* 10, 121–131. doi: 10.5194/tc-10-121-2016

Rivas, M. B., and Stoffelen, A. (2011). New Bayesian algorithm for sea ice detection with QuikSCAT. *IEEE Trans. Geosci. Remote Sens.* 49 (6), 1894–1901. doi: 10.1109/TGRS.2010.2101608

Rivas, M. B., Verspeek, J., Verhoef, A., and Stoffelen, A. (2012). Bayesian Sea Ice detection with the advanced scatterometer ASCAT. *IEEE Trans. Geosci. Remote Sens.* 50, 2649–2657. doi: 10.1109/TGRS.2011.2182356

Scharien, R. K., and Nasonova, S. (2022). Incidence angle dependence of texture statistics from sentinel-1 HH-polarization images of winter Arctic Sea ice. *IEEE Geosci. Remote Sens. Lett.* 19, 1–5. doi: 10.1109/LGRS.2020.3039739

Shen, X., Jie, Z., Xi, Z., Meng, J., and Ke, C. (2017b). Sea Ice classification using CryoSat-2 altimeter data by optimal classifier-feature assembly. *IEEE Geosci. Remote Sens. Lett.* 14, 1948–1952. doi: 10.1109/LGRS.2017.2743339

Shen, X. Y., Zhang, J., Meng, J. M., and Ke, C. Q. (2017a). "Sea Ice type classification based on random forest machine learning with cryosat-2 altimeter data," in *In 2017 International Workshop on Remote Sensing with Intelligent Processing (RSIP)*. (Shanghai, China: IEEE). 1–5. doi: 10.1109/RSIP.2017.7958792

Shi, Q., Su, J., Heygster, G., Shi, J., Wang, L., Zhu, L., et al. (2020). Step-by-Step validation of Antarctic ASI AMSR-e Sea-ice concentrations by MODIS and an aerial image. *IEEE Trans. Geosci. Remote Sens.* 59 (1), 392–403. doi: 10.1109/TGRS.2020.2989037

Shu, S., Zhou, X., Shen, X., Liu, Z., and Li, J. (2019). Discrimination of different sea ice types from CryoSat-2 satellite data using an object-based random forest (ORF). *Mar. Geod.* 5, 1–21. doi: 10.1080/01490419.2019.1671560

Wang, J. K., Aouf, L., Dalphinet, A., Li, B. X., Xu, Y., and Liu, J. Q. (2021). Acquisition of the significant wave height from CFOSAT SWIM spectra through a deep neural network and its impact on wave model assimilation. *J. Geophys. Res.: Oceans.* 126 (6), e2020JC016885. doi: 10.1029/2020JC016885

Wang, L., Ding, Z., Zhang, L., and Yan, C. (2019). Cfosat-1 realizes first joint observation of sea wind and waves. *Aerosp. China.* 20, 22–29. doi: 10.3969/j.issn.1671-0940.2019.01.004

Wang, J., Sun, W., and Zhang, J. (2021). Error characterization of satellite SSS products based on extended collocation analysis. *IEEE Trans. Geosci. Remote Sens.* 60, 1–11. doi: 10.1109/TGRS.2021.3107840

Xu, Y., Liu, J., Xie, L., Sun, C., and Xian, D. (2019). China-France Oceanography satellite (CFOSAT) simultaneously observes the typhoon-induced wind and wave fields. *Acta Oceanol. Sin.* 38, 158–161. doi: 10.1007/s13131-019-1506-3

Zakharova, E. A., Fleury, S., Guerreiro, K., Willmes, S., Rémy, F., Kouraev, A. V., et al. (2015). Sea Ice leads detection using SARAL/AltiKa altimeter. *Mar. Geodesy.* 38 (sup1), 522–533. doi: 10.1080/01490419.2015.1019655

Zhang, Z., Yu, Y., Li, X., Hui, F., Cheng, X., and Chen, Z. (2019). Arctic Sea ice classification using microwave scatterometer and radiometer data during 2002–2017. *IEEE Trans. Geosci. Remote Sensing.* 57 (8), 5319–5328. doi: 10.1109/TGRS.2019.2898872

Zhang, X., Zhu, Y., Zhang, J., Wang, Q., Shi, L., Meng, J., et al. (2021). Assessment of Arctic Sea ice classification ability of Chinese HY-2B dual-band radar altimeter during winter to early spring conditions. *IEEE J. Selected Topics Appl. Earth Observat. Remote Sens.* 14, 9855–9872. doi: 10.1109/JSTARS.2021.3114228

Zygmuntowska, M., Khvorostovsky, K., Helm, V., and Sandven, S. (2013). Waveform classification of airborne synthetic aperture radar altimeter over Arctic Sea ice. *Cryosphere* 7, 1315–1324. doi: 10.5194/tc-7-1315-2013

frontiers | Frontiers in Marine Science

TYPE Review
PUBLISHED 30 September 2022
DOI 10.3389/fmars.2022.971894

OPEN ACCESS

EDITED BY
Ludovic Brucker,
U.S. National Ice Center, United States

REVIEWED BY
Vanessa Lucieer,
University of Tasmania, Australia
Jan L. Lieser,
Bureau of Meteorology, Australia

*CORRESPONDENCE
Alvaro S. Scardilli
asscardilli@hidro.gov.ar

SPECIALTY SECTION
This article was submitted to Marine Affairs and Policy, a section of the journal Frontiers in Marine Science

RECEIVED 17 June 2022
ACCEPTED 14 September 2022
PUBLISHED 30 September 2022

CITATION
Scardilli AS, Salvó CS and Saez LG (2022) Southern Ocean ice charts at the Argentine Naval Hydrographic Service and their impact on safety of navigation
Front. Mar. Sci. 9:971894.
doi: 10.3389/fmars.2022.971894

Southern Ocean ice charts at the Argentine Naval Hydrographic Service and their impact on safety of navigation

Alvaro S. Scardilli*, Constanza S. Salvó and Ludmila Gomez Saez

Departamento Meteorología, Servicio de Hidrografía Naval, Buenos Aires, Argentina

Antarctica is a largely inhospitable and inaccessible continent that plays a key role in regulating the climate through ocean currents, winds, icebergs drift, and sea-ice concentration and thickness. The study area of this work corresponds to the Weddell Sea, Bellingshausen Sea and the South Atlantic Ocean. These areas are relevant because of supply operations to Antarctic stations and scientific and tourist activities. The Antarctic Peninsula is the most visited region of the continent for tourist and research vessels and requires special efforts in the development and dissemination of updated ice information for Safety of Navigation. For this purpose, it is critical to have information that discriminates the origin of the ice from land and open water, sea-ice concentration, and stage of development. The high recurrence of cloud cover over the Antarctic Peninsula during the summer hinders the operational use of visible/infra red satellite imagery, therefore access to Synthetic Aperture Radar (SAR) sensors is considered to be a high priority. Between 2018 and 2020, with the launch of the SAOCOM (Satélite Argentino de Observación Con Microondas) constellation, Argentina has evidenced an increase in the availability of SAR images for sea-ice operations. This paper presents the current state of routine production of operational ice charts at the Argentine Naval Hydrographic Service for mariners in the vicinity of the Antarctic Peninsula and South Atlantic Ocean and discuss future developments in place to prepare for expected increases in marine traffic in these areas.

KEYWORDS

ice chart, Antarctica, satellite imagery, icebergs, sea ice, GIS

Introduction

Antarctica is strategically valued as a natural laboratory, a reservoir of fresh water, and critical for understanding and monitoring the dynamics of global climate change. It is a continent surrounded by seas influenced by ocean currents, winds, and variations in the concentration and thickness of sea ice, that make it a unique place. Sea ice has a significant impact on climate regulation and the global energy balance. Formation of sea ice occurs when seawater freezes at temperatures of -1.8°C, a salinity of 27 ‰, and with favorable hydro-meteorological conditions for its growth (WMO No. 574, 2021). Sea ice can be found floating adrift on the ocean surface or lying along the coasts, in front of barriers, or surrounding grounded icebergs (WMO No. 259, 2014b).

Logistics and scientific activities in Antarctica are determined by the presence of sea ice and icebergs, making it essential to have the most accurate sea-ice information, allowing the planning of different tasks, and the means to carry out operational activities, such as the use of inflatable and medium-sized boats with landing ramps, or helicopters (Pope et al., 2017). Similarly, tourist activity in Antarctica has been developing since the late 1960s, with a primary focus on attractions in the vicinity of the Antarctic Peninsula and adjacent islands. Last period there was an increase in tourist activity at a rate of 8.6%, with more than 50,000 visitors on more than 50 vessels of different sizes and characteristics during the season October 2018 to March 2019 (International Association of Antarctica Tour Operators, 2020).

The position and drift of icebergs, sea-ice concentration, and extent of the ice field have been monitored using satellite data for decades, yet information on additional parameters such as sea-ice stage of development, thickness and areas of pressure ridging provide a better understanding of ice conditions to support navigational safety for mariners. However, monitoring sea ice and its geophysical parameters is difficult due to differences in snow cover, seasonal variability, vast areas without observations from ships or stations, among others. Additionally to these obstacles, typically only one set of satellite data is available at a given time (i.e. individual polar orbit satellites provides imagery one at a time) and optical data commonly limited by cloud cover and passive microwave data limited by horizontal resolution (Dierking, 2013).

To respond to the requirement of sea-ice monitoring, national ice services develop ice charts that are compiled using an exhaustive set of satellite observations to offer all the available information in a graphical, complete and simplified format. Ice charts are produced by sea-ice analysts following international standards (WMO No. 1215, 2014a) including additional sea-ice parameters and the presence of icebergs, that are not always clearly discernible from satellites. The development of ice charts originated to provide guidance and support to sailors in the Polar Regions, particularly in the Arctic, but also subpolar areas with high maritime traffic, such as the Baltic Sea, Barents Sea, Denmark Strait, Bering Strait, among others (Partington et al., 2003). Ice Services from Canada, Denmark, Finland, Germany, Norway, Russia, Sweden, and the USA, among others, have been developing ice charts for more than 4 decades; while in the Southern Hemisphere the countries that follow the same procedures are limited. These differences are mainly related to the extremely important commercial use of the polar and subpolar sea routes of the Northern Hemisphere where the presence of ice limits navigation with the consequent cost implications for naval transport. In the Southern Hemisphere, Antarctica and adjacent areas of the austral oceans, the greatest commercial activity is related to tourist cruises during the southern spring and summer and a still limited fishing activity. Pope et al. (2017) describe the work of the Ice Services or other National Organizations with ice chart production for the Southern Oceans: Argentina, Australia, Chile, China, Denmark, Germany, Norway, Russia and the USA. These organizations provide different ice chart products based on their mandate, financial capabilities and regions of interest. Common challenges related to limitations of the availability of satellite data also affects these Services.

Ice charts pre-date the satellite age (late 1960's with the onset of NIMBUS and other single sensor optical satellites), when routine products were produced using aerial reconnaissance, ship-based observations and local knowledge of sea ice areas, particularly closer to the land (Divine and Dick, 2006; Mahoney et al., 2008; Walsh et al., 2017). Since 1972 the U.S. National Ice Center (US NIC) has produced Arctic and Antarctic ice charts for operational purposes, including activity planning and nautical safety. The long consistent archive of operational charts has opened opportunities for numerous research projects that rely on ice chart databases for the validation of sea ice products developed for climate monitoring. For example, Kukla and Robinson (1980) use the ice charts for climatic studies of associated variables such as ice rim position, albedo, and snow depth. Knol et al. (2018) outline challenges in terms of changes in the information infrastructure of Ice Services in the Arctic, describing the different web services to access ice information in the Northern Hemisphere. For example, the Ocean and Sea Ice Satellite Application Facility (OSI SAF) generates derived products from climate records of gridded global ice concentration (Lavergne et al., 2019).

In order to provide ice charts suitable for navigational safety, it is essential to have the most up-to-date information on current sea-ice and iceberg conditions. To access this information during operations, or near real-time, satellite imagery from various sensors is used as the main source and paired with ship-based observations and coastal monitoring stations or aerial reconnaissance. But infrequent point observations have considerable limitations in terms of geographic coverage and frequency of acquisition and are therefore of relatively low importance from an operational point of view (Hall et al., 2002). There has been some development to automate ship-

based observations with the use of video cameras. Digital images acquired from the ice condition monitoring video cameras deployed on the NB Palmer icebreaker during the 2007 SIMBA expedition were subjected to modern image analysis techniques to verify and validate ice observationsand provided high temporal resolution of continuous observations, which may eventually be used to validate satellite-derived products, such as ice charts (Weissling et al., 2009). Observations from helicopters and aerial drones have been improving with a significant amount of information including roughness, thickness and concentration (Divine et al., 2016; Li et al., 2019)

In this regard, remotely sensed data, such as satellite images, have become a very valuable tool for Earth observation and have become fundamental to support better decision-making. The interpretation and analysis of the products of these sensors have allowed the planning, execution, monitoring and evaluation of projects to be carried out safe and more efficiently, optimizing resources and their sustainability (Arias Duarte et al., 2010). For this reason, improving the current procedures of how satellites are analyzed is essential for ice services to provide better support in greater detail and precision.

The Argentine Naval Hydrographic Service (Servicio de Hidrografia Naval, SHN) has been supporting Argentine Navy Ships since 1970s, but the ice information has not been publicly available until recently. In 2015, SHN introduced the publication of its ice charts to general maritime users and started working as a recognized National Ice Service (WMO 574 (2021)). SHN's routine products include the weekly production of ice charts for the Weddell Sea, Bellingshausen Sea and South Atlantic Ocean, iceberg drift charts, and detailed information through the Navtex and SafetyNet services for the safety of navigation.

The objective of this paper is to present the current state of SHN actions related to Ice Service duties, including a description of ice charting procedures, the satellite imagery processing and the analysis of different classes of sea ice and icebergs necessary for operations in Argentina's area of national responsibility. By giving visibility and clarification on the methods used for the analysis of sea-ice conditions and the presence of icebergs, the end-users can improve in the interpretation of this information for better decision-making in ice infested waters.

Data and methodology

Area of study

This paper is focused on the NAVAREA VI, the Argentine area of responsibility in terms of public service for Safety at Sea (Figure 1). This area includes the Antarctic Peninsula, Bellingshausen Sea, Weddell Sea and the Southwestern Atlantic Ocean. Ice charts are developed for the sub-areas detailed in Figure 2, including Scotia Sea, Weddell Sea and Bellingshausen Sea. Sea ice does not usually extend north of the 60° South latitude (Venegas and Drinkwater, 2001) yet, icebergs drift can extend to subtropical latitudes over the South Atlantic Ocean, thus it is necessary to have a separate iceberg analysis chart that includes all the NAVAREA VI.

The sub-areas of ice charting production presented in Figure 2 are considered to be high priority areas due to their relevance for research and tourist vessels, and multi-purpose operations that require more detailed sea-ice information.

Information sources

Information sources used as input for the production of ice charts are presented as the following:

Reconnaissance and *in situ* observations: coastal monitoring, ship-based and aircraft observations.

Observations from Argentine ships and coastal bases in Antarctica are conducted by personnel that undergo training procedures throughout the year, mandated by the SHN, to be approved as ice observers. Observations are collected and archived using the Glaciological Information System (SIGLAC, in Spanish) system, which registers sea ice parameters - such as concentration, stage of development, shape, topography and melting - and the amount of icebergs present. This software includes a quality control component during the observation input phase, that is converted into a numerical coded format for simplification and to unify the interpretation processes by analysts. Once the information is received, in near real-time, it is decoded and applied to second quality control, to be used in the validation of ice charts. All observations are stored in the SHN's ice database, not currently available for open access.

The advantage to recording observations by a well-trained crew is that it provides a reliable source of information from several places in Antarctica, especially those made from the vicinity of inlets, bays, or coves where vessels need to maneuver for operations. Currently, Argentina supports ice observations from 13 stations, between permanent and temporary ones, distributed throughout the Antarctic Peninsula, Bellingshausen Sea and the east of the Weddell Sea.

Additionally, international merchant vessels and those coming from the Southwestern Atlantic Ocean provide additional information by notifying SHN of the presence of icebergs. Though these observations are not made by trained personnel, they are usually accompanied by photographs and geolocation information that provides ground-truth to corresponding satellite images. This information is extremely valuable to track larger icebergs that are drifting outside Antarctic waters and represent a serious hazard to mariners.

Aircraft observations of sea ice and icebergs are registered during logistic flights. These are primarily used to calibrate and validate satellite imagery and to update general information

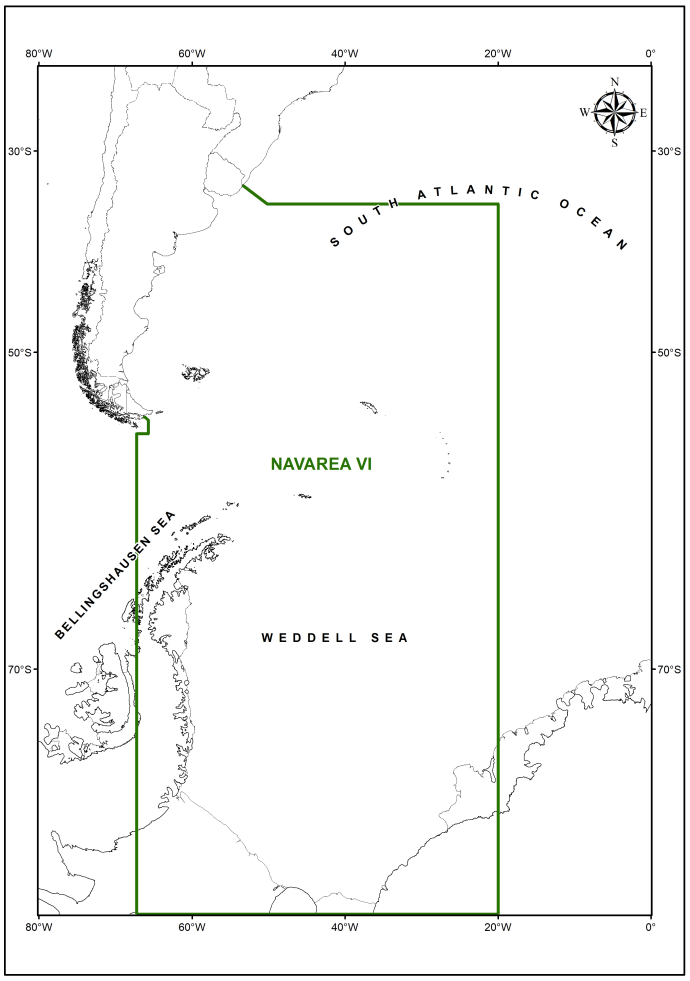

FIGURE 1
The NAVAREA VI, the Argentine area of responsibility for Safety at Sea information service, directed by the Naval Hydrographic Service.

about the sea ice pack position, concentration and iceberg tracking. Observations from aircraft do not follow the standard format as those from ships or bases, although they are geolocated photographs (Figure 3).

Optical satellite imagery (Visible and Infrared)

The primary sensor used for optical images analyzed at the SHN are the Moderate Resolution Imaging Spectroradiometer (MODIS), operational on the Terra and Aqua satellites, and the Visible Infrared Imaging Radiometer Suite (VIIRS) images from the Suomi National Polar-orbiting Partnership satellite (Suomi NPP). The MODIS and VIIRS imagery present multiple spatial resolutions, depending on the spectral bands. Resolutions corresponding to MODIS are 250 meters and 500 meters, while VIIRS has 375 meters and 750 meters,. Sea ice and icebergs are often identified using corrected reflectance in RGB composites of True and False Color. This optical imagery has the advantage of large spatial coverage with daily revisit for polar regions. However, in this type of image, the ice detection is obstructed by cloud cover or by the lack of solar light during the polar night in the winter season. In fact, high stratiform cloudiness can present spectral signatures similar to ice, which can make it difficult to distinguish, even with RGB combinations. The spectral bands that are frequently used go from the visible to the near-infrared region in the combination 3-6-7 and 7-2-1 for the MODIS Terra sensor, 7-2-1 for the MODIS Aqua sensor, and M11-I2-I1 and M3-I3-M11 for the VIIRS sensor. These combinations make it possible to easily detect ice or snow because of its spectral signature and filter the cloudiness which poses the main challenge when monitoring floating ice.

During low-light conditions, images from Day/Night Band (DNB) of the VIIRS sensor are often used, capturing low light emissions with those reflected by ice being sufficient for detection (Lee et al., 2006). The spatial resolution for this band

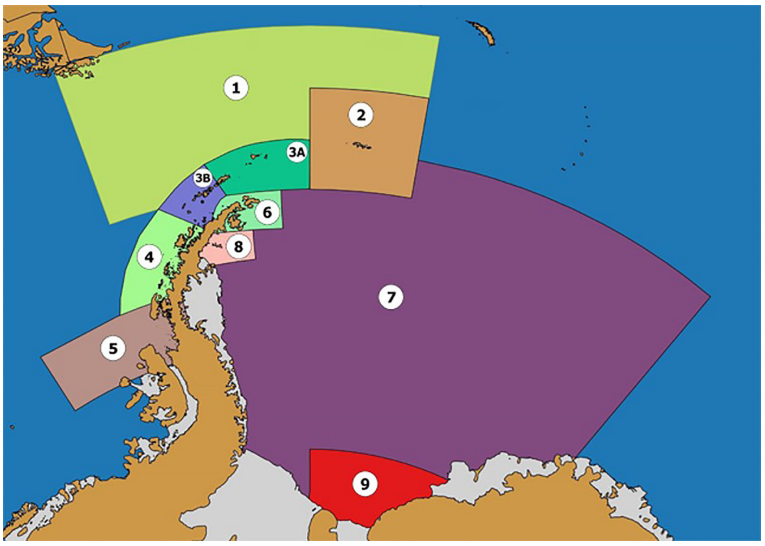

FIGURE 2
Sub-areas of ice charting production. Zone 1: Drake Passage. Zone 2: South Orkney Islands. Zone 3: Mar de la Flota Straight and South Shetland Islands (with sub-zones 3A and 3B). Zone 4: Channel to Belgrano Island. Zone 5: Bellingshausen Sea and Margarita Bay. Zone 6: Antarctic Strait and Erebus and Terror Gulf. Zone 7: Weddell Sea. Zone 8: Northwest Weddell Sea. Zone 9: South Weddell Sea (Halley station to Berkner Island).

is 750 meters with daily acquisitions and its combination with other optical images allows to obtain more information regarding the movement of cloud cover, taking advantage of the different schedules of satellite orbits.

Although the spatial resolution of optical satellites is low, as detailed on previous paragraphs, for a detailed analysis of sea ice and small icebergs, it makes it possible to have more regional information during the operational season for critical areas in the ice charts. Additionally, the aforementioned images can be obtained free of charge, provided by the Global Imagery Browse Services (GIBS) as part of the Earth Observing System Data and Information System (EOSDIS) of the National Aeronautics and Space Administration (NASA).

Microwave satellite imagery

Currently, the active microwave sensor Synthetic Aperture Radar (SAR) is the most essential instrument for monitoring floating ice and can be used under any weather and illumination conditions, especially over the polar regions where cloud cover and absence of sunlight in winter make observations difficult with other onboard satellite instruments.

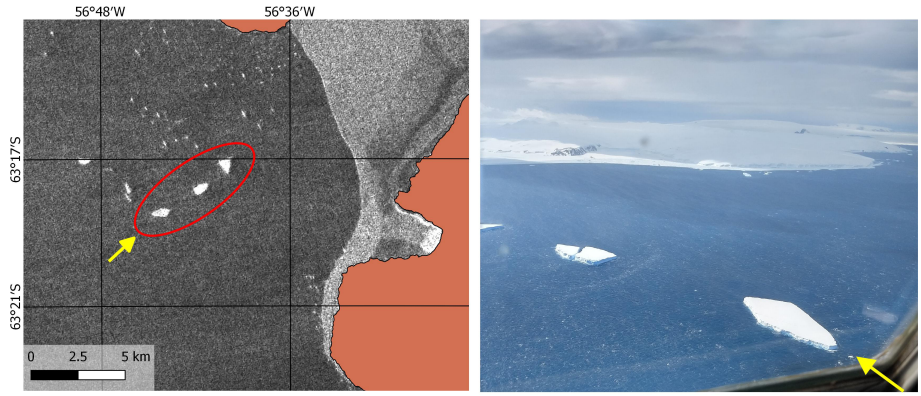

FIGURE 3
Observation of icebergs during a flight over Joinville Island (right) to validate SAOCOM image (left), from November 19, 2020. The yellow line correspond to the approximate route of the aircraft and the red circle marks the position of the observed icebergs (Satellite image provided by CONAE).

Different frequencies (bands) of the SAR systems are used for glaciology purposes, being mainly the X (8–12.5 GHz, 2.4–3.8 cm), C (4–8 GHz, 3.8–7.5 cm) and L (1–2 GHz, 15–30 cm) bands those with the highest application (Dierking, 2013). Current operational satellites are TerraSAR and COSMO-Skymed in X band, Sentinel-1 and RADARSAT-2 in C band; and ALOS-PALSAR-2 and SAOCOM-1 in L band. SAOCOM-1 consists of two Argentine satellites complementing the SIASGE constellation (Sistema Italo Argentino de Satélites para la Gestión de Emergencias, as in Spanish) with the Italian satellites COSMO-Skymed. SAOCOM-1, launched in 2018, has enabled Argentina to increase the amount of data analyzed for the production of ice charts (Figure 4).

SAR images have spatial resolutions that range from 3 to 100 m and wide swath from 20 to 400 km (depending on each satellite instrument and acquisition mode selected)-, allowing a high level of detail over a relatively large area (Dierking, 2013). The spatial resolution and size of the images will depend on the sensor and the acquisition mode. In general, acquisition modes in SAR systems are Spotlight, Stripmap, Scansar and the newer Topsar mode incorporated into Sentinel-1 and SAOCOM-1 satellites (De Zan and Monti Guarnieri, 2006). The Topsar and Scansar modes cover a larger area over Spotlight and Stripmap but yield lower spatial resolutions. Some SAR systems can also obtain polarimetry information for the observed surface using the polarization of received and transmitted signals combining the orientation of the vectorial electric field (Onstott and Shuchman, 2004; Dierking, 2013).

Unlike optical images, SAR images have specific geophysical characters that can affect photo interpretation, thus requiring analysis from specifically trained personnel. It is necessary to understand the scattering mechanisms from the objects of interest in response to the radar signal considering the dielectric properties and the roughness of the observed surface (Onstott and Shuchman, 2004). Characteristics of SAR systems such as the frequency (band) in which the sensor operates, the polarization and the incidence angle determine differences within a scene and must be considered by the ice analyst. Additionally, the coverage of SAR images is limited for regional areas, and the availability of scenes in Antarctic region depends on the frequency of acquisition of each satellite. Some images are usually provided free of charge for predetermined orbits (i.e., Sentinel 1) while others require on-demand and tailored acquisitions, usually at additional cost.

Products derived from passive microwave satellites are used for ice charts to observe sea-ice concentration using the Advanced Microwave Scanning Radiometer (AMSR-2) sensor onboard the GCOM-W satellite (Meier et al., 2018). Even though this data is available year-round, it is mostly used in the absence of illumination during the Southern Hemisphere winter for latitudes south of 60° S when optical images can no longer be used. The reason of this criteria in the use of AMSR-2 data is that the spatial resolution of 12 km is considered too low for a detailed analysis of ice conditions.

Elaboration of the ice charts

Currently, the SHN produces three types of ice charts: sea-ice concentration, ice edge, and iceberg; all three published weekly on the SHN website (www.hidro.gob.ar). Iceberg charts have been published since 2019 on the PolarView portal (www.

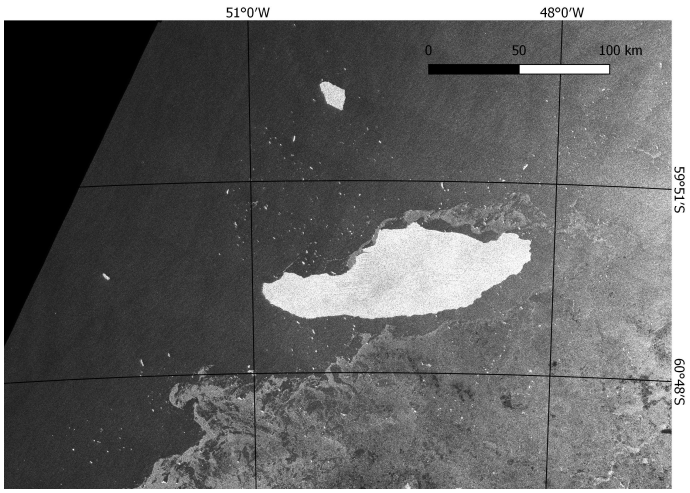

FIGURE 4
SAOCOM image from May 23 - 2020, showing A68A and A68C icebergs and sea ice in the Weddell Sea (Satellite image provided by CONAE).

polarview.aq), yet this is currently in trial mode. QGIS software (www.qgis.org) is used for ice charting production, a reliable, free and open-source solution to the requirements of the SHN. Satellite imagery analysis is performed by trained ice analysts with previous experience in data interpretation of optical and SAR imagery, and a comprehensive knowledge on Antarctic climatology and marine glaciology. The nomenclature and standards used in the generation of the ice charts described in this paper correspond to the publication WMO Sea Ice Nomenclature: Volume I – Terminology and Codes, Volume II – Illustrated Glossary and Volume III – International System of Sea Ice Symbols (WMO No. 259, 2014b). The methodology of ice charting and the description of the final product is explained in the Results section.

Result

Analysis of the information

The first step at the beginning of the charting procedure is to analyze the complete set of data that is available in near-real time. This begins with the ice analyst's work through visual interpretation of satellite images, combined with observations received from ships and stations in Antarctica. The characteristics to be identified are the extent, the stage of development, the shape and spatial distribution of sea ice. Icebergs presence are also analyzed in terms of their quantity and later tracking. To recognize these variables in the data, well trained analysts must have a good understanding of the object of study and the source of information used.

The object of study, sea ice and icebergs, is directly affected by different environmental variables. Wind and ocean currents determine drift, sea-surface temperature influences formation and melting processes and tidal currents have a local effect on sea-ice concentration in coves, bays and straits. A snow cover modifies the physics of the sea-ice surface and may obscure the stage of development. In order to have complete knowledge of the formation processes of snow cover and sea ice, the analyst needs to understand the climatological and glaciological regimes in the different regions of Antarctica.

Another subject to be covered in the training of ice analysts is the spatial and temporal scale of different satellite sensors and their integration with consistent criteria in the chart products. Additionally, observations from ships and stations are received in a coded format and need a proper training to rapidly understand the information, discriminate the relevant data and integrate them with the satellite imagery in the digitization of ice charts.

Optical images allow for an almost intuitive photo interpretation under cloud-free conditions when respective RGB composites are used. Clouds can obscure the surface and therefore present an obstacle in the identification of sea ice and icebergs, especially when the area of interest is below a dense stratiform cover. RGB composites that include bands from the visible and near-infrared channels can be of great help in distinguishing ice on the ocean from clouds in these situations. For example, the RGB combination of MODIS sensor Band 3-6-7 allows for enhancing the presence of snow and ice in reddish colorations, because these objects are reflective in band 3, corresponding to the visible spectrum, and absorbent in bands 6 and 7, infrared channel (Figure 5). Due to its spectral signature, a cloud cover is typically represented in white in the composite of those three mentioned bands and the open waters appear in dark colors. Therefore, it is possible to find a cloud-free location of sea ice and icebergs despite cloudiness. However, occasionally small ice crystals of Cirrus clouds appear in reddish orange with the aforementioned RGB composite, which means a detailed analysis is necessary to not confuse the ice on the ocean surface with that in the clouds.

On the other hand, SAR systems, by employing the transmission of electromagnetic pulses in the microwave range

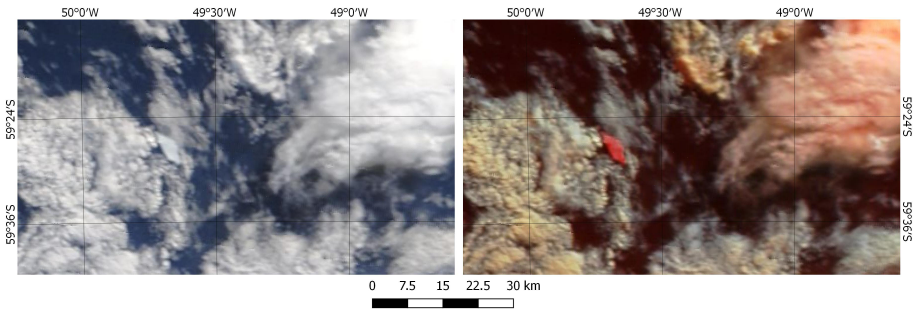

FIGURE 5
Iceberg and cloudiness in MODIS Terra image from April 5 - 2020, in true color (left) and RGB 3-6-7 composite (right).

to receive the energy backscattered from the surface, not only require trained personnel to understand the response of the objects to be analyzed, but also constant training and familiarization for the correct data.

Ice analysts can recognize the different types of ice in the SAR images by interpreting the intensity of the response, the texture and the shape of the different objects. The observed characteristics of those elements are integrated with the knowledge of the dielectric properties and the roughness of the surface of each class of ice. Also, radar frequency used is mainly considered, which determines the penetration of the signal into the surface and the angle of incidence of each image.

In large-scale SAR imagery (around 250 km swath coverage), such as ScanSAR and TopSAR, very small or large incidence angles can present difficulties in detecting ice, and in the worst-case scenario, the presence of ice is note noticeable in the SAR scene. Example of this can be seen in Figure 6, where sea-ice belt and strips are hardly detected. An ice analyst familiar with this type of image can determine the presence of the ice even when it is not as clearly defined by the sensor.

Information sources are not always updated at the time of the analysis, and some observations or satellite images may correspond to the previous 48 hours. Analyzes are carried out considering the variations that sea ice has suffered and the drift of icebergs in that period. Meteorological, oceanographic and even statistical climatological data must be incorporated in the charting process.

Sea-ice concentration charts

For the preparation of the sea-ice concentration charts, generally known as 'ice charts', homogeneous areas in the sea-ice concentration are identified. The World Meteorological Organization Nomenclature defines concentration as the fraction of the sea surface covered by ice, expressed in tenths (WMO No. 259, 2014b). The analysis of the area in which the different concentrations are divided will depend on the spatial scale used in the digitalization, the source of the information and the spatial resolution. The concentration is classified with categories ranging from 0/10 (open water) to 10/10 (the entire surface covered) of sea ice and polygons are generated in vector format files, following the definitions and standard colors of the Color Code Ice Chart Standard (WMO No. 1215, 2014a) (Figure 7).

The predominant form and stage of development of sea ice are coded using ice-chart symbology combined in the so-called Egg Code. This code is represented by an oval subdivided into four horizontal sections. The first one at the top indicates the total concentration of the sea ice in tenths. In the second section, partial concentrations are indicated, while in the third and fourth the stages of development and the forms, respectively, of each of the partial concentrations are reported. In those polygons where the presence of icebergs is detected, a black triangle is included on the side of the oval.

Figure 8 shows the ice chart for April 1 - 2020, corresponding to the Antarctic Strait and the Erebus and

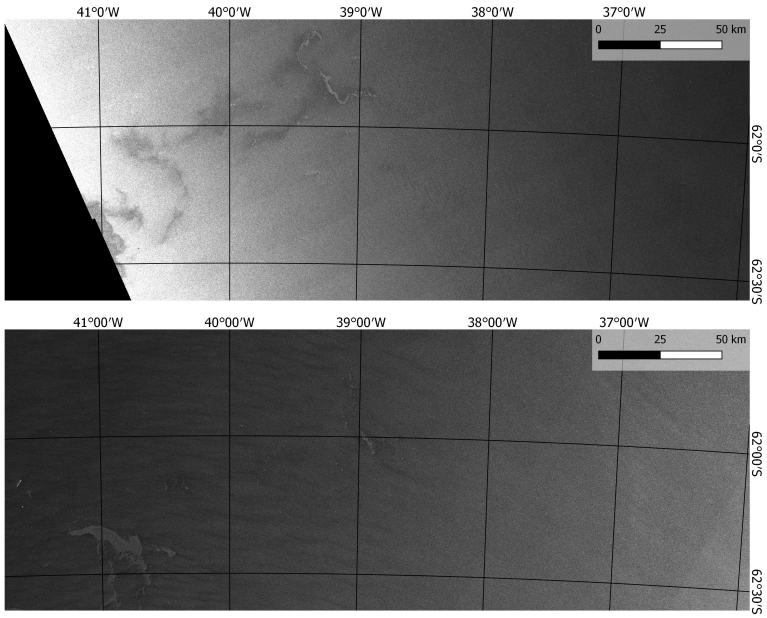

FIGURE 6
Belts and strips in Sentinel-1 image from April 4 (top) and April 5 (bottom), 2020 in the Weddell Sea. Near and far range of each image, respectively. Copernicus Sentinel data 2020, processed by ESA.

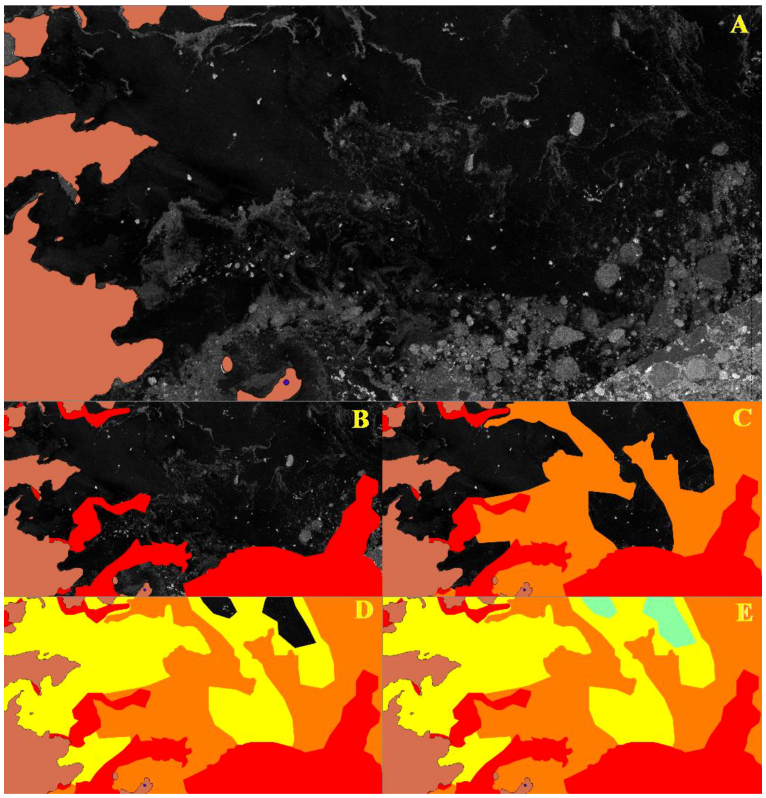

FIGURE 7
Digitization of sea-ice concentration polygons in the Erebus and Terror Gulf. **(A)** Sentinel-1 image from March 30, 2020. **(B)** Polygons with concentration 9-10/10, **(C)** adding polygons with concentration 7-8/10, **(D)** adding polygons with concentration 4-6/10 and **(E)** adding polygons with concentration 1-3/10. SHN 2020, contains modified Copernicus Sentinel data 2020, processed by ESA. Color code is available in Figure 8.

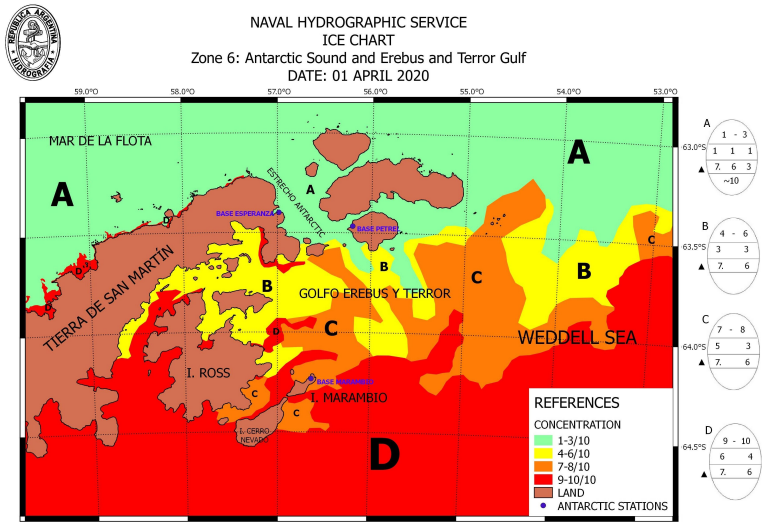

FIGURE 8
Ice chart dated April 1, 2020. Zone 6: Antarctic Strait and the Erebus and Terror Gulf.

Terror Gulf. Digitized ice concentrations for the area can be seen with Egg Codes for each polygon. In this particular situation, the polygon indicated with an A has a sea-ice concentration of 1-3/10 with egg code reporting partial concentrations of 1/10 for the stages of development '7. 6 3', corresponding to old, first year and young ice. The form in the fourth section is informed with (~ 10) symbology where strips and patches can be found in that concentration area. The black triangle indicates the presence of icebergs.

These ice charts provide detailed information on sea ice, but only indicate the presence or absence of icebergs in the egg code. Nine sea-ice concentration charts are generated weekly and in the case of significant changes due to environmental conditions, the frequency of updates increases; especially in the highly visited area of the Antarctic Peninsula.

Ice edge charts

The Ice Edge chart is made to establish the general limits of the ice edge and the marginal ice zone, allowing mariners to know which areas of navigable waters are free of sea ice. It is useful for ships that do not have intent to navigate in the Antarctic region but also need to make their way through the Drake Passage, which connects the South Atlantic Ocean with the South Pacific Ocean, or ships that sail north of the Antarctic Peninsula during spring and winter when the ice field extends the most to the northern waters.

As it was mentioned before, using the different satellite images, the presence of sea ice is observed and delimited with the digitization of polygons in vector format. In the analysis, the ice edge, compact and diffuse, and the marginal zone are distinguished. According to standardized nomenclature, the ice edge is the demarcation between the sea ice of any kind and the open sea. Operationally, this definition is considered for the delimitation of the ice edge and also the criterion is taken to consider those ice concentrations between 4-10/10. The marginal ice zone is defined as the region covered with ice that is affected by waves that penetrate the open areas of sea ice. For the digitization of the charts, concentration polygons of 1-3/10 are considered. Red polygons indicate the ice edge and yellow ones, the marginal ice zone (Figure 9).

In sectors where a diffuse ice edge is seen, broken sea-ice strips and belts may not be fully incorporated into the ice edge and belong in part to the marginal ice zone (Figure 9). The analyst should prioritize the areas to be included in these

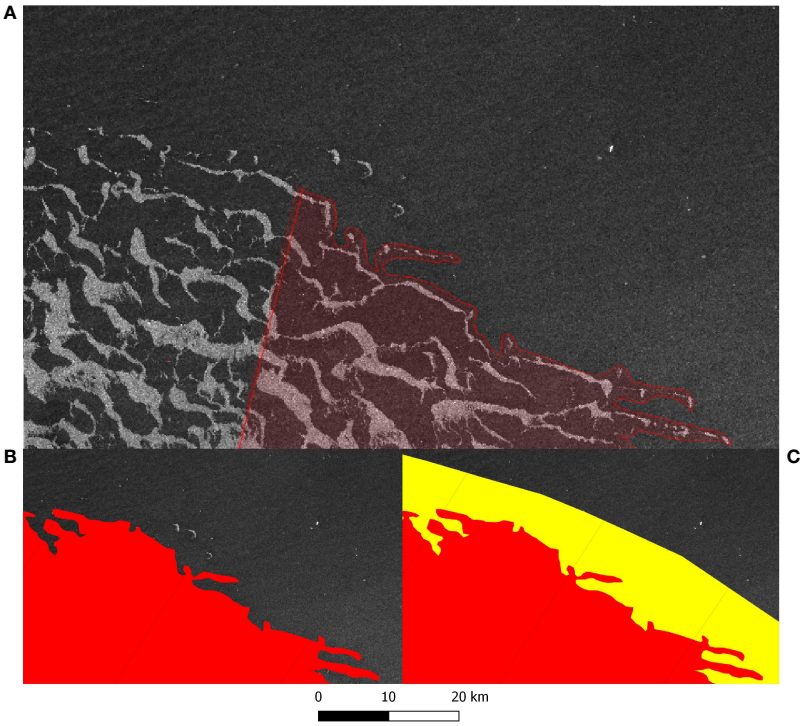

FIGURE 9
Generation of the ice edge chart using satellite images. **(A)** digitization of the Sentinel-1 image on March 31, 2020 in the Weddell Sea. **(B)** polygon of the ice edge (red) and **(C)** the addition of the marginal ice zone (yellow). SHN 2020, contains modified Copernicus Sentinel data 2020, processed by ESA. Color code is available in Figure 8.

polygons to clearly transmit the information about the sea-ice condition. The user should keep these considerations in mind, in case the only available information is the ice edge charts.

Two ice edge charts are generated weekly. Figure 10 presents a completed ice chart for May 26, 2020. It should be noted that this chart only refers to sea ice and does not indicate the presence or absence of icebergs, mariners should consult the iceberg chart so as not to incur risks during navigation nearby the sea-ice edge.

The same information is summarized in several waypoints and transmitted through SafetyNET and NAVTEX systems for duplication of communications to ensure that the location of sea-ice edge is acquired by all vessels in the NAVAREA VI and vicinities.

Iceberg charts

The Iceberg Chart identifies the position of icebergs in open waters or next to the sea-ice edge. Icebergs with dimensions greater than 10 nautical miles, named by the US NIC using a letter from the region of Antarctica where it calved, and a cumulative number, are indicated in the iceberg chart with colored dots. Icebergs with smaller dimension between10 and 2 nautical miles are marked with blue colored dots, differentiating them from internationally renowned (Figure 11).

Icebergs with smaller dimensions than 2 MN are include in areas indicating the risk of finding icebergs in a certain amount, named as 'Iceberg Risk Areas'. These areas are distinguished by the number of icebergs recorded in a grid cell of 1-degree latitude by 1-degree longitude. If the grid contains only 1 iceberg, it is classified as 'isolated icebergs' (green cells), between 2 and 6 icebergs it corresponds to 'few icebergs' (yellow cells), and for an amount of 7 icebergs or higher, it is called 'many icebergs' (red cells), as shown in Figure 11. Working with risk areas definitions saves operating time for the analysts by providing a large amount of detailed information for safety of navigation in waters infested by numerous icebergs.

Special focus is dedicated to those icebergs drifting in the Drake Passage or even further north in the Argentine Sea. The drift to the north and beyond the limits of the Antarctic Circumpolar Current is the consequence of the effect of the Malvinas Current that deflects to the north, towards warmer latitudes, representing a real hazard in regions of the South Atlantic Ocean where these floating objects are not expected by Officers on Watch at the bridge of a ship. Furthermore, warmer water generates a gradual decrease in the size of the iceberg due to melting and iceberg detection gets more difficult due to the spatial resolution of the available satellite data. In this situation, reports received by the vessels are extremely valuable information for the iceberg chart provided.

Figure 12 shows the iceberg chart from April 6, 2020. The compact ice edge is represented by the black line and white region, establishing that the risk areas analyzed are in open waters where icebergs constitute a bigger risk for navigation. Icebergs within the ice field are not represented on these specific charts.

As it was mentioned before, the iceberg chart is also uploaded on the PolarView(Figure 13), where it can also be overlaid with other shapes of information from different Ice Services around the world.

As for the ice edge, iceberg positions are also included in the SafetyNET and NAVTEX messages to mariners. Information on

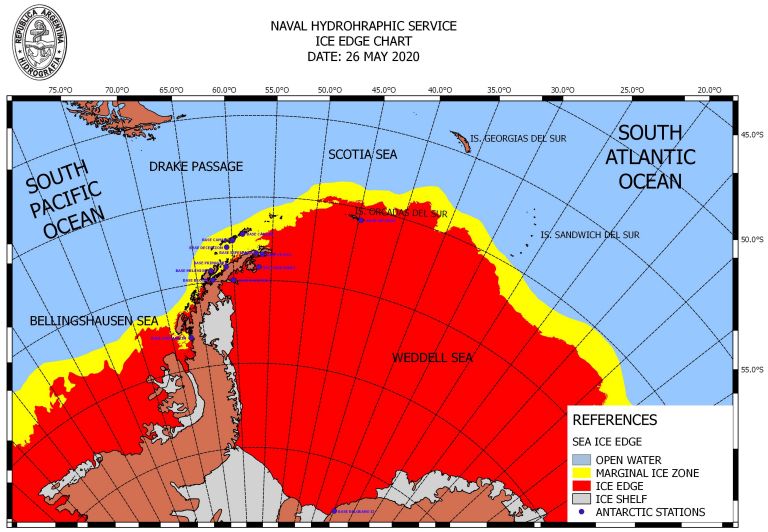

FIGURE 10
Ice edge chart from May 26, 2020. Ice edge is defined as the limit of sea-ice concentration above 4/10.

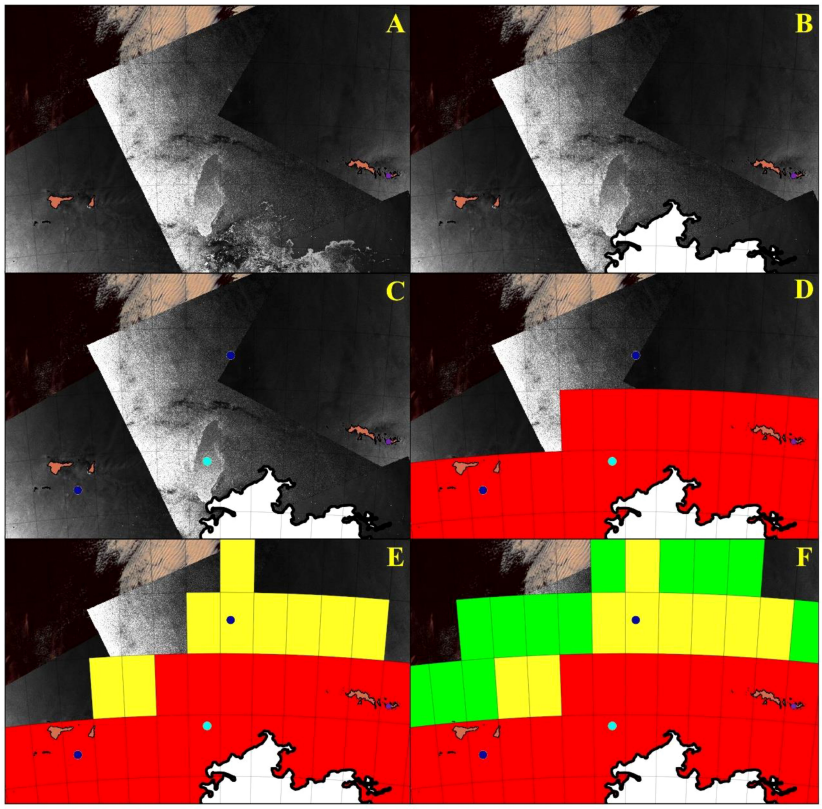

FIGURE 11
(A) Sentinel-1 image of April 2, 5 and 6 2020 and VIIRS Suomi NPP of March 28, 2020 in the South Orkney Islands sector. **(B)** Compact ice edge delimited in white. **(C)** A68A iceberg positioned with a cyan dot and smaller iceberg in blue dot. Digitized cells as a risk area for **(D)** 'many icebergs' **(E)** 'few icebergs' and **(F)** 'isolated icebergs'. SHN 2020, contains modified Copernicus Sentinel data 2020, processed by ESA.

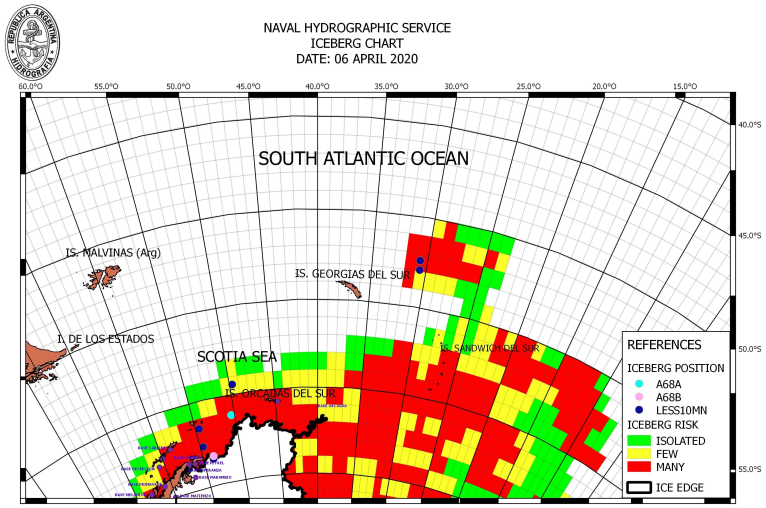

FIGURE 12
Iceberg chart from April 6, 2020. Grids are sized 1° x 1°. Isolated: only 1 iceberg, Few: from 2 to 6 icebergs and Many: more than 7 icebergs.

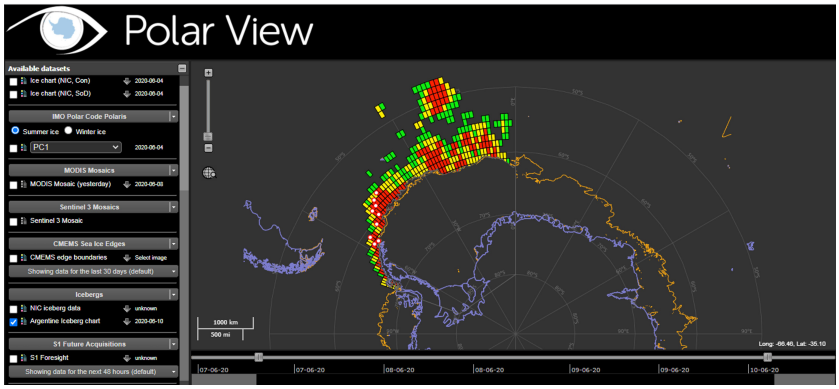

FIGURE 13
Argentine Iceberg Chart displayed on Polarview's website.

the position of all known icebergs is transmitted, with daily updates when satellite imagery is available, and areas with the presence of several icebergs by using the position of polygons vertices.

Discussion

The activities carried out on the Antarctic continent require a great logistical effort by all countries that have permanent or temporary stations, being executed mainly by marine transport. Although activities in polar waters of the Antarctic region are minimal compared to the Arctic Ocean, with well-defined trade routes and throughout the entire year, tourist activity and fishing in border regions of Antarctica increase annually. For that reason, it is imperative for countries closer to Antarctica, like Argentina, to provide reliable and accurate support information on the safety of navigation to all ships sailing this remote part of the globe. Even more, if we consider that if an incident occurs in polar or subpolar waters of the Southern Hemisphere, aid would be delayed for several days because of the long distances that exist between Antarctica and the Search and Rescue (SaR) Centers. It is important to inform that iceberg impacts are not the only hazard but also the presence of multi-year sea ice or the increase of pressure in the surrounding sea-ice field.

During the austral summer season, from November to April, the Argentine and Chilean Navy share SaR activities in the Antarctic Peninsula, ensuring the permanent presence of a rescue ship in the area with the highest marine traffic. However, for the rest of the year the aid could take weeks by ship to reach a remote area of Antarctica, with consequent implications of risking human lives or possible ecological disasters. Therefore, to ensure navigation in isolated and potentially dangerous areas subject to rapid variations due to the effect of meteorology and ocean currents, updated ice charts are necessary, which must be constantly improved with the development of new technological tools.

The mission of the Argentine Naval Hydrographic Service (SHN) as a public service is to provide information for safety of navigation in NAVAREA VI. One of these tasks is the provision of the best products and services for ice charting in the Antarctic and South Atlantic Ocean. Although this activity has been carried out uninterruptedly since the 1970s with the use of satellite products, since 2015 ice charts have been produced weekly, with a significant improvement in quality and precision according to the advancement of knowledge and technological tools.

The ice edge charts provide users with regional information on the extent and concentration of sea ice in the Weddell Sea and Bellingshausen Sea. When it is required to know in more detail the glaciological condition, the sea-ice concentration charts in the different areas can be consulted, which also present information on the stage of development and the forms of sea ice. The iceberg chart provides detailed information on icebergs all over the NAVAREA VI, with updated positions and risk areas giving information on their distribution and quantity.

In addition, the systematic and continuous production and storage of ice charts can provide a valuable source of information, validated and quantifiable, to map the detection of changes in the state and condition of both sea ice and icebergs. This information will be of particular interest to cryosphere researchers who are linking changes in sea-ice conditions and extent to climate models.

During the ice charting process, the training and experience of those who perform the analysis is essential. It is fundamental for the ice analysts to be familiar with the region of focus, with an emphasis on understanding the prevailing synoptic environmental variables - such as atmospheric, currents and tides - and climatological - such as glaciological regimes in the

formation or deterioration of the ice. Analysts must also be aware of the particularities of each information source to avoid making erroneous interpretations that could constitute a potential hazard to maritime navigation. Different characteristics of the ice (i.e., roughness, thickness or snow cover) may not be detected as easily as expected when the identification through the different types of satellite imagery must be done during operational times, knowing that dozens of vessels will depend on this information.

It should be noted that the manual drawing of ice charts has operator-dependent subjectivities. Partington et al. (2003) highlight that ice analysts have different skill levels according to their fieldwork experiences and knowledge on the specifics of ice. Alternatives to manually generated ice charts are being studied by automating the processes for the detection, classification and estimation of ice concentration (Moen et al., 2013). However, there is currently no conclusive evidence that the tasks of ice analysts can be replaced by automatic processes for operational activities.

As mentioned before, ice analysts have a major responsibility in the ice charting process. SHN's ice analysts have a rotation of about 5 years, allowing proper training with a high degree of experience in the manual elaboration of ice charts. Transferring experiences to new analysts is also an important concept in the personnel training. Generally, it is intended to incorporate one crew member per year with an increase from 2 to 7 expert analysts since 2015. Systematic errors can be reduced with a consolidated training program and continuous provision of personnel and the adjusted rotation in the assignment of tasks within the Ice Service responsibilities.

An advantage in the training of ice analysts from the SHN is the possibility of sailing in Antarctic waters on board Argentine Navy Ships – an icebreaker, polar supplies or research vessels - making it possible to personally experience navigation within sea ice or near icebergs of different sizes. In this sense, they become aware of the implications of providing the most accurate and updated ice information for nautical safety and the difficulties that mariners experience in the interpretation of ice charts.

Analog to the results obtained by Dedrick et al. (2001), the different ice charts that Argentina produces for Antarctica and NAVAREA VI have increased their quality and reliability remarkably from the following factors:

1. The increase in the availability of SAR imagery, starting with a higher acquisition frequency of Sentinel-1 and since 2018 with the Argentine SAOCOM satellite that represents a significant improvement in working capacity.
2. The ability to handle and process an increasing volume of information and to improve the quality controls of observations made by ships and stations.
3. The possibility of using the Night Vision mode of the SNPP satellite, allowed the improvement in the elaboration of ice charts during the austral polar night.
4. The increase in the number of personnel dedicated exclusively to the task of ice analysts.
5. The collaborative work between the different Ice Services and related organizations around the world, based on the links established through the incorporation to the International Ice Charting Working Group.

We conclude that the regular training of ice analysts in the correct use of information sources is essential and one of the key objectives of the SHN. This enables SHN to issue best quality products by integrating all near real-time information available and serve the public by providing relevant information for safety of navigation to mariners in Antarctic and South Atlantic waters. This paper is intended to make the information published in the ice charts visible for all end-users in order to enable a more in-depth interpretation.

Author contributions

Equal contribution: AS and CS. Last authorship: LS. All authors contributed to the article and approved the submitted version.

Acknowledgments

The authors acknowledge the support of WMO for the publication of this paper, as a contribution to better supporting sea ice services in the Southern Ocean. The authors acknowledge the use of imagery from NASA's Worldview application (https://worldview.earthdata.nasa.gov), part of NASA's Earth Observing System Data and Information System (EOSDIS).

Conflict of interest

The authors declare that the research was conducted in the absence of any commercial or financial relationships that could be construed as a potential conflict of interest.

Publisher's note

References

Arias Duarte, L. P., Santacruz Delgado, A. M., and Posada, E. (2010). Programa satelital colombiano de observación de la tierra: una estrategia de innovación y desarrollo tecnológico para Colombia. *Rev. del Instituto Geográfico Agustín Codazzi.* 44, 13–29.

Dedrick, K. R., Partington, K., Van Woert, M., Bertoia, C. A., and Benner, D. (2001). U.S. National/Naval ice center digital Sea ice data and climatology. *Can. J. Remote Sens.* 27:5, 457–475. doi: 10.1080/07038992.2001.10854887

De Zan, F., and Monti Guarnieri, A. (2006). TOPSAR: Observation by Progressive Scans. *IEEE Trans. Geosci. Remote Sens.* 44 (9), 2352–2360. doi: 10.1109/TGRS.2006.873853

Dierking, W. (2013). Sea Ice monitoring by synthetic aperture radar. *Oceanography* 26, 100–111. doi: 10.5670/oceanog.2013.33

Divine, D. V., and Dick, C. (2006). Historical variability of sea ice edge position in the Nordic seas. *J. Geophys. Res.* 111 (C01001). doi: 10.1029/2004JC002851

Divine, D. V., Pedersen, C. A., Karlsen, T. I., Faste Aas, H., Granskog, M. A., Hudson, S. R., et al. (2016). Photogrammetric retrieval and analysis of small scale sea ice topography during summer melt. *Cold Regions Sci. Technol.* 129, 77–84. doi: 10.1016/j.coldregions.2016.06.006

Hall, R. J., Hughes, N., and Wadhams, P. (2002). A systematic method of obtaining ice concentration measurements from ship-based observations. *Cold Regions Sci. Technol.* 34 (2), 97–102. doi: 10.1016/S0165-232X(01)00057-X

International Association of Antarctica Tour Operators (2020). Available at: https://iaato.org/.

Knol, M., Arbo, P., Duske, P., Gerland, S., Lamers, M., Pavlova, O., et al. (2018). Making the Arctic predictable: the changing information infrastructure of Arctic weather and sea ice services. *Polar Geogr.* 41:4, 279–293. doi: 10.1080/1088937X.2018.1522382

Kukla, G., and Robinson, D. (1980). Annual cycle of surface albedo. *Mon. Wea. Rev.* 108, 56–68. doi: 10.1175/1520-0493

Lavergne, T., Sørensen, A. M., Kern, S., Tonboe, R., Notz, D., Aaboe, S., et al. (2019). Version 2 of the EUMETSAT OSI SAF and ESA CCI sea-ice concentration climate data records. *Cryosphere* 13, 49–78. doi: 10.5194/tc-13-49-2019

Lee, T., Miller, S., Turk, F., Schueler, C., Julian, R., Deyo, S., et al. (2006). The NPOESS VIIRS Day/Night visible sensor. *Bull. Amer. Meteor. Soc* 87, 191–199. doi: 10.1175/BAMS-87-2-19

Li, T., Zhang, B., Cheng, X., Westoby, M. J., Li, Z., Ma, C., et al. (2019). Resolving fine-scale surface features on polar Sea ice: A first assessment of UAS photogrammetry without ground control. *Remote Sensing* 11 (7), 784. doi: 10.3390/rs11070784

Mahoney, R. A., Barry, R. G., Smolyanitsky, V., and Fetterer, F. (2008). Observed sea ice extent in the Russian arcti-2006. *J. Geophys. Res. Atmos.* 113 (C11). doi: 10.1029/2008JC004830

Meier, W. N., Markus, T., and Comiso, J. C. (2018). *AMSR-E/AMSR2 unified L3 daily 12.5 km brightness temperatures, Sea ice concentration, motion & snow depth polar grids, version 1* (Boulder, Colorado USA: NASA National Snow and Ice Data Center Distributed Active Archive Center). doi: 10.5067/RA1MIJOYPK3P

Moen, M.-A. N., Doulgeris, A. P., Anfinsen, S. N., Renner, A. H. H., Hughes, N., Gerland, S., et al. (2013). Comparison of feature based segmentation of full polarimetric SAR satellite sea ice images with manually drawn ice charts. *Cryosphere* 7, 1693–1705. doi: 10.5194/tc-7-1693-2013

Onstott, R., and Shuchman, R. (2004). "Chapter 3: Measurements of Sea ice," in *Synthetic aperture radar marine user's manual.* Eds. J. R. Apel and C. R. Jackson (Washington, DC. USA: National Oceanic and Atmospheric Administration).

Partington, K., Flynn, T., Lamb, D., Bertoia, C., and Dedrick, K. (2003). Late twentieth century northern hemisphere sea-ice record from U.S. national ice center ice charts. *J. Geophys. Res.* 108 (C11), 3343. doi: 10.1029/2002JC001623

Pope, A., Wagner, P., Johnson, R., Shutler, J., Baeseman, J., and Newman, L. (2017). Community review of southern ocean satellite data needs. *Antarctic Sci.* 29 (2), 97–138. doi: 10.1017/S0954102016000390

Venegas, S. A., and Drinkwater, M. R. (2001). Sea Ice, atmosphere and upper ocean variability in the weddell Sea, Antarctica. *J. Geophys. Res.* 106 (C8), 16747–16765. doi: 10.1029/2000JC000594

Walsh, J. E., Fetterer, F., Scott Stewart, J., and Chapman, W. L. (2017). A database for depicting Arctic sea ice variations back to 1850. *Geogr. Rev.* 107, 89–107. doi: 10.1111/j.1931-0846.2016.12195.x

Weissling, B., Ackley, S., Wagner, P., and Xie, H. (2009). EISCAM — digital image acquisition and processing for sea ice parameters from ships. *Cold Regions Sci. Technol.* 57, 49–60. doi: 10.1016/j.coldregions.2009.01.001

World Meteorological Organization (2014a) *Chart Colour Code Standard (WMO No. 1215).* Available at: https://library.wmo.int/index.php?lvl=notice_display&id=11296#.YppAa3bMI2w.

World Meteorological Organization (2014b) *Sea Ice Nomenclature (WMO No. 259, Volume I – Terminology and Codes, Volume II – Illustrated Glossary and Volume III – International System of Sea-Ice Symbols).* Available at: https://library.wmo.int/index.php?lvl=notice_display&id=6772#.YpoywXbMI2w.

World Meteorological Organization (2021) *Sea-ice Information and Services (WMO-No.574).* Available at: https://library.wmo.int/index.php?lvl=notice_display&id=7542#.YpodqHbMI2w.

frontiers | Frontiers in Marine Science

TYPE Correction
PUBLISHED 15 November 2022
DOI 10.3389/fmars.2022.1086751

OPEN ACCESS

EDITED BY
Ludovic Brucker,
U.S. National Ice Center, United States

REVIEWED BY
Vanessa Lucieer,
University of Tasmania, Australia
Jan L. Lieser,
Bureau of Meteorology, Australia

*CORRESPONDENCE
Alvaro S. Scardilli
asscardilli@hidro.gov.ar

SPECIALTY SECTION
This article was submitted to Marine Affairs and Policy, a section of the journal Frontiers in Marine Science

RECEIVED 01 November 2022
ACCEPTED 02 November 2022
PUBLISHED 15 November 2022

CITATION
Scardilli AS, Salvó CS and Saez LG (2022) Corrigendum: Southern Ocean ice charts at the Argentine Naval Hydrographic Service and their impact on safety of navigation. *Front. Mar. Sci.* 9:1086751. doi: 10.3389/fmars.2022.1086751

Corrigendum: Southern Ocean ice charts at the Argentine Naval Hydrographic Service and their impact on safety of navigation

Alvaro S. Scardilli*, Constanza S. Salvó and Ludmila Gomez Saez

Departamento Meteorología, Servicio de Hidrografía Naval, Buenos Aires, Argentina

KEYWORDS

ice chart, Antarctica, satellite imagery, icebergs, sea ice, GIS

A Corrigendum on:

Southern Ocean ice charts at the Argentine Naval hydrographic service and their impact on safety of navigation.

by Scardilli AS, Salvó CS and Saez LG (2022) Front. Mar. Sci. 9:971894. doi: 10.3389/fmars.2022.971894.

In the published article, there was an omission in the **Acknowledgments** section. "The authors acknowledge the support of WMO for the publication of this paper, as a contribution to better supporting sea ice services in the Southern Ocean" was not included. The correct statement appears as follows:

"The authors acknowledge the support of WMO for the publication of this paper, as a contribution to better supporting sea ice services in the Southern Ocean.

The authors acknowledge the use of imagery from NASA's Worldview application (https://worldview.earthdata.nasa.gov), part of NASA's Earth Observing System Data and Information System (EOSDIS)."

The authors apologize for this error and state that this does not change the scientific conclusions of the article in any way. The original article has been updated.

Publisher's note

All claims expressed in this article are solely those of the authors and do not necessarily represent those of their affiliated organizations, or those of the publisher, the editors and the reviewers. Any product that may be evaluated in this article, or claim that may be made by its manufacturer, is not guaranteed or endorsed by the publisher.

frontiers | Frontiers in Marine Science

TYPE Original Research
PUBLISHED 01 February 2023
DOI 10.3389/fmars.2023.979782

OPEN ACCESS

EDITED BY
John Falkingham,
International Ice Charting Working Group, Canada

REVIEWED BY
Qi Shu,
Ministry of Natural Resources, China
Thomas Rackow,
European Centre for Medium-Range Weather Forecasts, Germany
William Merryfield,
Environment and Climate Change Canada (ECCC), Canada

*CORRESPONDENCE
Leandro Ponsoni
leandro.ponsoni@vliz.be

SPECIALTY SECTION
This article was submitted to Marine Affairs and Policy, a section of the journal Frontiers in Marine Science

RECEIVED 27 June 2022
ACCEPTED 16 January 2023
PUBLISHED 01 February 2023

CITATION
Ponsoni L, Ribergaard MH, Nielsen-Englyst P, Wulf T, Buus-Hinkler J, Kreiner MB and Rasmussen TAS (2023) Greenlandic sea ice products with a focus on an updated operational forecast system. *Front. Mar. Sci.* 10:979782. doi: 10.3389/fmars.2023.979782

Greenlandic sea ice products with a focus on an updated operational forecast system

Leandro Ponsoni[1,2]*, Mads Hvid Ribergaard[1], Pia Nielsen-Englyst[1,3], Tore Wulf[1], Jørgen Buus-Hinkler[1], Matilde Brandt Kreiner[1] and Till Andreas Soya Rasmussen[1]

[1]Danish Meteorological Institute (DMI), Copenhagen, Denmark, [2]Flanders Marine Institute (VLIZ), Marine Robotics Centre (MRC), Ostend, Belgium, [3]DTU-Space, Technical University of Denmark (DTU), Lyngby, Denmark

Sea ice information has traditionally been associated with Manual Ice Charts, however the demand for accurate forecasts is increasing. This study presents an improved operational forecast system for the Arctic sea ice focusing on the Greenlandic waters. In addition, we present different observational sea ice products and conduct inter-comparisons. First, a re-analysis forced by ERA5 from 2000 to 2021 is evaluated to ensure that the forecast system is stable over time and to provide statistics for the users. The output is similar to the initial conditions for a forecast. Secondly, the sea ice forecast system is tested and evaluated based on two re-forecasts forced by the high resolution ECMWF-HRES forecast for the period from January 2019 to September 2021. Both the re-analysis and the re-forecasts include assimilation of sea surface temperatures and sea ice concentrations. We validate the re-analysis and the re-forecast systems for sea ice concentration against different remotely sensed observational products by computing the Integrated Ice Edge Error metric at the initial conditions of each system. The results reveal that the re-analysis and the re-forecast perform well. However, the summertime retreat of sea ice near the western Greenlandic coast seems to be delayed a few days compared with the observations. Importantly, part of the bias associated with the model representation of the sea ice edge is associated with the observational errors due to limitations in the passive microwave product in summertime and also near the coast. An inter-comparison of the observational sea ice products suggests that the model performance could be improved by assimilation of sea ice concentrations derived from a newly-developed automated sea ice product. In addition, analysis of persistence shows that the re-forecast has better skill than the persistence forecast for the vast majority of the time.

KEYWORDS

Greenland, sea ice conditions, sea ice edge, forecast, operational system, ocean modelling, satellite, sea ice charts

1 Introduction

The climate is rapidly changing in Polar Regions. These changes are remarkable in the Arctic, where positive trends in air temperature are reported to be about three to four times the global average (Chylek et al., 2022; Nielsen-Englyst et al., 2023). Aligned to changes in air temperature, the Arctic sea ice area and volume are declining at a fast pace both at regional and pan-Arctic scales (Onarheim et al., 2018). Negative sea ice trends have been observed for all months, being more pronounced at the end of the melt season in September (Serreze and Meier, 2019). Since this intense sea ice loss is projected to continue throughout the twenty-first century (Burgard and Notz, 2017), the navigability for the locals and the marine traffic are bound to change (Lindstad et al., 2016). The marine traffic will increase as local communities are accessible for longer periods of the year and new shipping routes become available. At the same time, cruise ship tourism (Snyder, 2007) and other economic activities are expected to intensify (e.g. mineral resource extraction (Gleick, 1989)). Due to this, the interest in sea ice predictability and variability is constantly increasing among scientists, policymakers, and society in general.

The above scenario leads to an augmentation in the demand for maritime weather, ocean, and sea ice services for the benefit of safety at sea and planning, especially in near-coastal waters. Consequently, operational services are required to provide better and more accurate sea ice information at time scales ranging from nowcasting through short-term forecasting and up to at least seasonal. The information at different time scales is important for near real-time maritime safety support and, on longer time scales, for the planning of voyages.

Historically (1893 to 1956), Danish Meteorological Institute (DMI) has collected information and produced ice charts for the summer months of the Arctic region (Underhill and Fetterer, 2012). However, the prime Arctic focus is on Greenlandic Waters, where DMI is the authority in charge of meteorological maritime safety information that assists mariners off the Greenlandic coast. In addition, DMI has offered in-person consultancy through the ice service with analysis focused on specific areas of the Greenlandic waters. For many years the ice service at DMI was based on *in situ* observations by helicopters and airplanes combined with manual interpretation of remotely sensed images that were converted into ice charts. The volume of remotely sensed data has increased and the Greenlandic ice service is now primarily based on remotely sensed data, although the portfolio of sea ice products has extended over time to include sea ice forecasting. In this direction, DMI has recently launched an improved operational, 5-km high-resolution sea ice forecast system with a focus on the waters surrounding Greenland (Figure 1).

This study introduces and conducts an inter-comparison of this forecast system and the latest operational remotely sensed-based sea ice services that DMI provides. The focus is on the sea ice edge location around Greenland as this is the main focus area for DMI and, at the same time, it is an essential diagnostic for mariners.

The article is organized as follows. Section 2 describes the materials and methods by introducing the high-resolution operational forecast system (Section 2.1), the re-analyses and the re-forecast experiments (Section 2.2), the atmospheric forcing (Section 2.3), the observational references (Section 2.4) used for evaluation purposes, and the verification metric (Section 2.5). The results related to the models' evaluation in terms of sea ice concentration (Section 3.1), edge location (Section 3.2), and persistence (Section 3.3) are described and discussed in Section 3. Section 4 summarizes the main aspects of this work.

2 Materials and methods

2.1 High-resolution operational forecast system

The newly-launched DMI sea ice operational forecast system (DMI-HYCOM-CICE) is based on the coupling of the 3D ocean model Hybrid Coordinate Ocean Model [HYCOM; Chassignet et al. (2007)] with the

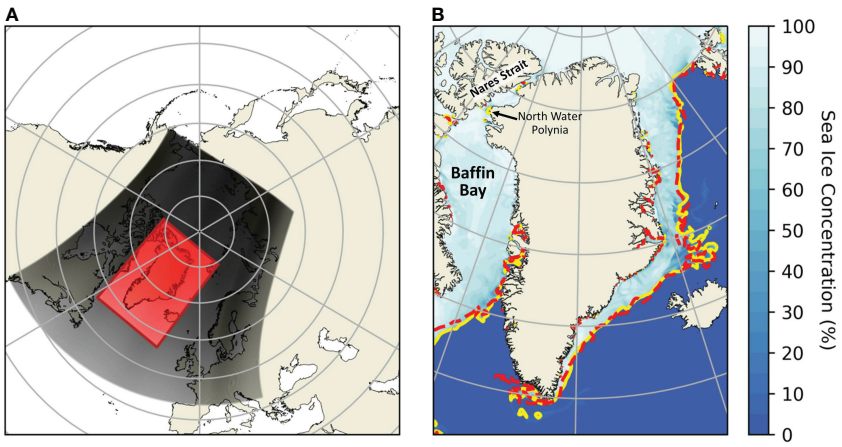

FIGURE 1
(A) Study region. Black and red shaded area define the operational model domain and the Greenland region from which the grid points are used in this study, respectively. **(B)** Demonstration-case (27/Apr/2021) of sea ice concentration estimated by the model (experiment v9; see below). The ice edge defined by the 15%-sea ice concentration contour is represented by the yellow line after the analysis at T=0 hours. The dashed red line shows the sea ice edge for the same forecast on day 6 forecast (T=144 hours; 03/May/2021).

Community Ice CodE model [CICE; Hunke et al. (2021)] through the Earth System Modeling Framework [ESMF; DeLuca et al. (2012)]. The system predicts the ocean and sea ice states. Compared to its previous version (Madsen et al., 2016), the model set-up has been updated on many fronts. It now adopts a finer nominal horizontal resolution of 5 km in the northern regions and includes new parameterized features. The sea ice component is improved with parameterizations of land fast sea ice (Lemieux et al., 2016b) and melt-ponds, as well as enhanced with prognostic sea ice salinity and improved thermodynamics schemes (Turner and Hunke, 2015).

Formation of sea ice occurs at the ocean freezing temperature, and ocean melts sea ice from below, when the ocean temperature exceeds the sea ice melting temperature, which is determined by the salt content of the lowest sea ice layer. The freshwater and ice discharge from Greenland are upgraded using a detailed dataset from the Geological Survey of Denmark and Greenland (Mankoff et al., 2019; Mankoff et al., 2020a; Mankoff et al., 2020b). We calculated monthly means for each of the ~ 50000 river-runoff outlets (29576 streams and 18902 "glacier margins", ie. glacier meltwater) and distribute these to the nearest coastal grid cell. Similar to this, ice calving from 267 glaciers (solid ice discharge) is transformed into equivalent freshwater fluxes, implying that the ice immediately melts at the nearest ocean grid cell. In reality, the solid ice (icebergs and growlers) will melt underway and gradually decrease the surface salinity and temperature within the fjords and offshore for the part that survives. The solid ice discharge used is on average 55%±32% of the total discharge for the 267 glaciers, but this number is an overestimation, as it also includes submarine melting at the glacier termini and melting between the termini and the gate upstream the glacier (Enderlin et al., 2014; Mankoff et al., 2020b). When compared to the previous version, the total freshwater discharge from Greenland is increased by a factor of 15, resulting in decreased near-shore salinity and increased baroclinicity. This is expected to contribute to improve the coastal ocean currents and, consequently, the sea ice transport nearshore Greenland.

The DMI-HYCOM-CICE set-up covers the Arctic and the Atlantic Ocean north of 15°S for the ocean, whereas the sea ice model only covers a northern fraction of the entire grid making the system more computationally efficient and less I/O demanding (Figure 1; black shaded area). It is forced by weather forecasts provided by the European Centre for Medium-Range Weather Forecasts (ECMWF) according to the performed experiment. To constrain model errors related to the sea ice, DMI-HYCOM-CICE assimilates satellite-based sea ice concentration provided at near real-time by the Ocean and Sea Ice Satellite Application Facility (OSI SAF), product OSI-401-b (OSI SAF, 2017). Similarly, DMI-HYCOM CICE assimilates satellite-based sea surface temperatures provided by the Group for High Resolution Sea Surface Temperature [GHRSST, https://podaac.jpl.nasa.gov/GHRSST, Høyer et al. (2012); Høyer et al. (2014)]. The assimilation system is a nudging system which is described in Rasmussen et al. (2018).

2.2 Experiments

To evaluate the performance of the model system three experiments were performed. They generated one re-analysis (v7) and two re-forecasts (v8 and v9). For details the reader is referred to Table 1 and Figure 2.

v7 is a re-analysis that assimilates sea surface temperature and sea ice concentration. The outputs from this simulation are comparable to the initial conditions of a forecast. This experiment spans Jan/2000-Aug/2021. v8 and v9 are re-forecasts that also assimilate sea surface temperatures and sea ice concentration from T=-24 to T=0, where T is hours from the initial conditions or the analysis. The v9 simulation continues from T=0 to T=144 (Figure 3). From T=0 to T=144 the re-forecast is comparable to the operational forecast run, except that the 144h atmospheric forecast consists of piece-wise 0-12h forecast slots rather than a full forecast from 0 to 144h. v8 spans Jan/2019-Sep/2021 and has been run for verification purposes. v9 also starts in Jan/2019 and keeps running to the present day as the operational version (Figure 2).

As the final product, a 144 hourly forecast of sea ice conditions is produced twice a day and released on the Polar Portal (http://polarportal.dk/en/home/) and DMI ocean web-page (http://ocean.dmi.dk/) following the forecast schedule shown in Figure 3.

2.3 Atmospheric forcing

Two different atmospheric products from ECMWF have been used for the three experiments described in Section 2.2 (Table 1). The first experiment (v7) is forced by ERA5 (Hersbach et al., 2020) re-analysis with a horizontal resolution of ~ 31 km. The second and third experiments (v8 and v9) are forced by ECMWF High-Resolution forecasts with ~ 9 km resolution (ECMWF-HRES cy47r3; https://www.ecmwf.int/en/publications/ifs-documentation).

The ERA5 atmospheric forcing is examined by Hudson et al. (2019) over the Arctic region. These authors found that the cloud cover is underestimated during spring, which leads to an overestimation of the short-wave radiation and (less pronounced) underestimation of the downward long-wave radiation. As a result of this, ERA5 has a positive bias in the total downward radiation in spring. Similarly, they found the downward heat flux during summer was too high. One of the main issues in the boundary conditions is the lack of snow in re-analysis such as ERA5 (Arduini et al., 2022). An earlier study by Rasmussen et al. (2018) used the ice surface temperature bias between remotely sensed ice surface temperatures and a coupled ocean and sea ice model in order to correct the 2 m temperature and, based on this, the near-surface forcing. A more advanced approach by Zampieri et al. (2022) uses level 2 remotely sensed surface temperature data and a machine learning approach in order to correct the biases of the atmospheric re-analysis.

In order to acknowledge the challenges of the atmospheric re-analysis, a series of experiments with atmospheric surface corrections was carried out and the ice coverage was compared on the Arctic scale. The most suitable and simple correction was to reduce the downward short-wave radiation over sea ice by 10% as reproduced in experiment v7. By doing so, we reduce the total downward heat flux to the sea ice during the season with incoming solar radiation, which in turn provides a direct heat flux reduction in Watts per square meter. This mimics the net effect of adding Arctic cloud cover during spring and summer. The same correction was added to the v8 experiment, whereas experiment v9 uses the ECMWF-HRES atmospheric forcing. Table 2 lists the atmospheric

TABLE 1 Description of the three experiments (v7, v8, and v9), their atmospheric forcing and its modifications performed for the development of the DMI-HYCOM-CICE operational system.

Experiments	Atmospheric forcing	Horiz. resolution	Shortwave radiation forcing modification factor	Time span
v7	ERA5	~31 km	0.9	Jan/2000-Aug/2021
v8	ECMWF-HRES	~9 km	0.9	Jan/2019–Sep/2021
v9	ECMWF-HRES	~9 km	not modified	Jan/2019–present

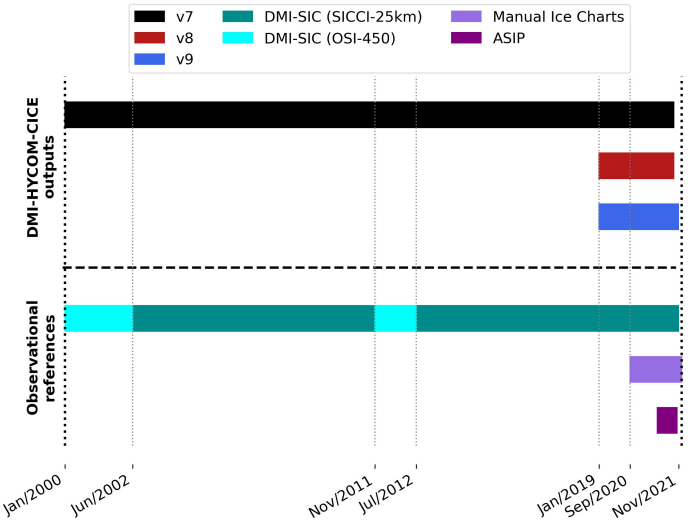

FIGURE 2
Data overview. Horizontal bars indicate the period covered by the DMI-HYCOM-CICE outputs (experiments v7, v8, and v9) and observational references (DMI-SIC, Manual Ice Charts, and Automated sea ice products (ASIP)). The period in which the DMI-SIC product derives from the SICCI-25km or OSI-450 product is also highlighted.

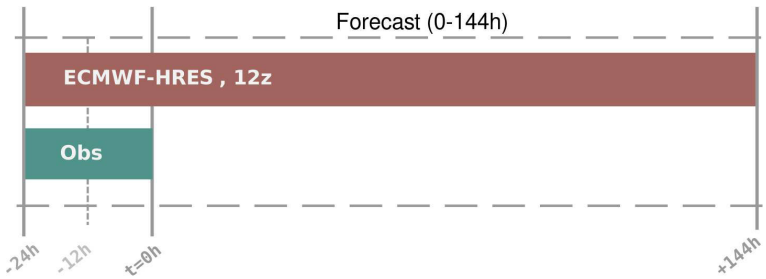

FIGURE 3
Overview of a forecast run. The brown bar indicates an 144 hours forecast that is initialized by 24h window when available observations (green bars) are assimilated. New forecasts are initiated with intervals of 12 hours and they are initiated from a restart file from the previous forecast.

forcing parameters and their GRIB field numbers for ERA5 and ECMWF-HRES. The specific humidity is calculated from pressure and dew temperature using the Arden Buck equation.

Traditionally, a short-term sea-ice forecast has been run as the DMI-HYCOM-CICE, where a coupled ocean-sea ice model has been forced by an atmospheric reanalysis (e.g. Sakov et al., 2012; Madsen et al., 2016; Lellouche et al., 2018; Smith et al., 2021). Sea ice concentration is seen as an initial value problem that evolves slowly and an evolving sea ice cover has therefore not been included until recently in the atmospheric short-term forecast. Most studies that investigate an evolving sea ice cover within a short-term forecast focus on the weather. However, some studies point towards issues within the ocean and sea ice properties as well. Pellerin et al. (2004) show that a fully coupled system is better at forecasting fast coastal processes such as the formation of polynyas. Day et al. (2022) describe how the forcing may create large fluxes in a forced ocean-sea ice model due to a misplaced ice edge. This will force the modelled ice edge to converge towards the sea ice inherited within the atmospheric forcing.

For this experiment, ERA5, ECMWF-HRES and DMI-HYCOM-CICE are all controlled by the OSI SAF data set either as a surface

TABLE 2 Forcing fields from ERA5 and ECMWF-HRES.

Forcing field	Grib number
Longwave radiation downward	175
Shortwave radiation downward	169
Total precipitation	228
2 meter temperature	167
2 meter dew point temperature	168
10m wind u-direction	165
10m wind v-direction	166
Mean sea level pressure	151

boundary condition (ERA5) or through assimilation (ECMWF-HRES and DMI-HYCOM-CICE). This should ensure that the location of the ice edge is rather similar to the initial condition of the forecast.

2.4 Observational references

Three state-of-the-art, satellite-based observational references are used in this work, as follows: (i) a newly-developed DMI sea ice concentration product (DMI-SIC); (ii) Manual Ice Charts produced at DMI, and (iii) automated sea ice product (ASIP) based on deep learning techniques also developed at DMI. Both (ii) and (iii) are distributed in the Copernicus Marine Service.

(i) The DMI-SIC product is a new release in which different sources of sea ice information have been combined and re-sampled onto a 0.05 ° regular latitude-longitude grid (Nielsen-Englyst et al., 2023). It is based on the EUMETSAT OSI SAF Global sea ice concentration CDR v2 product OSI-450 (covering 1979-2015) and the European Space Agency (ESA) Sea Ice Climate Change Initiative (SICCI) SICCI-25km sea ice concentration product (covering the following two periods: June 2002-October 2011 and July 2012-May 2017). An extension of the SICCI-25km processing was used to provide consistent sea ice concentration from May 2017 to May 2021 (hereafter referred to as SICCI-25km as well). The combined DMI-SIC product uses SICCI-25km whenever it is available and OSI-450 otherwise. Different filtering methods are used to improve the accuracy and consistency of the combined DMI-SIC product (Nielsen-Englyst et al., 2023).

(ii) The operational ice service at DMI produces ice charts based on manual interpretation of the satellite imagery, primarily from Synthetic Aperture Radar (SAR) sensors onboard the Copernicus Sentinel-1, but also other platforms such as Radarsat-2, the Radarsat Constellation Mission, TerraSAR-X and CosmoSkyMed. Optical and thermal infrared imagery from sensors onboard, e.g. Sentinel-2 and -3, are also used in the production when daylight and cloud cover is favorable. The ice charts are drawn within an ArcGIS production system with shape files as output. The ice charts map the ice concentration in polygons in 10s of % from 0-100% as defined by the World Meteorological Organization (WMO). The DMI ice charts do not have associated uncertainty estimates describing the ice concentration accuracy. However, a study of the differences between ice charts from the DMI ice service and the Norwegian ice service covering the same region shows a relatively large (up to 30%) standard deviation of the difference in ice concentration, especially at intermediate concentrations (20-80%), see Eastwood et al. (2022) (Appendix on ice chart uncertainty). The DMI ice charts are redistributed in the Copernicus Marine Service as gridded products resampled to 1 km × 1 km grid as the "Arctic Ocean - Sea Ice Concentration Charts - Svalbard and Greenland" (Dinessen et al., 2020), from which we use the "DMI overview ice chart" sub-product. The Overview ice charts are available through Copernicus Marine Service since September 2nd, 2020. The ice charts are produced twice weekly based on satellite data that is up to three days old, which is the time needed in order to cover our region of interest - Greenlandic waters.

(iii) The ASIP (Automated Sea Ice Products) sea ice concentration data set is produced by DMI using the ASIP deep learning algorithm, which is a further development of Malmgren-Hansen et al. (2021). The ASIP sea ice concentration products are automatically retrieved from Copernicus Sentinel-1 Synthetic Aperture Radar (SAR) satellite imagery (in Extra Wide (EW) and Interferometric Wide (IW) swath mode, both re-sampled to an 80 m grid, being close to the native spatial resolution in EW mode) by using a Convolutional Neural Network (CNN) that fuses the high-resolution SAR images with coarser resolution passive microwave observations from the AMSR2 sensor onboard JAXA's GCOM-W satellite in order to produce detailed maps of the sea ice conditions. The CNN is trained on DMI ice charts that are contained in the AI4Arctic/ASIP Sea Ice Dataset v2 (Saldo et al., 2021). This means that any bias introduced by the manual ice charting method (e.g. an overestimation of intermediate SICs) is inherent in the ASIP model. However, any inter- and intra-ice analyst variability are not reproduced by the ASIP algorithm. ASIP algorithm outputs sea ice products distributed within the Copernicus Marine Service as the "DMI-ASIP sea ice classification - Greenland" (Dinessen et al., 2022). For this study, 14-day mosaics were created from individual ASIP products, with the newest ASIP product on top", and with the mosaics' end-date corresponding to the datestamp of the DMI Overview ice charts. Although the ASIP mosaics are composed of up to 14 days of data, in practice, almost the entire Greenland waters are covered by data within 3 days.

It is worthwhile to mention that the observational references (DMI-SIC and the Manual Ice Charts) used for validation purposes are different from the data assimilated by the model (OSI-401-b) and also from themselves. Except for two relatively short periods when OSI-450 is merged into the DMI-SIC product (Jan/2000–Jun/2002 and Nov/2011–Jul/2012). These two periods do not overlap the v8 and v9 experiments. Figure 2 presents an overview of the model and observational data sets used in this work regarding their time coverage.

2.5 Verification metric

Observational products are interpolated onto the HYCOM-CICE grid to make the data from different sources straightforwardly comparable. We apply the Integrated Ice Edge Error [IIEE; Goessling et al. (2016)] as verification metric for evaluating the ability of the model in predicting the sea ice edge provided by the observational references, as well as to compare the observational references themselves. Hereafter, we adopt the definition in which the sea ice edge location is determined by the 15%-sea ice concentration threshold (note that this differs from the WMO Sea Ice Nomenclature definition of sea ice edge – 0%). The IIEE quantifies the total area where the predicted sea ice disagrees on the sea ice concentration being above or below 15%. Therefore, the IIEE is given by the sum of the areas from all grid cells where the modeled sea ice (or the second observational reference) overestimates (O) or underestimates (U) the "true" reference regarding the 15% threshold so that IIEE = O+U.

Figure 4 provides examples of the IIEE metric applied to our data sets for four different days (columns), one from each season. Comparisons are made between HYCOM-CICE (v9) *vs.* DMI-SIC, HYCOM-CICE (v9) *vs.* Manual Ice Charts, and DMI-SIC *vs.* Manual Ice Charts. As an assumption, we consider the later product from each pair of comparisons as the "true" reference. Therefore, red colors in Figure 4 indicate that the first product overestimates the sea ice edge of the reference product, while blue colors reveal the opposite.

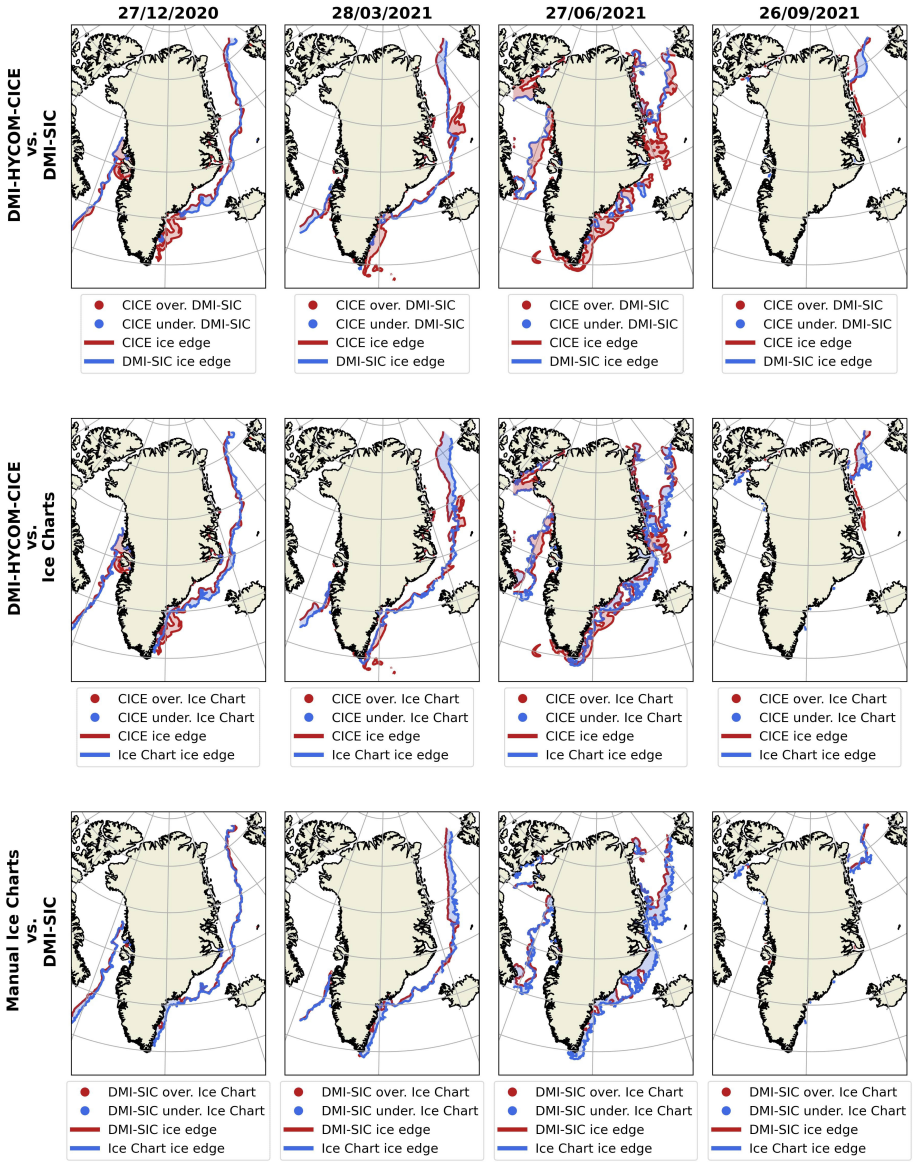

FIGURE 4
Snapshots of IIEE (see definition in section 2.5). Each column represents one day as displayed in the header. Top row: IIEE maps of DMI-HYCOM-CICE (V9) *vs.* DMI-SIC. Red and blue indicate whether DMI-HYCOM-CICE overestimates or underestimates the ice edge prescribed by DMI-SIC, respectively. Middle row: Same as top row but IIEE maps of DMI-HYCOM-CICE *vs.* Manual Ice Charts. Bottom row: Same as top row but it compares DMI-SIC *vs.* Manual Ice Charts (same order).

3 Results and discussion

Section 3.1 and Section 3.2 both focus on validation of the initial conditions, whereas Section 3.3 addresses the evaluation of the forecast skill.

3.1 Sea ice concentration

The sea ice edge is defined by the sea ice concentration field, therefore we will start by providing a first assessment of the DMI-HYCOM-CICE sea ice concentration outputs. We promote an averaged-based, month-by-month comparison of our v7 experiment against the DMI-SIC observational product. This comparison covers the period from Jan/2000 to Dec/2020, which represents the entire overlapping period of the two products (see Figure 2). Figure 5 shows that, on average, there is a good agreement between DMI-HYCOM-CICE and the observational reference. Overall, the model slightly underestimates the observations in almost all months outside of the melt season, as indicated by light shades of blue (differences smaller than 10%). Notice that from October to April, when sea ice is growing, the model underestimates the sea ice concentration near the sea ice edge in both the western and eastern Greenlandic coast.

On the other hand, the model overestimates the sea ice concentration near the southeastern Greenlandic coast whenever the region is sea ice covered, from December to July. The reason for this incongruence is in part linked to limitations of the observational reference itself, as discussed in section 3.2.3. DMI-HYCOM-CICE also overestimates the sea ice concentration in the Baffin Bay when the sea ice starts to melt around May with the

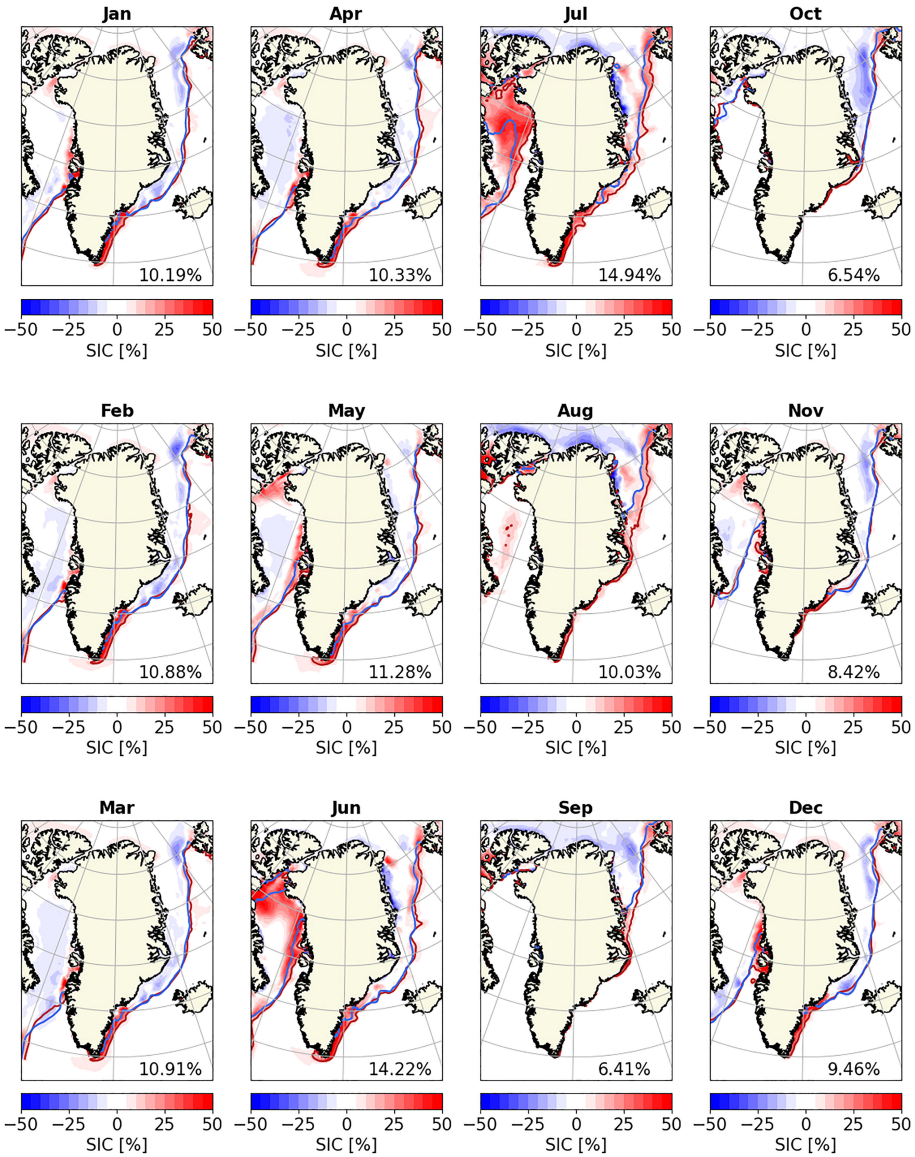

FIGURE 5
Mean difference (v7 - DMI-SIC) in sea ice concentration (%) estimated for each month (from Jan/2000 to Dec/2020) between the v7 experiment and the DMI-SIC reference product. Blue and red lines display the mean sea ice edge represented by the 15% sea ice concentration contour for the DMI-SIC and v7 outputs, respectively. The percentages given in the bottom right are the area-weighted root mean squared errors for the respective panels.

opening of the North Water Polynya in the northern extremity of the bay, between Greenland and Canada, and also adjacent to the western Greenlandic coast. The bias in the northern part of Baffin Bay is likely due to the sea ice model dynamics and the challenge of forming the ice bridge in the southern part of Nares Strait (e.g., Rasmussen et al., 2010; Dansereau et al., 2017; Plante et al., 2020). The approach by Shlyaeva et al. (2016) improved the challenges of modeling landfast sea ice by creating an ensemble member without sea ice dynamics. However, it does not improve the sea ice physics and it will cause problems if the ice bridge collapses during a forecast. The positive bias between model and observations grows throughout the melt season, but it vanishes in August and September when sea ice is entirely melted in that region including in the model outputs. Likewise, the model overestimates the sea ice concentration along the eastern sea ice edge around the same period.

The fact that the model underestimates the sea ice concentration from approximately October to April, and overestimates it during the melting season in the Baffin Bay and along the eastern Greenlandic coast, suggests that DMI-HYCOM-CICE is a few days delayed with the seawater freezing-up and sea ice breaking-/melting-up compared to the observations. Nevertheless, the relatively higher differences in June and July may partly be linked to higher uncertainties of the DMI-SIC product during these months, characterized by substantial melt-ponds coverage, as discussed in Section 3.2.3.

To provide a measure of the monthly differences shown in Figure 5, we calculated the area-weighted root mean squared errors (AW-RMSEs) for the monthly maps. The last four months of the year present smaller AW-RMSEs: 6.4% (September), 6.5% (October), 8.4% (November), and 9.5% (December). AW-RMSEs are similar from January to April, and August, ranging from 10.0% to 10.9%. Maximum AW-RMSEs take place in May (11.3%), June (14.2%), and July (14.9%), which is mainly due to the melting-season biases in the Baffin Bay discussed above.

3.2 Sea ice edge

3.2.1 Long-term IIEE

Figure 6A illustrates how the IIEE evolves from 01/Jan/2000 to 30/Sep/2021 when comparing the v7 experiment and the DMI-SIC product. In the long-term, the IIEE is stable and it does not present significant trends (Figure 6A, black line). From the mean IIEE = 2.61 (± 1.23) × 10^5 km^2 , the largest part of the standard deviation is the seasonal cycle rather than interannual variations or estimations of the mean. About 74% of the mean IIEE are due to the overestimation (Figure 6A, red line) of the sea ice edge by the model (O = 1.93(± 1.18)× 10^5 km^2), while the remaining 26% are due to an underestimation (blue line; U = 0.68(± 0.35)× 10^5 km^2).

The IIEE has a marked seasonal variation with values that grow throughout the melt season and peak in July when IIEE = 4.95(± 0.86)× 10^5 km^2 (Figure 6B). In the period from Sep–Mar, the IIEE is smaller than 2.60 × 105 km^2 . The IIEE growth in the melt season is mainly linked to the errors associated with an overestimation of the sea ice edge by the model (Figures 6A, B).

Even though the IIEE does not present a trend for the entire time span, and the higher errors in the warmer season are always explained by overestimation, the long-term time series shows two distinguished behaviours in the melt season. From Jan/2000 to Dec/2010, average values calculated from Sep-Mar indicate that errors due to overestimation (O = 1.56(± 0.60)× 10^5 km2) are higher than the

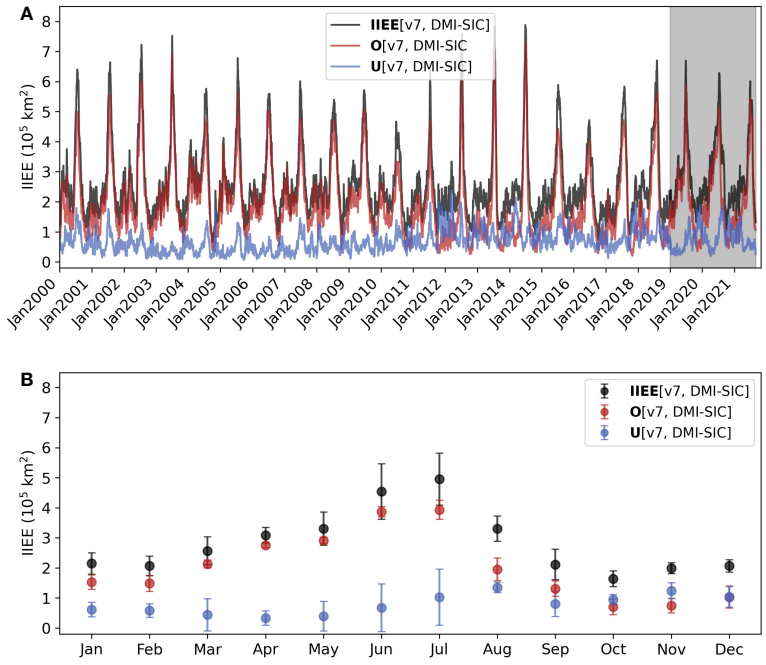

FIGURE 6
(A) Integrated Ice Edge Error (IIEE) estimated between the v7 experiment and DMI-SIC (black line), and its corresponding overestimated (red line) and underestimated (blue line) components. **(B)** Average monthly IIEE calculated for the time series displayed in **(A)**, calculated for the period Jan/2000–Dec/2020. Vertical bars indicate the 1-standard deviation interval.

underestimation (U = 0.47(± 0.23)× 10^5 km2) contribution. Nevertheless, from Jan/2011 to Dec/2018, the contributions to the IIEE are more equally distributed between overestimation (O = 0.99(± 0.39)× 10^5 km5) and underestimation (U = 0.89(± 0.35)× 10^5 km5) cases. We do not have a clear understanding for that behaviour.

As indicated by the mean sea ice edge contour for the individual months in Figure 7 (red and blue lines), there is a striking correspondence between model and observations throughout the year in terms of monthly averages. Figure 7 also displays the cumulative occurrence of days (in percentage) that v7 outputs disagree from the observations by overestimating or underestimating the sea ice edge. Again, the main differences are observed in the warmer seasons, mainly in June and July, in the northern Baffin Bay. Some mismatches also take place during summer off eastern Greenlandic coast, when the modeled ice edge is further offshore than the observed sea ice edge. Nevertheless, the maximum percentage of days in which mismatches take place in the eastern ice edge does not exceed 30–40% in August. Such a difference is even smaller in June, July, and September.

3.2.2 Impacts of differences in atmospheric forcing

To refine the model set-up for the operational forecast system, three different experiments are investigated using coarse resolution ERA5 atmospheric reanalysis with modified short wave radiation (v7), and similar using high resolution ECMWF-HRES forcing with (v8) and without (v9) short wave modifications as detailed in Section 2.3. The experiments overlap for almost 3 years from Jan/2019 to late 2021 (see Figure 2).

By comparing experiment v7 against v8, Figure 8A reveals that the two ECMWF forcings do not have a noticeable influence on the

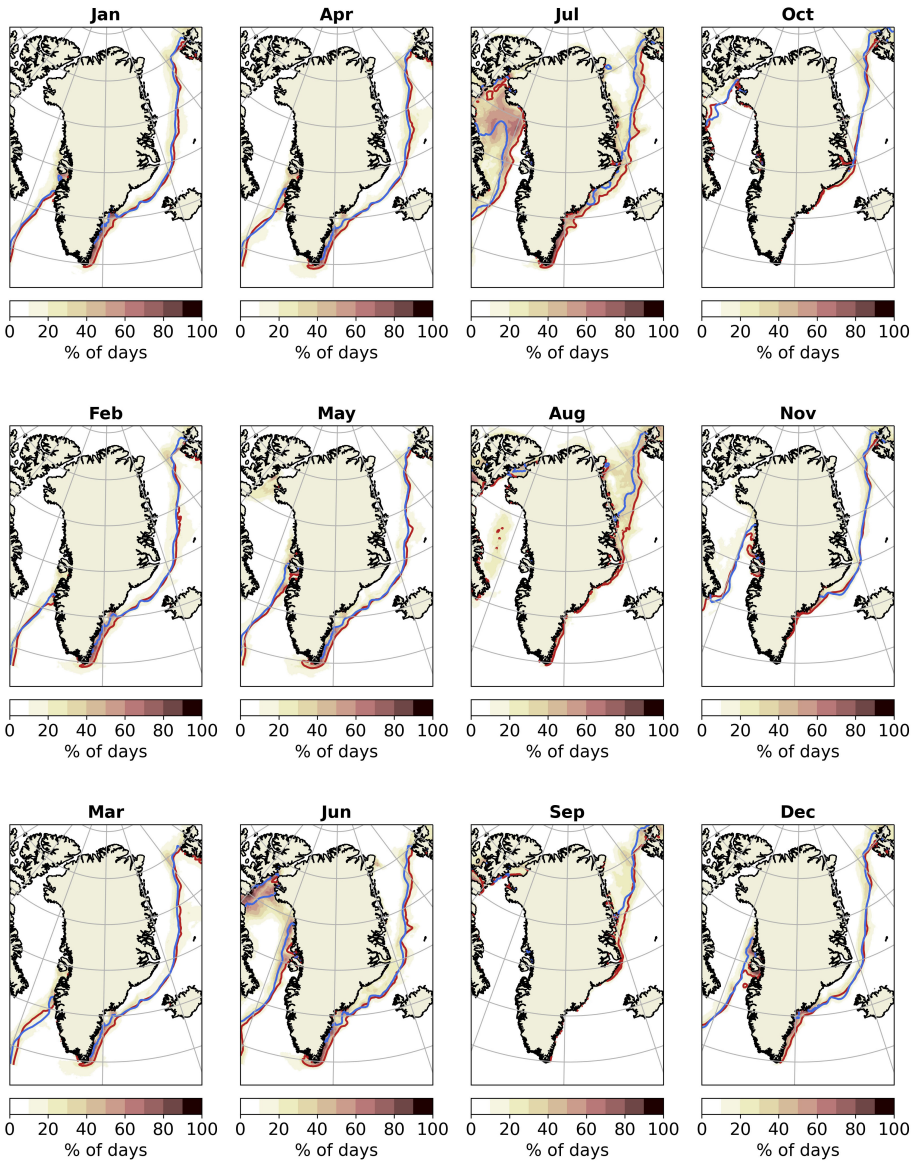

FIGURE 7
Cumulative occurrence of days (in percentage) in which the model outputs from v7 experiment overestimates or underestimates the DMI-SIC observational product based on the IIEE metric. The calculation spans for 21 years (Jan/2000-Dec/2020). Blue and red lines display the mean sea ice edge represented by the 15% sea ice concentration contour for the DMI-SIC and v7 outputs, respectively.

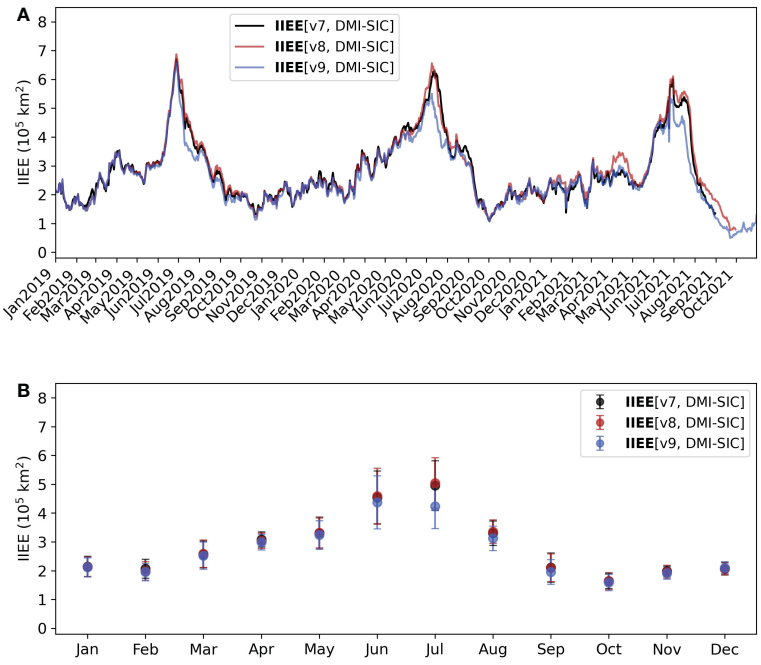

FIGURE 8
(A) Integrated Ice Edge Error (IIEE) estimated between the v7 (black line), v8 (red line), and v9 (blue line) experiments and DMI-SIC. **(B)** Average monthly IIEE calculated for the time series displayed in **(A)**, calculated for the period Jan/2000–Dec/2020. Vertical bars indicate the 1-standard deviation interval.

integrated errors associated with the forecast of the sea ice edge despite their different resolution. Regarding the shortwave modifications, the non-negligible improvement (smaller IIEE values) for v9 compared to v8 in summer (mainly in July) indicates that a 10% reduction in this variable may be a too strong forcing modification. It corroborates that the ECMWF-HRES does not need forcing modifications in the DMI-HYCOM-CICE standard version, at least for this study region and setup (Figures 8A, B).

By definition, the IIEE plotted over time in Figure 8 displays a diagnostic integrated for the entire study region. Therefore, this diagnostic does not specify the grid points where the model and observations agree, or not (over- or underestimate), in terms of sea ice edge location. Figure 9 overcomes this limitation by plotting the number of days (in percentage) in which the three experiments overestimate (first column) and underestimate (second column) the sea ice edge location provided by the observational reference. Figure 9's third column shows the total occurrence of days in which the model and observations disagree in either way. The three experiments present a marked resemblance regarding the number of days and regions of discrepancy. Over time, there is a clear pattern of how the sea ice edge mismatches are distributed in space, although the two data sets barely disagree in more than 30% of the total number of days. DMI-HYCOM-CICE slightly overestimates the sea ice edge in the Baffin Bay and off southeastern Greenlandic coast (Figure 9; first column) and underestimates it off northeastern Greenlandic coast (Figure 9; second column).

The spatial improvements highlighted by the dominance of shades of red in Figure 9's fourth column, associated with the smaller errors in summer shown in Figure 8, indicates that adopting the v9 experimental configuration upgrades the forecast skill of the sea ice edge for almost the entire domain, except in the north of Greenland. The clearest improvement is adjacent to the southeastern coast. Due to these improvements, the v9 configuration with ECMWF-HRES forcing and no forcing modification is selected as the operational version of our forecast system for sea ice conditions off Greenland.

3.2.3 Ice charts and observational uncertainties

Despite having a certain degree of subjectivity and being restricted in time, with twice-weekly releases available at the Copernicus Marine Services from Sep/2020 (120 images in total for this study), Manual Ice Charts provide a valuable opportunity for promoting an additional and independent evaluation of our forecast system as they are often considered to be the best available product, especially in terms of the ice edge. In addition to this, the recently developed ASIP product is included in the comparison. Considering these products also allow an estimation of the observational uncertainty itself through comparisons against the DMI-SIC product.

Figure 10A indicates that IIEE values resulting from the evaluation of v9 experiments are very similar when adopting either DMI-SIC (red dots) or Manual Ice Charts (blue dots) as observational reference. Interestingly, the IIEEs calculated between both observational products follow the same temporal pattern with values peaking in summer. This fact reveals that larger values of IIEE in summer, as shown in Figures 6, 8, are not only related to the model but in part resulting from observational uncertainties (Figure 10A, black dots). By comparing ASIP and Manual Ice Charts (Figure 10A, magenta crosses), two similar observational products, IIEE values are further reduced mainly in the (warm) summer season. Nevertheless, these results should be interpreted

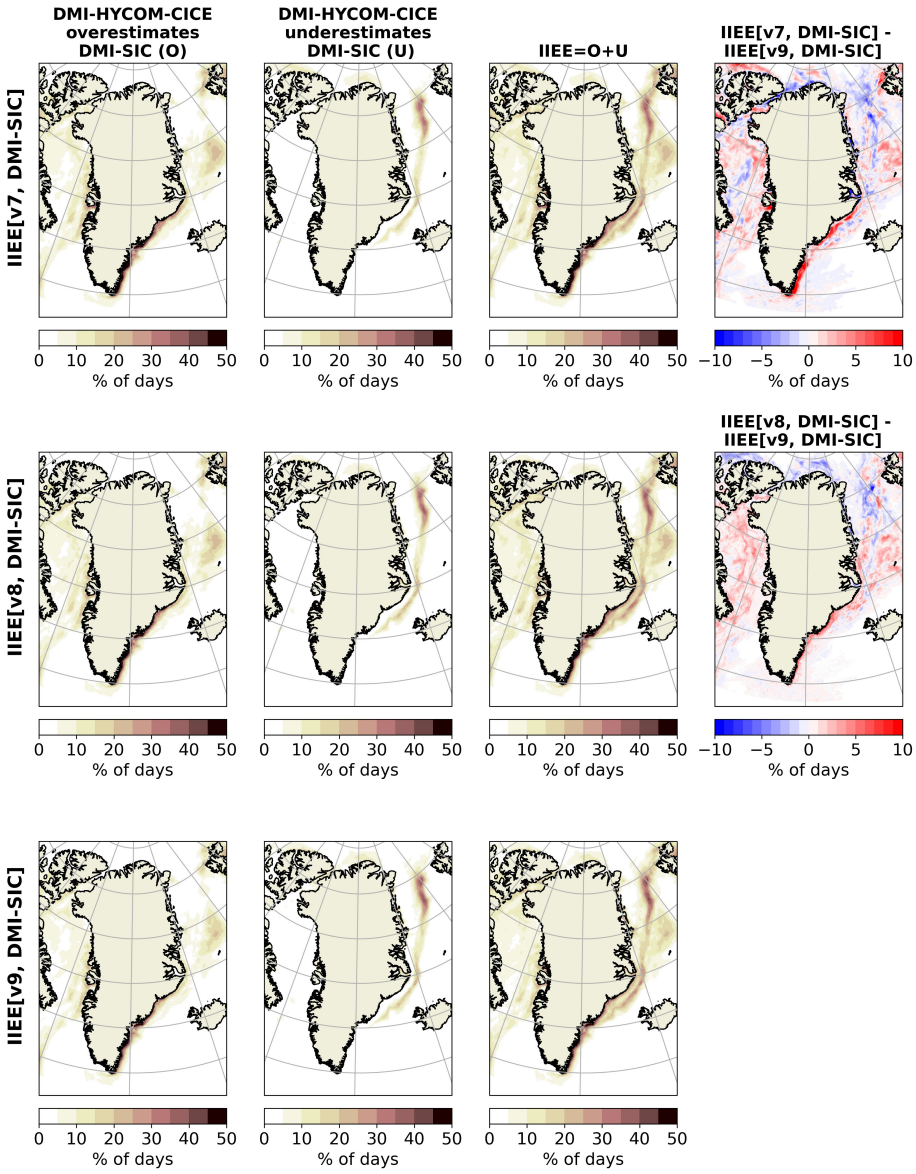

FIGURE 9
Cumulative occurrence of days (in percentage) in which the model outputs from v7 (first row), v8 (second row), and v9 (third row) experiments overestimate (first column) or underestimate (second column) the DMI-SIC observational product regarding the 15% sea ice concentration threshold. The third column shows both overestimation and underestimation cases. The fourth column shows the differences IIEE[v9, DMI-SIC] - IIEE[v7, DMI-SIC] (first row) and IIEE[v9, DMI-SIC] - IIEE[v8, DMI-SIC] (second row).

with caution since the ASIP algorithm is trained on Manual Ice Charts and might reproduce any systematic biases found in the charts, as described in Section 2.4.

Figure 10B reveals, by subtracting the observational uncertainty (IIEE[DMI-SIC, Manual Ice Charts]), that the relative IIEE is more stable over time and reduces by about 41% and 44% for the v9–DMI-SIC and v9–Manual Ice Charts comparisons. This indicates that assimilation of the ASIP product might improve the initial state of the operational sea ice model around Greenland, especially in summertime, when the largest bias occurs.

Analogously to Figure 9, but now comparing v9 *vs.* DMI-SIC, v9 *vs.* Manual Ice Charts, and DMI-SIC *vs.* Manual Ice Charts, Figure 11 shows the percentage of days in which a pair of sea ice concentration data sets disagree regarding the 15%-SIC threshold. Figure 11's first column shows that the IIEE due to the overestimation of the sea ice edge by the model (v9 experiment) is evident off the southeastern Greenlandic coast. This overestimation is higher when comparing v9 against DMI-SIC and attenuated when model outputs are compared against the Manual Ice Charts. Along the eastern and northeastern coast the errors are mainly associated with an underestimation of the sea ice edge by the model (Figure 11, second column). Reinforcing the results shown in Figure 10, the IIEE are smaller when comparing the observational products (Figure 11, fourth column). Also, the IIEE between the observational products are mainly due to an underestimation of the sea ice edge by the DMI-SIC product compared to the Manual Ice Charts (Figure 11, third row). DMI-SIC and other passive microwave products have issues near the coast where the satellite images are contaminated by land and provide

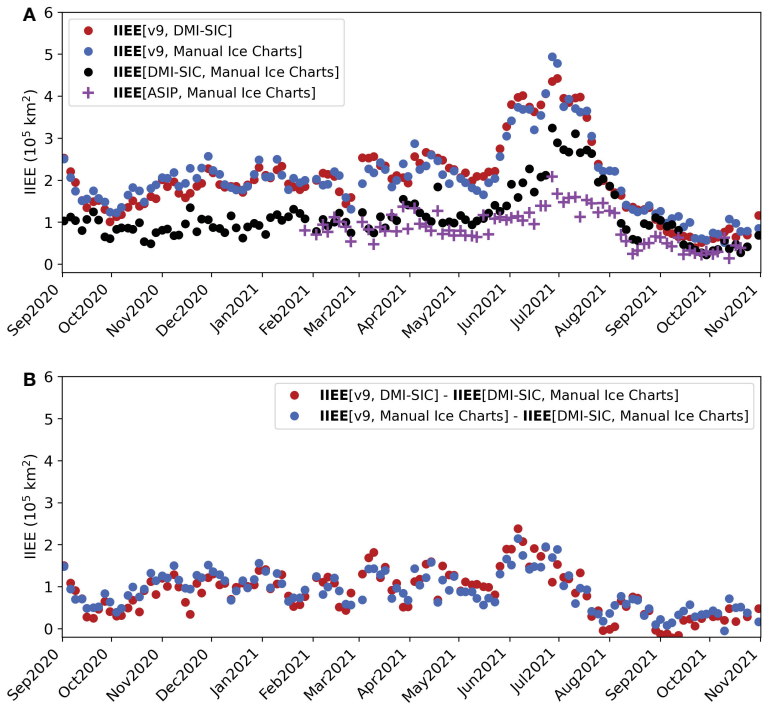

FIGURE 10
(A) Integrated Ice Edge Error **(IIEE)** estimated between the v9 experiment and the observational products: DMI-SIC (red dots) and Manual Ice Charts (blue dots). The black dots show the observational uncertainty given by the IIEE calculated between DMI-SIC and Manual Ice Charts and similar between ASIP and Manual Ice Charts given by the magenta plus markers. **(B)** Difference between the IIEE resulting from the comparison between model–observations and the observational uncertainty. The computation is performed only for dates in which Manual Ice Charts are available.

erroneous results. In the southeastern part of Greenland the sea ice cover is a near-coastal narrow band, which limits the information from passive microwave data.

To complement these results, the supplemental material of this manuscript brings an animation that displays the IIEE computation, partitioned in contributions due to overestimation and underestimation, between model outputs and observational products. It sequentially shows all 120 dates with available Manual Ice Charts. The animation makes it easier to visualize the results discussed throughout this manuscript. Nevertheless, it also allows us to identify other minor imperfections of the model. The most remarkable is the overestimation of the sea ice edge by the model in the southern tip of Greenland (e.g., 03/Feb/2021 and 07/Mar/2021). Given that these coastal seas have been marked out as the windiest location in the world ocean (Sampe and Xie, 2007), the likely explanation for this overestimation is related to the fact that the sea ice model does not account for the ocean waves and swells impinging the ice edge from offshore, and the system that provides the ECMWF-HRES forcing does not, either. These waves are recognized as an important agent for sea ice disintegration, mainly in the melt season (Squire et al., 1995; Squire, 2007; Li et al., 2021)

3.3 Persistence

An example of the evolution of a forecast is seen in Figure 1B. The yellow contour shows the forecast at the initial condition, whereas the dashed red contour shows the forecast at T=144. For this case, it is clear that compared to the total ice cover the changes are limited, however north of Iceland and in the southwestern corner of the domain near the ice edge the yellow and red contours differ.

In order to quantify the skill of the operational forecast, the experiment v9 is evaluated against persistence as in Lemieux et al. (2016a) and following Equation 1:

$$P_n - F_n = IIEE_{OBS_n,FC_0} - IIEE_{OBS_n,FC_n}, \quad (1)$$

where Pn and Fn denotes the IIEE calculated between observation (OBS) and forecast at day 0 (FC0) and day n (FCn), respectively. As observational reference, DMI-SIC is used, as it exists every day for the entire v9 period. If the solution for Equation 1 is positive, the forecast is better than persistence.

The temporal variation of the forecast skill against persistence is shown in Figure 12, and statistics are given in Table 3. The forecast is in general better than persistence. The improvement of the re-forecast skill compared to the persistence forecast increases by around 10% from the 1 day forecast (66%) to the 6 days forecast (76%). However, the initial IIEE is still the largest part of the bias, thus this should be a focus area in future developments. In summertime, when the biases are largest, the re-forecast skill towards persistence is also largest.

4 Summary

This article introduced the recently-launched, DMI operational forecast system for sea ice conditions off the Greenlandic coast. The system is built on the coupling of the ocean model HYCOM and the sea

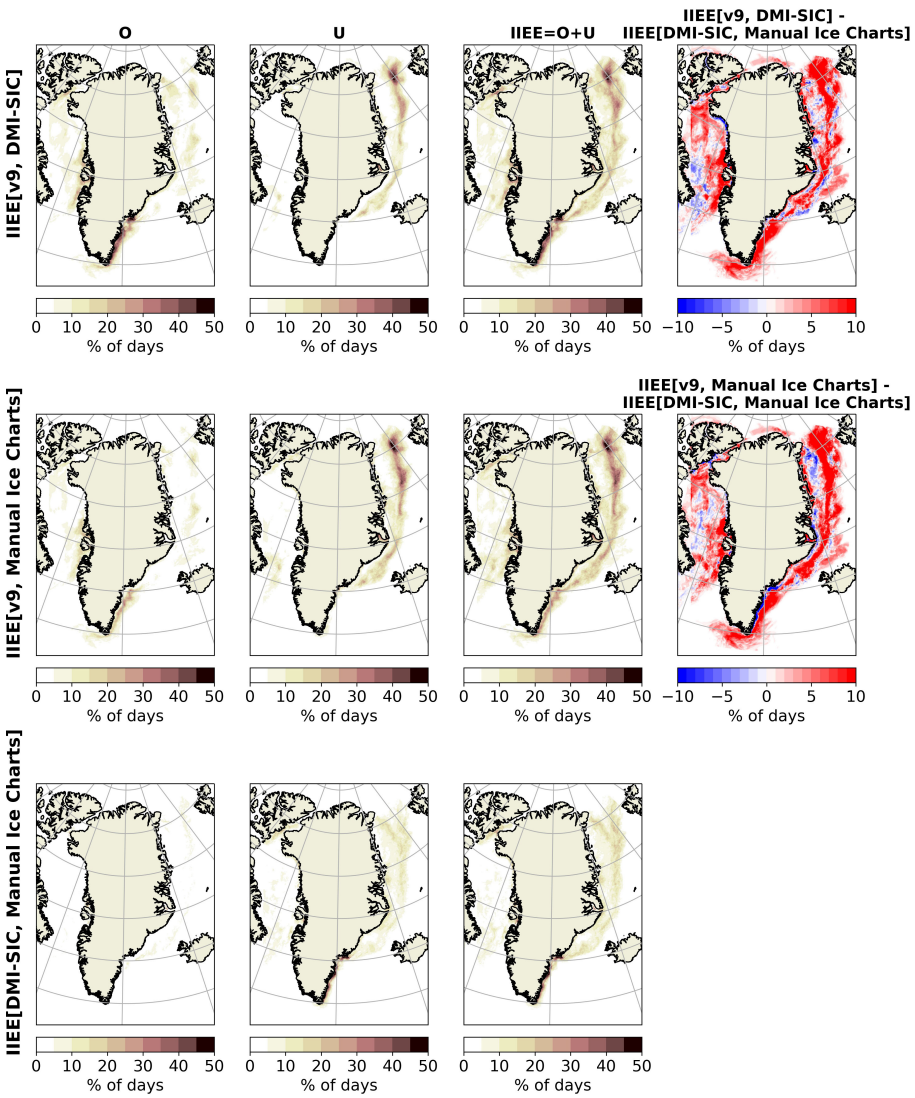

FIGURE 11
Same as Figure 9 but comparing the v9 experiments, and the DMI-SIC and Manual Ice Charts observational products.

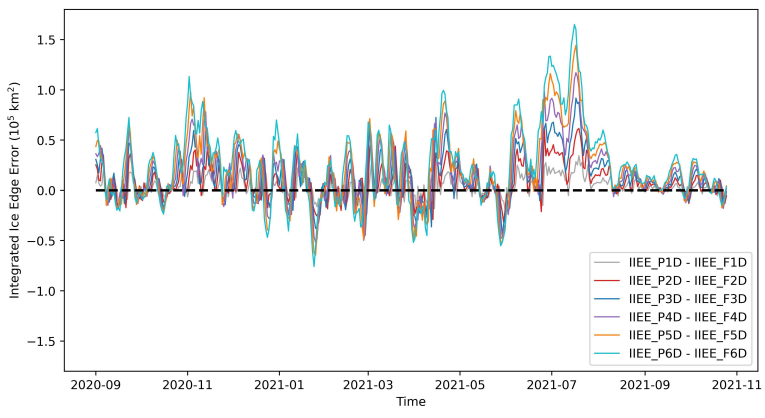

FIGURE 12
IIEE difference of persistence minus forecast for v9 experiment vs. DMI SIC product. The lines represent the result after 1 to 6 days.

TABLE 3 Persistence *vs.* forecast. First column is the forecast day. Second column is the number of days where forecast is better than persistence (out of 420 days). Third column is the IEEE for forecast against DMI-SIC (Fn), and the last column is the IEEE differences between persistence (Pn) and forecast (Fn).

FC days	no. days	$F_n[10^5\ km^2]$	$P_n - F_n[10^5\ km^2]$
0	–	2.30	0
1	279 (66%)	2.33	0.038
2	287 (68%)	2.36	0.082
3	297 (71%)	2.39	0.127
4	311 (74%)	2.41	0.172
5	311 (74%)	2.43	0.214
6	320 (76%)	2.45	0.255

ice model CICE. These are, in turn, forced by ECMWF deterministic atmospheric forcing and assimilate near-real-time satellite observations of sea ice concentration from OSI SAF (OSI-401-b). The model set-up for the operational version is chosen based on the evaluation of three experiments. It provides 144-hourly forecasts of sea ice conditions twice a day, supporting mariners with voyage planning and safety at sea (see Secs. 2.1 and 2.3).

We here provided a first evaluation of the forecast system by inspecting its ability to predict the sea ice edge location. To do so, we calculated the integrated ice edge error metric (see Section 2.5) between the DMI-HYCOM-CICE outputs against three satellite-based observational references: DMI-SIC, Manual Ice Charts, and ASIP (see Section 2.4). Since these products are based on different methods to convert retrievals of satellite observations into sea ice properties, it also allowed us to provide an estimate of the observational uncertainty.

Altogether the model provides robust forecasts of the sea ice edge throughout the year, although improvements during late spring and summer are desirable (see Section 3). In May, the forecast system is delayed a few days in reproducing the opening of the North Water Polynya in northern Baffin Bay. At the same time, the model is also delayed in the retreat of sea ice off the western Greenlandic coast. This delay in the model persists during summer when sea ice is melting in the entire Baffin Bay (see Figures 5, 7). Due to that, the highest values in the integrated ice edge error are observed in late spring and summer. The delay of the sea ice retreat may be linked to the warm currents along the western coast of Greenland not being properly modeled (Buch, 2002). Likewise, it could also be linked to the usage of passive microwave-based products, that can have issues with melt ponds during summer by interpreting them as open water, which lead to ice concentrations that are biased low (see Figures 6, 8).

The forecast of the ice edge was tested against persistence. The forecast is better than persistence in 66% of the days when the forecast is made with one day lead time and 76% percent of the days when the forecast is provided with 6 days lead time. The skill of the forecast is especially pronounced during summer, when the model biases are highest.

Off the southeastern coast of Greenland, the model also overestimates the observations in summer by predicting a sea ice edge further offshore (see Figures 5, 7). A potential reason for explaining this delay during the melt season is the fact that the model does not account for the waves interacting with the sea ice edge. Waves are important for the sea ice disintegration, especially considering that this area is extremely windy (Sampe and Xie, 2007). Nevertheless, part of the integrated ice edge errors found off the eastern Greenlandic coast might also be associated with observational uncertainties. Our results show that two independent observational references (DMI-SIC and Manual Ice Charts) also disagree in this region, especially in the area adjacent to the southeastern coast (see Figures 10, 11).

The inter-comparison between the remotely sensed products illustrated that the ASIP product and the Manual Ice Charts compare better than the latter against the DMI-SIC (see Figure 10A), especially in summer. This indicates that it would be beneficial to assimilate multi sensor products that consist at least of automated retrievals of SAR level 2 data (ASIP) and passive microwave level 2 data (OSI SAF). By doing so, the best solution is provided in terms of objectivity, resolution, available uncertainty estimates, and timeliness, especially when the ASIP product becomes Arctic wide.

Data availability statement

The raw data supporting the conclusions of this article will be made available by the authors, without undue reservation.

Author contributions

LP conducted the data processing, produced the figures, analysed the results, and wrote the manuscript based on discussion with MR and TR. MR and TR worked on the model development and implementation. MR performed the experiments and is responsible for making the operational data available for the users. PN-E

developed and produced the DMI-SIC product. TW developed and produced the ASIP product with support from JH and MK. MR and JH generated mosaics based on ASIP products. TR is the PI of the project. All authors provided comments on the manuscript. All authors contributed to the article and approved the submitted version

Funding

All authors were funded by the Danish State through the National Centre for Climate Research (NCKF) and the Act of Innovation foundation in Denmark through the MARIOT project (Grant Number 9090 00007B). PN-E was also partly funded by the Copernicus Marine Environment Monitoring Service (CMEMS).

Acknowledgments

We wish to acknowledge three reviewers for their constructive and valid comments including the proposed validation of the model forecast against persistence, which strengthen the article.

Conflict of interest

The authors declare that the research was conducted in the absence of any commercial or financial relationships that could be construed as a potential conflict of interest.

Publisher's note

Supplementary material

The Supplementary Material for this article can be foundonline at: https://www.frontiersin.org/articles/10.3389/fmars.2023.979782/full#supplementary-material

References

Arduini, G., Keeley, S., Day, J. J., Sandu, I., Zampieri, L., and Balsamo, G. (2022). On the importance of representing snow over sea-ice for simulating the Arctic boundary layer. *J. Adv. Modeling Earth Syst.* 14, e2021MS002777. doi: 10.1029/2021MS002777

Buch, E. (2002). "Present oceanographic conditions in Greenland waters," in *DMI scientific report 02-02* (Danish Meteorological Institute).

Burgard, C., and Notz, D. (2017). Drivers of Arctic ocean warming in CMIP5 models. *Geophys. Res. Lett.* 44, 4263–4271. doi: 10.1002/2016GL072342

Chassignet, E. P., Hurlburt, H. E., Smedstad, O. M., Halliwell, G. R., Hogan, P. J., and Wallcraft, A. J. (2007). The HYCOM (Hybrid coordinate ocean model) data assimilative system. *J. Mar. Syst.* 65, 60–83. doi: 10.1016/j.jmarsys.2005.09.016

Chylek, P., Folland, C., Klett, J. D., Wang, M., Hengartner, N., Lesins, G., et al. (2022). Annual mean 455 Arctic amplification 1970–2020: Observed and simulated by CMIP6 climate models. *Geophysical Res. Lett.* 49, e2022GL099371. doi: 10.1029/2022GL099371

Dansereau, V., Weiss, J., Saramito, P., Lattes, P., and Coche, E. (2017). Ice bridges and ridges in the maxwell-eb sea ice rheology. *Cryosphere* 11, 2033–2058. doi: 10.5194/tc-11-2033-2017

Day, J. J., Keeley, S., Arduini, G., Magnusson, L., Mogensen, K., Rodwell, M., et al. (2022). Benefits and challenges of dynamic sea ice for weather forecasts. *Weather Climate Dynamics* 3, 713–731. doi: 10.5194/wcd-3-713-2022

DeLuca, C., Theurich, G., and Balaji, V. (2012). *The earth system modeling framework* (Berlin, Heidelberg: Springer Berlin Heidelberg), 43–54. doi: 10.1007/978-3-642-23360-96

Dinessen, F., Hackett, B., and Kreiner, M. B. (2020). "Product user manual: For regional high resolution sea ice charts Svalbard and Greenland region," in *Copernicus Marine service, product SEAICE ARC SEAICE L4 NRT OBSERVATIONS*. 011 002 2.9. doi: 10.48670/moi-00128

Dinessen, F., Korosov, A., Wettre, C., Lavergne, T., and Kreiner, M. B. (2022). "Product user manual: Arctic sea ice concentration arctic sea ice type greenland sea ice concentration," in *Copernicus Marine service, product SEAICE ARC PHY AUTO L4 NRT*. 011 015 1.1. doi: 10.48670/moi-00122

Eastwood, S., Karvonen, J., Dinessen, F., Fleming, A., Pedersen, L., Saldo, R., et al. (2022). "Quality information document for sea ice products," in *Copernicus Marine service SI TAC, ref. cmems-si-quid-011- 402001to007-009to015-018 2.14.*

Enderlin, E. M., Howat, I. M., Jeong, S., Noh, M.-J., van Angelen, J. H., and van den Broeke, M. R. (2014). An improved mass budget for the Greenland ice sheet. *Geophysical Res. Lett.* 41, 866–872. doi: 10.1002/2013GL05901

Gleick, P. H. (1989). The implications of global climatic changes for international security. *Clim. Change* 15, 309–325. doi: 10.1007/BF00138857

Goessling, H. F., Tietsche, S., Day, J. J., Hawkins, E., and Jung, T. (2016). Predictability of the Arctic sea ice edge. *Geophys. Res. Lett.* 43, 1642–1650. doi: 10.1002/2015GL067232

Høyer, J. L., Karagali, I., Dybkjær, G., and Tonboe, R. (2012). Multi sensor validation and error characteristics of Arctic satellite sea surface temperature observations. *Remote Sens. Environ.* 121, 335–346. doi: 10.1016/j.rse.2012.01.013

Høyer, J. L., Le Borgne, P., and Eastwood, S. (2014). A bias correction method for Arctic satellite sea surface temperature observations. *Remote Sens. Environ.* 146, 201–213. doi: 10.1016/j.rse.2013.04.020

Hersbach, H., Bell, B., Berrisford, P., et al. (2020). The ERA5 global reanalysis. *Q. J. R. Meteorol. Soc* 146, 1999–2049. doi: 10.1002/qj.3803

Hudson, S. R., Granskog, M. A., Walden, V. P., Rinke, A., Graversen, R. G., Segger, B., et al. (2019). Evaluation of six atmospheric reanalyses over Arctic sea ice from winter to early summer. *J. Clim.* 32, 4121–4143. doi: 10.1175/JCLI-D-18-0643.1

Hunke, E., Allard, R., Bailey, D. A., Blain, P., Craig, A., Dupont, F., et al. (2021). *Cice-consortium/cice: Cice version 6.3.0* (Zenodo). doi: 10.5281/zenodo.5423913

Lellouche, J.-M., Greiner, E., Le Galloudec, O., Garric, G., Regnier, C., Drevillon, M., et al. (2018). Recent updates to the Copernicus marine service global ocean monitoring and forecasting real-time 1/12 high-resolution system. *Ocean Sci.* 14, 1093–1126. doi: 10.5194/os-14-1093-2018

Lemieux, J.-F., Beaudoin, C., Dupont, F., Roy, F., Smith, G. C., Shlyaeva, A., et al. (2016a). The regional ice prediction system (RIPS): verification of forecast sea ice concentration. *Q. J. R. Meteorological Soc.* 142, 632–643. doi: 10.1002/qj.2526

Lemieux, J.-F., Dupont, F., Blain, P., Roy, F., Smith, G. C., and Flato, G. M. (2016b). Improving the simulation of landfast ice by combining tensile strength and a parameterization for grounded ridges. *J. Geophysical Research: Oceans* 121, 7354–7368. doi: 10.1002/2016JC012006

Li, J., Babanin, A. V., Liu, Q., Voermans, J. J., Heil, P., and Tang, Y. (2021). Effects of wave-induced sea ice break-up and mixing in a high-resolution coupled ice-ocean model. *J. Mar. Sci. Eng.* 9. doi: 10.3390/jmse9040365

Lindstad, H., Bright, R. M., and Strømmanb, A. H. (2016). Economic savings linked to future Arctic shipping trade are at odds with climate change mitigation. *Transp. Policy* 45, 24–34. doi: 10.1016/j.tranpol.2015.09.002

Madsen, K. S., Rasmussen, T. A. S., Ribergaard, M. H., and Ringgaard, M. (2016). High resolution sea-ice modelling and validation of the Arctic with focus on south greenland waters 2004–2013. *Polarforschung* 85, 101–115. doi: 10.2312/polfor.2016.006

Malmgren-Hansen, D., Pedersen, L. T., Nielsen, A. A., Kreiner, M. B., Saldo, R., Skriver, H., et al. (2021). A convolutional neural network architecture for sentinel-1 and AMSR2 data fusion. *IEEE Trans. Geosci. Remote Sens.* 59, 1890–1902. doi: 10.1109/TGRS.2020.3004539

Mankoff, K. D., Colgan, W., Solgaard, A., Karlsson, N. B., Ahlstrøm, A. P., van As, D., et al. (2019). Greenland Ice sheet solid ice discharge from 1986 through 2017. *Earth Syst. Sci. Data* 11, 769–786. doi: 10.5194/essd-11-769-2019

Mankoff, K. D., Noel, B., Fettweis, X., Ahlstrøm, A. P., Colgan, W., Kondo, K., et al. (2020a). Greenland Liquid water discharge from 1958 through 2019. *Earth Syst. Sci. Data* 12, 2811–2841. doi: 10.5194/essd-12-2811-2020

Mankoff, K. D., Solgaard, A., Colgan, W., Ahlstrøm, A. P., and Khan, S. A. (2020b). Greenland Ice sheet solid ice discharge from 1986 through march 2020. *Earth Syst. Sci. Data* 12, 523 1367–1383. doi: 10.5194/essd-12-1367-2020

Nielsen-Englyst, P., Høyer, J. L., Kolbe, W. M., Dybkjær, G., Lavergne, T., Tonboe, R. T., et al. (2023). A combined sea and sea-ice surface temperature climate dataset of the arctic 1982–2021. *Remote Sens. Environ.* 284, 113331. doi: 10.1016/j.rse.2022.113331

Onarheim, I. H., Eldevik, T., Smedsrud, L. H., and Stroeve, J. C. (2018). Seasonal and regional manifestation of Arctic sea ice loss. *J. Clim.* 31, 4917–4932. doi: 10.1175/JCLI-D-17-0427.1

OSI SAF (2017). "EUMETSAT ocean and Sea ice satellite application facility: Global Sea ice concentration climate data record 1979–2015 (v2.0) - multimission," in *EUMETSAT SAF on ocean and Sea ice*. doi: 10.15770/EUMSAFOSI0008

Pellerin, P., Ritchie, H., Saucier, F. J., Roy, F., Desjardins, S., Valin, M., et al. (2004). Impact of a two-way coupling between an atmospheric and an ocean-ice model over the gulf of st. *lawrence. Monthly Weather Rev.* 132, 1379–1398. doi: 10.1175/1520-0493(2004)132⟨1379:IOATCB⟩2.0.CO;2

Plante, M., Tremblay, B., Losch, M., and Lemieux, J.-F. (2020). Landfast sea ice material properties derived from ice bridge simulations using the Maxwell elasto-brittle rheology. *Cryosphere* 14, 2137–2157. doi: 10.5194/tc-14-2137-2020

Rasmussen, T. A. S., Høyer, J. L., Ghent, D., Bulgin, C. E., Dybkjær, G., Ribergaard, M. H., et al. (2018). Impact of assimilation of sea-ice surface temperatures on a coupled ocean and sea-ice model. *J. Geophysical Research: Oceans* 123, 2440–2460. doi: 10.1002/2017JC013481

Rasmussen, T. A., Kliem, N., and Kaas, E. (2010). Modelling the sea ice in the nares strait. *Ocean Model.* 35, 161–172. doi: 10.1016/j.ocemod.2010.07.003

Sakov, P., Counillon, F., Bertino, L., Lisæter, K. A., Oke, P. R., and Korablev, A. (2012). TOPAZ4: an ocean-sea ice data assimilation system for the north Atlantic and Arctic. *Ocean Sci.* 8, 633–656. doi: 10.5194/os-8-633-2012

Saldo, R., Kreiner, M. B., Buus-Hinkler, J., Pedersen, L. T., Malmgren-Hansen, D., Nielsen, A. A., et al. (2021). *AI4Arctic / ASIP Sea ice dataset - version 2*. doi: 10.11583/DTU.13011134.v3

Sampe, T., and Xie, S.-P. (2007). Mapping high sea winds from space: A global climatology. *BAMS* 88, 1965–1978. doi: 10.1175/BAMS-88-12-1965

Serreze, M. C., and Meier, W. N. (2019). The arctic's sea ice cover: trends, variability, predictability, and comparisons to the Antarctic. *Ann. N. Y. Acad. Sci.* 1436, 36–53. doi: 10.1111/nyas.13856

Shlyaeva, A., Buehner, M., Caya, A., Lemieux, J.-F., Smith, G. C., Roy, F., et al. (2016). Towards ensemble data assimilation for the environment canada regional ice prediction system. *Q. J. R. Meteorological Soc.* 142, 1090–1099. doi: 10.1002/qj.2712

Smith, G. C., Liu, Y., Benkiran, M., Chikhar, K., Surcel Colan, D., Gauthier, A.-A., et al. (2021). The regional ice ocean prediction system v2: a pan-Canadian ocean analysis system using an online tidal harmonic analysis. *Geoscientific Model. Dev.* 14, 1445–1467. doi: 10.5194/gmd-14-1445-2021

Snyder, J. (2007). "Tourism in the polar regions," in *The sustainability challenge* (United Nations Environment Programme).

Squire, V. A. (2007). Of ocean waves and sea-ice revisited. *Cold Regions Sci. Technol.* 49, 110–133. doi: 10.1016/j.coldregions.2007.04.007

Squire, V. A., Dugan, J. P., Wadhams, P., Rottier, P. J., and Liu, A. K. (1995). Of ocean waves and sea ice. *Annu. Rev. Fluid Mechanics* 27, 115–168. doi: 10.1146/annurev.fl.27.010195.000555

Turner, A. K., and Hunke, E. C. (2015). Impacts of a mushy-layer thermodynamic approach in global sea-ice simulations using the cice sea-ice model. *J. Geophysical Research: Oceans* 120, 1253–1275. doi: 10.1002/2014JC010358

Underhill, V., and Fetterer, F. (2012). *Arctic Sea Ice charts from Danish meteorological institute 1893–1956, version 1*. doi: 10.7265/N56D5QXC

Zampieri, L., Arduini, G., Holland, M., Keeley, S., Mogensen, K. S., and Tietsche, S. (2022). A machine learning correction model of the clear-sky bias over the arctic sea ice in atmospheric reanalyses. *Earth Space Sci. Open Arch.* 33. doi: 10.1002/essoar.10511269.1

frontiers | Frontiers in Marine Science

TYPE Original Research
PUBLISHED 09 May 2023
DOI 10.3389/fmars.2023.1148899

OPEN ACCESS

EDITED BY
Pierre Yves Le Traon,
Mercator Ocean, France

REVIEWED BY
Laurent Bertino,
Nansen Environmental and Remote Sensing Center, Norway
Gilles Garric,
Mercator Ocean, France

*CORRESPONDENCE
François Massonnet
francois.massonnet@uclouvain.be

RECEIVED 20 January 2023
ACCEPTED 17 April 2023
PUBLISHED 09 May 2023

CITATION
Massonnet F, Barreira S, Barthélemy A, Bilbao R, Blanchard-Wrigglesworth E, Blockley E, Bromwich DH, Bushuk M, Dong X, Goessling HF, Hobbs W, Iovino D, Lee W-S, Li C, Meier WN, Merryfield WJ, Moreno-Chamarro E, Morioka Y, Li X, Niraula B, Petty A, Sanna A, Scilingo M, Shu Q, Sigmond M, Sun N, Tietsche S, Wu X, Yang Q and Yuan X (2023) SIPN South: six years of coordinated seasonal Antarctic sea ice predictions. *Front. Mar. Sci.* 10:1148899. doi: 10.3389/fmars.2023.1148899

SIPN South: six years of coordinated seasonal Antarctic sea ice predictions

François Massonnet[1*], Sandra Barreira[2], Antoine Barthélemy[1], Roberto Bilbao[3], Edward Blanchard-Wrigglesworth[4], Ed Blockley[5], David H. Bromwich[6], Mitchell Bushuk[7], Xiaoran Dong[8], Helge F. Goessling[9], Will Hobbs[10], Doroteaciro Iovino[11], Woo-Sung Lee[12], Cuihua Li[13], Walter N. Meier[14], William J. Merryfield[12], Eduardo Moreno-Chamarro[3], Yushi Morioka[7,15,16], Xuewei Li[8], Bimochan Niraula[9], Alek Petty[17], Antonella Sanna[18], Mariana Scilingo[2], Qi Shu[19], Michael Sigmond[12], Nico Sun[11], Steffen Tietsche[20], Xingren Wu[21], Qinghua Yang[8] and Xiaojun Yuan[13]

[1]Earth and Climate Centre, Earth and Life Institute (ELI), Université catholique de Louvain, Louvain-la-Neuve, Belgium, [2]Departamento Meteorologia, Servicio de Hidrografia Naval (SHN), Buenos Aires, Argentina, [3]Earth Sciences Department, Barcelona Supercomputing Center (BSC), Barcelona, Spain, [4]Department of Atmospheric Sciences, University of Washington, Seattle, WA, United States, [5]Oceans and Cryosphere, Met Office Hadley Centre, Exeter, United Kingdom, [6]Byrd Polar and Climate Research Center, Ohio State University, Columbus, OH, United States, [7]Geophysical Fluid Dynamics Laboratory, National Oceanic and Atmospheric Administration, Princeton, NJ, United States, [8]School of Atmospheric Sciences, Sun Yat-sen University, Southern Marine Science and Engineering Guangdong Laboratory, Zhuhai, China, [9]Alfred Wegener Institute, Helmholtz Center for Polar and Marine Research, Bremerhaven, Germany, [10]Australian Antarctic Program Partnership, Institute for Marine and Antarctic Studies, University of Tasmania, Hobart, TAS, Australia, [11]Ocean Modeling and Data Assimilation Division, Fondazione Centro Euro-Mediterraneo sui Cambiamenti Climatici - CMCC, Bologna, Italy, [12]Canadian Centre for Climate Modelling and Analysis, Environment and Climate Change Canada, Victoria, BC, Canada, [13]Lamont-Doherty Earth Observatory, Columbia University, Palisades, NY, United States, [14]National Snow and Ice Data Center, Cooperative Institute for Research in Environmental Sciences, University of Colorado, Boulder, CO, United States, [15]Application Laboratory, Research Institute for Value-Added-Information Generation (VAiG), Japan Agency for Marine-Earth Science and Technology (JAMSTEC), Yokohama, Kanagawa, Japan, [16]Atmospheric and Oceanic Sciences Program, Princeton University, Princeton, NJ, United States, [17]Earth System Science Interdisciplinary Center, University of Maryland, College Park, MD, United States, [18]Climate Simulations and Predictions Division, Fondazione Centro Euro-Mediterraneo sui Cambiamenti Climatici - CMCC, Bologna, Italy, [19]First Institute of Oceanography, Key Laboratory of Marine Science and Numerical Modeling, Ministry of Natural Resources, Qingdao, China, [20]Department of Research, European Centre for Medium-Range Weather Forecasts (ECMWF), Bonn, Germany, [21]Axiom at Environmental Modeling Center, National Centers for Environmental Prediction, National Oceanic and Atmospheric Administration, College Park, MD, United States

Antarctic sea ice prediction has garnered increasing attention in recent years, particularly in the context of the recent record lows of February 2022 and 2023. As Antarctica becomes a climate change hotspot, as polar tourism booms, and as scientific expeditions continue to explore this remote continent, the capacity to anticipate sea ice conditions weeks to months in advance is in increasing demand. Spurred by recent studies that uncovered physical mechanisms of Antarctic sea ice predictability and by the intriguing large variations of the

observed sea ice extent in recent years, the Sea Ice Prediction Network South (SIPN South) project was initiated in 2017, building upon the Arctic Sea Ice Prediction Network. The SIPN South project annually coordinates spring-to-summer predictions of Antarctic sea ice conditions, to allow robust evaluation and intercomparison, and to guide future development in polar prediction systems. In this paper, we present and discuss the initial SIPN South results collected over six summer seasons (December-February 2017-2018 to 2022-2023). We use data from 22 unique contributors spanning five continents that have together delivered more than 3000 individual forecasts of sea ice area and concentration. The SIPN South median forecast of the circumpolar sea ice area captures the sign of the recent negative anomalies, and the verifying observations are systematically included in the 10-90% range of the forecast distribution. These statements also hold at the regional level except in the Ross Sea where the systematic biases and the ensemble spread are the largest. A notable finding is that the group forecast, constructed by aggregating the data provided by each contributor, outperforms most of the individual forecasts, both at the circumpolar and regional levels. This indicates the value of combining predictions to average out model-specific errors. Finally, we find that dynamical model predictions (i.e., based on process-based general circulation models) generally perform worse than statistical model predictions (i.e., data-driven empirical models including machine learning) in representing the regional variability of sea ice concentration in summer. SIPN South is a collaborative community project that is hosted on a shared public repository. The forecast and verification data used in SIPN South are publicly available in near-real time for further use by the polar research community, and eventually, policymakers.

KEYWORDS

sea ice, seasonal prediction, Southern Ocean, Antarctica, forecasting & simulation

1 Introduction

Antarctic sea ice rarely fails to spur our curiosity. By the mid-2000s, sea ice extent anomalies (Figure 1) had exhibited no substantial change despite the global warming context. By contrast, in the Northern Hemisphere, significant reductions in Arctic sea ice extent were already evident year-round (Cavalieri et al., 2003). From 1979 to the mid-2010s, there was a positive trend in Antarctic sea ice extent, leading to a series of hypotheses that could explain such unexpected behavior (see, e.g., Hobbs et al. (2016) for a review). However, in spring-summer 2016-2017, the sign of sea ice anomalies drastically switched from positive to negative, canceling the gradual accumulation that had prevailed since the late 1970s (Parkinson, 2019). Sea ice extent conditions have remained low since then for all months of the year, with an absolute record low set in February 2022 and then in February 2023 (Raphael & Handcock, 2022; Wang et al., 2022; Liu et al., 2023). The interpretation of the summer 2022 and 2023 records is not obvious, given the strong positive phase of the Southern Annular Mode in summer 2021-2022, a mode that is normally associated with positive sea ice extent anomalies (Verfaillie et al., 2022; their Figure S2). Several ocean and atmospheric mechanisms have been hypothesized to explain the 2016-2017 chain of events (Stuecker et al., 2017; Schlosser et al., 2018; Meehl et al., 2019; Purich and England, 2019; Zhang et al., 2022). It is speculated that the recent decline of Antarctic sea ice extent could foreshadow more profound changes in the Southern Ocean system (Eayrs et al., 2021).

Sea ice is a key variable of the high-latitude Southern Hemisphere. While the Southern Ocean is known as a major carbon sink for the atmosphere, having accounted for up to 40% of the uptake of cumulative anthropogenic carbon emissions (DeVries, 2014), sea ice processes can act both as a source or a sink of atmospheric carbon depending on the season (Delille et al., 2014; Gray et al., 2018). Sea ice growth (melt) is associated with salt (freshwater) fluxes to the upper ocean that directly control its stratification on seasonal to decadal timescales (Martinson, 1990; Goosse and Zunz, 2014; Goosse et al., 2018). Sea ice also dampens horizontal ocean transport processes such as storm-generated waves (Kohout et al., 2014). Recent sea ice loss around the Antarctic Peninsula, for example, has been identified as a possible cause of ice shelf disintegration through enhanced ocean swells (Massom et al., 2018). Finally, sea ice mitigates heat transfers between the ocean and the atmosphere and, as such, plays a key role in the energy balance in polar regions. The year-to-year

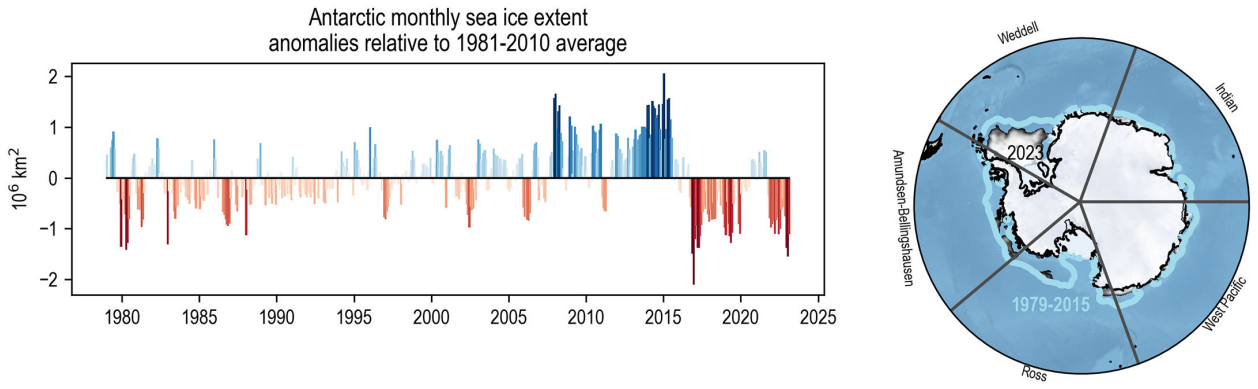

FIGURE 1
(Left) Antarctic monthly mean sea ice extent anomalies relative to the 1981-2010 mean seasonal cycle, from January 1979 to December 2022 (OSI-SAF sea ice index OSI-420; Lavergne et al., 2019). (Right) The 1979-2015 February climatological sea ice edge, defined as the 15% sea ice concentration contour of the average sea ice concentration field (light blue line), and the February mean 2023 sea ice conditions (white shading). The names of the regions introduced in Section 2.5 are given on this map.

fluctuations of sea ice at the regional and circumpolar levels might thus have consequences on a longer term and on a global scale. In view of this, the recent sequence of negative anomalies (Figure 1), and our ability to predict these anomalies ahead of time, should be given increased attention.

The interest for sea ice is not limited to the physical environments. Sea ice hosts a stock of bacteria, algae, and grazers which, upon melting, are released in the upper ocean and impact the biological activity including phytoplankton blooms (Brierley and Thomas, 2002). The variations in Antarctic sea ice extent significantly affect marine productivity and fisheries (Liu et al., 2022). Besides, sea ice conditions represent a real risk for all vessels operating in high-latitude marine areas (COMNAP, 2015). This is especially true for commercial operations - most notably fisheries (e.g. krill) and tourism - which tend to use ice-strengthened vessels rather than icebreakers. As the number and variety of tourist activities increase in the high-latitude Southern Ocean (Tejedo et al., 2022), considering sea ice related hazards, even in the middle of austral summer, has become a priority. For all these applications (and many more not mentioned here), a short-term notice (say, a few weeks to months) of the anomalous character of sea ice conditions in a given region would likely represent significant added value over the currently used information that consists of climatological forecasts or interpretation of real-time ice charts. Such information could be valuable as the system appears to be in a non-stationary state where climatology is, by definition, not meaningful.

The feasibility of skillful seasonal sea ice predictions rests on predictability mechanisms operating at sub-seasonal to seasonal time scales. In contrast to historical Arctic sea ice, Antarctic sea ice is almost entirely seasonal and is thinner on average, suggesting possibly different mechanisms. The first estimates of initial-value predictability (i.e., predictability associated with initial conditions or 'of the first kind') of Antarctic sea ice are credited to Holland et al. (2013). They investigated the characteristics of an ensemble of sea ice trajectories of the Community Climate System Model version 3 (CCSM3), each initialized on January 1st from the model's own state but subject to small perturbations at the initial time. They identified an eastward traveling signal of predictability of the Antarctic sea ice edge position with an associated timescale of 3-9 months depending on the region considered. They also noticed a temporary loss of predictability during the ice retreat season followed by an increase in predictability in the second year during the ice advance season. This phenomenon of 're-emergence' of predictability was confirmed in other model setups (Marchi et al., 2019): significant correlations between sea surface temperature (SST) anomalies in two successive winter seasons were diagnosed in a six-model ensemble despite the absence of correlation during summer. The re-emergence phenomenon is explained by the storage of surface information below the ocean mixed layer in the spring and summer seasons and the fact that these anomalies resurface when the mixed layer deepens in autumn and winter. A key finding of the Marchi et al. study is that the predictability horizon appears to be mean-state dependent: climate models with deeper oceanic mixed layers tend to exhibit longer predictability. In an Arctic-Antarctic intercomparison, Ordoñez et al. (2018) showed that Antarctic sea ice area predictability is less influenced by the initial sea ice volume anomalies than in the Arctic. Sea ice predictability is inherently tied to the vertical structure of the properties of the underlying ocean (Libera et al., 2022), which can explain why different estimates of predictability have been obtained with different general circulation models but also why these estimates may vary from one region to another.

In parallel to idealized predictability studies that employ model output without reference to the observed sea ice state, several studies have attempted to determine predictability content using observational and reanalysis datasets or using retrospective predictions (hindcasts). Chen and Yuan (2004) developed the first seasonal forecast for Antarctic sea ice concentration with a statistical model using a reanalysis of atmospheric variables and satellite-observed sea ice data. This linear Markov model showed considerable skill in predicting the anomalous sea ice concentration up to one year in advance in the western Antarctic, and especially high skill in austral winter. Chevallier et al. (2019) estimated that

Antarctic sea ice extent anomalies have a typical decorrelation time scale of up to two months in all seasons, except in austral spring (October to December) where it can drop to 3 weeks. Using reanalyses and satellite products, Holland et al. (2017) identified a 5-month relationship between springtime (October) zonal wind anomalies in the Amundsen-Bellingshausen Seas and the March sea ice area in the western Ross Sea: stronger westerlies in spring increase sea ice divergence, favor shortwave absorption and heat storage in the upper ocean and delay autumn sea ice advance. Such a coupled mechanism was, however, not found in state-of-the-art climate models (Holland et al., 2017). Recently, Morioka et al. (2019; 2021) reported skillful prediction of summertime sea ice conditions in the Weddell Sea owing to the initialization of winter sea ice concentration and thickness, pointing to the potentially increased contribution of thickness/volume anomalies to predictability at regional scales. Using a suite of coupled dynamical models, Bushuk et al. (2021) found that predictions of wintertime sea ice edge position are improved when taking into account the zonal advection of upper-ocean heat content anomalies. They also found that the initialization of sea ice concentration and thickness played a key role in summer prediction skill. The Weddell Sea was found to be a hotspot for summertime prediction (up to 9 months out) and less skill was found in the Ross Sea. Payne et al. (2022) also found the largest forecast skill in the Weddell Sea, with moderate skill in the Ross, Amundsen and Bellinghausen Seas, and lowest skill in the Indian and West Pacific sectors. They also found an important role of initial sea ice thickness for August to December predictions. Finally, Zampieri et al. (2019) found that current subseasonal to seasonal (S2S) prediction systems, not specifically geared towards polar prediction, display skill that rarely beats trivial forecasts beyond a few weeks. A key aspect of the Zampieri et al. (2019) study is that they apply a stringent skill metric that penalizes the spatial discrepancies between forecast and observed sea ice edges.

In summary, only a few studies have examined seasonal Antarctic sea ice predictability, and it can be summarized that: (1) predictability estimates vary regionally and seasonally; (2) the upper ocean is key to carrying sea ice predictability over seasons and regions; (3) ocean stratification and the vertical structure of its properties affects estimates of predictability in climate models; (4) predictability and skill are likely conditionally dependent on the baseline mean state; and (5) in model experiments, skill is generally high in the Weddell Sea and varies from one study to another in the Ross Sea. We note that the Weddell Sea is the sector of the Southern Ocean with the largest summer sea ice extent on climatological average. This sector, unlike the others, hosts at least 1 million km^2 of sea ice every summer, approximately 50% of the circumpolar total (Parkinson, 2019).

The satellite record of observed sea ice extent anomalies (Figure 1) suggests that, since the mid-2000s, Antarctic sea ice could have entered a new regime characterized by increased variance, increased persistence, and lower frequency. From the angle of predictability, the current epoch could well be a 'window of opportunity' in which longer-lived sea ice anomalies push the horizon of predictability well beyond the levels that had been prevailing before. Indeed, Payne et al. (2022) showed that hindcast skill increased substantially when the hindcasts include the 2010s.

In that context, the objective of SIPN South is to quantify the skill of the available sea ice prediction systems with a focus on the recent summers. Specifically, we aim to provide an initial answer to three scientific questions:

1. Does the SIPN South ensemble exhibit systematic forecast errors?
2. Do SIPN South forecasts provide added value over a climatological forecast?
3. Is there a relationship between the forecasting approach and skill?

We discuss in Section 2 the SIPN South protocol and the different forecasting approaches taken by the contributors. In Section 3, we attempt to answer the three questions raised above by analyzing the forecasts made from 2017 until 2023. We finish by discussing the limitations of the study and avenues for future work.

2 Methods

We describe the historical context of the SIPN South project and the generic protocol for contributions. Then, we briefly review the different approaches followed by the SIPN South contributors. Finally, we review the products and methods used for forecast verification.

2.1 SIPN South background

SIPN South was initially designed to be a 3-yr (2017-2019) activity taking place within the Southern Hemisphere component of the Year of Polar Prediction (YOPP-SH) project (Jung et al., 2016; Bromwich et al., 2020). SIPN South was created for the scientific reasons described in the introduction, but also to initiate a parallel effort to the (Arctic) Sea Ice Prediction Network (Steele et al., 2021). The project was extended beyond the initial period and now runs every year. SIPN South has briefly been described in Abrahamsen et al. (2020) and Bromwich et al. (2020), and in technical reports published after each forecasting season, all available on the project website (see "Data and code availability" section below).

Around mid-November each year, a call for contributions is issued on various mailing lists related to polar research, and on social media. The call itself contains the protocols to be followed, which we now briefly summarize. The forecasts cannot use data beyond the 1st of December and must be submitted within the first 10 days of December. The forecasts must cover the period 1st December to 28th February (90 days). The method of forecasting is free but must be documented. Up to four diagnostics can be submitted, by order of descending priority and for each of the 90 days of the forecasting period. These diagnostics are: (i) the integrated Antarctic sea ice area, (ii) the sea ice area in each successive 10° longitude band starting from 0°, (iii), the sea ice concentration (provided on the contributor's native grid), and (iv) the effective sea ice thickness, i.e. sea ice volume per unit grid cell area, also provided on the contributor's native grid. SIPN South allows the submission of ensembles of forecasts to reflect aspects of uncertainty in

the experimental setup. Finally, the call document specifies the two observational products that will be used as references for verification, (see "Observational references" section below).

There are several differences between the protocol followed in the SIPN South protocol and that followed in the (Arctic) sea ice outlooks (SIO) that have been conducted by the Sea Ice Prediction Network (Hamilton and Stroeve, 2016; Steele et al., 2021; https://www.arcus.org/sipn/sea-ice-outlook) since 2008. One difference is the systematic request for daily data in SIPN South (versus monthly in general for the SIO, up to a few exceptions). Having the daily temporal resolution is key to diagnosing the biases that develop at the sub-seasonal time scale, see Section 3.1. Another difference is that SIPN South only issues one call per summer while the Arctic SIO issues four (June, July, August, and September), which allows studying the influence of lead time on the skill. Finally, SIPN South requests explicit probability distributions estimates through individual ensemble members, while the SIO requests aggregated statistics (median and range). Several co-authors of this study are also involved in the SIO and ensure frequent exchanges on best practices in the respective communities.

The year-to-year evolution of the contribution statistics is shown in Figure 2. The latest forecasting exercise documented in this manuscript (2022-2023) has seen a record number of contributions but a slight decrease in the number of files contributed compared to the previous season, due to one group usually contributing more than 50 ensemble members for all diagnostics not being able to submit forecasts for this latest exercise.

In order to avoid over-interpretation of the results there are four caveats to the structure of SIPN South that need to be acknowledged before any comparison to observations is performed. First, only six years are available, which is very limiting when meaningful statistics need to be drawn. With so few data points, systematic inconsistencies between forecasts and verification datasets can be difficult to detect. Second, an agreement between forecasts and verification data is not a guarantee that the skill is obtained for good reasons. Besides the issue of limited statistical sampling, the SIPN South ensemble can be viewed as an 'ensemble of opportunity', i.e., a set of forecasts obtained after asking for output from anyone who is willing to contribute (Tebaldi and Knutti, 2007). The implication is that the range of forecasts contributed to SIPN South is not necessarily representative of the full range of uncertainty for all prediction systems that exist. The results presented here might be updated when more groups contribute to the effort. Third, because forecasting systems are constantly improving and evolving (e.g., physical models, data assimilation methods, observations used, ensemble perturbation methods), contributions labeled identically might correspond to slightly different underlying methods. Finally, no constraint was imposed regarding important aspects that make up prediction systems such as the dataset used for initialization or to train statistical models, the method of ensemble perturbation or uncertainty estimation, the values of specific parameters, or the application of bias correction step. The reason is that SIPN South aims to intercompare prediction systems each with its own design choices. This approach is similar to what has been done in the Arctic SIO (Blanchard-Wrigglesworth et al., 2015; Hamilton and Stroeve, 2016; Blanchard-Wrigglesworth et al., 2023).

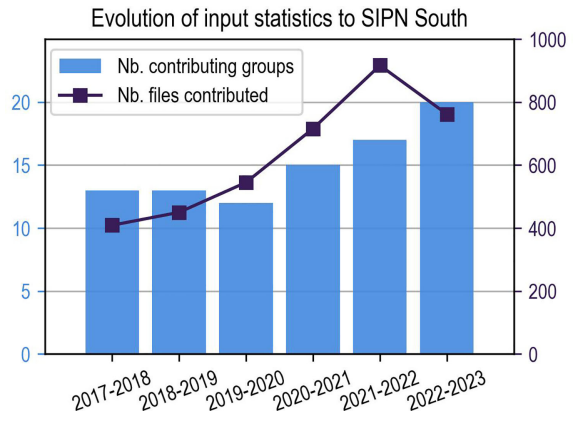

FIGURE 2
The number of individuals or groups that contributed forecasts to the SIPN South project for each of the austral summers since the beginning of the project (bars, left y-axis) and the total number of files contributed by all groups over the same period (line with squares, right y-axis).

2.2 Description of the forecasting systems

Since the approach to forecast is at the discretion of each contributing group, unsurprisingly there is a large variety in the types of forecasting systems used. Other initiatives to collect real-time seasonal predictions like the Seasonal Hurricane Prediction project (https://seasonalhurricanepredictions.bsc.es) and the Arctic Sea Ice Outlook introduced above also face a high diversity in forecasting approaches. For these two projects, forecasts have been categorized as either 'dynamical' or 'statistical' approaches (Caron et al., 2020; Steele et al., 2021). Dynamical approaches gather predictions made using process-based models, i.e., models based on first physical principles, that are initialized from observationally constrained initial states. These dynamical approaches include general circulation models (GCMs), either only for the ocean (including sea ice) or also coupled to an atmospheric model. By contrast, statistical approaches gather predictions made using data-based models, i.e., exploiting statistical predictor-predictand relationships in past data. This characterization onto dynamical and statistical models could be criticized, since in practice dynamical model predictions are often corrected a posteriori with statistical methods, and statistical forecasts often draw from climate model output or reanalyses to build empirical relationships. A description of the approach followed by SIPN South contributors is given in Table 1. For simplicity, we have assigned a group to 'dynamical' approach if it uses a GCM as the foundation of their prediction system, and to 'statistical' approach otherwise.

A group forecast is finally included in the analyses. The group forecast is constructed as an ensemble forecast of size n with n the number of contributors that provided data for a given year. For contributors providing ensemble members, these ensemble members are first averaged together.

TABLE 1 List of contributors to the SIPN South austral summer forecasts over the six seasons 2017-2018 to 2022-2023 and description of the method.

Long (+ short) name, country, approach type	Brief method description
AWI-SDAP, Germany, Statistical	The forecast consists in a gridded probability of sea ice presence (presence defined as sea ice concentration (SIC) >15%) based on Spatial Damped Anomaly Persistence (SDAP) using observed OSI-SAF (Lavergne et al., 2019) SIC of the previous ten years. A distinctive feature of the SDAP method is that it does not operate on individual grid cells. Instead, initial-state anomalies of the ice-edge are spatially "inherited" from the initial ice-edge location to the surroundings, gradually relaxing from the binary initial state towards the climatological probability of sea-ice presence while accounting for the seasonal migration of the climatological ice-edge location distribution, as detailed in Niraula and Goessling (2021). This contribution could not be used for diagnostics involving sea ice areas because it is not possible to derive sea ice area from the probability of ice presence; see more comments in the discussion. No bias-correction is applied.
Sandra Barreira et al. (barreira), Argentina, Statistical	The model is a three-level (two-level for the earlier version) neural network based on a principal component analysis (PCA). The first level has 17 neurons (i.e., principal components) and the second has 2204 neurons (each PCA separated in 12 different months). The third level has 18336 neurons but only 1344 had enough data until now to be trained. Each neuron was trained with a backward-forward learning technique: the neurons learn how a month has a determined PCA pattern according to what had happened the months before the occurrence of this pattern (the backward process); and the neurons also learn what will happen after a given pattern over the next three months (the forward process). After this supervised learning, the forecast system continues the training automatically (the automatic learning). No bias-correction is applied. The initial data are obtained from the NSIDC every month (monthly and daily data). The results of the operative version of the model are published every month at the SHN webpage: http://www.hidro.gov.ar/smara/SB/sb.asp
Barcelona Supercomputing Center (BSC), Spain, Dynamical	The forecast is taken from the BSC Decadal Prediction System based on the EC-Earth3 Earth System Model in its standard resolution. The atmospheric component is the IFS (from the ECMWF) with a T255 horizontal resolution (approximately 80 km) and 91 vertical levels, and the ocean component is NEMO3.6 and the LIM3 sea ice model, both run with an ORCA1 configuration (1° horizontal nominal resolution) and 75 vertical levels. The forecast system consists of a 10-member ensemble of 10-year-long predictions initialized every year in November from 1960 to present. The components have been initialized using full-field initialization: the atmospheric initial conditions are from the ERA5 reanalysis and the oceanic initial conditions come from a NEMO3.6-LIM3 simulation forced with historical ERA5 surface fluxes that assimilates ORA-S5 ocean temperature and salinity at the surface and EN4 temperature and salinity below the surface. The procedure is very similar to the one described in Bilbao et al. (2021) but with different observational products. The daily Antarctic values were produced by quadratically interpolating the monthly values. No bias correction was applied to the forecasts.
Environment and Climate Change Canada (CanSIPSv2 and Modified-CanSIPS), Canada, Dynamical	Three distinct contributions have been submitted to SIPN South. Modified-CanSIPS provided forecasts for 2017-2018, 2018-2019 and 2019-2020 based on two fully coupled models, CanCM3 and CanCM4, described in Merryfield et al. (2013). The atmospheric component of CanCM3 is CanAM3 with T63 horizontal resolution and 31 levels, and that for CanCM4 is CanAM4, also T63, with 35 levels. Sea ice is represented on the atmospheric grid for both models, and both employ the CanOM4 ocean component with 1.41°/0.94°resolution in longitude/latitude and 40 vertical levels. Initial conditions for the atmosphere, sea ice concentration and ocean temperature are drawn from ECCC's operational analyses, whereas sea ice thickness is initialized using the SMv3 statistical model described in Dirkson et al. (2017). CanSIPSv2, which provided forecasts for 2020-2021 and 2021-2022, is also based on two fully coupled models, CanCM4i and GEM-NEMO, described in Lin et al. (2020). CanCM4i employs the same model and initialization as CanCM4 in Modified-CanSIPS, whereas GEM-NEMO is based on the GEM atmospheric model with 1.41° resolution and 79 vertical levels, and the NEMO version 3.1 ocean model with nominal 1° resolution and 50 vertical levels. GEM-NEMO atmosphere, ocean and sea ice initial conditions are drawn from ECCC's operational analyses. Forecasts from all of these models employed 10 ensemble members for each model, and were initialized on 30th of November. Daily values for integrated Antarctic sea ice area and the sea ice area in 10° longitude bands until 28th of February are bias corrected by adding daily anomalies calculated for each ensemble member to the NSIDC Climate Data record observed 1981-2010 daily climatology. For 2022-23, CanSIPSv2.1 was used, which differs from CanSIPSv2 in that GEM-NEMO has been updated to GEM5-NEMO.
Centro Euro-Mediterraneo sui Cambiamenti Climatici (cmcc), Italy, Dynamical	CMCC-SPS3.5 is a fully coupled seasonal forecasting system, based on the CMCC-CM2 coupled climate model (Cherchi et al., 2019). CMCC-SPS3.5 consists of CAM (atmosphere), CLM (land), NEMO (ocean), and CICE (sea ice) sub-components, coupled using the cpl7/mct coupler. CMCC-SPS3.5 forecasts cover a 185-day forecast period, with an ensemble size of 50 members. The system is initialized using ten atmospheric EDA analyses, three land-analyses (CLM stand-alone forced runs) and nine 3D-var ocean analyses. The 50 initial conditions are randomly chosen among the 270 available uniquely defined. Sea ice concentration and thickness are assimilated through a nudging scheme. No bias correction is used.
Centre National de Recherches Météorologiques (CNRM), France, Dynamical	The forecast is based on Météo-France seasonal forecasting system 8, which is based on a high-resolution version of the CNRM-CM GCM (Voldoire et al., 2019). The model uses the ARPEGE-Climat atmospheric model, the SURFEX surface component, the NEMO ocean component, and the GELATO sea ice component that are coupled through the OASIS coupler. A full description of the model and the system is described in a technical documentation available here: http://www.umr-cnrm.fr/IMG/pdf/system8-technical.pdf. A summary of System 8 characteristics can be found on the C3S Confluence website: https://confluence.ecmwf.int/display/CKB/Description+of+System8-v20210101+C3S+contribution. Sea ice concentration is corrected using a simple per-pair bias correction method using the 1993-2016 re-forecast period and NSIDC data https://nsidc.org/data/G02202/versions/3. Bias correction was applied for the 2020-2021 season but not for other seasons, as the bias correction appeared to have undesirable effects due to the non-stationarity of the observed mean state over the past years.
European Centre for Medium-Range Weather Forecasts SEAS5 (ecmwf), Europe, Dynamical	The forecast is based on the ECMWF seasonal forecasting system SEAS5 as described in Johnson et al. (2019). The atmospheric component of SEAS5 is the IFS model cycle 43R1 on a cubic octahedral T319 grid (ca. 36 km horizontal resolution) and 91 vertical levels. The ocean component is NEMO3.4 with LIM2 as a sea-ice model, using the ORCA025 grid (ca. 25 km spatial resolution) with 75 vertical levels. The forecast is an ensemble of 51 members. Initial conditions for the atmosphere come from the ECMWF ensemble of data assimilations (EDA) augmented with singular vectors, and initial conditions for the ocean come from the 5-member ECMWF ocean reanalysis/analysis system OCEAN5. Model uncertainty is represented by applying stochastic perturbations to the physical tendencies (SPPT) in the atmosphere. No bias correction has been applied to the daily sea-ice concentration fields prior to computing regional and pan-Antarctic sea ice extent.

(Continued)

TABLE 1 Continued

Long (+ short) name, country, approach type	Brief method description
National Centers for Environmental Predic–ion - CFSv2 (emc), USA, Dynamical	The forecast is based on CFSv2, a fully coupled sub-seasonal to seasonal forecast system which was implemented for operation in April 2011 (Saha et al., 2014). CFSv2 consists of the component models of the NCEP GFS atmosphere with a T126 horizontal resolution (approximately 100 km) and 64 vertical levels, NOAH land (the same model grid as the atmospheric model), GFDL MOM4 ocean model and sea ice simulator (with slight modifications). The ocean model uses tripolar grids, northward of 65°N it uses a rotated bipolar grid that places two poles over land, thus eliminating the singularity in the northern ocean, while southward of 65°N it uses a regular latitude × longitude grid. The horizontal layout is a staggered Arakawa B grid. The zonal resolutio½s 1/2°, the meridional resolutio¼s 1/4° between 10°S and 10°N, gradually increasin½o 1/2° poleward of 30°S and 30°N. There are 40 layers in the vertical. The sea ice grid is the same as the ocean. CFSv2 is run daily with 16 ensemble ensembles for 45 days, 7 ensemble members for 3 months and 4 members for 9 months, with 6-hourly output. No bias correction is applied to the forecast.
First Institute of Oceanography Earth System Model (FIO-ESM), China, Dynamical	Satellite-derived daily sea surface temperature and sea level anomaly are assimilated into the fully-coupled model FIO-ESM using an Ensemble adjustment Kalman Filter (Qiao et al., 2013; Chen et al., 2016) to initialize the model. The FIO-ESM is based on the CAM3.0 atmospheric model, on the CLM3.5 land model, on the CICE4 sea ice model and on the POP2.0 ocean model. 10 ensembles were generated by a tiny-perturbing method. Bias correction is used through removing the monthly sea ice area biases.
Antarctic Gateway Partnership (Gateway), Australia, Statistical	The historical seasons (Jun-Oct) with the most similar sea ice area growth rates as the current ones are retained. These seasons are then used these to extrapolate to February next year.
Geophysical Fluid Dynamics Laboratory (gfdl), USA, Dynamical	The forecast is based on the fully-coupled global atmosphere-land-ocean-sea ice model SPEAR_MED (1° ice-ocean resolution, 0.5° atmosphere-land resolution; see Delworth et al. (2020)) that is initialized on December 1 using a weakly coupled ensemble data assimilation system (Lu et al., 2020). 30 ensemble members are integrated for one year. Daily sea ice area predictions are bias corrected using a lead-dependent linear regression adjustment based on a suite of retrospective seasonal predictions (Bushuk et al., 2021). Sea ice concentration predictions are not bias corrected.
Columbia University Sea Ice Group (Lamont), USA, Statistical	The forecast consists of a linear Markov model that predicts Antarctic SIC at the seasonal timescale using monthly atmospheric reanalysis variables and satellite-observed sea ice concentration data. The model was trained in the multivariate space of seven NCEP/NCAR atmospheric variables (SAT, SLP, Uslp, Vslp, 300mb heights and U300, V300) and NASA-Team SIC for the period of 1980 to 2000. The predictions were made by the linear Markov process for several leading MEOF modes. Cross-validated model experiments evaluated the prediction skill (Chen and Yuan, 2004). No bias correction is applied to the forecast. The daily values are obtained by quadratic interpolation of the monthly values provided.
NSIDC Meier (Meier-NSIDC), USA, Statistical	The model extrapolates daily sea ice loss from the initialization date through the end of the season. Daily sea ice loss for the extrapolation is based on the average daily loss from 2007 through the most recent year. Because there is high variability in ice daily ice loss, early season (e.g., 3-month) predictions are not expected to have high skill, but skill increases with shorter forecast times. The method provides a shrinking envelope of the likely range of values and provides a baseline for comparison of more sophisticated methods. The source data are the NSIDC Sea Ice Index (http://nsidc.org/data/seaice_index/). Daily extent values are used here because concentration/area are underestimated by the NASA Team algorithm used in the Sea Ice Index; thus, extent likely provides a better indication of true ice coverage. No bias-correction is applied.
Met Office GloSea (MetOffice), UK, Dynamical	The forecasts are obtained from the fully coupled seasonal forecasting system GloSea based upon the HadGEM3 coupled climate model (MacLachlan et al., 2015). GloSea uses the MetUM (atmosphere) and JULES (land) models at N216 resolution (~60 km in midlatitudes), coupled to the NEMO (ocean) and CICE (sea ice) models (~1/4° resolution) coupled using OASIS. GloSea forecasts are run daily out to 210 days and initialized using Met Office operational analyses (mixed 4DVar and 3DVar). Sea ice concentration is assimilated but not yet sea ice thickness. GloSea uses a lagged ensemble approach where 2 ensemble members are run each day and combined with members from previous days to create a 42-member ensemble. No bias correction is used.
MPAS CESM (mpas-cesm), USA, Dynamical	The CESM-CAM-MPAS v1.4.b7 is run as a fully-coupled atmosphere-land-ocean-sea ice model with MPAS as the atmospheric dynamical core on a quasi-uniform 60km grid and the rest of the components ~1 degree grid spacing. Forecasts are initialized on ^{De}c 1st using GFS analysis for the atmosphere and analog restarts from the CESM Large Ensemble for the other components.
NASA GMAO (nasa-gmao), USA, Dynamical	The NASA GMAO seasonal forecasts are produced with the Goddard Earth Observing System (GEOS) AOGCM (GEOS-S2S_2.1) (Rienecker, 2008; Molod et al., 2015). The atmospheric component is a recent version of the GEOS atmospheric model, run at 0.5°horizontal resolution with 72 vertical layers. This version includes two-moment cloud microphysics and an interactive aerosol chemistry model. The ocean component is version 5 of the GFDL Modular Ocean Model (MOM5) (Griffies, 2012) implemented here at a horizontal resolution of 0.5 degree with 40 vertical layers. The land component is the Catchment Land Surface Model (Koster et al., 2000). Sea ice is represented with the Los Alamos Sea Ice model (CICE4) (Hunke and Lipscomb, 2010). The system is initialized using MERRA-2 atmospheric reanalysis (Gelaro et al., 2017) and the GMAO Interim Ocean Analysis. The analysis incorporates sub-surface temperature and salinity data from available CTDs and Argo floats, temperature data from XBTs and moored arrays, and along-track altimetry. The analysis is nudged to the Operational Sea Surface Temperature and Sea Ice Analysis (OSTIA, Donlon et al. (2012)) sea surface temperatures, and uses the EUMETSAT OSI-SAF sea ice concentration provided with OSTIA. Ensemble members are produced with initializations on 12-Nov, 17-Nov, 22-Nov, and 27-Nov. An additional 6 ensemble members are initialized on 27-Nov using ocean and/or atmosphere analysis perturbations.

(Continued)

TABLE 1 Continued

Long (+ short) name, country, approach type	Brief method description
NASA-GSFC, USA, Statistical	The forecast is obtained from a statistical model that uses monthly sea ice concentration (SIC) data (1979-present day), derived from passive microwave brightness temperatures using the NASA Team algorithm. The historical SIC data for the given forecast month are detrended in-time for each grid-cell using linear regression as is the historical sea ice extent (SIE) for the month being forecast. A least-squares linear regression model is fit from the detrended SIE data and the mean detrended SIC data (weighted by the correlation coefficient to focus on regions of higher predictability). The monthly mean/detrended SIC data from the given forecast year are applied to the linear regression model to produce a seasonal forecast. The approach is the same as in the seasonal Arctic forecasts of Petty et al. (2017). To produce the daily Antarctic forecasts, multiple months are forecast and a quadratic curve is fit to interpolate the monthly values to daily.
Nico Sun (NicoSun), Europe, Statistical	The forecast model is based on sea ice persistence. It uses incoming solar radiation and sea ice albedo derived from a predicted Sea Ice Concentration (SIC) value to calculate daily thickness losses for every NSIDC 25km grid cell. The initial thickness is calculated from GIOMAS sea ice volume and NSIDC SIC data. The mean forecast uses the mean SIC over the previous 10 years (1/3 weight) and mean SIC change per day (2/3 weight) to predict future SIC. The low forecast reduces the predicted SIC by 0.25 standard deviation for previously observed SIC for this day. The high forecast increases the predicted SIC by 0.33 standard deviations.
SINTEX-F2, Japan, Dynamical	The forecast is based on the fully coupled seasonal prediction system based on ECHAM5 (~1 deg, 31 levels) atmospheric model and NEMO3 (0.5 deg, 31 levels) ocean-sea ice model (Doi et al., 2016). SINTEX-F2 seasonal prediction system used in this study was run monthly on Earth Simulator with SST and sea ice concentration (SIC) initializations, in which the model's SST and SIC are nudged to the OISSTv2 dataset. 24 ensemble members with SST (12 members) and SST-SIC (12 members) initializations are analyzed.
Sun-Yat Sen University (SYSU), China, Statistical	Three distinct contributions have been submitted to SIPN South. SML-kNN: A machine learning algorithm (kNN for K-Nearest Neighbors) is used in this prediction. The model was trained using daily Antarctic SIC in a 25 × 25 km grid obtained from the NSIDC for the period of January 1989 to March of the initialization year. The climatological annual cycle of SIC had been subtracted at each grid point prior to the training. To produce the daily Antarctic forecasts, the principle is to find the K nearest neighbors of the input variables from the training library. The prediction is then obtained by point-by-point calculation, and the Euclidean distance was set as distance weighting. No bias correction is applied to the forecast. SML-ConvLSTM: A Convolutional Long Short-Term Memory networks (ConvLSTM)[1] is used in the way of self-supervised learning in this prediction. ConvLSTM combines the (Convolutional Neural Network)CNN which can extract the spatial information, with LSTM, which is a kind of Recurrent Neural Network(RNN) and can extract the time information. In this way, ConvLSTM networks are powerful tools for intricate spatial-temporal sequence prediction problems. The NSIDC-0051/0081 SIC data are used in this experiment. The model tries to extract the spatial-temporal relationship from 15861 samples of 90days-90days sequence, in which the later 90-day is 90-day lag for the former 90-day. After training, we use the 90-day data before 1st December, 2022 as the feature data, and acquire the label data predicted from 1st December, 2022 to 28th February, 2023. We also acquire the long term by the same way, changing the time resolution from daily to monthly, initializing in November, 2022, and changing the length of time series from 90-day to 24-month. Our long-term prediction period is from December, 2022 to December, 2024. Reference: (Shi et al., 2015) SML-MLM: A multivariate linear Markov model is used in this prediction. The model use sea ice concentration, surface air temperature, sea level pressure, surface winds,300-hPa winds and 300-hPa geopotential height as predictors. We use the above parameters from 1989 to 2019 to train our model.
UCLouvain (ucl), Belgium, Dynamical	An ocean-sea ice model (NEMO3.6 ocean model, LIM3 sea ice model, ~1° resolution; Barthélemy et al. (2018)) simulation is forced by atmospheric reanalyses (JRA-55) until the 1st of November. Then, 10 ensemble members are integrated until 28th of February. Each member is using a distinct atmospheric forcing from the 10 previous years. No bias correction is applied to the forecast. The method is similar to that applied to the Arctic Sea Ice Outlook.
University of Washington (UW), United States, Dynamical	The UW forecast is made with the CESM1-CAM5 fully-coupled model at a nominal 1-degree resolution and 30 layers in the vertical in the atmosphere model. We run the model up to Nov 30, 2022, under RCP8.5 forcing and with winds above the boundary layer nudged to observations (ERA-5 reanalysis) poleward of 45 degrees (extending the runs described in Blanchard-Wrigglesworth et al, 2021). The nudged runs capture a significant portion of sea ice and SST variability, and serve to 'initialize' the forecast runs, which are run from November 30, 2022, to Dec 2024 in a 'free-running' mode (without nudging). The SIPN South forecasts are computed by calculating a sea ice area forecast anomaly of the forecast runs with respect to CESM1-Large Ensemble, and then the forecast anomaly is applied to the observed climatology of sea ice area.

Note that not all contributors participated in all six forecasting seasons.

2.3 Observational references

Two observational references were used for verification of the forecasts: the NSIDC-0081 product using the NASA Team algorithm for sea ice concentration reprocessing (Meier et al., 2022) and the OSI-401b product using the Bristol/Bootstrap algorithm (Tonboe et al., 2017). The choice of these products was made based on the near-operational availability of the datasets, but also to test the possible dependence of target diagnostics (sea ice area and concentration) on the choice of the reprocessing algorithms (NASA Team vs Bristol/Bootstrap). Our choice of using two products for forecast verification is motivated by the fact that observational errors introduce variability in skill metrics (Massonnet et al., 2016; Ferro, 2017; Mortimer et al., 2020; Lin et al., 2021).

The two products also display non-negligible differences in land-sea masks: for instance, the area covered by ocean south of 60°S differs by about 7.5% between the two products (46.93 million

km^2 for NSIDC-0081 vs 50.76 million km^2 for OSI-401b), likely due to differences in spatial resolution and in the treatment of landfast ice and ice shelves. These differences in land-sea masks and in reprocessing algorithms in observational references are to be kept in mind when interpreting SIPN South forecast errors, as these forecast errors can also have a component originating from the verification data itself.

NSIDC-0081 does not extend back prior to 2015 and OSI-401b does not extend back prior to 2005. Long-term climatologies were thus estimated with a third product, namely the OSI-450 dataset (Lavergne et al., 2019) recently superseded by the OSI-450a product, over the period 1979-2015. Note that the estimated climatologies are relatively insensitive to the choice of the observational product (see, e.g., Figure 1A of Roach et al. (2020) or Figure 3B of Lin et al. (2021)).

2.4 Climatological forecast

When assessing forecast skill, it is advisable to define a benchmark forecast (also known as the 'baseline' or 'reference' forecast) that is cheap to construct. The goal of such a benchmark forecast is to help establish whether the other forecasts outperform a naive prediction. In our case, the benchmark forecast is defined as the climatological forecast, comprising a 30-member ensemble corresponding to the 30 sea ice states of the 30 years preceding the target season. For example, the benchmark forecast for the 2020-2021 December-January-February forecasting season consists of the observed sea ice areas and concentrations of the December-January-February 1990-1991, 1991-1992, … 2019-2020 seasons. The climatological forecast is based on the OSI-401b product of sea ice concentration after 2015, and on the OSI-450 product before 2015. It is labeled "climatology" in the figures.

We are aware that other benchmark forecasts could have been introduced at this stage, such as: the trend extrapolation (sea ice area at day D is extrapolated from the linear or quadratic trend fitted to the previous areas at day D from previous years), the persistence forecast (sea ice area at day D is equal to the sea ice area at the initial time, i.$^{e.}$, 1st of December), the anomaly persistence forecast (sea ice area at day D is the sea ice area anomaly at the initial time added to the climatological sea ice area at day D), the damped anomaly persistence forecast (wherein the previous forecast is weighted by the auto-correlation of the time series), and many more. While looking simple in their formulations, these alternative benchmark forecasts are not always straightforward to implement for timeseries that are characterized by marked seasonal cycles in the mean, in the trend, and in the variability of sea ice concentration. In addition, producing ensembles of forecasts is not straightforward as these alternative benchmarks are deterministic by nature. Constructing ensemble statistics for these alternative benchmarks would require making assumptions on the statistical structure of the anomalies (e.g., accounting for autocorrelation in the time series, gaussianity or not, heteroscedasticity or not), which would in turn mean that we have created a new statistical model in its own right. For these reasons, we stick to the climatological forecast that requires no assumptions other than the number of years included. Note also that, since the long term trend of Antarctic sea ice extent is near-zero, a climatology benchmark is appropriate (unlike in the Arctic).

2.5 Domain boundaries

For regional analyses, we split the Southern Ocean into five regions following common definitions used in previous studies (Massonnet et al., 2013). The relevant regions are the Weddell Sea sector (60W-20E), the Indian sector (20E-90E), the West Pacific sector (90E-160E), the Ross Sea sector (160E-130W), and the Amundsen-Bellingshausen Seas sector (130W-60W). We refer to "Antarctic" or "circumpolar" when we mean the full 180W-180E. The five regions are shown on the map of Figure 1.

2.6 Data and code availability

The SIPN South project is intended to be a community project whereby anyone can produce diagnostics and analyses based on the data contributed. All the scripts, codes, and data are available from the SIPN South GitHub repository. The figures shown in this paper were generated from the release https://github.com/fmassonn/sipn-south-public/releases/tag/published.

3 Results and discussion

3.1 Does the SIPN South ensemble exhibit systematic forecast errors?

To answer that first question, we consider the forecast distribution of February mean sea ice area at the regional and circumpolar scales, along with the two verification datasets introduced in Sec. 2.3 (Figure 3). The plots presented in the figure summarize the bulk of the forecast distribution (group median and 10-90% range) as well as forecasts outside this range. Figure 3 also displays the historical distribution of the corresponding observed sea ice areas (1979-2015) following the same conventions as the forecast distributions. These historical distributions confirm that sea ice area in the six previous years has been anomalously low, in line with Figure 1. All regions have contributed to create these circumpolar negative anomalies. The Ross Sea has featured the largest reductions.

The first result is that observational uncertainty (indicated by the difference between the pair of black dots in Figure 3) is generally small in comparison to forecast uncertainty, apart from the Indian Sector, where it can be comparable to the 10-90% forecast range, as in 2020. The Indian Sector is, however, the region with the smallest climatological sea ice area (~5% of the circumpolar area). In absolute value, the observational spread is comparable to the observational spread in other sectors (~0.1 million km^2 maximum), but the apparent spread is magnified by the fact that the amount of sea ice to predict is very limited.

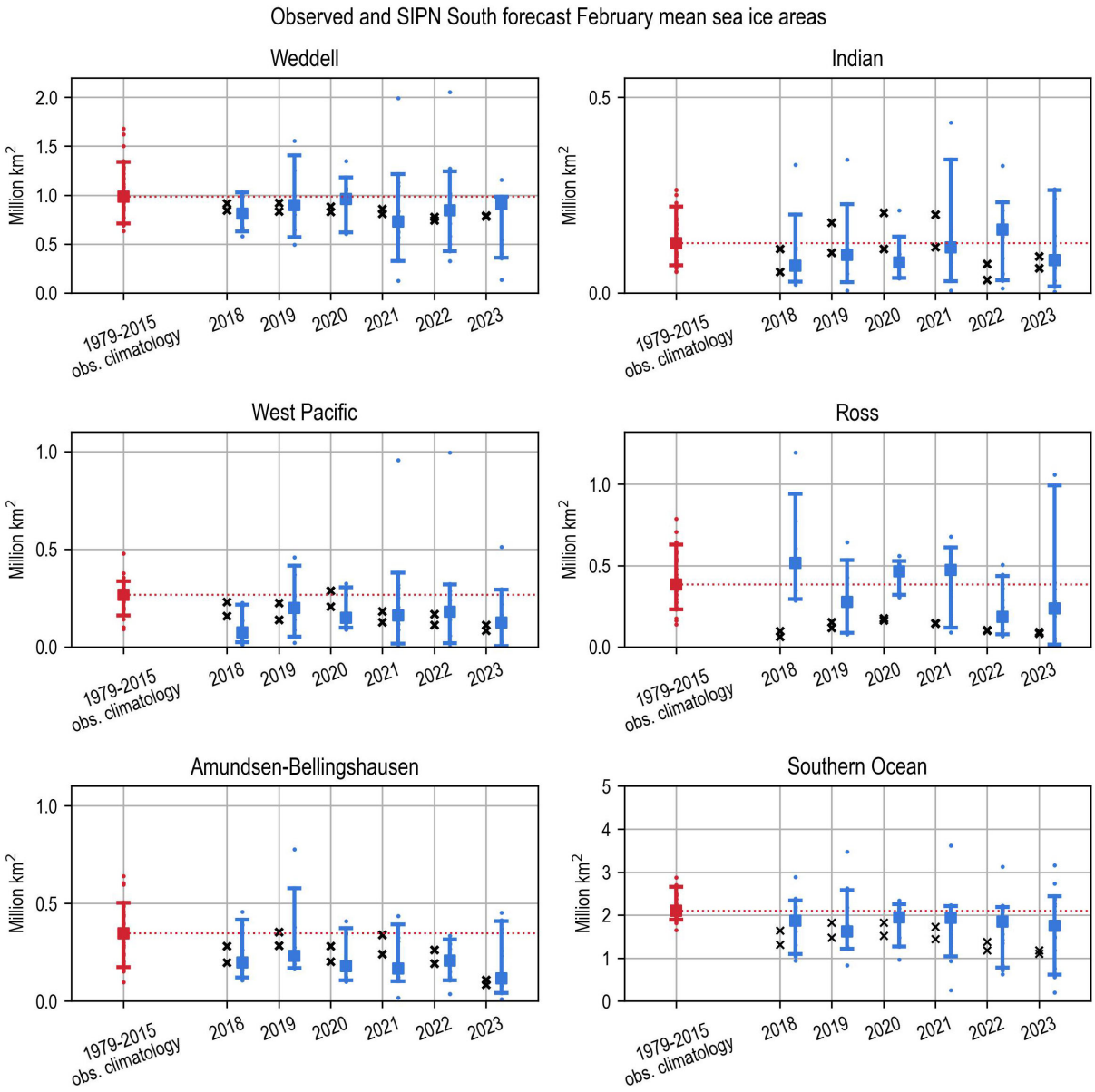

FIGURE 3
Distribution of the SIPN South forecasts and observed February mean sea ice areas for each of the forecasting seasons. The blue intervals represent the SIPN South distribution (10-90%), with the blue square referring to the ensemble median. The blue dots are those forecasts falling outside the 10-90% bulk of the distribution. The two black crosses denote the observational references. The red interval, square, and dots are the corresponding estimates for the climatological forecast. The light horizontal dotted line is drawn from the median to facilitate the comparison between the forecasts and the climatological state.

A second result is that the circumpolar SIPN South range of sea ice areas bracket observations for all years (Figure 3). The SIPN South forecast ensemble is therefore not incompatible, in a statistical sense, with the observations for the total sea ice area. Interestingly, for each year, the medians lie below the 1979-2015 climatological median (horizontal dashed line), suggesting that as a group, the SIPN South forecasts capture well the tendency since 2015 of sea ice area to lie on the low side of the climatological distribution. This gives credit to the SIPN South forecast ensemble having added value over a trivial climatological forecast. We note finally that the historical climatological distribution would be a poor forecast given that all six recently observed states lie below the 10th climatological percentile.

Analyzing regional forecasts allows us to establish whether the total circumpolar sea ice area forecast skill is obtained for the right reasons or thanks to error compensations at the regional scale. The SIPN South forecasts perform generally well in the Weddell Sea, in the West Pacific, and in the Amundsen-Bellingshausen Seas sectors: in those regions, the two observational datasets fall within the forecast range. We have deliberately not reported skill statistics as the sample size (n = 6 years) is very low. The Ross Sea stands out as the region with large systematic errors. The median systematically

overestimates the observed values and the observations lie at the edge, if not outside, of the 10-90% forecast range, for reasons that we will discuss in the next section.

Since Figure 3 displays February means, it does not convey information about how the sea ice area was forecast between initialization time (1st of December) and the target month of February. Figure 4 shows the daily evolution of the circumpolar sea ice area (forecast and observed) for the 2022-2023 exercise, for the subset of statistical and dynamical contributions. A striking pattern, also seen for all five previous forecasting seasons (see Supplementary Material), is clear: on average, the SIPN ensemble starts biased high for the circumpolar area; then, from mid-December to mid-January, melt rates are largely overestimated compared to observational references (Figure 4, right column). This feature is particularly evident for dynamical model contributions but is also shared by one statistical contribution.

In dynamical model contributions, several reasons can explain this general overestimation of sea ice area at initial time: issues in the initialization procedure or biases in the winter mean state. Regarding the initialization procedure, at least one group (Met Office) follows a "lagged" approach meaning that the ensemble of initial conditions is drawn from the 21 previous days' (twice a day) states before the initialization date (1st of December). Due to the seasonality of the sea ice area, all corresponding 42 states display a larger sea ice area than the one on Dec 1. For other contributions (e.g., ucl), the source of the problem is different. The ocean–sea ice model exhibits a well-known positive late winter bias in sea ice area (Barthélemy et al., 2018; Massonnet et al., 2019) causing excessive melt rates during the spring season. The origins of this winter bias have not been identified yet but appear to be common to other dynamical models. In statistical contributions, the initial overestimation is less evident: the forecasts appear to be more clustered around the observed state at initial time. An interesting feature

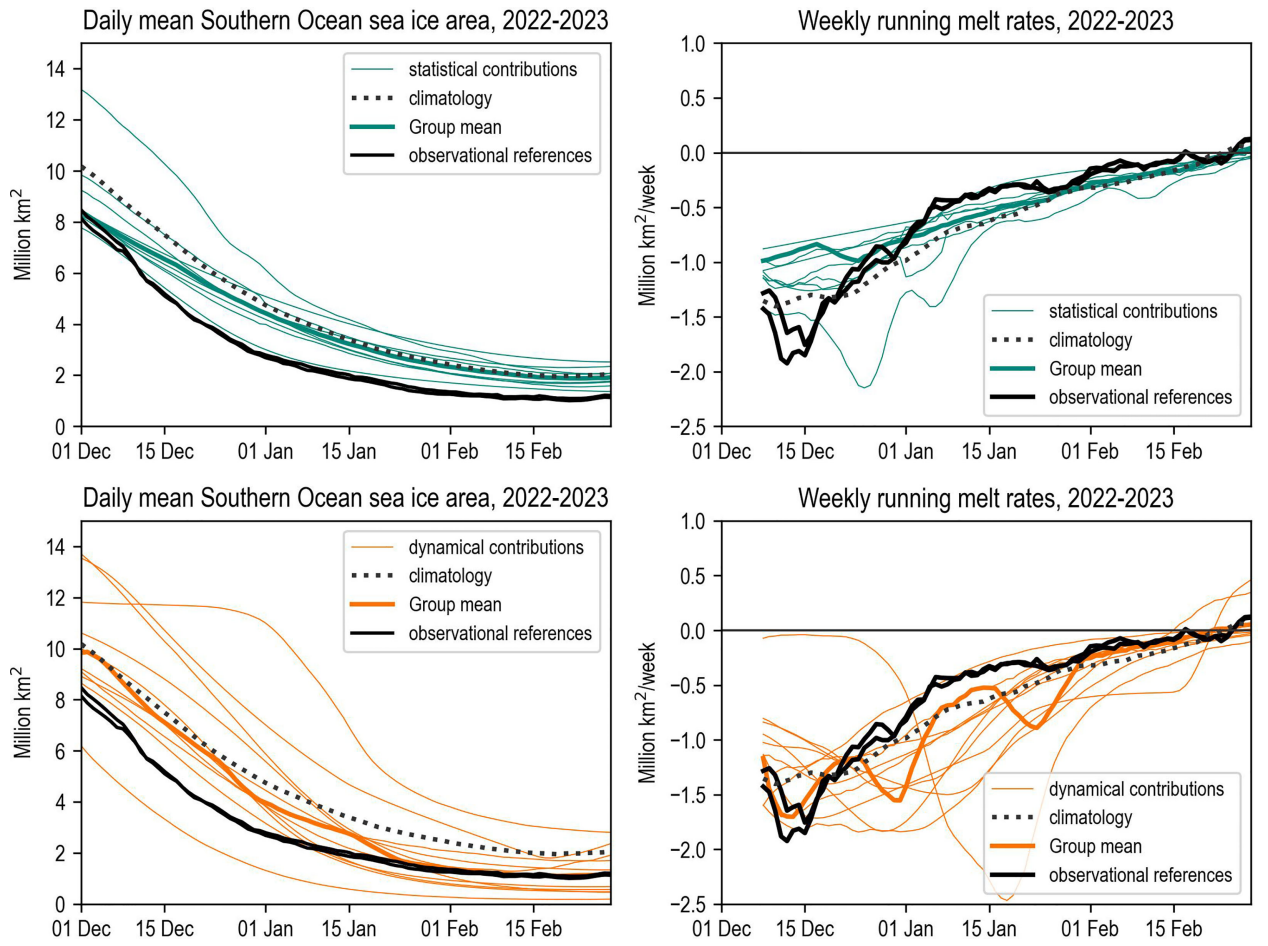

FIGURE 4
(Left column) Daily Antarctic sea ice area forecast by the groups participating in the 2022-2023 exercise, separated in (top) statistical contributions and (bottom) dynamical contributions. When several ensemble members are submitted by a group, the mean of the distribution is considered. The verifying observational references are shown as thick black lines. The climatological forecast is shown as the black dotted line. (Right column) Running weekly melt rates, computed for day *d* as the value of the timeseries of the left panel at day *d* minus the value at day *d* – 7. The same figures for previous years are shown in the Supplementary Material.

is that the climatological forecast itself is biased high on December 1st, consistently with the recent negative anomalies displayed in Figure 1.

3.2 Do SIPN South forecasts provide added value over climatological benchmarks?

With only six seasons of forecasts (2017-2018 to 2022-2023), delivering firm statements on the ability of forecasts to predict interannual variations in sea ice area skill is beyond reach. However, most contributions consist of ensembles of forecasts, so a few conclusions can at least be drawn on the appropriate dispersion properties of individual submissions. To exemplify several aspects of forecast characteristics, we show in Figure 5 the fitted probability density functions of the February mean sea ice area for all groups that participated in the 2022-2023 forecasting season as well as for the climatological forecast. We first note that, in general, statistical model contributions provide fewer ensemble members than dynamical model contributions. A possible reason is that delivering ensemble forecasts has long been standard practice in the weather and climate prediction communities, which frequently construct ensembles to produce probabilistic assessments. Statistical approaches are based on simpler models where it is not always clear how uncertainty should be sampled. All members (colored crosses) in Figure 5 should be viewed as equally plausible forecasts within each submission, except for the NicoSun contribution where each member corresponds to three scenarios of high melt, medium melt, and low melt, respectively.

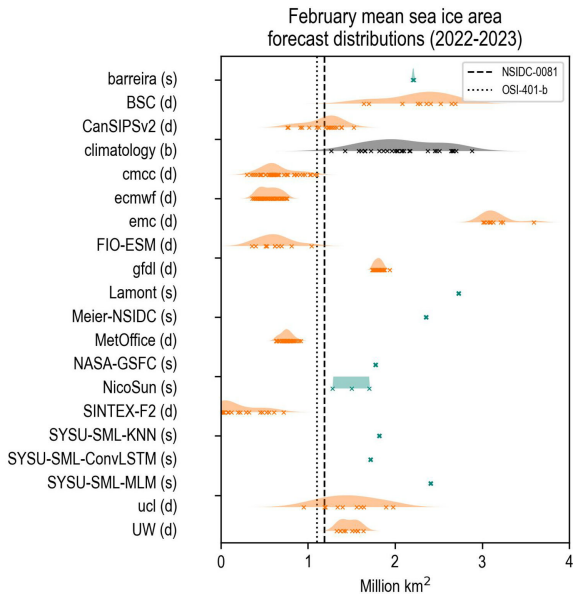

FIGURE 5
Distribution of the February mean circumpolar sea ice areas forecast by the groups participating in the 2022-2023 season and the verifying observations (vertical dashed lines). The color coding follows the same conventions as in Figure 4. The probability density functions are drawn with a kernel-density estimate using Gaussian kernels.

The first feature that is apparent from Figure 5 is the large variability in the shapes of the forecast distributions. Several contributions are underdispersive (or overconfident) in the sense that the observed value is statistically incompatible with the forecast distribution (e.g., barreira, gfdl). The lack of bias correction is one plausible reason for this behavior. Other contributions are overdispersive (or underconfident) in the sense that the forecast distribution is much wider than the climatology (e.g., SINTEX-F2). Neither underdispersive nor overdispersive ensemble forecasts are desirable from a decision-making point of view: underdispersive forecasts are sharp but most often do not include the actual outcome, while overdispersive forecast distributions most often include the actual outcome but are overly flat.

Striking a good balance between bias (i.e., how far the forecast mean is compared to the verification value) and spread (i.e., how uncertain is the forecast) is essential in ensemble forecasting. The ability to reach a good tradeoff can be measured with a single metric, namely the continuous rank probability (CRPS). The CRPS is a generalization of the Brier Score to continuous variables (Jolliffe and Stephenson, 2003) and measures the area under the squared difference between the cumulative density function of the forecast distribution and the cumulative density function of the observations, i.e., a step function at the observed value. The CRPS is a convenient metric because it penalizes forecasts that are systematically biased high or low, but also forecasts that are excessively spread out. According to the definition, a CRPS value of zero is obtained for a perfect forecast with the mass of the distribution centered at the verifying observation value, and larger CRPS values correspond to less skillful forecasts.

The CRPS values for all six forecasting seasons are reported in Table 2. Caution should be exercised when interpreting the results in this table since the CRPS, like any metric of performance, is sensitive to sampling issues. Nevertheless, several interesting features are noted. First, no obvious relationship emerges between the type of forecasting approach and the CRPS metric: the statistical and dynamical sub-groups score an average value of 0.57 and 0.49 million km^2 squared for the six forecasting seasons, respectively. Second, we note that 51% (42 out of 82) predictions are superior, in a CRPS sense, to the climatological forecast. This proportion raises to 65% (22 out of 34) for the last two seasons when an all-time minimum occurred (2021-2022 and then 2022-2023). Several individual contributions systematically outperform that benchmark forecast. Finally, the group forecast, obtained by aggregating individual forecasts (see Sec. 2.3) is systematically more skilled than the climatological forecast and more skilled than most of the individual forecasts. We also note that the CRPS of the statistical and dynamical sub-group forecast is more skilled than the average CRPS within each respective group. This behavior is reminiscent of what is observed with the multi-model mean in climate change simulations, and is likely explained by the cancellation of random errors that characterize individual forecasts.

TABLE 2 Continuous Rank Probability Scores (CRPS) for the February mean Antarctic sea ice area forecasts, for each of the forecasting seasons of the SIPN South project.

	2017-2018	2018-2019	2019-2020	2020-2021	2021-2022	2022-2023
climatology	0.37	0.20	0.19	0.24	0.51	0.66
Statistical models						
barreira	/	1.64	0.41	0.51	0.80	1.02
Gateway	0.71	/	/	/	/	/
Lamont	**0.22**	0.79	**0.17**	0.42	0.77	1.54
Meier-NSIDC	/	/	/	/	0.69	1.17
NASA-GSFC	0.47	**0.15**	0.42	0.38	**0.51**	**0.59**
NicoSun	**0.22**	**0.20**	**0.15**	**0.12**	**0.25**	**0.22**
SYSU-SML-KNN	/	/	/	**0.18**	**0.49**	**0.63**
SYSU-SML-ConvLSTM	/	/	/	/	/	**0.53**
SYSU-SML-MLM	/	/	/	/	/	1.22
Statistical group forecast	**0.18**	0.30	0.21	**0.20**	0.52	**0.65**
Dynamical models						
BSC	/	/	/	/	**0.10**	0.88
CanSIPSv2	/	/	/	**0.13**	**0.14**	**0.05**
cmcc	/	**0.12**	/	0.65	0.57	**0.43**
CNRM	/	/	**0.08**	1.68	1.61	/
ecmwf	0.49	0.92	0.43	0.32	0.69	**0.56**
emc	1.14	/	/	/	/	1.89
FIO-ESM	0.52	0.30	0.57	0.31	**0.44**	**0.46**
gfdl	/	/	/	/	**0.49**	**0.60**
MetOffice	**0.04**	0.45	0.26	**0.08**	**0.51**	**0.39**
Modified-CanSIPS	**0.21**	**0.20**	0.36	/	/	/
mpas-cesm	0.70	/	/	/	/	/
nasa-gmao	**0.28**	0.56	0.79	/	/	/
SINTEX-F2	/	/	/	1.36	**0.39**	0.86
ucl	**0.09**	**0.13**	**0.10**	**0.13**	**0.28**	**0.16**
UW	/	/	/	/	/	**0.23**
Dynamical group forecast	**0.19**	0.27	**0.18**	**0.20**	**0.17**	**0.22**
Group forecast	**0.18**	**0.19**	**0.13**	**0.15**	**0.24**	**0.31**

Units are million km^2 squared. The contributions are separated into statistical and dynamical sub-groups. The CRPS are in bold font when the forecast performs better than the climatological forecast. The "Statistical group forecast", the "Dynamical group forecast" and the "Group forecast" rows show the CRPS obtained by aggregating the data from the corresponding sub-groups or entire ensemble, respectively (see Sec. 2.2).

3.3 Is there a relationship between forecasting approach and skill?

The previous section has hinted at the fact that, from a circumpolar point of view, no sub-group of forecasts (statistical or dynamical) outperforms the other. The results have also suggested the value of aggregating the individual forecasts to produce a group forecast. On the other hand, Section 3.1 has shown that the skill is region-dependent in the SIPN South ensemble. To assess the ability of the prediction systems to capture the regional distribution of sea ice concentration, we compute the Integrated Ice Edge Error (IIEE, Goessling et al. (2016)). The IIEE is the areal integral of all grid cells where the forecast and the verification

disagree on a certain event, defined here as sea ice presence (SIC > 15%). For one-member forecasts, the calculation of the IIEE is straightforward: the spatial fields of SIC are converted to 1 or 0 based on the 15% SIC threshold and the resulting binary field is compared to the observed binary field of ice presence. The areas of grid cells where sea ice is present in observations but absent in the forecasts, or absent in observations but present in the forecasts are then summed. For multi-member forecasts, the calculation is slightly different: binary fields of sea ice presence are defined for each member individually, and a probability of sea ice presence is calculated by averaging the binary fields across the ensemble. The areas of grid cells where sea ice present in observations but present with < 50% probability in the ensemble, or absent in observations but present with > 50% in the ensemble, are then summed. To compute the IIEE, all forecasts and verification data were first remapped (nearest-neighbor interpolation) to a 2° by 2° regular grid.

The IIEEs for the 2022-2023 forecasting season are shown in Figure 6. In line with Figure 4 (circumpolar sea ice area daily time series), dynamical predictions in general exhibit larger initial errors than statistical predictions. These initial errors in dynamical predictions develop throughout the melting season until ~1st of January, before a sharp reduction towards the month of February. For that month, no type of prediction appears to be superior to another for the IIEE metric. The group forecast has an IIEE that is among the lowest from early February, confirming at the regional scale the conclusions obtained at the circumpolar scale.

4 Conclusions, perspectives, and recommendations

The SIPN South project was initiated in 2017, i.e., one year after the beginning of a series of anomalously low sea ice conditions in the Southern Ocean (Figure 1). The non-stationary character of sea ice area anomalies suggests that climatological forecasts could be of limited value for seasonal prediction. An important finding of this study is that several prediction systems, based on both statistical and dynamical modeling, are consistently more skillful than the climatological forecast. The group forecast, obtained by aggregating all individual forecasts, is found to outperform the climatological forecast and the majority of individual forecasts themselves for two standard metrics of performance, the continuous rank probability score and the integrated ice edge error.

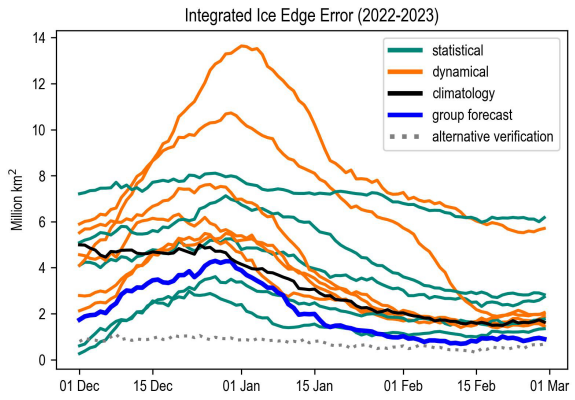

FIGURE 6
Integrated Ice Edge Error (see the text for definition) for the contributions providing the sea ice concentration information. The color coding follows the same conventions as in Figure 4. The black curve is the benchmark climatological forecast (see Section 2.4) and the thick blue curve is the IIEE of the group forecast. The reference product for the IIEE calculation is the NSIDC-0081 product, and the grey curve shows the IIEE of the alternative verification product OSI-401-b.

The Ross Sea appears to be the sector where sea ice prediction is the most challenging and where spread is the largest, although a recent study (Payne et al., 2022) demonstrates moderate skill in the sector with a dynamical model. While we have not attempted here to understand the sources of prediction errors and why they vary regionally, we can formulate hypotheses. The Ross Sea summer sea ice concentration anomalies are linked to the spring sea ice drift and thickness anomalies in the neighboring Amundsen Sea sector. In observations, westward coastal currents transport sea ice toward the Ross ice shelf during the spring season, and sea ice is then advected offshore by the dominant southerly winds (e.g., Holland and Kimura, 2016). This coupled dynamical process is difficult to simulate at the resolution of current ocean-sea ice dynamical models (Holland et al., 2014). In addition, the statistical models participating in SIPN South (Table 1) do not consider the initial sea ice thickness as a predictor except for one (NicoSun), which turns out to be performing relatively well. The poor performance of forecasts in the Ross Sea could also be explained by the fact that predictability is inherently lower there compared to other sectors. In dynamical model predictions, ensemble spread is usually the largest in the Ross sea (not shown), which supports this idea of limited initial-value predictability in that sector.

Several studies have reported long-range (>1 yr) sea ice predictability thanks to mechanisms of reemergence (e.g., Holland et al., 2013; Marchi et al., 2019) and the results of SIPN South might appear disappointing, at least in light of the initial prospects raised in these perfect predictability studies. The ocean-to-sea ice connection that brings the long-range predictability of surface conditions is more direct in winter (since the deep mixing causes direct interaction), whereas the summer connection requires simulation of more complex process (mixed layer shoaling, ice-albedo feedback, vertical mixing, etc.), which is likely not captured by the current models.

The results of this study have highlighted that dynamical models, even when they are initialized with observed or reanalyzed ocean-sea ice states, exhibit a positive bias in sea ice area at initial time but no bias at the sea ice minimum, implying excessive sea ice area losses during the melting season. The reason could be that the dynamical contributions are initialized with different products from the ones used for verification. More diagnostics (e.g., tendencies in sea ice concentration due to thermodynamic and dynamic processes) would be required to pinpoint the deficient physical mechanisms in these models.

For the metrics of performance introduced in this paper, the statistical models appear to perform better than the dynamical models for predicting the spatial information during the melting season (December and January, see the IIEE curves in Figure 6). Nonetheless, a limitation of statistical contributions is that most of them are deterministic, i.e., provide only one prediction (the NicoSun is an exception, providing forecasts as a range of three scenarios: low melt, medium melt, high melt). The deterministic nature of most statistical forecasts is contrasted by the large ensemble size in dynamical models, exceeding 50 ensemble members for several dynamical contributions,

and can be regarded as a serious limitation to the use of these statistical predictions by stakeholders. Stakeholder-relevant diagnostics like the probability of sea-ice presence (i.e., the probability of observing sea ice concentration above 15% at a given point at a given day) cannot be reliably estimated with statistical models alone when they provide only one or even three ensemble members. In this context it is worth mentioning that one of the statistical SIPN South contributions, AWI-SDAP, provided just that probability of sea ice presence instead of sea ice concentration (although only for one year). However, this contribution could not be included in all analyses because it is not possible to derive sea-ice area from the probability of ice presence. In future intercomparison studies, we might thus recommend submitting forecasts of the probability of sea ice presence directly.

The conclusions presented here draw on six seasons of coordinated sea ice predictions since 2017. One of the novel aspects of SIPN South is that it collects predictions done in a real-time context with the best possible information available at the time of submission by each group. These predictions differ from hindcasts (retrospective forecasts) that are less constrained by data unavailability (since ocean/atmosphere/sea ice reanalyses are released with a couple of weeks or months of delay). Also, hindcasts might exhibit larger skill than real-time forecasts due to the fact that the models are, consciously or not, continuously adapted and tuned to represent new climatic situations.

The principal value of the SIPN South community effort is to identify and engage contributors on best practices, while exploring the current skill in forecasting austral summer sea ice conditions. We are aware that we might miss potential contributions from individuals, groups, or institutions that are not registered on those lists or on social media. We will continue to regularly collect forecasts for the summer season, and are currently expanding the protocol for other seasons. The possibility to submit more diagnostics such as sea ice drift and thickness, oceanic mixed layer depth and heat content, will be added to the SIPN South protocol to better partition forecast errors between initial-condition uncertainty and model uncertainty. We will also consider developing near-operational benchmark datasets beyond simple climatology. Future work will also include a more systematic evaluation of skill at the regional scale, will accept longer forecasts (out to fall and winter), and will allow contributors to re-submit forecasts in a hindcast context, i.e. when all datasets at initial times are available.

Data availability statement

The datasets presented in this study can be found in online repositories. The names of the repository/repositories and accession number(s) can be found in the article/Supplementary Material.

Author contributions

All co-authors provided the data. FM wrote the manuscript, all co-authors edited and commented it. All authors contributed to the article and approved the submitted version.

Funding

QY, XL and XD are supported by the National Key R&D Program of China (No. 2022YFE0106300) and the National Natural Science Foundation of China (No. 41941009, 42106233). WaM is supported by the NASA Earth Science Data Information System (ESDIS) Project through the NASA Snow and Ice Distributed Active Archive Center (DAAC) at NSIDC. WH is supported by grant funding from the Australian Government as part of the Antarctic Science Collaboration Initiative program. HG and BN acknowledge the financial support by the Federal Ministry of Education and Research of Germany in the framework of SSIP (grant 01LN1701A). EB-W was funded by National Science Foundation grant NSF-RAPID OPP-2233016.

Acknowledgments

FM is a F.R.S.-FNRS Research Associate. EB was supported by the Met Office Hadley Centre Climate Programme funded by BEIS and Defra. XY and CL are supported by Lamont-Dohert Earth Observatory of Columbia University and a private donor (Ying). YM is supported by JSPS KAKENHI Grant Number 22K03727 and Princeton University/NOAA GFDL Visiting Research Scientists Program. SINTEX-F2 seasonal forecast was performed on Earth Simulator at JAMSTEC. AS was supported by Copernicus Climate Change Service (C3S2_370) Operational Seasonal Predictions, DI by the Foundation Euro-Mediterranean Center on Climate Change (CMCC, Italy).

Conflict of interest

The authors declare that the research was conducted in the absence of any commercial or financial relationships that could be construed as a potential conflict of interest.

Publisher's note

Supplementary material

The Supplementary Material for this article can be found online at: https://www.frontiersin.org/articles/10.3389/fmars.2023.1148899/full#supplementary-material

References

Abrahamsen, E. P., Barreira, S., Bitz, C. M., Butler, A., Clem, K. R., Colwell, S., et al. (2020). Antarctica And the southern ocean. *Bull. Am. Meteorol. Soc.* 101 (8), S287–S320. doi: 10.1175/BAMS-D-20-0090.1

Barthélemy, A., Goosse, H., Fichefet, T., and Lecomte, O. (2018). On the sensitivity of Antarctic sea ice model biases to atmospheric forcing uncertainties. *Climate Dynamics.* 51 (4), 1585–1603. doi: 10.1007/s00382-017-3972-7

Bilbao, R., Wild, S., Ortega, P., Acosta-Navarro, J., Arsouze, T., Bretonnière, P.-A., et al. (2021). Assessment of a full-field initialized decadal climate prediction system with the CMIP6 version of EC-earth. *Earth Syst. Dynamics.* 12 (1), 173–196. doi: 10.5194/esd-12-173-2021

Blanchard-Wrigglesworth, E., Bushuk, M., Massonnet, F., Hamilton, L. C., Bitz, C. M., Meier, W. N., et al. (2023). Forecast skill of the Arctic Sea ice outlook 2008–2022. *Geophys. Res. Lett.* 50 (6), e2022GL102531. doi: 10.1029/2022GL102531

Blanchard-Wrigglesworth, E., Cullather, R. I., Wang, W., Zhang, J., and Bitz, C. M. (2015). Model forecast skill and sensitivity to initial conditions in the seasonal Sea ice outlook. *Geophys. Res. Lett.* 42 (19), 8042–8048. doi: 10.1002/2015GL065860

Brierley, A. S., and Thomas, D. N. (2002). Ecology of southern ocean pack ice. *Adv. Mar. Biol.* 43, 171–276. doi: 10.1016/s0065-2881(02)43005-2

Bromwich, D. H., Werner, K., Casati, B., Powers, J. G., Gorodetskaya, I. V., Massonnet, F., et al. (2020). The year of polar prediction in the southern hemisphere (YOPP-SH). *Bull. Am. Meteorol. Soc.* 101, E1653–E1676. doi: 10.1175/BAMS-D-19-0255.1

Bushuk, M., Winton, M., Haumann, F. A., Delworth, T., Lu, F., Zhang, Y., et al. (2021). Seasonal prediction and predictability of regional Antarctic sea ice. *J. Climate* 1 (aop), 1–68. doi: 10.1175/JCLI-D-20-0965.1

Caron, L.-P., Massonnet, F., Klotzbach, P. J., Philp, T. J., and Stroeve, J. (2020). Making seasonal outlooks of Arctic Sea ice and Atlantic hurricanes valuable–not just skillful. *Bull. Am. Meteorol. Soc.* 101 (1), E36–E42. doi: 10.1175/BAMS-D-18-0314.1

Cavalieri, D. J., Parkinson, C. L., and Vinnikov, K. Y. (2003). 30-year satellite record reveals contrasting Arctic and Antarctic decadal sea ice variability. *Geophys. Res. Lett.* 30 (18), 1–4. doi: 10.1029/2003GL018031

Chen, H., Yin, X., Bao, Y., and Qiao, F. (2016). Ocean satellite data assimilation experiments in FIO-ESM using ensemble adjustment kalman filter. *Sci. China Earth Sci.* 59 (3), 484–494. doi: 10.1007/s11430-015-5187-2

Chen, D., and Yuan, X. (2004). A Markov model for seasonal forecast of Antarctic Sea ice. *J. Climate* 17, 13. doi: 10.1175/1520-0442(2004)017<3156:AMMFSF>2.0.CO;2

Cherchi, A., Fogli, P. G., Lovato, T., Peano, D., Iovino, D., Gualdi, S., et al. (2019). Global mean climate and main patterns of variability in the CMCC-CM2 coupled model. *J. Adv. Modeling. Earth Syst.* 11 (1), 185–209. doi: 10.1029/2018MS001369

Chevallier, M., Massonnet, F., Goessling, H., Guémas, V., and Jung, T. (2019). *Sub-Seasonal. to Seasonal. Prediction.*, 201–221. doi: 10.1016/B978-0-12-811714-9.00010-3

COMNAP (2015) *COMNAP sea ice challenges workshop report : Hobart, Tasmania, Australia, 12-13 may 2015*. Available at: https://static1.squarespace.com/static/61073506e9b0073c7eaaf464/t/615a56981ab568669d8e4554/1633310364849/COMNAP_Sea_Ice_Challenges_BKLT_Web_Final_Dec2015.pdf.

Delille, B., Vancoppenolle, M., Geilfus, N.-X., Tilbrook, B., Lannuzel, D., Schoemann, V., et al. (2014). Southern ocean CO2 sink : the contribution of the sea ice. *J. Geophys. Res.: Oceans.* 119 (9), 6340–6355. doi: 10.1002/2014JC009941

Delworth, T. L., Cooke, W. F., Adcroft, A., Bushuk, M., Chen, J., Dunne, K. A., et al. (2020). SPEAR : the next generation GFDL modeling system for seasonal to multidecadal prediction and projection. *J. Adv. Modeling. Earth Syst.* 12 (3). doi: 10.1029/2019MS001895

DeVries, T. (2014). The oceanic anthropogenic CO2 sink : storage, air-sea fluxes, and transports over the industrial era. *Global Biogeochem. Cycles.* 28 (7), 631–647. doi: 10.1002/2013GB004739

Dirkson, A., Merryfield, W. J., and Monahan, A. (2017). Impacts of Sea ice thickness initialization on seasonal Arctic Sea ice predictions. *J. Climate* 30 (3), 1001–1017. doi: 10.1175/JCLI-D-16-0437.1

Doi, T., Behera, S. K., and Yamagata, T. (2016). Improved seasonal prediction using the SINTEX-F2 coupled model. *J. Adv. Modeling. Earth Syst.* 8 (4), 1847–1867. doi: 10.1002/2016MS000744

Donlon, C. J., Martin, M., Stark, J., Roberts-Jones, J., Fiedler, E., and Wimmer, W. (2012). The operational Sea surface temperature and Sea ice analysis (OSTIA) system. *Remote Sens. Environ.* 116, 140–158. doi: 10.1016/j.rse.2010.10.017

Eayrs, C., Li, X., Raphael, M. N., and Holland, D. M. (2021). Rapid decline in Antarctic sea ice in recent years hints at future change. *Nat. Geosci.* 14, 1–5. doi: 10.1038/s41561-021-00768-3

Ferro, C. A. T. (2017). Measuring forecast performance in the presence of observation error : measuring forecast performance in the presence of observation error. *Q. J. R. Meteorol. Soc.* 143 (708), 2665–2676. doi: 10.1002/qj.3115

Gelaro, R., McCarty, W., Suárez, M. J., Todling, R., Molod, A., Takacs, L., et al. (2017). The modern-era retrospective analysis for research and applications, version 2 (MERRA-2). *J. Climate* 30 (14), 5419–5454. doi: 10.1175/JCLI-D-16-0758.1

Goessling, H. F., Tietsche, S., Day, J. J., Hawkins, E., and Jung, T. (2016). Predictability of the Arctic sea ice edge. *Geophys. Res. Lett.* 43 (4), 1642–1650. doi: 10.1002/2015GL067232

Goosse, H., Kay, J. E., Armour, K. C., Bodas-Salcedo, A., Chepfer, H., Docquier, D., et al. (2018). Quantifying climate feedbacks in polar regions. *Nat. Commun.* 9 (1), 1–13. doi: 10.1038/s41467-018-04173-0

Goosse, H., and Zunz, V. (2014). Decadal trends in the Antarctic sea ice extent ultimately controlled by ice–ocean feedback. *Cryosphere.* 8 (2), 453–470. doi: 10.5194/tc-8-453-2014

Gray, A. R., Johnson, K. S., Bushinsky, S. M., Riser, S. C., Russell, J. L., Talley, L. D., et al. (2018). Autonomous biogeochemical floats detect significant carbon dioxide outgassing in the high-latitude southern ocean. *Geophys. Res. Lett.* 45 (17), 9049–9057. doi: 10.1029/2018GL078013

Griffies, S. M. (2012). *Elements of the modular ocean model. GFDL ocean group technical report no. 7* (Princeton: NOAA/Geophysical Fluid Dynamics Laboratory), 632.

Hamilton, L. C., and Stroeve, J. (2016). 400 predictions : the SEARCH Sea ice outlook 2008–2015. *Polar. Geogr.* 39 (4), 274–287. doi: 10.1080/1088937X.2016.1234518

Hobbs, W. R., Massom, R., Stammerjohn, S., Reid, P., Williams, G., and Meier, W. (2016). A review of recent changes in southern ocean sea ice, their drivers and forcings. *Global Planet. Change* 143, 228–250. doi: 10.1016/j.gloplacha.2016.06.008

Holland, M. M., Blanchard-Wrigglesworth, E., Kay, J., and Vavrus, S. (2013). Initial-value predictability of Antarctic sea ice in the community climate system model 3. *Geophys. Res. Lett.* 40 (10), 2121–2124. doi: 10.1002/grl.50410

Holland, P. R., Bruneau, N., Enright, C., Losch, M., Kurtz, N. T., and Kwok, R. (2014). Modeled trends in Antarctic Sea ice thickness. *J. Climate* 27 (10), 3784–3801. doi: 10.1175/JCLI-D-13-00301.1

Holland, P. R., and Kimura, N. (2016). Observed concentration budgets of Arctic and Antarctic Sea ice. *J. Climate* 29 (14), 5241–5249. doi: 10.1175/JCLI-D-16-0121.1

Holland, M. M., Landrum, L., Raphael, M., and Stammerjohn, S. (2017). Springtime winds drive Ross Sea ice variability and change in the following autumn. *Nat. Commun.* 8 (1), 731. doi: 10.1038/s41467-017-00820-0

Hunke, E. C., and Lipscomb, W. H. (2010). *CICE: the Los alamos sea ice model documentation and software user's manual* (Los Alamos: T-3 Fluid Dynamics Group, Los Alamos National Laboratory), 76.

Johnson, S. J., Stockdale, T. N., Ferranti, L., Balmaseda, M. A., Molteni, F., Magnusson, L., et al. (2019). SEAS5 : the new ECMWF seasonal forecast system. *Geosci. Model. Dev.* 12 (3), 1087–1117. doi: 10.5194/gmd-12-1087-2019

I. T. Jolliffe and „. D. B. Stephenson (Eds.) (2003). *Forecast verification : a practitioner's guide in atmospheric science* (Chichester, West Sussex, England and Hoboken, NJ: J. Wiley).

Jung, T., Gordon, N. D., Bauer, P., Bromwich, D. H., Chevallier, M., Day, J. J., et al. (2016). Advancing polar prediction capabilities on daily to seasonal time scales. *Bull. Am. Meteorol. Soc.* 97 (9), 1631–1647. doi: 10.1175/BAMS-D-14-00246.1

Kohout, A. L., Williams, M. J. M., Dean, S. M., and Meylan, M. H. (2014). Storm-induced sea-ice breakup and the implications for ice extent. *Nature* 509 (7502), 604–607. doi: 10.1038/nature13262

Koster, R. D., Suarez, M. J., Ducharne, A., Stieglitz, M., and Kumar, P. (2000). A catchment-based approach to modeling land surface processes in a general circulation model : 1. model structure. *J. Geophys. Res.: Atmospheres.* 105 (D20), 24809–24822. doi: 10.1029/2000JD900327

Lavergne, T., Sørensen, A. M., Kern, S., Tonboe, R., Notz, D., Aaboe, S., et al. (2019). Version 2 of the EUMETSAT OSI SAF and ESA CCI sea-ice concentration climate data records. *Cryosphere.* 13 (1), 49–78. doi: 10.5194/tc-13-49-2019

Libera, S., Hobbs, W., Klocker, A., Meyer, A., and Matear, R. (2022). Ocean-Sea ice processes and their role in multi-month predictability of Antarctic Sea ice. *Geophys. Res. Lett.* 49 (8), e2021GL097047. doi: 10.1029/2021GL097047

Lin, X., Massonnet, F., Fichefet, T., and Vancoppenolle, M. (2021). SITool (v1.0) – a new evaluation tool for large-scale sea ice simulations : application to CMIP6 OMIP. *Geosci. Model. Dev.* 14 (10), 6331–6354. doi: 10.5194/gmd-14-6331-2021

Lin, H., Merryfield, W. J., Muncaster, R., Smith, G. C., Markovic, M., Dupont, F., et al. (2020). The Canadian seasonal to interannual prediction system version 2 (CanSIPSv2). *Weather. Forecasting.* 35 (4), 1317–1343. doi: 10.1175/WAF-D-19-0259.1

Liu, H., Yu, W., and Chen, X. (2022). Melting Antarctic Sea ice is yielding adverse effects on a short-lived squid species in the Antarctic adjacent waters. *Front. Mar. Sci.* 9. doi: 10.3389/fmars.2022.819734

Liu, J., Zhu, Z., and Chen, D. (2023). Lowest Antarctic sea ice record broken for the second year in a row. *Ocean-Land-Atmosphere. Res.* 0 (ja). doi: 10.34133/olar.0007

Lu, F., Harrison, M. J., Rosati, A., Delworth, T. L., Yang, X., Cooke, W. F., et al. (2020). GFDL's SPEAR seasonal prediction System : initialization and ocean tendency adjustment (OTA) for coupled model predictions. *J. Adv. Modeling. Earth Syst.* 12 (12), e2020MS002149. doi: 10.1029/2020MS002149

MacLachlan, C., Arribas, A., Peterson, K. A., Maidens, A., Fereday, D., Scaife, A. A., et al. (2015). Global seasonal forecast system version 5 (GloSea5) : a high-resolution seasonal forecast system. *Q. J. R. Meteorol. Soc.* 141 (689), 1072–1084. doi: 10.1002/qj.2396

Marchi, S., Fichefet, T., Goosse, H., Zunz, V., Tietsche, S., Day, J. J., et al. (2019). Reemergence of Antarctic sea ice predictability and its link to deep ocean mixing in global climate models. *Climate Dynamics.* 52 (5–6), 2775–2797. doi: 10.1007/s00382-018-4292-2

Martinson, D. G. (1990). Evolution of the southern ocean winter mixed layer and sea ice : open ocean deepwater formation and ventilation. *J. Geophys. Res.* 95 (C7), 11641. doi: 10.1029/JC095iC07p11641

Massom, R. A., Scambos, T. A., Bennetts, L. G., Reid, P., Squire, V. A., and Stammerjohn, S. E. (2018). Antarctic Ice shelf disintegration triggered by sea ice loss and ocean swell. *Nature* 558 (7710), 383–389. doi: 10.1038/s41586-018-0212-1

Massonnet, F., Barthélemy, A., Worou, K., Fichefet, T., Vancoppenolle, M., Rousset, C., et al. (2019). On the discretization of the ice thickness distribution in the NEMO3.6-LIM3 global ocean–sea ice model. *Geosci. Model. Dev.* 12 (8), 3745–3758. doi: 10.5194/gmd-12-3745-2019

Massonnet, F., Bellprat, O., Guemas, V., and Doblas-Reyes, F. J. (2016). Using climate models to estimate the quality of global observational data sets. *Science* 354 (6311), 452–455. doi: 10.1126/science.aaf6369

Massonnet, F., Mathiot, P., Fichefet, T., Goosse, H., König Beatty, C., Vancoppenolle, M., et al. (2013). A model reconstruction of the Antarctic sea ice thickness and volume changes over 1980–2008 using data assimilation. *Ocean. Model.* 64, 67–75. doi: 10.1016/j.ocemod.2013.01.003

Meehl, G. A., Arblaster, J. M., Chung, C. T. Y., Holland, M. M., DuVivier, A., Thompson, L., et al. (2019). Sustained ocean changes contributed to sudden Antarctic sea ice retreat in late 2016. *Nat. Commun.* 10 (1), 14. doi: 10.1038/s41467-018-07865-9

Meier, W., Stewart, J. S., Wilcox, H., Hardman, M. A., and Scott, D. J. (2022) *Near-Real-Time DMSP SSMIS daily polar gridded Sea ice concentrations, version 2.* Available at: https://nsidc.org/data/nsidc-0081.

Merryfield, W. J., Lee, W.-S., Boer, G. J., Kharin, V. V., Scinocca, J. F., Flato, G. M., et al. (2013). The Canadian seasonal to interannual prediction system. part I : models and initialization. *Monthly. Weather. Rev.* 141 (8), 2910–2945. doi: 10.1175/MWR-D-12-00216.1

Molod, A., Takacs, L., Suarez, M., and Bacmeister, J. (2015). Development of the GEOS-5 atmospheric general circulation model : evolution from MERRA to MERRA2. *Geosci. Model. Dev.* 8 (5), 1339–1356. doi: 10.5194/gmd-8-1339-2015

Morioka, Y., Doi, T., Iovino, D., Masina, S., and Behera, S. K. (2019). Role of sea-ice initialization in climate predictability over the weddell Sea. *Sci. Rep.* 9 (1), 2457. doi: 10.1038/s41598-019-39421-w

Morioka, Y., Iovino, D., Cipollone, A., Masina, S., and Behera, S. K. (2021). Summertime sea-ice prediction in the weddell Sea improved by sea-ice thickness initialization. *Sci. Rep.* 11 (1), 11475. doi: 10.1038/s41598-021-91042-4

Mortimer, C., Mudryk, L., Derksen, C., Luojus, K., Brown, R., Kelly, R., et al. (2020). Evaluation of long-term northern hemisphere snow water equivalent products. *Cryosphere.* 14 (5), 1579–1594. doi: 10.5194/tc-14-1579-2020

Niraula, B., and Goessling, H. F. (2021). Spatial damped anomaly persistence of the Sea ice edge as a benchmark for dynamical forecast systems. *J. Geophys. Res.: Oceans.* 126 (12), e2021JC017784. doi: 10.1029/2021JC017784

Ordoñez, A. C., Bitz, C. M., and Blanchard-Wrigglesworth, E. (2018). Processes controlling Arctic and Antarctic Sea ice predictability in the community earth system model. *J. Climate* 31 (23), 9771–9786. doi: 10.1175/JCLI-D-18-0348.1

Parkinson, C. L. (2019). A 40-y record reveals gradual Antarctic sea ice increases followed by decreases at rates far exceeding the rates seen in the Arctic. *Proc. Natl. Acad. Sci.* 116 (29), 14414–14423. doi: 10.1073/pnas.1906556116

Payne, G., Martin, J., Monahan, A., and Sigmond, M. (2022). *Seasonal predictions of regional and pan-Antarctic sea ice with a dynamical forecast system*. (Victoria, British Columbia, Canada).

Petty, A. A., Schröder, D., Stroeve, J. C., Markus, T., Miller, J., Kurtz, N. T., et al. (2017). Skillful spring forecasts of September Arctic sea ice extent using passive microwave sea ice observations. *Earth's. Future* 5 (2), 254–263. doi: 10.1002/2016EF000495

Purich, A., and England, M. H. (2019). Tropical teleconnections to Antarctic Sea ice during austral spring 2016 in coupled pacemaker experiments. *Geophys. Res. Lett.* 46 (12), 6848–6858. doi: 10.1029/2019GL082671

Qiao, F., Song, Z., Bao, Y., Song, Y., Shu, Q., Huang, C., et al. (2013). Development and evaluation of an earth system model with surface gravity waves. *J. Geophys. Res.: Oceans.* 118 (9), 4514–4524. doi: 10.1002/jgrc.20327

Raphael, M. N., and Handcock, M. S. (2022). A new record minimum for Antarctic sea ice. *Nat. Rev. Earth Environ.* 3, 1–2. doi: 10.1038/s43017-022-00281-0

Rienecker, M. (2008). *GEOS-5 data assimilation system–documentation of versions 5.0.1, 5.1.0, and 5.2.0. technical report series on global modeling and data assimilation, NASA/TM–2008–104606*, Vol. 27. 1–118.

Roach, L. A., Dörr, J., Holmes, C. R., Massonnet, F., Blockley, E. W., Notz, D., et al. (2020). Antarctic Sea Ice area in CMIP6. *Geophys. Res. Lett.* 47 (9). doi: 10.1029/2019GL086729

Saha, S., Moorthi, S., Wu, X., Wang, J., Nadiga, S., Tripp, P., et al. (2014). The NCEP climate forecast system version 2. *J. Climate* 27 (6), 2185–2208. doi: 10.1175/JCLI-D-12-00823.1

Schlosser, E., Haumann, F. A., and Raphael, M. N. (2018). Atmospheric influences on the anomalous 2016 Antarctic sea ice decay. *Cryosphere.* 12 (3), 1103–1119. doi: 10.5194/tc-12-1103-2018

Shi, X., Chen, Z., Wang, H., Yeung, D.-Y., Wong, W., and WOO, W. (2015). Convolutional LSTM Network : a machine learning approach for precipitation nowcasting. *Adv. Neural Inf. Process. Syst.* 28.

Steele, M., Eicken, H., Bhatt, U., Bieniek, P., Blanchard-Wrigglesworth, E., Wiggins, H., et al. (2021). Moving Sea ice prediction forward Via community intercomparison. *Bull. Am. Meteorol. Soc.* 1 (aop), 1–7. doi: 10.1175/BAMS-D-21-0159.1

Stuecker, M. F., Bitz, C. M., and Armour, K. C. (2017). Conditions leading to the unprecedented low Antarctic sea ice extent during the 2016 austral spring season. *Geophys. Res. Lett.* 44 (17), 9008–9019. doi: 10.1002/2017GL074691

Tebaldi, C., and Knutti, R. (2007). The use of the multi-model ensemble in probabilistic climate projections. *Philos. Trans. R. Soc. A: Mathematical. Phys. Eng. Sci.* 365 (1857), 2053–2075. doi: 10.1098/rsta.2007.2076

Tejedo, P., Benayas, J., Cajiao, D., Leung, Y.-F., De Filippo, D., and Liggett, D. (2022). What are the real environmental impacts of Antarctic tourism? unveiling their importance through a comprehensive meta-analysis. *J. Environ. Manage.* 308, 114634. doi: 10.1016/j.jenvman.2022.114634

Tonboe, R., Lavelle, J., Pfeiffer, R. H., and Howe, E. (2017) *Product user manual for OSI SAF global Sea ice concentration (Product OSI-401-b)*. Available at: http://osisaf.met.no/docs/osisaf_cdop3_ss2_pum_ice-conc_v1p6.pdf.

Verfaillie, D., Pelletier, C., Goosse, H., Jourdain, N. C., Bull, C. Y. S., Dalaiden, Q., et al. (2022). The circum-Antarctic ice-shelves respond to a more positive southern annular mode with regionally varied melting. *Commun. Earth Environ.* 3 (1), Article 1. doi: 10.1038/s43247-022-00458-x

Voldoire, A., Saint-Martin, D., Sénési, S., Decharme, B., Alias, A., Chevallier, M., et al. (2019). Evaluation of CMIP6 DECK experiments with CNRM-CM6-1. *J. Adv. Modeling. Earth Syst.* 11 (7), 2177–2213. doi: 10.1029/2019MS001683

Wang, J., Luo, H., Yang, Q., Liu, J., Yu, L., Shi, Q., et al. (2022). An unprecedented record low Antarctic Sea-ice extent during austral summer 2022. *Adv. Atmospheric. Sci.* 39, 1591–1597. doi: 10.1007/s00376-022-2087-1

Zampieri, L., Goessling, H. F., and Jung, T. (2019). Predictability of Antarctic Sea ice edge on subseasonal time scales. *Geophys. Res. Lett.* 46 (16), 9719–9727. doi: 10.1029/2019GL084096

Zhang, L., Delworth, T. L., Yang, X., Zeng, F., Lu, F., Morioka, Y., et al. (2022). The relative role of the subsurface southern ocean in driving negative Antarctic Sea ice extent anomalies in 2016–2021. *Commun. Earth Environ.* 3 (1), Article 1. doi: 10.1038/s43247-022-00624-1

frontiers | Frontiers in Marine Science

TYPE Original Research
PUBLISHED 29 June 2023
DOI 10.3389/fmars.2023.1171958

OPEN ACCESS

EDITED BY
John Falkingham,
International Ice Charting Working Group, Canada

REVIEWED BY
Jan L. Lieser,
Bureau of Meteorology, Australia
David Jackson,
Retired, Ottawa, ON, Canada

*CORRESPONDENCE
Lucy S. Vlietstra
Lucy.S.Vlietstra@uscga.edu

†PRESENT ADDRESS
Alexandra Darden,
Data and Digital Innovation, National Geospatial-Intelligence Agency, Springfield, VA, United States

RECEIVED 22 February 2023
ACCEPTED 17 May 2023
PUBLISHED 29 June 2023

CITATION
Vlietstra LS, Hinrichs KR, Bernstein ER, Darden A and Martino M (2023) Polar class ship accessibility to Arctic seas north of the Bering Strait in a decade of variable sea-ice conditions.
Front. Mar. Sci. 10:1171958.
doi: 10.3389/fmars.2023.1171958

Polar class ship accessibility to Arctic seas north of the Bering Strait in a decade of variable sea-ice conditions

Lucy S. Vlietstra[1*], Kayla R. Hinrichs[2], E. Rachel Bernstein[2], Alexandra Darden[3†] and Matthew Martino[3]

[1]Department of Marine Science, United States Coast Guard Academy, New London, CT, United States, [2]Research Directorate, National Geospatial-Intelligence Agency, Springfield, VA, United States, [3]United States National Ice Center, National Oceanic and Atmospheric Administration, Suitland, MD, United States

Surface atmospheric temperatures over the Arctic Ocean are rising faster than the global average, and sea-ice coverage has declined, making some areas newly accessible to ocean-going ships. Even so, Arctic waters remain hazardous to ships, in part, because of the highly variable nature of sea-ice formation and drift in some areas. In this study, we investigated interannual variability in polar class (PC) ship accessibility in the northern Bering Sea and seas north of the Bering Strait (East Siberian, Chukchi, Beaufort) from February 2012 to February 2022. We used sea-ice charts from the U.S. National Ice Center and calculations of the Risk Index Outcome *(RIO)* for PC3, PC5, and PC7 ships to characterize spatiotemporal trends in PC ship accessibility during the months of February, June, September, and November over the last 10 to 11 years. We also characterized shipping activity on select days in 2021. Overall, PC ship accessibility during the months of February and June increased over the last decade, especially for PC7 ships. However, areas that became more accessible over time did not support heavy ship traffic, possibly because they were not located on preferred transit routes or because they were surrounded by unnavigable ice, which made them inaccessible in practice. Ship accessibility was highly variable in the northernmost, offshore regions of the study site. During June, PC7 ship accessibility was interannually variable in waters south of the Bering Strait, and ships were active in those regions (most were fishing vessels), indicating potentially hazardous conditions during this time of year. Accessibility was considerably less variable over space and time (months, years) for PC5 (ice capable) ships and for PC3 ships (heavy icebreakers). Information from this study can be used by PC ship operators planning safe and successful shipping routes and by coastal states preparing emergency services to protect the maritime community. As governments and the private sector build out fleets of ice-capable ships, knowledge of interannual variability in ship accessibility will also help planners match PC ship capabilities to mission requirements.

KEYWORDS

Arctic, icebreakers, climate change, sea ice, Polar Code

1 Introduction

Surface atmospheric temperatures over the Arctic Ocean are rising 2–8 times faster than average global temperatures, driving pronounced declines in sea-ice coverage in recent decades (Meier, 2017; Stroeve and Notz, 2018; Årthun et al., 2021; Isaksen et al., 2022). Sea-ice declines are making some areas of the Arctic Ocean more accessible to ocean-going vessels, and ship traffic in the region has increased (Aksenov et al., 2017; PAME, 2020; Gunnarsson, 2021; Gunnarsson and Moe, 2021; PAME, 2021; Min et al., 2021). From 2013 to 2019, for example, the number of ships operating in the Arctic Ocean as defined by the International Code for Ships Operating in Polar Waters [Polar Code, International Maritime Organization (2017)] increased by 25%, and the distance sailed increased by 75% (PAME, 2020).

Expanding Arctic maritime traffic has prompted growing concern over risks to maritime transportation systems and mariner safety as shipping in the region remains dangerous, even for ice-strengthened ships (Marchenko et al., 2018; Vanhatalo et al., 2021). Among the hazards is the highly variable nature of sea-ice development and drift (Stephenson et al., 2013). Not only are changes occurring in the amount of sea-ice coverage over the Arctic Ocean as a whole, but smaller-scale processes, such as sea-ice formation and advection by surface currents, promote significant variability in ice concentration and thickness over local and regional spatial scales (Eicken, 2013; Meier, 2017).

Challenges that variable sea-ice conditions pose to vessel operators in the modern day are underscored by recent incidents of ships becoming beset in sea ice during Arctic operations (Kubat et al., 2013; Kubat et al., 2015). For example, more than 58 besetting incidents took place on the Northern Sea Route between 2013 and 2017 (Vanhatalo et al., 2021). In 2021, at least 18 ships were beset on the Northern Sea Route during the month of November alone. Some were frozen for weeks and required icebreaker support before they could resume their voyage (Bennetts, 2021).

Most ships have specific design limitations that restrict safe operation to open, ice-free water or, in the case of polar class (PC) ships, to ice of a certain concentration and thickness. Understanding where sea-ice conditions permit navigation for certain ships and the extent to which ice conditions are consistent (predictable) from month-to-month and year-to-year is critical for safe and efficient maritime transportation and operational planning, especially route planning for multi-day voyages or transits. Such awareness is also important for fleet managers, who need to understand operational conditions if they are to ensure sufficient ship design and capability requirements for newly built ships.

In this study, we characterize interannual variability in ship accessibility relating to sea-ice conditions in a 3.6 million km^2 region of the Arctic Ocean encompassing the northern Bering Sea, Chukchi Sea, western Beaufort Sea, and East Siberian Sea (Figure 1). The region includes the Bering Sea north of the Pribilof Islands and the Bering Strait, which serves as a chokepoint for vessel entry into

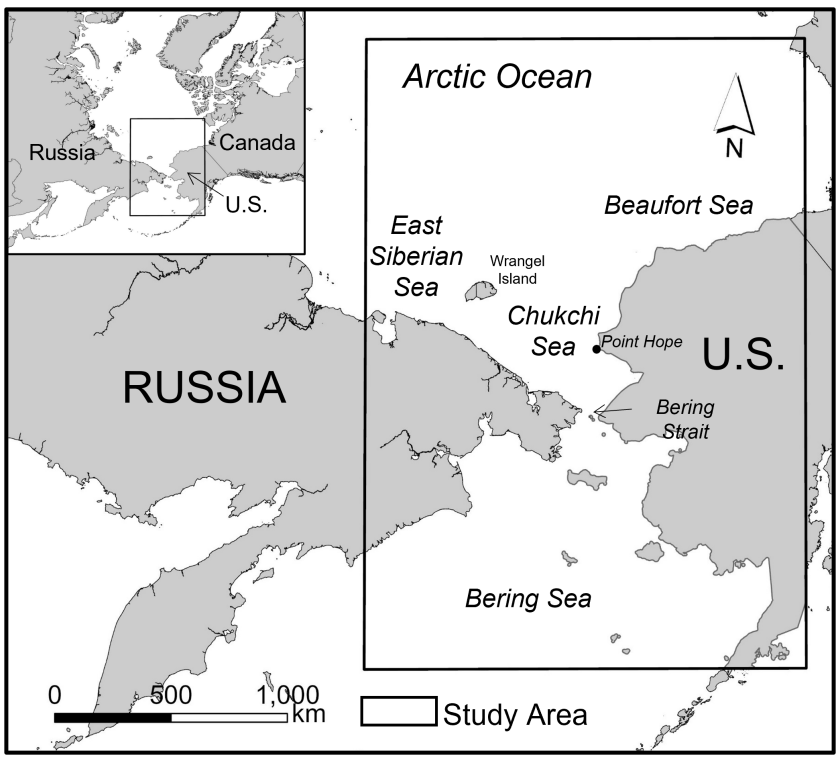

FIGURE 1
Study site, including the northern Bering Sea, Chukchi Sea, Beaufort Sea, and East Siberian Sea (Esri, 2022a).

the Arctic region. The region also supports a growing volume of commercial maritime traffic, a trend that is projected to continue with the ongoing decline in sea-ice coverage (U.S. Committee on the Marine Transportation System, 2019). Specifically, we address the following questions:

(1) How has the area accessible to PC ships within the study site changed over the last decade?
(2) When and where is interannual variability in PC ship accessibility the greatest?
(3) To what extent do ships (PC and other vessels) currently operate in newly accessible areas or areas with high interannual variability in ship accessibility?

We chose to focus on accessibility for PC ships during the months of February, June, September, and November over the last 10 years. Ships with a PC rating are built to safely navigate a defined range of ice conditions, which determines their assigned rating (PC1–PC7) within the *Unified Requirements for PC Ships* (International Association of Classification Societies, 2016). Not all ships built for ice operations have ratings defined by the PC system; some regions of the world use other classification systems, and the PC rules do not apply to ship built prior to July 2007. However, the polar classes serve as an effective proxy for most ice-strengthened ships (PC6–PC7), ice-capable ships (PC4–PC5), and icebreakers (PC1–PC3).

The four months used in this analysis were chosen because they represent the time of year when Arctic sea ice is near the annual maximum extent and ships are active in the region (Feb), when the Arctic shipping season typically begins (Jun), when sea ice reaches the annual minimum extent (Sep), and when the shipping season typically ends (Nov; Eguíluz et al., 2016). An analysis of ship accessibility during these months should provide operators and planners with key insights into ship capabilities required for desired operational ranges during the most restrictive and the most permissive ice conditions in the study area.

We recognize that risk posed to vessels by interannual fluctuations in ice conditions is a function of not only sea-ice conditions but also of ship activity in those regions. If ships do not operate in areas where ice conditions are highly variable, then risk posed by those conditions is likely minimal. To evaluate this possibility for the most recent calendar year, we overlaid shipping activity on select days during February, June, September, and November 2021 onto maps of interannual variability in ship accessibility developed in the first part of the study.

2 Materials and methods

We conducted this study with sea-ice information from the U.S. National Ice Center and a model developed in Python (IceMaps.py). The model converts sea-ice conditions into measures of ship accessibility for a range of PC ships. The conversion is based on design characteristics of PC ships known to affect a vessel's ability to operate in ice. Characteristics are defined by the International Association of Classification Society's *Unified Requirements for Polar Class Ships*, which establishes seven categories of PC ships: PC1, PC2, PC3, PC4, PC5, PC6, and PC7 (Table 1). The PC system is not based on a ship's functional role (e.g., breaking ice, escorting other ships) but rather on its design specifications and whether the ship can safely operate in a particular ice environment. We limited the analysis to PC3 (heavy icebreakers), PC5 (light icebreakers), and PC7 (ice-capable) ships because they represent the range of ice-strengthened vessels for which movements are most likely restricted by ice conditions in the Arctic Ocean. We did not consider PC2 and PC1 ships because they are capable of navigating most ice conditions.

Sea-ice information was obtained from ice charts produced by the U.S. National Ice Center. These charts are based on ice observations made from synthetic aperture radar satellite imagery, optical imagery, and other ancillary data. To produce the charts, trained ice analysts use a standardized methodology to classify imagery according to observed ice concentration (in a range of tenths) and stage of ice development. Stage of development relates to new ice, young ice, thin first-year ice, first-year medium ice, first-year thick ice, old (multi-year) ice, and glacial ice. On November 1, 2021, analysts replaced the categories for first-year ice (thin, medium, thick) with a single category, first-year ice. This update affects PC5 and PC7 calculations in November 2021 and February 2022, but the impact on our results appeared minimal and did not affect key findings.

Each sea-ice chart contains multiple polygons identifying various sea-ice characteristics, including sea-ice concentration and stage of development. This work was performed for the entire Arctic Ocean on a weekly basis before November 1, 2021, and on a bi-weekly basis thereafter. The results are shared as shapefiles and other geospatial products on the U.S. National Ice Center website.[1]

We obtained sea-ice charts for the first available dates in the months of interest for each year between February 1, 2012, and February 3, 2022 (Table 2; Figure 2). By stratifying the analysis by the first week of each month, we sought to minimize variability due to within-season trends in ice cover. To produce PC ship-accessibility maps from the ice charts, we ran the IceMaps.py model with the ice charts as inputs. The model used an established algorithm for calculating the Risk Index Outcome *(RIO)* from sea-ice concentration and stage of development (i. e., ice type):

$$RIO = \sum_{i=1}^{n} (C_i \times RV_i),$$

where

C_i = concentration (in tenths) of ice type i within an ice regime, and

RV_i = risk value for a given ship's PC designation for ice type i.

The *RIO* is a single value representing operational risk for a PC ship traveling through an area with a given ice regime, or combination of ice types within a region of interest. The metric was originally developed as an ice numeral *(IN)* for the Transport Canada Arctic Ice Regime Shipping System (AIRSS) (Transport

1 https://usicecenter.gov/Products/ArcticData

TABLE 1 Description of sea ice navigable by ships in each polar class.

Polar Class (PC)	Ice Description
PC 1	Year-round operation in all polar waters
PC 2	Year-round operation in moderate multi-year ice (>120 cm) conditions
PC 3	Year-round operation in second-year ice (>120 cm), which may include multi-year ice inclusions
PC 4	Year-round operation in thick first-year ice (>120 cm), which may include old ice inclusions
PC 5	Year-round operation in medium first-year ice (70–120 cm), which may include old ice inclusions
PC 6	Summer/autumn operation in medium first-year ice (70–120 cm), which may include old ice inclusions
PC 7	Summer/autumn operation in thin first-year ice (30–70 cm), which may include old ice inclusions

Measurements refer to sea-ice thickness (cm).
Ice descriptions are from on World Meteorological Organization Sea Ice Nomenclature (WMO, 2014).

Canada, 1998). The AIRSS system was later updated to align with the Polar Operational Limitations Assessment Risk Indexing System (POLARIS), which reflects capabilities of the PC classification system. Like the *IN* in AIRSS, the *RIO* in POLARIS considers characteristics of all ice types in the regime and known capabilities of a ship to safely navigate those conditions (Stoddard et al., 2016).

In POLARIS, PC ship capabilities for ice operations are reflected in the risk value *(RV)* parameter. The *RV* is a known value ranging from -3 to +3 for PC1–7 ships, indexed to a ship's structural characteristics determining its ability to navigate ice of a certain developmental stage. Positive risk values are used when a ship is structurally capable of navigating a particular ice type. Negative values are used when a ship is not structurally capable. Values of C_i range from 1 to 10 and represent the concentration (in tenths) of ice type i and the portion (in tenths) of sea surface that is ice-free. In this study, "ice-free" refers to water where ice concentrations are < 10% (i.e., up to 1/10 surface coverage). This terminology follows ice classification protocols used by the U.S. National Ice Center.[2] Because a given ice regime may contain several ice types, the products of C and RV are summed across all ice types in the regime, including the area occupied by ice-free water, to derive a single *RIO* value ranging from -30 to +30. If $RIO \geq 0$, the regime as a whole is considered accessible. If $RIO < 0$, the regime is considered inaccessible.

In this study, we used risk values prescribed by the International Maritime Organization's Polar Code Advisory (American Bureau of Shipping, 2016), with one exception: $RV = -1$ was applied to PC3 ships encountering both light and heavy multi-year ice, because the original sea-ice files did not distinguish between categories of multi-year ice. Ship-accessibility maps produced in this study consisted of multiple polygons, each representing the associated *RIO* calculated for a PC ship of interest. An example of ship-accessibility maps produced for a single date in 2021 is shown in Figure 3.

Spatio-temporal patterns in ship accessibility were visualized in ArcGIS Pro 2.9.3 (Esri, 2022b), where we uploaded ship-accessibility maps clipped to the study site. For each PC ship type, we summed the total area encompassed by polygons classified as ice-free water ($RIO = 30$), accessible ice cover ($0 \leq RIO < 30$), and inaccessible ice cover ($RIO < 0$). Outside of ArcGIS, we used analysis of variance (ANOVA) to compare the monthly mean area of the study site accessible to PC3, PC5, and PC7 ships over the 10-11 years of the study. We used a Student's t-test for two-sample comparisons when ANOVA results indicated significant differences in accessibility among months.

We then overlaid a 10-km^2 mesh grid (51,164 cells) onto the study site and used the spatial join geoprocessing tool ArcGIS to associate the *RIO* value calculated for each polar class with each grid cell. This was done separately for each month, February, June, September, and November. We used a non-parametric Mann-Kendall trend test in MATLAB (The MathWorks Inc., 2021) to identify cells with significantly increasing or decreasing *RIO* values over the 10-11 years of the study. Results were visualized in ArcGIS for each month x PC ship type combination. All statistical tests were performed with $\alpha = 0.05$.

Interannual variability in ship accessibility was also calculated from ship-accessibility maps. In ArcGIS, we used the same 10-km^2 mesh grid to calculate the range of *RIO* values (RIO_{range}) in each cell (j), for each month (k), and each PC ship type (l) across all years of the study:

$$RIO_{range} = RIO_{max,jkl} - RIO_{min,jkl}$$

where

$RIO_{max,jkl}$ = maximum *RIO* value in cell j during month k for PC l, and

$RIO_{min,jkl}$ = minimum *RIO* value in cell j during month k for PC l.

Spatial patterns in interannual variability in PC ship accessibility were visualized by mapping RIO_{range} in each 10-km^2 cell across the study site for each $k \times l$ combination.

We used satellite-based Automatic Identification System (AIS) data provided by the U.S. Coast Guard Navigation Center to assess the extent to which ships operated in areas of high interannual variability or consistent gain/loss in ship accessibility. The AIS is a broadcast system in which certain ships carry Class A very high frequency (VHF) transceiver-receptors that transmit the ship's position (latitude–longitude) and other information to satellites and coastal ground stations at regular time intervals while the ship

2 Distributed ice fragments in areas where sea ice is present in concentrations <10% represent a safety hazard for non-ice-class ships; but small amounts of ice in areas that are largely ice-free may be difficult to detect in satellite imagery. Most ice fragments in the Bering Sea study region consist of relatively young ice. Glacial ice (e.g., icebergs, bergy bits, and growlers), on the other hand, is older and denser and therefore potentially more damaging to ship structures if struck. Glacial ice is less common in the Bering Sea than in other regions of the Arctic.

10.3389/fmars.2023.1171958

TABLE 2 Dates of weekly sea-ice shapefiles used in this study.

Year	Season (Northern Hemisphere)			
	Winter	Spring	Summer	Autumn
2012	Feb 13	Jun 04	Sep 10	Nov 05
2013	Feb 11	Jun 03	Sep 09	Nov 07
2014	Feb 06	Jun 05	Sep 02	Nov 06
2015	Feb 05	Jun 04	Sep 03	Nov 05
2016	Feb 04	Jun 02	Sep 01	Nov 03
2017	Feb 02	Jun 01	Sep 07	Nov 02
2018	Feb 01	Jun 07	Sep 06	Nov 01
2019	Feb 01	Jun 06	Sep 05	Nov 08
2020	Feb 07	Jun 04	Sep 03	Nov 05
2021	Feb 04	Jun 04	Sep 02	Nov 04
2022	Feb 03	—	—	—

is underway (Fournier et al., 2018; U.S. Coast Guard, 2022). The International Maritime Organization mandates that certain ships (e.g., ≥ 300 GT on international voyage) utilize Class A AIS transceivers. Class B transceivers are carried by other vessels on a voluntary basis. For this study, we obtained position reports produced by all ships, both PC and non-ice-strengthened, with Class A and Class B transceivers that were present in the study area on February 3–5, 2021, June 3–5, 2021, September 1–3, 2021, and November 3–5, 2021. These dates coincide with the date (± 24 hr) when 2021 ice charts were available from the U.S. National Ice Center. We focused on shipping activity in 2021 because it was the most recent calendar year for which AIS data were available in all four months.

Automatic Identification System datasets were pre-processed to remove duplicate reports as well as reports from non-ship platforms (e.g., buoys, beacons) and ships with <10 position reports during the month of interest. We uploaded the position reports into ArcGIS and overlaid them on maps of significant gain/loss of PC7 ship accessibility and interannual variability (RIO_{range}). Maps for PC7 ships were used for this comparison because their capabilities for ice navigation most closely resemble those of commercial ships, which are not ice-strengthened but compose the majority of ships in the

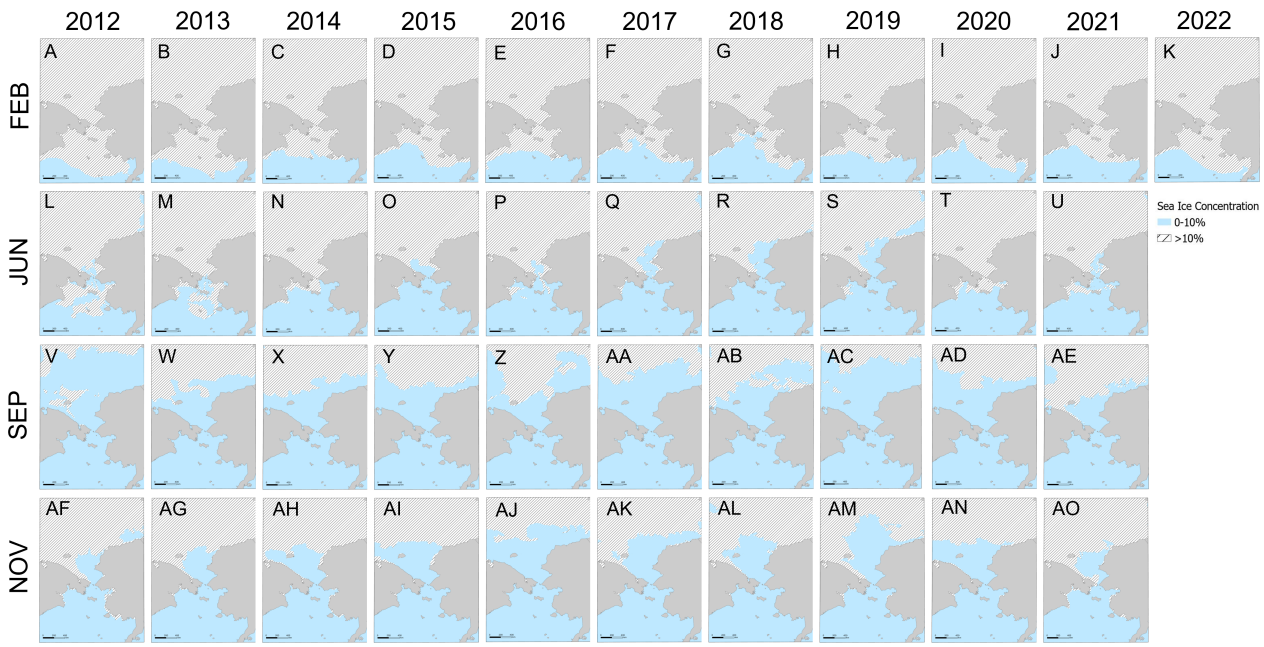

FIGURE 2
Sea-ice maps for select dates in February (A–K), June (L–U), September (V–AE), and November (AF–AO). Table 2 lists dates for which sea-ice coverage is depicted in each map. Hatched regions show areas where ice concentration is >10%.

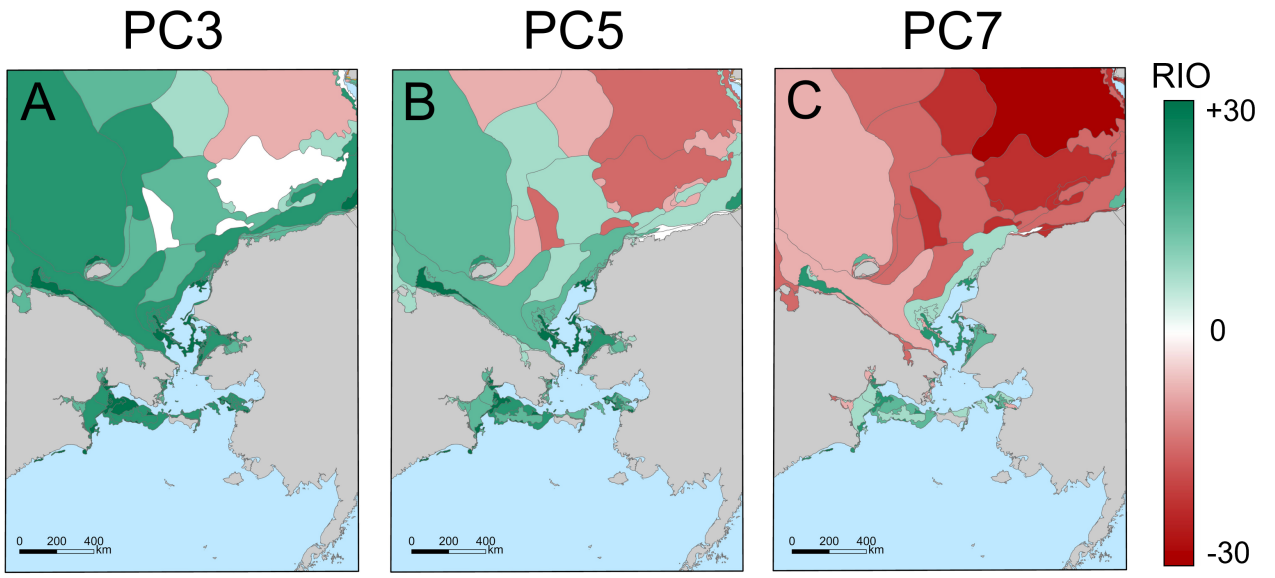

FIGURE 3
Ship-accessibility maps for PC3 **(A)**, PC5 **(B)**, and PC7 **(C)** ships on June 4, 2021. Polygons depict RIO_{range} values on a scale ranging from -30 to +30. Ice-free water is shown in light blue.

study area. We used the spatial join geoprocessing tool to identify the RIO_{range} coincident with each position report to quantify extent of overlap with interannual variability.

We defined areas of "high" interannual variability as those with RIO_{range} > 30. These values signified areas that shifted between accessible and inaccessible to a PC7 ship between two or more years during the study. To evaluate whether ships operated in these areas, we used the spatial join processing tool in ArcGIS to calculate the number and proportion of all vessels present where RIO_{range} > 30.

3 Results

3.1 Changes in spatial extent of accessible area

Hereafter, we use the term "accessible" to refer to areas of either ice-free water or water that was ice-covered but navigable for a particular PC ship. Ice-free water was accessible to all ships, but access to ice-covered water varied among the polar classes. This led to differences in the total area (km^2) accessible to PC3, PC5, and PC7 ships when all four months were combined ($F_{2,122}$ = 30.34, P< 0.001, Figure 4).

On average, more area within the study site was accessible to PC3 ships (3.26 × 10^6 km^2) than to PC5 ships (2.94 x 10^6 km^2; t_{80} = 4.38, P< 0.001), and more area was accessible to PC5 ships than to PC7 ships (2.46 x 10^6 km^2; t_{80} = 4.05, P< 0.001). This pattern was driven mainly by seasonal (monthly) differences in accessibility , with less area accessible to PC5 and PC7 ships in February and June than in September and November (PC7, $F_{3,40}$ = 71.57, P< 0.001; PC5, $F_{3, 40}$ = 9.73, P< 0.001). June was especially restrictive to PC7 ships (Figure 5). In contrast, the area accessible to PC3 ships was relatively uniform across the four months ($F_{3, 40}$ = 2.37, P = 0.086). The area accessible to ships in all three polar classes was similar in November ($F_{2, 29}$ = 0.80, P = 0.460, Figure 5).

We found a weak but increasing linear trend in the area of the study site accessible to PC3, PC5, and PC7 ships during February and June over the 10–11-year study period and to PC3 and PC5 ships in September. The rate of increase was greatest for PC7 ships in February (76,998 km^2/yr, Figure 6A; Table 3) and is equivalent to PC7 ships gaining access to an additional 21% of the study site over a period of 10 years. Positive trends were also substantial in June (PC3: +59,117 km^2/yr; PC5: +57,145 km^2/yr, Figure 6B; Table 3). Temporal trends were only slightly positive or moderately negative in September. Accessibility declined in November for all three polar classes, with the greatest rate of decline evident for PC7 ships (Figures 6C, D; Table 3).

Consistent with increasing trends in ship accessibility at the spatial scale of the study site, we detected significant (P< 0.05) positive and negative trends in *RIO* values at smaller (10-km^2) spatial scales within the study site. These areas are shown in Figure 7, in dark green and red, respectively. Areas that were always accessible to a given PC ship are shown in light green. Areas that were always inaccessible are shown in dark gray.

The total areal extent of the study site in which ship accessibility trended from inaccessible to accessible far exceeded those which shifted from accessible to inaccessible. When the four months were combined, the ratio of area gained to area lost (gain:loss) was 32:1 for PC3 ships, 16:1 for PC5 ships, and 25:1 for PC7 ships (Figure 8). Significant trends in accessibility were only seen north of the Bering Strait. The areal extent of positive *RIO* trends was greatest for PC7 ships, especially in February. These areas include waters off the coast of the Russian Far East, including those south and northwest of Wrangel Island, as well as Chukchi Sea waters north of Point Hope, Alaska (Figure 7I). In June, areas where PC7 ships gained access included the Chukchi Sea region immediately adjacent to a

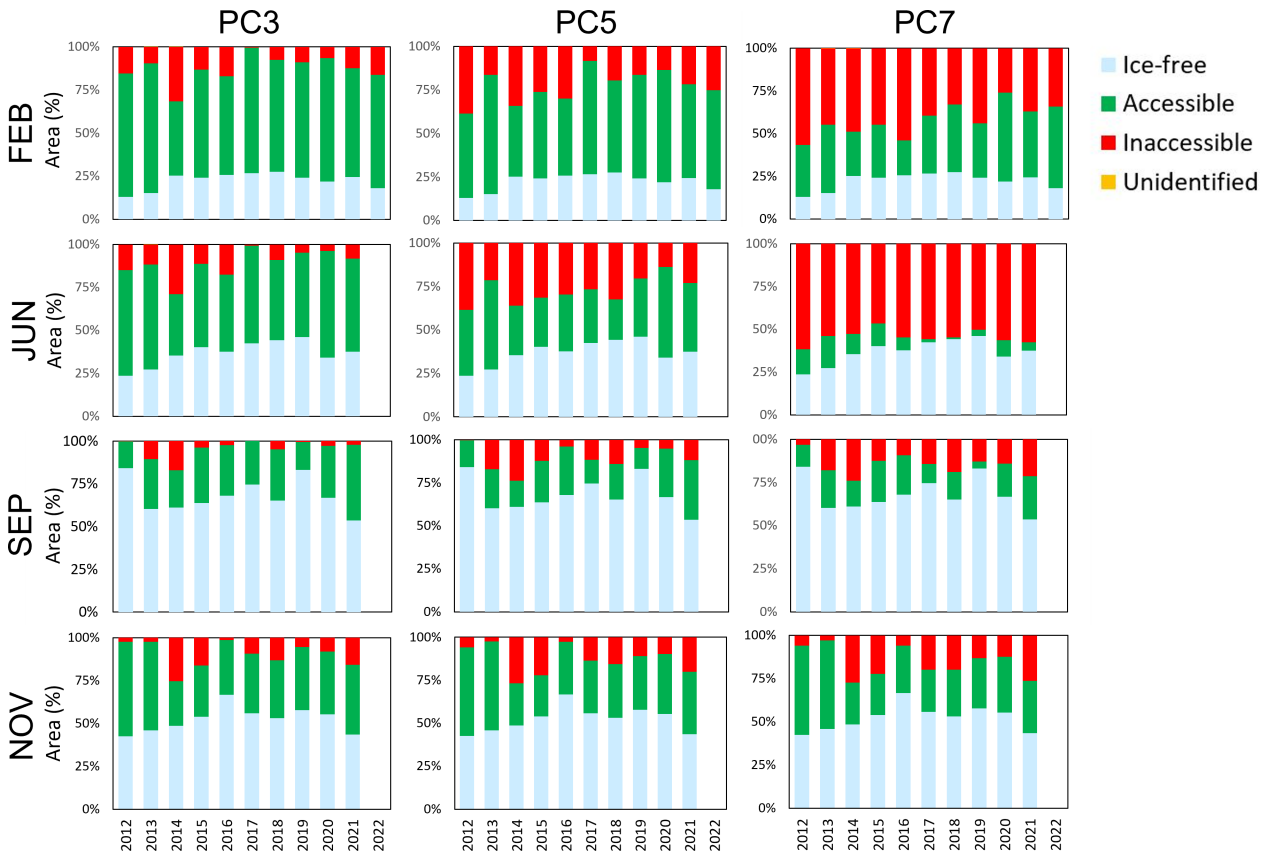

FIGURE 4
Percentage of the study site that was ice-free (*RIO* = 30), ice-covered but accessible (0≤ *RIO* < 30), and inaccessible (*RIO* < 0) due to ice conditions in February, June, September, and November. Small portions of the study site (< 0.04%) lacked information on ice stage of development in February 2013, June 2013, and June 2014. We report ship accessibility in those areas as "unidentified."

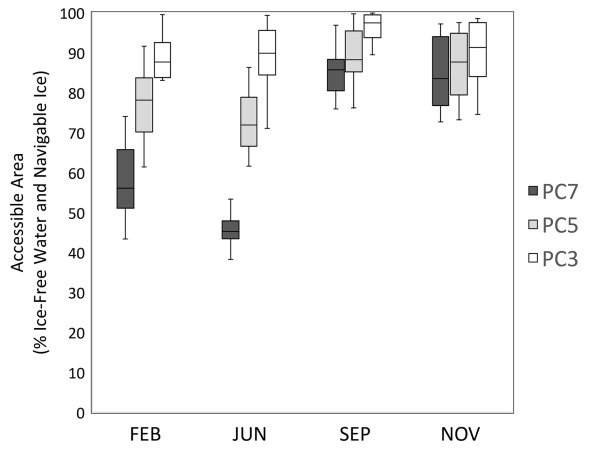

FIGURE 5
Box plot of the percentage of the study site that was accessible (ice-free or ice-covered but navigable) to PC3, PC5, and PC7 ships. Within each box, the horizontal line denotes the median value. Boxes extend from the 25th to the 75th percentile of each group's distribution of values. Bars denote the minimum and maximum values. FEB = February, JUN = June, SEP = September, NOV = November.

large region of inaccessible sea ice (Figure 7J). Gains for PC5 and PC3 ships were greatest in June and included some areas that were inaccessible to PC7 ships in every year throughout the study period (Figures 7B, F).

In September and November, areas with significant change were considerably smaller than those in February or June, and areas where accessibility increased over time were roughly similar in size to areas where accessibility decreased (Figure 8). In addition, cells that gradually shifted from accessible to inaccessible, i.e., negative *RIO* trends, were located only in the northernmost reaches of the study site (Figure 7).

3.2 Interannual variability in ship accessibility

Figure 9 shows the distribution and magnitude of interannual variability in PC3, PC5, and PC7 ship accessibility in the months of February, June, September, and November. Areas that were ice-free every year of the study are shown in light blue. Areas that were always accessible, i.e., either open water or navigable ice cover (*RIO* = 0–30) every year, are shown in light green. Dark grey areas were always inaccessible, i.e., unnavigable ice cover (*RIO* < 0) every year.

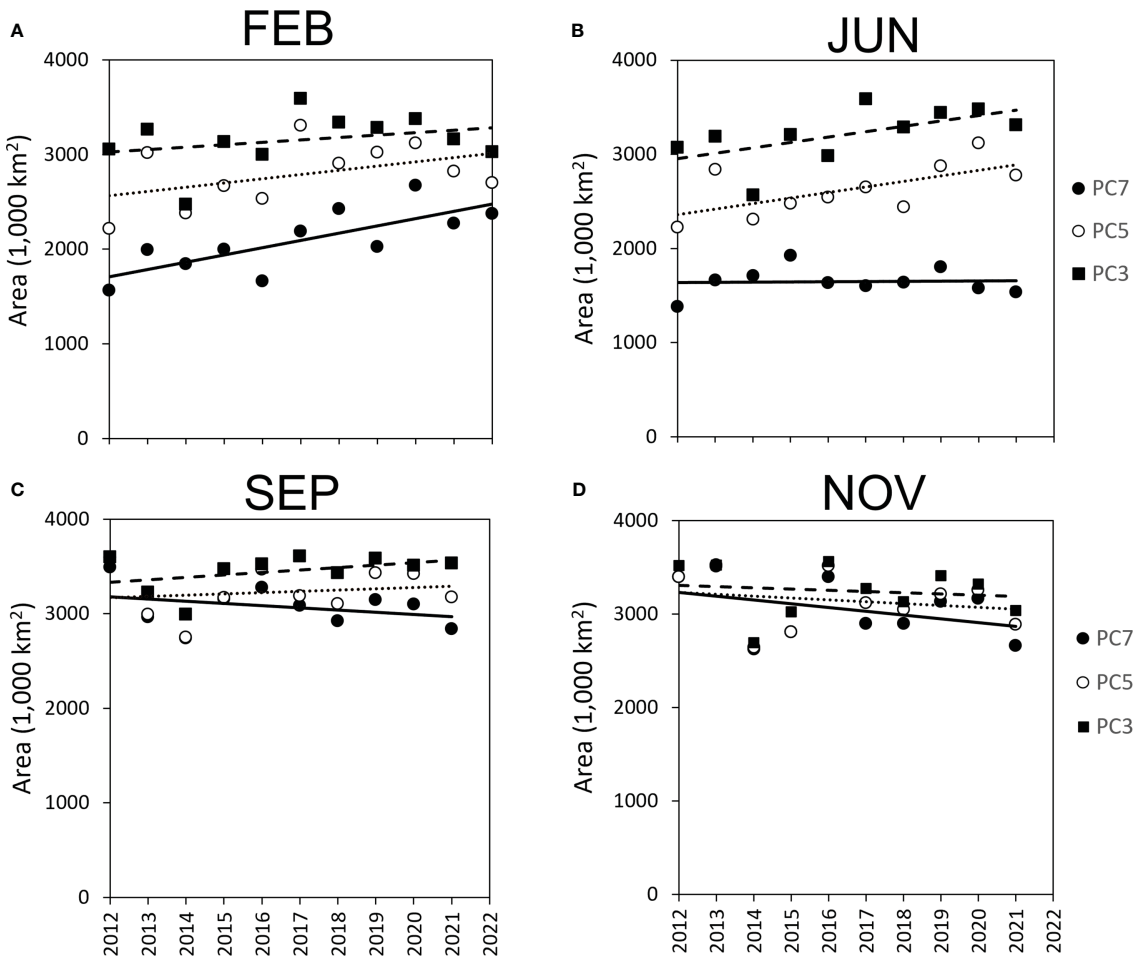

FIGURE 6
Area of the study site accessible (ice-free or ice covered but accessible) to PC3, PC5, and PC7 ships in the months of **(A)** February, **(B)** June, **(C)** September, and **(D)** November.

Areas in graduated shades of orange fluctuated between accessible ($RIO \geq 0$) and inaccessible ($RIO < 0$) at least once during the study period. Darker shades of orange indicate cells with higher values of RIO_{range}, with the maximum RIO_{range} being 60.

Overall, interannual variability in ship accessibility was greatest for PC7 ships, with RIO_{range} values routinely exceeding 40 (Figures 9I–L). For ships in all three polar classes, the month of February was least variable (Figures 9A, E, I). In June, interannual variability for PC7 ships was high ($RIO_{range} > 30$) in the southern portion of the study site, south of the Bering Strait. These areas were located immediately adjacent to consistently ice-free water. A large region north of the Bering Strait was always inaccessible to PC7 ships during the month of June, which included the region adjacent to the coastline of the Russian Far East and water surrounding Wrangel Island (Figure 9J). Also in June, PC7 ship accessibility was highly variable from year to year in the Chukchi Sea, north of Alaska, with $RIO_{range} > 50$ (Figure 9J).

In September, much of the water in the northern Bering Sea (south of the Bering Strait) and southern Chukchi Sea was always ice-free over the last decade (Figures 9C, G, K). However, the majority of ocean surface north of the Chukchi Sea, from the East Siberian Sea to the Beaufort Sea, showed a high degree of interannual variability, especially for PC7 ships (Figure 9K). Most of the region was characterized by $RIO_{range} > 30$. A similar pattern occurred in November, with one important difference being the presence of small regions of the Beaufort Sea, offshore northern Alaska, with the maximum observed RIO_{range} (Figure 9L). This value signifies a region where, over the last ten years, PC7 ships would have encountered at least one year of maximum inaccessibility due to ice conditions ($RIO = -30$) and at least one year of maximum accessibility in ice-covered water and/or ice-free water ($RIO = 30$). Also notable about November was the relatively large portion of the Chukchi Sea that was always either ice-free or ice-covered yet still accessible to PC7 ships (Figure 9L).

Interannual variability in ship accessibility for PC3 and PC5 ships was similar to that for PC7 ships in terms of spatial and seasonal patterns; however, the RIO_{range} was comparatively lower for PC3 and PC5 ships (Figure 9). For example, Figure 9 shows large areas that were always accessible to PC5 and PC3 ships (i.e., light green areas) but inaccessible to, or highly variable for, PC7 ships (Figures 9I, L). In general, RIO_{range} values were often roughly 10 units lower for PC5 ships than for PC7 ships. In all months, RIO_{range}

TABLE 3 Area (%, 1,000 km^2) of the study site that was ice-free or ice-covered but accessible to PC3, PC5, and PC7 ships.

Month	Polar Class (PC)	% Area Ice-Free or Ice-Covered and Accessible (2012–2022)	Annual Rate of Change (1,000 km^2/yr)
February	PC3	68–100%	+25.6
	PC5	61–92%	+44.9
	PC7	43–74%	+77.0
June	PC3	71–99%	+57.1
	PC5	62–86%	+59.1
	PC7	38–53%	+2.2
September	PC3	83–100%	+26.2
	PC5	76–100%	+13.3
	PC7	76–97%	-23.2
November	PC3	75–99%	-13.1
	PC5	73–98%	-19.8
	PC7	73–97%	-40.5

Annual rate of change in ice-free and accessible regions is derived from the slope of the linear trendline.

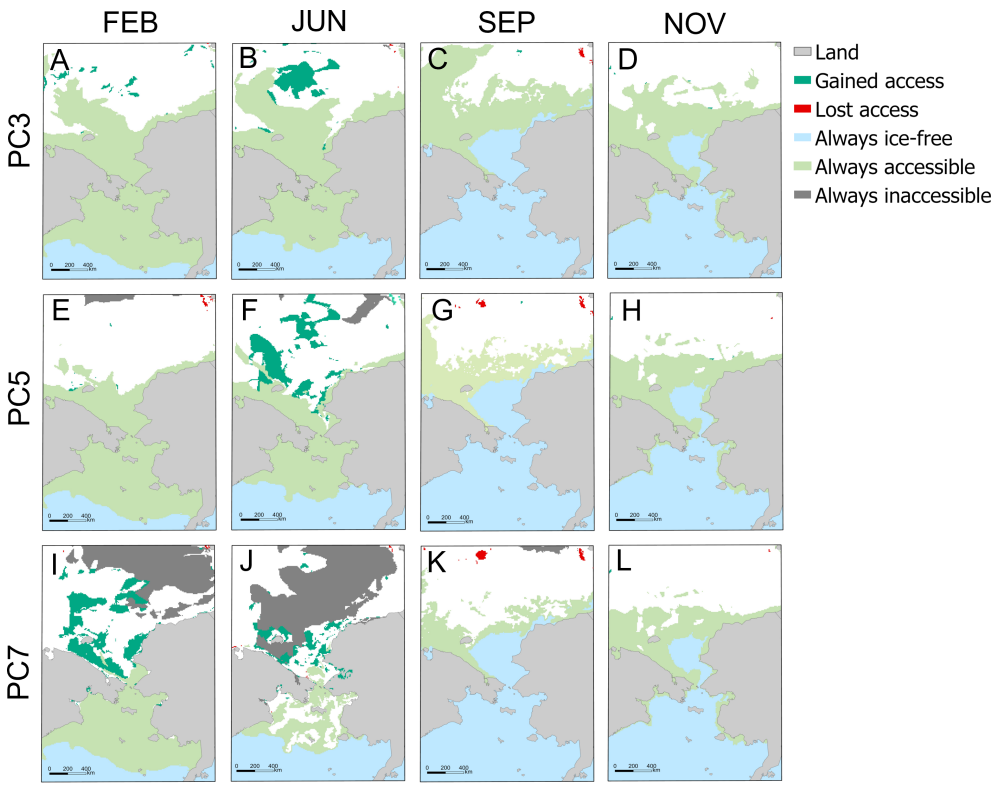

FIGURE 7
Significant trends in Risk Index Outcome (*RIO*) calculated for PC3 **(A–D)**, PC5 **(E–H)**, and PC7 **(I–L)** ships in the months of February (n = 11 yr), June (n = 10 yr), September (n = 10 yr), and November (n = 10 yr). Dark green indicates positive accessibility trends (from inaccessible to accessible), and red indicates negative accessibility trends (from accessible to inaccessible) (Mann-Kendall Trend test: $P < 0.05$).

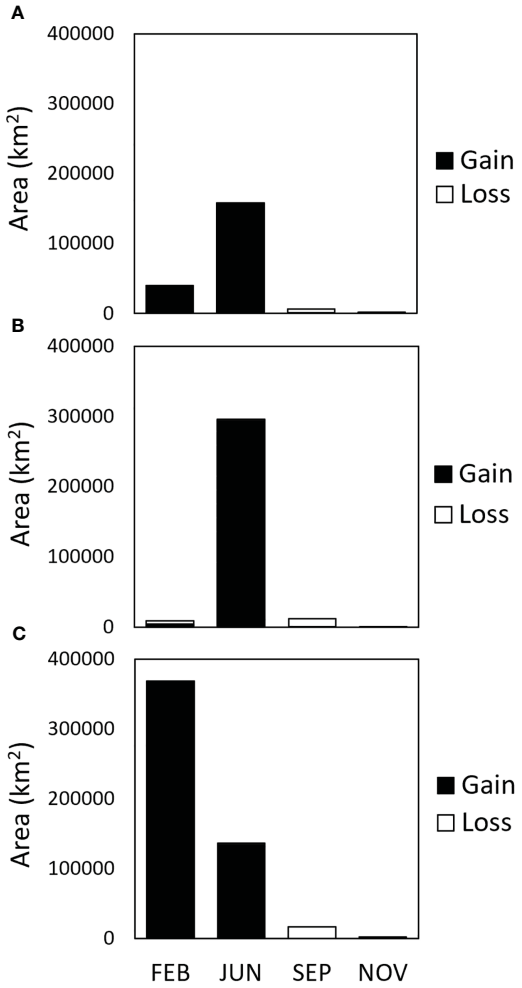

FIGURE 8
Area (km^2) of the study site where PC3 **(A)**, PC5 **(B)**, and PC7 **(C)** ships gained access and lost access due to changing sea-ice conditions from February 2012 to February 2022.

values in the northernmost regions of the study site were often roughly 10 units lower for PC3 ships (Figures 9A, D) than for PC5 ships (Figures 9E, H).

3.3 Case study: shipping activity in 2021

Ships were present both north and south of the Bering Strait during the three-day periods examined in February, June, September, and November 2021 (Figure 10). The vast majority of position reports (>99.6% of 3,159,888 reports) were produced by ships with Class A transceivers. The greatest number of vessels in the study site occurred on the three days of interest in September (n = 348 ships), followed by June (n = 255 ships), November (n = 161 ships), and February (n = 151 ships, Figure 10).

Most ship traffic in this analysis took place south of the Bering Strait (Figure 10). This region was usually ice-free or covered in ice accessible to PC7 ships but not to non-ice-strengthened vessels, such as most commercial ships. All ships present south of the Bering Strait on February 3–5, 2021, operated in areas of open water or water that was ice-covered but still accessible to PC7 ships. The same is true of most ships (95% of 348 ships) present during September 1–3, 2021 (Figures 10C, G) and November 3–5, 2021 (94% of 161 ships; Figures 10D, H). In contrast, over one-third (35% of 255 ships) of ships present during June 3–5, 2021, operated where interannual variability in PC7 ship accessibility was high (Figure 10F). Of those, over two-thirds (68% of 90 vessels) were commercial fishing vessels, which are usually not ice-strengthened (Table 4).

Relatively few ships were active north of the Bering Strait in February and June. In February, one ship travelled in the East Siberian Sea, where interannual variability in PC7 ship accessibility was low, passing through an area where accessibility had significantly increased since 2012. In June, one ship was underway on the Chukchi Sea, and two ships operated within 20 km of the northern coast of Alaska. September and November had heavier maritime traffic north of the Bering Strait (Figures 10C, D, G, H), when multiple vessels travelled within 200 km of the northern coastline of Russia and the United States (Alaska). None of these areas showed significant increasing or decreasing trends in accessibility over time (Figures 10C, D). In September, four ships were underway > 500 km offshore mainland Russia in the East Siberian Sea and central Arctic Ocean, where PC7 ship accessibility was highly variable from year to year (Figure 10G).

4 Discussion

This study takes a practical approach to understanding interannual variability in PC ship accessibility in a region of the Arctic Ocean known to support a growing volume of maritime traffic (U.S. Committee on the Marine Transportation System, 2019). Although we do not directly address accessibility for ships that are not ice-strengthened, and there are many operating in the region, our results do have applications for maritime planning in general, since PC ships represent the upper limit of operational capabilities for any vessel underway in the Arctic. Specifically, we identify overall trends in PC ship accessibility related to ice conditions encountered by ships in the northern Bering Sea, Chukchi Sea, East Siberian Sea, and Beaufort Sea over the last 10-11 years. We also identify ocean areas where PC ship accessibility has been most unpredictable from year to year and areas where it has been most predictable. We also identify areas that have become more accessible and those that have become less accessible to PC ships over time. We do not, however, provide prescriptive recommendations or a formal risk evaluation for a given ship class. Rather, we offer comprehensive information on ship accessibility relative to spatiotemporal trends in sea-ice coverage to enable situational awareness of the operational environment in ice-prone waters. This information could be incorporated into future analyses of maritime risk.

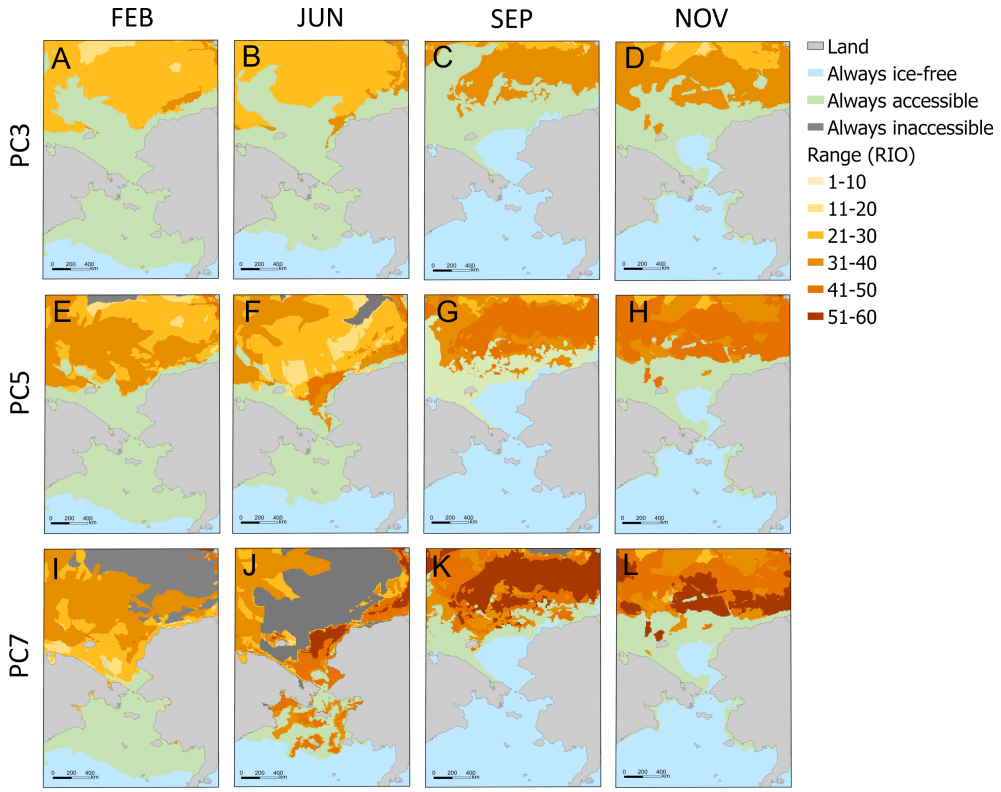

FIGURE 9
Range of Risk Index Outcomes (RIO_{range}) calculated for PC3 **(A–D)**, PC5 **(E–H)**, and PC7 **(I–L)** ships in the months of February, June, September, and November during the study period.

4.1 Spatial extent of accessible area

Seasonal patterns in PC7 ship accessibility were generally consistent with well-documented seasonal patterns in sea-ice coverage across the Arctic Ocean as a whole, namely, sea-ice development in the autumn and winter and sea-ice melt in the spring and summer. In general, PC7 ships are built to operate in thin, first-year ice, and we found they had access to a relatively small portion of the study site in the winter and spring months of February and June compared to later months. This is around the time when sea-ice extent in the Arctic Ocean reaches an annual maximum (February–March). In the spring (May–June), seasonal ice thaws, breaking up near the ice edge. During the months of both February and June over the last 10 to 11 years, we found a positive linear trend in PC ship accessibility, with *RIO* values increasing fastest for PC7 ships. The trend suggests a long-term decline in ice concentration and thickness in the region during winter and spring months, which aligns with patterns in winter sea-ice extent across the greater Arctic Ocean. The National Snow and Ice Data Center reports that winter sea-ice extent has declined at a rate of 2.6–2.8% per decade since 1979 (Stroeve and Notz, 2018; NSIDC, 2022a). Some of the areas within the study site that became more accessible to PC7 ships over the last 10 to 11 years include offshore locations in the East Siberian Sea, Chukchi Sea, and Beaufort Sea. Represented in dark green color in Figure 7, these regions occur up to 900 km offshore and are most widespread during February and June. They represent grid cells in which *RIO* values gradually shifted from mostly negative values to mostly positive values, indicating a progressive decline in sea-ice concentration or a trend away from older (thicker) ice and toward younger (thinner) ice.

Areas where PC5 and PC3 ship accessibility progressively increased also occurred in the northernmost regions of the study site but were smaller than areas of increase in PC7 ship accessibility. They were also more prominent in June than in February, which is different from the PC7 pattern. Some of the regions becoming more accessible to PC5 and PC3 ships in June remained inaccessible to PC7 ships, reinforcing the idea that at least some gains in PC5 and PC3 ship accessibility in the Arctic Ocean were due to reductions in sea-ice concentration and stage of development (i.e., thickness) as opposed to the total loss of sea-ice coverage in those regions. This is important because it shows that changes over time in PC ship accessibility to the Arctic may not be detected in charts of sea-ice extent alone.

During September and November, a larger portion of the study site was accessible to all three PC ship types compared to conditions in February and June. During September, warmer atmospheric and sea surface temperatures drive sea ice to its annual minimum spatial extent. In October and November, temperatures drop, and sea ice re-freezes at the seaward edge of multi-year ice. Reductions in sea-ice extent during the month of September over recent decades are well documented, with total extent declining at a rate of 12.6% per decade since 1979 (NASA, 2022). In contrast to this trend, PC7 ship

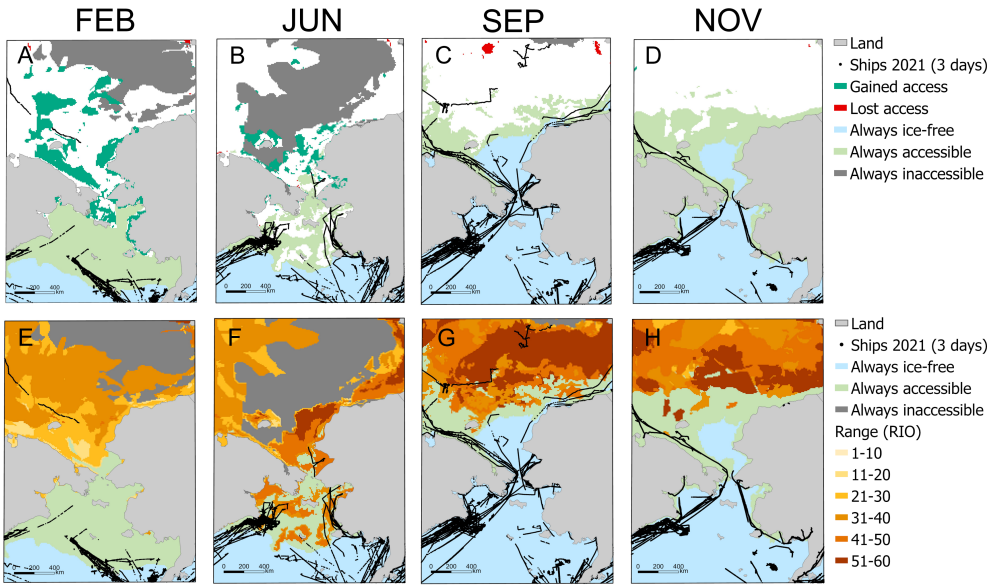

FIGURE 10
Automatic Identification System (AIS) position reports generated by vessels in the study site on February 3-5, 2021 **(A, E)**, June 3-5, 2021 **(B, F)**, September 1-3, 2021 **(C, G)**, and November 3-5, 2021 **(D, H)**. Position reports are overlaid on maps of Gain/Loss **(A–D)** and RIOrange **(E, F)** for PC7 ships.

accessibility in this study failed to show a long-term increase as it did in February and June. Instead, PC7 ship accessibility declined in September and remained relatively constant in November. This observation may be due, at least in part, to the historically low sea-ice extent recorded in September 2012, which was the first year in our time series. Minimum sea-ice extent that year was the lowest seen across the Arctic Ocean in 44 years (1979–2022), dropping to 3.6×10^6 km^2 in total extent, compared to the typical (interdecile) range of $5.1–7.2 \times 10^6$ km^2 in previous and subsequent years (Parkinson and DiGirolamo, 2021; NSIDC, 2022b). This made September 2012 an unusually low reference point against which we compared September ship accessibility in later years.

It is also possible, however, that physical processes acting over the spatial scale of the study site as opposed to over the Arctic Ocean as a whole caused ice concentration and/or ice thickness to increase locally in some areas, leading to a genuine decline in PC7 ship accessibility within the study site over the last decade. For example, the Beaufort Gyre is known to move multi-year ice from seas north of Greenland into the Beaufort Sea, which lies within the study site. Moore et al. (2022) reported an anomalous increase in multi-year ice transported into the Beaufort Sea by the Beaufort Gyre in the summers of 2020 and 2021, resulting in older, thicker ice present in the Beaufort Sea in those years and in the Chukchi Sea in 2021. This would have made conditions less permissible to ships, especially those with little ice strengthening, such as PC7 vessels. Babb et al. (2022) also reports that the amount of multi-year sea ice transported by the gyre appears to have been increasing over the last 20 years; however, a substantial portion (up to one third) of it now melts while in the Beaufort Sea, so the role of the Beaufort Gyre in the decline in accessibility we observed remains unclear.

With respect to accessibility for the more capable PC3 and PC5 ships, our results suggest that these ships are considerably less sensitive to seasonal variability in the sea-ice landscape than are PC7 ships. Not only was PC3 ship accessibility similar from month to month despite seasonal fluctuations in sea-ice extent, concentration, and stage of development, but PC5 and PC3 accessibility increased at a slower rate in February and June than it did for PC7 ships. Moreover, relatively few areas within the study site shifted from inaccessible to accessible (or vice versa) to these ships over the last decade, suggesting that greater changes in the ice environment are needed to influence areas where PC5 and PC3 ships can navigate compared to environmental changes affecting accessibility for PC7 ships.

TABLE 4 Number of ships in the study site on February 3–5, 2021, June 3–5, 2021, September 1–3, 2021, and November 3–5, 2021, including the number of ships in areas where RIO_{range} > 30 and, of those, the number that were commercial fishing vessels.

	No. Ships		
	Total	RIO_{range} >30	Fishing vessels, RIO_{range} >30
February	155	1	0
June	255	90	61
September	348	9	0
November	161	4	0

While accessibility differences among the polar classes in February and June were expected given that the PC system is based on structural capabilities related to ice operations, the absence of such differences during the month of November was initially surprising. However, inspection of the ship-accessibility maps in Figure 9 shows that the similarities during November may simply reflect the relatively large portion of the study area covered by ice-free water during this month. As sea ice melts, the ice edge moves north during the summer, making the study site accessible to a wider range of ice-strengthened ships than in previous months. Even the sea ice present is largely accessible to the three polar classes, as much of it is thin, first-year ice, which, during October and November, usually forms on the southern seaward edge of thicker, multi-year ice to the north during autumn freeze-up (Wadhams, 2003; Stroeve and Notz, 2018).

Ice formation during autumn can have serious implications for PC ship accessibility in the future given ongoing climate change. Based on a 40-year time series analysis of satellite-based sea-ice data, Zheng et al. (2021) noted a strong correlation between the timing of autumn freeze-up in the Laptev Sea, East Siberian Sea, Chukchi Sea, and Beaufort Sea and total sea-ice extent during the previous June. Specifically, early summers with little ice coverage were followed by autumns with delayed seasonal ice formation. If continued summer sea-ice loss in the Arctic region continues in upcoming years, then ice formation in November may routinely occur later in the year than it has in the past. Unusually slow autumn freeze events in the Arctic Ocean documented during 2016 and 2020 are consistent with this potential future trend (NSIDC, 2022a). In a scenario where autumn refreeze is delayed, ship accessibility in November, which is already similar among the PC3, PC5, and PC7 ships, may become even less reliant upon the need for ice-strengthened ships. Should vessels without ice-hardening expand northern operations under this assumption, years with an unusually early refreeze event could present dangerous conditions for ship operators and their crew.

Seasonal differences in accessibility among the polar classes, or lack thereof, may also have implications for maritime planners forecasting needs for shipping operations in a rapidly changing Arctic Ocean. Heavy icebreakers (i.e., PC2, PC3 ships) are considerably more costly to build and operate than ships with lower PC ratings, which are, in turn, more costly to build and operate than non-ice-strengthened ships. For example, Solakivi et al. (2018) estimated that PC ships could be up to 3 times more costly to build than non-ice-strengthened ships and approximately 1.5 times more costly to operate due to higher fuel costs.

The shipping industry might avoid these costs by hiring an icebreaker to provide escort service for a non-ice-strengthened ship, but such services can be costly and the availability of icebreakers is limited (Lindborg and Andersson, 2020). Managers therefore have a financial incentive to optimize ship design or to plan shipping operations that avoid the need for ice-capable ships when possible. Our results suggest that knowledge of seasonal differences in PC ship accessibility to a region of interest, such as during February and June, or the absence of such differences, such as during September and November, could help managers make decisions about how to balance the need for minimum ship capabilities with operational costs. This is especially relevant to ships operating on established routes (e.g., from Russia's Yamal Peninsula to greater Asia), where knowledge of the likelihood of a route remaining accessible during a voyage can inform decisions about the need to acquire PC ships and how to minimize operational costs while prioritizing safety of navigation. If ice conditions observed over the last 10-11 years are indicative of future conditions, PC ship accessibility to established trade routes through Arctic seas north of the Bering Strait may not be too different for PC3 and PC5 ships. In this case, commercial operators may benefit from prioritizing new construction of PC5 ships over that of PC3 icebreakers.

4.2 Interannual variability in ship accessibility

Polar maritime safety is in many ways reliant upon ship operators selecting routes that minimize the likelihood of encountering ice conditions that exceed a ship's physical capabilities for safe navigation. Ideally, routes are planned for areas where ice conditions are predictable and do not exceed the range for which the ship was built. Nonetheless, ships may encounter unexpected ice conditions in locations and during times of year when sea-ice coverage exhibits a high degree of seasonal or interannual variability. At best, these encounters require the ship to take an alternate route and incur additional costs and time delays. At worst, encounters damage structural elements of the ship and threaten mariner safety (Kujala and Arughadhoss, 2012; Kubat et al., 2015). Numerous recent incidents in which ships have become beset in sea ice on major Arctic shipping routes underscore the importance of situational awareness with respect to spatiotemporal variability in ice conditions (Kubat et al., 2013; Bennetts, 2021; Vanhatalo et al., 2021).

In this study, February was the least variable month in terms of PC ship accessibility. June, September, and November showed considerable interannual variability. Interannual variability in ship accessibility during June differed from other months in that high variability in PC7 accessibility was observed as far south as the northern Bering Sea. While sea ice in February also extended as far south as it did in June, it did so in the form of thin, first-year ice and was consistently navigable by PC7 ships. On the other hand, in June, ice thaws and ice sheets break up into separate segments or floes that are more susceptible than pack ice to movement by surface winds and currents (Hwang et al., 2017).

Polar class ship accessibility in June was also relatively variable on an interannual basis in waters north of the Bering Strait, especially in coastal regions adjacent to mainland Russia and the United States (Alaska). Waters in the western Beaufort Sea, encompass the westernmost portion of the Northwest Passage, which has hosted more shipping activity in recent years from commercial traffic, e.g., bulk carriers and general cargo ships, and from passenger vessels, e.g., cruise ships and pleasure craft (Boylan and Elsberry, 2019; Gunnarsson, 2021; PAME, 2021). These vessel types typically lack ice strengthening, and passenger vessels in particular plan voyages well in advance of getting underway,

making this maritime sector potentially more prone than others to unexpected and unsafe encounters with ice hazards.

In contrast, large areas of the East Siberian Sea were consistently ice covered in June, making the region always inaccessible to PC7 ships. This region includes the eastern portion of the Northern Sea Route. Knowledge among ship operators that conditions are always unfavorable for PC7 ships in this region during June could inform route planning and real-time decisions to avoid the area, mitigating potential risk. In contrast, the region was always accessible to PC5 and PC3 ships in the four months that we examined. In September and November, vast regions of the study site north of the Bering Strait exhibited high interannual variability for all three polar classes, but especially for PC7 ships. Maximum RIO_{range} values calculated for PC7 ships were observed off northern Alaska during November. While climate-driven declines in sea-ice coverage in the Arctic Ocean may create opportunities for polar maritime traffic in general, our results show that the Arctic environment remains highly unpredictable on smaller (regional and local) spatial scales. Real possibilities exist for planning miscalculations. Shipping industry leaders have said that Arctic shipping routes will remain undesirable for commercial maritime traffic (Lasserre, 2018) due, in part, to the high degree of variability in transit time caused by shifting ice conditions and unpredictable weather. This could be especially problematic for maritime sectors driven by a just-in-time supply model, which is less accommodating of time delays caused by ships using alternate routes to avoid unexpected and unfavorable ice conditions (as cited in Roscoe et al., 2014). Consider November 2021, when the media reported that at least 20 commercial ships, including 18 cargo vessels and two oil tankers without ice strengthening, were beset in sea ice while transiting the Northern Sea Route. The incidents occurred when ships were underway north of Russia in early November, and the annual autumn freeze-up occurred earlier and faster than in previous years (Bennetts, 2021). If Arctic shipping continues to expand, regardless of whether ships are ice-strengthened, planners may consider the need for greater ice breaker support capabilities and emergency response assets in key areas to improve maritime safety where and when ice conditions are most unpredictable.

4.3 Case study: shipping activity in 2021

Most ship operators concerned with balancing safety risks with economic factors may already practice due caution in ice-prone regions of the Arctic Ocean and avoid areas where ice conditions are unpredictable from year to year. If so, unpredictable ice conditions may pose less of a risk to mariners than otherwise thought. To determine the extent to which ships have been recently operating in newly accessible areas or highly variable areas, we superimposed shipping activity over three-day periods in February, June, September, and November 2021 onto PC7 ship-accessibility maps. Because most commercial ships are not ice-strengthened, ship-accessibility maps for PC7 vessels were likely most representative of conditions encountered by the maritime community as a whole.

In general, ships were active mainly in ice-free water south of the Bering Strait. This result was expected given that most ships are commercial vessels that are not ice-strengthened. Some ships operated in water that was accessible to PC7 ships in some years but inaccessible in others; however, RIO_{range} was relatively low (<30) in these areas during the study. With the exception of June, few ships occurred where interannual variability was high (RIO_{range} > 30). However, during June, nearly half of all ships south of the Bering Strait in June operated in highly variable areas. Of those, 68% were commercial fishing vessels. Already one of the world's most dangerous industries, fishing vessels accidents are among the most frequent reasons for emergency response calls in the U.S. Bering Sea region (U.S. Coast Guard, 2008). We suggest that fishing vessel exposure to ice hazards in this region is not likely to decline in the future as fishing vessels often operate near the ice edge to gain early access to newly exposed fishing grounds in the spring (Rampal et al., 2009).

Moreover, several authors have documented poleward shifts in the distribution of important commercial groundfish species, such as walleye pollock (*Gadus chalcogrammus*) and Pacific cod (*G. macrocephalus*), which make up the bulk of targeted commercial fish in the Bering Sea (Stevenson and Lauth, 2019; Rooper et al., 2021). Similar poleward range shifts have been seen in small pelagic fishes of commercial interest, including juvenile sockeye salmon (*Oncorhynchus nerka*; Yasumiishi et al., 2020). If our results from June 2021 reflect commercial fishing vessel distribution typical for the month, climate change may provide incentive for ships to follow fish populations further north into regions with highly variable ice conditions from year to year. If so, maritime authorities may consider prioritizing emergency response capabilities for the northern Bering Sea region during June and other early-summer months.

North of the Bering Strait, ships were uncommon during February and June, and few operated in areas of gradually increasing accessibility or high interannual variability. Only two ships were present in areas where accessibility significantly increased over time, but they only passed through these areas as opposed to exhibiting a preference for them. Areas opening up to ship traffic in northern Arctic seas may be undesirable to ship operators if they occur in regions off the beaten path where there is no cost or time incentive to travel. Newly accessible areas may also be unavailable to ships in a practical sense if they are surrounded by ice that is inaccessible. This was the case for most areas in the Chukchi Sea and East Siberian Sea that had become more accessible to PC3, PC5, and PC7 ships over the last 10-11 years. This finding highlights the need for future projections about Arctic shipping based on sea-ice declines to incorporate a spatially explicit, network-based approach to evaluating whether ships can access seas becoming navigable for the first time under the new climate regime as well as the costs and benefits of travelling there. Related to this observation is that most shipping activity north of the Bering Strait in September and November occurred in the southernmost regions of the Arctic, along coastlines and in open water or thin first-year ice even though waters to the north were accessible. In September 2021, only four vessels (of 348 ships total) were active in the study site's highest latitudes, where PC7 ship accessibility was highly variable or where PC7 could not safely access. Presumably, those ships had PC ratings higher than PC7.

In conclusion, global climate change continues to promote rapid change in the Arctic marine landscape, driving sea-ice declines that allow for shipping activity at the world's highest northern latitudes. Our study shows that ice coverage affecting access by PC ships has been

variable, sometimes highly so, over seasonal and interannual temporal scales. How long these conditions will persist into the future as climate change continues to drive sea-ice loss in the Arctic Ocean remains to be seen. Long-term predictions for ship accessibility in the Arctic Ocean vary among climate models (Stephenson et al., 2013), but spatiotemporal variability is a common feature of most projections (e.g., Stephenson and Smith, 2015). Even so, shelf areas of the Arctic Ocean are forecast to be ice-free during summer within the next 25–30 years (Årthun et al., 2021), and the Arctic Ocean as a whole is expected to be ice-free in summer months by 2100 (Boé et al., 2009). In the winter months, some areas, such as the Barents Sea, may be ice-free by the turn of the century (Årthun et al., 2021). If so, spatiotemporal variability in ship accessibility described in this study could represent a transitional state in a long-term progression toward an ice-free Arctic. If projections are correct and commercial ship traffic continues to expand poleward (Stephenson et al., 2013; Huntington et al., 2015; Aksenov et al., 2017; U.S. Committee on the Marine Transportation System, 2019; Min et al., 2021), a similar analysis of ship accessibility trends should be conducted for non-ice-strengthened ships and for other regions of the Arctic Ocean.

Data availability statement

Sea-ice shapefiles are publicly available on the U.S. National Ice Center website. Inquiries regarding the availability of the model used to generate ship-accessibility maps can be directed to the U.S. National Ice Center.

Author contributions

LV: Data curation, Formal analysis, Writing -original draft, Writing – review and editing. KH: Conceptualization, Writing -original draft, EB: Conceptualization, Writing – review and editing. AD, MM: Data curation, Formal analysis, Writing – review and editing. All authors contributed to the article and approved the submitted version.

Funding

This research was supported by an appointment to the Visiting Faculty Scientist Program at the National Geospatial-Intelligence Agency (NGA), administered by the Oak Ridge Institute for Science and Education through an interagency agreement between the United States Department of Energy and NGA.

Acknowledgments

We are grateful for contributions from M. Ortiz, B. McDonald, D. Holland, and G. Pavur, who assisted in developing the analytical tools and data products used in this study. We also thank the two reviewers for their constructive feedback on the original manuscript.

Conflict of interest

The authors declare that the research was conducted in the absence of any commercial or financial relationships that could be construed as a potential conflict of interest.

Publisher's note

References

Aksenov, Y., Popova, E. E., Yool, A., Nurser, A. J. G., Williams, T. D., Bertino, L., et al. (2017). On the future navigability of Arctic sea routes: high resolution projections of the Arctic ocean and sea ice. *Mar. Policy* 75, 300317. doi: 10.1016/j.marpol.2015.12.027

American Bureau of Shipping (2016). *IMO Polar code advisory* (Houston, TX: American Bureau of Shipping), 68.

Årthun, M., Onarheim, I. H., Dörr, J., and Eldevik, T. (2021). The seasonal and regional transition to an ice-free Arctic. *Geophys. Res. Lett.* 48, e2020GL090825. doi: 10.1029/2020GL090825

Babb, D. G., Galley, R. J., Howell, S. E. L., Landy, J. C., Stroeve, J. C., and Barber, D. G. (2022). Increasing multi-year sea ice loss in the Beaufort Sea: a new export pathway for the diminishing multiyear ice cover of the Arctic ocean. *Geophys. Res. Lett.* 49, e2021GL097595. doi: 10.1029/2021GL097595

Bennetts, M. (2021) *Early Arctic sea freeze traps Arctic ships in ice near Russia* (The Times). Available at: http://www.thetimes.co.uk/article/early-arctic-sea-freeze-traps-18-ships-in-ice-near-russia-c93lz7fkx (Accessed February 1, 2023).

Boé, J., Hall, A., and Qu, X. (2009). September Sea-ice cover in the Arctic ocean projected to vanish by 2100. *Nat. Geosci.* 2, 341343. doi: 10.1038/NGEO467

Boylan, B. M., and Elsberry, D. T. (2019). *Increased maritime traffic in the Arctic: implications for international cooperation and security* (Fairbanks, USA: Center for Arctic Policy Studies, University of Alaska).

Eguíluz, V. M., Fernández-Gracia, J., Irigoien, X., and Duarte, C. M. (2016). A quantitative assessment of Arctic shipping in 2010–2014. *Nat. Sci. Rep.* 6, 30682. doi: 10.1038/srep30682

Eicken, H. (2013). Arctic Sea ice needs better forecasts. *Nature* 497, 431433. doi: 10.1038/497431a

Esri (2022a). *World countries (Generalized)* [shapefile]. Available at: https://hub.arcgis.com/datasets/esri::world-countries-generalized/about (Accessed May 22, 2023).

Esri (2022b). ArcGIS Pro: Release 2.9.3. Redlands, CA: Environmental Systems Research Institute.

Fournier, M., Hilliard, R. C., Rezaee, S., and Pelot, R. (2018). Past, present, and future of the satellite-based automatic identification system: areas of applications, (2004 –2016). *WMU J. Maritime Affairs* 17, 311345. doi: 10.1007/s13437-018-0151-6

Gunnarsson, B. (2021). Recent ship traffic and developing shipping trends on the northern Sea route – policy implications for future Arctic shipping. *Mar. Policy* 124, 104369. doi: 10.1016/j.marpol.2020.104369

Gunnarsson, B., and Moe, A. (2021). Ten years of international shipping on the northern Sea route: trends and challenges. *Arctic Rev. Law Politics* 12, 430. doi: 10.23865/arctic.v12.2614

Huntington, H. P., Daniel, R., Hartsig, A., Harun, K., Heiman, M., Meehan, R., et al. (2015). Vessels, risks, and rules: planning for safe shipping in Bering strait. *Mar. Policy* 51, 119127. doi: 10.1016/j.marpol.2014.07.027

Hwang, B., Wilkinson, J., Maksym, T., Graber, H. C., Schweiger, A., Horvat, C., et al. (2017). Winter-to-summer transition of Arctic sea ice breakup and floe size distribution in the Beaufort Sea. *Elementa: Sci. Anthropocene* 5, 40. doi: 10.1525/elementa.232

International Association of Classification Societies (2016) *IACS unified requirements for PC ships. IACS requirements 2011*. Available at: https://iacs.org.uk/publications/unified-requirements/ur-i/ (Accessed May 1, 2023).

International Maritime Organization. (2017). *International code for ship operating in polar waters (POLAR CODE)*. (MEPC 68/21) Geneva, Switzerland.

Isaksen, K., Nordli, Ø., Ivanov, B., Køltzow, M. A. Ø., Aaboe, S., Gjelten, H. M., et al. (2022). Exceptional warming over the barents area. *Sci. Rep.* 12, 9371. doi: 10.1038/s41598-022-13568-5

Kubat, I., Fowler, D., and Sayed, M. (2015). "Chapter 18: floating ice and ice-pressure challenge to ships," in *Snow and ice-related hazards, risks, and disasters*. Eds. J. F. Chroder, W. Haeberli and C. Whiteman (Waltham, MA, USA: Elsevier, Inc.), 641–669.

Kubat, I., Sayed, M., and Babaei, M. H. (2013). "Analysis of besetting incidents in Frobisher bay during 2012 shipping season," in *Proceedings of the 22nd International Conference on Port and Ocean Engineering under Arctic Conditions*, Espoo, Finland.

Kujala, P., and Arughadhoss, S. (2012). Statistical analysis of ice-crushing pressures on a ship's hull during hull-ice interaction. *Cold Regions Sci. Technol.* 70, 111. doi: 10.1016/j.coldregions.2011.09.009

Lasserre, F. (2018). "Chapter 20: Arctic shipping: more ships will come but not for transit," in *From science to policy in the Eastern Canadian artic: an integrated regional impact study (IRIS) of climate change and modernization*. Eds. T. Bell and T. M. Brown (Quebec City: ArcticNet), 509521.

Lindborg, E., and Andersson, P. (2020). The costs of icebreaking services: an estimation based on Swedish data. *WMU J. Maritime Affairs* 19, 125142. doi: 10.1007/s13437-019-00191-x

Marchenko, N., Andreassen, N., Borch, O. J., Kuznetsova, S. Y., Ingimundarson, V., and Jakobsen, U. (2018). Arctic Shipping and risks: emergency categories and response capacities. *TransNav* 12, 1. doi: 10.12716/1001.12.01.12

Meier, W. N. (2017). "Losing Arctic sea ice: observations of the recent decline and the long-term context," in *Sea Ice*, *3rd ed*. Ed. D. N. Thomas (West Sussex, U.K: John Wiley & Sons), 290303.

Min, C., Yang, Q., Chen, D., Yang, Y., Zhou, X., Shu, Q., et al. (2021). The emerging Arctic shipping corridors. *Geophys. Res. Lett.* 49, e2022GL099157. doi: 10.1029/2022GL0991574

Moore, G. W. K., Steele, M., Schweiger, A. J., Zhang, J., and Laidre, K. L. (2022). Thick and old sea ice in the Beaufort Sea during summer 2020/21 was associated with enhanced transport. *Commun. Earth Environ.* 3, 198. doi: 10.1038/s43247-022-00530-6

National Aeronautical and Space Agency (NASA) (2022) *Arctic Sea Ice minimum extent*. Available at: https://climate.nasa.gov/vital-signs/arctic-sea-ice/ (Accessed February 1, 2023).

NSIDC (National Snow and Ice Data Center) (2022a) *Arctic Sea ice maximum at tenth lowest record in satellite history*. Available at: http://nsidc.org/arcticseaicenews/2022/03/ (Accessed February 1, 2023).

NSIDC (National Snow and Ice Data Center) (2022b) *Charctic interactive sea ice graph*. Available at: https://nsidc.org/arcticseaicenews/charctic-interactive-sea-ice-graph/ (Accessed February 1, 2023).

PAME (Protection of the Arctic Marine Environment) (2020) *The increase in Arctic shipping 20132019. Arctic shipping status report (ASSR) 1*. Available at: https://www.pame.is/projects-new/arctic-shipping/pame-shipping-highlights/411-arctic-shipping-status-reports (Accessed February 1, 2023).

PAME (Protection of the Arctic Marine Environment) (2021) *Shipping in the Northwest passage. Arctic shipping status report (ASSR) 3*. Available at: https://www.pame.is/projects-new/arctic-shipping/pame-shipping-highlights/411-arctic-shipping-status-reports (Accessed February 1, 2023).

Parkinson, C. L., and DiGirolamo, N. E. (2021). Sea Ice extents continue to set new records: Arctic, Antarctic, and global results. *Remote Sens. Environ* 267, 112753. doi: 10.1016/j.rse.2021.112753

Rampal, P., Weiss, J., and Marsan, D. (2009). Positive trend in the mean speed and deformation rate of Arctic sea ice 1979–2007. *J. Geophys. Res.* 114, C05013. doi: 10.1029/2008JC005066

Rooper, C. N., Ortiz, I., Hermann, A. J., Lamean, N., Chang, W., Kearney, K., et al. (2021). Predicted shifts of groundfish distribution in the Eastern Bering Sea under climate change, with implications for fish populations and fisheries management. *ICES J. Mar. Sci.* 78 (1), 220234. doi: 10.1093/icesjms/fsaa215

Roscoe, H. C., Campagna, P. F., and McNulty, D. (2014). Improving arctic safety in the U.S. Arctic. *Joint Force Q.* 72, 82–87.

Solakivi, T., Kiiski, T., and Ojala, L. (2018). The impact of ice class on the economics of wet and dry bulk shipping in the arctic waters. *Maritime Policy Manage.* 45 (4), 530542. doi: 10.1080/03088839.2018.1443226

Stephenson, S. R., and Smith, L. C. (2015). Influence of climate model variability on projected Arctic shipping futures. *Earth Future* 3, 331343. doi: 10.1002/2015EF000317

Stephenson, S. R., Smith, L. C., Brigham, L. W., and Agnew, J. A. (2013). Projected 21st-century changes to Arctic marine access. *Climatic Change* 118, 885899. doi: 10.1007/s10584-012-0685-0

Stevenson, D. E., and Lauth, R. R. (2019). Bottom trawl surveys in the northern Bering Sea indicate recent shifts in the distribution of marine species. *Polar Biol.* 42, 407421. doi: 10.1007/s00300-018-2431-1

Stoddard, M. A., Etienne, L., Fournier, M., Pelot, R., and Beveridge, L. (2016). "Making sense of Arctic maritime traffic using the polar operational limits assessment Risk indexing system (POLARIS)," in *IOP Conference Series, Earth and Environmental Science*. 012034. doi: 10.1088/17551315/34/1/012034

Stroeve, J., and Notz, D. (2018). Changing state of sea ice across all seasons. *Environ. Res. Lett.* 13 (10), 103001. doi: 10.1088/1748-9326/ade56

Transport Canada (1998) *Arctic Ice regime shipping system (AIRSS) standards* (Ottawa: Transport Canada). Available at: https://tc.canada.ca/en/marine-transportation/marine-safety/arctic-ice-regime-shipping-system-airss (Accessed February 1, 2023).

The MathWorks Inc. (2021). MATLAB version: 9.10.0 (R2021a), Natick, Massachusetts: The MathWorks Inc.

U.S. Coast Guard (2008). *Analysis of fishing vessel casualties: a review of lost fishing vessels and crew fatalities 19932007* (U.S. Coast Guard, Washington, D.C: Compliance Analysis Division).

U.S. Coast Guard (2022) *Types of automatic identification systems (per ITU-r M.1371 and IEC standards)*. Available at: https://navcen.uscg.gov/types-of-ais (Accessed February 1, 2023).

U.S. Committee on the Marine Transportation System (2019). *A ten-year projection of maritime activity in the U.S. Arctic region 2020–2030* (Washington, D.C.), 118.

Vanhatalo, J., Huuhtanen, J., Bargström, M., Helle, I., Mäkinen, J., and Kujala, P. (2021). Probability of a ship becoming beset in ice along the northern Sea route – a Bayesian analysis of real-life data. *Cold Regions Sci. Technol.* 184, 103238. doi: 10.1016/j.coldregions.2021.103238

Wadhams, P. (2003) *How does Arctic sea ice form and decay*? Available at: https://www.pmel.noaa.gov/arctic-zone/essay_wadhams.html (Accessed February 1, 2023).

World Meteorological Organization (WMO) (2014) *Sea Ice nomenclature* (WMO). Available at: https://library.wmo.int/index.php?lvl=notice_display&id=6772#.ZF5xi3bMKUk (Accessed May 12, 2012). 5th Session of the JCOMM Expert Team on Sea Ice.

Yasumiishi, E. M., Cieciel, K., Andrews, A. G., Murphy, J., and Dimond, J. A. (2020). Climate-related changes in the biomass and distribution of small pelagic fishes in the eastern Bering Sea during late summer 2002–2018. *Deep Sea Res. Part II Trop. Stud. I Oceanogr.* 104907, 181182. doi: 10.1016/j.dsr2.2020.104907

Zheng, L., Cheng, X., Chen, Z., and Liang, Q. (2021). Delay in Arctic Sea ice freeze-up linked to early summer ice loss: evidence from satellite observations. *Remote Sens.* 13, 2162. doi: 10.3390/rs13112162

frontiers | Frontiers in Marine Science

TYPE Original Research
PUBLISHED 18 August 2023
DOI 10.3389/fmars.2023.1190164

OPEN ACCESS

EDITED BY
Penelope Wagner,
Norwegian Meteorological Institute,
Norway

REVIEWED BY
Xinyu Zhang,
Dalian Maritime University, China
Ru Chen,
Tianjin University, China

*CORRESPONDENCE
Yangjun Wang
wangyangjun18@nudt.edu.cn

†These authors share first authorship

RECEIVED 20 March 2023
ACCEPTED 31 July 2023
PUBLISHED 18 August 2023

CITATION
Liu Q, Wang Y, Zhang R, Yan H, Xu J and Guo Y (2023) Arctic weather routing: a review of ship performance models and ice routing algorithms.
Front. Mar. Sci. 10:1190164.
doi: 10.3389/fmars.2023.1190164

Arctic weather routing: a review of ship performance models and ice routing algorithms

Quanhong Liu[1†], Yangjun Wang[2*†], Ren Zhang[1], Hengqian Yan[1], Jing Xu[1] and Yutong Guo[1]

[1]College of Meteorology and Oceanography, National University of Defense Technology, Changsha, China, [2]College of Advanced Interdisciplinary Studies, National University of Defense Technology, Nanjing, China

With the accelerated melting of the Arctic sea ice, the opening of the Northeast Passage of the Arctic is becoming increasingly accessible. Nevertheless, the constantly changing natural environment of the Arctic and its multiple impacts on vessel navigation performance have resulted in a lack of confidence in the outcomes of polar automated route planning. This paper aims to evaluate the effectiveness of two distinct models by examining the advancements in two essential components of e-navigation, namely ship performance methods and ice routing algorithms. We also seek to provide an outlook on the future directions of model development. Furthermore, through comparative experiments, we have examined the existing research on ice path planning and pointed out promising research directions in future Arctic Weather Routing research.

KEYWORDS

arctic weather routing, ship speed model, shipping cost, navigation safety, D*-NSGA-III algorithm

1 Introduction

Considering global climate change and the acceleration of Arctic sea ice melting (Guemas et al., 2016), the opening of the Arctic Northeast Passage (NEP) will become a reality (Li et al., 2021a). The emergence of this new route will provide a new option for maritime trade between Asia and Europe. Not only will the journey distance be cut by about 40%, the voyage time will be reduced, and the economic costs will be lower (Chen et al., 2020; Tseng et al., 2021), but it will also ease the present strain on shipping on traditional shipping routes.

However, as a new route, the harsh nature of the environment makes polar navigation more challenging. To create safe, effective, and economic routes, an experienced skipper must pay close attention to the ice and ocean conditions of the Arctic waters. Is it possible to do this using a computer?

Automatic systems are increasingly employed in shipping. Weather routing is a way of planning and providing the operating state of a vessel under various sea conditions based

on the weather forecast and the vessel's technology (Simonsen et al., 2015). In traditional ocean voyages, the influences of sea, wind, and cyclone on the vessel maneuvering are taken into account in the weather routing to obtain a quick, economical, and safe route (Li et al., 2017; Perera and Soares, 2017; Fabbri and Vicen-Bueno, 2019). However, more influencing factors should be considered in Arctic weather navigation.

In Arctic waters, apart from the influences of wind, waves, and currents, there is also a need to take into consideration the impact of severe conditions like sea ice, freezing temperatures, and poor visibility. Sea ice has a multiscale impact on ship maneuvering in polar waters. For instance, perennial ice limits the normal passage of ships, first-year ice can slow down the boat, and floating ice can pose a threat to the security of the sea. Moreover, while the journey is reduced by polar navigation, sailing in an icy region will inevitably increase operating costs and the amount of fuel consumed, making it more difficult to assess the economic cost of shipping.

To sum up, a great challenge has been imposed on automatic route planning due to the rapid change of the natural environment of Arctic NEP and its multiscale impact on vessel navigation. The rationality and efficiency of weather routing in polar areas must be verified. Two aspects should be considered in this regard: first, the adequacy of the Ship Performance Models (SPMs); second, the feasibility of the Ice Routing Algorithms (IRAs). SPMs are mathematical models for ship velocity, cost, and security in a complicated polar environment, whereas IRAs describe a reasonable route design approach that can be adapted to the requirements of navigation and operation. This article gives an overview of the current studies on SPMs and IRAs.

The framework of this paper is as follows: Section 2 introduces the current research status of SPMs. The research progress of IRAs is discussed in Section 3, and then a dynamic multi-objective path algorithm adapted to polar regions is proposed for the existing problems. Section 4 validates the new algorithm, and Section 5 summarized the conclusions.

2 Literature review for SPMs

Due to the many factors affecting SPMs, the scope of this paper is limited to the direct impact of sea ice on ship navigation, including sea ice induced changes in navigation safety, navigation cost and speed. These factors are closely related to the development of polar shipping and are key useful functions for the optimal design of polar shipping routes. The remaining factors, such as ecological and environmental protection, geopolitical and military conflicts and other external influences, certainly have an impact on the development of polar shipping. However, such influences are macroscopic and indirect, so they are out of the scope of our study.

2.1 Polar ship speed models

Cargo is usually time-consuming for merchant ships, and the Arctic sea ice can have a significant effect on the speed of vessels. This requires reliable ice-speed models in e-navigation to allow route design within a reasonable time frame (Agarwal and Ergun, 2008).

In the Arctic, except for some specific routes where wind and waves need to be considered, such as the Kemi-Hamburg route (Lehtola et al., 2020), it is the impact of sea ice on navigation speed that is the most important and persistent.

The Polar Operational Limit Assessment Risk Indexing System (POLARIS), a polar navigation standard, clearly states that when sea ice concentration and ice thickness are above certain thresholds, navigation speed will inevitably be affected and may even need to be detoured (Engtrø et al., 2020).

According to the existing research, the current research on the inference of navigation speed in the Arctic sea is mainly divided into two categories: dynamic models and statistical models.

2.1.1 Dynamic model

The dynamic model is analyzed from the perspective of dynamics and kinematics. By analyzing the force relationships between the polar sea ice and the ship, the motion equations between the ship's speed and the sea ice are constructed, and the changes in the ship's motion state under different sea ice resistance are calculated. Its development phase includes four stages: semi-empirical formula, simulation of sea ice processes on ships using Discrete Element (DEM), or Finite Element Method (FEM), characterization of multiphase interactions between ships and marine elements by coupled Computational Fluid Dynamics (CFD) and DEM/FEM, and a hybrid scheme combining the above methods. The specific development process is shown in Figure 1:

The early ice resistance model utilized a semi-empirical formula to calculate the ice resistance (Riska et al., 1997). The formula was subsequently further elaborated by (Colbourne, 2000) as follows:

$$Fr_p = V/\sqrt{gh_iC} \tag{1}$$

$$R_P = 0.5C_p\rho_i Bh_i V^2 C^n \tag{2}$$

$$C_p = k_c Fr_p^{-b} \tag{3}$$

where Fr_p denotes the ice Froude number, h_i stands for the ice thickness, C represents the ice concentration, g symbolizes the acceleration of gravity, R_p indicates the ice resistance, C_p signifies the ice force coefficient, B and ρ_i are the ship beam and the ice density, and k_c, b, and n are constants relevant to ship parameters.

These research results made important contributions to ship design and operational planning (Juva and Riska, 2002). However, semi-empirical studies cannot solve the problem of maneuvering, so it is necessary to simplify the interaction between ship and ice in order to arrive at a viable solution (Li et al., 2020b).

Thus, high-fidelity computing models based on CFD, DEM, or FEM can improve individual ice resistance (Xue et al., 2020). A mathematical model for estimating ship speed was developed, which considers the ice-breaking process (Petri, 2001). Lubbad and Løset used a closed-form solution for ice-breaking modeling

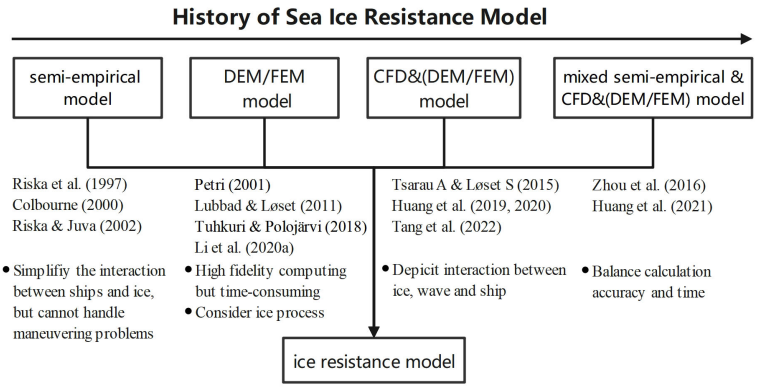

FIGURE 1
History of the dynamic model.

to simulate the dynamic processes of the ship as it broke through the ice. The velocity of a vessel in an icy region is calculated by a numerical simulation of the ice motion (Lubbad and Løset, 2011). More complex ice processes, such as ice rotation and ice submersion, were considered in current studies (Tuhkuri and Polojärvi, 2018). Although the descriptions of the different processes were still simple and not systematically validated, they were of great importance to guide (Li et al., 2020a).

Previous simulations of ship progress through ice floes ignored the effect of hydrodynamics, which was also a key factor in ship operation in icy water (Tsarau and Løset, 2015). Huang et al. (2020) first developed a CFD and DEM approach to simulate the ship-wave-ice interactions and provide reliable resistance prediction (Huang et al., 2020). In which, standard CFD models were used for ship propulsion in open water and DEM was used to simulate the interaction between ship structures and ice floes, and fluid forces were obtained from the CFD solution to achieve ship-wave-ice coupling. The original floe-distribution algorithm was developed to import the natural ice-floe fields into the CFD & DEM model, where the floes were randomly distributed and had a range of sizes according to field measurements. The accuracy of this approach in predicting the ice-floe resistance was experimentally confirmed (Tang et al., 2022).

Although a computation method is usually affordable, the CFD and DEM model is very costly. It is impractical to run the simulation every time a resistance estimation is required. Therefore, it is necessary to develop empirical equations to quickly estimate the ice resistance (Zhou et al., 2016; Huang et al., 2021), as follows:

$$R_{ice} = A \times \rho_i \times h \times D \times V^2 \times B/L_{pp} \times C^{1.5} \times Fr^{-0.8} \quad (4)$$

where A represents a coefficient dependent on ships, D denotes the ice diameter, and L_{pp} stands for the length between vertical lines.

So far, the dynamic method is highly accurate, and it can be utilized to simulate the variation of the load in a certain polar environment. However, due to the complicated relationship between the ice and the ocean in the polar region, there are many types of ice-strengthened vessels, and the sailing conditions are very varied. A dynamic model has to recreate all the options, and this requires a large number of computational resources. It is a small sample event with weak generalization ability, and it cannot meet the requirement of high-speed simulation in polar regions.

2.1.2 Data-driven model

The statistical models are mainly based on data driving, and the effects of sea ice and other factors on ships are investigated by statistical algorithms. For instance, the relationships between the displacement and the thickness of sea ice, the concentration of sea ice, and the ice sheet were established by regression analysis (Jeong et al., 2021).

Based on Automatic Identification System (AIS) ship data, as well as sea-ice data from satellite observations, Löptien and Axell (2014) calculated velocity using multivariate regression. The mapping relationship between the ice shelf and the ice sheet, as well as the displacement depth and direction angle, was built to predict the speed performance of the various vessels in the ice (Löptien and Axell, 2014).

As a result of the rapid development of machine learning technology, Milaković et al. (2020) applied artificial neural networks to speed up reasoning in Arctic areas. By characterizing the acceleration/deceleration effect of sea ice on the ship, the speed of the ship was calculated (Milaković et al., 2020).

The main limiting factor of data-driven speed is that sea ice data cannot be matched by ship information due to different data sources (Milaković et al., 2020). Because of the poor temporal and spatial resolution of the AIS model, it is difficult to describe the interglacial channel due to the low time and space resolution of the sea ice model. Thus, wrong velocity patterns are produced, and this influences the validity of the model training. In order to do so, Similä and Lensu (2018) utilized high-resolution Synthetic Aperture Radar images to precisely describe the polar seas. The AIS temporal and spatial data were employed to train stochastic forest models. The performance of the training was more consistent with the actual sailing speed of the vessel (Similä and Lensu, 2018).

Thus, the statistical model is to establish a general empirical relationship that can be applied to different types of ships in complex polar sea conditions. Since the model is based on ship and ice data, the results are more in line with the reality of

navigation. However, because of the uncertainty and randomness in the choice of variables, the reliability and stability of the proposed model should be validated.

2.1.3 Summary

Based on the above-mentioned literature review, different types of speed inference models and their errors in predicting ship speed are sorted out in Table 1.

In order to reduce the uncertainty of ship forecasts, improve their robustness, and save computational resources, the integration of dynamic and statistical models must be enhanced.

Figure 2 proposed a new framework where the dynamic and statistical models were combined. The framework adopted the concept of transfer learning with two stages (Zhang et al., 2022). In the first stage, the mixed dynamic models were incorporated to generate large samples of certain vessels at various operating conditions. A transfer network of ship speed in ice was constructed and pre-trained by these samples. In the second stage, it was possible to derive a quantitative relationship between environmental performance, vessel performance and velocity based on the historical navigational data through the statistical models, and thus corrected the pre-training pattern.

TABLE 1 Summary of ship speed inference models.

Type	Method	Ship speed error
Data-driven model	Regression analysis (Jeong et al., 2021)	2.7%-17.3%
Data-driven model	Artificial neural network (Milaković et al., 2020)	2.6%-9.4%
Data-driven model	Random forest (Similä and Lensu, 2018)	≤9%
Dynamic model	Mathematical ship model (Lubbad and Løset, 2011)	≈7%
Dynamic model	Ship performance model (Li et al., 2020a)	≤10%
Dynamic model	General empirical equation (Huang et al., 2021)	≥10%

2.2 Polar shipping cost

An important reason that the Arctic passage has attracted the world's attention is the potential cost advantage of shipping due to its short distance. This is not a simple linear problem with a negative connection with the route distance.

The economic cost of navigating in the NEP depends on the ability of the ship's ice resistance level, the cost of building the vessel, the cost of fuel (fuel consumption, fuel price, and fuel types), the operational expenses (staff wages, insurance, and repairs and maintenance), as well as the combination of several factors including piloting and ice-breaking charges (Theocharis et al., 2019). Apart from the determination of the voyage time and the area of the NEP, sea ice will also have an impact on the sailing speed, route design, and operating costs of vessels (Wang et al., 2021).

To adapt to the harsh weather and environmental conditions of the NEP, ships operating in the NEP require more powerful engines and sturdier hulls. This has resulted in higher ship-building costs compared to those of the traditional passage (Erikstad and Ehlers, 2012). As for operational costs, because of the high risk of Arctic maritime transport, extra maintenance and insurance costs have to be incurred to actively avoid accidents and mitigate risks. At the same time, crew members with ice sailing experience and the ability to cope with harsh conditions also need more salaries. Fuel cost is also one of the key factors affecting shipping costs. A ship's fuel consumption is determined by its size, hull structure, speed, durability, and design. Since the NEP is relatively short, it is advantageous in terms of fuel expenditure. In the Arctic, however, according to the International Maritime Organization's sulfur limit,

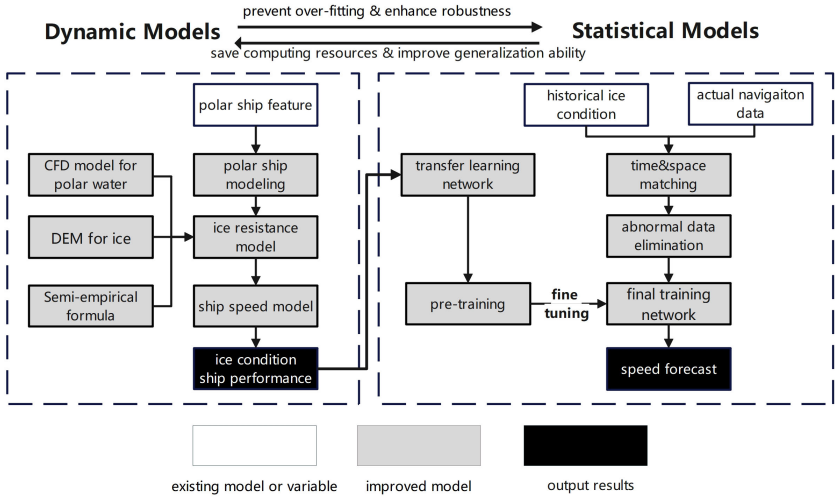

FIGURE 2
Speed reasoning network of coupled dynamic and statistical techniques.

ships have to utilize cleaner fuels at a higher cost compared to traditional fuels (Wan et al., 2018).

The estimate of the parameters in the current Arctic NEP potential evaluation models are very different and uncertain (Tables 2–4). On the one hand, the estimates of relevant factors in Arctic NEP (like ship-building, fuel, and operational costs) are highly subjective. Experts' different understandings of the problem and optimistic and conservative expectations for the future have resulted in controversial conclusions (Theocharis et al., 2018).

On the other hand, there is a lack of quantification of the multiscale effects of sea ice in the models (Wang et al., 2021). The effects of sea ice variability are usually used to determine the navigable time and navigable area. Few studies have considered the impact of sea ice changes on fuel consumption, route distance, and icebreaker charges. Models typically use many assumptions rather than parameters estimates. Although the computational complexity of the model is simplified in this way, it also brings uncertainty to the assessment. For instance, the thermal distance of the NEP is regarded as a constant, and the design of the channel does not change with changes in sea ice.

To address the aforementioned issue, Solakivi and his research team (2019) used Clarkson's World Fleet Register data to analyze the extra economic cost of NEP vessels with various sizes/ice classes (Solakivi et al., 2019). This included extra fuel costs, extra shipping costs, and extra operational expenses. However, the data quality, the choice of factors, and the differences in statistical models have resulted in uncertainty in the outcomes of data-driven assessments. Especially, the data from the above-mentioned documents were obtained in the winter, and the samples were not sufficiently representative. Furthermore, the 2015 figures were taken into account for transportation costs up to 2022 or beyond, with no consideration for changes in the economic cost over time.

To make full use of expert knowledge and data-driven analysis, Wang et al. (2023) proposed a new framework for economic analysis of marine transportation (see Figure 3), where uncertainty is given more attention than the current research (Wang et al., 2023). First, a new quantitative method was used in conjunction with an importance ranking method to capture uncertainty in the evidence and to perform multi-source evidence fusion. Second, a Bayesian network model was chosen as a tool to convey the uncertainty from one variable to another variable. Third, the Bayesian network was well-trained by the fused multi-source evidence, and was able to combine expert knowledge and statistical results in a probabilistic manner to achieve inference about the economic costs of future polar voyages. Finally, the trained network was used for sensitivity analysis and quantitative evaluation of key factors affecting the polar economy.

TABLE 2 Different conclusions regarding additional fuel costs.

considered Ice class category	Extra fuel consumption rate	Resource
IB	+67%	(Liu and Kronbak, 2010)
IA, IAS	+8%	(Lasserre, 2014)
Ice class	+8%; +10%; +30%	(Furuichi and Otsuka, 2014; Zhang et al., 2016; Wan et al., 2018)
IC; IB; IA, IAS	+2%; +3%; +10%	(Omre, 2012)

2.3 Polar navigation safety

For Arctic weather routing, in addition to considering the above navigation speed and navigation costs, the security of navigation is clearly of paramount importance. As a result of the unique geographical environment of the Arctic region, apart from the

TABLE 3 Different conclusions regarding additional shipbuilding costs.

considered Ice class category	Extra building cost	Resource
IB	+20%	(Liu and Kronbak, 2010)
IAS, IA	+20%	(Lasserre, 2014)
IAS-IA	+5-7%	(Pruyn, 2016)
IAS; IA; IB; IC	+12%; +9.5%; +7.5%; +6.5%	(Eide et al., 2010)
PC7 to PC4*	+20%	(Schøyen and Bråthen, 2011)
PC6	+20%	(Dvorak, 2009)
PC4	+30%	(Eide et al., 2010)
DAS+high	+30-40%	(Chernova and Volkov, 2010)
CAC3	+30%,+40%	(Somanathan et al., 2009)
Ice class	+10-35%; +20%; +25%; +30%; +30%; +36%	(Zhang et al., 2016; Kiiski, 2017; Wang et al., 2018)
Ice class	Derived based on the data from Clarkson's World Fleet Register	(Solakivi et al., 2019)

*According to the approximate equivalence of ice class classification systems, PC6 is equal to IAS and PC7 is equal to IA.

TABLE 4 Different conclusions regarding operating expenses (USD/day).

Payload (TEU)	Crew cost		Maintenance		Insurance		Other		Resource
	SCR	NSR	SCR	NSR	SCR	NSR	SCR	NSR	
3800	2740	+0%	1644	+100%	3288	+0%			(Omre, 2012)
4000	3333	+0%	1280	+100%	3344	+0%	1445		(Verny and Grigentin, 2009)
4000	2749	+10%	465	100%	803	+19%	3211	+0%	(Kiiski, 2017)
4000	2740	+0%			1321	+50%			(Furuichi and Otsuka, 2014)
4300	2500	+10%	1200	+100%	1400	+50%	1000	+50%	(Liu and Kronbak, 2010)
4500	4333	+10%	1667	+20%	2192	50%			(Lasserre, 2014)
5089	3767	+50%	2638	+10%	8990	+50%	1883	+10%	(Wan et al., 2018)
5500	3640	+10%	725	+20%	3080	24.6%	1250	+0%	(Zhang et al., 2016)
–	–	+11-14%		+150%		+50%			(Somanathan et al., 2009)

traditional factors such as wind, waves, and other factors, the influence of sea ice on safe navigation should be taken into account. Though the Arctic NEP is essentially navigable in the summer, there are still a few marine regions that are frozen.

There are two major types of risk evaluation in Arctic NEP. The first type is risk assessment by considering risk probability or empirical formula. The other type adopts a standardized risk quantification framework that combines critical navigation conditions (such as the sea ice index in the sea ice regional navigation system issued by Transport Canada, and the risk index in POLARIS issued by the International Maritime Organization) (Browne et al., 2022).

The benefit of risk assessment by considering risk probabilities or empirical formulas is that it is possible to draw probabilistic conclusions if the effect of sea ice is not sufficiently clear. The model of reasoning combined with the experience can provide assessment results that are consistent with general cognition. For example, Li et al. (2021b) employed the Dynamic Bayesian Network (DBN) approach to assess the navigational hazard of a particular route according to influencing factors like wind velocity, temperature, wave height, and ice depth (Li et al., 2021b). They built the network nodes according to subjective experience and computed the DBN time transmission probability. Through the dynamic time transfer nodes, the study could enable the dynamic risk assessment of probability changes as the background field changes. However, this method requires reliable expertise to determine probabilities for various types of ships, and its generality has to be reviewed. Besides, in the quantification of sea ice, the study only considered the effect of sea ice concentration, without taking into account the effect of factors like the thickness of the sea ice on the hazard and velocity of the vessel. Lehtola et al. (2019) applied a subjective experience formula to comprehensively consider the effects of sea ice concentration, thickness, and ice ridges on vessel navigation (Lehtola et al., 2019). Furthermore, the impact of sea ice on

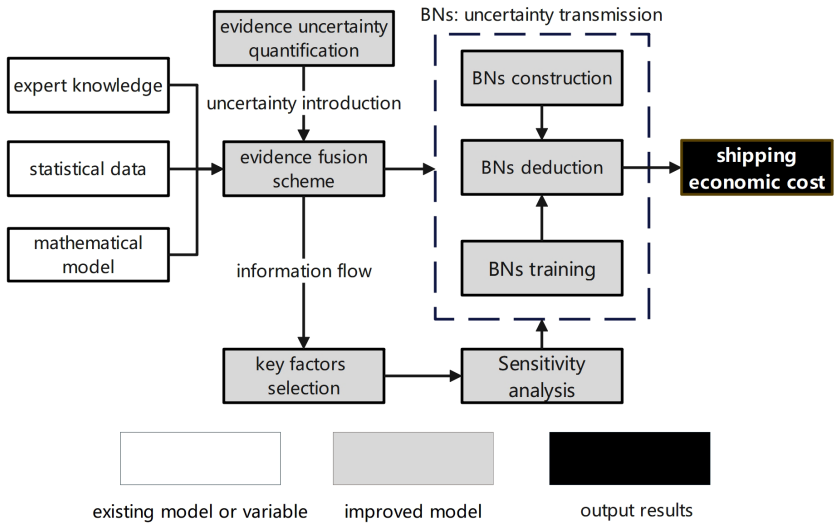

FIGURE 3
Multi-source heterogeneous economic cost inference model.

navigational risks was mapped to navigation speed for navigation. Compared with the probability of DBN, the empirical equation could provide a distinct hazard outcome. The study could also provide a reasonable quantification of factors, such as the concentration and thickness of sea ice, and the calculated results were very informative. However, the empirical formula is based on some necessary assumptions, such that calculated results are not correct and the real sailing conditions are not consistent. Moreover, the empirical formula is based on the fixed information of some factors, and it does not consider the subjective initiative of the crew in the actual voyage.

The second approach is based on determining the safe margin of navigation combined with critical navigational conditions. The POLARIS not only considers sea ice concentration and thickness data, which are the most important factors for navigation, but also takes into account seamen's subjective experience. POLARIS integrates the related experience with other techniques, such as the Canadian Arctic Ice Navigation System, the Russian Ice Zone Certificate, and the Assistance to the Pilot Ice Zone as described in the Navigation Regulations of the Northern Sea Route (Deggim, 2018). The formula for calculating the risk value is as follows:

$$RIO = (C_1 \times RIV_1) + (C_2 \times RIV_2) + (C_3 \times RIV_3) + \ldots + (C_n \times RIV_n) \quad (5)$$

where $C_1 \ldots C_n$ are the sea ice concentration, and $RIV_1 \ldots RIV_n$ are determined by the ice level of the ship and the thickness of the sea ice (see Table 5). As a framework for navigation guidance in polar areas, the POLARIS can evaluate the navigation risks under different ice conditions according to the ice level of the ship. Based on the navigation risks, navigation instructions such as the need to slow down or to recommend detours are presented in Table 6 (Engtrø et al., 2020). The system can be utilized as a risk restraint in ship navigation, and the recommended speed is based on the risk range (Table 7). For example, Li et al. (2020b) calculated the speed of the ship through ice resistance and introduced the risk index of the POLARIS as a navigation risk constraint in route planning (Li et al., 2020b). Route planning was carried out according to the thickness and concentration of sea ice to ensure the safe navigation of ships. Lee et al. (2021) computed the sailing power based on the ship's evaluation model and introduced the POLARIS into route planning (Lee et al., 2021). The research was based on POLARIS' guidance to constrain the sailing speed and to ensure the safety of the planning results. For Arctic meteorological navigation, the POLARIS can not only quantify the risk of sea ice cover for ship navigation but also can regulate the navigation of ships based on the quantified risk value, which has good applicability in meteorological navigation issues.

3 Literature review for IRAs

The components of a route-finding algorithm can be illustrated by formulating the task in terms of an optimization problem. The objective function models the cost for a ship to travel along a given path between destination A and destination B. This cost may be measured by the journey time, the shipping costs, or the voyage risk caused by the ice loading.

TABLE 5 Risk index values (Li et al., 2020b).

Ice Class	Ice-Free	New Ice	Grey Ice	Grey White Ice	Thin First Year Ice 1st Stage	Thin First Year Ice 2nd Stage	Medium First Year Ice less than 1 m thick	Medium First Year Ice	Thick First Year Ice	Second Year Ice	Light Multi Year Ice less than 2.5 m thick	Heavy Multi Year Ice
PC1	3	3	3	3	2	2	2	2	2	2	1	1
PC2	3	3	3	3	2	2	2	2	2	1	1	0
PC3	3	3	3	3	2	2	2	2	2	1	0	-1
PC4	3	3	3	3	2	2	2	2	1	0	-1	-2
PC5	3	3	3	3	2	2	1	1	0	-1	-2	-2
PC6	3	2	2	2	2	1	1	0	-1	-2	-3	-3
PC7	3	2	2	2	1	1	0	-1	-2	-3	-3	-3
IA Super	3	2	2	2	2	1	0	-1	-2	-3	-4	-4
IA	3	2	2	2	1	0	-1	-2	-3	-4	-5	-5
IB	3	2	2	1	0	-1	-2	-3	-4	-5	-6	-6
IC	3	2	1	0	-1	-2	-3	-4	-5	-6	-7	-8
Not Ice-Strengthened	3	1	0	-1	-2	-3	-4	-5	-6	-7	-8	-8

TABLE 6 Risk index outcome criteria (Bergström et al., 2022).

RIO	Ice classes PC1-PC7	Ice classes below PC7 or ships not assigned an ice class
RIO≥0	Normal operation	Normal operation
-10≤RIO<0	Elevated operational risk	Operation subject to special consideration
RIO<-10	Operation subject to special consideration	Operation subject to special consideration

TABLE 7 Recommended speed limits for elevated-risk operations (Bergström et al., 2022).

Ice Class	Recommended Speed Limit
PC1	11 knots
PC2	8 knots
PC3-PC5	5 knots
Below PC5	3 knots

3.1 Design of background field

First of all, unlike road planning, there is no fixed route in polar marine areas. The coastline map of the shipping area defines the objective functions, which can be based on various definitions, such as a grid or a diagram linking waypoints, and points in a Cartesian grid or in the form of a triangular-shaped grid (Piehl et al., 2017). Recently, several research studies have been devoted to the development of original ice routing approaches, such as the application of the Voronoi diagram (Liu et al., 2016), and the FEM-based potential theory (Piehl et al., 2017). Based on the existing research on Arctic sea route planning, the design of the background field can be divided into two categories.

One is the discrete background field, which is usually regarded as the standard grid of discretization. For example, Zhang et al. (2019) used a standard grid based on data resolution as the background field in the course simulation of multi-ship operations (Zhang et al., 2019). When Lee et al. (2021) used a genetic algorithm to plan the route in the Arctic sea, the grid of the background field is generated according to the longitude and latitude resolution of sea ice data (Lee et al., 2021). Depending on the latitude, the resolution of the grid also changes, as shown in Figure 4.

The use of discrete standard grids for background field design leads to rough routes obtained by the path planning algorithms, which need to be smoothed afterwards. Since there are only a few fixed choices of ship steering angles in a discrete background field, it is usually only possible to move from the current point to eight surrounding points (Nam et al., 2013). Some studies have interpolated sea ice elements to improve the grid resolution of the background field and reduce the roughness of the route (Kotovirta et al., 2009).

The other is the continuous background field, which is usually irregular. For example, Piehl et al. (2017) used the Delaunay triangulation method to divide the background field into fine irregular triangles, making the ship's turning angle freer (Piehl et al., 2017). The resulting visual continuity is shown in Figure 5 below.

Similarly, Liu et al. (2016) used the Voronoi diagram method to divide the background field into irregular polygons (Liu et al., 2016). This can improve the steering freedom of the ship in the route planning algorithm and make the calculated route smoother. In addition, there are also studies on route planning based on sailing distance and turning angle, which decompose the entire route into many short routes of different lengths and angles (Lee et al., 2018). A smooth route can also be obtained by this method when the route segmentation is fine.

Although routes generated based on discrete and continuous background fields have different roughness, they often need to be smoothed at a later stage. Several studies have shown that the difference in background field design has little effect on the results of route planning, but mainly affects the calculation time of the algorithm. Despite the concern that the convergence speed in continuous conditions is usually slower in comparison to the discrete conditions because more alternatives are involved in the former, the algorithms reach an optimal solution at a similar iteration (Choi et al., 2013).

3.2 Selection of path planning algorithm

In addition to the above background field design differences, the most significant difference between ice routing studies is the choice of a path planning algorithm. In the current research on ice route planning in the Arctic, the methods used can be roughly divided into the following:

The first is a direct search algorithm, such as the Powell method. This kind of algorithm has high computational efficiency, but it is easy to fall into local optimization, and algorithm convergence is difficult (Kotovirta et al., 2009).

The second is a greedy search algorithm, such as the Dijkstra algorithm. Nam et al. applied the Dijkstra algorithm to choose the best way on a set of segments along the Northern Sea Route (Nam et al., 2013). If there is no negative objective function value in the search area, the Dijkstra algorithm can achieve the global optimal solution by checking all the explored nodes. But for a large sea area, the search speed of this algorithm will be significantly reduced, and a lot of memory will be consumed.

The third is a heuristic algorithm, such as the A* heuristic algorithm. Ice route planning based on the A* heuristic algorithm has attracted much attention in recent years because of its high search efficiency (Guinness et al., 2014). Some studies contain modifications of the basic A* algorithm for better applicability to the considered problem (Wang et al., 2018). The heuristic search algorithm can measure the distance relationship between the search location and the target location. This makes the search direction preferentially oriented to the target location and improves search efficiency.

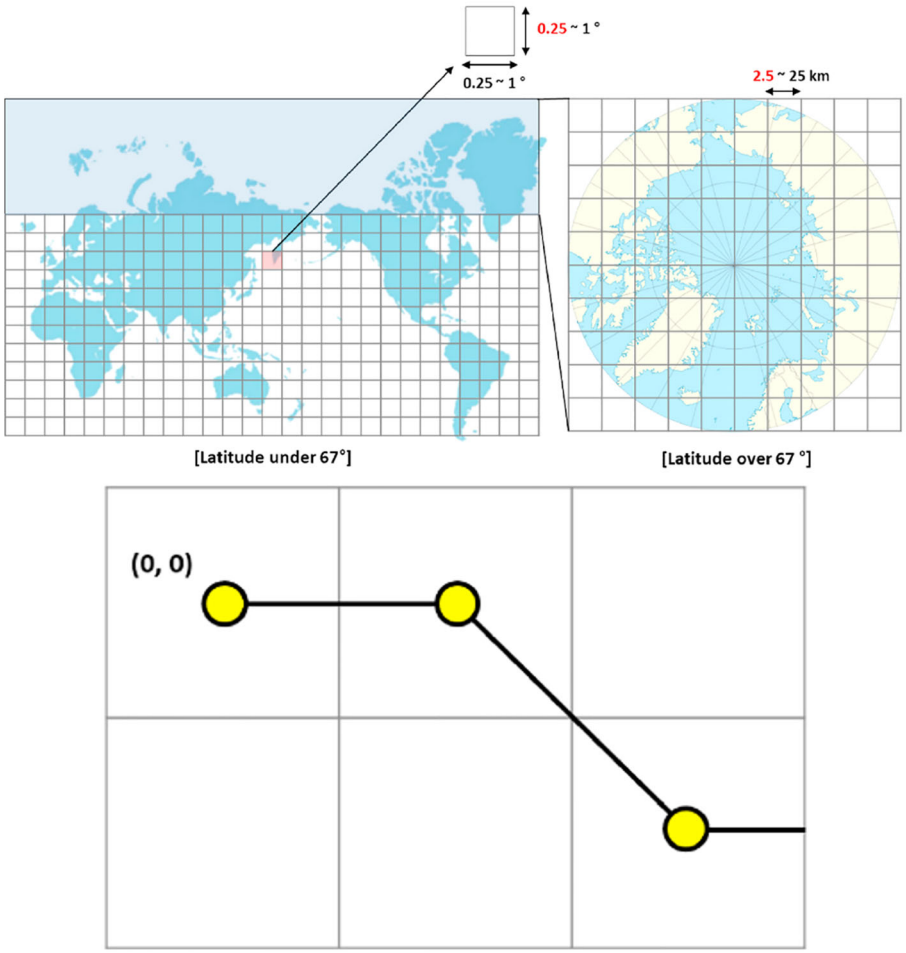

FIGURE 4
Background field of normalized grid points (Lee et al., 2021).

The fourth is a random search algorithm, such as the Genetic Algorithm (GA). Choi et al. contributed to the problem of ice routing by introducing the genetic optimization algorithm instead of the "greedy" one (Choi et al., 2013). This algorithm is suitable for multi-objective programming, especially when the weight of goals cannot be measured. The random search algorithm can get a good solution quickly. But the algorithm depends on parameter initialization, and the performance of the algorithm is greatly affected by the random search operator (Katoch et al., 2021). Therefore, it is difficult for the random search algorithm to achieve global optimization.

The algorithm in the above research mainly focuses on static route planning and cannot respond to the change of background field. In addition to the above algorithms, there are also LPA* and

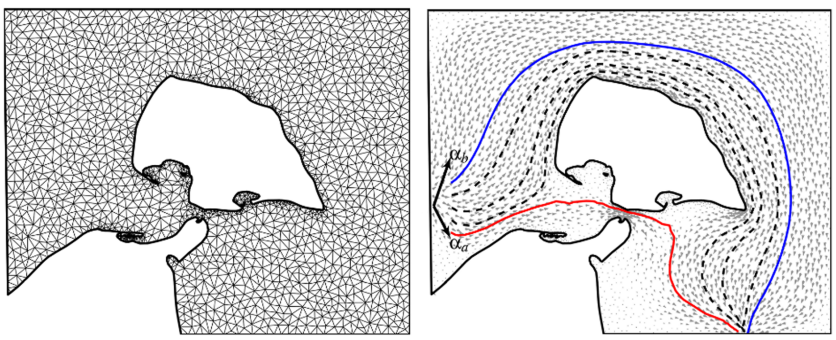

FIGURE 5
Background field of triangulated grid points (Piehl et al., 2017).

D*lite algorithms suitable for dynamic programming. The LPA* algorithm is a forward incremental search algorithm. In a dynamic environment, the LPA* algorithm can adapt to the change of obstacles in the environment. When the obstacles change, the distance information obtained previously is used for secondary planning without recalculating the entire environment. However, this algorithm cannot guarantee the pass ability of the unsearched area, because it can only be calculated based on the distance information from the current point to the starting point and the estimated information to the target point (Koenig and Likhachev, 2005). In the process of approaching the target point, the D*lite algorithm can deal with the emergence of dynamic obstacle points through static search in the local scope. The heuristic algorithm can guide the search direction to the target point in each search, which can further improve the search efficiency by replacing the limitation of the non-heuristic algorithm to walk around without rules (Jin et al., 2023).

Considering the changes of icefloes and icebergs in the Arctic Sea, the dynamic planning algorithm is more suitable for the route in the ice region. Elements such as icefloes and icebergs usually do not have fixed drift routes, so the location or short-term prediction must be carried out based on real-time observations. Therefore, in order to deal with the variables that change with time, a dynamic path planning algorithm should be introduced to optimize routes in the Arctic Sea. The algorithm can characterize the dynamic influence of dangerous elements such as icefloes and icebergs, and adjust the route based on the constantly updated forecast data (Choi, 2015).

The present dynamic path planning algorithm can be used to describe the variation of the dynamic barrier more effectively. However, dealing with the dynamic variation of the objective function because of the variation of the sea ice is not effective. In the Arctic Sea, the dynamic changes of sea ice not only affect the points of obstacles, but also have a significant impact on the navigable grid points. As the sea ice changes at different times, the objective functions such as the risk and speed change accordingly. For instance, as the sea ice becomes thicker and thicker, the associated navigational hazards and navigational speed will be decreased and increased with time. Even though the obstacles remain unchanged, the objective function has changed with time (Wang et al., 2018). Therefore, the current dynamic path planning algorithm has application problems in Arctic Weather Routing, which need to be further studied and improved.

3.3 Diversity of objective functions

Because of the special nature and ecology of the Arctic region, the route planning for the Arctic Sea should not only consider the changes in the environmental field, but also consider a variety of constraints. As far as the restriction is concerned, the terrain restriction is static and depends on the vessel's type and relative parameters (e.g., dimension, shape, and draft). In the future, the dynamic variation of sea ice is a critical factor that will limit the opening of NEP. (Zhang et al., 2017) presented a new approach to scheduling Arctic maritime routes with multiple constraints on physical and operational aspects.

As for the object function, the primary aim of Arctic Route Planning is to guarantee safe sailing and prevent damage to the ship due to the harsh environmental conditions. (Li et al., 2021b) adopted DBN to build a road safety assessment model based on environmental factors such as sea ice, which could be utilized to dynamically evaluate the voyage hazard. In addition to security, the cost of navigation should also be taken into consideration. (Topaj et al., 2019) utilized economical criteria to optimize the route design and to make sure that the target can be reached within the scheduled time. At the same time, they not only saved the cost of fuel and other costs but also avoided the problem of damages for violation of the contract due to excessive sailing time. Furthermore, the timeliness of navigation is also crucial. A number of studies have considered polar climates and have employed voyage time as an objective function when planning a path to minimize fuel consumption and to make sure that the destination port is reached on time (Kuhlemann and Tierney, 2020).

Based on the above-complicated constraints and objective functions, it is clear that the single-objective path planning algorithm has no capability. Thus, it is necessary to adopt multi-objective route planning. The existing research on multi-objective processing is mainly divided into two methods:

One is to introduce subjective knowledge optimization methods, such as the weighting method, constraint method, and linear programming method. Based on the theory of weights, constraints, and linear programming, a multi-objective function can be converted into a single-objective function. The multi-objective function is solved by the single-objective optimization method. Although this method makes the solution less difficult, it is possible to obtain only one solution, like (Lehtola et al., 2020) who implemented the auto-route optimization with the A * algorithm. Taking into account the timeliness and security characteristics of vessels operating in the Arctic NEP, this optimal framework was developed to assign different weights. In the actual decision-making process, the distribution of weighted values is more subjective. Conflicts may exist between objectives, and it is difficult to specify accurate weights to optimize them all at once.

The other one is based on Pareto optimal solution. This method can find a set of solutions that make each target value compromise, that is, the Pareto optimal solution, to provide a variety of alternative solutions according to different needs. For example, Zhang et al. (2021) used the improved ant colony evolution algorithm to build different types of multi-objective route planning models, aiming at route optimization among conflicting objectives (sailing time, additional navigation resistance, and navigation safety) (Zhang et al., 2021). Fabbri and Vicen-Bueno (2019) introduced the second-generation fast non-dominated genetic algorithm (NSGA-II) to solve the Pareto optimal set under multi-objective conditions (Fabbri and Vicen-Bueno, 2019).

However, the application of the multi-objective optimization method in the Arctic Sea is less. Considering that the multiple objective functions to be considered in the Arctic route planning are complicated, it is difficult to give weights based on subjective knowledge. Therefore, multi-objective optimization algorithms based on Pareto have high applicability, such as the NSGA-II algorithm. More research should be done on multi-objective optimization in Arctic Weather Routing.

4 Discussion

Since most of the research on IRAs in Section 3.2 used only one algorithm, the differences between algorithms were not compared. Therefore, we replicated and compared the existing algorithms with experiments based on the background field of normalized grid points to study the effects of different algorithms under different objective functions. In addition to the static path planning algorithm in Section 3.2, we also introduced the D*lite dynamic path planning algorithm here. The applicability of static and dynamic path planning algorithms in ice route planning was tested.

Further, through the literature review in Section 3, we identified the problem in the current research, i.e., how to deal with the dynamic multi-objective path planning in the Arctic Sea. There would be a variety of solutions to this problem, and we proposed a solution here, the D*-NSGA-III algorithm. We compared the dynamic multi-objective optimization capability of D*-NSGA-III algorithm based on the replication and comparison experiments of existing algorithms.

4.1 Data description

This experiment used the sea ice thickness data of PIOMAS (Pan-Arctic Ice-Ocean Modeling and Assimilation System) and the sea ice concentration data of NSIDC (National Snow and Ice Data Center). The spatial resolution was unified to a grid of 0.25°×0.25°, and the time resolution was one day. The ship navigation data of the IA ice class was derived from Automatic Identification System (AIS).

Sea ice concentration from the National Snow and Ice Data Center (NSIDC) is a daily grid data. The data was synthesized from the Nimbus-7 satellite and microwave detection data from the Defense Meteorological Satellite Program (DMSP) and DMSP-F17 satellite (Tschudi et al., 2020).

PIOMAS is an Arctic sea ice numerical simulation system that includes multiple elements of sea ice and ocean (Zhang and Rothrock, 2003). Improving numerical simulation results by assimilating sea surface temperatures from ice-free areas and using different ice strength parameters can provide daily grid data on sea ice thickness.

AIS is a modern navigational aid system that transmits information such as ship speed back to ground base stations. The frequency reported by the ship is generally 12 seconds/time, and when the course changes, it is generally 4 seconds/time. The AIS data set of 2018 was used in this experiment. The ice class of the ship was Class IA and the speed was up to 22 knots.

4.2 Design of experiment

This experiment is divided into two main parts. The first part of the experiment, based on four algorithms (D*lite, A*, Dijkstra, GA), takes navigation safety cost (RIO), sailing time cost (Time), and sailing distance cost (Distance) as a single objective function to test the effectiveness of the four algorithms.

In the second part of the experiment, the D*-NSGA-III algorithm is used to obtain the Pareto optimal solution set of the dynamic multi-objective path planning problem by considering the constraints of three objective functions, RIO, Time, and Distance, under the dynamic background field. By comparing with the results of the first part, we test whether the algorithm can be used to solve the dynamic multi-objective path planning problem in the Arctic Sea, and verify the effectiveness of the algorithm.

To control the variables, the following experiment takes the port of Petropavlovsk-Kamchatskiy (53°1′N,158°39′E) as the start point and the port of Rotterdam (51°55’ N, 4°29’E) as the endpoint. This experiment assumes November 2, 2020, as the departure time, and only two environmental factors, sea ice concentration and sea ice thickness, are considered. Navigation risk is calculated based on the RIO value of the POLARIS. The speed inference model is based on the random forest algorithm to fit the relationship between sea ice concentration, thickness and ship speed (Wang et al., 2021). The area where RIO is less than -10 is considered as an unnavigable obstacle. The area of RIO between -10 and 0 is considered to require icebreaker assistance, and the speed is fixed at 4 knots. The area of RIO between 0 and 30 is calculated by the random forest model. Areas of RIO greater than or equal to 30 are at full speed, with a speed of 22 knots.

In the first part of the experiment, only two variables of the algorithm (4 kinds) and the objective function (3 kinds) are changed in this study, and a total of 12 route planning results are obtained. Three aspects of work have been carried out:

Firstly, the effects of algorithms on ice route planning (taking A*, Dijkstra, GA as examples) are compared.

Secondly, the influence of different objective functions on the route planning algorithm is verified.

Thirdly, the applicability of static path planning algorithm and dynamic path planning algorithm (taking D*lite as an example) in ice route planning is tested.

In the second part of the experiment, this study uses the D*-NSGA-III algorithm to obtain the Pareto optimal solution set by taking RIO, Time, and Distance as multi-objective constraints. To clearly show the result of path planning, this paper only shows three optimal paths under different goals.

4.3 D*-NSGA-III

Because the D*lite algorithm only updates the values of adjacent or related points when the obstacle is changed. The remaining grid points which are always passable still retain historical values. Therefore, the objective function value of the passable point does not change with the background field, resulting in the feasible solution found by the algorithm not being the optimal solution.

In addition, D* lite has a problem with addressing multiple objectives during the planning. This algorithm takes the utility function as the basis of the choice of the route. Although the multi-pole utility function can be set at the same time, there is still a need to enhance the consistency and understanding of the various objectives. The NSGA algorithm performs well in multi-objective optimization. Furthermore, NSGA-III improves the crowding classification of population screening more than NSGA-III, thus allowing more diversity of algorithm results (Deb and Jain, 2014). The NSGA-III

algorithm is employed to randomly find the best solution in the solution space, and it is utilized to generate a new population. The algorithm is based on the Pareto theory and uses non-dominant sorting to sort and filter the crossed and mutated populations. The diversity of the screened populations is guaranteed through preset reference points. However, NSGA-III also has some problems with Arctic weather navigation. The population initialization is complicated, particularly in the Arctic meteorological navigation, and it is difficult to find a viable solution to accommodate the variations in the background field.

In summary, the optimization of the Arctic NEP should not only deal with the dynamic variation of the parameters and the utility function but also should deal with the multi-objective function constraints. To solve this dynamic multi-objective ice routing planning problem, we propose a possible solution. Based on the population iterative optimization framework of NSGA-III, we combine D*lite and NSGA-III algorithms to propose D*-NSGA-III algorithm. The technical flow of the algorithm is shown in Figure 6 below.

In the initialization module, the D*lite algorithm can smoothly generate the initial population, even though it is not necessarily the best estimate. Based on the population generated by D*lite initialization, NSGA-III can find the Pareto optimum through cross-variation and population selection. Ultimately, the D*-NSGA-III algorithm can come up with multiple sets of feasible solutions. The solution distributed on the leading edge of Pareto is the optimal solution under the multi-objective function constraints, and the appropriate route can be chosen based on the different navigation tasks.

4.4 Objective function

In this experiment, the calculation of safety cost is based on the RIO value in Section 2.3. The value of RIO in POLARIS ranges from -10 to 30. A larger value indicates more security. The safety cost of navigation adopts the cumulative RIO value method:

$$S = \sum_i (40 - (RIO_i + 10)) \tag{6}$$

Where i represents the grid point through which the route passes. Since the cost function in the algorithm should be as low as possible, we invert RIO when calculating the cumulative value of the cost function and adjust it to the range of 0~40.

The cost of route distance D is calculated based on the results of track planning as follows:

$$\begin{aligned} D &= \sum_i D_i \\ &= \sum_i R \times \arccos[\cos(y_{1i})\cos(y_{2i})\cos(x_{1i} - x_{2i}) + \sin(y_{1i})\sin(y_{2i})] \end{aligned} \tag{7}$$

where R is the radius of the earth, and (x_{1i}, y_{1i}), (x_{2i}, y_{2i}) are the latitude and longitude of the two points i in the segment. The distance is measured in nautical miles (nm).

The cost of sailing time T is calculated based on the distance and the average speed of the two points, as follows:

$$T = \sum_i D_i / (V_{1i} + V_{2i}) \tag{8}$$

Where D_i is the sailing distance between two points, V_{1i} and V_{2i} are the speed at two points of the course. The speed is obtained by the speed inference model established in Section 4.2. Sailing time is measured in hours.

4.5 Replication and comparison of existing studies

For the static planning algorithm (A*, Dijkstra, GA), since the algorithm could not consider the daily refresh of the background field, the sea ice concentration and thickness on November 2 are always used as the background field for navigation planning. The population number of the GA algorithm is 100 and the number of iterations is 300. As for the dynamic planning algorithm (D*lite), the algorithm can update the sea ice background field every day, and continue to plan the subsequent route according to the changes in obstacles.

The above four algorithms are executed three times and set as the objective functions of RIO, Time and Distance, respectively. Finally, 12 routes are obtained for comparison.

The navigability and objective function values of the above 12 routes are calculated under the actual dynamic navigation environment. From November 2, when the sailing time of the route accumulates for one day, the background field is refreshed to the sea ice value of the next day. The navigability and objective function values of each route are shown in Table 8 below.

The orange marks in Table 8 are the optimal results for the corresponding single-objective function. As can be seen from the table, when RIO is taken as the objective function, that is, the pursuit of the lowest cost of navigation safety, all routes of the 4 algorithms can be used, and the D*Lite algorithm has the best results. Among the static planning algorithms (A*, Dijkstra, GA), GA has the best effect.

However, taking the shortest time or shortest distance as the single-objective function will cause some statistical routes to be impassable. Because the routes with a short time or short distance tend to the high-latitude sea areas. However, most of the high-latitude sea areas are covered by sea ice and the sea ice changes significantly. Most of the existing studies on ice route planning are static algorithms, which can only consider a constant background field. However, when the high-latitude sea ice changes day by day, the sea ice in some areas may become thicker, resulting in some points in the static route being impassable.

All navigable routes are shown in Figure 7 below.

From the above figure, there are obvious differences in the route planning results of the same algorithm with different objective functions. Routes with lower navigation safety costs are mostly located in low-latitude sea areas, while routes with lower time cost and lower distance cost tend to be in high-latitude sea areas. To better reflect the relationship between dynamic changes of background field and route planning, we show the route planning process with RIO, SIC, and SIT as background in (Appendix Figures 10-12) .

The data resolution used in this experiment is 0.25°, which is undoubtedly rough for product applications. It can be seen from the experimental results that the rough resolution will lead to the obvious sawtooth of the route, as shown in Figure 6. However, the purpose of this experiment is to compare the applicability of different IRAs in the Arctic. A resolution of 0.25° or finer may affect the results of the algorithm, but it should not materially affect them.

In general, the existing research on ice route planning mostly uses static planning algorithms, and there are some cases of unnavigable routes in the actual dynamic background field of ice navigation. The dynamic path planning algorithm, such as D*Lite, can be applied to the dynamic changes of Arctic sea ice and has a good application prospect. However, D*Lite cannot refresh the objective function values of globally passable grid points, and its applicability needs to be further improved.

In addition, different objective functions will have different effects on the path planning results. The Arctic Weather Routing involves a variety of objective functions, so how to reasonably carry out multi-objective route planning is also an important research direction in the future.

4.6 Effectiveness of D* -NSGA-III

From November 2, 2020, the sea ice background field was updated daily along with the accumulation of time. The population size of the D*-NSGA-III model was set to 300. The initial population was generated by the D*Lite module based on different objective functions, and the path individuals were repeated to 300 to ensure that the individuals of the initial population were passable. In the course of crossing, two intersections of different routes were selected randomly to cross and swap paths in this section. The mutation node was randomly selected during mutation. After the node's position was changed, if a continuous route could still be found, the mutation would be considered successful. After 100 iterations, the effect of the model tended to be stable, and the individuals in the final population were all F1 individuals, that is, the Pareto optimal solution set. The Pareto surface formed by this solution set was shown in Figure 8 below:

TABLE 8 The navigability and single-objective function value of 12 routes (× represents that the route is actually impassable).

Algorithm \ Objective function	RIO	Time (hour)	Distance (nm)
D*Lite	22636.648	336.910	5943.144
A*	18995.475	333.935	×
Dijkstra	6754.590	327.152	×
GA	21387.928	×	6036.900

The shaded part represents the best value in the current column.

From the above graph, it can be observed that the optimal results of D*-NSGA-III have excellent population diversity. To pursue the shortest voyage, the lowest voyage risk, and the shortest voyage time, or to seek a compromise between several objectives, the Pareto surface, which consists of the above-mentioned points, may serve as a base for selecting routes.

Since there are multiple routes on the Pareto surface, to clearly show the route planning process and facilitate comparison with Tables 8, 9 only shows the three optimal individuals (Individual 1~3) in the optimal order of RIO, Time and Distance, respectively. Taking Individual 1 as an example, this individual has the lowest risk (the highest RIO) in the Pareto surface, as well as the best time and distance costs. Similarly, Individual 2 has the shortest time cost and Individual 3 has the shortest distance cost. The specific values are shown in Table 9.

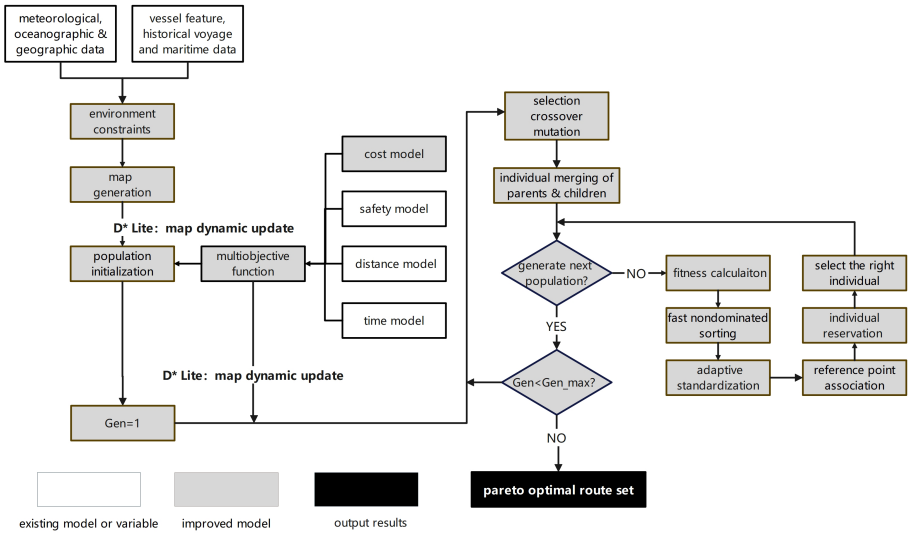

FIGURE 6
D*-NSGA-III dynamic multi-objective path planning model.

The green marks in Table 9 represent the individual results with the optimal objective value in the Pareto solution set when single-objective sorting (columns in the table). Because D*-NSGA-III is a multi-objective optimization algorithm, all individuals (rows in the table) have three target values. By comparison with Table 8, it can be seen that when only pursuing a certain objective is optimal, the result of D*-NSGA-III is superior to the other four algorithms. In addition, D* -NSGA-III can consider a variety of objectives, so that the other two objectives are also relatively optimal.

The dynamic process of the above three routes over time is shown in Figure 9 below, taking the RIO background field as an example:

As can be seen from Figure 9, D*-NSGA-III can provide the optimal route with multi-objective optimization according to different mission objectives. When in pursuit of the lowest risk of navigation (Individual 1) or the shortest voyage time (Individual 2), the two routes have high consistency, that is the mid-ocean route. It can not only avoid the time cost caused by long distances in low-latitude sea, but also avoid the time cost caused by high risks in high-latitude sea. When pursuing the shortest sailing distance (Individual 3), the route will be biased towards the high-latitude sea. At the same time, it can ensure the navigability of the route and the relatively optimal navigation risk and navigation time. In order to clearly show the route planning process, only 3 routes are shown here. The appendix shows the route planning process of all Pareto optimal solutions (Appendix Figures 13-15).

Based on the experiments, the D*-NSGA-III algorithm can satisfy the requirement of designing multi-target routing in Arctic waters. D*-NSGA-III can be employed as a guide for multi-target navigation missions.

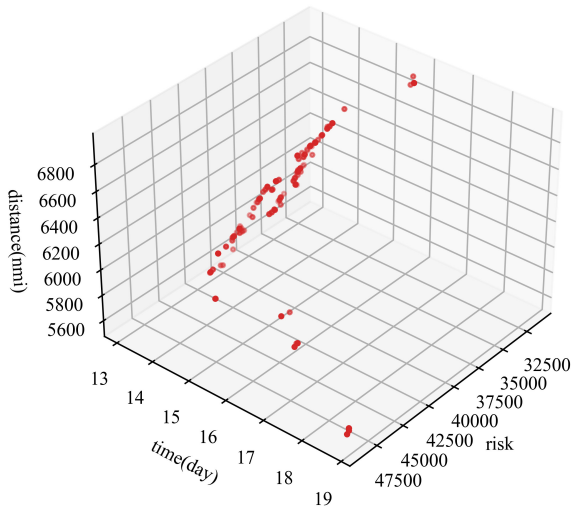

FIGURE 8
Distribution of optimal solution set of D*-NSGA-III. The points represent the fitness of the objective function for each path. Since all individuals are F1 individuals, the same color is used.

5 Conclusion

Our research team has been working on the development of two key components of e-navigation, namely the ship performance methods and ice routing algorithms. The validity of these two models was assessed separately, the shortcoming of existing research was pointed out, and further development of this model was also discussed. Based on the replication and comparison of experiments, we examined the existing research on ice routing planning and pointed out the application prospects of dynamic routing algorithms. This paper proposed a solution to the dynamic multi-objective planning problem in Arctic waters (D*-NSGA-III) and pointed out the future research directions for Arctic weather routes.

- Based on the concept of transfer learning, the combination of dynamic and statistical models contributes to improve the robustness and generalizability of velocity forecasting.

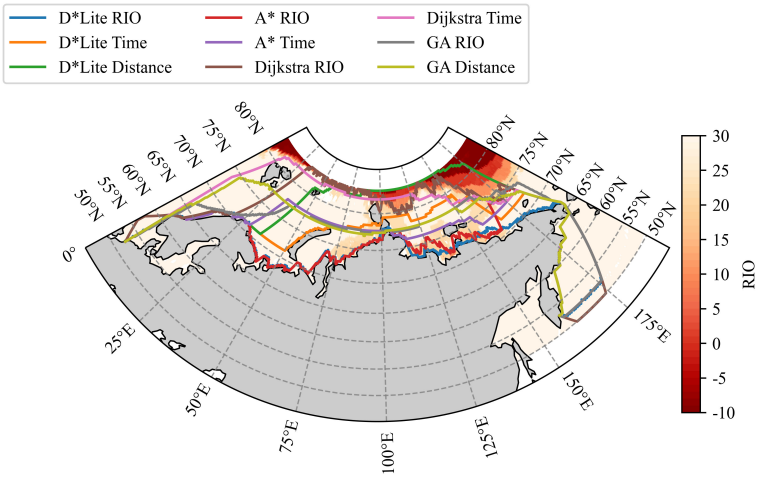

FIGURE 7
Passable route of path planning algorithm. The lines with different colors represent the route planning results of different algorithms (A*, Dijkstra, GA, D*Lite) under different single objective functions (RIO, Time, Distance).

TABLE 9 Multiple objective function values of 3 routes.

Individual \ Objective function	RIO	Time (hour)	Distance (nm)
Individual 1	24864.860	315.759	6077.283
Individual 2	24722.812	313.539	6048.870
Individual 3	11753.088	451.235	5572.599

The shaded part represents the best value in the current column.

- Leveraging expertise and statistics, and combining expertise with statistics in a probabilistic manner, enables the justification of the economic cost of polar navigation based on multi-source heterogeneous evidence.
- Forecasts based on sea ice concentration and sea ice thickness allow the estimation of navigational hazards under critical navigational conditions, making quantitative results more realistic.
- Dynamic route planning algorithm based on multi-objective optimization has a good application prospect in Arctic Weather Routing.

According to the review and analysis of IRAs, the present IRAs are not appropriate for the multi-scale dynamic variation in the Arctic NEP. Moreover, it is impossible to guarantee the diversity of the Pareto optimal solution set. Given these deficiencies, we presented a new adaptation of the IRA, named D*-NSGA-III. The validity of this algorithm was demonstrated by an example. It was proved that the proposed algorithm can achieve multi-objective optimization in the case of sea ice variation, which could satisfy the various requirements of marine transport.

However, because of the limitations of the current measurement techniques, large-scale measurements of sea ice concentration and thickness are mostly based on satellite inversion. There is still room for improvement in the accuracy of the satellite observation data, but the most significant issue is the resolution of the observed data. Different elements of sea ice often need to be observed from a distance. Besides, technical restrictions make it challenging to have accurate observations across the Arctic. Moreover, there is a spatial discontinuity in the background field data from various sources. Some of the background fields are thick, while others are thin. Therefore, it is necessary to deal with the placement and fusion of

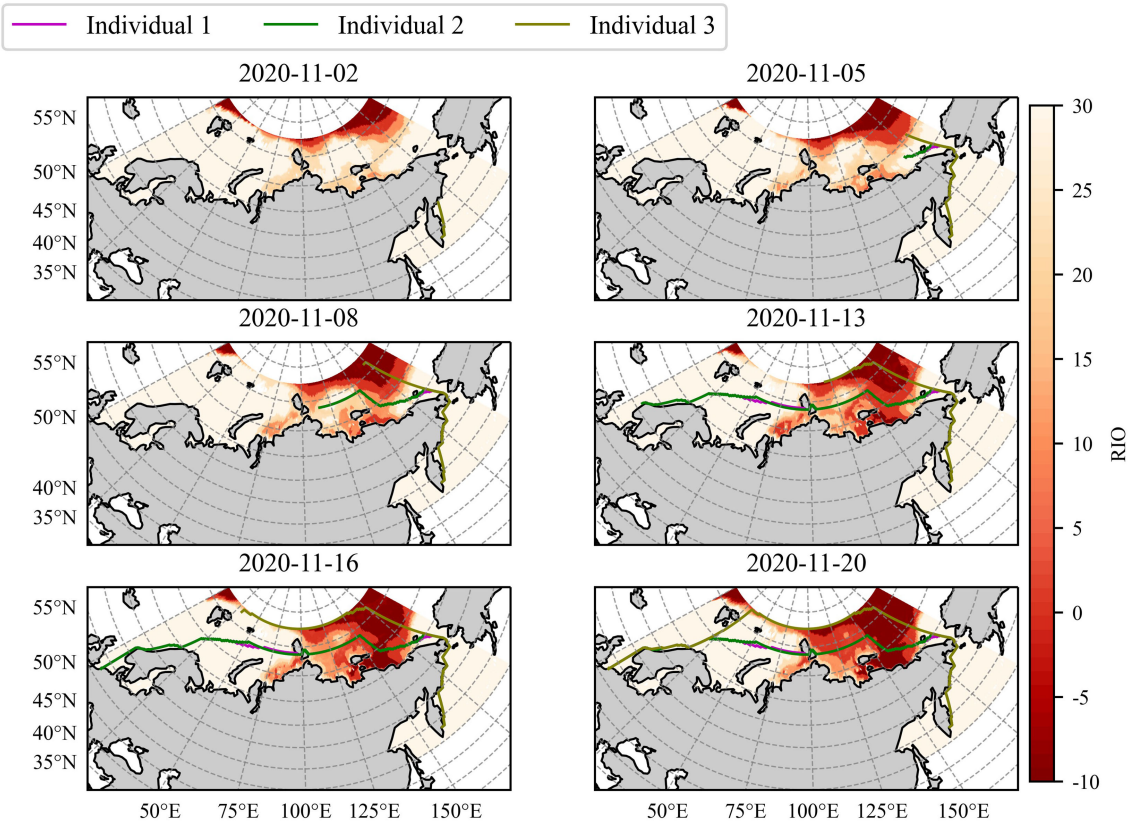

FIGURE 9
Individual 1~3 dynamic multi-objective route planning results. Individual 1 and 2 overlap for the most part.

different grids. Currently, the available resolution of sea-ice data (e.g., ERA5 reanalysis datasets) is usually 0.25° x 0.25°, which is unsuitable for weather navigation (Bormann et al., 2013). Though the SAR satellite has a high resolution, it is impossible to ensure continuous observation, and it is possible to observe only a tiny portion of the ocean.

In the future, the Arctic weather routing should nest grids of different resolutions based on background fields of different spatial resolutions to realize multiscale path planning. It is possible to employ the background field of the numerical model and build the background area of the route planning through multiple grid nets. Multigrid nesting has been applied in the weather model, where a coarse grid indicates the global situation and the nesting of one or more sub-regions (Krol et al., 2005). Likewise, when the background field of route planning is built, the edge region can be procured using thicker resolution data. A delicate mesh is embedded when the marine region or certain vessel region is highly resolved. Thus, it is possible to unify the data of different resolutions to construct a background field for multiscale planning.

Data availability statement

Publicly available datasets were analyzed in this study. This data can be found here: http://psc.apl.uw.edu/research/projects/arctic-sea-ice-volume-anomaly/data/model_grid https://nsidc.org/data/G02202/versions/4.

Author contributions

QL: methodology, algorithm implementation, literature collation. YW: methodology, writing- original draft preparation. RZ: supervision, conceptualization, language editing. HY: data curation, validation. JX: language editing.YG: literature collation. All authors contributed to the article and approved the submitted version.

Funding

The author(s) disclosed receipt of the following financial support for the research, authorship, and/or publication of this article: This work has received funding from the Chinese National Natural Science Fund (No. 41976188) and the Natural Science Foundation of Hunan Province of China (No. 2021JJ40669).

Conflict of interest

The authors declare that the research was conducted in the absence of any commercial or financial relationships that could be construed as a potential conflict of interest.

Publisher's note

Supplementary material

The Supplementary Material for this article can be found online at: https://www.frontiersin.org/articles/10.3389/fmars.2023.1190164/full#supplementary-material

References

Agarwal, R., and Ergun, Ö. (2008). Ship scheduling and network design for cargo routing in liner shipping. *Transp. Sci.* 42, 175–196. doi: 10.1287/trsc.1070.0205

Bergström, M., Li, F., Suominen, M., and Kujala, P. (2022). A goal-based approach for selecting a ship's polar class. *Mar. Struct.* 81, 103123. doi: 10.1016/j.marstruc.2021.103123

Bormann, N., Fouilloux, A., and Bell, W. (2013). Evaluation and assimilation of ATMS data in the ECMWF system. *J. Geophys. Res. Atmospheres* 118, 12,970–12,980. doi: 10.1002/2013JD020325

Browne, T., Tran, T. T., Veitch, B., Smith, D., Khan, F., and Taylor, R. (2022). A method for evaluating operational implications of regulatory constraints on Arctic shipping. *Mar. Policy* 135, 104839. doi: 10.1016/j.marpol.2021.104839

Chen, J., Kang, S., Chen, C., You, Q., Du, W., Xu, M., et al. (2020). Changes in sea ice and future accessibility along the Arctic Northeast Passage. *Glob. Planet. Change* 195, 103319. doi: 10.1016/j.gloplacha.2020.103319

Chernova, S., and Volkov, A. (2010). *Economic feasibility of the Northern Sea Route container shipping development*. Master's thesis. Norway: Bodø University College. 124.

Choi, M. (2015). Arctic sea route path planning based on an uncertain ice prediction model. *Cold Reg. Sci. Technol.* 109, 61–69. doi: 10.1016/j.coldregions.2014.10.001

Choi, M., Chung, H., Yamaguchi, H., and De Silva, L. W. A (2013). Application of Genetic Algorithm to Ship Route Optimization in Ice Navigation. in *Proceedings of the International Conference on Port and Ocean Engineering Under Arctic Conditions* (Espoo, Finland).

Colbourne, D. B. (2000). Scaling pack ice and iceberg loads on moored ship shapes. *Ocean. Eng. Int.* 4 (1), 39–45.

Deb, K., and Jain, H. (2014). An evolutionary many-objective optimization algorithm using reference-point-based nondominated sorting approach, part I: solving problems with box constraints. *IEEE Trans. Evol. Comput.* 18, 577–601. doi: 10.1109/TEVC.2013.2281535

Deggim, H. (2018)."The International Code for Ships Operating in Polar Waters (Polar Code)," in *Sustainable Shipping in a Changing Arctic WMU Studies in Maritime Affairs*. eds. L P. Hildebrand, L. W. Brigham and T. M. Johansson (Cham: Springer International Publishing), 15–35. doi: 10.1007/978-3-319-78425-0_2

Dvorak, R. E. (2009). *Engineering and economic implications of ice-classed containerships*. Thesis. Cambridge, MA: Massachusetts Institute of Technology, 93.

Eide, L. I., Eide, A., and Endresen, Ø. (2010). *Shipping across the Arctic Ocean: A feasible option in 2030-2050 as a result of global warming*. Research and Innovation Position Paper 04-2010. 2010. Available at: https://www.yumpu.com/en/document/view/10675657/shipping-across-the-arctic-ocean-positionpaper-dnv.

Engtrø, E., Gudmestad, O. T., and Njå, O. (2020). The polar code's implications for safe ship operations in the arctic region. *TransNav* 14, 655–661. doi: 10.12716/1001.14.03.18

Erikstad, S. O., and Ehlers, S. (2012). Decision support framework for exploiting northern sea route transport opportunities. *Ship Technol. Res.* 59, 34–42. doi: 10.1179/str.2012.59.2.003

Fabbri, T., and Vicen-Bueno, R. (2019). Weather-routing system based on METOC navigation risk assessment. *J. Mar. Sci. Eng.* 7, 127. doi: 10.3390/jmse7050127

Furuichi, M., and Otsuka, N. (2014). Economic feasibility of finished vehicle and container transport by NSR/SCR-combined shipping between East Asia and Northwest Europe. in *International Association of Maritime Economists Conference 2014* (Norfolk, USA).

Guemas, V., Blanchard-Wrigglesworth, E., Chevallier, M., Day, J. J., Déqué, M., Doblas-Reyes, F. J., et al. (2016). A review on Arctic sea-ice predictability and prediction on seasonal to decadal time-scales. *Q. J. R. Meteorol. Soc* 142, 546–561. doi: 10.1002/qj.2401

Guinness, R. E., Saarimaki, J., Ruotsalainen, L., Kuusniemi, H., Goerlandt, F., Montewka, J., et al. (2014). "A method for ice-aware maritime route optimization," in *2014 IEEE/ION Position, Location and Navigation Symposium - PLANS 2014* (Monterey, CA, USA: IEEE), 1371–1378. doi: 10.1109/PLANS.2014.6851512

Huang, L., Li, Z., Ryan, C., Ringsberg, J. W., Pena, B., Li, M., et al. (2021). Ship resistance when operating in floating ice floes: Derivation, validation, and application of an empirical equation. *Mar. Struct.* 79, 103057. doi: 10.1016/j.marstruc.2021.103057

Huang, L., Tuhkuri, J., Igrec, B., Li, M., Stagonas, D., Toffoli, A., et al. (2020). Ship resistance when operating in floating ice floes: A combined CFD&DEM approach. *Mar. Struct.* 74, 102817. doi: 10.1016/j.marstruc.2020.102817

Jeong, S. Y., Choi, K., and Kim, H. S. (2021). Investigation of ship resistance characteristics under pack ice conditions. *Ocean Eng.* 219, 108264. doi: 10.1016/j.oceaneng.2020.108264

Jin, J., Zhang, Y., Zhou, Z., Jin, M., Yang, X., and Hu, F. (2023). Conflict-based search with D* lite algorithm for robot path planning in unknown dynamic environments. *Comput. Electr. Eng.* 105, 108473. doi: 10.1016/j.compeleceng.2022.108473

Juva, M., and Riska, K. (2002). *On the power requirement in the Finnish-Swedish ice class rules* (Finland: Winter Navigation Research Board).

Katoch, S., Chauhan, S. S., and Kumar, V. (2021). A review on genetic algorithm: past, present, and future. *Multimed. Tools Appl.* 80, 8091–8126. doi: 10.1007/s11042-020-10139-6

Kiiski, T. (2017). *Feasibility of commercial cargo shipping along the Northern Sea Route*. Doctoral dissertation. Finland: Turku School of Economics.

Koenig, S., and Likhachev, M. (2005). Fast replanning for navigation in unknown terrain. *IEEE Trans. Robot.* 21, 354–363. doi: 10.1109/TRO.2004.838026

Kotovirta, V., Jalonen, R., Axell, L., Riska, K., and Berglund, R. (2009). A system for route optimization in ice-covered waters. *Cold Reg. Sci. Technol.* 55, 52–62. doi: 10.1016/j.coldregions.2008.07.003

Krol, M., Houweling, S., Bregman, B., van den Broek, M., Segers, A., van Velthoven, P., et al. (2005). The two-way nested global chemistry-transport zoom model TM5: Algorithm and applications. *Atmospheric Chem. Phys.* 5, 417–432. doi: 10.5194/acp-5-417-2005

Kuhlemann, S., and Tierney, K. (2020). A genetic algorithm for finding realistic sea routes considering the weather. *J. Heuristics* 26, 801–825. doi: 10.1007/s10732-020-09449-7

Lasserre, F. (2014). Case studies of shipping along Arctic routes. Analysis and profitability perspectives for the container sector. *Transp. Res. Part Policy Pract.* 66, 144–161. doi: 10.1016/j.tra.2014.05.005

Lee, H. W., Roh, M. I. L., and Kim, K. S. (2021). Ship route planning in Arctic Ocean based on POLARIS. *Ocean Eng.* 234, 109297. doi: 10.1016/j.oceaneng.2021.109297

Lee, S.-M., Roh, M.-I., Kim, K.-S., Jung, H., and Park, J. J. (2018). Method for a simultaneous determination of the path and the speed for ship route planning problems. *Ocean Eng.* 157, 301–312. doi: 10.1016/j.oceaneng.2018.03.068

Lehtola, V., Montewka, J., Goerlandt, F., Guinness, R., and Lensu, M. (2019). Finding safe and efficient shipping routes in ice-covered waters: A framework and a model. *Cold Reg. Sci. Technol.* 165, 102795. doi: 10.1016/j.coldregions.2019.102795

Lehtola, V. V., Montewka, J., and Salokannel, J. (2020). Sea captains' Views on automated ship route optimization in ice-covered waters. *J. Navig.* 73, 364–383. doi: 10.1017/S0373463319000651

Li, F., Goerlandt, F., and Kujala, P. (2020a). Numerical simulation of ship performance in level ice: A framework and a model. *Appl. Ocean Res.* 102, 102288. doi: 10.1016/j.apor.2020.102288

Li, Z., Hu, S., Gao, G., Yao, C., Fu, S., and Xi, Y. (2021b). Decision-making on process risk of Arctic route for LNG carrier *via* dynamic Bayesian network modeling. *J. Loss Prev. Process Ind.* 71, 104473. doi: 10.1016/j.jlp.2021.104473

Li, Z., Ringsberg, J. W., and Rita, F. (2020b). A voyage planning tool for ships sailing between Europe and Asia via the Arctic. *Ships Offshore Struct.* 0, 1–10. doi: 10.1080/17445302.2020.1739369

Li, X., Stephenson, S. R., Lynch, A. H., Goldstein, M. A., Bailey, D. A., and Veland, S. (2021a). Arctic shipping guidance from the CMIP6 ensemble on operational and infrastructural timescales. *Clim. Change* 167, 1–19. doi: 10.1007/s10584-021-03172-3

Li, X., Wang, H., and Wu, Q. (2017). "Multi-objective optimization in ship weather routing," in *2017 constructive nonsmooth analysis and related topics (dedicated to the memory of V.F. Demyanov) (CNSA)* (Saint Petersburg, Russia: IEEE), 1–4. doi: 10.1109/CNSA.2017.7973982

Liu, M., and Kronbak, J. (2010). The potential economic viability of using the Northern Sea Route (NSR) as an alternative route between Asia and Europe. *J. Transp. Geogr.* 18, 434–444. doi: 10.1016/j.jtrangeo.2009.08.004

Liu, X., Sattar, S., and Li, S. (2016). Towards an automatic ice navigation support system in the arctic sea. *ISPRS Int. J. Geo-Inf.* 5, 36. doi: 10.3390/ijgi5030036

Löptien, U., and Axell, L. (2014). Ice and AIS: ship speed data and sea ice forecasts in the Baltic Sea. *Cryosphere* 8, 2409–2418. doi: 10.5194/tc-8-2409-2014

Lubbad, R., and Løset, S. (2011). A numerical model for real-time simulation of ship-ice interaction. *Cold Reg. Sci. Technol.* 65, 111–127. doi: 10.1016/j.coldregions.2010.09.004

Milaković, A. S., Li, F., Marouf, M., and Ehlers, S. (2020). A machine learning-based method for simulation of ship speed profile in a complex ice field. *Ships Offshore Struct.* 15, 974–980. doi: 10.1080/17445302.2019.1697075

Nam, J.-H., Park, I., Lee, H. J., Kwon, M. O., Choi, K., and Seo, Y.-K. (2013). Simulation of optimal arctic routes using a numerical sea ice model based on an ice-coupled ocean circulation method. *Int. J. Nav. Archit. Ocean Eng.* 5, 210–226. doi: 10.2478/IJNAOE-2013-0128

Omre, A. (2012). *An economic transport system of the next generation integrating the northern and southern passages*. Master's thesis. Norway: Institutt for marin teknikk, Trondheim, 89.

Perera, L. P., and Soares, C. G. (2017). Weather routing and safe ship handling in the future of shipping. *Ocean Eng.* 130, 684–695. doi: 10.1016/j.oceaneng.2016.09.007

Petri, V. (2001). The resistance of ships in level ice. *Trans. - Soc Nav. Archit. Mar. Eng.*, 53–83.

Piehl, H., Milaković, A.-S., and Ehlers, S. (2017). A finite element method-based potential theory approach for optimal ice routing. *J. Offshore Mech. Arct. Eng.* 139, 061502. doi: 10.1115/1.4037141

Pruyn, J. F. J. (2016). Will the Northern Sea Route ever be a viable alternative? *Marit. Policy Manage.* 43, 661–675. doi: 10.1080/03088839.2015.1131864

Riska, K., Wilhelmson, M., Englund, K., and Leivisk ä, T. (1997). *Performance of merchant vessels in the baltic. ship laboratory, winter navigation research board* (Espoo, Finland: Helsinki University of Technology).

Schøyen, H., and Bråthen, S. (2011). The Northern Sea Route versus the Suez Canal: cases from bulk shipping. *J. Transp. Geogr.* 19, 977–983. doi: 10.1016/j.jtrangeo.2011.03.003

Similä, M., and Lensu, M. (2018). Estimating the speed of ice-going ships by integrating SAR imagery and ship data from an automatic identification system. *Remote Sens.* 10, 1132. doi: 10.3390/rs10071132

Simonsen, M. H., Larsson, E., Mao, W., and Ringsberg, J. W. (2015). "State-of-the-art within ship weather routing," in *ASME 2015 34th International Conference on Ocean, Offshore and Arctic Engineering* (St. John's, Newfoundland, Canada). doi: 10.1115/OMAE2015-41939

Solakivi, T., Kiiski, T., and Ojala, L. (2019). On the cost of ice: estimating the premium of Ice Class container vessels. *Marit. Econ. Logist.* 21, 207–222. doi: 10.1057/s41278-017-0077-5

Somanathan, S., Flynn, P., and Szymanski, J. (2009). The northwest passage: A simulation. *Transp. Res. Part Policy Pract.* 43, 127–135. doi: 10.1016/j.tra.2008.08.001

Tang, X., Zou, M., Zou, Z., Li, Z., and Zou, L. (2022). A parametric study on the ice resistance of a ship sailing in pack ice based on CFD-DEM method. *Ocean Eng.* 265, 112563. doi: 10.1016/j.oceaneng.2022.112563

Theocharis, D., Pettit, S., Rodrigues, V. S., and Haider, J. (2018). Arctic shipping: A systematic literature review of comparative studies. *J. Transp. Geogr.* 69, 112–128. doi: 10.1016/j.jtrangeo.2018.04.010

Theocharis, D., Rodrigues, V. S., Pettit, S., and Haider, J. (2019). Feasibility of the Northern Sea Route: The role of distance, fuel prices, ice breaking fees and ship size for the product tanker market. *Transp. Res. Part E Logist. Transp. Rev.* 129, 111–135. doi: 10.1016/j.tre.2019.07.003

Topaj, A. G., Tarovik, O. V., Bakharev, A. A., and Kondratenko, A. A. (2019). Optimal ice routing of a ship with icebreaker assistance. *Appl. Ocean Res.* 86, 177–187. doi: 10.1016/j.apor.2019.02.021

Tsarau, A., and Løset, S. (2015). Modelling the hydrodynamic effects associated with station-keeping in broken ice. *Cold Reg. Sci. Technol.* 118, 76–90. doi: 10.1016/j.coldregions.2015.06.019

Tschudi, M. A., Meier, W. N., and Scott Stewart, J. (2020). An enhancement to sea ice motion and age products at the National Snow and Ice Data Center (NSIDC). *Cryosphere* 14, 1519–1536. doi: 10.5194/tc-14-1519-2020

Tseng, P. H., Zhou, A., and Hwang, F. J. (2021). Northeast passage in Asia-Europe liner shipping: an economic and environmental assessment. *Int. J. Sustain. Transp.* 15, 273–284. doi: 10.1080/15568318.2020.1741747

Tuhkuri, J., and Polojärvi, A. (2018). A review of discrete element simulation of ice–structure interaction. *Philos. Trans. R. Soc Math. Phys. Eng. Sci.* 376, 20170335. doi: 10.1098/rsta.2017.0335

Verny, J., and Grigentin, C. (2009). Container shipping on the northern sea route. *Int. J. Prod. Econ.* 122, 107–117. doi: 10.1016/j.ijpe.2009.03.018

Wan, Z., Ge, J., and Chen, J. (2018). Energy-saving potential and an economic feasibility analysis for an arctic route between shanghai and rotterdam: case study from China's largest container sea freight operator. *Sustainability* 10, 921. doi: 10.3390/su10040921

Wang, Y., Liu, K., Zhang, R., Qian, L., and Shan, Y. (2021). Feasibility of the Northeast Passage: The role of vessel speed, route planning, and icebreaking assistance determined by sea-ice conditions for the container shipping market during 2020–2030. *Transp. Res. Part E Logist. Transp. Rev.* 149, 102235. doi: 10.1016/j.tre.2021.102235

Wang, Y., Zhang, R., Liu, K., Fu, D., and Zhu, Y. (2023). Framework for economic potential analysis of marine transportation: A case study for route choice between the suez canal route and the northern sea route. *Transp. Res. Rec. J. Transp. Res. Board* 2677, 1–16. doi: 10.1177/03611981221144286

Wang, Y., Zhang, R., and Qian, L. (2018). An improved A* Algorithm based on hesitant fuzzy set theory for multi-criteria arctic route planning. *Symmetry* 10, 765. doi: 10.3390/sym10120765

Xue, Y., Liu, R., Li, Z., and Han, D. (2020). A review for numerical simulation methods of ship–ice interaction. *Ocean Eng.* 215, 107853. doi: 10.1016/j.oceaneng.2020.107853

Zhang, Y., Meng, Q., and Ng, S. H. (2016). Shipping efficiency comparison between Northern Sea Route and the conventional Asia-Europe shipping route *via* Suez Canal. *J. Transp. Geogr.* 57, 241–249. doi: 10.1016/j.jtrangeo.2016.09.008

Zhang, J., and Rothrock, D. A. (2003). Modeling global sea ice with a thickness and enthalpy distribution model in generalized curvilinear coordinates. *Mon. Weather Rev.* 131, 845–861. doi: 10.1175/1520-0493(2003)131<0845:MGSIWA>2.0.CO;2

Zhang, X., Wang, H., Wang, S., Liu, Y., Yu, W., Wang, J., et al. (2022). Oceanic internal wave amplitude retrieval from satellite images based on a data-driven transfer learning model. *Remote Sens. Environ.* 272, 112940. doi: 10.1016/j.rse.2022.112940

Zhang, G., Wang, H., Zhao, W., Guan, Z., and Li, P. (2021). Application of improved multi-objective ant colony optimization algorithm in ship weather routing. *J. Ocean Univ. China* 20, 45–55. doi: 10.1007/s11802-021-4436-6

Zhang, M., Zhang, D., Fu, S., Yan, X., and Zhang, C. (2017). A method for planning arctic sea routes under multi- constraint conditions. in *Proceedings of the 24th International Conference on Port and Ocean Engineering under Arctic Conditions* (Busan, Korea).

Zhang, W., Zou, Z., Goerlandt, F., Qi, Y., and Kujala, P. (2019). A multi-ship following model for icebreaker convoy operations in ice-covered waters. *Ocean Eng.* 180, 238–253. doi: 10.1016/j.oceaneng.2019.03.057

Zhou, Q., Peng, H., and Qiu, W. (2016). Numerical investigations of ship-ice interaction and maneuvering performance in level ice. *Cold Reg. Sci. Technol.* 122, 36–49. doi: 10.1016/j.coldregions.2015.10.015

frontiers | Frontiers in Marine Science

TYPE Original Research
PUBLISHED 27 September 2023
DOI 10.3389/fmars.2023.1255425

OPEN ACCESS

EDITED BY
Pierre Yves Le Traon,
Mercator Ocean, France

REVIEWED BY
Xuebo Zhang,
Northwest Normal University, China
Nick Hughes,
Norwegian Meteorological Institute, Norway

*CORRESPONDENCE
Constanza S. Salvó
csalvo@agro.uba.ar

†These authors have contributed equally to this work and share the first authorship

RECEIVED 08 July 2023
ACCEPTED 06 September 2023
PUBLISHED 27 September 2023

CITATION
Salvó CS, Gomez Saez L and Arce JC (2023) Multi-band SAR intercomparison study in the Antarctic Peninsula for sea ice and iceberg detection.
Front. Mar. Sci. 10:1255425.
doi: 10.3389/fmars.2023.1255425

Multi-band SAR intercomparison study in the Antarctic Peninsula for sea ice and iceberg detection

Constanza S. Salvó*†, Ludmila Gomez Saez† and Julieta C. Arce

Departamento Meteorología, Servicio de Hidrografía Naval, Buenos Aires, Argentina

Synthetic aperture radar (SAR) systems are one of the best resources to gather information in polar environments, but the detection and monitoring of sea ice types and icebergs using them is still a challenge. Limitations using single-frequency images in sea ice characterization are well known, and using different SAR bands has been revealed to be useful. In this paper, we present the quantitative results of an intercomparison experiment conducted by the Argentine Naval Hydrographic Service (SHN) using X-, C-, and L-bands from COSMO-SkyMed, Sentinel-1, and SAOCOM satellites, respectively. The aim of the experiment was to evaluate SAOCOM for its use on SHN products. There were 25 images with different SAR parameters that were analyzed, incorporating the diversity in the information that everyday Ice Services attend to. Particularly, iceberg detections, fast first-year ice, and belts and strips were studied in the Antarctic Sound, the surroundings of Marambio Island, and Erebus and Terror Gulf. The results show that the HV polarization channel of the L-band provides useful information for iceberg detection and fast first-year ice surface feature recognition and is a promising frequency for the study of strip identification under windy sea conditions and snow accumulation on first-year ice.

KEYWORDS

SAOCOM, L-band, Sentinel-1, C-band, COSMO-SkyMed, X-band, multifrequency analysis, operational monitoring

1 Introduction

In a climate change context, Ice Services are facing new challenges for operational monitoring, with unusual dynamics and changes in old regimes of sea ice and icebergs. This scenario reveals the significance of having the most updated information available in operational times, in which any source is valuable, either provided by satellite imagery or, less frequently, from *in situ* observations. The capability of synthetic aperture radar (SAR) systems to monitor the polar environments is known; nevertheless, the complexity of sea ice forms, the different properties and surface features of the ice, the variability in environmental conditions, and the great diversity in SAR parameters still make its use a challenge (Onstott and Shuchman, 2004; Dierking, 2013).

The broad scientific literature use SAR for sea ice characterization and iceberg detection (Dierking, 2013; Lyu et al., 2022); however, the incidence angles used are generally bounded to a few degrees of variability or its effect is not considered (Lyu et al., 2022), the image acquisition modes are the ones with the best spatial resolution or only one type of acquisition mode are used (Zakhvatkina et al., 2012; Casey et al., 2016; Johansson et al., 2018; Wang and Li, 2021), full polarization SAR images are considered (Drinkwater et al., 1991; Johansson et al., 2017; Singha et al., 2018), and the few multifrequency analyses that exist are commonly done using the same remote platform, without the limitation of the time gaps between the acquisitions (Matsuoka et al., 2001; Lyu et al., 2022).

Since the launch of the SAR SAOCOM (Satélite Argentino de Observación COn Microondas) in 2018, the Argentine Naval Hydrographic Service (Servicio de Hidrografía Naval, SHN) has incorporated the L-band in its ice charts (Scardilli et al., 2022). Studies with SAOCOM have been done for calibration (Azcueta et al., 2022), surface deformation (Roa et al., 2021; Viotto et al., 2021; De Luca et al., 2022), digital surface model generation (Seppi et al., 2021), soil salinity and moisture estimation (MaChado and Solorza, 2020; Anconitano et al., 2022), forest biomass retrieval (Blomberg et al., 2018), and glacial movement (Ferreyra et al., 2021). However, there were not published results of SAOCOM for sea ice and iceberg conditions (Lyu et al., 2022).

The synergistic use of multifrequency SAR systems has been proven beneficial for ice charting and iceberg detection (Drinkwater et al., 1991; Singha et al., 2018; Dierking, 2021; Dierking et al., 2022). Analysis of multiple SAR frequencies contributes additional information on the observed target due to the different interaction between the ice surface and the signal, with the scattering mechanism and the penetration depth depending on the length scales of the radar waves (Onstott and Shuchman, 2004; Dierking, 2013). The C-band operates in wavelengths of 3.8–7.5 cm, and it is the accepted frequency for all-season sea ice monitoring in the scientific literature and at the Ice Services (Maillard et al., 2005; Arkett et al., 2007; Flett et al., 2008; Dierking, 2013; Scardilli et al., 2022). It was widely studied for sea ice concentration, characterization, drift, thickness, and melt detection, and for iceberg detection (Kwok et al., 2003; Zakhvatkina et al., 2012; Dierking, 2013; Wang and Li, 2021; Lyu et al., 2022).

The X-band, with a wavelength of 2.4–3.8 cm, is less used to Ice Services in daily ice charts because of its similar response to the C-band, although it was suggested that it is more sensitive to the ice surface's properties (Dierking, 2013; Han et al., 2020). In regard to the L-band, a wavelength of 15–30 cm, it was mentioned that it shows superior performance for iceberg detection in rough seas and inside a sea ice field in HV polarization, showing a brighter response (Dierking et al., 2022). Furthermore, it showed a greater distinction between deformed and smooth sea ice, with higher sensitivity to the surface topography such as ridges, hummocks, and rubble fields (Dierking and Busche, 2006; Dierking et al., 2022), and the use of the L-band during the melt season was proposed since it is less sensitive to the first stages of melting (Arkett et al., 2008; Casey et al., 2016).

In 2020, the SHN carried out an Intercomparison Experiment (IE-2020) using different SAR frequencies to test the L-band for its inclusion in daily products and ice advisory. The experiment used the L-band from SAOCOM, the C-band from Sentinel-1, and the X-band from COSMO-SkyMed ("COnstellation of small Satellites for the Mediterranean basin Observation") in the north of Peninsula Antarctica. Ice analysts from the SHN interpreted the images in each frequency making deductions, along with meteorological data and sea ice information from the Argentine Antarctic stations at the time of the SAR image acquisition. Conclusions to the IE-2020 were presented at the 21st meeting of the International Ice Charting Working Group and published in Salvó et al. (2022).

From an operational and maritime point of view, the SHN identified different ice conditions that are relevant for the generation of products of safety at sea. Among them are mentioned the following: (i) the amount of iceberg in an area, which is to date manually identified by ice analysts in the iceberg chart (Scardilli et al., 2022); (ii) fast ice features that can be sensitive to the SAR response but not operationally relevant for the ice chart production, making the information in the images difficult to interpret by the ice analyst; and (iii) the belts and strips that represent a hazard to the vessels that navigate in polar waters and are a challenge to monitor by SAR since they can be formed in a couple of hours from not detectable disperse brash ice and camouflage in windy sea ice condition with only one SAR polarization.

In this paper, we present a quantitative study, a less subjective approach, to the qualitative results found in the SHN IE-2020. The information presented in the following sections is divided into the three typical sea ice and iceberg operational conditions relevant to the ice charting production: (i) icebergs, (ii) fast ice features, and (iii) belts and strips.

2 Materials and methods

2.1 Study area and data

The study area corresponds to the north of the Antarctic peninsula (Figure 1), site where the SHN IE-2020 took place, and zone of strategic relevance in the operational tasks of the SHN. Two main areas of interest were analyzed: the first site was the Antarctic Sound with open water and a sea ice regime arranged in strips and belts, and the second area was in Marambio Island and Erebus and Terror Gulf where different stages of development and forms of sea ice occurred, with a high density of icebergs. All the sea ice and iceberg dynamics and characteristics in the study area were known from the monitoring and information of the SHN.

There were 25 images in the X-, C-, and L-bands that were analyzed corresponding to the COSMO-SkyMed, Sentinel-1, and SAOCOM satellites (Table 1). The center frequency in which the satellites operate is 9.6 GHz, 5.405 GHz, and 1.275 GHz, respectively. The images were acquired between May and September 2020. Sentinel-1 images were downloaded from the Copernicus Open Access Hub from the European Space Agency (ESA) https://scihub.copernicus.eu/dhus/. SAOCOM images were requested by the SAOCOM catalog from the Comisión Nacional de Actividades Espaciales (CONAE) https://catalog.saocom.conae.gov.ar/catalog/, and the COSMO-SkyMed images were acquired by the Agenzia Spaziale Italiana (ASI) and provided to the SHN by CONAE. The level of processing of the SAR images was in High-Resolution Ground Range Detected for Sentinel-1, Detected Image for

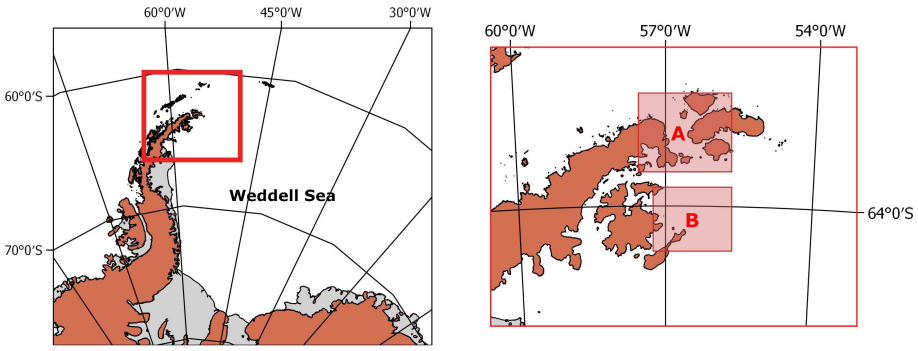

FIGURE 1
Study area in the north of the Antarctic peninsula (left) and detailed representation (right), showing the **(A)** Antarctic Sound and **(B)** Marambio Island and Erebus and Terror Gulf.

SAOCOM, and Single-look Complex Slant for COSMO-SkyMed. For the intercomparison analysis, the dataset was divided into five groups based on an acceptable time gap between acquisitions concerning the ice regimes under study (Table 1). The use of the different groups is detailed in the next subsections.

The SAR images were processed using the Python Snappy module of ESA's Sentinel Application Platform (SNAP) version 8 http://step.esa.int. Orbit correction was applied to Sentinel-1 data, and then Sentinel-1 and COSMO-SkyMed images were radiometrically calibrated to sigma naught. The exception with SAOCOM in the calibration step was because the images were obtained in Detected Image Level-1B (data projected to ground range, radiometrically calibrated, and georeferenced). Multi-looking was applied to all the images, and looks in range and azimuth were calculated using the higher range and azimuth spacing of the dataset. Subsequently, an ellipsoid correction was applied and the final projection used was the Antarctic Polar Stereographic (EPSG: 3031). To afford a comparable dataset in space resolution for the intercomparison, each image was resampled to a square pixel, the final pixel size corresponded to the largest of all the images (58.4 meters). At last, the backscatter coefficient values were converted into decibels (dB).

Meteorological data provided by the Argentine Meteorological Service (Servicio Meteorológico Nacional SMN) was used to validate the sea ice conditions. The observations were acquired from three Antarctic stations: Esperanza station (63°23′50″S 56° 59′54″W) situated in the Antarctic Sound, Marambio station (64° 14′50.6″S 56°37′39.3″W) in Marambio Island, and Carlini station (62°14′27.4″S 58°40′01.1″W) located in the north of the Peninsula. These stations provided measurements of air temperature, wind speed, wind direction, and precipitation (liquid or solid state) every 3 h in order to accredit the synoptic atmospheric situation.

2.2 Icebergs

The SAR response to the density of icebergs in a given area was analyzed in different SAR frequencies. All the SAR images of groups 1, 4, and 5 were used (Table 1). Particularly from group 2, the Sentinel-1 and SAOCOM images were selected, and for group 3, only the Sentinel-1 ones. The icebergs were counted in polygons of 1 km^2 in a fast first-year ice using the Sentinel-2 image of the 30th August 2020 near the Marambio station as a reference (Figure 2). The polygons were distributed in the fast ice covering a wide range of iceberg density, from 0 to 48 in the highest-density areas. The Sentinel-2 image, downloaded from the Copernicus Open Access Hub from the ESA, was the only optical image available in the area of high resolution and cloud-free for the period of study. Since the icebergs were trapped in fast sea ice and part of them are in a grounded area, corroborated by the SHN in the Argentine Antarctic Summer Campaign 2019-2020, the Sentinel-2 optical image was considered as a reliable source of validation.

The mean and standard deviation values of the X-, C-, and L-band backscattering coefficients for HH and HV polarization were extracted from the polygons. Explanatory analysis was performed to examined the correlation among the data using the Pearson's correlation coefficient (Equation 1).

$$r = \frac{\Sigma((x-\bar{x})(y-\bar{y}))}{\sqrt{(\Sigma(x-\bar{x})^2 * \Sigma(y-\bar{y})^2)}} \quad (1)$$

where r represents the Pearson correlation coefficient, x and y are the number of icebergs and the backscatter coefficient in each polygon, $\bar{x}$ is the mean of the x-values, and $\bar{y}$ is the mean of the y-values. The standard deviations of the x-values and y-values are represented in the denominator of the equation. The influence of the incidence angle in the samples was also extracted and examined. In every SAR frequency, to each SAR acquisition, a linear least-square regression model was applied to obtain the relationship between the number of icebergs and the mean backscatter values (Equation 2).

$$Y = b_0 + b_1 X \quad (2)$$

where Y is the dependent variable to predict, represented here as the backscatter coefficient, b_0 and b_1 are the intercept and the slope of the regression line, and X is the independent variable representing the number of icebergs per 1 km^2.

10.3389/fmars.2023.1255425

TABLE 1 Description of SAR image acquisitions.

Sensor	Acquisition time (UTC)	Group	Polarization	Acquisition mode	Pixel spacing original Rg x Az (m)	Incidence angle
SENTINEL-1	2020-05-10 07:51	1	HH-HV	EW	25.0 × 25.0	17.99–45.92
SENTINEL-1	2020-05-10 07:52		HH-HV	EW	25.0 × 25.0	17.74–45.74
SAOCOM 1-A	2020-05-10 11:09		HH-HV-VV-VH	TOPSAR Wide	58.4 × 58.4	17.60–35.49
COSMO-SkyMed	2020-05-11 19:10		HH-HV	PINGPONG	6.95 × 2.31	56.00–57.16
SENTINEL-1	2020-05-13 08:16	2	HH-HV	EW	25.0 × 25.0	17.94–45.78
SAOCOM 1-A	2020-05-13 19:57		HH-HV	TOPSAR Wide	31.2 × 31.2	24.9– 48.70
COSMO-SkyMed	2020-05-13 20:09		HH-HV	PINGPONG	2.76 × 2.34	18.94–22.21
SAOCOM 1-A	2020-05-21 11:15	3	HH-HV-VV-VH	TOPSAR Wide	58.4 × 58.4	17.62–35.49
COSMO-SkyMed	2020-05-21 19:45		HH-HV	PINGPONG	5.33 × 2.33	39.74–41.78
SENTINEL-1	2020-05-22 07:51		HH-HV	EW	25.0 × 25.0	17.99–45.92
SENTINEL-1	2020-05-22 07:52		HH-HV	EW	25.0 × 25.0	17.73–45.74
SENTINEL-1	2020-08-21 07:44	4	HH-HV	EW	40.0 × 40.0	17.76–45.73
SAOCOM 1-A	2020-08-23 20:09		HH-HV	TOPSAR Narrow	23.0 × 23.0	24.9–38.29
SAOCOM 1-A	2020-08-25 11:15		HH-HV	TOPSAR Wide	31.2 × 31.2	24.9–48.70
SENTINEL-1	2020-08-26 07:51		HH-HV	EW	40.0 × 40.0	17.99–45.92
SENTINEL-1	2020-08-26 07:52		HH-HV	EW	40.0 × 40.0	17.73–45.74
SAOCOM 1-A	2020-08-26 11:33		HH-HV	Stripmap	5.2 × 5.2	38.20–41.29
COSMO-SkyMed	2020-09-06 19:22	5	HH-HV	PINGPONG	6.53 × 2.31	50.57–52.21
SENTINEL-1	2020-09-06 23:51		HH	EW	25.0 × 25.0	17.94–45.80
SENTINEL-1	2020-09-07 07:51		HH-HV	EW	25.0 × 25.0	17.99–45.92
SENTINEL-1	2020-09-07 07:52		HH-HV	EW	25.0 × 25.0	17.73–45.74
SAOCOM 1-A	2020-09-08 20:09		HH-HV	TOPSAR Narrow	23.0 × 23.0	24.9–32.29
COSMO-SkyMed	2020-09-10 19:22		HH-HV	PINGPONG	6.53 × 2.31	50.57–52.21
SENTINEL-1	2020-09-10 08:16		HH-HV	EW	25.0 × 25.0	17.93–45.78
SAOCOM 1-A	2020-09-13 20:03		HH-HV	TOPSAR Narrow	23.0 × 23.0	24.9–38.29

2.3 Fast ice features

In view of what was seen in SHN IE-2020, where spatial patterns were recognized in the different SAR frequencies, the fast ice's features were studied at each sensor to quantify this variability. First, the hole fast ice area was jointly analyzed considering all the sea ice features together in the platform without differentiation ice characteristics. Second, the presence of snow on the fast ice and its differences observed in the SAR images were analyzed.

The analysis of the hole fast sea ice around Marambio Island was analyzed using all the SAR images of groups 1, 4, and 5 (Table 1). Specifically, from group 2 the Sentinel-1 and SAOCOM images were selected, and for group 3, only the Sentinel-1 ones. The fast ice was delineated to its minimum extent covering all the dates present in the images mentioned. For delineating the polygon, photointerpretation of the SAR images was performed and optical imagery was used as validation when available from the Sentinel-2 or MODIS (Moderate Resolution Imaging Spectroradiometer). Sentinel-2 was obtained as mentioned in Section 2.2, and MODIS was consulted on NASA (National Aeronautics and Space Administration) Worldview application https://worldview.earthdata.nasa.gov, part of NASA's Earth Observing System Data and Information System (EOSDIS). After the delimitation of the fast ice area, values were extracted to all the images and the frequency distribution of the data was analyzed.

The analysis of the presence of the snow cover on the fast ice was done comparing the backscatter of bare and snow-covered first-year ice near Cockburn Island in the Erebus and Terror Gulf. From the Sentinel-2 image of the 30th August 2020, snow-covered and

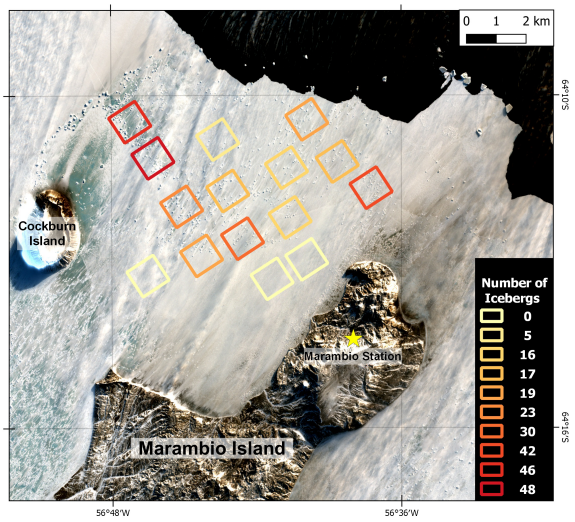

FIGURE 2
Iceberg sampled in the fast ice near the Marambio station. Sentinel-2 MSI 30th August 2020, bands 4-3-2. Copernicus Sentinel data 2020.

bare sea ice were identified and circular samples were collected with a 50 m radius (Figure 3). Mean values were calculated to each sample; afterward, to each SAR image, mean values for the snow-covered areas and bare ice were evaluated, and the difference of the same were performed following Equation 3:

$$\mathrm{Diff}_{s-b} = 10^{*}\log_{10}(\sigma_s - \sigma_b) \quad (3)$$

where $\mathrm{Diff}_{s\text{-}b}$ is the difference between the snow-covered and bare ice areas as the difference of the power per unit area of the snow-covered ice σ_s and the power per unit area of the bare ice σ_b, converted in decibels. The SAR images used to calculate this difference were from the 21st August to 13th September corresponding to groups 4 and 5 (Table 1).

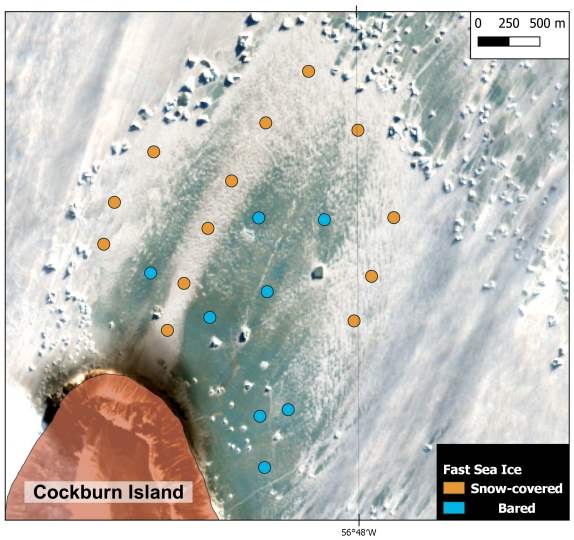

FIGURE 3
Snow-covered and bare samples on the fast ice north of Cockburn Island. Sentinel-2 MSI 30th August 2020, bands 4-3-2. Copernicus Sentinel data 2020.

Meteorological data were used to validate the use of optical imagery as ground truth. Meteorological observations were taken from the Marambio station with 51 days of accumulated days of precipitation registered, showing 102.1 mm of snow recorded since the formation of the fast ice. Maximum and minimum temperatures were below 0°C with a prevailing wind direction from the south to southwest, accumulating 48% of the daily observations in that direction. Patterns in the snow cover to the north of Cockburn Island were visualized in the Sentinel-2 image, confirming the recorded observations (Figure 3).

2.4 Belts and strips

Strips and belts present in the Antarctic Sound were analyzed, and the images used correspond to groups 2 and 3. In order to compare backscatter values for sea and water around, strip and water samples were selected at similar incidence angles (Figure 4). The samples were determined visually using HH and HV polarization of each band. Boxplots were plotted for each pair of samples (strips and water) and for each band so as to facilitate the comparison between samples (comparison of backscatter values and standard deviation). To ensure a detailed analysis of the backscatter values of strips and water, the wind speed and direction data were taken from the Esperanza station, corresponding to the dates of image acquisition (Table 1).

3 Results and discussion

3.1 Icebergs

The Pearson correlation coefficients were low for all the SAR frequencies and above zero, determining a positive weak relation between the number of icebergs and the backscattering coefficients in the X-, C-, and L-bands for each polarization (Figure 5). The C- and L-bands showed a wider value range in the backscattering coefficient since more image acquisition was analyzed in those frequencies.

To quantify the nature of the relationship between the number of icebergs per km^2 and the backscatter coefficient in different SAR frequencies, linear regression models were performed. The coefficient of determination of the models (R^2) was low for most of the acquisition in HH polarization in all the frequencies and with p-values that were only significant to 0.05 for two images of three in the X-band, five images of eight in the C-band, and six images of seven in the L-band (Table 2). HV polarization showed higher R^2 values than HH polarization with only one image in the X-band, three in the C-band, and one in the L-band with lower values than 0.7; all p-values were significant (Table 2). The slope for the linear model was higher in the L-band than in the X- and C-bands.

The incidence angle where the polygons were located was contrasted with its response in the HH and HV channels. The difference in the backscatter coefficient for areas with low vs. high amounts of icebergs increases with the incidence angle in both polarizations (Figure 6). Because the availability in C- and L-band imagery was larger than the X-band, a broader range of incidence angles was presented in the dataset for those frequencies, making the analysis of the X-band inconclusive for evaluating the effect of

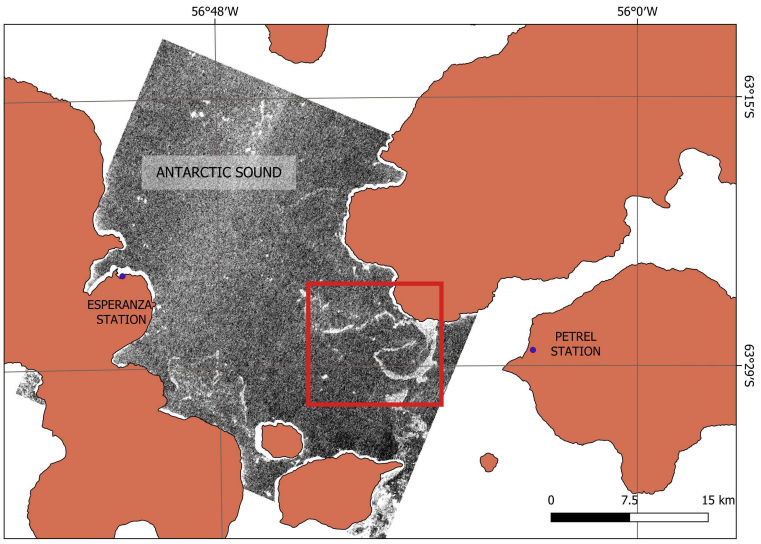

FIGURE 4
The study area for the analysis of strips and belts. The red box shows the area where the samples of ice and water were taken. The satellite image correspond to the SAOCOM image of 15th May 2020. SAOCOM® Product – ©CONAE – 2020. All Rights Reserved.

the incidence angle. The L-band showed a large interval between the minimum and maximum of backscatter values in HV polarization. The standard deviation range obtained for the backscattering coefficient in HH polarization was 1.24–1.6 dB for the X-band, 1.14–2.07 dB for the C-band, and 1.75–3.03 dB for the L-band; meanwhile, for HV, polarization was 1.33–1.78 dB for the X-band, 1.13–2.08 dB for the C-band, and 2.5–6.18 dB for the L-band.

The higher variability of the L-band in HV polarization evidences greater sensitivity of the L-band to the presence of icebergs than the C- and X-bands, with the exception of one TOPSAR Narrow image, in which thermal noise was observed on one of the sub-swaths, the position in which the samples were taken. Additional analysis of the TOPSAR Narrow mode is required to ameliorate the effect or reduce the thermal noise in the sub-swath.

3.2 Fast ice features

The fast ice around Marambio Island contains multiyear ice, north of Marambio station, which was grounded prior to freezing

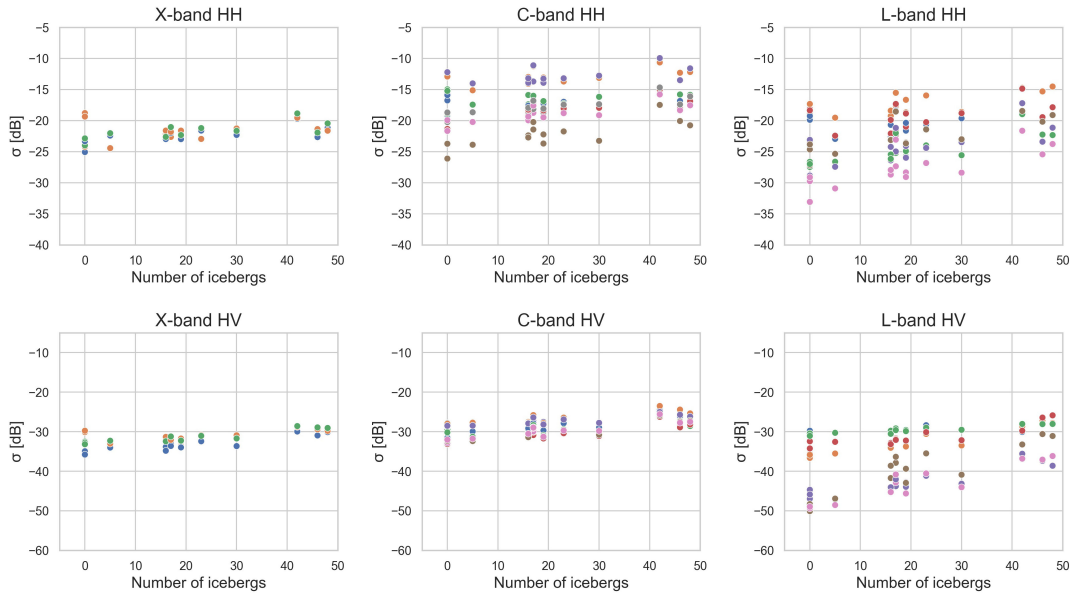

FIGURE 5
X-, C-, and L-band backscattering coefficients in dB for HH (top) and HV (bottom) polarization vs. different numbers of icebergs in 1 km^2. Different colors identify different SAR acquisitions.

TABLE 2 Mean and standard deviation for each linear regression per image acquisition in each SAR frequency.

	HH			HV		
	X	C	L	X	C	L
Slope (dB)	0.04 ± 0.02	0.05 ± 0.02	0.10 ± 0.03	0.08 ± 0.02	0.09 ± 0.02	0.18 ± 0.09
Intercept (dB)	−22.86 ± 0.66	−18.27 ± 3.20	−24.35 ± 3.68	−33.53 ± 1.40	−30.81 ± 1.71	−39.55 ± 7.04
R^2	0.36 ± 0.24	0.39 ± 0.20	0.48 ± 0.15	0.66 ± 0.25	0.68 ± 0.13	0.79 ± 0.13
p-value	0.21 ± 0.29	0.06 ± 0.08	0.02 ± 0.05	0.01 ± 0.02	0.00 ± 0.00	0.00 ± 0.00

(Figure 7). Of all the frequencies, the L-band was the one that showed a closer representation of HH polarization to the optical images, accurately following the fast sea ice composition and evolution, highlighting the variety of features in the ice (Figure 7).

The distribution of the backscattering response in dB was analyzed for each intercomparison group in the fast ice area (Figure 8). Conclusions about the range of the backscattering coefficient cannot be done because of the wide range in the incidence angles present in the dataset. In HH polarization, the L-band from SAOCOM showed higher variability in the backscatter values as can be seen in the histograms for all the intercomparison dates (Figure 8). The standard deviation in dB obtained for HH polarization in the first group was 3.58 for the X-band, 3.58 for the C-band, and 3.61 for the L-band. For the second and third groups, it was 3.21–3.28 for the C-band and 4.48 for the L-band. Lastly, in the fourth group, the standard deviation was 3.29–3.47 for the C-band and 4.31–5.6 for the L-band, and for the fifth group it was 3.93–4.13 for the X-band and 3.18–4.36 and 4.1–5.26 for the L-band.

HV polarization presented less variability in the data distribution than HH polarization, with similar curves for each frequency, with the exception of SAOCOM images from the fourth and fifth intercomparison groups, corresponding to two images with incidence angles upper 33°, Stripmap and TOPSAR Narrow mode, and a TOPSAR Wide image with a nominal incidence angle of 25.5° in the fast ice area. SAOCOM images from 23rd August and 8th September showed a bimodal distribution that was caused by

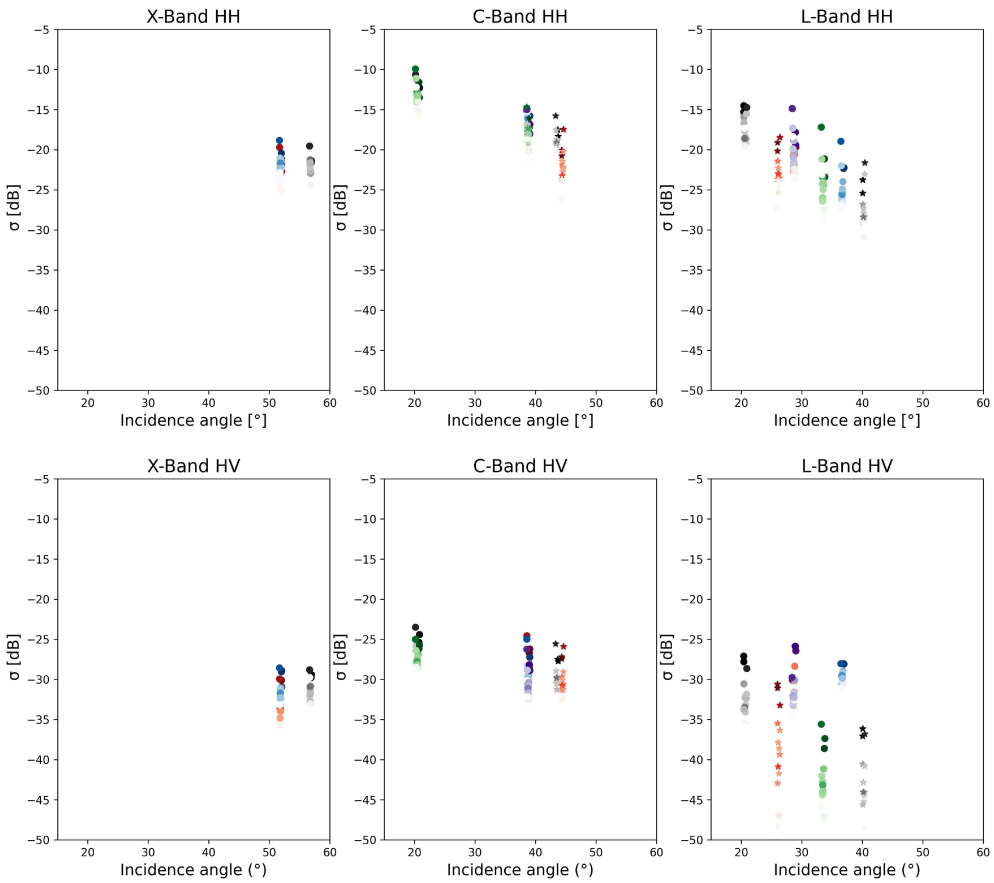

FIGURE 6
X-, C-, and L-band backscattering coefficients in dB for HH and HV polarization vs. incidence angle in degrees. Each color represents one SAR image, and the saturation corresponds to the increase in the number of icebergs sampled.

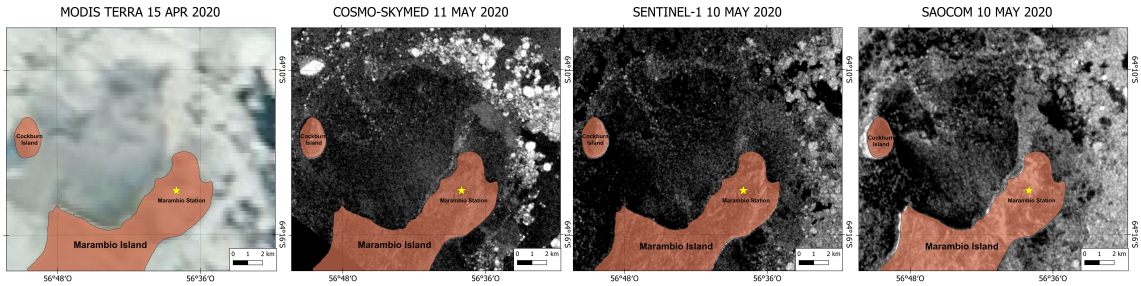

FIGURE 7
Fast ice's formation near Marambio Island on MODIS Terra. The same area in the X-, C-, and L-band images, backscattered in dB for HH polarization. Copernicus Sentinel data 2020. SAOCOM® Product – © CONAE – 2020, All Rights Reserved. COSMO-SkyMed Product – © ASI 2020 processed under license from ASI – Agenzia Spaziale Italiana, All Rights Reserved, and distributed by CONAE.

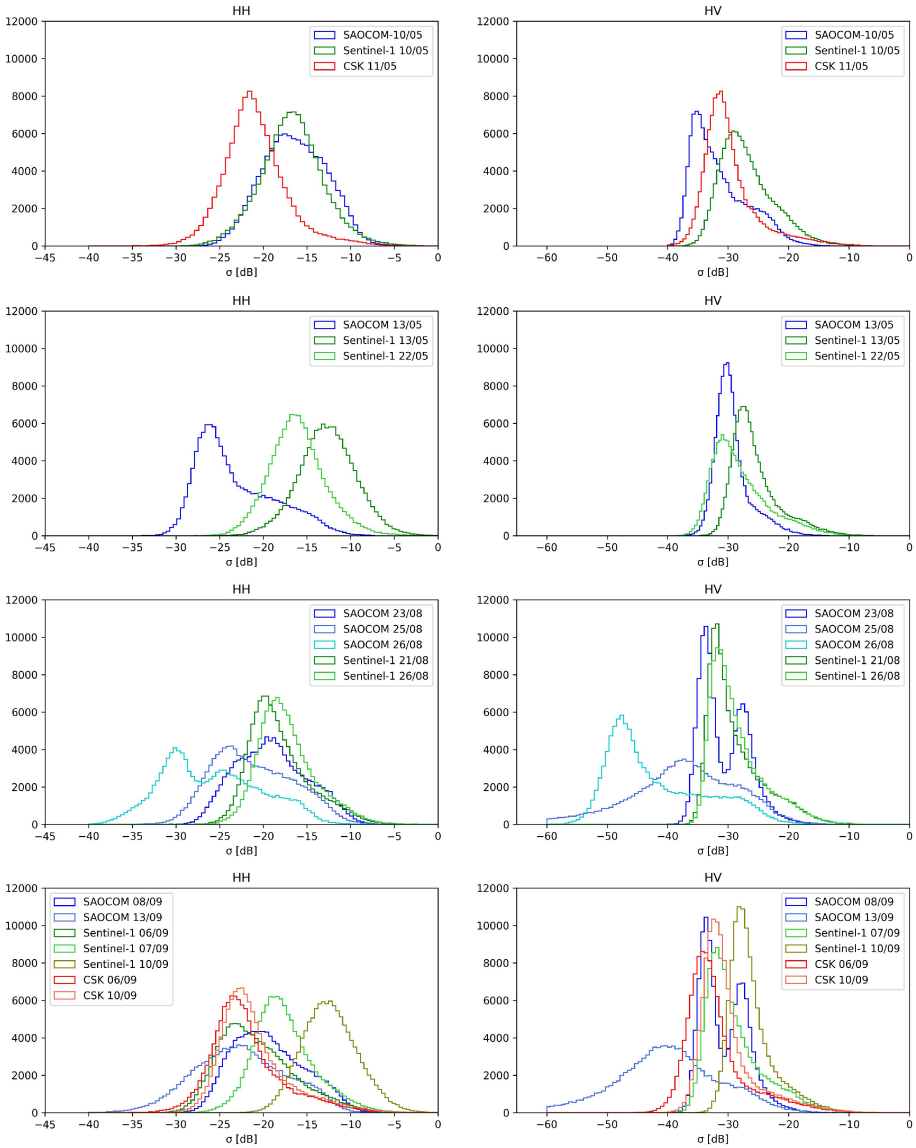

FIGURE 8
Histogram distribution of SAR images in the X-, C-, and L-bands for (from top to bottom) groups 1, 2 and 3, 4, and 5. HH polarization is represented to the left and HV to the right.

the thermal noise in one of the sub-swaths of the TOPSAR Narrow Mode, as it was explained in the previous subsection.

For the analysis of the snow presence on the fast ice, the SAR frequency did not show a distinction between the backscatter coefficient of bare and snow-covered first-year ice, and the variability observed in the results was attributed to differences in the SAR parameters. However, the polarization channel showed an impact on the snow detection with all the differences between the bare and snow-covered positive in HH polarization, 75% of the images above 2 dB of difference (Figure 9). In HV polarization, the differences were lower, with three images from SAOCOM and from COSMO-SkyMed below zero (Figure 9). Patterns in the variability presented in the results considering the SAR frequency, incidence angle, resolution of the image, direction of the antenna in relation to the area sampled, and weather conditions were studied; nonetheless, causes cannot be attributed because the differences in the dataset and more images need to be included to reach conclusions.

In HH polarization, SAOCOM showed an increase in the bare and snow-covered difference between 23rd and 26th August, a period in which snowfalls occurred, and a similarity in the bare and snow-covered difference from 8th to 13th September, a date interval without precipitation (Figure 9). Further research needs to be done on the L-band, since the results revealed a sensitivity to snow precipitation but the dataset is not large enough to conclude.

3.3 Belts and strips

Figure 10 shows the images analyzed on the Antarctic Sound; the backscatter values of strips and water were compared, and the result is shown in Figure 11.

For most of the analyzed cases, the HV polarization showed an advantage for strip detection with respect to HH polarization; this result was noted in the visual and quantitative analyses (Figure 11) where the backscatter values for the water box were below the values for the strip ice box. A clear example was found in the C-band image from 13th May, where it was not possible to distinguish the presence of ice in HH (both samples had similar backscatter values), whereas in HV the presence of strips was observed. This advantage of HV polarization may be due to a higher sensitivity of HH polarization to the wind effect on the ocean surface. This result is consistent with previous studies where the water backscatter values in HV are lower than those of HH even under wind roughened conditions (Shuchman and Flett, 2003; Arkett et al., 2007).

In some cases, the sea surface presented more backscattering than sea ice like X-band image from 13th May, where sea ice had dark tones and the backscatter values for the strip ice box were below the values for the water box. This could be a result of a greater roughness of the sea surface with respect to the ice surface. The dark tones for sea ice in SAR images must be taken into account by the ice analysts when the presence of sea ice is analyzed. This effect was

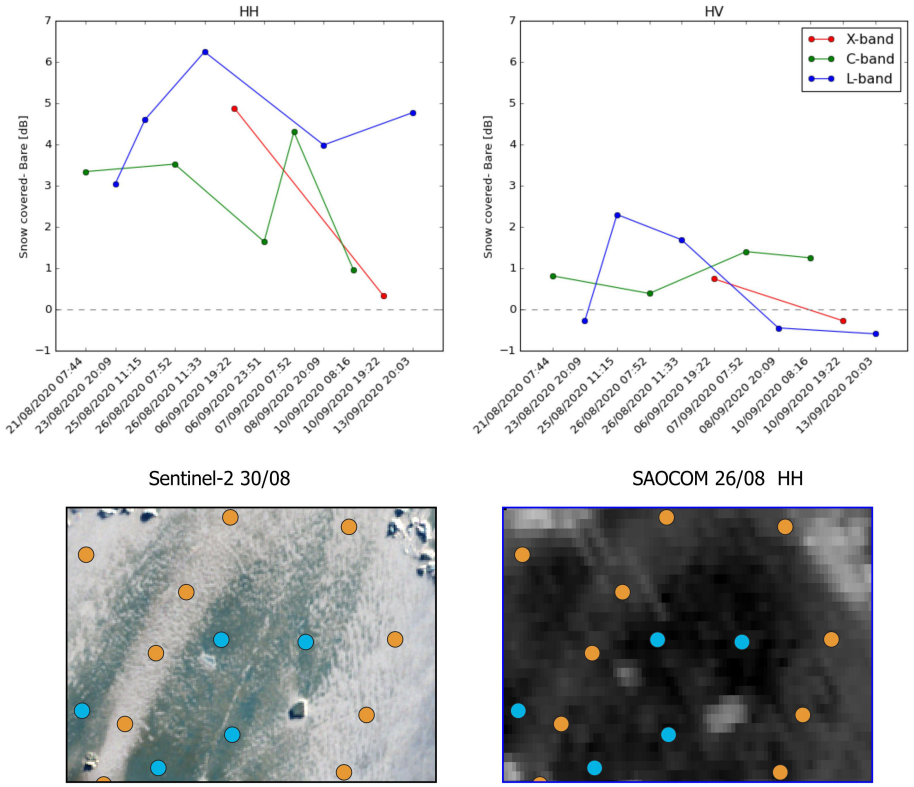

FIGURE 9
Difference between snow-covered and bare samples mean on the fast ice north of Cockburn Island for HH and HV polarization in the X-, C-, and L-bands. Copernicus Sentinel data 2020. SAOCOM® Product – © CONAE – 2020, All Rights Reserved.

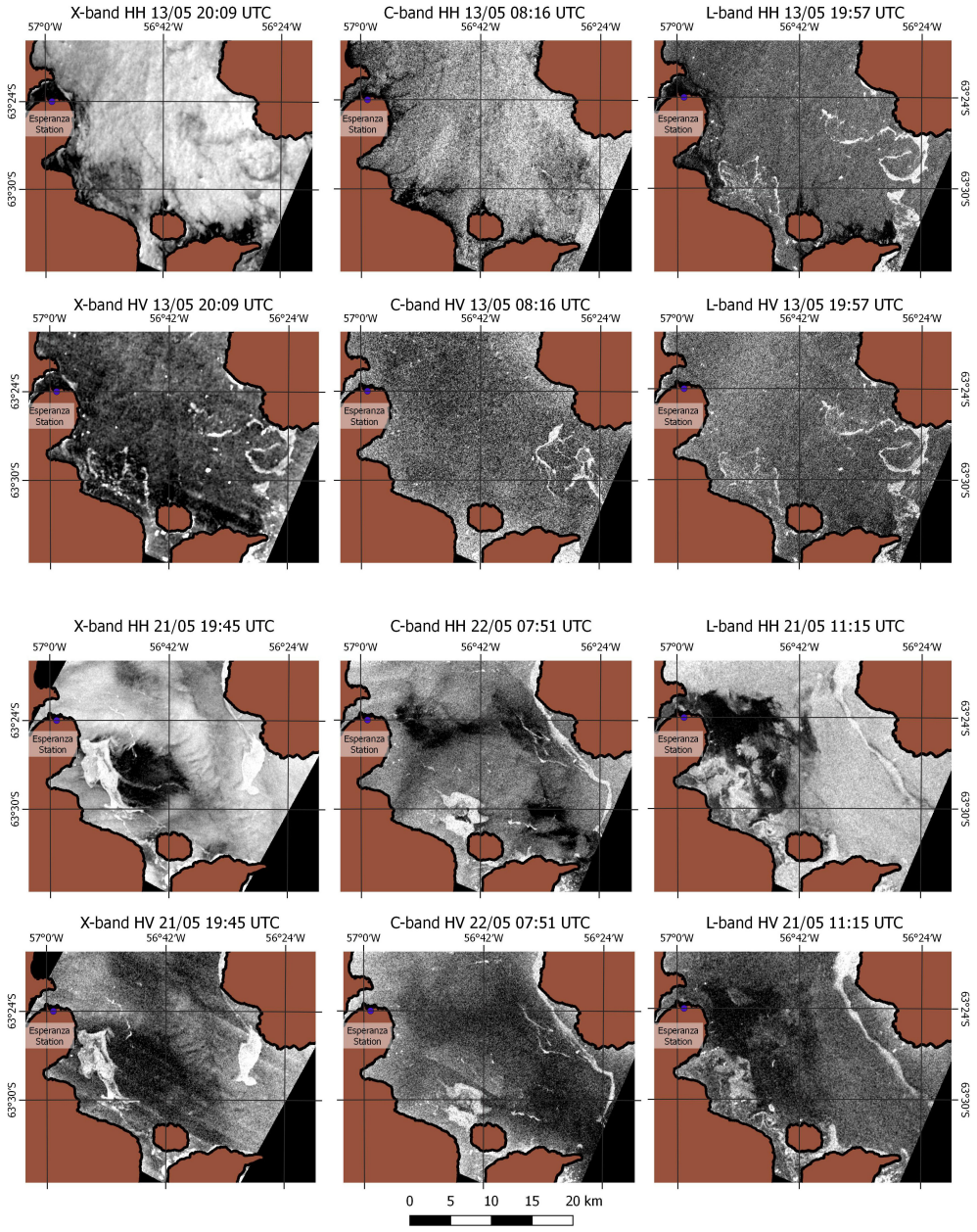

FIGURE 10
X-, C-, and L-band backscattering coefficients in dB for HH and HV polarization. Copernicus Sentinel data 2020. SAOCOM® Product – © CONAE – 2020, All Rights Reserved. COSMO-SkyMed Product – © ASI 2020 processed under license from ASI – Agenzia Spaziale Italiana, All Rights Reserved, and distributed by CONAE.

reported previously in the ice edge zone by Onstott and Shuchman (2004) and by Arkett et al. (2007).

In the inter-band analysis, it was observed that in the case of group 2, in the C-band image with HH polarization, it was not possible to identify and differentiate the sea ice from the water around it, unlike the X- and C-band images with HH polarization. According to the wind measurements reported at the closest meteorological station to the study area, there was a decrease of approximately 60% in the intensity of the wind between the acquisition of the C-band and X- and L-band images (Figure 12). An increase in the intensity of the wind over the sea produces a growth in the roughness of the sea surface, in turn increasing the backscattering of the surface. This results in sea surface roughness, and its response could be limiting the detection of sea ice at HH polarization.

The X- and L-band images of group 2 were acquired within 12 min apart, and no evidence was found that the meteorological conditions were significantly modified in that time period. However, a better distinction was noted for L-band both visually and in the boxplots, with a greater difference between samples. The differences between X- and L-band could be due to the intrinsic characteristics of each band. This would represent an advantage for

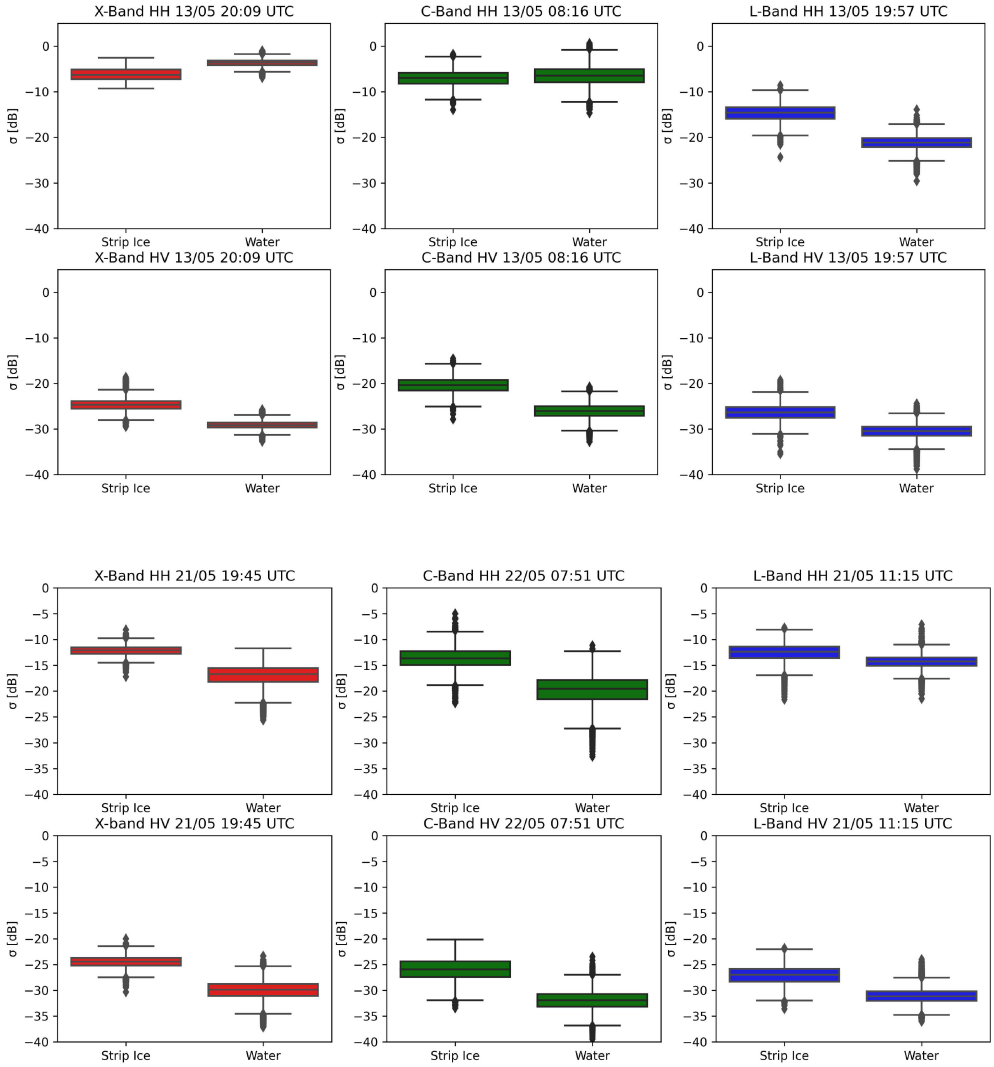

FIGURE 11
Boxplots of backscatter at X-, C-, and L-bands for open water and strips.

the L-band in distinguishing sea ice strips from water, being L-band less sensitive to the wind or the sea state compared with X-band as Dierking et al., 2022 indicated in their study. However, differences in the incidence angles of each acquisition make it difficult to determine a conclusive cause.

For the acquisition dates of group 3, no significant variations in wind intensity (Figure 12) or a particular pattern in wind behavior were found. In all the bands, it was possible to identify and differentiate the water from the strips. The differences between bands may be due to the characteristics of each image acquisition (space resolution and incidence angle).

4 Conclusion

This paper presents the quantitative results obtained from a detailed previous Intercomparison Experiment carried out in 2020 (IE-2020) by the Argentine Naval Hydrographic Service using the X-, C-, and L-bands from the COSMO-SkyMed, Sentinel-1, and SAOCOM, respectively. The analysis was performed following typical sea ice and iceberg operational conditions: (i) icebergs, (ii) fast ice features, and (iii) belts and strips.

The results found with the HV polarization of SAOCOM suggested the L-band as a convenient frequency for the detection of areas with a high density of icebergs surrounded by first-year ice. The number of icebergs showed positive but weak correlations with the backscatter coefficient in HH polarization for all the sensors; however, significant results were obtained in HV polarization, even under different SAR parameters such as image acquisition and different incidence angles. The linear regressions presented showed the L-band as the frequency with a higher slope and coefficient of determination, being significant in HV polarization, with good results even under spatial resolutions of around 100 m for the TOPSAR Wide Quad polarization mode.

As it was seen from visual interpretation in the IE-2020, the analysis of the fast first-year ice near Marambio Island revealed a

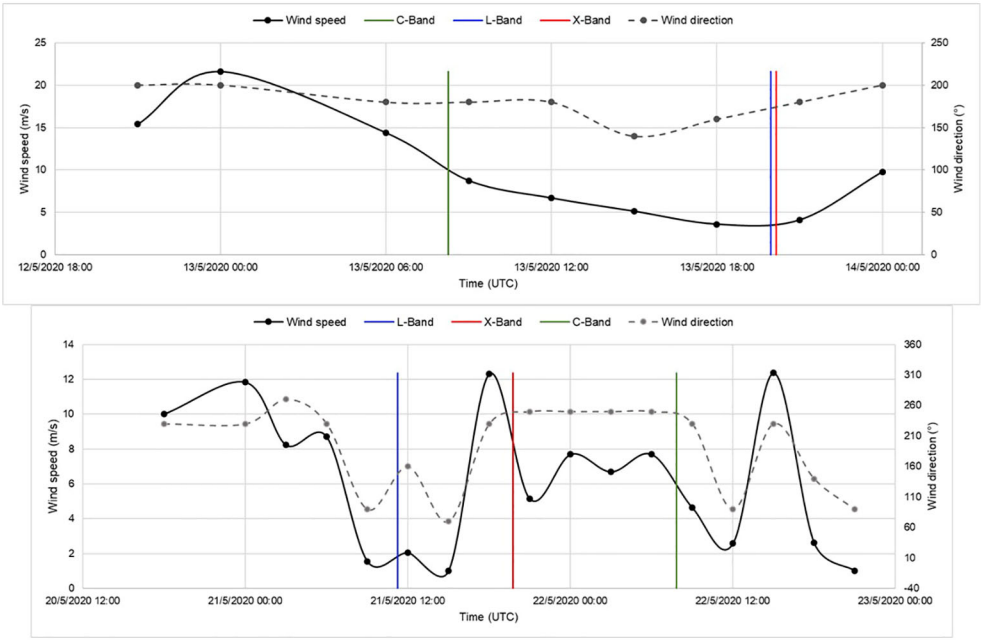

FIGURE 12
Evolution for wind parameters in Esperanza station during May.

higher sensitivity to the surface features of the L-band, consistent with the evolution and composition of the fast ice. No influence in the backscattering coefficient was observed on the different SAR frequencies in relation to the snow layer on the first-year ice; nevertheless, polarization was important in its detections, with measurable differences in the HH channel.

The identification of strips and belts in seawater depended on the sea state and wind conditions in the area. The HV polarization represented an advantage in the identification in relation to HH polarization because of the lower sensitivity to the surface water roughness. The L-band showed to be less sensitive to the roughness of the sea surface; however, further analysis is needed to determine a benefit in the detection of strips with the L-band. Additionally, future research has to be done to incorporate in the SAOCOM image processing workflow the reduction in sub-swath thermal noise, as was seen in two TOPSAR Narrow images from our dataset.

In addition to the limitation in part of the results found, the dataset used in this intercomparison showed the typical operational situation in the Ice Services, where any SAR acquisition is valuable to approach the last most updated condition of the sea ice and icebergs. Further research still needs to be developed in view of incorporating the broad variability in SAR parameters, such as diversity in acquisition modes, resolution, polarization, incidence angle, different environmental conditions, and season of the year to generate useful outcomes for decision-making.

Data availability statement

The raw data supporting the conclusions of this article will be made available by the authors, without undue reservation.

Author contributions

CS: Writing – original draft, Writing – review & editing. LG: Writing – original draft, Writing – review & editing. JA: Writing – original draft, Writing – review & editing.

Funding

We would like to thank the World Meteorological Organization (WMO) for all the support that has been provided to the Argentine Hydrographic Service over the years, and for the financial support that has made this publication possible and open to the scientific community and operational users.

Acknowledgments

We would like to thank the Comisión Nacional de Actividades Espaciales (CONAE) for the provision of the SAOCOM® Product – © CONAE – 2020 All Rights Reserved, and to all personnel that helped us during the process of incorporating the SAOCOM satellite in our Ice Service, especially Laura Frulla, Mario Camuyrano, and Marcela Jauregui, and the great support from the technical support team with the SAOCOM catalog. We acknowledge Copernicus Sentinel data 2020, and COSMO-SkyMed Product – © ASI 2020 processed under license from ASI – Agenzia Spaziale Italiana, All Rights Reserved, distributed by CONAE. We acknowledge the use of imagery from the Worldview Snapshots application (https://wvs.earthdata.nasa.gov), part of the Earth Observing System Data and Information System (EOSDIS). Finally, we are grateful to the

reviewers whose comments contributed to the readability and clarity of this paper.

Conflict of interest

The authors declare that the research was conducted in the absence of any commercial or financial relationships that could be construed as a potential conflict of interest.

Publisher's note

All claims expressed in this article are solely those of the authors and do not necessarily represent those of their affiliated organizations, or those of the publisher, the editors and the reviewers. Any product that may be evaluated in this article, or claim that may be made by its manufacturer, is not guaranteed or endorsed by the publisher.

References

Anconitano, G., Acuña, M. A., Guerriero, L., and Pierdicca, N. (2022). "Analysis of multi-frequency SAR data for evaluating their sensitivity to soil moisture over an agricultural area in Argentina," in *IGARSS 2022 - 2022 IEEE International Geoscience and Remote Sensing Symposium*, Kuala Lumpur, Malaysia, pp. 5716–5719. doi: 10.1109/IGARSS46834.2022.9884232

Arkett, M., Flett, D. G., and Abreu, R. D. (2007). "B-band multiple polarization SAR for ice monitoring - What can it do for the Canadian ice Service," in *Proceedings of the Envisat Symposium 2007 Montreux, Switzerland (ESA SP-636, July 2007)*. pp. 23–27.

Arkett, M., Flett, D., Abreu, R. D., Clemente-Colon, P., Woods, J., and Melchior, B. (2008). "Evaluating ALOS-PALSAR for ice monitoring—What can L-band do for the North American ice service?" in *IGARSS 2008 - 2008 IEEE International Geoscience and Remote Sensing Symposium*, Boston, MA, USA, pp. V-188–V-191. doi: 10.1109/IGARSS.2008.4780059

Azcueta, M., Gonzalez, J. P. C., Zajc, T., Ferreyra, J., and Thibeault, M. (2022). "External calibration results of the SAOCOM-1A commissioning phase,". *IEEE Trans. Geosci. Remote Sens.* 60, 1–8. doi: 10.1109/TGRS.2021.3075369. 2022, Art no. 5207308.

Blomberg, E., Ferro-Famil, L., Soja, M. J., Ulander, L. M. H., and Tebaldini, S. (2018). "Forest biomass retrieval from L-band SAR using tomographic ground backscatter removal,". *IEEE Geosci. Remote Sens. Lett.* 15 (7), 1030–1034. doi: 10.1109/LGRS.2018.2819884

Casey, J. A., Howell, S. E. L., Tivy, A., and Haas, C. (2016). Separability of sea ice types from wide swath C- and L-band synthetic aperture radar imagery acquired during the melt season. *Remote Sens. Environ.* 174, 314–328. doi: 10.1016/j.rse.2015.12.021

De Luca, C., Roa, Y., Bonano, M., Casu, F., Manunta, M., Manzo, M., et al. (2022). "On the first results of the DInSAR-3M project: A focus on the interferometric exploitation of saocom SAR images," in *IGARSS 2022 - 2022 IEEE International Geoscience and Remote Sensing Symposium*, Kuala Lumpur, Malaysia, pp. 4502–4505. doi: 10.1109/IGARSS46834.2022.9884715

Dierking, W. (2013). Sea ice monitoring by synthetic aperture radar. *Oceanography* 26 (2), 100–111. doi: 10.5670/oceanog.2013.33

Dierking, W., and Busche, T. (2006). Sea ice monitoring by L-band SAR: an assessment based on literature and comparisons of JERS-1 and ERS-1 imagery. *IEEE Trans. Geosci. Remote Sens.* 44 (4), 957–970. doi: 10.1109/TGRS.2005.861745

Dierking, W. (2021). "Synergistic use of L- and C-band SAR satellites for sea ice monitoring," in *2021 IEEE International Geoscience and Remote Sensing Symposium IGARSS*, Brussels, Belgium, pp. 877–880. doi: 10.1109/IGARSS47720.2021.9554359

Dierking, W., Iannini, L., and Davidson, M. (2022). "Joint use of L-and C-band spaceborne SAR data for sea ICE monitoring," in *IGARSS 2022 - 2022 IEEE International Geoscience and Remote Sensing Symposium*, Kuala Lumpur, Malaysia, pp. 4711–4712. doi: 10.1109/IGARSS46834.2022.9884133

Drinkwater, M. R., Kwok, R., Winebrenner, D. P., and Rignot, E. (1991). Multi-frequency polarimetric synthetic aperture radar observations of sea ice. *J. Geophys. Res.* 96 (C11), 20,679–20,698. doi: 10.1029/91JC01915

Ferreyra, J., Solorza, R., Teverovsky, S., and Soldano, A. (2021). "Estimación de dirección y velocidad superficial en glaciares de la Patagonia Austral utilizando datos de la constelación SIASGE." in *2021 XI Congreso Argentino Tecnología Espacial*, pp. 7–9.

Flett, D., De Abreu, R., Arkett, M., and Gauthier, M.-F. (2008). "Initial evaluation of Radarsat-2 for operational sea ice monitoring," in *IGARSS 2008 - 2008 IEEE International Geoscience and Remote Sensing Symposium*, Boston, MA, USA, pp. I-9–I-12. doi: 10.1109/IGARSS.2008.4778779

Han, H., Kim, J. I., Hyun, C. U., Kim, S. H., Park, J. W., Kwon, Y. J., et al. (2020). Surface roughness signatures of summer arctic snow-covered sea ice in X-band dual-polarimetric SAR. *GIScience Remote Sens.* 57 5, 650–669. doi: 10.1080/15481603.2020.1767857

Johansson, A. M., Brekke, C., Spreen, G., and King, J. A. (2018). X-, C-, and L-band SAR signatures of newly formed sea ice in Arctic leads during winter and spring. *Remote Sens. Environ.* 204, 162–180. doi: 10.1016/j.rse.2017.10.032

Johansson, A. M., King, J. A., Doulgeris, A. P., Gerland, S., Singha, S., Spreen, G., et al. (2017). Combined observations of Arctic sea ice with near-coincident colocated X-band, C-band, and L-band SAR satellite remote sensing and helicopter-borne measurements. *J. Geophysical Research: Oceans* 122 (1), 669–691. doi: 10.1002/2016JC012273

Kwok, R., Cunningham, C. F., and Nghiem., S. V. (2003). A study of the onset of melt over the Arctic Ocean in RADARSAT synthetic aperture radar data. *J. Geophysical Res.* 108, 3363. doi: 10.1029/2002JC001363

Lyu, H., Huang, W., and Mahdianpari, M. (2022). "A meta-analysis of sea ice monitoring using spaceborne polarimetric SAR: advances in the last decade," in *IEEE Journal of Selected Topics in Applied Earth Observations and Remote Sensing*, 15, 6158–6179. doi: 10.1109/JSTARS.2022.3194324

MaChado, F., and Solorza, R. (2020). "Feasibility of the inversion of electromagnetic models to estimate soil salinity using SAOCOM data," in *2020 IEEE Congreso Bienal de Argentina (ARGENCON)*, Resistencia, Argentina, pp. 1–8. doi: 10.1109/ARGENCON49523.2020.9505383

Maillard, P., Clausi, D. A., and Deng, H. (2005). Operational map-guided classification of SAR sea ice imagery IEEE Trans. *Geosci. Remote Sens.* 43 (12), 2940–2951. doi: 10.1109/TGRS.2005.857897

Matsuoka, T., Uratsuka, S., Satake, M., Kobayashi, T., Nadai, A., Umehara, T., et al. (2001). CRL/NASDA airborne SAR (Pi-SAR) observations of sea ice in the Sea of Okhotsk. *Ann. Glaciology* 33, 115–119. doi: 10.3189/172756401781818734

Onstott, R. G., and Shuchman, R. A. (2004). "SAR measurements of sea ice," in *Synthetic Aperture Radar:Marine User's Manual*. Eds. C. R. Jackson and J. R. Apel (Washington, DC: Synthetic Aperture Radar MarineUser's Manual. NOAA), 81–115.

Roa, Y., Rosell, P., Solarte, A., Euillades, L., Carballo, F., García, S., et al. (2021). First assessment of the interferometric capabilities of SAOCOM-1A: New results over the Domuyo Volcano, Neuquén Argentina. *J. South Am. Earth Sci.* 106, 102882. doi: 10.1016/j.jsames.2020.102882. ISSN 0895-9811.

Salvó, C. S., Gómez Saez, L., Scardilli, A., and Salgado, H. (2022). "Incorporación del Sar Saocom para el monitoreo operativo del hielo marino y témpanos," in *Centro de Estudios de Prospectiva Tecnológica Militar TEC 1000 / 1a ed.*. (Ciudad Autónoma de Buenos Aires: Universidad de la Defensa Nacional), 216, 173–182. Available at: https://www.fie.undef.edu.ar/ceptm/wp-content/uploads/2022/10/TEC1000-2021-Digital.pdf.

Scardilli, A. S., Salvó, C. S., and Gomez Saez, L. (2022). Southern Ocean ice charts at the Argentine Naval Hydrographic Service and their impact on safety of navigation. *Front. Mar. Sci.* 9. doi: 10.3389/fmars.2022.971894

Seppi, S. A., Casanova, E. S., Roa, Y. L. B., Euillades, L., and Gaute, M. (2021). On the feasibility of applying orbital corrections to SAOCOM-1 data with free open source software (foss) to generate digital surface models: a case study in Argentina. *Int. Arch. Photogrammetry Remote Sens. Spatial Inf. Sci.* 46, 167–174. doi: 10.5194/isprs-archives-XLVI-4-W2-2021-167-2021

Shuchman, R. A., and Flett, D. G. (2003). "SAR measurement of sea ice parameters: sea ice session overview paper". in *Proceedings of the Second Workshop on Coastal and Marine Applications of SAR (CMASAR)*, 8 – 12 September 2003, Svalbard, Norway (ESA SP-565, June 2004). p. 151–160.

Singha, S., Johansson, M., Hughes, N., Hvidegaard, S., and Skourup, H. (2018). Arctic sea ice characterization using spaceborne fully polarimetric L-, C- and X-band SAR with validation by airborne measurements. *IEEE Trans. Geosci. Remote Sens.* 56 (7), 3715–3734. doi: 10.1109/TGRS.2018.2809504

Viotto, S., Bookhagen, B., Toyos, G., and Torrusio, S. (2021). "Assessing ground deformation in the Central Andes (NW Argentina) with Interferometric Synthetic Aperture Radar analyses: First results of SAOCOM data and Sentinel-1 data," in *EGU General Assembly 2021, online,* 19–30 Apr 2021, EGU21–12474. doi: 10.5194/egusphere-egu21-12474

Wang, Y. R., and Li, X. M. (2021). Arctic sea ice cover data from spaceborne synthetic aperture radar by deep learning. *Earth Syst. Sci. Data* 13, 2723–2742. doi: 10.5194/essd-13-2723-2021

Zakhvatkina, N. Y., Alexandrov, V. Y., Johannessen, O. M., Sandven, S., and Frolov, I. Y. (2012). Classification of sea ice types in ENVISAT synthetic aperture radar images. *Geosci. RemoteSensing* 51 (5), 2587–2600. doi: 10.1109/TGRS.2012.2212445

frontiers | Frontiers in Marine Science

TYPE Original Research
PUBLISHED 11 April 2024
DOI 10.3389/fmars.2024.1366002

OPEN ACCESS

EDITED BY
John Falkingham,
International Ice Charting Working Group, Canada

REVIEWED BY
Longjiang Mu,
Laoshan Laboratory, China
John Yackel,
University of Calgary, Canada

*CORRESPONDENCE
Keguang Wang
keguang.wang@met.no

RECEIVED 05 January 2024
ACCEPTED 18 March 2024
PUBLISHED 11 April 2024

CITATION
Wang K, Wang C, Dinessen F, Spreen G, Ricker R and Tian-Kunze X (2024) Multisensor data fusion of operational sea ice observations.
Front. Mar. Sci. 11:1366002.
doi: 10.3389/fmars.2024.1366002

Multisensor data fusion of operational sea ice observations

Keguang Wang[1]*, Caixin Wang[1], Frode Dinessen[2], Gunnar Spreen[3], Robert Ricker[4] and Xiangshan Tian-Kunze[5]

[1]Department of Research and Development, Norwegian Meteorological Institute, Oslo, Norway, [2]Department of Research and Development, Norwegian Meteorological Institute, Tromsø, Norway, [3]Institute of Environmental Physics, University of Bremen, Bremen, Germany, [4]NORCE Norwegian Research Centre, Tromsø, Norway, [5]Division of Sea Ice Physics, Alfred Wegener Institute, Bremerhaven, Germany

Multisensor data fusion (MDF) is a process/technique of combining observations from multiple sensors to provide a more robust, accurate and complete description of the concerned object, environment or process. In this paper we introduce a new MDF method, multisensor optimal data fusion (MODF), to fuse different operational sea ice observations around Svalbard. The overall MODF includes regridding, univariate multisensor optimal data merging (MODM), multivariate check of consistency, and generation of new variables. For MODF of operational sea ice observations around Svalbard, the AMSR2 sea ice concentration (SIC) is firstly merged with the Norwegian Meteorological Institute ice chart. Then the daily SMOS sea ice thickness (SIT) is merged with the weekly CS2SMOS SIT to form a daily CS2SMOS SIT, which is further refined to be consistent with the SIC through consistency check. Finally sea ice volume (SIV) and its uncertainty are calculated based on the merged SIC and fused SIT. The fused products provide an improved, united, consistent and multifaceted description for the operational sea ice observations, they also provide consistent descriptions of sea ice edge and marginal ice zone. We note that uncertainties may vary during the regridding process, and therefore correct determination of the observation uncertainties is critically important for MDF. This study provides a basic framework for managing multivariate multisensor observations.

KEYWORDS

multisensor optimal data fusion (MODF), regridding, multisensor optimal data merging (MODM), sea ice concentration (SIC), sea ice thickness (SIT), sea ice volume (SIV), sea ice edge (SIE), marginal ice zone (MIZ)

1 Introduction

Sea ice refers to any form of ice found at sea originated from the freezing of seawater (WMO, 2014). The annual mean global sea ice area is approximately 23×10^6 km^2, being approximately 4.5% of the Earth's surface and approximately 6.4% of the world's oceans. The majority of sea ice is in the Arctic and Southern oceans, with some additional seasonal sea ice in the Baltic, Black, Okhotsk, and Bohai seas.

Sea ice plays an important role in the Earth's climate system. Due to the much higher surface albedo compared with seawater (Perovich et al., 2002), sea ice reflects much of the incident solar radiation back to the atmosphere, thus keeping the underlying ocean cooler in summer than it would be in open water. The presence of sea ice prevents rapid exchange of heat and mass between the underlying water and the overlying atmosphere. Freezing and melting of sea ice alters the oceanic salinity, thus influencing the global ocean circulation and freshwater budget (Liu et al., 2019b; Ferster et al., 2022). Polar sea ice is one of the largest ecosystems on Earth (Arrigo, 2014), playing an important role in the global ecosystem. It constitutes a unique habitat for many biota, providing feeding grounds and nurseries for microbes, meiofauna, fish, birds, and mammals (Steiner et al., 2021).

A large number of satellite sensors have been developed for different sea ice observations. However, most sea ice remote sensing products contain defects due to the limitations of individual sensors. For example, due to many factors (including smooth surface, absence of snow, brine content), the sea ice concentration (SIC) of thin sea ice (<30 cm) is commonly underestimated by most passive microwave radiometer (PMR) SIC algorithms (Cavalieri, 1994; Kern et al., 2019). For sea ice thickness (SIT) remote sensing, the Soil Moisture and Ocean Salinity (SMOS) has high uncertainty for measuring thick (over 1 m) sea ice (Tian-Kunze et al., 2014) whereas the CryoSat-2 has high uncertainty for measuring thin (below 1 m) sea ice (Ricker et al., 2017). In order to overcome such shortcomings, there have been some studies to merge multisensor data, such as the merging of SMOS SIT and CryoSat-2 SIT (Ricker et al., 2017; Wang et al., 2020); merging of SSMIS SIC, AMSR2 SIC, and ice chart (Wang et al., 2020); merging of AMSR2 SIC and MODIS SIC (Ludwig et al., 2020); and fusion of AMSR2 SIC and SAR SIC (Khachatrian et al., 2023).

Multisensor data fusion (MDF) is a process/technique of combining observations from multiple sensors to provide a more robust, accurate, and complete description of an object, environment, or process. An extensive review of the MDF approaches and its applications is presented in Khaleghi et al. (2013). The purpose of fusing multisensor data is to obtain better estimates of geophysical parameters or new information that could not be obtained with any single sensors. In this study, we introduce a new MDF method, multisensor optimal data fusion (MODF), to fuse operational sea ice observations around Svalbard.

In sea ice research, MDF and multisensor data merging (MDM) are often interchangeably used. However, they are thus far only applied for univariate applications (e.g., Ricker et al., 2017; Ludwig et al., 2020; Wang et al., 2020; Khachatrian et al., 2023). In the present study, we confine the MDM or merging only for combination of univariate multisensor observations; that is, all the data from the multisensors describe the same variable or parameter. By contrast, the MDF or fusion is denoted for combination of multivariate multisensor observations, in which the observations are composed of different variables or parameters. MDF can be seen as an extension of MDM, where the univariate multisensor observations are a subset of the multivariate multisensor observations (see details in Section 3). As far as the authors know, there has been no such MDF study for sea ice.

A full MDF of sea ice observations shall include all aspects of sea ice parameters, for example sea ice concentration (extent, area, thickness, type, volume, age, drift, deformation, ridges, leads, polynyas, melt ponds, salinity) and sea ice surface albedo (roughness, temperature, emissivity). As a starting study of MDF for operational purposes, here we focus on the two most important parameters: SIC and SIT. These two variables are the central for the determination of ship categories navigating in the polar waters. Another sea ice parameter, sea ice volume (SIV), is also included here which can be deduced from the combination of SIC and SIT. SIV is important in sea ice modeling and data assimilation, as it is a basic variable in sea ice models (Hunke et al., 2015; Wang et al., 2023). Our main purpose here is to generate a united, consistent, and multifaceted daily sea ice observations for monitoring and prediction applications. Such a framework shall also be useful for the construction of consistent sea ice Essential Climate Variables (Lavergne et al., 2022; Sandven et al., 2023), which include more sea ice parameters.

The paper is organized as follows. In section 2, we introduce the study area and the data. In section 3, we describe the theoretical framework of the multisensor optimal data fusion (MODF) for fusing the multivariate operational sea ice observations. Some critical navigational information such as sea ice edge (SIE) and marginal ice zone (MIZ) are also introduced here as extra information from the fusion of SIC and SIT observations. The MODF results are presented in section 4, with the focus on a consistent observation and estimate of the operational sea ice conditions around Svalbard. In section 5, we discuss some issues on the evaluation and future applications. The conclusions are summarized in section 6.

2 Study area and data

Svalbard is the northernmost territory of Norway, composed of the Svalbard Archipelago in the Arctic Ocean about midway between mainland Norway and the North Pole (Figure 1). Compared with other areas at similar latitudes, the climate of Svalbard and the surrounding seas is considerably milder, wetter, and cloudier, due mainly to the atmospheric heat and moisture transport associated with the Icelandic low and the warm West Spitsbergen Current (AMAP, 2017). As a result of the mild climate and the rich marine bioresources, Svalbard waters have long been an area of more maritime activities from a pan-Arctic perspective (Olsen et al., 2020). Along with the reducing Arctic sea ice, there is a continuous growth in marine activities such as shipping, fisheries, tourism, and oil and gas exploration around Svalbard (AMAP, 2017; Olsen et al., 2020), with remarkable increases in the operational seasons and navigational areas (Stocker et al., 2020; Müller et al., 2023). It is therefore critically important to frequently monitor and accurately predict the sea ice conditions to assist safe

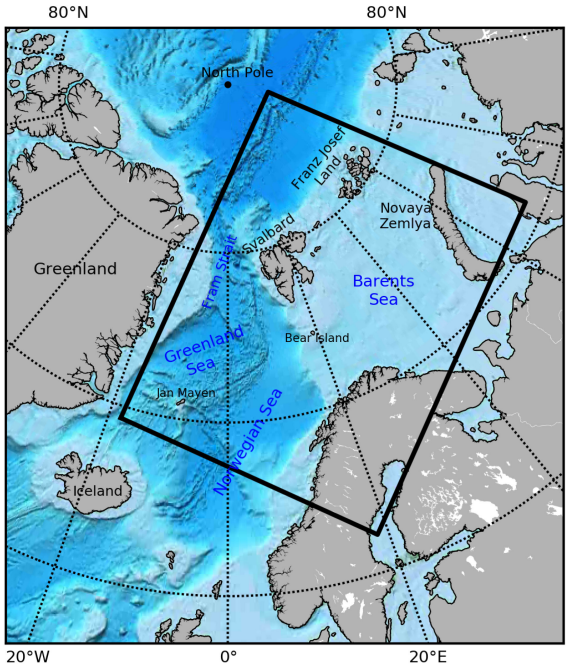

FIGURE 1
Study area: Barents-2.5km model domain shown by the thick rectangle.

operations for ship traffic, fisheries, search and rescue, and other marine operations.

The MDF of operational sea ice observations is performed for the sea areas around Svalbard, as shown by the thick rectangle in Figure 1. This is the model domain for the Barents-2.5-km operational ocean and sea ice forecast model at the Norwegian Meteorological Institute (Duarte et al., 2022; Röhrs et al., 2023), with the horizontal model grid resolution of 2.5 km. The Barents-2.5-km model does not contain ocean and sea ice information in the Baltic Sea. For consistency, we have also removed the sea ice in the Baltic Sea in this study. The fused sea ice observations will be further utilized for operational analysis and forecast.

2.1 SIC observations

There have been a large number of SIC observation through remote sensing (Kern et al., 2019). In this study, we use two high-resolution operational SIC products. One is the AMSR2 SIC data produced at the University of Bremen, and the other is sea ice chart from the Norwegian Meteorological Institute's Ice Service (NIS). Figure 2 shows an example of the original SIC and standard deviation (SD) from these two data sets for 16/03/2022, as a typical winter sea ice condition in the Arctic.

2.1.1 AMSR2 SIC

The AMSR2 microwave radiometer onboard the GCOM-W1 satellite measures the microwave emission from the Earth, at a nominal incident angle of 55° and a swath width of 1,450 km. The AMSR2 SIC dataset we used here is version 5.4 with a grid resolution of 3.125 km, which utilizes the highest spatially resolving AMSR2 channels at 89 GHz (Melsheimer, 2019). It uses the same ARTIST sea ice (ASI) algorithm, as it was developed for the AMSR-E 89 GHz channel (Spreen et al., 2008). It has a higher spatial resolution than most other AMSR2 SIC datasets, but the atmospheric influence can be higher. The uncertainty is calculated following the same procedure in Spreen et al. (2008), where the overall error sums from three sources: the radiometric error from the bright temperature, the variability of the tie points, and the atmospheric opacity. The uncertainty is expressed in terms of SD. It is noted that this uncertainty does not account for individual, spatially varying atmospheric and surface effects as for example discussed in Rückert et al. (2023) and Rostosky and Spreen (2023).

2.1.2 NIS ice chart

Due to the large uncertainties in the PMRs for low SIC conditions (Cavalieri, 1994; Kern et al., 2019), we choose the NIS sea ice chart to mitigate the defect. The ice chart is produced based on manual interpretation of satellite data (Dinessen and Hackett, 2018), being a typical manually analyzed product. The ice charting employs a variety of satellite observations to obtain a more realistic SIE and MIZ. The main satellite data used are the weather-independent SAR data from RadarSat-2 and Sentinel-1. The analyst also uses visual and infrared data from METOP, NOAA, and MODIS in cloud-free conditions. These satellite data cover the charting area several times a day and are resampled to 1-km grid spacing. The NIS ice chart includes seven ice categories following the WMO sea ice nomenclature (WMO, 2014): fast ice (SIC = 10/10), very closed drift ice (9–10/10), closed drift ice (7–8/10), open drift ice (4–6/10), very open drift ice (1–3/10), open water (<1/10), and ice free (0). For practical use, a mean value is applied to denote the different ice categories in the ice chart. The uncertainty is approximated as the half of the range of the corresponding ice category, except being 0.01 for the fast ice. Apparently, this uncertainty is a very coarse estimate.

2.2 SIT observations

Remote sensing of SIT is much more difficult. There is thus far no sub-daily to daily SIT observation covering the whole Barents-2.5-km domain. The daily SMOS SIT has a high temporal resolution but with limitations of no observation north of 85°N and large uncertainties for SIT over 1 m. The weekly CS2SMOS SIT has better spatial coverage but has a limitation of weekly temporal resolution. In this study, we use these two products to generate a daily SIT data to cover the whole domain.

2.2.1 SMOS SIT

The SMOS SIT is retrieved from brightness temperature measured at the L-band (1.4 GHz) from ESA's SMOS mission.

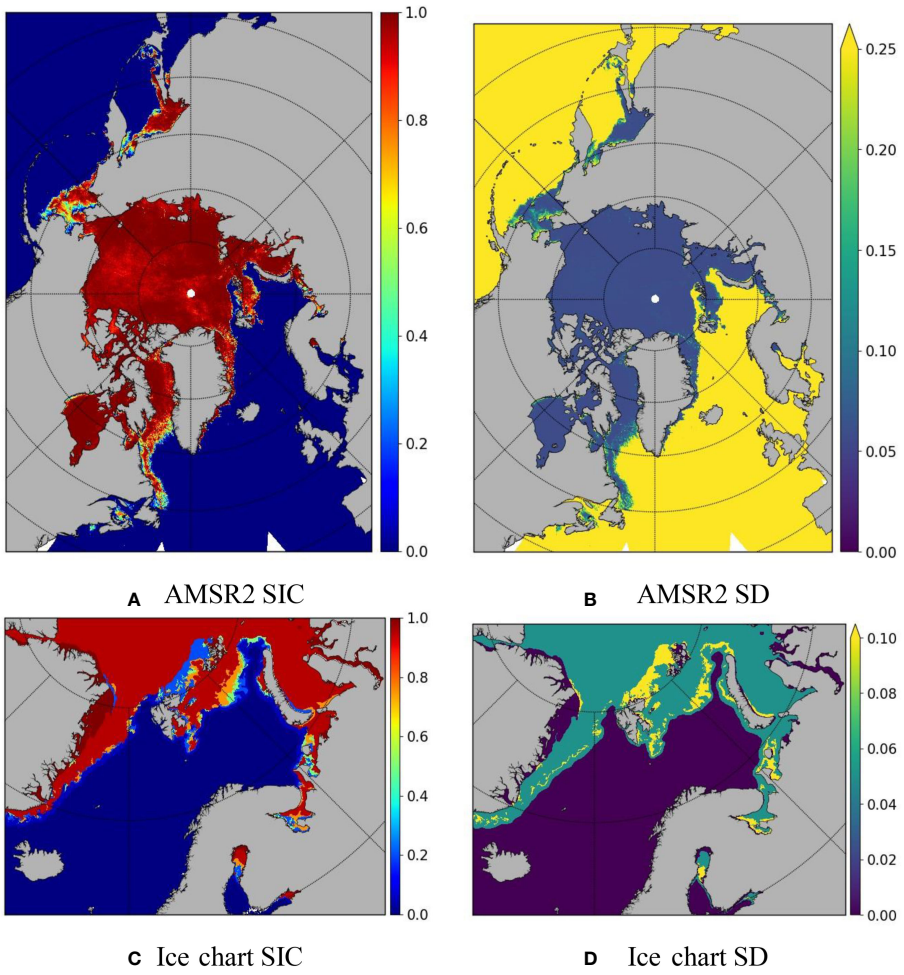

FIGURE 2
Original AMSR2 SIC and SD (**A,B**) and NIS ice chart (SIC and SD (**C, D**)) on 16/03/2022. The AMSR2 data is obtained from the University of Bremen, and the NIS ice chart is from the Norwegian Meteorological Institute.

The retrieval algorithm is based on a thermodynamic sea ice model and a three-layer radiative transfer model, which applies an iterative method to calculate SIT using bulk ice temperature and bulk ice salinity (Tian-Kunze et al., 2014). The SMOS SIT uncertainty is calculated based on the following factors: uncertainty of the measured brightness temperature, uncertainties of the auxiliary data sets (JRA55 reanalysis and sea surface salinity climatology), and the assumptions made for the radiation and thermodynamic models. The uncertainty increases rapidly with increasing SIT, and it is strongly recommended to use only data with a saturation ratio (provided in the dataset) less than 100% (Tian-Kunze et al., 2014). The data is gridded at the 12.5-km grid spacing on polar stereographic projection and is available from mid-October to mid-April in the Arctic. During winter seasons, the data is generated operationally by Alfred Wegener Institute (AWI), Germany, on daily basis with 24-h latency. SMOS SIT is obtained from ESA data collections (ESA, 2023a, version 3.3, accessed on 07.07.2023). As an example, the SMOS SIT and its SD on 16/03/2022 are shown in Figures 3A, B.

2.2.2 Weekly CS2SMOS SIT

The weekly CS2SMOS SIT is also produced by AWI and distributed *via* the ESA web portal (ESA, 2023b, version 2.05, accessed on 07.07.2023). CS2SMOS provides weekly SIT retrievals from merging daily SMOS thin SIT retrievals (Tian-Kunze et al., 2014) and SIT retrievals from CryoSat-2 (Hendricks and Paul, 2023), using an optimal interpolation approach (Ricker et al., 2017). The uncertainty of the CS2SMOS SIT is a natural part of the optimal interpolation. The data are projected onto the 25-km EASE2 Grid, based on a polar aspect spherical Lambert azimuthal equal-area projection. Figures 3C, D show the weekly CS2SMOS SIT and its SD on 16/03/2022, being an estimate of SIT and its SD during 13–19/03/2022.

3 MODF method

In this section, we describe the theoretical framework of MODF, which includes regridding, univariate multisensor optimal data merging (MODM), multivariate consistency check, and generation

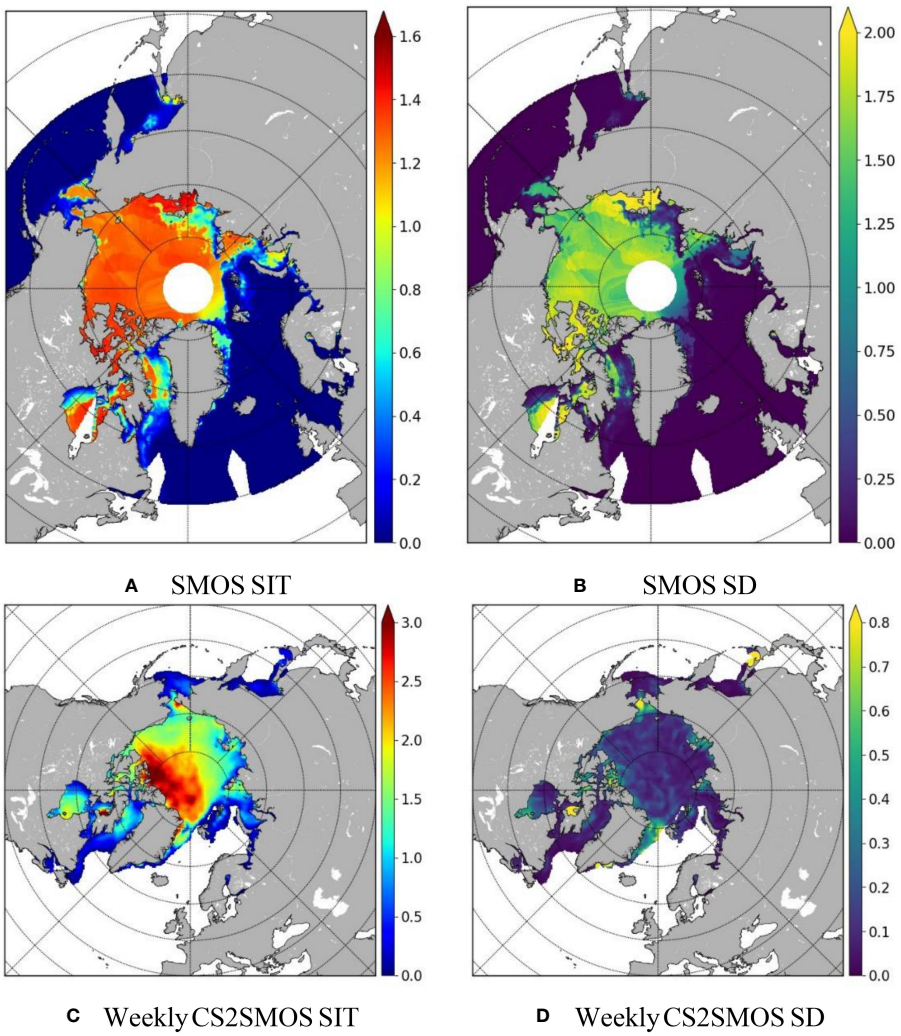

FIGURE 3
Original SMOS SIT and SD **(A, B)** and weekly CS2MSOS SIT and SD **(C, D)** on 16/03/2022. The weekly CS2SMOS SIT and SD are an estimate of weekly mean SIT and its SD during 13–19/03/2022. All the data are from AWI *via* ESA. The units are meters for both SIT and SD.

of new variables. The MODM has been used to optimally merge univariate multisensor observations (Wang et al., 2020), and it is here integrated as an important component of MODF.

3.1 Regridding

It is common that different remote sensing products have different projections and grids. Similarly, different applications would also have their own special projections and grids. For solving a certain desired application, we would thus need to remap the different satellite observations to the dedicated grid of the application. There are two common methods for such remapping: regridding and resampling. The essential difference between regridding and resampling lies in that regridding is performed on the grids, whereas resampling is performed on the points. Whether to use the regridding or resampling method depends mainly on the properties of the desired parameters. For example, if we need to remap the SIC, which is the fraction of the ice-covered area to the total area in a grid, then the regridding method shall be used. By contrast, if we need to remap the sea ice velocity field, then the resampling method shall be used at the grid points. In this case, the velocity inside a grid can be well-interpolated from the surrounding grid points, whereas using the grid-mean velocity is generally uncommon. In this study, for remapping the SIC and SIT, we use the regridding method, which can generally be separated in upgridding and downgridding.

3.1.1 Upgridding and downgridding

Upgridding refers to the process of regridding a source field to a finer-resolution destination field. This applies to both temporal and spatial fields. In this study, regridding of the weekly mean CS2SMOS SIT to daily would require upgridding in the temporal space, whereas both of the SMOS SIT (spatial resolution 12.5 km) and the CS2SMOS SIT (spatial resolution 25 km) would need upgridding of the two-dimensional spatial SIT to the Barents-2.5-km domain. Upgridding is generally performed through the

interpolation technique, which is typically composed of nearest neighbor, linear, and cubic interpolations.

In contrast to the upgridding, downgridding is the process of regridding a source field to a coarser-resolution destination field. In the present study, the sea ice chart SIC has a spatial resolution of 1 km, and it would require downgridding to the relatively coarser resolution for the Barents-2.5-km domain. While the common interpolation methods, such as the nearest neighbor, linear, and cubic interpolation, are generally applicable for downgridding, conservative interpolation methods are preferred for some special cases which require high accuracy for tiny changes (Pletzer and Fillmore, 2015).

3.1.2 Effect of regridding on uncertainty

Due to the importance of observation uncertainty on data assimilation, it is essential to accurately determine the uncertainties of satellite observations due to regridding. To the authors' knowledge, such an effect has not been considered thus far in the data assimilation community.

The effect of downgridding on the uncertainty may be derived as follows. Denote $x_1, x_2, \ldots, x_l$ as l independent observations with SDs $\sigma_1, \sigma_2, \ldots, \sigma_l$, then the total is

$$S = x_1 + x_2 + \cdots + x_l \tag{1}$$

which has variance

$$\mathrm{Var}(S) = \mathrm{Var}(x_1) + \mathrm{Var}(x_2) + \cdots + \mathrm{Var}(x_l) = \sum_{k=1}^{l} \sigma_k^2 . \tag{2}$$

The mean of these measurements $\bar{x}$ is simply given by

$$\bar{x} = S/l . \tag{3}$$

The variance of the mean can then be calculated according to the Equations (1–3) such that

$$\mathrm{Var}(\bar{x}) = \mathrm{Var}(S/l) = \frac{1}{l^2}\mathrm{Var}(S) = \frac{1}{l^2}\sum_{k=1}^{l}\sigma_k^2 . \tag{4}$$

From Equation (4) we get the corresponding SD

$$\sigma_{\bar{x}} = \frac{\sqrt{\sum_{k=1}^{l}\sigma_k^2}}{l} . \tag{5}$$

If the uncertainties of all the l observations are equal, namely, $\sigma_k = \sigma$ then Equation (5) can be simplified as

$$\sigma_{\bar{x}} = \frac{\sigma}{\sqrt{l}} . \tag{6}$$

Due to different manipulations of data, the effect of upgridding on the uncertainty may differ between temporally and spatially. For temporal upgridding such as the weekly CS2SMOS SIT into daily SIT, an inverse process to the downgridding shall be applied. If we assume that the daily SIT observations are independent on each other and their uncertainties are approximately equal, then the daily uncertainty σ can be estimated from the weekly uncertainty $\sigma_{\bar{x}}$ such that

$$\sigma = \sqrt{l}\sigma_{\bar{x}}, \tag{7}$$

where $l = 7$ in this case.

Equations (5–7) indicate the resulting uncertainty tends to decrease during downgridding and increase during upgridding. However, spatial upgridding of satellite observations may need special attention. It is noted that, for satellite products such as the AMSR2 SIC, SMOS SIT, and CS2SMOS SIT, their spatial resolutions may already be at the highest of the products. Therefore, upgridding does not produce more independent observations. As a consequence, the uncertainty would be unlikely to increase as significantly as the temporal upgridding. Further studies are needed to accurately determine the uncertainty variations for this situation. In this study, the uncertainties are assumed unchanged during the spatial upgridding.

3.2 MODM

Using the regridding method above, we can remap the individual sea ice observations to the dedicated area (here the Barents-2.5-km domain). These regridded multiple observations can be merged for the same univariate observations, using the MODM method (Wang et al., 2020). MODM here is used as a component of MODF. For self-containment, the main theoretical framework of MODM is described here with some minor modifications.

3.2.1 General solution

Consider a state variable vector x (column vector) such as SIC for a certain spatial domain such as the Barents-2.5-km domain (Figure 1), on a regular grid with the total grid number of n. Suppose we have m observations $\mathrm{x}_k, k = 1, \ldots, m$, for the true state vector x_t. These observations are assumed to be taken with different instruments, and their error vector associated with each measurement is $\epsilon_k = \mathrm{x}_k - \mathrm{x}_t$. We note that the observations are also assumed independent during the temporal regridding process in section 3.1.2. However, those observations are generally obtained using the same instrument but differ in the temporal distributions.

We assume that all the observations have been regridded and that all the error vectors are random, unbiased, and normally distributed. Thus, for the kth observation error vector, we have the mean $\mu = E(\epsilon_k) = 0$ and covariance $\mathbf{R}_k = E(\epsilon_k \epsilon_k^T)$, where E denotes expectation operation and the superscript "T" denotes transpose. The probability density function (PDF) of such a error vector can be expressed as,

$$f(\epsilon_k) = \frac{1}{(2\pi)^{1/2}|\mathbf{R}_k|^{1/2}} \exp\left(-\frac{1}{2}\epsilon_k^T \mathbf{R}_k^{-1} \epsilon_k\right), \tag{8}$$

where $|\mathbf{R}_k|$ denotes the determinant of $\mathbf{R}_k$. If we further assume that the observation error vectors are not mutually correlated, that is, $E(\epsilon_j \epsilon_k^T) = 0$, when $j \neq k$, the PDF of the joint multivariate normal distribution for all the observation error vectors can be extended from Equation (8) and expressed as (Todling, 1999)

$$f(\epsilon_1, \epsilon_2, \cdots, \epsilon_m) = \prod_{k=1}^{m} \frac{1}{(2\pi)^{m/2}|\mathbf{R}_k|^{1/2}} \exp\left(-\frac{1}{2}\epsilon_k^T \mathbf{R}_k^{-1} \epsilon_k\right), \quad (9)$$

where Π denotes the multiplication operator. It is thus easy to see from Equation (9) that the maximum likelihood estimate of $f(\epsilon_1, \epsilon_2, \ldots, \epsilon_m)$ is obtained by equivalently minimizing the following cost function

$$J(x) = \sum_{k=1}^{m} \epsilon_k^T \mathbf{R}_k^{-1} \epsilon_k = \sum_{k=1}^{m} (x - x_k)^T \mathbf{R}_k^{-1} (x - x_k), \quad (10)$$

where the optimal estimate is considered as an approximate to the true value. Differentiate $J(x)$ in Equation (10) against x and set it as 0,

$$\frac{\partial}{\partial x} J(x) = \frac{\partial}{\partial x} \sum_{k=1}^{m} (x - x_k)^T \mathbf{R}_k^{-1} (x - x_k) = 2 \sum_{k=1}^{m} \mathbf{R}_k^{-1} (x - x_k) = 0. \quad (11)$$

From Equation (11) we thus have the optimal estimate x_o vector

$$x_o = \left(\sum_{k=1}^{m} \mathbf{R}_k^{-1}\right)^{-1} \sum_{k=1}^{m} \mathbf{R}_k^{-1} x_k, \quad (12)$$

and the optimal observation error vector

$$\epsilon_o = x_o - x_t = \left(\sum_{k=1}^{m} \mathbf{R}_k^{-1}\right)^{-1} \sum_{k=1}^{m} \mathbf{R}_k^{-1} \epsilon_k . \quad (13)$$

Since all the estimates are assumed as unbiased, normally distributed, and not mutually correlated, from Equation (13) we get the optimal observation error covariance

$$\mathbf{R} = E(\epsilon_o \epsilon_o^T) = \left(\sum_{k=1}^{m} \mathbf{R}_k^{-1}\right)^{-1}. \quad (14)$$

The optimal estimate Equation (12) can be rewritten as

$$x_o = \mathbf{R} \sum_{k=1}^{m} \mathbf{R}_k^{-1} x_k . \quad (15)$$

It is noted that the error covariance is symmetric and semi-positive definite. Consider the process for two data sets to be merged with the error covariance being $\mathbf{R}_1$ and $\mathbf{R}_2$, respectively. According to Equation (14), the merged data error covariance is

$$\begin{aligned} \mathbf{R} &= (\mathbf{R}_1^{-1} + \mathbf{R}_2^{-1})^{-1} = [\mathbf{R}_1^{-1}(\mathbf{R}_1 + \mathbf{R}_2)\mathbf{R}_2^{-1}]^{-1} = \mathbf{R}_2(\mathbf{R}_1 + \mathbf{R}_2)^{-1}\mathbf{R}_1 \\ &= \mathbf{R}_1 - \mathbf{R}_1(\mathbf{R}_1 + \mathbf{R}_2)^{-1}\mathbf{R}_1 = \mathbf{R}_2 - \mathbf{R}_2(\mathbf{R}_1 + \mathbf{R}_2)^{-1}\mathbf{R}_2 . \end{aligned} \quad (16)$$

From Equation (16) and consider the properties of positive definite matrix, we see that the trace of $\mathbf{R}$ has the following property:

$$tr(\mathbf{R}) \leq tr(\mathbf{R}_1), tr(\mathbf{R}_2) . \quad (17)$$

Equation (17) indicates that the sum of the error variance of merged data is no larger than any of the individual observations. For more observations, we can use this analysis successively. With more and more observations, the sum of the merged error variance will become smaller and smaller. Therefore, the MODM process is to combine multiple observations with reducing uncertainty and increasing confidence. In addition, the MODM method can significantly reduce the computational cost and storage for data assimilation, as assimilating the merged multisensor observations is equivalent to assimilating the individual observations concurrently (Wang et al., 2020).

3.2.2 Simplification of MODM

In recent years, more and more sea ice remote sensing observations begin to provide local variance or SD as a measure of uncertainty (Tian-Kunze et al., 2014; Ricker et al., 2017; Tonboe et al., 2016; Lavergne et al., 2019). Accordingly, the MODM method may be simplified by further assuming that each observation error vector is spatially uncorrelated. In this case, the kth error covariance, $\mathbf{R}_k$ (Equation 14), becomes

$$\mathbf{R}_k = E(\epsilon_k \epsilon_k^T) = \begin{bmatrix} \sigma_{1,k}^2 & & & \\ & \ddots & & \\ & & \sigma_{j,k}^2 & \\ & & & \ddots \\ & & & & \sigma_{n,k}^2 \end{bmatrix}, \quad (18)$$

where $\sigma_{j,k}$ is the SD of the kth observation at the jth grid, where $k = 1, \ldots, m$ and $j = 1, \ldots, n$. In this case, the error covariance (Equation 14) and the optimal estimate (Equation 15) of the multisensor observations can be expressed on individual grid (Equation 18),

$$\sigma_j = \left(\sum_{k=1}^{m} \sigma_{j,k}^{-2}\right)^{-1/2}, \quad (19)$$

$$x_j = \sigma_j^2 \sum_{k=1}^{m} x_{j,k} \sigma_{j,k}^{-2}, \quad (20)$$

where $j = 1, \ldots, n$ is the grid ordinal number. Equations (19) and (20) are used in this study for MODM of SIC and SIT.

3.3 Multivariate consistency

Due to the inherent defect of PMRs in the observation of low SIC, it is common that some of the sea ice close to the SIE is underestimated or even removed by weather filters. For such situations, the SIC can be improved by using a sea ice chart which is based on a large variety of sea ice satellite observations. However, there is no similar observations yet for the SIT; therefore, a reasonable treatment must be presented to mitigate the deficiency. One such solution is the empirical relationship between SIC and SIV for thin sea ice (Fritzner et al., 2018), which is based on a non-linear regression for SIT up to 0.4 m. The corresponding SIT can thus be easily obtained *via* SIT = SIV/SIC as follows (Wang et al., 2023):

$$h_m = 0.02e^{2.8767 a_m}, \quad (21)$$

where a and h denote SIC and SIT, h_m denotes the missing SIT, and a_m denotes the SIC in the areas where $a > 0$ but the original SIT $h_0 = 0$. It is noted that the valid SIC range in Equation (21) is also slightly extended such that $a_m \in (0, 1]$ (Wang et al., 2023). The corresponding uncertainty for this newly created SIT h_m can be estimated through the Gaussian propagation of uncertainty together with Equation (21) such that

$$\sigma_{h_m} = 2.8767 h_m \sigma_{a_m}. \quad (22)$$

Thus, the overall fused SIT uncertainty can be approximated as

$$\sigma_h = (\sigma_{h_m}^2 + \sigma_{h_0}^2)^{1/2}, \quad (23)$$

where σ_{h0} is the SD of the original SIT h_0.

3.4 Generation of new variables

One of the main purposes of the MDF is to generate new variables that are not possible with any single variables. Here, we show from the combination of SIC and SIT, we can obtain a series of more robust, accurate, and complete description of the sea ice conditions.

3.4.1 Sea ice volume

Sea ice volume (SIV) is not directly observed, and there has been no studies to estimate the SIV uncertainty. Here, we deduce the formulation for SIV (V) based on the observed SIC (a) and SIT (h) and their SDs $\sigma_a$and σ_h. It is generally reasonable to assume that a and h are two independent random variables; thus, V can be simply expressed as

$$V = ha, \quad (24)$$

and its SD can be calculated according to the variance of the products (Goodman, 1960)

$$\sigma_V = (h_{mean}^2 \sigma_a^2 + a_{mean}^2 \sigma_h^2 + \sigma_a^2 \sigma_h^2)^{1/2}, \quad (25)$$

where the subscript "mean" denotes the mean values of SIC and SIT. It is noted that Equation (25) is the exact variance of products, whereas the Gaussian propagation of uncertainty is an approximate solution after neglecting high-order derivatives and cross-correlated terms.

3.4.2 Sea ice edge

According to the World Meteorological Organization (WMO, 2014), SIE is defined as the demarcation at any given time between open sea and sea ice of any kind. It can generally be separated into two types: compacted and diffuse. The compacted SIE refers to the close and clear-cut SIE, which is compacted by wind or current, usually on the windward side of an area of drift ice. The diffuse SIE refers to the poorly defined SIE, which has an area of dispersed ice, usually on the leeward side of an area of drift ice. In practical usages, SIE is often defined as the demarcation where SIC = 0.15 in the sea ice and climate modeling communities. By contrast, it is often defined as the demarcation where SIC = 0.1 in the sea ice charting community, such as the NIS ice chart (https://cryo.met.no) and US National Ice Center (NIC) ice chart (https://usicecenter.gov/Products). Wang et al. (2023) argue that choosing SIC = 0.1 as the demarcation for SIE has several benefits. Most importantly, it has a clear physical representation that distinguishes open water (SIC<1/10) and very open drift ice (SIC in 1–3/10). In addition, it provides a consistent definition for the joint sea ice modeling and charting community. In this study, we also use SIC = 0.1 as the demarcation for SIE.

3.4.3 Marginal ice zone

MIZ is generally referred to the transition region from open water to dense pack ice that is affected by open ocean processes (Wadhams, 1986; Johannessen et al., 1987), although its accurate definition is still under intensive discussion from different viewpoints and concerns. Typical MIZ conditions are found along the southern edges of the ice pack in the Bering, Greenland, and Barents seas, in the Baffin Bay, and along the complete northern edge of the Antarctic ice cover (Røed and O'Brien, 1983). There have been several definitions for the MIZ. The most widely used one is solely based on SIC, commonly defined as the region where SIC $\in$ [0.15,0.8]. In order for a consistent definition in both ice charting and sea ice modeling, the MIZ is here defined as follows

$$\mathrm{MIZ}_t = \text{regions where } a \in [0.1, 0.8] \quad (26)$$

where a is the SIC, and the subscript "t" denotes traditional. This traditional definition has been applied in a variety of applications, such as sea ice charting (e.g., the NIC ice chart), satellite observations (e.g., Strong, 2012; Liu et al., 2019a), sea ice modeling (e.g., Wang et al., 2023), primary productions (e.g., Barber et al., 2015), marine ecosystems (e.g., Wassmann, 2011; Arrigo, 2014), and ship navigation (e.g., Palma et al., 2019).

The above traditional definition of MIZ provides a reasonable quantification of the MIZ extent. However, it is often inadequate for a detailed description of MIZ dynamics (see Bennetts et al., 2022 and references therein). In such cases, the effect of waves must be taken into consideration. To observe the dynamical MIZ, Dumont (2022) suggests three approaches, in which sea ice displays vortical motions, wavy motion, or a dominant floe size less than an upper value (in the order of 200 m–500 m). We comment that the vortical and wavy motions are generally unstable features, so they are not proper for a consistent determination of the dynamical MIZ. For example, the ice eddies or waves in the ice could be temporally diminished in the MIZ whereas the ice floes remain unchanged. In such cases, the extent of the MIZ should remain according to the floe size method, rather than vanished according the other two methods. Therefore, the floe size method appears to be the most appropriate method for observing the dynamical MIZ.

The sea ice floe size is not operationally observed for the sea areas around Svalbard. As an alternative, we approximate the dynamical MIZ using combined SIC and SIT based on the model results from a coupled wave and ice model (Dumont et al., 2011),

$$\mathrm{MIZ}_d = \text{regions where} \begin{cases} a \in [0.1, 0.85],\ h \le 2.0 \\ \text{or} \\ a > 0.85,\ h \le 10.5 - 10a \end{cases} \quad (27)$$

where a and h denote SIC and SIT and the subscript "d" denotes dynamical. The lower SIC bound of 0.1 is here used to be consistent with the SIE. Compared with the traditional MIZ_t the dynamical MIZ_d also includes part of the very close drift ice, although the SIT tends to be thinner with increasing SIC.

It is noted that the dynamical MIZ formulation Equation (27) is solely based on the simulation results at the Fram Strait of a 1D coupled wave-ice model (Dumont et al., 2011). Its accuracy and validity for other sea areas needs further verification. The upper SIC bound of 0.85 is used here to be consistent with the simulation results (Dumont et al., 2011), which is slightly larger than the traditional upper bound of 0.8 (see Equation 26). This difference can partly be explained by the constraint $h \leq 2.0$ in Equation (27). For $h > 2.0$ m, the upper SIC bound is supposed to become lower than 0.85 and approach to 0.8.

4 Results

In this section, we fuse the AMSR2 SIC, NIS ice chart, SMOS SIT, and weekly CS2SMOS SIT to generate a united, consistent, and multifaceted daily description of the sea ice for the Barents-2.5-km area. The corresponding data are available at https://doi.org/10.5281/zenodo.10726427.

4.1 MODF of SIC

The original SIC and their SD of the AMSR2 and NIS ice chart are shown in Figure 2. The AMSR2 covers the whole northern hemisphere, whereas the NIS ice chart only covers the European Arctic. The regridding of the SIC and SD is performed using the nearest neighbor interpolation method. The effects of spatial regridding on the uncertainties are ignored. The regridded SIC and SD in the Barents-2.5-km domain are shown in Figures 4A–D. While the overall sea ice distributions are similar, there are noticeable differences between the AMSR2 SIC and the NIS ice chart. One notable difference is the very open drift ice (SIC 1–3/10) north of Svalbard and Franz Josef Land, which is clearly recognized in the ice chart, but identified as ice free (SIC = 0) in the AMSR2 SIC. This is the shortcoming commonly in the PMWs, which have low capabilities in accurately determining low SIC (Cavalieri, 1994; Kern et al., 2019). It is noted that such high uncertainty is very well described in the AMSR2 product (Figure 4B). Application of a large variety of remote sensing products in the ice charting effectively improves the identification of the very open drift ice. Another prominent difference is the fine features within the very close drift ice (9–10/10), which are clearly seen in the AMSR2 SIC (Figures 4A, B), but missing in the ice chart (Figures 4C, D). This is one shortcoming in the manual ice charting, as such features could often be ignored by the analyst.

In order to compensate for the missing features in the very close drift ice in the ice chart, one feasible method is to increase the corresponding uncertainty. In this study, we have set the SD for the very close drift ice in the ice chart as 0.3 during the SIC MODM. This seems to be a reasonable estimate based on the merged SIC and its SD (Figures 4E, F). Merging of the AMSR2 SIC and ice chart SIC follows Equations (19) and (20). On the whole, the merged SIC SD resembles the NIS ice chart SD (cf. Figures 4F, D), due mainly to the much higher uncertainties in the AMSR2 open water and ice free areas (Figure 4B). The fine features in the AMSR2 are very well maintained in the merged SIC (cf. Figures 4A, E). Similarly, SIC (lower). The data in the Baltic Sea have been removed according to the Barents-2.5-km model setting. The very open drift ice in the north of Svalbard and Franz Josef Land and in the northeast Barents Sea is very well preserved (cf. Figures 4C, E).

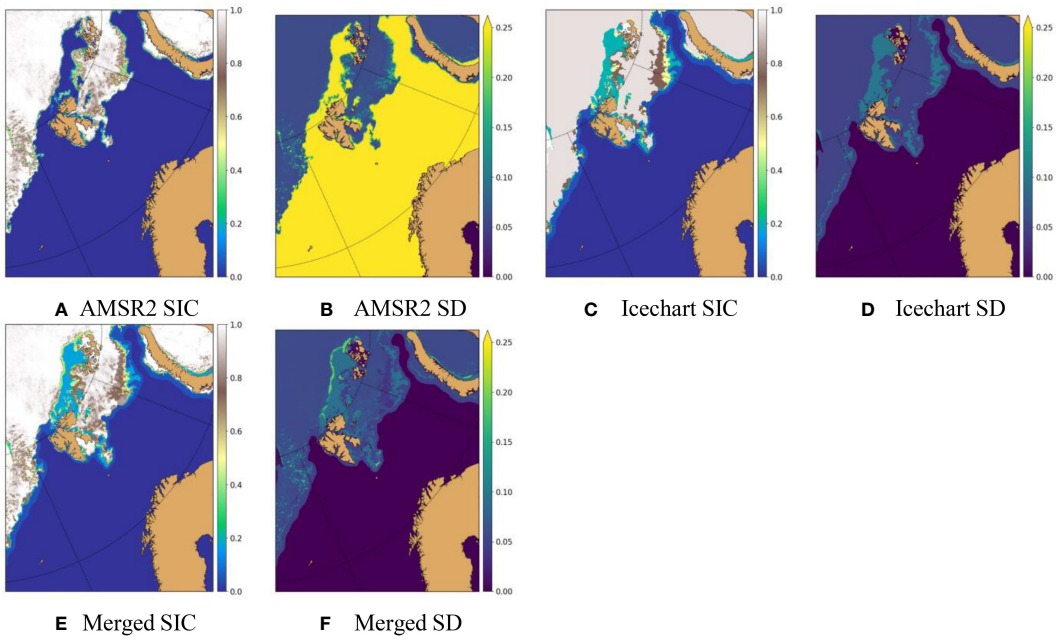

FIGURE 4
SIC and its SD on 16/03/2022: regridded AMSR2 (**A, B**), ice chart (**C, D**) and merged (**E, F**).

there is a noticeable difference in the Arctic central pack ice in the AMSR2 SIC and ice chart, particularly north of the very open drift ice between Svalbard and Franz Jozef Land. It was observed as very close drift ice in the ice chart but identified as ice free in the AMSR2 SIC. This difference is most probably caused by the different time of the observations. The relatively large SD also suggests a strong diurnal variation there (Figure 4F). The merged SIC along this high SD area is around 0.45 (Figure 4E), being a weighted average between the AMSR2 SIC and the ice chart SIC.

4.2 MODF of SIT

The MODF of SIT includes two parts. The first part is the MODM of daily SMOS SIT and weekly CS2SMOS SIT to form a merged daily CS2SMOS SIT, and the second part is a consistency check of the merged daily CS2SMOS SIT with the merged SIC.

4.2.1 MODM of SIT

The MODM of SIT follows much of the same procedure for the SIC. The original SIT and SD for the daily SMOS and weekly CS2SMOS are shown in Figure 3, both covering the whole northern hemisphere, with the spatial resolutions of 12.5 km and 25 km, respectively. These two SIT products are firstly upgridded to the Barents-2.5-km domain using the nearest-neighbor interpolation (Figures 5A–D). For clarity purposes, the uncertainties have both remained unchanged during the regridding. It can be seen that there are considerable differences in these two products (Figure 5). The SMOS SIT has a relatively large data hole around the North Pole. The uncertainty increases rapidly when the observed SIT is over 1 m, as can also be seen in Figures 5A, B. By contrast, the weekly CS2SMOS SIT has a full coverage of the whole domain, with the SIT generally up to 3 m (Figure 5C). The CryoSat-2 SIT has large uncertainties when it is thinner than 1 m (Ricker et al., 2017), and the weekly CS2SMOS SIT effectively reduces the overall uncertainty by combining the CryoSat-2 SIT and the SMOS SIT.

It is noteworthy that the weekly CS2SMOS SIT is a weekly mean; therefore, it can be biased when used for daily purposes. One such case can be seen in the north Greenland Sea, west of Svalbard (cf. Figures 5A, C). We can see that the thin SMOS SIT there is generally approximately 0.5 m (Figure 5A), whereas the weekly CS2SMOS SIT is mostly over 1 m (Figure 5C). This discrepancy is due mainly to the weekly average of the CryoSat-2 SIT and SMOS SIT over the whole week, in which both thin and thick ice drifting before and after the day are accounted for. Therefore, for daily usage, a more accurate estimate of the thin ice should be closer to the daily SMOS SIT. It is apparent that assimilation of such weekly SIT as a daily data would introduce considerable systematic bias.

The merged daily CS2SMOS SIT and SD with and without the temporal upgridding effect are shown in Figures 5E–H, in which the subscript "0" denotes no temporal upgridding effect. It is seen that the merged SD is noticeably larger than SD_0 (cf. Figures 5F, H), particularly for the larger SIT areas in the Arctic Ocean and Greenland Sea. By contrast, the merged SIT is slightly lower than SIT_0 (cf. Figures 5E, G). On the whole, the merged daily CS2SMOS SIT is closer to the SMOS SIT, whereas the SIT_0 is closer to the weekly CS2SMOS SIT, although the thick ice in both SIT and SIT_0 are close to the weekly CS2SMOS SIT.

The merged thin SIT to the west of Svalbard is very close to that in the SMOS SIT (cf. 5e and 5a), showing a successful merging as discussed above. However, the overall distributions of the merged SIT and SIT_0 in the Kara Sea (east of Novaya Zemlya) appear much closer to the weekly CS2SMOS ST than the SMOS SIT, although more similarities are seen to the SMOS SIT when considering the temporal upgridding effect (cf. Figures 5A, C, E, G). Since the SIT there is generally approximately 0.7 m–0.9 m, a reasonable result would be that the merged SIT is closer to the SMOS SIT rather than the weekly CS2SMOS SIT. The most probable reason for the discrepancy is that the uncertainty there in the weekly CS2SMOS SIT (Figure 5D) is underestimated. This is confirmed by the weekly CS2SMOS SIT SD, which is generally less than 0.06 m in this area (Figure 5D). It is much lower than the SMOS SIT SD (generally approximately 0.7 m as shown in Figure 5B), even after the temporal downgridding from daily to weekly. A further refinement of the weekly CS2SMOS SIT uncertainty would be highly desirable.

4.2.2 Check of consistency

The fused SIT and its SD are generally similar to the merged ones in much of the domain (cf. Figures 5I, J, E, F). Their differences are calculated according to Equations (22) and (23), and shown in Figures 5K, L. The differences are mainly located near the SIE, with the additional thin SIT in several cm and additional SD below 1 cm. Such a supplementary effectively overcomes the shortcoming of the PMRs, thus generating a more consistent and accurate observation of the SIE and MIZ compared with the merged SIT and SD. The application of the ice chart also removes some coastal sea ice along the mainland Norway (Figures 5K, L).

4.3 MODF of SIV

Direct observations of SIV and its SD are so far not feasible, so they are calculated according to Equations (24) and (25) with the observed SIC and SIT. Since SIC is a dimensionless variable, the unit of SIV is the same as that of SIT, representing the mean SIT of the concerned grid. On the whole, the SIV resembles the fused SIT (cf. Figures 6A, 5I for reference). This is partly due to the fact that the majority of the sea ice is very close drift ice (Figure 4E), with the SIC close to 1. Different from the SIV, its uncertainty is nonlinearly dependent on the SIC, SIT, and their uncertainties (Equation 20). The overall distribution of the SIV SD is also close to the SIT SD (Figures 6B vs. 5J).

4.4 SIE and MIZ

SIE and MIZ are byproducts of operational sea ice observations. In this study, we focus mainly on their distributions; their uncertainties are not estimated. As an example, Figure 7 shows the MIZ distributions on 16/03/2022. The traditional MIZ_t is solely

10.3389/fmars.2024.1366002

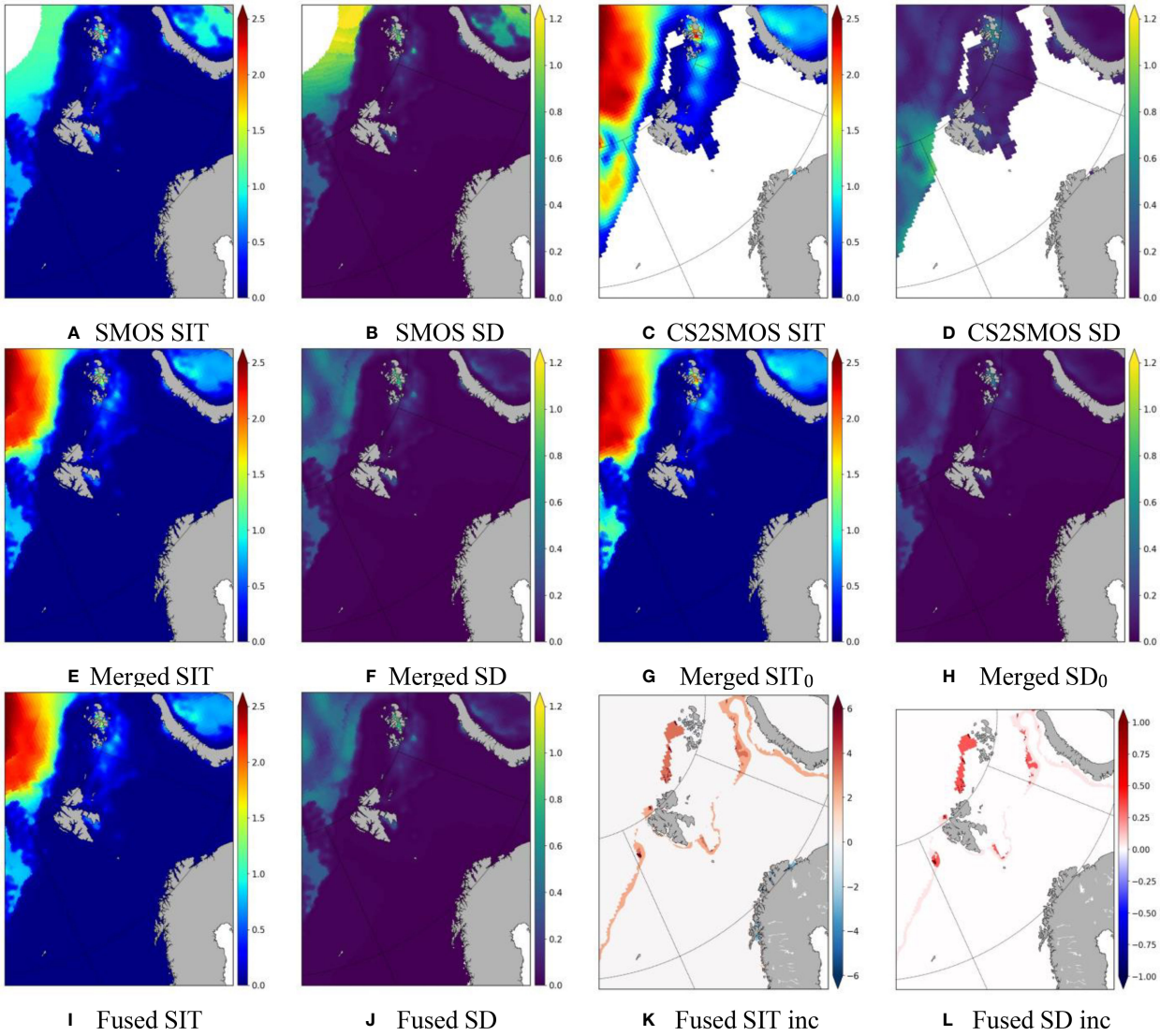

FIGURE 5
SIT and its SD on 16/03/2022: regridded daily SMOS SIT **(A, B)**, regridded weekly CS2SMOS SIT **(C, D)**, merged daily CS2SMOS SIT with temporal upgridding effect **(E, F)**, merged daily CS2SMOS SIT without temporal upgridding effect **(G, H)**, fused SIT and increment **(I–L)**. The fused increments denote the SIT and SD differences of fused−merged. The units of the SIT and SD are m; the units of the increments are cm.

based on SIC (Equation 26), whereas the dynamical MIZ_d is based on a combination of SIC and SIT (Equation 27). In this study, we have set the SIE as the lower bound of MIZ, being the demarcation where SIC = 0.1. The extra condition of SIT<2.0 m for MIZ_d in Equation (27) generally has a minor effect on the SIE. As can be seen from Figure 7, when using the same data sources, there are no noticeable differences in the SIE between the MIZ_t and MIZ_d.

There are significant differences in the MIZ_t and MIZ_d. The most prominent difference is the very close drift ice in the Barents Sea, which was identified as dense pack ice in the MIZ_t (Figures 7A–C), but as MIZ in the MIZ_d (Figures 7D–F). Such difference also occurs in the Kara Sea and Greenland Sea. The SIT in these areas are generally less than 0.8 m (Figure 5E). This indicates that either lower SIC or low SIT can contribute to the MIZ_d.

Different data sources have a strong impact on the determination of MIZ. This can be clearly seen in the three traditional MIZ_t (Figures 7A–C). As mentioned in section 4.1, a large patch of very open drift ice in the ice chart north of Svalbard and Franz Josef Land (Figure 7B) was identified as open water in the AMSR2 MIZ_t (Figure 7A). By contrast, some fine features identified by the AMSR2 SIC were missing in the ice chart (cf. Figures 7A, B). Similar to the merging of SIC (Figure 4), the merged MIZ_t also includes the very open drift ice identified in the NIS ice chart and the fine features identified in the AMSR2 SIC. It remains to be further discussed whether such fine features should be included in the MIZ_t.

The MIZ_d is seen very sensitive to the SIC. A large part of the sea ice in the Kara Sea is identified as dense pack ice according to the

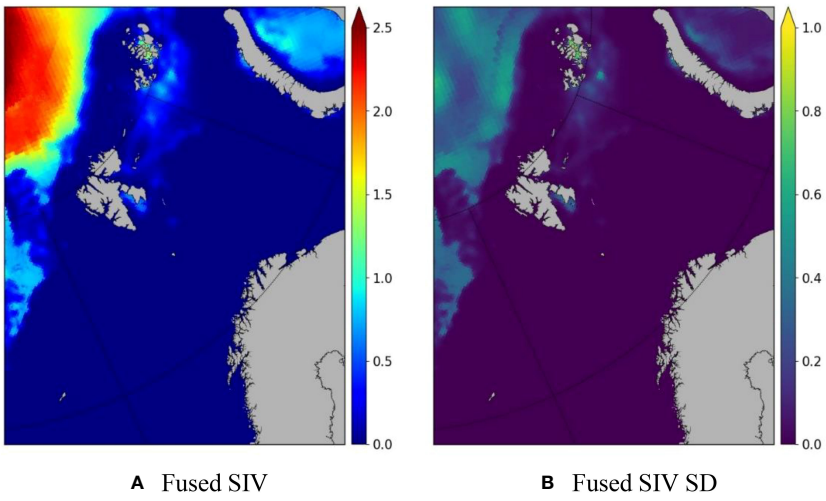

FIGURE 6
Fused SIV (**A**) and its SD (**B**) per m^2 on 16/03/2022. The units are meters for both SIV and its SD.

AMSR2 SIC (Figure 7D), whereas the ice in the whole Kara Sea is classified as MIZ according to the ice chart (Figure 7E), both using the fused SIT (Figure 5F). Since we use the same SIT for determining the MIZ_d, the differences are mainly caused by the difference in the SIC. The SIC in the ice chart is 0.95, whereas the SIC in the AMSR2 is very close to 1 for the dense pack ice region. Similar results occur in the Greenland Sea, where some small patches of the very close sea ice are identified as dense pack ice (Figures 7D, F), whereas it is almost all identified as MIZ when using the NIS ice chart (Figure 7E). This indicates that the NIS SIC is generally of coarse resolution in the SIC space and would be insufficient for the accurate determination of the MIZ_d. It is noted that the current MIZ_d is parameterized based on the simulations from one-dimensional wave-ice coupled model (see Equation 27) at

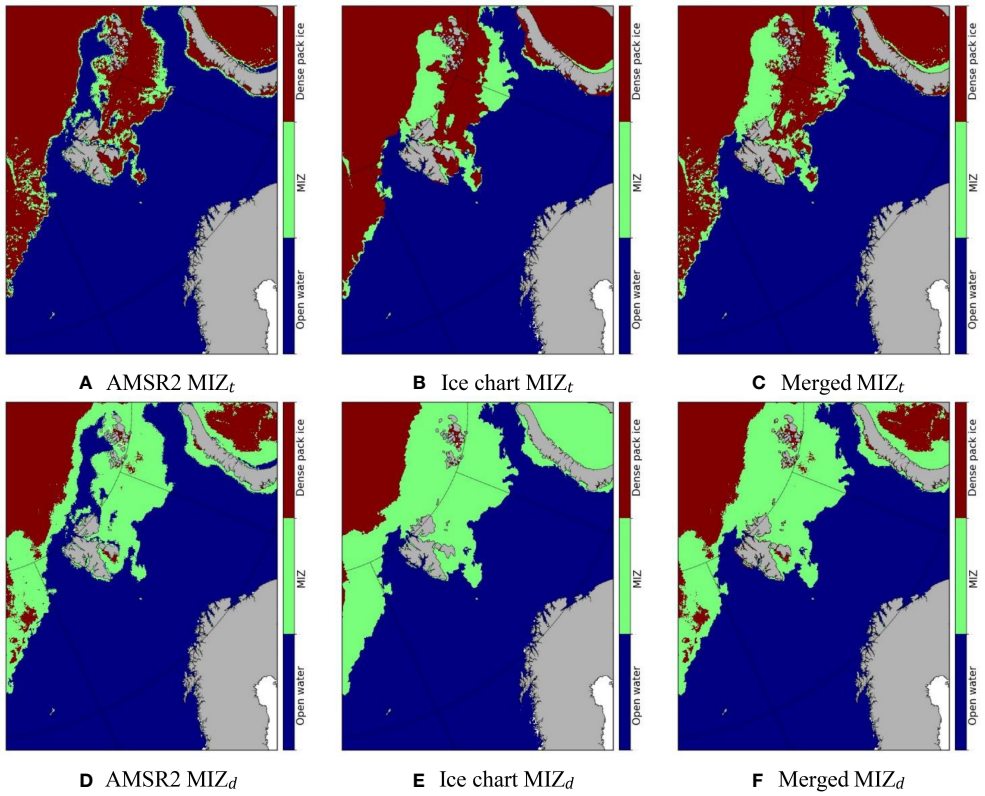

FIGURE 7
MIZ distribution on 16/03/2022: traditional MIZ_t from **(A)** AMSR2, **(B)** NIS ice chart, and **(C)** merged SIC, and dynamical MIZ_d from **(D)** AMSR2, **(E)** NIS ice chart, and **(F)** merged SIC. For the determination of MIZ_d, the fused SIT are used in all the three cases **(D–F)**.

the Fram Strait. Its feasibility and reliability remains to be further verified for the whole Barents-2.5km area.

5 Discussion

5.1 Evaluation

No formal evaluation is performed in this study. This is partly due to the fact that all the data are from observations, which are so far among the best available data for sea ice observations. In such a case, it is very difficult to find better observation data for evaluation, and it is generally of limited values to evaluate the results with lower-quality data (Wang et al., 2023).

Nevertheless, the natural limitations of the observations can help justify the advantage of the MODF, as can be clearly seen from the results. For example, for the MODF of SIC (Figure 4), it is well known that the passive microwave remote sensing products have a general shortcoming when applying for low SIC conditions (e.g., Cavalieri, 1994; Spreen et al., 2008; Kern et al., 2019), whereas the manually analyzed sea ice chart tends to ignore some fine features within the ice pack. Such deficiencies are almost perfectly mitigated in the merged SIC. Compared with the original AMSR2 SIC and NIS ice chart, the merged SIC clearly preserves the fine features in the AMSR2 SIC and the very open drift ice observed in the ice chart (Figure 4).

Similarly, for the MODF of SIT (Figure 5), the SMOS SIT only covers a limited area with very large uncertainties for SIT over 1 m, whereas the weekly CS2SMOS SIT only provides a weekly mean, which is generally not adequate for accurate daily description, particularly for sea ice under rapid movement or thermal growth. In the present case, the weekly CS2SMOS SIT tends to overestimate a patch of daily SIT in the Greenland Sea, which is corrected by merging the SMOS SIT. The SIT is further improved *via* the multivariate consistency check. With the improvements in both SIC and SIT, it is straightforward to know that the fused SIV is improved.

5.2 Observation uncertainties

As shown in Equations (12, 19, and 20), the merged value is strongly dependent on the original observation uncertainties. Therefore, accurate determination of the original observation uncertainties is critical to the final merged and fused results. In this study, the SD of the AMSR2 SIC for the open water is approximately 0.25, which results from three sources (Spreen et al., 2008). Such a high value correctly depicts the large uncertainties of PMRs for low SIC conditions (Cavalieri, 1994; Kern et al., 2019). Similarly, we used a large uncertainty of 0.3 for the very close drift ice in the NIS ice chart to account for the often neglected fine features. On the whole, such high uncertainties provide an important foundation for the successful SIC merging.

One special deficiency is noteworthy in the sea ice satellite remote sensing: the uncertainty is often underestimated. For the SIC merging case mentioned above, we have also tested using low uncertainties for the low AMSR2 SIC and the NIS very close drift ice. In such a case, the resulting merged SIC captures neither the very open drift ice north of Svalbard and Franz Josef Land nor the fine features observed in the AMSR2 SIC. Similar underestimate occurs in the merging of SIT in the Kara Sea, where the weekly CS2SMOS SIT is approximately 0.7 m with an SD below 0.06 m (Figure 5). The resulting merged daily CS2SMOS SIT tends to be closer to the weekly mean rather than the daily SMOS SIT. A further study of the case would be highly desirable.

5.3 Further expansion of the observations

In this study, we have focused on the fusion of SIC, SIT, and SIV for the operational purpose. This is due to the fact that for marine operations such as the sea area around Svalbard, SIC, SIT, SIE, and MIZ are the most important sea ice parameters for safe operations. As can be seen in the analysis, SIE and MIZ can be deduced from the observed SIC and SIT. SIV can also obtained from the combination of SIC and SIT, which is important for sea ice modeling and assimilation, as well as for overall sea ice mass estimate. In general, sea ice velocity, temperature, and age are also important for safe operations but considered as secondary. In particular, initial sea ice velocity would soon lose its inertia in several hours. Therefore, accurate prediction of sea ice velocity would strongly rely on the initial SIC and SIT, as well as the model quality rather than its initial velocity. Nevertheless, these parameters can be included if they are necessary.

Accurate and consistent description of sea ice is an important part of climate studies. A comprehensive set of sea ice variables, such as SIC, SIT, SIV, sea ice drift, sea ice age, melt pond fraction, and sea ice surface albedo, would be valuable for climate analysis, simulation, evaluation, and prediction. There are emerging discussions on such needs (e.g., Lavergne et al., 2022; Sandven et al., 2023). The present framework can be naturally expanded with more variables, longer time scale, and larger spatial coverage, thus generating united, consistent, and multifaceted climate data sets.

6 Conclusions

Sea ice is one of the most severe threats to the marine operations around Svalbard. With the continuous increasing of marine activities around Svalbard, monitoring and prediction of sea ice is urgently needed for safe and sustainable development. In this study, we introduced a new MDF method, MODF, and applied it to fuse the operational sea ice observations around Svalbard, with the focus on the SIC and SIT. The results will be further used in the operational Barents-2.5-km model (Duarte et al., 2022; Röhrs et al., 2023) at the Norwegian Meteorological Institute.

The overall MODF method includes regridding, univariate MODM, multivariate consistency check, and generation of new variables. Individual SIC or SIT operational products have their own spatial and temporal coverages and resolutions, which are often different from the concerned applications. Regridding (upgridding or downgridding) is therefore needed to remap such products to the desired coverage and resolution. In this study, we have used a simple nearest neighbor interpolation method for both upgridding and downgridding. While the uncertainty would be theoretically altered during the regridding, it is only considered during the temporal upgridding of the weekly CS2SMOS SIT in this study. Further studies are desirable to investigate the exact regridding effect on the uncertainties.

The univariate MODM is here used to merge multisensor observations of the same variable following Wang et al. (2020). The advantage of the MODM is to extract the most confident parts of the observations to form a refined variable. In this study, the NIS ice chart has a higher capability to accurately depict the low SIC area, whereas the AMSR2 SIC has the advantage to describe the SIC more continuously and accurately away from the low SIC area. Similarly, the weekly CS2SMOS SIT has low uncertainty for thick sea ice, whereas SMOS SIT has low uncertainty for thin sea ice. Merging of SMOS SIT and weekly CS2SMOS SIT thus provides a refined daily SIT observation for both thin and thick sea ice. The univariate MODM therefore provides a very efficient method to combine different sensors for observing the same sea ice variable.

The multivariate MODF is an extension of the univariate MODM, from single variable to multiple variables. For each variable, the univariate MODM is firstly applied to form a refined variable. A further combination of the multiple variables is performed during the multivariate MODF *via* consistency checks. Such consistency checks can supplement extra information for the observations (Figure 5). In addition, new variables such as SIV, SIE, and MIZ can be generated, which provide extra insight into the sea ice observations.

The present study provides a fundamental framework for managing multivariate multisensor observations. The main focus here has been on the data fusion of operational sea ice observations (SIC, SIT, SIV, and their uncertainties), which are the most important for operational sea ice monitoring and predictions. It is straightforward to extend the present data sets to include more variables for climate studies, such as sea ice age, sea ice drift, melt pond fraction, and snow depth (Lavergne et al., 2022; Sandven et al., 2023). The MODF is also applicable for other environmental observations in order to form a consistent, multifaceted, and more robust and accurate description.

Data availability statement

The AMSR2 SIC is available at https://seaice.uni-bremen.de/data/amsr2/. The NIS ice chart is available at https://doi.org/10.48670/moi-00128. The SMOS SIT and the weekly mean CS2SMOS SIT are available at ftp://smos-diss.eo.esa.int/SMOS/. The corresponding data regridded on the Barents-2.5-km grid and their merged and fused data are available at https://doi.org/10.5281/zenodo.10726427.

Author contributions

KW: Conceptualization, Formal analysis, Funding acquisition, Investigation, Methodology, Project administration, Software, Validation, Visualization, Writing – original draft, Writing – review & editing. CW: Formal analysis, Funding acquisition, Investigation, Writing – review & editing. FD: Writing – review & editing, Data curation, Investigation. GS: Data curation, Investigation, Writing – review & editing. RR: Data curation, Investigation, Writing – review & editing. XT-K: Data curation, Investigation, Writing – review & editing.

Funding

The author(s) declare financial support was received for the research, authorship, and/or publication of this article. This study was supported by the Norwegian FRAM Flagship program project SUDARCO (grant No. 551323), the Nordic Council of Ministers project NOCOS DT (grant no. 102642), and the Norwegian Research Council project 4SICE (grant no. 328886).

Conflict of interest

The authors declare that the research was conducted in the absence of any commercial or financial relationships that could be construed as a potential conflict of interest.

Publisher's note

References

AMAP (2017). *Adaptation Actions for a Changing Arctic (AACA) - Barents Area Overview report, Arctic Monitoring and Assessment Programme (AMAP)* (Oslo, Norway: AMAP), pp. 24. https://www.amap.no/documents/doc/adaptation-actions-for-a-changing-arctic-aaca-barents-area-overview-report/1529

Arrigo, K. R. (2014). Sea ice ecosystems. *Annu. Rev. Mar. Sci.* 6, 439–467. doi: 10.1146/annurev-marine-010213-135103

Barber, D., Hop, H., Mundy, C., B., E., Dmitrenko, I., Tremblay, J., et al. (2015). Selected physical, biological and biogeochemical implications of a rapidly changing arctic marginal ice zone. *Prog. Oceanogr.* 139, 122–150. doi: 10.1016/j.pocean.2015.09.003

Bennetts, L., Bitz, C., Feltham, D. L., Kohout, A. L., and Meylan, M. H. (2022). Theory, modelling and observations ofmarginal ice zone dynamics: multidisciplinary perspectives and outlooks. *Phil.Trans.R.Soc* 380, 20210265. doi: 10.1098/rsta.2021.0265

Cavalieri, D. J. (1994). A microwave technique for mapping thin sea ice. *J. Geophys. Res.* 99, 12561–12572. doi: 10.1029/94JC00707

Dinessen, F., and Hackett, B. (2018). *Product user manual for regional high resolution sea ice charts Svalbard region* (Ramonville-Saint-Agne, France: EU Copernicus Marine Service), pp. 16. Available at: http://marine.copernicus.eu/documents/PUM/CMEMS-OSI-PUM-011-002.pdf

Duarte, P., Brændshøi, J., Shcherbin, D., Barras, P., Albretsen, J., Gusdal, Y., et al. (2022). Implementation and evaluation of open boundary conditions for sea ice in a regional coupled ocean (roms) and sea ice (cice) modeling system. *Geosci. Model. Dev.* 15, 4373–4392. doi: 10.5194/gmd-15-4373-2022

Dumont, D. (2022). Marginal ice zone dynamics: history, definitions and research perspectives. *Phil. Trans. R. Soc A* 380, 20210253. doi: 10.1098/rsta.2021.0253

Dumont, D., Kohout, A., and Bertino, L. (2011). A wave-based model for the marginal ice zone including a floe breaking parameterization. *J. Geophys. Res.-Oceans* 116, C04001. doi: 10.1029/2010JC006682

ESA (2023a). *SMOS L3 sea ice thickness, version 3.3*. doi: 10.57780/sm1-5ebe10b

ESA (2023b). *SMOS-CryoSat L4 sea ice thickness, version 206*. doi: 10.57780/sm1-4f787c3

Ferster, B. S., Simon, A., Fedorov, A., Mignot, J., and Guilyardi, E. (2022). Slowdown and recovery of the atlantic meridional overturning circulation and a persistent north atlantic warming hole induced by arctic sea ice decline. *Geophys. Res. Lett.* 49, e2022GL097967. doi: 10.1029/2022GL097967

Fritzner, S., Graversen, R., Wang, K., and Christensen, K. (2018). Comparison between a multi-variate nudging method and the ensemble kalman filter for sea-ice data assimilation. *J. Glaciol.* 64, 387–396. doi: 10.1017/jog.2018.33

Goodman, L. (1960). On the exact variance of products. *J. Amer. Stat. Ass.* 55, 708–713. doi: 10.2307/2281592

Hendricks, S., and Paul, S. (2023). Product user guide algorithm specification - awi cryosat-2 sea ice thickness (version 2.6) issued by (v2.6). Zenodo. doi: 10.5281/zenodo.10044554

Hunke, E., Lipscomb, W., Turner, A., Jeffery, N., and Elliott, S. (2015). *CICE: the Los Alamos Sea Ice Model Documentation and Software User's Manual, Version 5.1*. Los Alamos, USA: Los Alamos National Laboratory.

Johannessen, J. A., Johannessen, O. M., Svendsen, E., Shuchman, R., Manley, T., Campbell, W. J., et al. (1987). Mesoscale eddies in the fram strait marginal ice zone during the 1983 and 1984 marginal ice zone experiments. *J. Geophys. Res.-Oceans* 92, 6754–6772. doi: 10.1029/JC092iC07p06754

Kern, S., Lavergne, T., Notz, D., Pedersen, L., Tonboe, R., Saldo, R., et al. (2019). Satellite passive microwave sea-ice concentration data set intercomparison: closed ice and ship-based observations. *Cryosphere* 13, 3261–3307. doi: 10.5194/tc-13-3261-2019

Khachatrian, E., Dierking, W., Chlaily, S., Eltoft, T., Dinessen, F., Hughes, N., et al. (2023). Sar and passive microwave fusion scheme: A test case on sentinel-1/amsr-2 for sea ice classification. *Geophys. Res. Lett.* 50, e2022GL102083. doi: 10.1029/2022GL102083

Khaleghi, B., Khamis, A., Karray, F., and Razavi, S. (2013). Multisensor data fusion: A review of the state-of-the-art. *Inf. Fusion* 14, 28–44. doi: 10.1016/j.inffus.2011.08.001

Lavergne, T., Kern, S., Aaboe, S., Derby, L., Dybkjaer, G., Garric, G., et al. (2022). A new structure for the sea ice essential climate variables of the global climate observating system. *BAMS* 103, E1502–E1521. doi: 10.1175/BAMS-D-21-0227.1

Lavergne, T., Sørensen, A. M., Kern, S., Tonboe, R., Notz, D., Aaboe, S., et al. (2019). Version 2 of the eu-metsat osi saf and esa cci sea-ice concentration climate data records. *Cryosphere* 13, 49–78. doi: 10.5194/tc-13-49-2019

Liu, J., Scott, K. A., and Fieguth, P. W. (2019a). Detection of marginal ice zone in synthetic aperture radar imagery using curvelet-based features: a case study on the canadian east coast. *J. Appl. Remote Sens.* 13, 1–14. doi: 10.1117/1.JRS.13.014505

Liu, W., Fedorov, A. V., and Sevellec, F. (2019b). The mechanisms of the atlantic meridional overturning circulation slowdown induced by arctic sea ice decline. *J. Clim.* 32, 977–996. doi: 10.1175/JCLI-D-18-0231.1

Ludwig, V., Spreen, G., and Pedersen, L. (2020). Evalution of a new merged sea-ice concentration dataset at 1 km resolution from thermal infrared and passive microwave satellite data in the arctic. *Remote Sens.* 12, 3183. doi: 10.3390/rs12193183

Melsheimer, C. (2019). *ASI version 5 sea ice concentration user guide, version v0.92* (Bremen, Germany: Unversity of Bremen). Available at: https://data.seaice.uni-bremen.de/amsr2/ASIuserguide.pdf

Müller, M., Knol-Kauffman, M., Jeuring, J., and Palerme, C. (2023). Arctic shipping trends during hazardous weather and sea-ice conditions and the polar code's effectiveness. *NPJ Ocean Sustain.* 2, 12. doi: 10.1038/s44183-023-00021-x

Olsen, J., Hovelsrud, G., and Kaltenborn, (2020). "Increasing shipping in the arctic and local communities' engagement: A case from longyearbyen on svalbard," in *Arctic Marine Sustainability*. Eds. E. Pongrácz, V. Pavlov and N. Hänninen (Cham: Springer), 305–331. doi: 10.1007/978-3-030-28404-6_14

Palma, D., Varnajot, A., Dalen, K., Basaran, I. K., Brunette, C., Bystrowska, M., et al. (2019). Cruising the marginal ice zone: climate change and arctic tourism. *Polar Geogr.* doi: 10.1080/1088937X.2019.1648585

Perovich, D. K., Grenfell, T. C., Light, B., and Hobbs, P. (2002). Seasonal evolution of the albedo of multiyear arctic sea ice. *J. Geophys. Res.* 107, 8044. doi: 10.1029/2000JC000438

Pletzer, A., and Fillmore, D. (2015). Conservative interpolation of edge and face data on n dimensional structured grids using differential forms. *J. Comp. Phys.* 302, 21–40. doi: 10.1016/j.jcp.2015.08.029

Ricker, R., Hendricks, S., Kaleschke, L., Tian-Kunze, X., King, J., and Haas, C. (2017). A weekly arctic sea-ice thickness data record from merged cryosat-2 and smos satellite data. *Cryosphere* 11, 1607–1623. doi: 10.5194/tc-11-1607-2017

Røed, L. P., and O'Brien, (1983). A coupled ice-ocean model of upwelling in the marginal ice zone. *J. Geophys. Res.* 88, 2863–2872. doi: 10.1029/JC088iC05p02863

Röhrs, J., Gusdal, Y., Rikardsen, E., Duran Moro, M., Brændshøi, J., Kristensen, N. M., et al. (2023). Barents-2.5km v2.0: An operational data-assimilative coupled ocean and sea ice ensemble prediction model for the barents sea and svalbard. *Geosci. Model. Dev.* 16, 5401–5426. doi: 10.5194/gmd-16-5401-2023

Rostosky, P., and Spreen, G. (2023). Relevance of warm air intrusions for Arctic satellite sea ice concentration time series. *Cryosphere* 17, 3867–3881. doi: 10.5194/tc-17-3867-2023

Rückert, J. E., Rostosky, P., Huntemann, M., Clemens-Sewall, D., Ebell, K., Kaleschke, L., et al. (2023). Sea ice concentration satellite retrievals influenced by surface changes due to warm air intrusions: A case study from the MOSAiC expedition. *Elem. Sci. Anth.* 11, 1. doi: 10.1525/elementa.2023.00039

Sandven, S., Spreen, G., Heygster, G., Girard-Ardhuin, F., Farrell, S., Dierking, W., et al. (2023). Sea ice remote sensing–recent developments in methods and climate data sets. *Surveys Geophys.* 44, 1653–1689. doi: 10.1007/s10712-023-09781-0

Spreen, G., Kaleschke, L., and Heygster, G. (2008). Sea ice remote sensing using amsr-e 89-ghz channels. *J. Geophys. Res. Oceans* 113, C02S03. doi: 10.1029/2005jc003384

Steiner, N. S., Bowman, J., Campbell, K., Chierici, M., Eronen-Rasimus, E., Falardeau, M., et al. (2021). Climate change impacts on sea-ice ecosystems and associated ecosystem services. *Elementa* 9, 7. doi: 10.1525/elementa.2021.00007

Stocker, A., Renner, A., and Knol-Kauffman, M. (2020). Sea ice variability and maritime activity around svalbard in the period 2012–2019. *Sci. Rep.* 10, 17043. doi: 10.1038/s41598-020-74064-2

Strong, C. (2012). Atmospheric influence on arctic marginal ice zone position and width in the atlantic sector, february–april 1979–2010. *Clim. Dyn.* 39, 3091–3102. doi: 10.1007/s00382-012-1356-6

Tian-Kunze, X., Kaleschke, L., Maaß, N., Mäkynen, M., Serra, N., Drusch, M., et al. (2014). Smos-derived thin sea ice thickness: algorithm baseline, product specifications and initial verification. *Cryosphere* 8, 997–1018. doi: 10.5194/tc-8-997-2014

Todling, R. (1999). "Estimation theory and foundations of atmospheric data assimilation," in *Office Note Series on Global Mo deling and Data Assimilation*, vol.). Ed. R. Atlas (DAO office Note 1999-01, Maryland, USA: NASA), 1–25.

Tonboe, R. T., Eastwood, S., Lavergne, T., Sørensen, A. M., Rathmann, N., Dybkjær, G., et al. (2017). The EUMETSAT sea ice concentration climate data record. *The Cryosphere* 10, 2275–2290. doi: 10.5194/tc-10-2275-2016, 2016

Wadhams, P. (1986). The Seasonal Ice zone. In: Untersteiner, N. (eds). *The geophysics of sea Ice. NATO ASI Series*. Boston, MA: Springer. doi: 10.1007/978-1-4899-5352-0_15

Wang, K., Ali, A., and Wang, C. (2023). Local analytical optimal nudging for assimilating amsr2 sea ice concentration in a high-resolution pan-arctic coupled ocean (hycom 2.2.98) and sea ice (cice 5.1.2) model. *Cryosphere* 17, 4487–4510. doi: 10.5194/tc-17-4487-2023

Wang, K., Lavergne, T., and Dinessen, F. (2020). Multisensor data merging of sea ice concentration and thickness. *Adv. Polar Sci.* 31, 1–13. doi: 10.3189/2013aog62a138

Wassmann, P. (2011). Arctic marine ecosystems in an era of rapid climate change. *Prog. Oceanography* 90, 1–17. doi: 10.1016/j.pocean.2011.02.002

WMO (2014). SEA ICE NOMENCLATURE. *No. 259* (Geneva: WMO).

frontiers | Frontiers in Marine Science

TYPE Review
PUBLISHED 24 July 2024
DOI 10.3389/fmars.2024.1339610

OPEN ACCESS

EDITED BY
Ed Blockley,
Met Office, United Kingdom

REVIEWED BY
Till Andreas Soya Rasmussen,
Danish Meteorological Institute (DMI), Denmark
Meijie Liu,
Qingdao University, China

*CORRESPONDENCE
Jürgen Holfort
juergen.holfort@bsh.de

RECEIVED 16 November 2023
ACCEPTED 31 May 2024
PUBLISHED 24 July 2024

CITATION
Aldenhoff W and Holfort J (2024) Information on operational sea ice products and current and future activities of the German ice service. *Front. Mar. Sci.* 11:1339610. doi: 10.3389/fmars.2024.1339610

Information on operational sea ice products and current and future activities of the German ice service

Wiebke Aldenhoff and Jürgen Holfort*

Abteilung für Meereskunde, Referat Eisdienst und Wasserstandsdienst Ostsee, Bundesamt für Seeschifffahrt und Hydrographie, Rostock, Germany

The ice service at the German Federal Maritime and Hydrographic Agency and its predecessors has been committed to the safety and easiness of ship navigation for more than 100 years. Within this paper, an overview of the operational products issued by the German ice service on a daily to weekly basis throughout the northern hemisphere winter season is given. These comprise written reports, ice charts, NAVTEX messages, and messages via the Global Telecommunication System to inform about the sea ice situation in German coastal waters, the Baltic Sea, and worldwide. Furthermore, the ice service has systematically collected ice observation data along the German North Sea and Baltic Sea coast since the winter of 1896/1897. The history of the German ice service is presented to put the sea ice data into context of the observation technologies used in the course of the existence of the ice service. These long-term observations enable climatological analyses of the sea ice cover in German coastal waters necessary for the safe operation of offshore infrastructure. An evaluation of the data shows a recent decline in sea ice occurrence in the Baltic Sea and German Bight. Current work is ongoing to preserve more of the historic data in digital form and also to transform the products to conform to modern standards in digital technologies and interactive solutions for the customers.

KEYWORDS

ice service, ice charts, sea ice, Baltic Sea, North Sea

1 Introduction

For more than a hundred years, the German ice service has been committed to the safety and ease of shipping in German coastal waters and ice-infested waters worldwide. The ice service started its regular ice observation and ice information service in the winter of 1896/1897 as part of the “Deutsche Seewarte”. Ice observing stations along the coast sent daily ice information in coded form by telegraph that were published as part of the marine weather report. In the 1920s, international cooperation intensified between countries bordering the Baltic Sea and resulted in the first standardized sea ice code used for sea

ice observations. In 1928/1929, the publication of the "Eisbericht", the first stand-alone ice report, started. Until today, this is the main written publication of sea ice information in the Baltic Sea and German Bight published by the German ice service. The creation of ice charts started in the winter of 1927/1928. From the end of World War II until the German reunification, independent ice services existed in the Federal Republic of Germany and the German Democratic Republic, each taking responsibility for their respective sea areas. Since the reunification in 1990, the German ice service is part of the Federal Maritime and Hydrographic Agency [Bundesamt für Seeschifffahrt und Hydrographie (BSH)] and today is located in Rostock. The operation of the ice service is legally delegated to the BSH by the Federal Maritime Responsibilities Act (§1 paragraph 9c and §5 paragraph 1). The main task of the ice service is the delivery of sea ice information along the German North Sea and Baltic Sea coasts as well as the Baltic Sea to mariners and the public. To fulfill its duties, the ice service publishes several different operational ice products, i.e., written ice reports, ice charts, and NAVTEX or Global Telecommunication System (GTS) (WMO, 2015) messages, throughout the ice season, usually from about October to June.

In the early years of the ice service, manual ice observations at the different ice stations were the primary source of information. Sea ice information outside coastal areas were only accessible as long as ship traffic was possible. With advances in aeronautics, air reconnaissance started to be a valuable source of information after World War I. Space-borne optical imagery became available in the course of the 1960s (Strübing, 1970). Cloud cover and lack of solar illumination in higher latitudes, however, limited the use of such imagery for ice observations. Passive microwave radiometry overcame these limitations and has been the main source for systematical monitoring of the world's sea ice cover since 1979. Microwave radiation is almost unaffected by the atmosphere and independent of solar illumination, thus delivering year-round information. The relative coarse resolution, however, limits the use for navigation in ice-infested waters and general observations of sea ice in coastal waters. Synthetic aperture radar (SAR) imagery starting operationally with ERS-1 in 1991 took available sea ice information to the next level. Nowadays, especially with the freely available data from the Copernicus Sentinel Program and a number of commercial and state-owned SAR-carrying satellites, SAR imagery is the prime information source not only for the German ice service but also for ice services around the world. Furthermore, optical remote sensing data is a great asset of high-resolution information if the cloud cover is not too dense. Manual ice observations are, however, still a valuable source of information in coastal areas and harbors and maintain the long-time series of station observations. At present, the availability of remote sensing data is rapidly increasing in space and time. This challenges the ice services to convey the latest available information to the customers. This is of great importance as sea ice is constantly changing and up-to-date, and timely information are therefore necessary to ensure safe navigation.

Sea ice is also an import indicator of climate change (Garcia-Soto et al., 2021). The interannual variability of sea ice occurrence in German waters requires a long time series to separate climate and weather effects. More-than-a-century-long history of sea ice observations provide a valuable data source to evaluate recent changes in the sea ice cover along the German coasts and the Baltic Sea. Parts of the historical sea ice data and ice charts are already digitized and available in a database for public access (https://login.bsh.de/fachverfahren/?lang=en). Nevertheless, there is still a large amount of data hidden in archives especially for the beginning of the 20th century. Furthermore, there is an increased interest in ice climatological data in the German exclusive economic zone for the installation of offshore infrastructure, e.g., wind turbines. Permission for the installation requires the consideration of sea ice impact on the structure. Therefore, it is necessary to make statistical information about sea ice coverage in German waters available to the customers.

The following sections give a detailed overview of the current operational and non-operational sea ice products as well as historical sea ice data available at the BSH. Furthermore, a summary of changes in the sea ice cover in German coastal waters is presented. The paper concludes with an outlook onto challenges the ice service is currently facing as well as the planned activities in the near future.

2 Products, publications, and data

2.1 Operational sea ice products

The German ice service produces several operational products to inform about sea ice conditions in German waters, the Baltic Sea, German Bight, and worldwide. An overview of the operational ice products and data, their publishing language, publication frequency, and data availability is shown in Table 1.

Underlying ice information are obtained from a variety of different sources including remote sensing data, ice observers, meteorological data, and reports of other ice services around the world. Nowadays, the main information source especially outside coastal areas is remote sensing data from optical, microwave, and infrared sensors. Since the start of the Copernicus Program in 2014, the availability of timely and high-resolution data has greatly increased and improved the quality of sea ice products. In coastal areas and harbors, ice observers are, however, still an invaluable source of information. Therefore, a network of around 120 ice observing stations is maintained along the German coasts. The network and some historic ice stations are shown in Figure 1. These stations are operated by volunteers, often with a maritime background, or by administrative assistants from harbors or vessel traffic service centers. The advantages of ice observers are information about the beginning of ice formation, timeliness, and the possibility of thickness measurements, which are difficult to obtain from remote sensing data. The ice observers report ice conditions daily according to the Baltic Sea Ice Code, a four-digit code where each digit provides encoded information about ice coverage, stage of development, form of the ice, and navigation conditions, respectively (Koslowski, 1981). Additionally, ice thickness may be measured and other relevant observations, e.g., leads in the ice or accumulation of ice at shallows, can be reported. The information are checked for plausibility on reception, and an additional quality control is carried

TABLE 1 Overview of operational ice products, their publishing language, publication frequency, and data availability.

Operational products	Language	Frequency	Availability since	
			Analog	Digital
Amtsblatt - Ice Report Baltic Sea	English (older publications German or German/English)	Weekdays	1928/29	2004/05
Ostseebericht (Baltic Sea report)	German	Weekdays		2005/06
Nordseebericht (North Sea report)	German	Weekdays		2010/11
Wochenbericht (weekly report)	German	Weekly		2003/04
Ice winter report	German and English	Yearly	uncertain	2004/05
Ice chart Baltic Sea	English (older publications German or German/English)	Weekly[a]	1927/28	1960/61 (gridded) 2005/06 (polygons)
Regional ice chart Western Baltic and North Sea	English (older publications German or German/English)	Daily[b]	Uncertain	1960/61 (polygons, digitized) 2004/05 (polygons)
Regional Ice Chart German Baltic Sea	English (older publications German or German/English)	Daily[b]	Uncertain	1956/57 (gridded) 2004/05 (polygons)
German ice report	English	Daily[b]	Uncertain	2004/05
Navtex German Bight	German and English	Daily[b]	No archive	
Navtex German Baltic Sea	German and English	Daily[b]	No archive	
Observation data				
Ice observing stations	Baltic Sea Ice Code (older observations ice code used at that time)	Daily	~ 1896/97	1939/40 for daily data of many stations

[a]Day of best data coverage.
[b]Ice occurrence in the respective sea area.

FIGURE 1
Ice observing stations in the North Sea and Baltic Sea (image courtesy: T. Moltmann).

out at the end of the season. The history of official ice observations dates back to the winter of 1896/1897.

Remote sensing data from optical, microwave, and infrared sensors are the prime information source for larger-scale information. Optical images provide high-resolution information that is easy to assess for humans but suffer from cloud cover and require solar illumination. Sources include Copernicus Sentinel-2 and Sentinel-3, MODIS from Aqua and Terra and Landsat-8/9. Lower-resolution optical data is obtained from MetOP satellites. SAR imagery provides high-resolution information independent from weather and solar illumination. Sentinel-1 is the main source for this kind of data, but other providers are used if data is available to the ice service.

The operational ice products are discussed in more detail in the following subsections. The products target different customers and therefore vary in detail and language. All products are available in digital form from the official website (www.bsh.de/ice), free of charge.

2.1.1 Ice report (Eisbericht, Amtsblatt des Bundesamtes für Seeschifffahrt und Hydrographie)

The main product throughout the winter season in the Baltic Sea and German Bight is the ice report (Eisbericht, Amtsblatt des Bundesamtes für Seeschifffahrt und Hydrographie) (BSH, 1928). The report informs in text form about the current ice conditions in the Baltic Sea and the German Bight. It was first published in the winter of 1928/1929. The report is divided into sections corresponding to sea areas with ice occurrence. Each section consists of a brief description of sea ice conditions and a short outlook of the expected development of the ice conditions in the next 24 h or 72 h on weekdays and Fridays, respectively. Furthermore, the ice report contains information about current and upcoming traffic restrictions as well as icebreaker activity published by national ice services. The report is concluded by a list of international ice observing stations and the respective observations coded by the four digit Baltic Sea Ice Code. The report is issued on weekdays and is written in English to reach a broader range of customers. Publication starts with the first persistent ice in the Baltic Sea and ends when the last ice has vanished or the last restrictions are retracted and only ice remnants are present.

2.1.2 Ice charts

There are three types of ice charts regularly published by the German ice service: an overview ice chart of the Baltic Sea, a regional ice chart of the German Baltic Sea, and a regional ice chart of the western Baltic and North Sea. Generally, each ice chart consist of two pages: the first shows sea ice concentration and the second sea ice stage of development. The ice charts follow the WMO Ice Chart Colour Code Standard (WMO, 2004). Color codes for rotten fast ice and hatching for different new ice concentrations are added to better reflect the ice conditions in the Baltic Sea. Furthermore, the ice charts contain contour lines of modeled sea surface temperature and meteorological information from coastal stations. All ice charts are, at present, manually drawn by an ice analyst using the geographic information system software QGIS (QGIS.org, 2022). The ice analyst draws polygons of similar ice types and assigns the ice concentration and ice thickness as the main parameters. Furthermore, information about the melt status, e.g., rotten ice, as well as point symbols for features like ridged ice areas, leads too small to outline, or brash ice barriers can be added. The decisions are mostly based on information from remote sensing imagery as well as auxiliary information from ice observers and other ice services. The ice charts are projected into WGS 84/World Mercator (EPSG:3395). The standard output file format of the published ice charts is PDF, but since the past several years, the charts are also delivered in S-411 format for Electronic Chart Display and Information Systems (ECDIS) (JCOMM, 2014). The original polygonal data is stored as shapefiles as well as in a geographical database for further use, processing, and analysis.

2.1.2.1 Overview ice chart of the Baltic Sea

The overview ice chart of the Baltic covers an area from approximately 53.5° N, 9.5° E to 66° N, 30.2° E. The page with the ice stage of development contains a table with actual restrictions to navigation. Furthermore, active icebreakers are annotated in the ice chart. Figure 2 shows an example of the ice chart from 2022-02-03. The overview ice chart is published weekly on the day with best data coverage. The focus is to produce an ice chart with a high level of detail and as accurate as possible at the time of data acquisition.

2.1.2.2 Regional ice charts of the German Baltic Sea and the western Baltic Sea and North Sea

Regional ice charts of the German Baltic Sea and the western Baltic Sea and North Sea are produced daily in case of ice occurrence as operational ice charts for the German coastal waters. Publication time is around noon, local time. The ice chart of the German Baltic Sea covers an area from approximately 53.5° N, 8° E and 55.8°, N 15°E. Figure 3 shows an example from 2021-02-17. The ice chart for the western Baltic Sea and North Sea covers an area from approximately 53.5° N, 7° E to 60° N, 15° E. Figure 4 presents an example from 2021-02-17.

2.1.3 German ice report and NAVTEX messages

With ice occurrence along the German coasts, mariners are informed daily about sea ice conditions via the GTS and the NAVTEX service. The German ice report with information about the ice conditions in German coastal waters is transmitted via GTS. It contains the Baltic Sea Ice Code of the German fairway stations and a brief description of the ice situation in areas of interest for navigation in English. NAVTEX messages are very brief summaries of the ice conditions in German waters. They are published separately for the German Bight and the Baltic Sea in German and English before 10:30 a.m.

2.1.4 North Sea report (Nordseebericht) and Baltic Sea report (Ostseebericht)

North Sea report (Nordseebericht) and Baltic Sea report (Ostseebericht) are two publications that describe the ice situation along the German coasts. The reports are issued Monday to Friday when ice occurs at the respective coasts and are written in German. They

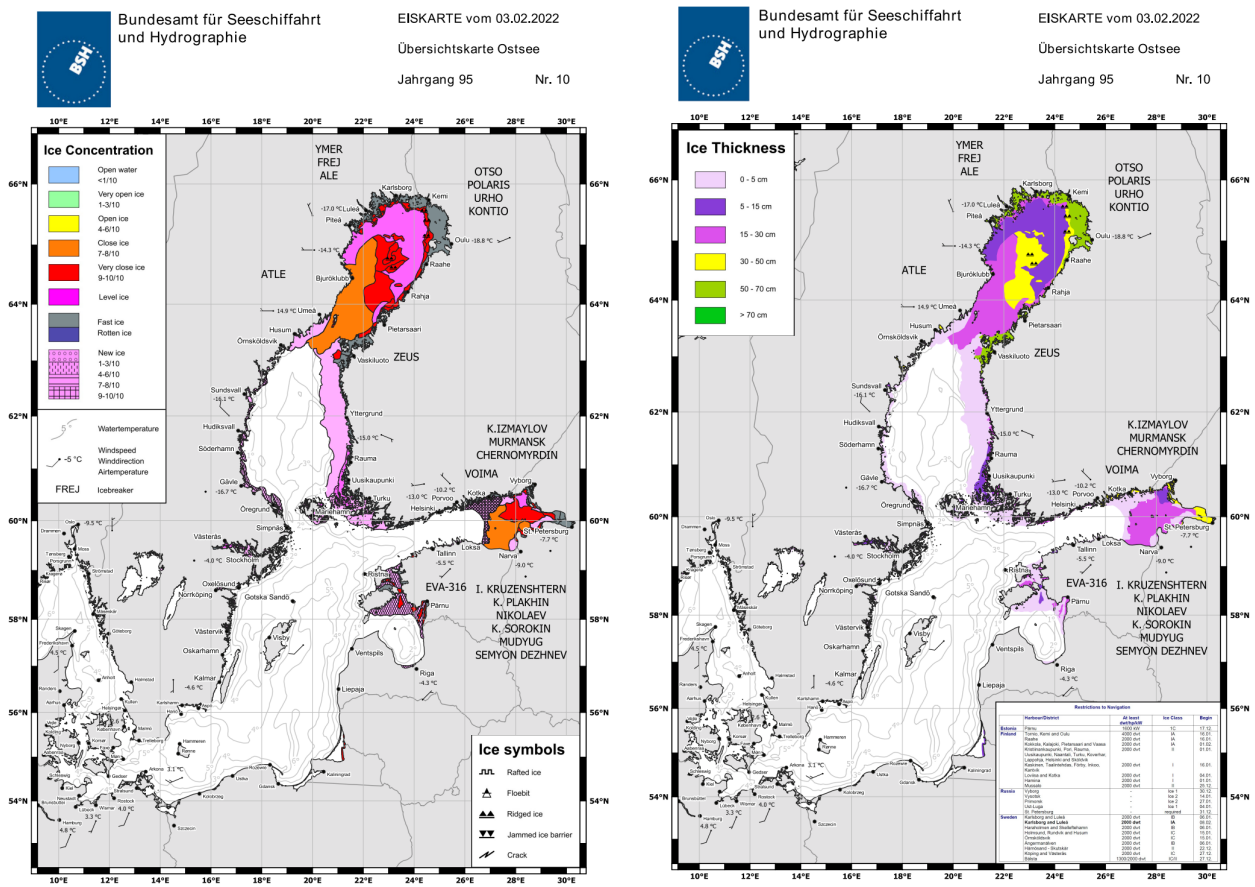

FIGURE 2
Overview ice chart of the Baltic Sea example from 2022-02-03.

contain information about the ice conditions for the main fairways and specific regional areas along the coasts that are more detailed compared to the Eisbericht and German ice report. The reports conclude with an outlook of the expected development of the ice situation. In case of restrictions to navigation in German waters, these are given at the end of the report. Sometimes the report starts with a brief statement of recent changes to the ice situation. The reports are available for download free of charge at the website (www.bsh.de/ice).

2.1.5 Weekly report

The weekly report (Wochenbericht) is a weekly report about the sea ice conditions and ice-related traffic restrictions in the Baltic Sea

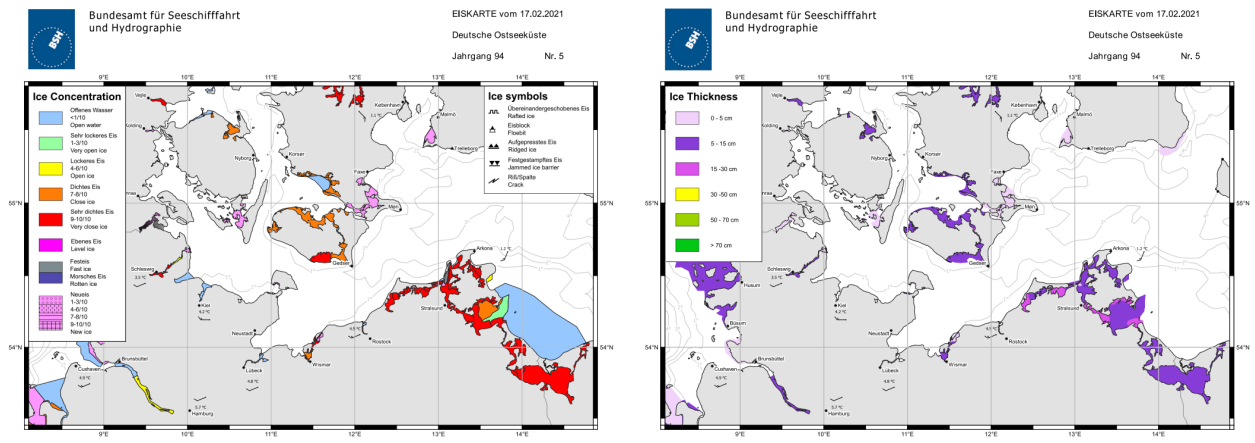

FIGURE 3
Ice chart of the German Baltic Sea example from 2021-02-17.

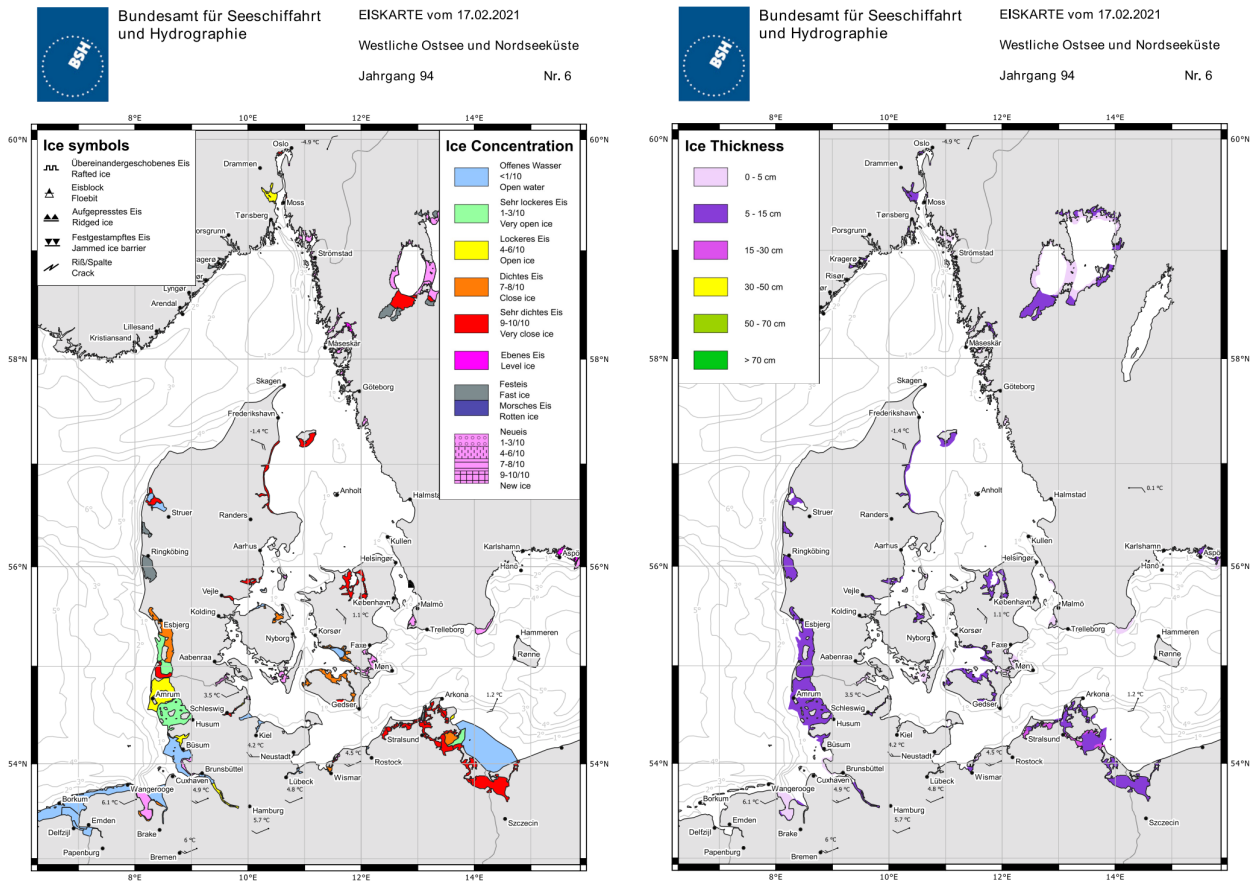

FIGURE 4
Ice chart of the German Bight, Skagerrak and western Baltic Sea example from 2021-02-17.

and German Bight. The weekly report briefly describes the current ice situation in the Baltic Sea and German Bight and gives an overview on current and upcoming navigational restrictions, ice breaker activities, and the expected development of the ice situation in the upcoming week. Since the winter of 2021/2022, it contains a brief section about general ice conditions in the Arctic and Antarctica. For the first time in 2022, this report has been continued through the northern summer months with information about ice conditions in the Arctic and Antarctica with a focus on typical areas for navigation, e.g., northern sea route, North West passage, and the western Antarctic Peninsula. The report is usually published on Mondays throughout the year. The publication language is German.

2.1.6 Ice winter report

The ice winter report summarizes the entire winter season and puts the ice winter into context of the long-term time series of winter observations. This report describes in detail the course of the ice winter along the German coasts as well as the meteorological and hydrographic situation. Furthermore, the bygone ice winter is assessed in the long-term context of previous winters. The central metric used for the German coast is the areal ice volume sum that categorizes the ice winter in weak, mild, severe, very severe, and extremely severe winters (Koslowski, 1989). The areal ice volume sum takes the concentration and thickness of the ice cover into account and is accumulated over the winter. A time series of this measure has been calculated for ice climatological stations in the Baltic Sea since 1879 and in the North Sea since 1897. The ice winter in the entire Baltic Sea is reviewed more briefly. The ice winter severity is assessed by the maximum sea ice extent derived from ice charts, and the time series dates back to 1971. Appended to the report is a graphical representation of the Baltic Sea Ice Code of the German ice observing stations as well as some key statistical parameters for each station. The report is available in German and English and is published after the ice season has ended.

2.2 Non-periodical publications

The ice service regularly contributes its expertise about sea ice to national nautical publications. Two regularly updated publications are the Nordsee-Handbuch (North Sea Handbook) and Ostsee-Handbuch (Baltic Sea Handbook) that provide a wide variety of information of the respective sea areas to mariners (BSH, 2020, 2021). The environmental conditions chapter contains a section about sea ice conditions relevant for navigation. On the one hand, these publications give information about ice formation and melting with respect to typical meteorological and oceanographic conditions and situations. On the other hand, climatological ice

information are provided to ease the planning of shipping operations. These publications are in German.

Two ice atlases covering German waters and adjacent sea areas are available: one for the western and southwestern Baltic Sea (Schmelzer and Holfort, 2012) and one for the German Bight and Limfjord (Schmelzer and Holfort, 2015). These publications aim to give an overview of the geographic and yearly distribution of sea ice and its changes throughout the study period from 1961 to 2010. They comprise information such as the beginning/end of ice occurrence, number of days with ice, length of ice season, frequency of ice occurrence, ice thicknesses, and means of ice concentration as charts of the region and for selected stations. Furthermore, statistical parameters are calculated for 30-year periods (1961–1990, 1971–2000, and 1981–2010) to provide information about changes in sea ice coverage. Currently, work is ongoing to calculate the new climatological period from 1991 to 2020. Findings about changes of the sea ice cover are discussed in detail in Section 3.

2.3 Historical ice data and ice database

The German ice service has systematically collected ice information from ice observing stations along the North Sea and Baltic Sea coast since 1896/1897. The observation area comprises the North Sea coast from Emden in the west to the island Sylt in the north. The Baltic Sea coast was covered from about Flensburg in the north to Klaipeda in the east. The observation area, however, changed slightly with the borders of the German Reich. After World War II until today, the observation stations covered the coastal area of nowadays Germany. Most of the historical data is stored as written originals in the archives of the ice service. The data was usually received daily in coded form by telegraph from the ice observing stations. Additionally, the ice code plus valuable other information, i.e., weather data, ice thickness, and tides, was collected in monthly reports and sent to the ice service. For each winter season, a compilation of the stations' monthly reports plus statistical analysis, about the length of the ice season, days with ice, and restrictions for navigation, exists in the archives. A written report containing these statistical winter summaries was usually published yearly in "Annalen der Hydrographie und Maritimen Meteorologie" from about 1905 to 1944 (Deutsche Seewarte, 1905–1944).

Parts of this historical data have been digitized to make it easily accessible and to facilitate its analysis. Data of stations east of Travemünde prior to the winter of 1939/1940 exists to date only in the analog archive. Winter summaries for stations along the North Sea and in the Baltic Sea from Flensburg to Travemünde have been digitized for the winters since 1901. Daily station data is available in digital format for the stations along the German coast since the winter of 1939/1940. The data is stored in the ice code used at the time of observation. This code changed with time to accommodate for more detailed ice information about the size and thickness of the ice. There exist rules to transform the ice code to comply with the ice objects catalog. Nowadays, the observation data is continuously transferred to an electronic ice database that exists since the early 1980s. Additionally, the Baltic Sea Ice Code of international ice stations is injected regularly in this database as received via GTS.

The historical station data has been used to calculate a time series of ice winter strength using the accumulated areal ice volume for the North Sea coast and the Baltic Sea coast (Koslowski, 1989). A total of 13 ice climatological stations have been used for each coast, respectively. These time series date back to 1879 for the Baltic Sea and to 1897 for the North Sea. This gives a good overview of the changes of the ice winter severity for more than a century. Additionally a time series of ice winter strength of the western Baltic has been created from 1301 to 2001 (Koslowski and Glaser, 1999; Koslowski and Schmelzer, 2007; Schmelzer and Holfort, 2011). Information was derived from historical sources of many kinds that enable conclusions about ice conditions, e.g., ship traffic, transportation over ice, or notes about sea ice cover. The results will be discussed in more detail in the next section.

Besides the ice observations, ice charts have been produced operationally for the North Sea and the Baltic Sea since the winter 1927/1928. In the beginning, ice charts of the Baltic Sea were produced daily. Sea ice information was given in different classes roughly resembling the ice concentration and relevance for navigation. Overview ice charts of the Baltic Sea are produced until today. The periodicity of the publication varied with the years, but usually one to two ice charts per week were produced since the 1950. Since the beginning of the 1980s, the ice charts use the WMO standards for sea ice concentration, which is still in use today (WMO, 2004), and additionally an ice thickness range is given.

The ice charts of the Baltic have been digitized on a 0.5° × 0.5° grid for the years 1957 to 2005 and cover an area north of 56°N. The ice charts of the German coast have been digitized in the course of the production of the ice atlases on a 2′ latitude × 4′ longitude grid that resembles roughly 2 NM by 2 NM. The paper charts for the years 1960-2006 were digitized. The ice charts of the German Bight have been redrawn and stored in shapefiles for all winters since 1960/1961. In the process, ice thickness information was added, and missing or incorrect data has been corrected. All ice charts contain information about concentration, but ice charts prior to the winter of 1981/1982 did not contain any information about ice thickness. Ice charts are readily stored as shapefiles since the winter of 2005/2006, with each polygon containing information about concentration and ice thickness as well as information such as rotten ice.

The ice service is currently working on transferring all the digitized data, including the ice chart information, into a geodatabase that will be accessible for the public. The database will contain daily station data, ice charts, restrictions to navigation (data included only for recent years), and winter summaries/simple statistics for the German stations.

3 Changes of sea ice occurrence in German coastal waters

Figures 5 and 6 show the time series of the areal ice volume sum from 13 ice observing stations along the North Sea and Baltic Sea coast, respectively. The black lines in the figure denote the boundaries for weak, moderate, severe, very severe, and extremely severe ice winters. The figures show not only a large interannual variability of the ice winter strength at the German coasts but also that ice winter strength at the different coasts correlate well with each other. However, the ice winters along the North Sea coast are generally milder than at the Baltic Sea due to the influence of the

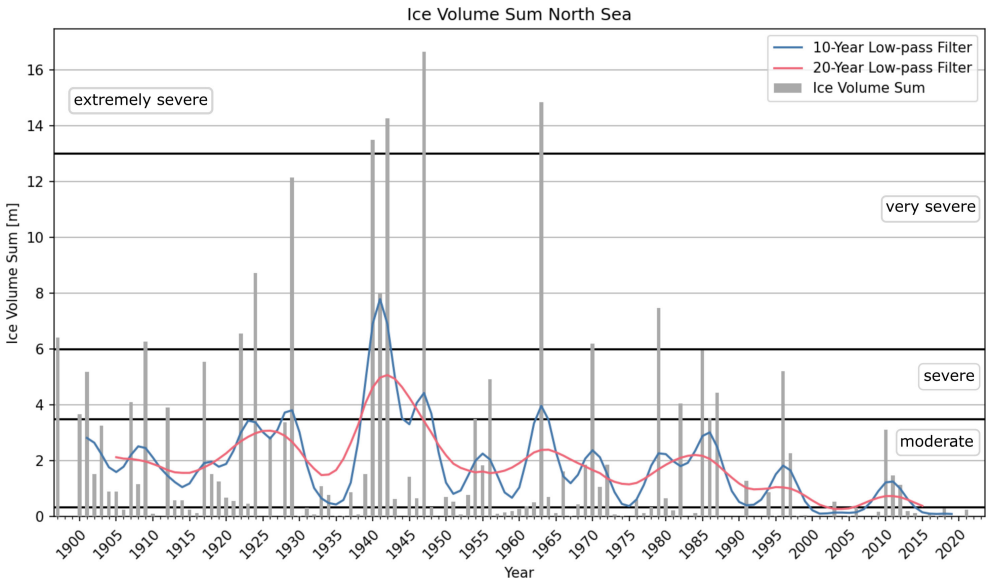

FIGURE 5
Time series of ice volume sum at the German North Sea coast from winter 1896/97 to 2022/23. The black lines denote the boundaries for weak, moderate, severe, very severe, and extremely severe ice winters.

warmer water and tidal effects. Furthermore, there was a peak of very and extremely severe winters in the early 1940s. Since the beginning of the 21st century, there was no severe winter in the North Sea, and only the winter of 2010 has been severe at the Baltic Sea coast. Generally, a decreasing trend in ice winter severity can be observed for the ice winter strength in recent years.

While these time series give a general view of the ice winter strength, they do not contain any information about the regional and yearly distribution of sea ice occurrence in different sea areas. These information are, however, of importance for navigation and installation of offshore infrastructure. The results and figures presented in the following section are a summary of information contained in the published ice atlases for the western and southwestern Baltic (Schmelzer and Holfort, 2012) and the German Bight and Limfjord (Schmelzer and Holfort, 2015). The presented cartographic information are based on ice charts and station observations produced in Germany, Denmark, and Poland.

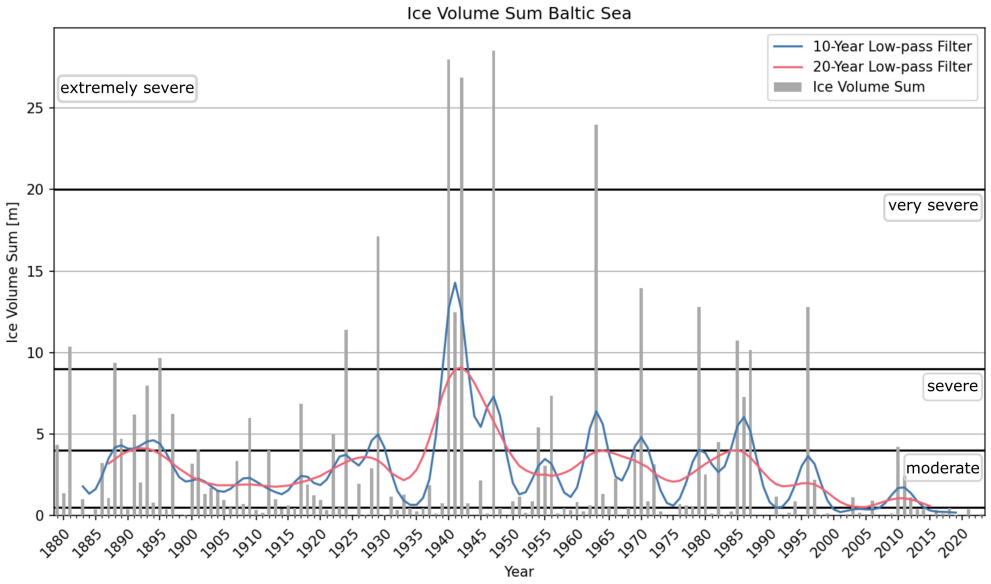

FIGURE 6
Time series of ice volume sum at the German Baltic Sea coast from winter 1878/79 to 2022/23. The black lines denote the boundaries for weak, moderate, severe, very severe, and extremely severe ice winters.

Figures 7 and 8 show the probability of ice occurrence in the southwestern Baltic Sea and North Sea for the three time periods 1961–1991, 1971–2001, and 1981–2010, respectively. In both sea areas, there is a decrease in sea ice occurrence especially at the open sea. Areas that usually have been covered with sea ice every year in all three epochs, like the Schlei, the Bodden waters around Rügen, and the Szczecin Lagoon, do not show a diminishing probability of ice occurrence. Nevertheless, the diminishing winter strength in these areas can be seen as a decrease in the mean number of days with ice and in the mean length of the season.

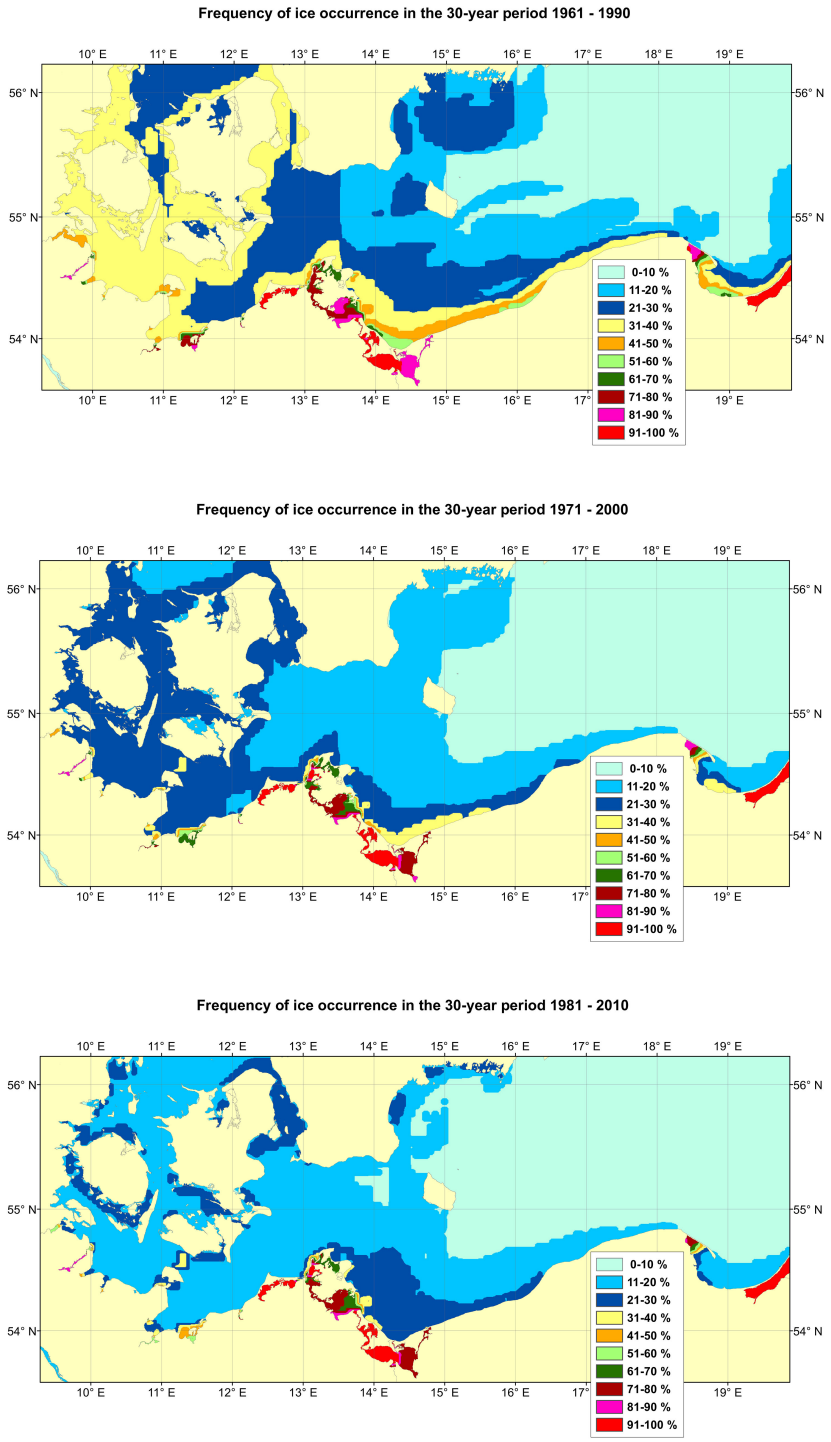

FIGURE 7
Charts of ice occurrence in the southwestern Baltic for the three epochs 1961-1990, 1971-2000, and 1981-2010. A decrease of ice occurrence with time is visible for almost all regions (Schmelzer and Holfort, 2012).

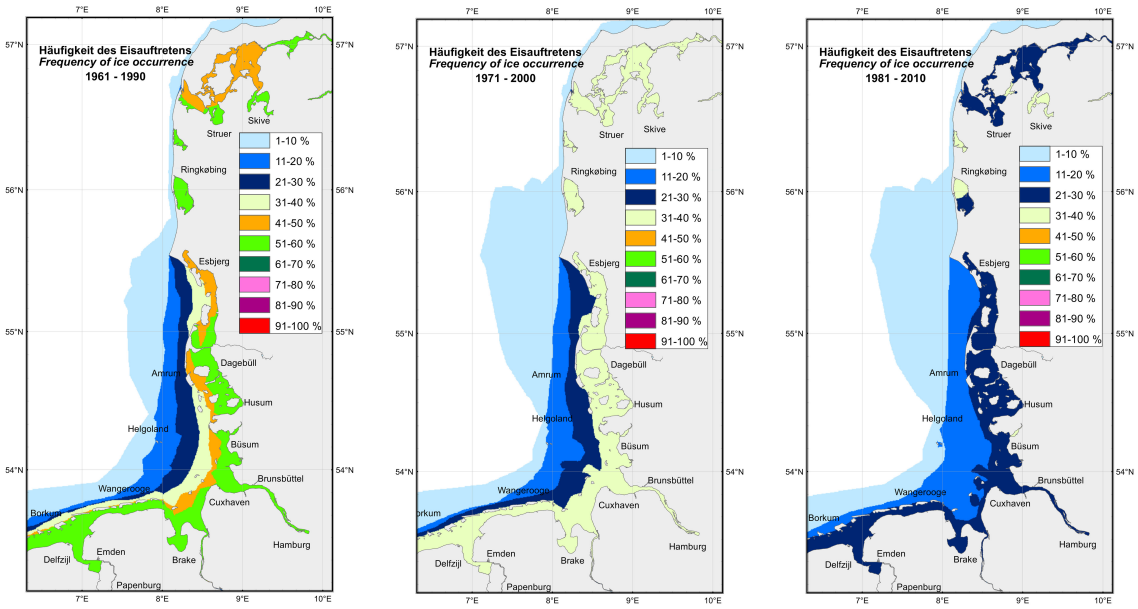

FIGURE 8
Charts of ice occurrence in the North Sea for the three epochs 1961-1990, 1971-2000, and 1981-2010. A decrease of ice occurrence with time is visible for almost all regions (Schmelzer and Holfort, 2015).

4 Future outlook

The German ice service will continue the production of its current operational sea ice products in the coming years. This ensures the distribution of well-established and international standardized products and use of worldwide proven communication methods. Digitalization, information availability, and advances in telecommunication capacities, however, increase the demand on timely and high-resolution information for safe and optimal navigation in ice-infested waters. Therefore, it is necessary to offer products that extend today's static and often text-based products to the digital age. Electronic Chart Display and Information Systems (ECDIS) allow the integration of sea ice information into on-board navigation. The improvement of usability requires the further development of international standards, i.e., IHO/WMO S-411, for the display of sea ice information. S-411, in its actual version 1.1, was published in 2014 based on the version 1 of the underlying S100 standard. Although many ice charts are available in S411, the standard has to be updated to comply with the actual S100 version 5. Within the needed update, new features, especially for portrayal, will be implemented. Therefore, routines for scale-dependent display of sea information need to be established and internationally standardized. In addition, it will be necessary to adapt the current ice information, especially the actual ice charts, to comply with these future standards. Furthermore, the ice service is currently working on a web mapping tool to make ice station data, harbor restrictions, ice charts, and text information available on a scalable map. This facilitates the easy access to relevant sea ice information especially for the public.

A longer-term project includes forecast charts based on numerical models with assimilation of sea ice information from automatically classified satellite data. In principle, the needed tools (operational ocean models including ice, data assimilation, and satellite classification) are available at the BSH. However, much work is still needed before the quality and performance of these tools are good enough for general use.

During the time of its existence, the ice service has collected a long time series of historical sea ice information. Parts of this data are digitized and stored in a database alongside most recent sea ice information. To date, this data is only available on direct request from the ice service. For customers, it is not possible to explore the data and to obtain knowledge of the availability of sea ice information. The geospatial database currently under development will provide a user interface that allows customers to search the available information and download exactly the data of interest. These comprise, among others, ice observations from stations, statistical summaries of the ice winter for the stations, and ice charts. Other ice services have direct access to the database and the possibility to update/change their countries data. This will greatly simplify the access to historical sea ice data and make it accessible for a broad range of customers. However, there are still large amounts of data that have not yet been digitized, inspected, or evaluated. If workload permits, conservation and digitalization of this valuable data will be carried out in the future.

Climatological ice information are of great interest not only to evaluate climate change but also for the design of offshore infrastructure. The ice atlases of the western and southern Baltic Sea as well as the German Bight provide information for the 50-year period from 1961 to 2010. The ice service is currently working to update the data for the next 30-year period from 1991 to 2020. This is important to keep track of the most recent changes of sea ice cover and to provide the most up-to-date information to the customers.

Author contributions

WA: Conceptualization, Data curation, Formal analysis, Investigation, Methodology, Software, Writing – review & editing, Visualization, Writing – original draft. JH: Conceptualization, Data curation, Formal analysis, Investigation, Methodology, Project administration, Software, Supervision, Writing – review & editing.

Funding

The author(s) declare that no financial support was received for the research, authorship, and/or publication of this article.

Conflict of interest

The authors declare that the research was conducted in the absence of any commercial or financial relationships that could be construed as a potential conflict of interest.

Publisher's note

All claims expressed in this article are solely those of the authors and do not necessarily represent those of their affiliated organizations, or those of the publisher, the editors and the reviewers. Any product that may be evaluated in this article, or claim that may be made by its manufacturer, is not guaranteed or endorsed by the publisher.

References

Bundesamt für Seeschiffahrt und Hydrographie (BSH). (1928). *Eisbericht: Amtsblatt des Bundesamtes für Seeschifffahrt und Hydrographie* (Hamburg: Bundesamt für Seeschiffahrt und Hydrographie).

Bundesamt für Seeschifffahrt und Hydrographie (BSH). (2020). *Nordsee-Handbuch, südöstlicher Teil. 6th edn* (Hamburg and Rostock).

Bundesamt für Seeschifffahrt und Hydrographie (BSH). (2021). *Ostsee-Handbuch, südwestlicher Teil. 24th edn* (Hamburg and Rostock).

Deutsche Seewarte. (1905–1944). *Annalen der Hydrographie und Maritimen Meteorologie* (Hamburg und Berlin).

Garcia-Soto, C., Cheng, L., Caesar, L., Schmidtko, S., Jewett, E. B., Cheripka, A., et al. (2021). An overview of ocean climate change indicators: sea surface temperature, ocean heat content, ocean pH, dissolved oxygen concentration, Arctic sea ice extent, thickness and volume, sea level and strength of the AMOC (Atlantic meridional overturning circulation). *Front. Mar. Sci.* 8. doi: 10.3389/fmars.2021.642372

JCOMM. (2014). *Ice Information Product Specification. Edition 1.1.0* (Monaco: JCOMM TR), 81.

Koslowski, G. (1981). *Der Ostsee-Eiskode von 1980* Vol. 42 (Hamburg: Der Seewart), 176–184.

Koslowski, G. (1989). Die flächenbezogene Eisvolumensumme, eine neue Maßzahl für die Bewertung des Eiswinters an der Ostseeküste Schleswig-Holsteins und ihr Zusammenhang mit dem Charakter des meteorologischen Winters. *Deutsche Hydrographische Z.* 42, 61–80. doi: 10.1007/BF02226421

Koslowski, G., and Glaser, R. (1999). Variations in reconstructed ice winter severity in the western Baltic from 1501 to 1995, and their implications for the North Atlantic oscillation. *Climate Change* 41, 175–191. doi: 10.1023/A:1005466226797

Koslowski, G., and Schmelzer, N. (2007). *Ice Winter Severity in the Western Baltic Sea in the Period 1301–1500*, Hamburg and Rostock: Bundesamt für Seeschifffahrt und Hydrographie. Vol. 42. 47–56, Hamburg and Rostock: Berichte des BSH.

QGIS.org. (2022). *QGIS Geographic Information System* (QGIS Association). Available at: http://www.qgis.org.

Schmelzer, N., and Holfort, J. (2011). Ice winter severity in the western Baltic Sea in the period of 1301–1500: comparison with other relevant data. *Int. J. Climatol.* 31, 1094–1098. doi: 10.1002/joc.2337

Schmelzer, N., and Holfort, J. (2012). *Climatological Ice Atlas for the western and southern Baltic Sea (1961–2010)*. Hamburg and Rostock: Bundesamt für Seeschifffahrt und Hydrographie.

Schmelzer, N., and Holfort, J. (2015). *Climatological Ice Atlas for the German Bight and Limfjord (1961-2010)*. Hamburg and Rostock: Bundesamt für Seeschifffahrt und Hydrographie.

Strübing, K. (1970). Satellitenbild und meereiserkundung. *Deutsche Hydrographische Z.* 23, 193–213. doi: 10.1007/BF02311139

WMO. (2004). *Ice Chart Colour Code Standard, World Meteorological Organization*, Geneva: World Meteorological Organization. WMO/TD-No. 1215.

WMO. (2015). *Manual on the Global Telecommunication System*. Geneva: World Meteorological Organization. WMO-No. 386.

frontiers | Frontiers in Marine Science

TYPE Review
PUBLISHED 08 August 2024
DOI 10.3389/fmars.2024.1400479

OPEN ACCESS

EDITED BY
Kum Fai Yuen,
Nanyang Technological University, Singapore

REVIEWED BY
Leandro Ponsoni,
Flanders Marine Institute, Belgium
Jan L. Lieser,
Bureau of Meteorology, Australia

*CORRESPONDENCE
William Copeland
williamjp@met.no

RECEIVED 13 March 2024
ACCEPTED 10 July 2024
PUBLISHED 08 August 2024

CITATION
Copeland W, Wagner P, Hughes N, Everett A and Robertsen T (2024) The MET Norway Ice Service: a comprehensive review of the historical and future evolution, ice chart creation, and end user interaction within METAREA XIX. *Front. Mar. Sci.* 11:1400479. doi: 10.3389/fmars.2024.1400479

The MET Norway Ice Service: a comprehensive review of the historical and future evolution, ice chart creation, and end user interaction within METAREA XIX

William Copeland*, Penelope Wagner, Nick Hughes, Alistair Everett and Trond Robertsen

Værvarslinga divisjon for Nord-Norge, Norwegian Meteorological Institute, Tromsø, Norway

The MET Norway Ice Service (NIS) celebrated its fiftieth year as a formal operational sea ice information provider in 2020. Prior to the 1970's, support to navigation had started off with *ad-hoc* observations from coastal stations on Svalbard in the 1930's, before developing as a research programme in the 1960's. Activity in the region has steadily increased, and now the NIS also supports a large number of research, tourist, and resource exploration vessels, in addition to the ice chart archive being a resource for climate change research. The Ice Service has always been at the forefront in the use of satellite Earth Observation technologies, beginning with the routine use of optical thermal infrared imagery from NASA TIROS and becoming a large user of Canadian RADARSAT-2 Synthetic Aperture Radar (SAR), and then European Copernicus Sentinel-1, in the 2000's and 2010's. Initially ice charts were a weekly compilation of ice information using cloud-free satellite coverage, aerial reconnaissance, and *in situ* observations, drawn on paper at the offices of the Norwegian Meteorological Institute (MET Norway) in Oslo. From 1997 production moved to the Tromsø office using computer-based Geographical Information System (GIS) software and the NIS developed the ice charting system *Bifrost*. This allowed the frequency of production to be increased to every weekday, with a greater focus on detailed sea ice concentrations along the ice edge and coastal zones in Eastern Greenland and in the Svalbard fjords. From 2010, the NIS has also provided a weekly austral summer ice chart for the Weddell Sea and Antarctic Peninsula. To further develop its capabilities, NIS engages in a number of national and international research projects and led the EU Horizon 2020 project, Key Environmental monitoring for Polar Latitudes and European Readiness (KEPLER). This paper summarises the overall mandate and history of the NIS, and its current activities including the current state of routine production of operational ice charts at the NIS for maritime safety in both the Arctic and Antarctic, and future development plans.

KEYWORDS

sea ice (Arctic), Arctic, Norway, Svalbard, Barents, Fram Strait, Ice Service, sea ice operations

1 Introduction

The main aim of this paper is to give an overview of the activities of the MET Norway Ice Service (NIS) at the Norwegian Meteorological Institute (MET Norway) and address the current limitations and future prospects for the NIS in a changing Arctic. Not only will this serve as a historical record, but it will also aid our end users to better understand our products and processing chains.

1.1 Arctic navigation: challenges and opportunities

The Arctic Ocean is a nearly landlocked ocean consisting of two deep central basins, i.e. Eurasian and Amerasian, bordered by seven epicontinental seas, i.e. The Greenland Sea, Lincoln Sea, Beaufort Sea, Chukchi Sea, East Siberian Sea, Laptev Sea, Kara Sea and Barents Sea Jakobsson et al., 2003, 2012). The presence of multiyear sea ice coverage is consistent throughout the year in the northern Canadian and northern Fram Strait regions, although this is rapidly decreasing due to climate change (Massonnet et al., 2012; Babb et al., 2022; Regan et al., 2023). The presence of ice is not restricted to only Arctic latitudes, forming during the winter season within the Okhotsk, Baltic, Bering, Labrador Seas and Baffin and Hudson Bay, with significant inter annual variability (Serreze and Meier, 2018; Matveeva and Semenov, 2022). It is in regions with seasonal sea ice where reliable charting is of most interest, due to a combination of active year round maritime traffic and in some areas a very dynamic ice pack/ice edge (Babb et al., 2021). Despite declining sea ice, the trend is not spatially uniform, meaning regional trends can be masked by a pan Arctic approach (Onarheim and Årthun, 2017; Arthun et al., 2021).

Shipping in ice infested waters around the Arctic consists of a variety of maritime operators. These include, but are not limited to, fisheries, research, tourism, military, energy exploration and production, and cargo transport (Wagner et al., 2020). Calving glaciers and the creation of icebergs along the coasts of Svalbard and Greenland are an additional hazard, especially those icebergs that drift into the highly frequented waters of the Barents Sea, where they are particularly hazardous due to their small size (Løset and Carstens, 1996; Nesterov et al., 2023). This makes them difficult to detect. It was the sinking of the RMS *Titanic* in 1912 in the waters off of Newfoundland which was the catalyst for the International Convention for the Safety Of Life At Sea (SOLAS), which still governs maritime safety today International Maritime Organization, 1974, and resulted in the formation of the International Ice Patrol (IIP) (Murphy and Cass, 2012).

Climate change has caused a significant decline in the Arctic ice cover, resulting in more open water and increased accessibility to Arctic regions for maritime traffic and geopolitical purposes (Huntington et al., 2021; Meier and Stroeve, 2022). Over the last 4 decades, sea ice extent has decreased 40% in September and 10% in March (Meleshko et al., 2020). However, it is important to consider interannual variability when discussing operational sea ice forecasting, as such fluctuations in ice cover can pose a significant risk to maritime users (Mioduszewski et al., 2019; Stocker et al., 2020). The reduction of sea-ice thickness and extent does not translate to decreased risk of ice hazard along maritime routes, rather this results in an increased risk due to drift of residual multiyear ice embedded within the seasonal sea ice cover, which is difficult to detect both in satellite images and on shipboard radar. This is exemplified by the large inter-annual variability in open navigation days along the Northern Sea Route (NSR), with a marked increase from 2016 to an 88 day opening in 2020, followed by a drastic reduction to 0 in 2021 (CHNL, 2020). Consequently, a number of vessels became trapped, necessitating a protracted rescue period of multiple vessels over 2–3 months (Müller et al., 2023). Meanwhile on the North West Passage an increase in maritime traffic is observed due to the decrease in overall sea ice year on year. However, increasingly thinning multiyear ice drifting south onto the route through the summer, and an increase in lower ice class vessels operating in the region, has increased navigational risk (Dawson et al., 2022).

It's also important to note that the term "ice free" when referring to the Arctic is a misnomer, because ice-free includes < 1 million km^2 of sea ice (Kim et al., 2023) The term "ice free" is defined by a threshold for sea-ice extent, which indicates the area of ocean with at least 15 percent sea-ice concentration, as measured by the assimilation passive microwave sensor used by climate modellers (Overland and Wang, 2013). This terminology originated due to the limitation of models to assimilate sea ice data accurately, yet conflicts with the definition in the Sea Ice, 2014 *Sea Ice Nomenclature*. Due to the models being limited by this constraint, the risk to maritime activities increases significantly when the sea ice extent falls below this limit with ice that does not appear in the forecasts moving rapidly in regional areas. The increased outflow of multiyear ice through the Fram Strait and a propensity for more highly dynamic first year ice in the Barents sea and around Svalbard, raises the risks of navigational hazards in these regions.

Furthermore, tourism is opening up a wide variety of route possibilities, with summer cruises to the North Pole, and more daring expeditions into remote areas where there is a lack of historical *in situ* sea ice data. Over the last decade ship traffic across the Arctic has doubled, with the most significant increase observed in the Svalbard region (Stocker et al., 2020). Increased traffic opens up not only issues with regards to maritime safety, but also involves geopolitical tensions and ecological impacts for the region (Marchenko et al., 2015; Hovelsrud et al., 2023).

1.2 A brief history of the Norwegian Ice Service

Ice charting of the ice edge has been of particular interest to mariners since the beginning of the hunting industry in the Atlantic sector of the high Arctic during the mid 16th Century (Divine and Dick, 2006; Mö et al., 2020). The NIS has a partial ice observation catalogue spanning back to the 1500s created by the manual digitizing of early observations from ship logbooks and other

records up to 2002, concluding with a collection of over 6000 charts, that can be viewed using GIS software (ACSYS, 2003). Sea ice observation and reporting grew in importance especially during the era of polar exploration, when sea ice conditions played a role in some of the most well-known expeditions led by the likes of the Norwegian explorers Fridthjof Nansen and Roald Amundsen. Svalbard became part of Norwegian territory in 1925, and from 1933 official sea ice bulletins were released from the newly built Isfjord Radio on Svalbard by the Norwegian Svalbard and Arctic Ocean Survey (NSIU) headed by Adolf Hoel. Hoel, a Norwegian polar region scientist, political activist and trade/industry promoter, led multiple expeditions to Svalbard and Greenland (Hoel, 1929; Drivenes, 1994). Reporting of sea ice continued right up until the beginning of World War Two, when operations temporarily ceased. In 1948, the NSIU was renamed to the Norwegian Polar Institute (NPI) as a result of post war structural change, and as of 1963, sea ice reporting started anew, led by the NPI from both Bjørnøya and Isfjord Radio.

In 1969 the meteorological institute in Oslo began to download NASA Television Infrared Observation Satellite (TIROS) analogue thermal infrared (TIR) satellite imagery, and in 1970 the NIS was formed.

Reporting from the stations Bjørnøya and Hopen were fairly routine and sent to the Meteorological Institute in Oslo for analysis in the early days of satellite imagery (Figures 1A-C). Satellite imagery allowed for a greater overview of the region, and approximate ice edge position data was sent from the meteorological institute to the stations during the 1970s. In addition to this there were *ad hoc* ice observation flights along the ice edge from Andøya to Svalbard. Ice edge locations were plotted, along with identification of icebergs as show in Figures 1D, E. If visibility was greatly reduced, the flight radar was used to calculate the rough position of the ice edge.

Today the NIS is the mandated authority for provision of sea ice and iceberg information in WMO/IOC JCOMM GMDSS METAREA-XIX. The service is also tied to the SOLAS

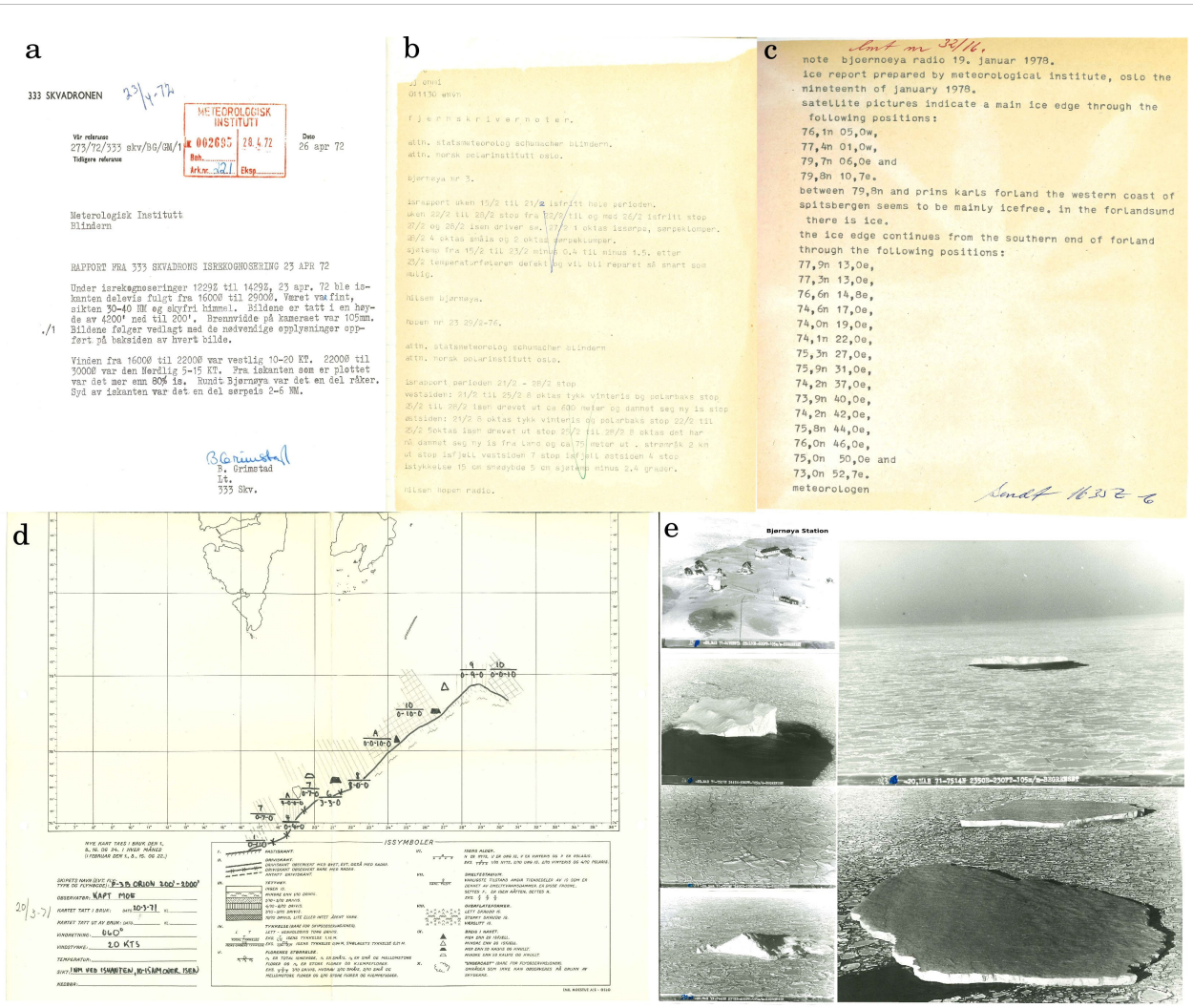

FIGURE 1
(A) Flight report from flyover 23rd April 1972, **(B)** Ice observations from Bjørnøya and Hopen sent to the Meteorological Institute February 1976, **(C)** Ice edge positions sent out from the meteorological institute using TIROS satellite imagery as a guide, **(D)** Ice edge plot map with icebergs from a flyover on 20th March 1971, **(E)** Aerial photographs complementing the plotting map for the same date as panel **(D)**.

convention, which has the main aim to ensure the safety of life and property at sea, designated by the International Maritime Organization (IMO) and the International Hydrographic Organization (IHO). To fulfil this mandate, the NIS provides standardised sea ice and weather information, forecasts and warnings. This includes daily (working day, Monday-Friday) ice concentration charts with an emphasis on Svalbard, the Barents Sea and eastern Greenland. The NIS also provides a weekly (on Mondays) ice chart for the Weddell and Bellingshausen Seas of the Antarctic during the austral summer (October to April) as part of the "Collaborative Antarctic Char" project between Norway, Russia and the United States. Several short-term sea ice forecast models are being evaluated on a pre-operational basis to assess their suitability for use in the Ice Service. These include: (a) U.S. Naval Research Laboratory GOF3.1 (Metzger et al., 2017), (b) Copernicus Marine Service (CMEMS) neXtSIM (Williams et al., 2021), and (c) the MET Norway Barents Ensemble Prediction System (Barents-EPS) model (Röhrs et al., 2023).

2 Area of study

2.1 METAREA XIX

The NIS provides ice charts for METAREA-XIX, covering the northern Norwegian mainland coastline, a large portion of the Greenland Sea, and the western Barents Sea, and the sector of the Arctic Ocean north of these areas up to the North Pole (see Figure 2) The ice charts include the entirety of this region with extension to include the entire Barents Sea, northern Baltic Sea, and the southern Greenland Sea, including the Denmark Strait. Ice charts also cover the Skagerrak, Kattegat and Outer-Oslofjord which can become ice covered in severe winters. The Svalbard region is the primary area of operations due to high ship traffic and where many of our end users operate.

European Arctic users of ice information are diverse, ranging from land communities, maritime navigators on leisure crafts to expert ice pilots. The foundations of user needs in METAREA XIX

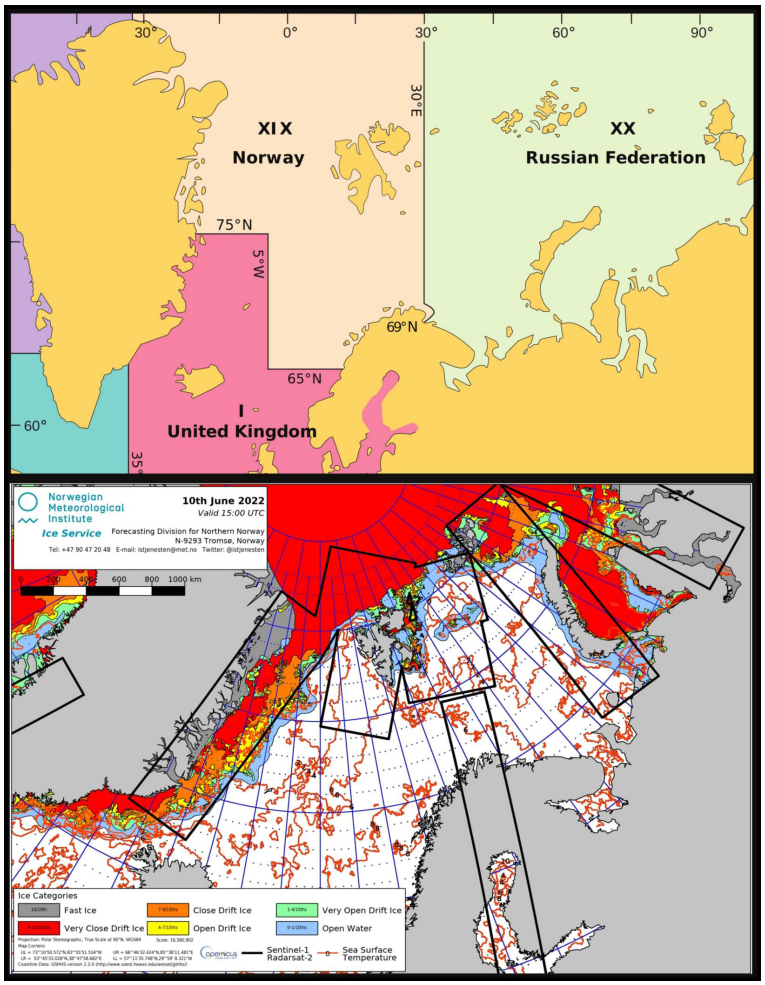

FIGURE 2
METAREA XIX along with the boundary area for NIS ice charts. Highest priority is given to the mandated area of the NIS, however maps are produced for further afield to complement ice charts created by other ice services e.g. AARI and Greenland ice service. Black boxes in the ice chart highlight available Sentinel 1 SAR imagery for the specific date.

began with the fishing and hunting industry but quickly evolved to include tourism, the offshore energy sector, research expeditions, military activities, search-and-rescue (SaR) and general navigational vessels. Tourism is becoming a significant user base in this region, fuelled by a combination of increasing adventure tourism demand and increased duration of accessibility during the shoulder seasons (Stocker et al., 2020; Müller et al., 2023). The varying experience amongst ice pilots and increasingly dynamic ice conditions in this region during the shoulder months, raises the possibility of dangerous maritime incidents (Parsons and Progoulaki, 2014). The Svalbard and Barents region have especially dynamic ice conditions, arguably the greatest in the entire Arctic (Koenigk et al., 2008; Docquier et al., 2020).

During the Spring and Summer seasons the European Arctic experiences its highest vessel traffic, coinciding with sea ice retreat and rapidly changing ice movement. During this time, non-ice reinforced vessels are able to travel along and within the marginal ice zone (MIZ) and ice edge because the ice is often of low concentration. This allows for ships to travel to areas (i.e. fjords and narrow channels) that are normally inaccessible during the freeze-up and winter seasons. Meanwhile within the pack ice north of Svalbard, and more especially North East Greenland, first (FYI), second (SYI) and multiyear ice (MYI) cover presents itself with thick ridging, multi-year ice floes and potential for embedded icebergs throughout the year (Renner et al., 2013; Krumpen et al., 2016). Although this is changing as a result of climate change, with thinner ice becoming more predominant (Sumata et al., 2023), this environment continues to pose significant safety risks for the inexperienced and unprepared, especially those that do not fall under the goal-based polar code requirements (Müller et al., 2023).

One of the most challenging aspects for predicting sea ice conditions in METAREA XIX is inter-annual variability of sea ice in the region. This poses major challenges for long term route planning and predictability of the ice edge on a seasonal basis, that has traditionally relied upon climate based monitoring capabilities. Weather, and more especially sustained wind direction, plays a major role in changing sea ice extent, where thinner ice is more susceptible to wind and wave action. With a lack of *in situ* meteorological observational data in the Arctic region, models struggle to predict weather systems as comprehensively as they do in temperate and equatorial regions (Jung et al., 2016). This compounds the issues surrounding long term route planning for ships, especially tourist vessels that use the ice edge as their primary target, as forecasting resources and capabilities are greatly hindered.

2.2 The Antarctic

Although the mandate of the NIS does not extend to the Antarctic region, the NIS actively participates in the "Collaborative Antarctic Chart" project between Norway, Russia and the United States. During the austral summer, from the beginning of October to the end of April, weekly charts for the Weddell Sea and Antarctic Peninsula region are created every Monday, aligning with the summer tourist season in the region (Figure 3). Most importantly, the NIS contributes to the Antarctic Iceberg Database, with naming supplemented by the U.S. National Ice Center, 2024.

In the Antarctic, FYI is the predominant stage of development (SoD). This SoD is susceptible to rapid development and decay, rendering its temporal evolution difficult to ascertain solely from sporadic satellite data (Eayrs et al., 2019). Conversely, old ice, which has persisted over multiple years, is relatively scarce in the Antarctic, primarily confined to limited regions in the Weddell

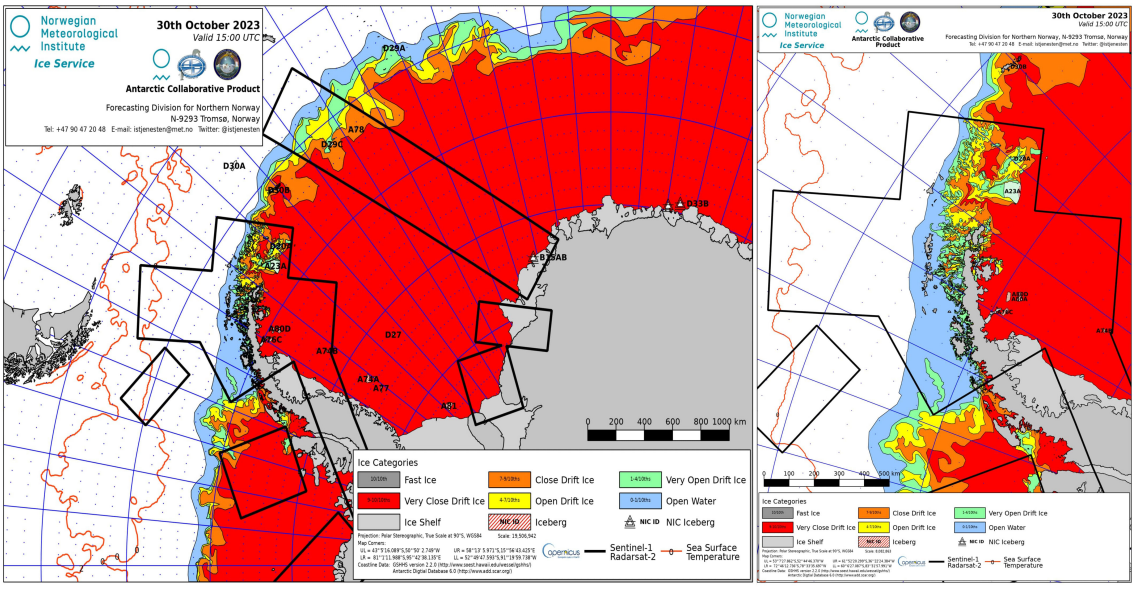

FIGURE 3
Antarctic ice chart area primarily focusing on the Weddell Sea and Peninsula region where the highest ship traffic takes place during the austral summer.

and Ross Sea gyres. However, this is reducing due to the impact of climate change (Turner et al., 2020; Shi et al., 2021; Melsheimer and Spreen, 2022).

Despite the SoD not being of primary concern in the creation of ice charts of SIC, the dominance of FYI, drift and the ice edge creates challenges in accurately monitoring ice in near real time (NRT) (Eayrs et al., 2019). This highlights the high competence needed for sea ice analysts with regards to weather patterns and local knowledge, especially where weather has significant interplay with oceanographic or topographic features. Polynya formations are a well-known feature of Antarctic sea ice throughout the formation and melt seasons (Barber and Massom, 2007; Kern, 2009; Campbell et al., 2019).

An additional hazard is the very high density of icebergs, bergy bits and growlers around Antarctica, extending many 10s of km away from the ice shelves. Monitoring of icebergs is carried out by the U.S. NIC and the Argentine Naval Hydrographic Service, where the latter uses both *in situ* and satellite observations (Scardilli et al., 2022).

3 User needs for ice information in METAREA XIX

Changes in sea-ice regimes in the polar regions are driven by the changing climate, retreating sea ice in some areas and more importantly shifting weather patterns on regional scales that contributes to a high level of variability. There has been an increase in the number of ships observed in polar waters, and this trend is expected to continue in all areas of the Arctic, based on ship-building statistics from the Russian Maritime Register of Shipping, 2024 and Dawson et al., 2022.

Extensive studies have been conducted on the needs of mariners and land-based users in the European Arctic (Kepler D1.1 (Wagner et al., 2019), 1.2 (Mustonen et al., 2019), 1.4 (Hughes et al., 2020), D4.1 (Kangas et al., 2020), 4.3 (Tietsche et al., 2020); Jeuring and Knol-Kauffman, 2019; Jeuring et al., 2019; Stewart et al., 2019; Stocker et al., 2020; Veland et al., 2021; Blair et al., 2022).The recurring theme among end-users is a growing provision for augmented sea-ice products that significantly enhance current operational sea ice information. This includes parameters such as sea-ice SoD/ice type, areas of deformation, sub-daily ice concentration information, and, most Importantly, short-term sea ice forecasts on the spatial scales relevant to the users (Wagner and Hegelund, 2020; Veland et al., 2021).

3.1 Tailoring ice services to diverse user needs

Ice services directly engage with users and stakeholders, regularly documenting user feedback as part of their service. In the European Arctic, users of ice information vary significantly based on their activities, which can be related to maritime or land-based community requirements, as well as their individual levels of expertise. Land-based users require information about the ice's location and its stability over water. Maritime users navigate through different ice regimes, which may be within the ice pack, around the outer ice pack area, along the edges of ice-encumbered regions, or with the goal of avoiding ice conditions altogether. User needs are not straightforward because they depend on the specific activity, and often, the information requirements and activities overlap in terms of spatial and temporal scales.

One aspect of the IMO Polar Code (Deggim, 2018) concerns the voyage planning component, where the vessel master must be well-prepared for any environmental conditions along the planned route and ensure that the ship is equipped in accordance with the Polar Code. A basic level of competency for the crew is essential, and it is expected that the vessel receives regular and high-quality updates on weather, ocean, and ice conditions for navigational safety and situational awareness.

The ice information requirements of end-users and stakeholders in the European Arctic are influenced by their proximity to the ice edge or ice-covered areas and their varying levels of skill and vessel capabilities. The International Ice Chart Working Group (IICWG) mariner survey provides a concise overview of how these factors relate to how users perceive ice information Table 1 (Veland et al., 2021).

TABLE 1 Overview of the findings from the IICWG Mariner Survey 2019; Veland et al., 2021 and summer seasons (Sandven et al., 2023).

Factors relevant to the differences in skill among mariners in the Arctic	
Ship Capabilities	No ice class to Polar class (1–7) travelling through various ice regimes (e.g., ice edge, marginal ice zone, outer pack ice, etc.)
Vessel Size	Small leisure vessels to icebreakers
Ship Operator/ Navigator	Calm and ice free to extremely harsh with no visibility and areas blocked by ice
Seasonality	Calm and ice free to extremely harsh with no visibility and areas blocked by ice
Ice regime	- Ice free to multiple stages of FYI Combination of FYI/SYI/MYI mixed ice regimes (including icebergs)
Mariner Training	- IMO requirements for navigators are vague - Training facilities for Polar Code certificates are not standardised
Mariner needs relative to their distance from the ice edge	
Location far from any ice	- Iceberg information on limit and clusters Ice edge and distribution - Sea ice and iceberg information on spatial scales between 200m-10km
Location near coastal zones and ice edges	- High spatial resolution and short-term sea ice forecasts (< 100 resolution) - Iceberg positions - Sub-daily nowcasts and forecasts
Location within ice	- Ice information (e.g., stage of development, pressure, deformation, drift, strength, and leads) - Sub-daily nowcasts, 24h forecasts Scalable file formats to onboard systems Satellite images < 1km spatial resolution.

3.2 User hazards and mitigating ice service requirements

Operating conditions on or around sea ice can turn hazardous at any time due to prevailing weather conditions, and require that ice services ensure information that is sent out is relevant, representative of actual conditions, reliable and accessible. These are part of mitigating measures that underpin the usefulness of the data for end-users. Figure 4 summarises the spatial and temporal scales relevant for the various applications and operations.

Ships operating in the Arctic Seas continue to experience limited communication bandwidth when at high latitudes (over 75N [with exceptions]) or when ships are travelling in mountainous coastal regions with narrow fjords. This means product dissemination should be clear so the user understands the difference between products, including the quality and relevance to their activity. All ice services aim to provide daily and sub-daily ice information for critical areas (near harbours, choke points); and high resolution products (< 1km) that represent sea ice at the scale necessary to observe features such as ice edges, SoD, deformation and areas of open water. This is particularly challenging given the geophysical caveats observed during the melting of snow on sea ice. As the snow transitions into water on the ice surface, microwave sensors struggle to effectively separate open water, thin and thick ice, impacting the ability to measure sea-ice volume, a key factor in understanding changing sea-ice trends (Tilling et al., 2018; Landy et al., 2021). These limitations are especially pronounced during the melt.

Maritime traffic is increasing with the melting sea ice, especially in the European Arctic, where a mixing of old and new ice regimes continue to be susceptible to ocean and wind forcing. For this reason, a high level of quality control is required to oversee sea ice information that analysts in ice services use prior to being disseminated to the public. Ice analysts closely monitor ice along northeast Greenland where a combination of new melting ice from breakup of the fast ice and old ice flowing out of the Arctic through Fram Strait begin to mix to create larger ice floes. Generally, the thick compact first year ice and old ice north of Svalbard begins to become less compact as the melt season advances towards the summer. This introduces a higher risk for ice advection in the fjords to the north, as well as along the eastern part Nordaustlandet where the ice can be pushed up Hinlopen Strait, depending on local weather conditions.

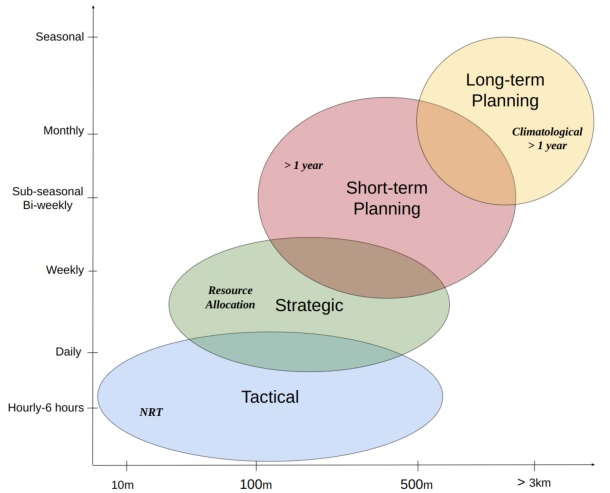

FIGURE 4
Different situations and corresponding spatial and temporal scales required by the maritime and land use sectors. (Taken from Hughes et al., 2020).

The vulnerability of sea ice to unexpected displacement during this period creates a misunderstanding between where there are areas of open ice and opportunities for maritime activity in the Arctic. With a lack of observational data in the polar regions, reliability of weather and ice forecasts is reduced (Lawrence et al., 2019; Laroche and Poan, 2021). On the one hand the possibility for more areas of open ice encourages a higher potential for various types of vessels to traverse through regions that are normally ice covered throughout the year. On the other hand, from a user perspective, this creates an operational challenge because in the event of sudden or unpredictable weather conditions, commonly occurring in polar regions, ice can become a hazard if large amounts are quickly moved in the area of a vessel that does not have the appropriate ice class, or if the maritime activity is operating in an area and is unable to obtain appropriate ice information to safely navigate to a safer area.

Therefore there is a critical need for ice services to increase their portfolio to include a variety of relevant products and services that can address a broad group of users with targeted and relevant sea-ice information. The ideal ice service includes the following attributes:

- Ice information that is specific to the METAREA where known areas of high traffic are routinely monitored and where the predominant user/stakeholder community is closely aligned with the ice service products and mandate.
- Sea ice information provided at required resolutions for maritime navigation.
- High update frequency with capabilities to observe hazardous ice (scale: 100–200m or less, sub-daily updates for certain regions).
- Full coverage of satellite data at sub-kilometre resolution for ice charting.
- Tailored/high resolution ice information provision for certain dynamic or critical locations linking to early warning systems.
- Ice information products that can be translated or integrated into risk assessment schemes.
- Local/regional high spatial resolution sea ice forecast products covering 24–48 hours for safe/efficient navigation in/near ice.
- Improved access to scalable ice information and maintain graphical formats for other displays.
- Extended access to automated/annotated satellite Quicklooks.

4 International and national collaboration

The NIS works as a bridge between institution-based projects which aim to develop new products through deep learning/AI

methods, and ice service end users. Our role is primarily to provide input from an operational standpoint and help evaluate the algorithms for usability in the operational community. Collaborative efforts are taken both internationally and nationally. Within the NIS the internal development structure provides a crucial role in evaluating product performance. This involves utilising large data volumes and utilising the expertise of the ice analysts, to identify areas for improvement and streamlining the product-to-service chain.

Since the inception of IICWG in 1999, the NIS has been a key member of the Group. The NIS takes part in, and leads, a number of task teams with diverse objectives, including iceberg modelling, implementation of new satellite sensors for operational use, best practises, their usage, gaps and opportunities.

Close collaboration also exists between the International Hydrographic organisation (IHO), International Maritime Organisation (IMO) and the World Meteorological Organisation (WMO). Within the WMO, the NIS plays an active role within the Global Cryosphere Watch (GCW), Sea ice Watch (SIW) which strives to consolidate requirements for sea-ice monitoring, analysis and forecasting, as well as updating WMO guides for instruments and observation best practices. The NIS is also in the Standing Committee on Marine Meteorological and Oceanographic Services (SC-MMO) where the Expert Team on Maritime Safety (ET-MS) maintains the documentation and data standards on sea-ice reporting, including the Sea Ice Nomenclature laid out by the Sea Ice 2014; JCOMM Expert Team on Sea Ice, 2014; International Hydrographic Organization (IHO), 2014).

5 Information sources for ice charting

The creation of ice charts is primarily reliant on the delivery of timely and reliable satellite image data. This is supplemented with *in situ*, ship-based and aircraft observations, that are sparse in the region due to the logistical challenges posed by the remoteness of data collection in polar regions. All of these data sources are assessed by experienced ice analysts and the information collated into the ice charts.

5.1 Information sources

Over time, the availability of satellite data has significantly expanded, resulting in a wide variety of increasingly higher spatial resolution imagery with varying sensor capabilities. Figure 5 illustrates the evolution of satellite missions, while Table 2 provides a more in-depth overview of the capabilities of SAR imagery specifically. The European Sentinel-1A is currently heavily relied upon for its daily imaging capacity due to a malfunction of its twin satellite Sentinel-1B in December 2021. Improved coverage will be restored when Sentinel-1C is successfully launched (scheduled for November 2024) and after a 6 month commissioning phase.

Presently, any gaps in orbital coverage in Sentinel-1A imagery are filled using supplementary SAR imagery from RADARSAT-2, RADARSAT Constellation Mission (RCM), COSMO-SkyMed, as well as optical images from VIIRS, Sentinel-2, Sentinel-3, and

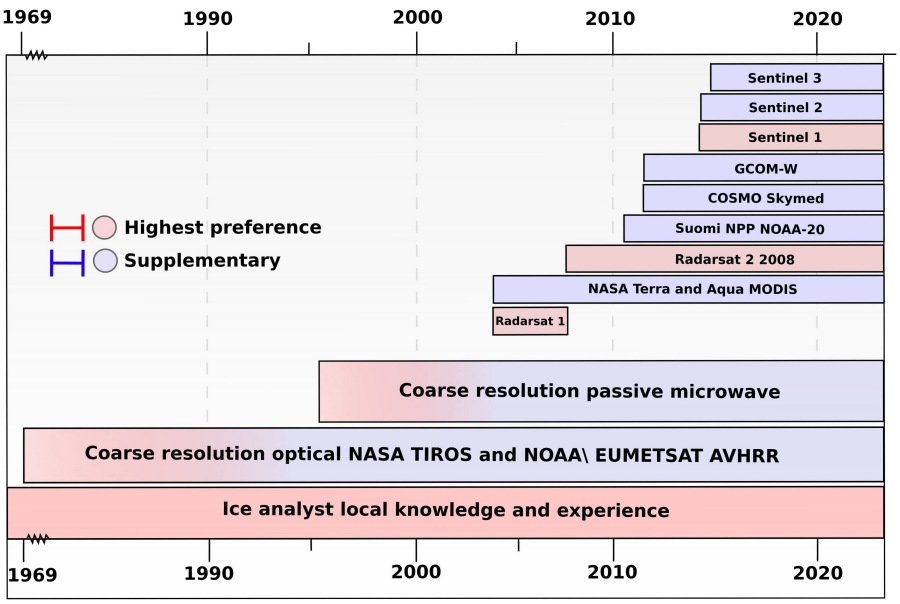

FIGURE 5
List of satellite data sources as of summer 2022, ranked in order of preference (highest first). Note that ice analyst local knowledge and experience is ranked as highest preference throughout the time period and will continue to be so into the near future even with the initiation of AI and machine learning techniques.

TABLE 2 SAR sources.

Satellite	Operator/ Provider	Band and polarisation	Spatial resolution (Footprint)
Sentinel-1	Copernicus	C-band SAR images Typically these are dual (HH +HV) polarisation.	Extended Wide (EW) and Interferometric Wide (IW) modes at 40 m and 10 m resolution respectively.
RADARSAT-2	MDA/ Copernicus	C-band SAR Typically these are dual (HH +HV) polarisation.	Images in ScanSAR Wide mode covering the Svalbard area at 50 m resolution.
RADARSAT Constellation Mission	CSA/ Copernicus	C-band SAR. Typically these are dual (HH +HV) polarisation.	Images covering the European sector of the Arctic with image modes between 16m and 50m resolution
COSMO-SkyMed	ASI/ Copernicus	X-band single polarisation (HH) SAR	Images in HugeRegion and Himage modes at 100 m and 3 m resolution respectively.
ICEYE	ICEYE/ Copernicus	X-band single polarisation (V V)	SAR images in ScanSAR mode at 15 m resolution.

METEOSAT Advanced Very High Resolution Radiometer (AVHRR), provided that weather and lighting conditions allow. Passive microwave imagery from AMSR2 is also employed as a guide and supplement to the above-mentioned sources.

5.1.1 Synthetic Aperture Radar

Since the 1980s, Synthetic Aperture Radar (SAR) has emerged as the preferred sensor type for global ice services, first as airborne systems and later on satellites (Haykin et al., 1994). SAR is favoured for its independence from the restrictions imposed by cloud cover and daylight, which hinder the use of optical imagery (Sandven et al., 2023). With resolutions ranging from 3 to 100 meters and wide swath widths of 20 to 400 kilometres, SAR allows for detailed analysis of large areas, depending on the satellite acquisition mode. This capability enables ice analysts to cover extensive regions without the need for secondary sources (Dierking, 2013).

SAR systems can utilize polarimetry to provide information on the orientation of the electromagnetic field vectors, allowing for enhanced analysis of the geophysical properties of the observed surface (Shuchman et al., 2004; Dierking, 2013). A multi-frequency and multi-sensor approach has demonstrated the capability to derive automated sea ice concentration and SoD products that support operational ice services (Singha et al., 2018; Khachatrian et al., 2021; Salvó et al., 2023). This approach can potentially resolve regional and seasonal challenges that have notably hindered the accuracy of sea ice monitoring, particularly during the spring and summer seasons, due to the melting snow atop sea ice and melt ponds (Casey et al., 2016).

The penetration depth of the SAR C, L, and X-band frequencies varies, enabling more accurate 3-D mapping of the ice. Optical and infrared visible sensors complement this data to provide a more realistic observation of sea ice SoD (Lohse et al., 2020) and concentration (Singha et al., 2018; Zhang and Hughes, 2023).

At the NIS, C-band Sentinel-1 and RADARSAT-2 are the primary sources of microwave imagery for ice chart production.

L-band SAR is expected to offer significant improvements for SoD classification, and we have evaluated data from ALOS-2 (Singha et al., 2018; Færch et al., 2023) and SAOCOM satellites in preparation for expanded coverage expected from the future NISAR and ROSE-L missions, set to launch in early 2024 and 2028, respectively.

5.1.2 Optical satellite imagery (infrared and visible)

When available, optical imagery is the preferred supplement to SAR images for ice analysts because features and boundaries are more defined and are easier to identify compared to other forms of imagery. However, its use is limited by the constraints of the polar night and periodic cloud cover.

The main sources for optical imagery are listed in Table 3. The NIS utilizes optical satellite data sources from the Visible Infrared

TABLE 3 Optical imagery sources.

Satellite	Sensor	Type	Operator/ Provider	Description
Sentinel-2	MSI	Optical	Copernicus	Visible and near-infrared optical images at high (10 m) resolution from the EU Copernicus programme Sentinel-2A satellite.
Suomi NPP NOAA-20	VIIRS	Optical	NOAA	Multichannel medium resolution optical and infrared, at 375 m or 750 m resolution.
Sentinel-3	OLCI and SLSTR	Optical	Copernicus	Multichannel medium resolution visible (OLCI) at 375 m resolution, and infrared (SLSTR) at 1 km resolution.
NOAA-15/18–19 Metop-B/C	AVHRR	Optical	NOAA and EUMETSAT	Multichannel visible and infrared at 1 km resolution.

Imaging Radiometer Suite (VIIRS) on the NASA/NOAA Suomi National Polar-orbiting Partnership (Suomi NPP) and NOAA-20 satellites, the Ocean and Land Color Instrument (OLCI), and Sea and Land Surface Temperature Radiometer (SLSTR) on Copernicus Sentinel-3, and AVHRR due to their abundance and frequent overpasses. Previously, the Moderate Resolution Imaging Spectroradiometer (MODIS) on the NASA Terra and Aqua satellites was also used. The Copernicus Sentinel-2 satellite carries the Multi-Spectral Imager (MSI) with 13 spectral bands and has a 10-meter resolution within the visible spectrum and a 60-meter resolution in the near-infrared bands. This provides analysts with a very high-resolution overview of the ice conditions in specific locations, complementing the resolution available from SAR. This high resolution is especially important within the complex fjord systems of the Svalbard and North East Greenland regions, where small-scale features such as icebergs can also be identified.

5.1.3 Passive microwave

Passive microwave sensors (Table 4) provide valuable data products that are utilised primarily in climate analysis, particularly for observing sea-ice concentration and extent over long time scales, and more recently, thin sea ice thickness through L-band radiometry (Heygster et al., 2009). Despite being available year-round, this data is typically only used as an aid to ice charting during the Northern Hemisphere winter for latitudes north of 60°N, when optical images are no longer viable due to limited daylight hours, or in the Southern Hemisphere, where SAR coverage is sparse. The Advanced Microwave Scanning Radiometer (AMSR-2) sensor, onboard the GCOM-W satellite, is the primary used in these instances (Meier and Stroeve, 2022). When the data from AMSR-2's 89 GHz channels are processed to 3.125km (e.g. Spreen et al., 2008), the data can be of use with quality control from an analyst and in the absence of SAR and optical imagery.

6 Sea ice analyst knowledge on local and regional scales

Ice analysts not only interpret satellite imagery but also apply their inherent understanding of weather conditions and utilise past experience, and local knowledge when creating an ice chart. This section aims to emphasise the importance of having ice analysts in all ice service teams to ensure the most reliable ice chart is delivered to our end users, even with the advent of artificial intelligence (AI) and machine learning techniques.

6.1 Sea-ice development, dynamics and decay

Interpreting sea-ice conditions from satellites requires skill that involves integrating insights from local environmental systems to understand ice formation and decay. This entails having a proficient understanding of how sea ice develops, encompassing seasonal and regional variations. We provide a short summary here, but the interested reader is referred to the International Hydrographic Organization (IHO), 2014 webpage and Wadhams, 2000.

A typical sea-ice SoD cycle in the northern hemisphere starts in mid to late September, with freeze-up, and continues through to the next summer. Freeze-up begins when the surface sea water is cooled to around -1.8 °C, for water with average salinity of 35 psu (practical salinity units). The first indication of sea ice formation begins with small ice crystals, frazil ice, forming in the water. Under calm conditions, these coalesce into grease ice, and in the presence of waves, into pancake ice. Both of these types of sea ice are distinctly recognisable, both visually, and in SAR images. Further cooling under calm conditions results in increased ice thickness, and a thin sheet called Nilas ice is developed. This can be subdivided into dark (thin, up to 5 cm) and light (thicker, up to 10 cm) nilas. Waves result in increasingly thick, and large floes of, pancake ice. Both nilas and pancake ice may thicken further and floes freeze together to form grey (up to 15 cm) and grey-white (up to 30 cm) ice. So far the ice crystals in all these types of sea ice, collectively known as Young Ice, are still randomly orientated due to their frazil origin.

The next stage of development is FYI, and thickening occurs through columnar ice crystal growth on the underside of ice floes. Thin FYI is 30–70 cm thick, medium FYI is 70–120 cm, and thick FYI is up to 200 cm, a limit imposed by onset of melting in the spring. All of these types of FYI are also distinct in high resolution satellite images, with thin FYI having smooth surfaces, often confused with calm water in SAR images, medium FYI having small ridges, and thick FYI having large ridges. In areas of high snow accumulation, typically in the Antarctic but also in some locations in the Arctic, the snow load can push the ice surface below sea level, resulting in flooding and the growth of superimposed ice.

When air temperatures go above 0°C in late spring or early summer, the melt season begins. Snow that has accumulated on the ice surface melts and forms puddles, called melt ponds. These are darker than the surrounding ice and absorb solar radiation, causing enlargement of the melt pond and eventually penetrating through to form thaw holes. For this reason, analysts consider that the melt and freeze-up periods are expected to vary regionally, when assessing the current ice situation.

TABLE 4 Passive microwave imagery source.

Satellite	Sensor	Type	Operator/ Provider	Band and polarisation (footprint)
GCOM-W	AMSR2	Passive Microwave	JAXA/ U. Bremen	Sea ice concentrations processed from JAXA AMSR-2 passive microwave 89 GHz data Channels at 3.125 km resolution provide background global coverage and are used in areas that do not require tactical information or cloud-free optical images are unavailable. The use of this requires local knowledge of ice analysts to know the history of the ice at a given location.

FYI can survive a summer melt season and is then classified as Old Ice. This can be divided into SYI and MYI. The melt season causes the ice to become less saline due to brine drainage, and air pockets in the ice being removed. This increases the hardness of the ice, and MYI embedded within FYI is therefore a significant hazard to marine users. MYI is also distinct from FYI in both optical and SAR satellite images.

An example of some varying ice regimes and types can be seen in Figure 6 from the CIRFA cruise in Spring 2022. These were observed both by Sentinel-2 optical and Sentinel-1 SAR and compared to *in-situ* imagery taken as part of the Ice Watch program Ice Watch ASSIST Data Network, 2006.

6.2 Inter-annual variability

Within METAREA XIX, interannual variability is becoming increasingly prevalent in response to climate change (Serreze and Stroeve, 2015; Onarheim et al., 2018; Lundesgaard et al., 2021; Luo et al., 2023; Sumata et al., 2023). Figure 7 shows the variability of ice conditions from the ice charts over the period 2012–2023 for the end of various months through the year around Svalbard. It is evident that interannual variability can be significant, creating challenges in providing reliable long term forecasting of ice edge positions on an annual to interdecadal time scales. Most of these large variations are due to shifts in weather patterns which need to be understood by ice analysts in order to update the ice chart accordingly.

6.3 Regional sea ice changes due to weather impacts

Over short time scales (1–7 days) the effect of large fluctuations in temperature and wind and wave action can have a significant impact on the ice edge and how sea ice and surrounding ice free

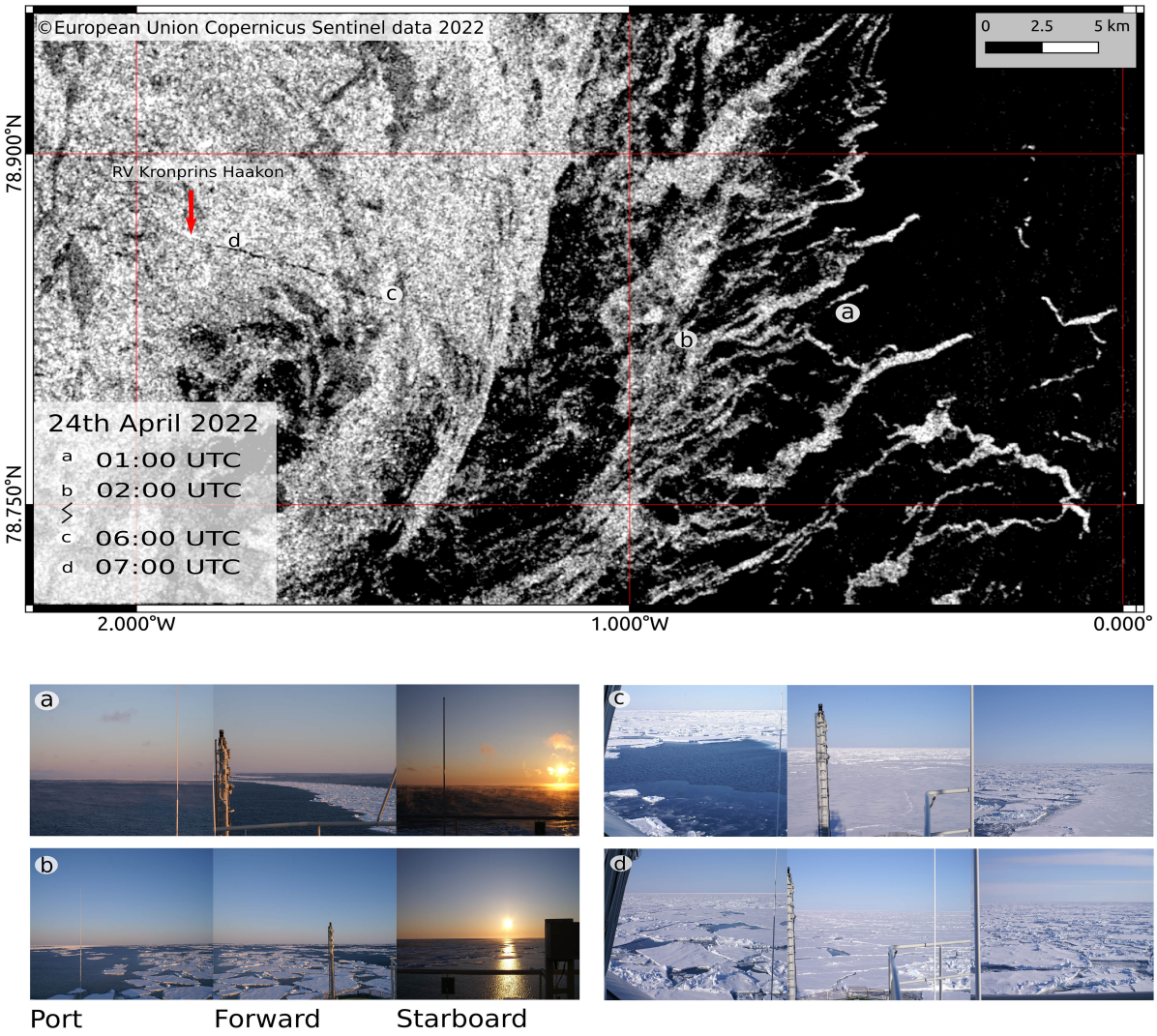

FIGURE 6
SAR imagery for 24th April 2022. Ice Watch imagery location aligned with satellite imagery to show in situ conditions (Ice Watch ASSIST Data Network, Norwegian Meteorological Institute, 2023). The markers a-d show the locations at which photographs were taken, which can be seen under the satellite image. (Copernicus sentinel data 2022, processed by ESA).

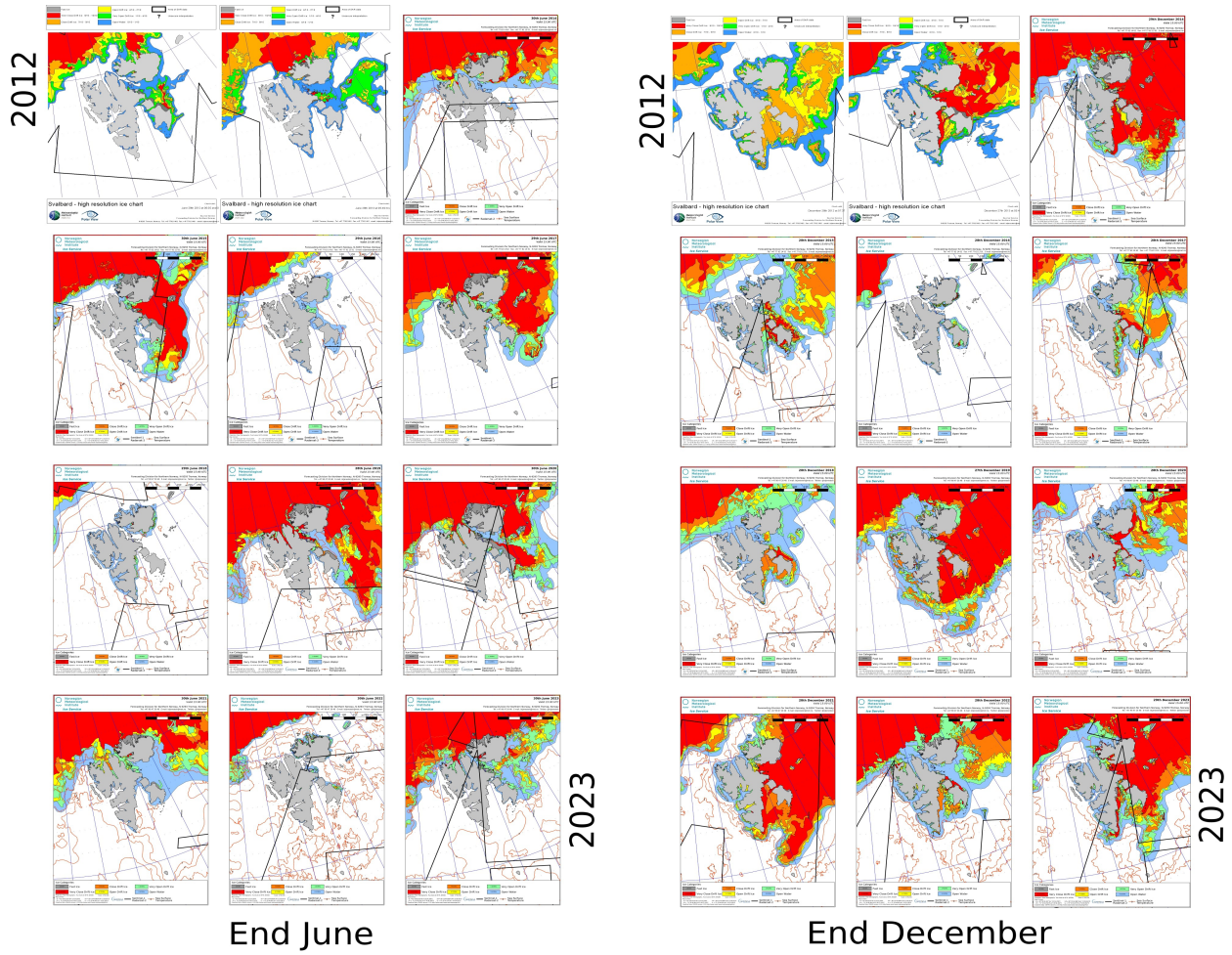

FIGURE 7
Variability of ice conditions from the ice charts for summer conditions (late June - 28-30th) and winter conditions (late December - 27-29th) over the period 2012–2023 around Svalbard. There is quite clearly a large range of inter-annual variability over the last decade, which can be explained by prevailing winds over the course of weeks or months resulting in drift and formation of ice around the archipelago.

water appears in satellite imagery. This is where the skill of the ice analyst is vital, as they are able to distinguish between ice and water, and identify surface characteristic changes of the ice. AI and machine learning techniques struggle to find consistent patterns that accurately represent the current ice situation, emphasizing the importance of tracking ice history through ice analysts as displayed in the Extreme Earth Project, 2021. During intense weather events, the risk of ice advection in unexpected areas rises. Therefore, timely and reliable ice information is crucial.

METAREA XIX experiences significant weather fluctuations due to its exposure to Atlantic low pressure systems. In addition, very cold air masses moving over the warmer waters that flow northward into the West Spitsbergen Current create the perfect environment for polar lows, a defining polar weather system that can rapidly affect the sea ice edge state of an area within the space of just a few hours (Rojo et al., 2015; Mallet et al., 2017).

Figure 8 shows the effects of strong katabatic winds flowing south eastward from north east Greenland creating a polynya along the fast ice (FI) edge in early May 2022. Sea surface temperatures and air temperatures were conducive to sea ice formation. There is a clear indication of pancake ice formation due to the combination of strong wind and ocean forcings. As a result, the corresponding SAR image demonstrates challenges to decipher the presence of sea ice in a given area, due to rough surface conditions/reflectance. By the 4th May, winds had calmed slightly allowing pancake ice to cement, significantly reducing wave action and therefore resulting in a more flat reflectance signal in the SAR imagery. As can be seen in the optical imagery (left), both days have similar sea-ice concentrations within the polynya, however, this is difficult to perceive from SAR imagery alone. Without analyst knowledge of the area, weather conditions and continuity in monitoring, misinterpretation of these two images without the help of optical imagery (such as in the winter or with cloudy skies) would be very likely.

7 Construction of sea ice charts

The NIS produces routine ice charts for the Arctic from Monday through Friday, as part of its operational mandate for METAREA XIX. The ice charts nomenclature and colour code

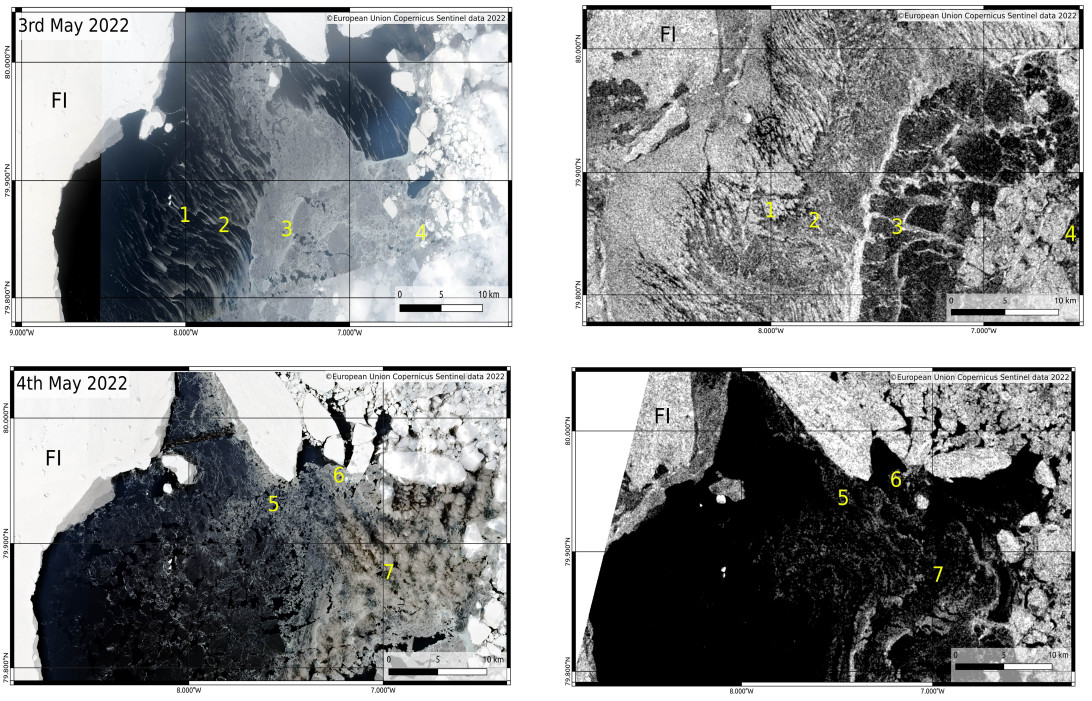

FIGURE 8
Ice watch observations versus satellite imagery for 2 consecutive days. Sea ice SoD and concentration (expressed in 10ths) stated for specific locations along the track of RV *Kronprins Haakon* in Spring 2022. (Copernicus sentinel data 2022, processed by ESA) (CIRFA research cruise 2022).

standards follow the WMO, 2004 Ice Chart Colour Code Standard (WMO/TD-No. 1215) and Sea Ice, 2014 Sea Ice Nomenclature (WMO-259) documents used at all ice services. Ice chart production at the NIS relies on manual analysis from expert ice analysts due to the geophysical limitations of sea ice monitoring as outlined in section 5. Currently, the sea ice charts represent sea ice concentration, ice edge and delineation of fast ice areas.

7.1 Tools and systems

Geographical Information Systems (GIS) software serves as the standard ice charting system for all ice services. It allows for scalable data representation and standardized vector data formats that seamlessly convert to S-411 (ice information product specifications laid out by the IHO) and sea ice grid (SIGRID) standards. This compatibility is vital for users needing information to be transmitted through electronic navigational charts (ENC) onboard ships or in the field. The analysts are supported by a selection of systems designed to automate a number of tasks and aid in the production of an ice chart. At NIS these are set up as part of the Bifrost system and run on various parts of the infrastructure at MET Norway.

The NIS developed an ice charting system using QGIS, an open source geographic information system (QGIS Development Team, 2023). QGIS includes tools for drawing and editing polygons and overlaying various satellite products. It is also compatible with digital drawing tablets, which some analysts prefer over using the mouse. NIS employs customised QGIS profiles which are installed on the analyst work stations. Each day a project is automatically generated with all the required layers available such that an analyst can quickly begin drawing polygons. On Mondays, a fresh ice chart is generated using only the fast ice extent and the ice edge from the previous Friday, while on subsequent days of the week the chart is a copy from the previous day which is then updated to match current conditions.

The various satellite products outlined in Section 4 are downloaded and processed on MET Norway's high performance computing cluster. These are then made available on the analyst's workstation where they can open and view images in QGIS (Figure 9). This processing is almost entirely automated, with the exception of some more bespoke satellite products. Other data used by the analysts, such as weather models and observations are viewed using Diana, a meteorological visualisation and production software developed at MET Norway.

While the ice chart is being drawn, the analyst can run scripts which validate the ice polygons and check for errors which may not be obvious to the naked eye. After the ice chart is completed, the analyst must go through a quality control (QC) process to check the chart, and after this the ice chart can be sent for further processing.

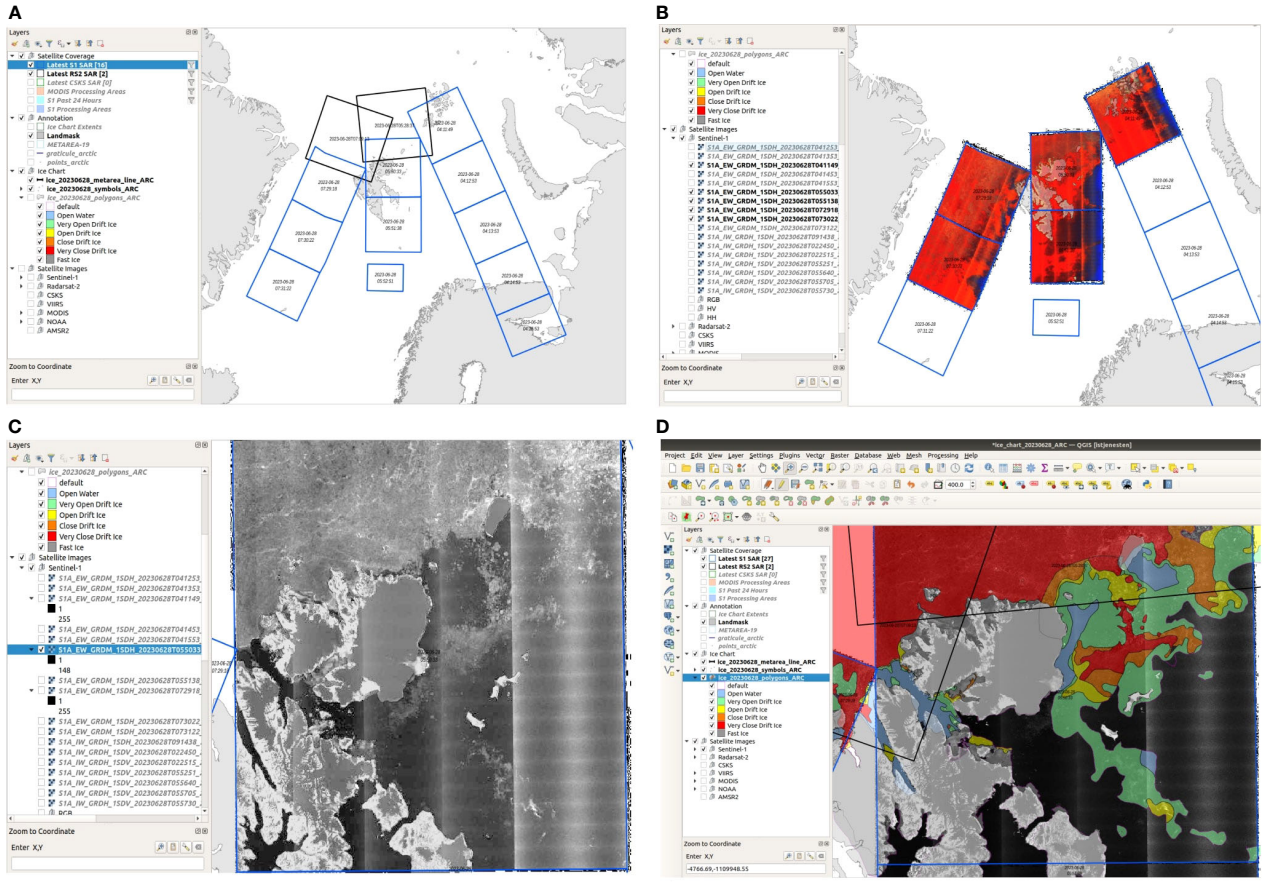

FIGURE 9
Screen shots showing various stages of the ice chart creation process. **(A)** Shows the satellite imagery timestamps loaded automatically on opening of the QGIS project. **(B)** Pre-rendered sentinel 1 SAR imagery selected for the area of interest. **(C)** Zoomed in and rendered Sentinel 1 SAR image from NE Svalbard. Image rendered by changing render type from multiband colour to single band grey and choosing Band 2 (green band), along with increasing the brightness and contrast under colour rendering. **(D)** An underway ice chart for the satellite image in c where the analyst is using their knowledge and experience to identify areas of differing ice concentration.

This primarily involves the production of the various products outlined in the following section, as well as distribution via email and uploads to various other distribution channels.

Inter comparison between analysts and comparison studies of ice charts against models have been carried out with regards to the inherent subjectivity of ice chart creation, showing positive results (Moen et al., 2013; Karvonen et al., 2015; Cheng et al., 2020).

7.2 The sea ice analyst's workflow

Producing an ice chart begins with reviewing weather, wind patterns and temperatures from the previous day. The fast ice, attached to land, is updated as needed throughout the week, unlike drift ice, which requires more frequent updates. Ice analysts align with the Canadian Ice Service, 2005 Manual of Standard Procedures for Observing and Reporting Ice Conditions (MANICE).

Using the satellite imagery, the analyst constructs the ice chart by subdividing a large initial polygon into smaller polygons denoted by primary, secondary and tertiary. Each smaller polygon is then assigned its respective ice concentration in tenths.

Additionally, high-resolution satellite images from the previous night are downloaded, particularly those covering eastern Greenland, to mitigate gaps in satellite coverage later in the day. Analysts receive individual SAR swaths beginning over Nova Zemlya and proceeds westward, ending at NE Greenland. Satellite imagery delivery of individual swaths follow the satellite acquisition from the orbit and the latency is typically less than 3 hours from acquisition to delivery to BiFrost. In exceptional cases, the acquisition is less than one hour for priority swaths from the Collaborative Ground Segment in Norway, or orders through Kongsberg Satellite Services (KSAT).

When drawing the ice chart, analysts prioritize high-traffic areas, focusing on detailed analysis. This includes considering the capabilities of vessels with low or no ice class that travel around Svalbard and snowmobile excursions around Spitsbergen. The sea-ice concentration within individual polygons is determined by tenths of the total ice concentration of an ice

area, adhering to the criteria outlined in MANICE and the WMO Egg Code.

Analysts use all available satellite data to assess the current ice situation. Upon completion of analysis on all imagery, the polygons are quality checked for any invalid polygons or nodes. In areas with gaps in SAR coverage, lower spatial resolution satellite data may be used to supplement. However, analysts possess inherent knowledge of ice precision and can adjust for ambiguities, especially at the Marginal Ice Zone (MIZ) and ice edge. When the ice chart analysis is completed, the Metarea XIX line from southwest Greenland to the eastern part of Franz Joseph Land is drawn. After a quality check for any data errors, the ice chart distributed online. The METAREA XIX line is sent separately into the meteorological weather system. The ice edge coordinates are sent to the coastal radio centre for distribution to fishing vessels. It is important to note that the operational definition of the "ice edge" is considered the line separating open sea from any type of sea ice at a specific time as outlined by the WMO, 2004.

Alternatively, the typical threshold used in climate monitoring is 15 percent, or more, within a 12 - 25km pixel or grid cell. If a pixel or grid cell exceeds 15 percent ice concentration, it is considered ice covered; otherwise it is deemed as ice free. It is important to clarify this distinction when communicating with end-users and stakeholders.

7.3 NIS products

A general ice chart is generated for the entire region, while regional charts for the Baltic, Barents sea, Denmark Strait, Fram Strait, Oslofjord and Svalbard (Figure 10) are also generated from the analyst's daily chart.

The SIGRID-3 file format is currently the standard for all ice services due to its two main advantages of being compact and scalable. This means vector data typically requires less disk space and can be displayed at varying scales without loss of quality. For ice information relevant for users, this allows for information to be easily retained and catalogued for easy access for maritime users, particularly in the field, which has resulted in the development of the IHO S-411 format for use in Electronic Navigational Chart (ENC) systems.

Users can receive ice charts via email covering any of the available regions in PNG, JPG or PDF format, depending on their available bandwidth. Zipped SIGRID-3 and S-411 files can also be provided to users, but require some GIS or ENC knowledge to use. The ice edge position for METAREA-XIX is communicated via telex. All archived ice charts from 1997-present are stored and available on the website for the ice service, available in JPG format, and as Shapefile upon request. Earlier ice charts from 1967 to 2002 can also be found in ACSYS, 2003. Further products provided by

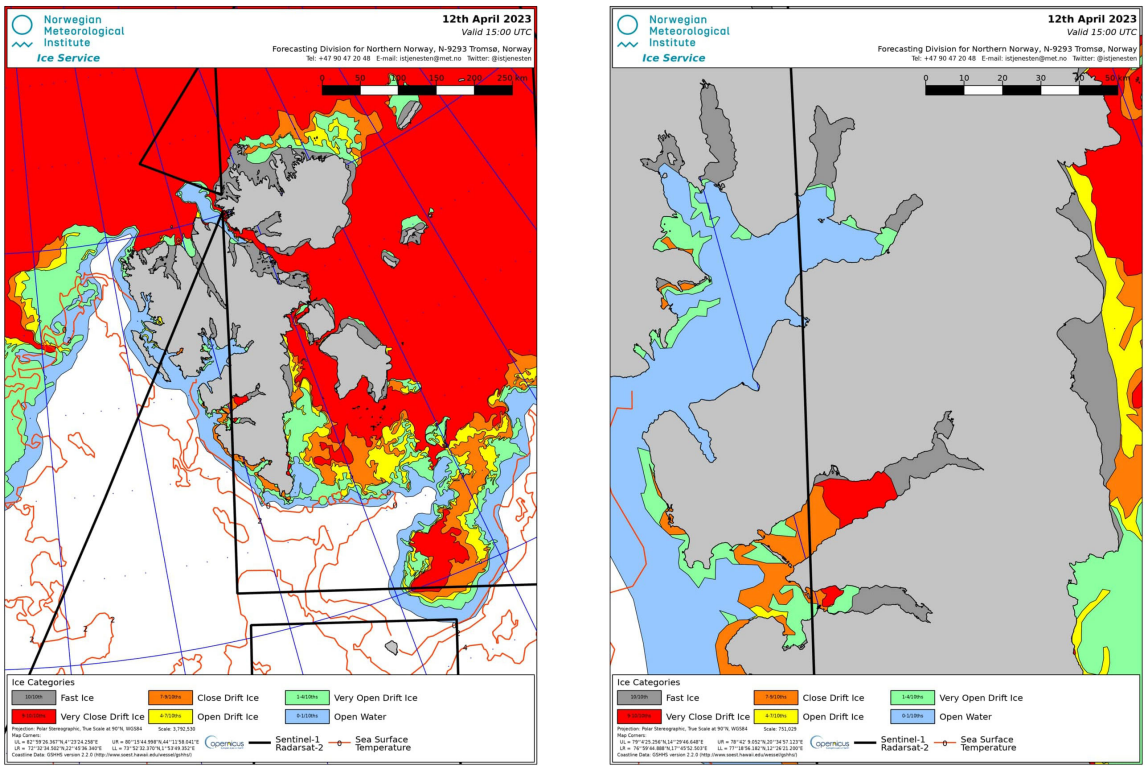

FIGURE 10
Example of a completed regional specific ice chart for Svalbard. Black bounding boxes highlight where satellite imagery was available during construction of the chart to allow for users to know where the greatest reliability of sea ice information is present. Red contour lines delineating sea surface temperatures are taken from a combination of thermal imagery sources according to the data from E.U. Copernicus Marine Service Information (CMEMS), 2023.

the NIS as of 2023 are listed below and can be found at the MET Norway Ice Service webpage.

- Applications of Research to Operations at Mesoscale (AROME) weather prediction and the Regional Ocean Modeling System (ROMS) ocean prediction models integrate NIS gridded data into their systems, and these are distributed publicly through the MET Norway Thredds server. The gridded products are also disseminated via the EU Copernicus Marine Environment Monitoring Service (CMEMS).
- High resolution charts are available for the Svalbard (Isfjord) area.
- A weekly (Monday) Antarctic chart has been produced during austral summers (October to April) since the 2010/2011 season. In addition, a high-resolution chart is issued for the Bransfield Strait and Adelaide Island areas of the Antarctic Peninsula. These charts are produced in collaboration with the U.S. National Ice Center and Russian Arctic and Antarctic Research Institute.
- Visualisations of external short range, 10 day or less, sea ice forecasts at intervals of 24, 48, 72, 96, 120, 144 and 168 hours. The Global Ocean Forecast System version 3.1 (GOFS3.1), Nansen Center Sea Ice Model (neXtSIM) and Barents-25km models are used due to their spatial resolutions being better than 5km, therefore approaching a scale that can better represent finer sea ice edge detail and conditions within the Svalbard fjords. These products are considered as experimental at this stage due to their external creation, meaning the NIS cannot guarantee availability or accessibility of this product.

8 Discussion - future of the NIS

8.1 Ice charting automation

A number of projects have focused on the automation of ice charting procedures with varying degrees of success so far (Dierking, 2020). However, as of yet there is still no algorithm or products that are used for year round sea ice charting and operationally in ice services. The scope of research and literature addressing this work is vast and out of the scope of the paper but relevant information can be found at (KEPLER Project, 2020; Extreme Earth Project, 2021). The more advanced products are in the beta-testing phase and will require further understanding of how they address specific inter-annual and regional variability within each METAREA as highlighted in the Extreme Earth Project, 2021. The challenges are due to a combination of the complexity of satellite images through the shifting seasons (especially spring and summer) and the patchwork nature of SAR imagery in a given region. Another factor limiting automation of ice charting is the time in which analysts have to create an ice chart. Time constraints leave little time for analysts to evaluate an algorithm output and provide quality control for all the inaccuracies, whereby more time is spent on correcting errors than using the traditional manual method. Continued work with improved coverage of relevant satellite sensors, advanced intelligent AI and machine learning algorithms for sea ice mapping and forecasting, and assessments of the seasonal robustness and applicability to seasonal variability, will lead to more semi-automated ice services and enhanced capacity to service users (Karmakar et al., 2023; Khachatrian et al., 2023; Lima et al., 2023). Iceberg detection is also showing promising results with the Constant False Alarm Rate (CFAR) algorithm for object detection. In combination with known Automatic Identification Data (AIS) which can provide input when carrying out high resolution iceberg forecasting. Meanwhile drift models are providing information about areas of all known ice that can be useful in risk assessment and situational awareness for iceberg forecasting (Kubat et al., 2005; Dagestad et al., 2018; Færch et al., 2023).

8.2 Stage of development charts

Sea ice SoD is currently not routinely included in the ice charts at the NIS, however, ice analysts do take into account the ice age and type during the creation of the concentration charts. This is necessary to provide forecasts to users where they can anticipate drift dynamics in changing weather conditions (e.g. old thick ice is much less likely than thin new ice to drift rapidly with changing wind directions).

8.3 User need for reliable sea ice forecasts

There is an overall need from the operational marine community to have reliable, understandable and easily accessible sea-ice forecasts available at multiple time scales. They assist with strategic and route planning (short-term and sub-seasonal), as well as being valuable for long-term planning or logistics (seasonal). Sea ice forecasts typically assimilate data on the spatial scale of sea-ice climate mapping and models, although more advanced techniques for sea-ice thickness allow for resolutions of 5 or more kilometres. While this is felt by some developers to be inadequate, there are few attempts to push for datasets that are more representative of actual ice conditions due to the time and resources used in setting up and running these models (Blockley et al., 2020; Hunke et al., 2020; Wagner et al., 2020; Andersson et al., 2021; Veland et al., 2021; Müller et al., 2023). Drifting sea ice poses a challenge for sea-ice forecasts to accurately assimilate certain parameters such as sea ice SoD or thickness, and concentration, particularly during the late spring and summer seasons due to snow melt. It is especially difficult to convey sea ice in forecasts at the MIZ and along the coastal areas where due to the merging of satellite products from multiple time points and with varying sensor frequency footprints, there is often a smearing of the ice edge and any features of potential interest. A full review of the current state of sea-ice forecasts is out of the scope of this manuscript but refer to Smith et al., 2019 and Fox-Kemper et al., 2019) for a further overview.

It has been demonstrated that assimilation of ice charts improves prediction accuracy of short term forecasts by providing quality controlled and regularly updated information on ice

concentration and potentially stage of development (when available) (Posey et al., 2015; Kvanum et al., 2024). The use of ice charts for initialization into models and forecasts can enable real-time adjustments, that significantly boosts forecasting precision and maritime safety (Hunke et al., 2020).

8.4 Exploitation of new ESA satellite missions

Over the next few years, multiple new satellite missions aim to introduce availability of L-Band SAR. For the NIS, the NASA/Indian Space Research Organisation (ISRO) Synthetic Aperture Radar (NISAR) and Copernicus Radiometer Occultation Scattering Experiment - Lite (ROSE-L) are of most interest. After successful deployment of the satellites, evaluation must take place over the course of the next few years, meaning there is still a delay after the launch date before these satellites are operational. In preparation NIS is engaged in evaluations of the benefits of L-band SAR for sea ice mapping and iceberg detection (Dierking et al., 2022; Færch et al., 2023).

Studies were carried out during the KEPLER project to ascertain the spatial resolution requirements of end users. Results show that the spatial resolution of sea-ice information is of particular concern. The current state of information provision cannot always provide details on sea ice features such as ice type and deformation on the scale that would improve support for the operational marine community; unless it is administered by private or commercial services that need to be prepared in advance. There is a collective need for spatial and temporal resolutions for the Arctic and Baltic operators. New and improved products for the maritime sector are consistently requested in order to provide high resolution ice products based on SAR as well as information on ice thickness and ice type. Table 1 shows the level of interest in spatial scales for different parameters based on whether these were for tactical or planning purposes. High-resolution products for tactical purposes, where high resolution is understood to be on the sub-kilometre scale, are highly sought after. Spatial resolutions on the kilometre scale are of interest at the planning stage for most users, and more commonly in the research community. End-users deemed the kilometre scale too coarse for navigational and tactical use due to the difficulty in detecting features important for maritime operations such as ice concentration at the edge, the marginal ice zone and coastal zones, ice concentration, leads, polynyas and icebergs. In addition, a number of intermediate users noted that this spatial resolution was an impediment to the development of regional forecast products applicable to end-user demands.

In addition to SAR, new missions such as the Copernicus Land Surface Temperature Monitoring (LSTM) are expected to provide TIR imaging at much higher (30–50m) spatial resolution than is presently available, and will be of significant benefit to complement SAR and improve the ability to provide automatic classification at the scales necessary for maritime safety.

8.5 A future ice service process chain

Figure 11 shows the Ice Service process chain, highlighting the impact of preprocessed automated products on the future direction of the Service. The vision for the NIS into the future is a sustainable value chain incorporating high resolution (< 1km) automated sea ice charting algorithms, NRT *in-situ* observations (Ice Watch, 2023) and sea ice analysts in tandem. This will free up time for analysts to give more specific end user support and lay the foundations for production of routine SoD in charts. A more in depth overview of

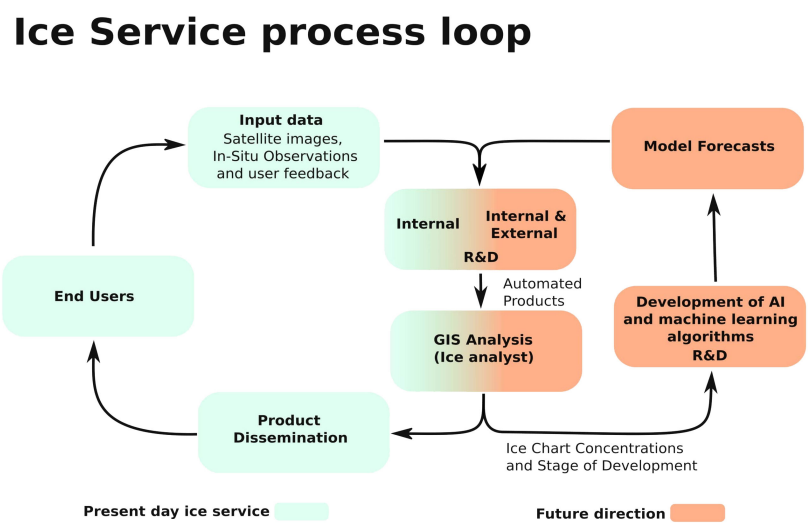

FIGURE 11
The NIS service process chain currently (green) and the direction for the future (red). The hope is that automated products will provide a more regulatory constrained data format to feed into forecast models and eventually to aid in the creation of model forecasts than what is currently available from hand drawn ice charts. This will be aided by an increase in satellite data availability and *in situ* observations from increased boat traffic in the region, especially with regards to the NIS hosted Ice Watch program.

the ice service value chain can be found at the National Snow and Ice Data Center, 2024 webpage.

Ice analysts possess extensive training and experience in comprehending local conditions, meteorological patterns, and the intricate dynamics of ice drift. These factors present ongoing challenges for automation and modelling in comparison to real-world observations. Looking optimistically toward the future, the vision for ice services is to develop products that incorporate pertinent validation metrics, with input from seasoned ice analysts. Such an approach which will enrich and expand our repository of ice-related information.

Author contributions

WC: Writing – review & editing, Writing – original draft, Investigation, Data curation, Conceptualization. PW: Writing – review & editing, Writing – original draft. NH: Writing – review & editing, Writing – original draft. AE: Writing – review & editing, Writing – original draft. TR: Writing – review & editing, Writing – original draft.

Funding

The author(s) declare that financial support was received for the research, authorship, and/or publication of this article. Funding for this article was received from the Research Council of Norway.

Conflict of interest

The authors declare that the research was conducted in the absence of any commercial or financial relationships that could be construed as a potential conflict of interest.

Publisher's note

All claims expressed in this article are solely those of the authors and do not necessarily represent those of their affiliated organizations, or those of the publisher, the editors and the reviewers. Any product that may be evaluated in this article, or claim that may be made by its manufacturer, is not guaranteed or endorsed by the publisher.

References

ACSYS. (2003). *ACSYS Historical Ice Chart Archive, (1553-2002)* (Tromsø, Norway: Arctic Climate System Study). IACPO Informal Report No. 8.

Andersson, T. R., Hosking, J. S., Pe´rez-Ortiz, M., Paige, B., Elliott, A., Russell, C., et al. (2021). Seasonal Arctic sea ice forecasting with probabilistic deep learning. *Nat. Commun.* 12. doi: 10.1038/s41467-021-25257-4

Arthun, M., Onarheim, I. H., Dörr, J., and Eldevik, T. (2021). The seasonal and regional transition to an ice-free Arctic. *Geophys. Res. Lett.* 48, e2020GL090825. doi: 10.1029/2020GL090825

Babb, D. G., Galley, R. J., Howell, S. E. L., Landy, J. C., Stroeve, J. C., and Barber, D. G. (2022). Increasing multiyear sea ice loss in the Beaufort sea: A new export pathway for the diminishing multiyear ice cover of the Arctic ocean. *Geophys. Res. Lett.* 49, e2021GL097595. doi: 10.1029/2021GL097595

Babb, D. G., Kirillov, S., Galley, R. J., Straneo, F., Ehn, J. K., Howell, S. E. L., et al. (2021). Sea ice dynamics in Hudson strait and its impact on winter shipping operations. *Journal Geophys. Res.: Oceans* 126, e2021JC018024. doi: 10.1029/2021JC018024

Barber, D. G., and Massom, R. A. (2007). "Chapter 1 The Role of Sea Ice in Arctic and Antarctic Polynyas," in *Polynyas: Windows to the World*, vol. 74 . Eds. W. O. Smith and D. G. Barber (Amsterdam, Netherlands: Elsevier), 1–54. doi: 10.1016/S04229894(06)74001-6

Blair, B., Andrea, M. U. G., Jelmer, J., Steffen, M. O., and Machiel, L. (2022). Mind the gap! A consensus analysis of users and producers on trust in new sea ice information products. *Climate Serv.* 28, 100323. doi: 10.1016/j.cliser.2022.100323

Blockley, E., Vancoppenolle, M., Hunke, C. Bitz E., Feltham, D., Lemieux, J., Losch, M., et al. (2020). The future of sea ice modeling: where do we go from here?" In. *Bull. Am. Meteorol. Soc.* 101, E1304–E1311. doi: 10.1175/BAMS-D-20-0073.1

Campbell, E. C., Wilson, E. A., Moore, G. W. K., Riser, S. C., Brayton, C. E., Mazloff, M. R., et al. (2019). Antarctic offshore polynyas linked to Southern Hemisphere climate anomalies. *Nature* 570, 319–325. doi: 10.1038/s41586-019-1294-0

Canadian Ice Service. (2005). *MANICE: Manual of Standard Procedures for Observing and Reporting Ice Conditions. Ninth Edition* (Ottawa, Ontario: Crown copyrights reserved. Meteorological Service of Canada). Available at: https://publications.gc.ca/site/eng/9.646757/publication.html. Environment Canada.

Casey, J. A., Howell, S. E. L., Tivy, A., and Haas, C. (2016). Separability of sea ice types from wide swath C- and L-band synthetic aperture radar imagery acquired during the melt season. *Remote Sens. Environ.* 174, 314–328. doi: 10.1016/j.rse.2015.12.021

Cheng, A., Casati, B., Tivy, A., Zagon, T., Lemieux, J.-F., and Tremblay, L. B. (2020). Accuracy and inter-analyst agreement of visually estimated sea ice concentrations in Canadian ice service ice charts using single-polarization RADARSAT-2. *Cryosphere* 14, 1289–1310. doi: 10.5194/tc-14-1289-2020

CHNL. (2020). *Northern Sea Route Information Office*. Available online at: https://arctic-lio.com/.

Dagestad, K. F., Röhrs, J., Breivik, Ø., and Ådlandsvik, B. (2018). OpenDrift v1. 0: a generic framework for trajectory modelling. *Geosci. Model. Dev.* 11, 1405–1420. doi: 10.5194/gmd-11-1405-2018

Dawson, J., Cook, A., Holloway, J., and Copland, L. (2022). "Analysis of Changing Levels of Ice Strengthening (Ice Class) among Vessels Operating in the Canadian Arctic over the Past 30 Years. *ARCTIC* 75 (4), 413–430. doi: 10.14430/arctic75553

Deggim, H. (2018). The international code for ships operating in polar waters (Polar Code). *Sustain. shipping changing Arctic*, 15–35. doi: 10.1007/ 978-3-319-78425-0_2

Dierking, W. (2013). Sea ice monitoring by synthetic aperture radar. *Oceanography* 26, 100–111. doi: 10.5670/oceanog

Dierking, W. (2020). "Maritime Surveillance with Synthetic Aperture Radar, Sea Ice and Icebergs," in *SAR Handbook: Comprehensive Methodologies for Forest Monitoring and Biomass Estimation*. University of Naples Federico II, Naples, Italy: Institution of Engineering and Technology, pp. 173–225. doi: 10.1049/SBRA521E

Dierking, W., Iannini, L., and Davidson, M. (2022). "Joint use of L-and C-band spaceborne SAR data for sea ICE monitoring," in *IGARSS 2022 - 2022 IEEE International Geoscience and Remote Sensing Symposium*, Kuala Lumpur, Malaysia. 4711–4712. doi: 10.1109/IGARSS46834.2022.9884133

Divine, D. V., and Dick, C. (2006). Historical variability of sea ice edge position in the Nordic Seas. *J. Geophys. Res.* 111. doi: 10.1029/2004JC002851

Docquier, D., Fuentes-Franco, R., Koenigk, T., and Fichefet, T. (2020). Sea ice—Ocean interactions in the Barents sea modeled at different resolutions. *Front. Earth Sci.* 8. doi: 10.3389/feart.2020.00172

Drivenes, E.-A. (1994). Adolf Hoel – polar ideologue and imperialist of the Polar Sea. *Acta Borealia* 11, 63–72. doi: 10.1080/08003839408580437

Eayrs, C., Holland, D., Francis, D., Wagner, T., Kumar, R., and Li, X. (2019). Understanding the seasonal cycle of Antarctic sea ice extent in the context of longer-term variability. *Rev. Geophys.* 57, 1037–1064. doi: 10.1029/2018RG000631

E.U. Copernicus Marine Service Information (CMEMS). (2023). *Arctic Ocean - Sea and Ice Surface Temperature*. Toulouse, France.

Extreme Earth Project. (2021). *Implementation and evaluation of the Polar use case - version II* (Extreme Earth Project). Available online at: https://earthanalytics.eu/deliverables.html (Accessed 2024-06-24). Deliverable D5.5.

Færch, L., Dierking, W., Hughes, N., and Doulgeris, A. P. (2023). A comparison of CFAR object detection algorithms for iceberg identification in L- and C-band SAR imagery of the Labrador sea. *Cryosphere Discuss.* 2023, 1–26. doi: 10.5194/tc-2023-17

Fox-Kemper, B., Adcroft, A., Böning, C. W., Chassignet, E. P., Curchitser, E., Danabasoglu, G., et al. (2019). Challenges and prospects in ocean circulation models. *Front. Mar. Sci.* 6. doi: 10.3389/fmars.2019.00065

Haykin, S., Lewis, E. O., Raney, R.K., and Rossiter, J. R. (1994). *Remote sensing of sea ice and icebergs* Vol. 13 (Hoboken, New Jersey, USA: John Wiley & Sons).

Heygster, G., Hendricks, S., Kaleschke, L., Maass, N., Mills, P., Stammer, D., et al. (2009). *L-Band Radiometry for Sea-Ice Applications, Executive Summary of Final Report for ESA ESTEC Contract 21130/08/NL/EL*. Germany: University of Bremen.

Hoel, A. (1929). *The Norwegian Svalbard Expeditions 1906-1926*.

Hovelsrud, G. K., Olsen, J., Nilsson, A. E., Kaltenborn, B., and Lebel, J. (2023). Managing Svalbard tourism: inconsistencies and conflicts of interest. *Arctic Rev. Law Polit.* 14, 86–106. doi: 10.23865/arctic.v14.5113

Hughes, N., Qvistgaard, K., Seppänen, J., Eriksson, P., Kangas, A., Grönfeldt, I., et al. (2020). *KEPLER Deliverable Report: Overall Assessment of Stakeholder Needs*. Available online at: https://kepler-polar.eu/deliverables/index.html.

Hunke, E., Allard, R., Blain, P., Blockley, E., Feltham, D., Fichefet, T., et al. (2020). Should sea-ice modeling tools designed for climate research be used for short-term forecasting? *Curr. Climate Change Rep.* 6, 121–136. doi: 10.1007/s40641-020-00162-y

Huntington, H. P., Zagorsky, A., Kaltenborn, B. P., Shin, H. C., Dawson, J., Lukin, M., et al. (2021). Societal implications of a changing Arctic Ocean. *Ambio* 51 (2), 298–306. doi: 10.1007/s13280-021-01601-2

Ice Watch. (2023). Norwegian Meteorological Institute. Available online at: https://icewatch.met.no/.

Ice Watch ASSIST Data Network, Norwegian Meteorological Institute. (2006). *Ice Watch Program for Sea Ice Observations*. Available online at: https://icewatch.met.no/ (Accessed January 1st 2024).

International Hydrographic Organization (IHO). (2014). *Ice Information Product Specification* (Monaco: JCOMM). Tech. rep. S-411.

International Maritime Organization. (1974). *International Convention for the Safety of Life At Sea* (United Kingdom: International Maritime Organization). Available at: https://www.refworld.org/legal/agreements/imo/1974/en/46856.

Jakobsson, M., Grantz, A., Kristoffersen, Y., and Macnab, R. (2003). Physiographic provinces of the Arctic Ocean seafloor. *Geol. Soc. America Bull.* 115, 1443–1455. doi: 10.1130/B25216.1

Jakobsson, M., Mayer, L. A., Coakley, B., Dowdeswell, J. A., Forbes, S., Fridman, B. E., et al. (2012). The international bathymetric chart of the Arctic ocean (IBCAO) version 3.0. *Geophys. Res. Lett.* 39. doi: 10.1029/2012GL052219

JCOMM Expert Team on Sea Ice. (2014). *SIGRID-3: a vector archive format for sea ice georeferenced information and data. Version 3.0. JCOMM Technical Report 23* (Geneva, Switzerland: WMO & IOC), 40. doi: 10.25607/OBP-1498.2

Jeuring, J., and Knol-Kauffman, M. (2019). *Mapping Weather, Water, Ice and Climate Knowledge & Information Needs for Maritime Activities in the Arctic Survey report*. Available online at: https://salienseas.com/wp-content/uploads/2019/09/SALIENSEAS-Mapping-WWICKnowledge-and-Information-Needs-for-Maritime-Activities-in-the-Arctic_FINAL_20190830.pdf.

Jeuring, J., Knol-Kauffman, M., and Sivle, A. (2019). Toward valuable weather and sea-ice services for the marine Arctic: exploring user–producer interfaces of the Norwegian Meteorological Institute. *Polar Geogr.* 43, 139–159. doi: 10.1080/1088937x.2019.1679270

Jung, T., Gordon, N. D., Bauer, P., Bromwich, D. H., Chevallier, M., Day, J. J., et al. (2016). Advancing polar prediction capabilities on daily to seasonal time scales. *Bull. Am. Meteorol. Soc.* 97, 1631–1647. doi: 10.1175/BAMS-D-14-00246.1

Kangas, A., Seppa¨nen, J., Eriksson, P., Grönfeldt, I., Wagner, P., Hughes, N., et al. (2020). *KEPLER Deliverable Report: Harmonisation and improvement of sea ice mapping products* (Finnish Meteorological Institute Finnish Ice Service). Available at: https://keplerpolar.eu/deliverables/index.html.

Karmakar, C., Dumitru, C. O., Hughes, N., and Datcu, M. (2023). A visualization framework for unsupervised analysis of latent structures in SAR image time series. *IEEE J. Select. Topics Appl. Earth Observ. Remote Sens.* 16, 5355–5373. doi: 10.1109/JSTARS.2023.3273122

Karvonen, J., Vainio, J., Marnela, M., Eriksson, P., and Niskanen, T. (2015). A comparison between high-resolution EO-based and ice analyst-assigned sea ice concentrations. *IEEE J. Select. Topics Appl. Earth Observ. Remote Sens.* 8, 1–9. doi: 10.1109/JSTARS.4609443

KEPLER Project (2020). *Key Environmental Monitoring for Polar Latitudes and Environmental Readiness*. Available online at: https://kepler-polar.eu/deliverables/ (Accessed 2024-06-24).

Kern, S. (2009). Wintertime Antarctic coastal polynya area: 1992–2008. *Geophys. Res. Lett.* 36. doi: 10.1029/2009GL038062

Khachatrian, E., Chlaily, S., Eltoft, T., Dierking, W., Dinessen, F., and Marinoni, A. (2021). Automatic selection of relevant attributes for multi-sensor remote sensing analysis: A case study on sea ice classification. *IEEE J. Select. Topics Appl. Earth Observ. Remote Sens.* 14, 9025–9037. doi: 10.1109/JSTARS.2021.3099398

Khachatrian, E., Dierking, W., Chlaily, S., Eltoft, T., Dinessen, F., Hughes, N., et al. (2023). SAR and passive microwave fusion scheme: A test case on sentinel-1/AMSR-2 for sea ice classification. *Geophys. Res. Lett.* 50, e2022GL102083. doi: 10.1029/2022GL102083

Kim, Y. H., Min, S. K., Gillett, N. P., Notz, D., and Malinina, E. (2023). Observationally constrained projections of an ice-free Arctic even under a low emission scenario. *Nat. Commun.* 14, 3139. doi: 10.1038/s41467-023-38511-8

Koenigk, T., Mikolajewicz, U., Jungclaus, J. H., and Kroll, A. (2008). Sea ice in the Barents Sea: seasonal to interannual variability and climate feedbacks in a global coupled model. *Climate Dynam.* 32, 1119–1138. doi: 10.1007/s00382008-0450-2

Krumpen, T., Gerdes, R., Haas, C., Hendricks, S., Herber, A., Selyuzhenok, V., et al. (2016). Recent summer sea ice thickness surveys in Fram Strait and associated ice volume fluxes. *Cryosphere* 10, 523–534. doi: 10.5194/tc-10-523-2016

Kubat, I., Sayed, M., Savage, S. B., and Carrieres, T. (2005). An operational model of iceberg drift". *Int. J. Offshore Polar Eng.* 15, 26–30.

Kvanum, A. F., Palerme, C., Müller, M., Rabault, J., and Hughes, N. (2024). Developing a deep learning forecasting system for short-term and high-resolution prediction of sea ice concentration. doi: 10.5194/egusphere-2023-3107

Landy, J., Bouffard, J., Wilson, C., Rynders, S., Aksenov, Y., and Tsamados, M. (2021). Improved arctic sea ice freeboard retrieval from satellite altimetry using optimized sea surface decorrelation scales. *J. Geophys. Res.: Oceans* 126, e2021JC017466. doi: 10.1029/2021JC017466

Laroche, S., and Poan, E. (2021). Impact of the arctic observing systems on the ECCC global weather forecasts. *Q. J. R. Meteorol. Soc.* 148, 252–271. doi: 10.1002/qj.4203

Lawrence, H., Bormann, N., Sandu, I., Day, J., Farnan, J., and Bauer, P. (2019). Use and impact of Arctic observations in the ECMWF Numerical Weather Prediction system. *Q. J. R. Meteorol. Soc.* 145, 3432–3454. doi: 10.1002/qj.3628

Lima, R., Vahedi, B., Hughes, N., Barrett, A. P., Meier, W., and Karimzadeh, M. (2023). Enhancing sea ice segmentation in Sentinel-1 images with atrous convolutions. *Int. J. Remote Sens.* 44, 5344–5374. doi: 10.1080/01431161.2023.2248560

Lohse, J., Doulgeris, A. P., and Dierking, W. (2020). Mapping sea-ice types from Sentinel-1 considering the surface-type dependent effect of incidence angle. *Ann. Glaciol.* 61, 260–270. doi: 10.1017/aog.2020.45

Løset, S., and Carstens, T. (1996). Sea ice and iceberg observations in the western Barents sea in 1987. *Cold Reg. Sci. Technol.* 24, 323–340. doi: 10.1016/0165-232X(95)00029-B

Lundesgaard, Ø., Sundfjord, A., and Renner, A. H. H. (2021). Drivers of interannual sea ice concentration variability in the Atlantic water inflow region North of Svalbard. *J. Geophys. Res. Oceans* 126, e2020JC016522. doi: 10.1029/2020JC016522

Luo, B., Luo, D., and Ge, Y. (2023). Origins of Barents-Kara sea-ice interannual variability modulated by the Atlantic pathway of El Niño–Southern oscillation. *Nat. Commun.* 14, 585. doi: 10.1038/s41467-023-36136-5

Mallet, P. E., Claud, C., and Vicomte, M. (2017). North Atlantic polar lows and weather regimes: do current links persist in a warmer climate? *Atmos. Sci. Lett.* 18, 349–355. doi: 10.1002/asl.763

Marchenko, N., Borch, O. J., Markov, S. V., and Andreassen, N. (2015). "Maritime activity in the high north - The range of unwanted incidents and risk patterns"," in *Proceedings International Conference on Port and Ocean Engineering under Arctic Conditions 2015*, Trondheim, Norway.

Massonnet, F., Fichefet, T., Goosse, H., Bitz, C. M., Philippon-Berthier, G., Holland, M. M., et al. (2012). Constraining projections of summer Arctic sea ice. *Cryosphere* 6, 1383–1394. doi: 10.5194/tc-6-1383-2012

Matveeva, T. A., and Semenov, V. A. (2022). Regional features of the Arctic sea ice area changes in 2000-2019 versus 1979-1999 periods. *Atmosphere* 13, 2073–4433. doi: 10.3390/atmos13091434

Meier, W. N., and Stroeve, J. (2022). An updated assessment of the changing Arctic sea ice cover. *Oceanography* 35, 10–19. doi: 10.5670/oceanog

Meleshko, V. P., Pavlova, T., Bobylev, L. P., and Golubkin, P. (2020). Current and projected sea ice in the Arctic in the twenty-first century. *Sea Ice Arctic: Past present Future*, 399–463. doi: 10.1007/ 978-3-030-21301-5_10

Melsheimer, C., and Spreen, G. (2022). Remote sensing of multiyear ice in the Antarctic. *DAC H2022. Leipzig Deutschland* , 21–25. doi: 10.5194/dach2022-284

Metzger, E. J., Helber, R. W., Hogan, P. J., Posey, P. G., Thoppil, P. G., Townsend, T. L., et al. (2017). *Global Ocean Forecast System 3.1 Validation Testing* (Naval Research Laboratory, Stennis Space Center, MS). Tech. rep. NRL/MR/7320–17-9722. Approved for public release; distribution is unlimited.

Mioduszewski, J. R., Vavrus, S., Wang, M., Holland, M., and Landrum, L. (2019). Past and future interannual variability in Arctic sea ice in coupled climate models. *Cryosphere* 13, 113–124. doi: 10.5194/tc-13-113-2019

Mö, N.-A., Solheim, J.-E., Humlum, O., and Falk-Petersen, S. (2020). Changes in Barents Sea ice Edge Positions in the Last 440 years: A Review of Possible Driving Forces. *Int. J. Astronom. Astrophys.* 10, 97–164. doi: 10.4236/ijaa.2020.102008

Moen, M. A., Doulgeris, A. P., Anfinsen, S. N., Renner, A. H., Hughes, N., Gerland, S., et al. (2013). Comparison of feature based segmentation of full polarimetric SAR satellite sea ice images with manually drawn ice charts. *Cryosphere* 7, 1693–1705. doi: 10.5194/tc-7-1693-2013

Müller, M., Batrak, Y., Dinessen, F., Grote, R., and Wang, K. (2023). Challenges in the description of sea ice for a kilometer-scale weather forecasting system. *Weather Forecast.* 38, 1157–1171. doi: 10.1175/WAF-D-22-0134.1

Murphy, D. L., and Cass, J. L. (2012). The international ice patrol: safeguarding life and property at sea". *Coast. Guard J. Saf. Secur. at Sea* 69.

Mustonen, T., Mustonen, K., Saijets, J., Feodoroff, P., Kirillov, J., Mikaelsson, S., et al. (2019). *Report on Deliverable D1.2: Community-Based Observation and Societal Needs*

(EU Project Kepler, Work Package Report). Available at: https://kepler-polar.eu/deliverables/index.html.

National Snow and Ice Data Center. (2024). *International Ice Charting Working Group*. Available online at: https://nsidc.org/noaa/iicwg (Accessed 2024).

Nesterov, A. V., Gavrilov, Y. G., Buzin, I. V., Skutin, A. A., Gudoshnikov, Y. P., Kornishin, K. A., et al. (2023). "Icebergs detection and characterization capabilities: field trials in the Arctic seas," in *33rd International Ocean and Polar Engineering Conference*, Ottawa, Canada: International Society of Offshore and Polar Engineers. doi: 10.17736/10535381

Onarheim, I. H., and Årthun, M. (2017). Toward an ice-free Barents sea. *Geophys. Res. Lett.* 44, 8387–8395. doi: 10.1002/2017GL074304

Onarheim, I. H., Eldevik, T., Smedsrud, L. H., and Stroeve, J. C. (2018). Seasonal and regional manifestation of Arctic sea ice loss. *J. Climate* 31, 4917–4932. doi: 10.1175/JCLI-D-17-0427.1

Overland, J. E., and Wang, M. (2013). When will the summer Arctic be nearly sea ice free? *Geophys. Res. Lett.* 40, 2097–2101. doi: 10.1002/grl.50316

Parsons, J., and Progoulaki, M. (2014). "Promoting safety and managing risks in arctic marine transportation: A best practices approach and the polar code," in *Proceedings of the ASME 2014 33rd International Conference on Ocean, Offshore and Arctic Engineering*. San Francisco, California, USA: American Society of Mechanical Engineers (ASME). doi: 10.1115/OMAE2014-23271

Posey, P., Metzger, E., Wallcraft, A., Hebert, D., Allard, R., Smedstad, O., et al. (2015). Improving arctic sea ice edge forecasts by assimilating high horizontal resolution sea ice concentration data into the US navy's ice forecast systems. *Cryosphere* 9, 1735–1745. doi: 10.5194/tc-9-1735-2015

QGIS Development Team. (2023). *QGIS Geographic Information System. Open Source Geospatial Foundation Project. Version 3.22.* Available at: https://qgis.org [Accessed 20 September 2023].

Regan, H., Rampal, P., Ólason, E., Boutin, G., and Korosov, A. (2023). Modelling the evolution of Arctic multiyear sea ice over 2000–2018. *Cryosphere* 17, 1873–1893. doi: 10.5194/tc-17-1873-2023

Renner, A. H. H., Hendricks, S., Gerland, S., Beckers, J., Haas, C., and Krumpen, T. (2013). Large-scale ice thickness distribution of first-year sea ice in spring and summer north of Svalbard. *Ann. Glaciol.* 54, 13–18. doi: 10.3189/2013AoG62A146

Röhrs, J., Gusdal, Y., Rikardsen, E. S. U., Durán Moro, M., Brændshøi, J., Kristensen, N. M., et al. (2023). Barents-2.5km v2.0: an operational data-assimilative coupled ocean and sea ice ensemble prediction model for the Barents Sea and Svalbard. *Geosci. Model. Dev.* 16, 5401–5426. doi: 10.5194/gmd-16-5401-2023

Rojo, M., Claud, C., Mallet, P.-E., Noer, G., Carleton, A. M., and Vicomte, M. (2015). Polar low tracks over the Nordic Seas: a 14-winter climatic analysis. *Tellus A: Dynam. Meteorol. Oceanogr.* 67 (1), 24660. doi: 10.3402/tellusa.v67.24660

Russian Maritime Register of Shipping (2024). *Russian Maritime Register of Shipping*. Available online at: https://rs-class.org/en/.

Salvó, C. S., Gomez Saez, L., and Arce, J. C. (2023). Multi-band SAR intercomparison study in the Antarctic Peninsula for sea ice and iceberg detection. *Front. Mar. Sci.* 10, 1255425. doi: 10.3389/fmars.2023.1255425

Sandven, S., Spreen, G., Georg, H., Girard-Ardhuin, F., Farrell, S. L., Dierking, W., et al. (2023). Sea ice remote sensing—Recent developments in methods and climate data sets. *Surv. Geophys.* 44, 1653–1689. doi: 10.1007/s10712-023-09781-0

Scardilli, A. S., Salvó, C. S., and Saez, L. G. (2022). Southern Ocean ice charts at the Argentinian Naval Hydrographic Service and their impact on safety of navigation. *Front. Mar. Sci.* 9. doi: 10.3389/fmars.2022.971894

Sea Ice, JCOMM Expert Team on. (2014). sea-ice nomenclature: Snapshot of the WMO sea ice nomenclature WMO No. 259, volume1–terminology and codes; volume II–illustrated glossary and III–international system of sea-ice symbols.

Serreze, M. C., and Meier, W. N. (2018). The Arctic's sea ice cover: trends, variability, predictability, and comparisons to the Antarctic. *Ann. New York Acad. Sci.* 1436, 36–53. doi: 10.1111/nyas.13856

Serreze, M. C., and Stroeve, J. (2015). Arctic sea ice trends, variability and implications for seasonal ice forecasting. *Phil. Trans. R. Soc A* 373, 20140159. doi: 10.1098/rsta.2014.0159

Shi, Q., Yang, Q., Mu, L., Wang, J., Massonnet, F., and Mazloff, M. R. (2021). Evaluation of sea-ice thickness from four reanalyses in the Antarctic Weddell Sea. *Cryosphere* 15, 31–47. doi: 10.5194/tc-15-31-2021

Shuchman, R. A., Onstott, R. G., Johannessen, O. M., Sandven, S., and Johannessen, J. A. (2004). Processes at the ice edge: the arctic". *Synth. Aperture Radar Mar. user's manual*, 373–395.

Singha, S., Johansson, M., Hughes, N. F., Hvidegaard, S. M., and Skourup, H. (2018). Arctic sea ice characterization using spaceborne fully polarimetric L-, C-, and X-band SAR with validation by airborne measurements. *IEEE Trans Geosci Remote Sens.* 56, 3715–3734. doi: 10.1109/TGRS.36

Smith, G. C., Allard, R., Babin, M., Bertino, L., Chevallier, M., Corlett, G., et al. (2019). Polar ocean observations: A critical gap in the observing system and its effect on environmental predictions from hours to a season. *Front. Mar. Sci.* 6. doi: 10.3389/fmars.2019.00429

Spreen, G., Kaleschke, L., and Heygster, G. (2008). Sea ice remote sensing using AMSR-E 89-GHz channels". *J. Geophys. Res.* 113. doi: 10.1029/2005JC003384

Stewart, E. J., Liggett, D., Lamers, M., Ljubicic, G., Dawson, J., Thoman, R., et al. (2019). Characterizing polar mobilities to understand the role of weather, water, ice and climate (WWIC) information. *Polar Geogr.* 43, 95–119. doi: 10.1080/1088937X.2019.1707319

Stocker, A. N., Renner, A. H. H., and Knol-Kauffman, M. (2020). Sea ice variability and maritime activity around Svalbard in the period 2012-2019. *Sci. Rep.* 10, 17043. doi: 10.1038/s41598-020-74064-2

Sumata, H., de Steur, L., and Divine, D. V. (2023). Regime shift in Arctic ocean sea ice thickness. *Nature* 615, 443–449. doi: 10.1038/s41586-022-05686-x

Tietsche, S., Mueller, M., Bertino, L., Garric, G., Goessling, H., Pedersen, L. T., et al. (2020). *KEPLER Deliverable Report: Recommendations for more user-relevant sea-ice forecasts* (European Centre for Medium-Range Weather Forecasts (ECMWF). Available at: https://kepler-polar.eu/deliverables/index.html.

Tilling, R. L., Ridout, A., and Shepherd, A. (2018). Estimating Arctic sea ice thickness and volume using CryoSat-2 radar altimeter data. *Adv. Space Res.* 62, 1203–1225. doi: 10.1016/j.asr.2017.10.051

Turner, J., Guarino, M. V., Arnatt, J., Jena, B., Marshall, G. J., Phillips, T., et al. (2020). Recent decrease of summer sea ice in the Weddell sea, Antarctica. *Geophys. Res. Lett.* 47, e2020GL087127. doi: 10.1029/2020GL087127

U.S. National Ice Center. (2024). (U.S. National Ice Center). Available online at: https://usicecenter.gov/ (Accessed 05 March 2024).

Veland, S., Wagner, P., Bailey, D., Everett, A., Goldstein, M., Rivas, H. R., et al. (2021). Knowledge needs in sea ice forecasting for navigation in Svalbard and the High Arctic. doi: 10.13140/RG.2.2.11169.33129

Wadhams, P. (2000). *Ice in the Ocean. 1st* (Boca Raton, Florida, USA: CRC Press/Taylor and Francis Group). doi: 10.1201/9781482283082

Wagner, P. M., and Hegelund, O. J. (2020). *Key Environmental Monitoring for Polar Latitudes and Environmental Readiness*. Available online at: https://kepler-polar.eu/deliverables/.

Wagner, P. M., Hegelund, O. J., Hughes, N., Qvistgaard, K., Seppänen, J., Eriksson, P., et al. (2019). *Report on Deliverable D1.1: Stakeholder Needs: Maritime Sector Needs* (Norwegian Meteorological Institute - Norwegian Ice Service). Available at: https://kepler-polar.eu/deliverables/index.html.

Wagner, P. M., Hughes, N., Bourbonnais, P., Stroeve, J., Rabenstein, L., Bhatt, U., et al. (2020). Sea-ice information and forecast needs for industry maritime stakeholders. *Polar Geogr.* 43, 160–187. doi: 10.1080/1088937X.2020.1766592

Williams, T., Korosov, A., Rampal, P., and Olasoń, E. (2021). Presentation and evaluation of the Arctic sea ice forecasting system neXtSIM-F. *Cryosphere* 15, 3207–3227. doi: 10.5194/tc-15-3207-2021

WMO. (2004). *Ice chart colour code standard - 259*. Available online at: https://library.wmo.int/records/item/37175-ice-chart-colourcode-standard.

Zhang, Q., and Hughes, N. (2023). Towards a manual-free labelling approach for deep learning-based ice floe instance segmentation in airborne and high-resolution optical satellite images. *EGUsphere.* 2023, 1–27. doi: 10.5194/egusphere-2023-295

frontiers | Frontiers in Marine Science

TYPE Policy and Practice Reviews
PUBLISHED 28 April 2025
DOI 10.3389/fmars.2025.1563900

OPEN ACCESS

EDITED BY
Wolfgang Dierking,
Alfred Wegener Institute Helmholtz Centre for Polar and Marine Research (AWI), Germany

REVIEWED BY
Torbjorn Eltoft,
UiT The Arctic University of Norway, Norway
Jan L. Lieser,
Bureau of Meteorology, Australia
Day Qvistgaard,
Danish Meteorological Institute (DMI), Denmark

*CORRESPONDENCE
John Falkingham
john.falkingham@rogers.com

RECEIVED 20 January 2025
ACCEPTED 06 March 2025
PUBLISHED 28 April 2025

CITATION
Falkingham J (2025) The International Ice Charting Working Group: the first twenty-five years.
Front. Mar. Sci. 12:1563900.
doi: 10.3389/fmars.2025.1563900

The International Ice Charting Working Group: the first twenty-five years

John Falkingham*

International Ice Charting Working Group, Ottawa, ON, Canada

Since 1999, the International Ice Charting Working Group (IICWG) has successfully worked as a forum for the operational ice services and helped them to better meet the needs of their national and international maritime clients through coordination and cooperation in data sharing, standards, training, product development, and research activities. The annual meeting has proven to be a valuable opportunity for the national ice services to meet, along with their partners and clients, to share information about new research developments, implementation successes and failures, and advances in ice information products and services. This paper presents a brief overview of the first twenty-five years of the IICWG, including its raison d'être, the history of its formation, its organization, and its accomplishments.

KEYWORDS

sea ice, iceberg, polar, marine, shipping

1 Introduction

This paper was written on the 25th anniversary of the first meeting of the International Ice Charting Working Group (IICWG). Its purpose is to document its history and celebrate its accomplishments.

Over 25 years, the IICWG has been successful at developing a collegial working relationship amongst the world's ice information services – those governmental organizations that provide information about sea ice, lake ice and icebergs for the safety of marine operations. Several of the original founders have passed away. Many others have retired or moved on to other endeavours and been replaced by their successors. This infusion of new talents and ideas is critical to continuing success but comes with a loss of historical context and appreciation for the founding principles of the IICWG. The intention here is to help preserve that organizational memory as a foundation for the future.

2 What is the IICWG?

2.1 Mission

The IICWG was formed as an *ad-hoc* working group of northern hemisphere national ice services, primarily for the purpose of exchanging information and ideas to help one another better serve their clients. The preamble to the Terms of Reference (IICWG, 2016), adopted at the very first meeting in 1999, clearly and succinctly defines why the IICWG exists and what it does:

> *"Recognizing the ongoing interest of the nations influenced by ice covered seas in the use and protection of these seas; and further recognizing the value and economics of cooperative activities in operational ice services supporting maritime navigation; the ice charting nations of the world hereby form the* International Ice Charting Working Group.

> *"The International Ice Charting Working Group provides a forum for coordination of ice matters, including icebergs, acts as an advisory body for the relevant international sea organizations and programs, in particular, WMO/IOC JCOMM, CLiC, GCOS and IHO, and offers non-binding recommendations to senior management as appropriate …".*

Following the preamble, the Terms of Reference outline the activities that are of interest to the IICWG:

- Data and Product Exchange.
- Terminology, Data and Mapping Standards.
- Operations and Customer Support.
- Training.
- Technology for Analysis and Forecasting.
- Applied Science, Research and Development.

Of central importance in defining the IICWG's mission is the notion that it is concerned primarily with "operational ice services supporting maritime navigation". While research activities and climatological investigations are critical components of an ice service, they are not the focus of the IICWG. The IICWG founders felt that these peripheral aspects were adequately addressed in other fora. It was in the coordination and development of *operational* services that the IICWG was filling a gap and where it should focus its attention. This intention is instilled throughout the Terms of Reference.

2.2 Vision and strategic goals

By 2017, the IICWG felt that a rejuvenation was needed. Many original issues that provided focus had been resolved but changes in the environment, technology, and relationships with other organizations were demanding more and more energy. Under the leadership of co-chairs Diane Campbell, Marianne Thyrring, and Tom Cuff, a concise statement of the IICWG's vision and strategic goals was adopted at the Helsinki meeting in 2018. This was further developed, at the 25th meeting in 2024, into the Vision, Mission, Values and Strategic Goals (IICWG, 2024) attached at Appendix A.

2.3 Members/participants

Throughout its history, the IICWG has been an open group without a sense of requirement for formal membership. Representatives of the national ice services form the core of participation in the annual meetings and undertake the bulk of its work. However, private ice services have also taken an active role in the Working Group. Space agencies, as the suppliers of ice monitoring data, are regular participants in a two-way dialogue with the ice services – providing information about earth observation programs and accepting requirements for ice monitoring. Client groups take part in the IICWG to inform the ice services of their information needs and to influence the services' activities and initiatives accordingly. Research communities join in the Group to share their findings and learn of operational requirements that can help direct their research towards useful ends.

2.4 Clients

From its beginning, the IICWG has maintained a strong focus on the clients of the ice services. Marine transportation operators and regulators, including national maritime administrations and icebreaker operators, shipping companies, Coast Guards, Navies, offshore oil and gas operations, fishing fleets and field research campaigns, are the primary customers of the ice services that participate in the IICWG. Meteorological organizations, policy-makers, marine engineers, and residents in ice-affected regions represent more diverse client sectors. The IICWG tries to understand the needs of their clients by offering, at the yearly meetings, a forum for them to interact directly with the ice services. The Group has shared many instances of best practices in serving clients and has undertaken actions to improve the availability and usability of ice information globally.

2.5 IICWG relationship with legal authorities

As an *ad-hoc* working group, the IICWG is independent and free to establish its own working rules, set its own agenda and act in areas its participants deem worthwhile. Individuals and organizations participate at their own expense. The IICWG has no budget of its own and can reach its objectives only when its individual participants are willing and able to undertake the necessary work. This "*ad-hoc-ness*" has both good and bad aspects. On the positive side, it has allowed the Group to work

quickly to address concerns without the burden of overhead imposed by a bureaucratic organizational structure. However, it also presents difficulties for some participants to get support for IICWG initiatives within their parent (national) organizations and has the disadvantage of uncertain support for on-going activities. To respond to these downsides, the IICWG has positioned itself as an *advisory body* to the established, legal, international authorities.

For the first two decades, the primary connection was with the Joint WMO/IOC Technical Commission for Oceanography and Marine Meteorology (JCOMM) Expert Team on Sea Ice (ETSI) (JCOMM, 2023). JCOMM was a joint commission of the Intergovernmental Oceanographic Commission (IOC) and the World Meteorological Organization (WMO) and enjoyed the support of both of those esteemed bodies. However, as a result, the ETSI was encumbered by IOC/WMO rules, finances, membership limitations and infrequent meetings. The IICWG is not so encumbered and therefore was well positioned to react quickly to arising needs, undertake necessary groundwork and subsequently have a solution incorporated into international practice by referring it to the ETSI for international deliberation and acceptance. Coordination between the IICWG and the ETSI was achieved by maintaining a high degree of overlap in membership and participation.

The JCOMM was dissolved in 2019 and its responsibilities assumed mainly by the WMO. In the recently re-structured WMO organization, the Expert Team on Maritime Safety (ETMS) within the Standing Committee on Marine Meteorology and Oceanography (SC-MMO) is the primary focus for the IICWG. The IICWG has active members in the MMO and ETMS as well as the WMO Global Cryosphere Watch, ensuring continued collaboration and cooperation.

After 25 years of continuing engagement and success, and recognition as an important advisory body by international authorities, including the WMO, International Maritime Organization, and International Hydrographic Organization, it has been suggested that *ad-hoc* is no longer an appropriate description of the IICWG. *"Non-aligned"* might be more accurate.

3 History

3.1 Origins

Prior to the formation of the IICWG, the only global body focusing on operational sea ice information services was the World Meteorological Organization's Sub-Group on Sea Ice (SGSI), a working group of the WMO Commission for Marine Meteorology. Dating from the 1960's, the SGSI was responsible for developing the WMO Sea Ice Nomenclature, the International Sea Ice Symbology and SIGRID – the Sea Ice Grid format for archiving ice chart information in a digital format for climatological purposes. The SGSI also initiated the Global Digital Sea Ice Data Bank (GDSIDB) project to assemble and integrate ice charts from many countries. However, by the 1990's, the SGSI was meeting less frequently and was primarily focused on the GDSIDB. As a result, communication, and coordination between the national ice services on operational matters had suffered.

The countries bordering the Baltic Sea had been meeting regularly in the Baltic Sea Ice Meeting (BSIM) since 1925. Since the 1980s, the United States and Canada had developed a robust forum for collaboration between their ice services in the U.S.-Canada Joint Ice Working Group (JIWG - forerunner of the North American Ice Service). At the 1998 JIWG meeting, the co-chairs, Nancy Cutler (Canada) and Helen Wood (U.S.), noted the success of the JIWG and challenged the group to extend it in an international forum. At a Seattle workshop on ice charts for Arctic climate studies later that same year, Cheryl Bertoia of the U.S. National Ice Center, and Keld Qvistgaard of the Danish Meteorological Institute (DMI) together with Mike Manore of the Canadian ice service and Dennis Conlon of the U.S. Office of Naval Research-Europe (ONR-Europe) discussed the possibility of extending the JIWG concept to other national ice services. The outcome of that discussion was an invitation from DMI to host a meeting under the sponsorship of the three organizations with funding from ONR-Europe.

The first meeting of the International Ice Charting Working Group was held October 5-7, 1999, at the DMI offices in Copenhagen (Figure 1). Forty participants from 11 ice services including Canada, Denmark, Finland, Germany, Iceland, Japan, Norway, Sweden, Russia, the United States, and the International Ice Patrol gathered under the chairmanship of David Grimes (Canada), Helen Wood (U.S.) and Erik Boedtker (Denmark). The focus of the first meeting was largely on information exchange as the Group tentatively explored areas of common interest and how this new group might complement the more formal SGSI. The agenda sessions of that first meeting are instructive as to the interests and intentions of the founders:

FIGURE 1
Inaugural IICWG meeting. Reproduced with permission from https://nsidc.org/iicwg/iicwg-meetings, October 1999 IICWG-I Participant Group Photo — Credit: Vasily Smolyanitsky.

- Sea Ice Observation, Data Sources and Analysis Techniques – report from each service.
- Satellites for Sea Ice Monitoring.
- Ice Operations, Analysis and Forecasting Techniques.
- International Ice Terminology and Symbology.
- Use of Geographic Information Systems (GIS) in Ice Chart Production.
- Icebergs.
- The Future of Ice Information in Electronic Navigation Chart Systems.

The first meeting also discussed the future of the Group and, in agreeing that it could fulfil an important need, decided upon a Terms of Reference, and established two standing committees. Co-chair David Grimes stated in his closing remarks that he "believed that the meeting had been a rousing success." The participants agreed and accepted Iceland's invitation to host a second meeting the following year.

3.2 Annual meetings

In October 2000, the IICWG convened in Reykjavik. The meeting was hosted by the Icelandic Meteorological Office and was chaired by Trausti Jónsson (Iceland), David Grimes (Canada) and Zdenka Willis (USA). As testament to the rapid recognition of the IICWG's importance, this second meeting attracted 53 participants representing 25 organizations in 11 countries, as well as the World Meteorological Organization. Thus began a familiar pattern for IICWG meetings. Representatives from the northern hemisphere national ice services formed the core participation with regular involvement from other organizations including space agencies and satellite data suppliers, universities and research organizations, client groups, and international organizations with interests in Arctic marine activities. The linkage between operations and science was discussed from the beginning and, starting with IICWG-III, Science Workshops became a regular feature of the meetings.

As early as 2010, participants in the IICWG were raising the idea of extending the Group's reach to the southern hemisphere. In contrast to the Arctic, there were no organized public ice services for the Antarctic. Ship traffic was mainly confined to Antarctic research station re-supply with voyage-specific ice information provided by the host nation.

That is not to say that international cooperation was absent when situations demanded. When the M/V "Magdalena Oldendorff" became beset in Antarctic pack ice in June 2002, several ice services cooperated in the successful rescue operation.

However, the decade leading up to 2010 saw a boom in cruise ship tourism in the Antarctic with large cruise ships carrying thousands of passengers into icy waters, often with little or no ice information. The sinking of the cruise ship *M/V Explorer* on 23 November 2007, fortunately without loss of life, underlined the need for improved ice information around Antarctica.

In 2011, the annual IICWG meeting was hosted by the British Antarctic Survey. It marked the beginning of a concerted effort to include the southern hemisphere states responsible for marine safety in Antarctic waters. The first meeting in the southern hemisphere was hosted by Chile in 2014, beginning a pattern of regular southern meetings.

The COVID pandemic forced the IICWG to hold the annual meetings by videoconference in 2020 and 2021. As virtual meeting technology became easier to access and use, subsequent meetings have been conducted in a hybrid format with participants in the room joined by many others on-line. This has permitted access to the meetings from a much wider audience.

Participation in the annual meetings up until 2019 averaged 70-80 individuals, representing some 30 organizations from 15 countries. With the advent of virtual meetings in 2020, participation nearly doubled, a level that has been maintained with hybrid meetings. At the 25th meeting in 2024, 70 ice experts met at the U.S. Naval Postgraduate School with another 70 participating on-line. Fifty-five organizations from 20 countries were represented at that meeting (IICWG, 2024).

The IICWG has issued a press release at each annual meeting since 2007, when the first record low sea ice extent was observed in the Arctic Ocean. Press releases provided brief highlights of the global ice shipping seasons along with some details about that year's meeting. The press releases are available on the IICWG website (https://nsidc.org/noaa/iicwg#anchor-participating-agencies).

Appendix B has a list of the meetings held in the first 25 years.

4 Organization

4.1 The charter

At the 6th meeting in 2005, the IICWG undertook a review of its first five years and determined that its accomplishments were impressive enough to warrant continuing. It was decided that commitment to the Group should be formalized and, over the next two years, the Charter was developed. At the 8th meeting in 2007, hosted by the European Space Agency in Frascati, Italy, in a rather low-key ceremony, the Charter was signed by the original nine participating ice services, including the:

- Canadian Ice Service (Environment Canada).
- Finnish Ice Service (Finnish Institute for Marine Research).
- German Ice Service (Federal Maritime and Hydrographic Agency).
- Greenland Ice Service (Danish Meteorological Institute).
- Norwegian Ice Service (Norwegian Meteorological Institute).
- Arctic and Antarctic Research Institute (Russian Federal Service for Hydrometeorology and Environmental Monitoring).
- Swedish Ice Service (Swedish Meteorological and Hydrological Institute).
- National Ice Center (United States National Oceanographic and Atmospheric Administration).
- International Ice Patrol (United States Coast Guard).

The Charter is a rather innocuous document that merely states the intention of the signatories to "participate in the activities of the IICWG to the best of their abilities" with no legal or financial obligation. Nevertheless, it has served the Group well in solidifying the commitment of the signatories and establishing the IICWG as a significant force in the sea ice and iceberg community.

The Charter has come to represent membership in the Working Group. While many actions are proposed and opinions offered during the open meeting, it is the Charter signatories who decide on what positions to adopt and what actions to undertake. To date, six more ice services have signed the Charter, including:

- Icelandic Meteorological Office, 2008.
- British Antarctic Survey, 2011.
- Polish Institute of Meteorology and Water Management, 2012.
- Argentine Naval Hydrographic Service, 2015.
- Chilean Directorate of Maritime Safety, 2016.
- Australian Bureau of Meteorology, 2023.

A copy of the Charter is attached at Appendix C.

4.2 Terms of reference

Absent from the original Terms of Reference was any prescription for how the IICWG would organize itself and operate. Partly, this reflected its origins. There was a sense that bureaucratic encumbrance was one of the reasons that the WMO Sub-Group on Sea Ice had lost touch with the operational ice services. The Group wanted to maintain its flexibility and "*ad-hoc-ness*" to avoid that pitfall. Undoubtedly, there was also some uncertainty about the sustainability of the new Group.

As the IICWG matured and proved itself to be a valuable continuing Group, an Annex to the Terms of Reference was adopted in 2007 to establish a more formal arrangement for the IICWG co-chairs. Until that time, the appointment of co-chairs had been somewhat arbitrary with Canada and the U.S. taking a primary role along with a third co-chair from the host organization. The Terms of Reference Annex sets out that there should be two co-chairs – one from Eurasia and the other from the Americas. It also specifies that the co-chairs should be at an organizational level higher than the heads of the represented ice services, prescribes the responsibilities of the co-chairs, and stipulates that the co-chairs should rotate every three years, preferably not at the same time.

4.3 Committees and task groups

At the first meeting in 1999, the IICWG established two standing committees - the Applied Science and Research Standing Committee (ASRSC) and the Data, Information and Customer Support Standing Committee (DICSSC). The somewhat unwieldy names of the committees reflect the discussion that led to their creation. Considering the activities of interest as outlined in the Terms of Reference, as many as seven standing committees were initially proposed. However, accepting the realities of IICWG participation possible from each ice service, it was agreed that two committees were most appropriate but that these two committees should embrace the range of IICWG interests. The ASRSC and DICSSC have informally been known as the "science committee" and "data committee" ever since.

Concurrent with the development of the vision and strategic goals in 2018, the IICWG decided to replace the committee structure with a number of dynamic task groups. It was felt that, after 18 years, the committees had become "dumping grounds" for items that lingered on with little action. Task groups were to be focused on specific issues, would have a relatively short life, and had to be led by a "champion". A Co-Chairs' Coordination Committee was established to bring the task group leaders together on a quarterly basis to track progress.

Since 2018, there have been 32 task teams formed, 21 of which completed their work within 1-3 years. The eleven active teams were all initiated in 2021-2023. At time of writing, they are at various stages of completion. A listing of the task teams is attached at Appendix D.

4.4 Secretariat

In 2008 as the IICWG matured, the members decided that a secretariat was needed for more consistency in reporting and follow-up on actions. Previously, this had been the responsibility of rotating meeting hosts. John Falkingham, recently retired from the Canadian ice service, was appointed as the first secretariat and served until 2022 when he was succeeded by John Parker, also retired from Canada's Marine and Ice Services. The secretariat is funded on an informal basis by member organizations, primarily Canada and the United States.

4.5 Website

The IICWG website has been hosted by the U.S. National Snow and Ice Data Center (NSIDC) since 2000 (Figure 2). IICWG business is documented as much as possible on this site and includes reports from the annual meetings, press releases, lists of action items, reports that have been prepared, and relevant documents that have been collected. The site is open freely to the public at large in the spirit of education and cooperation.

5 Accomplishments

There is a lengthy list of accomplishments of the IICWG over its first 25 years. A short list includes implementation of common standards for ice charting globally, advocacy with space agencies for commitments to satellite observations of sea ice and icebergs, collaboration in ice analyst and forecaster training, mutual assistance in operational ice charting including joint international production of ice information, development of ice information

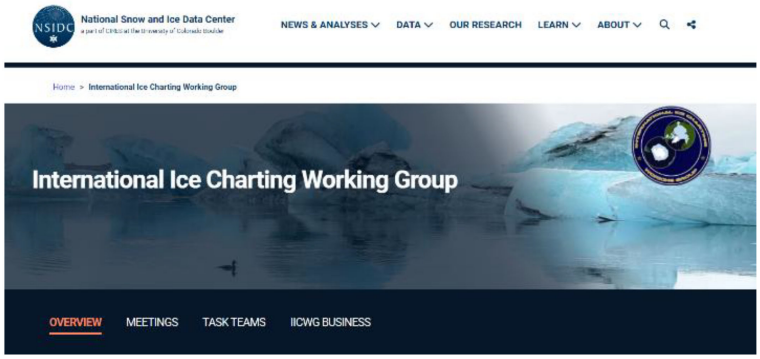

FIGURE 2
IICWG website home page. (http://nsidc.org/noaa/iicwg/).

products for Electronic Navigation Charts, and engagement with mariners to further develop ice information services that are relevant and valuable.

The following section expands on these accomplishments.

5.1 Ice information standards

5.1.1 International ice chart colour standard

One of the first collaborative initiatives that the IICWG undertook was to standardize the colours used on ice charts. In 1999, even though many ice services had started to produce ice charts in colour, there was no common standard for the use of colour. After three years of deliberation and negotiation, a colour code scheme was adopted by the IICWG (Figure 3). In its first formal act as an "advisory body," the IICWG recommended this colour code as an international ice chart standard to the JCOMM Expert Team on Sea Ice. It was subsequently adopted as such and published as JCOMM Technical Report No. 24 in 2004 (JCOMM Expert Team on Sea Ice, 2004).

5.1.2 SIGRID-3: a vector archive format for sea ice charts

The Sub-Group on Sea Ice had previously developed the SIGRID ("Sea Ice Grid") format for archiving ice chart information. SIGRID-1 and -2 both used grid-point schemes for capturing the information on an ice chart. While this format was amenable to digital archiving and large-scale climatological analysis,

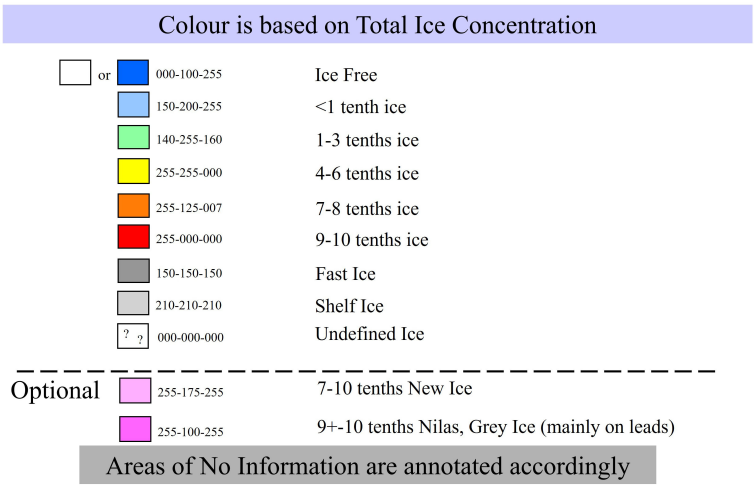

FIGURE 3
International ice concentration colour code. Adapted from JCOMM – Joint WMO-IOC Technical Commission for Oceanography and Marine Meteorology: Ice Chart Colour Code Standard Version 1.0, 2014, Tech. Rep. JCOMM-TR-024, WMO/TD-NO. 1215, World Meteorological Organization and Intergovernmental Oceanographic Commission, https://doi.org/10.25607/OBP-1077, 2014. a, b.

it represented a serious loss of chart information. At IICWG-II, a proposal was made for a new archive format based on vector shapefiles, an open Geographic Information System (GIS) format that could be used to faithfully reproduce the original chart. SIGRID-3 was adopted by the IICWG in 2003 and recommended to the ETSI as an international ice chart archiving and exchange standard. It was subsequently adopted as such and published as JCOMM Technical Report No. 23 (JCOMM Expert Team on Sea Ice, 2004 & 2010 Revision). It remains in use in 2024 to transfer ice charts electronically and is the basis for converting digital ice charts to Electronic Navigation System formats.

5.1.3 Navtex terminology

IICWG formed a working group at its meeting in 2010 to develop and test a standard set of terminology and abbreviations for NAVTEX safety bulletins extending Baltic Sea practice globally. These were adopted the following year and referred to JCOMM. JCOMM accepted the recommendation at its 4th meeting in 2012 and directed the Manual on Marine Meteorology be updated accordingly.

5.1.4 Ice hazard warning standards

In the late 2010s, several ice services, including the International Ice Patrol, were working on ways to depict hazards, specifically for icebergs and sea ice pressure. The aim was to make risk assessment, a requirement of the Polar Code for every voyage near ice, easier for mariners. In 2021, IICWG created two task teams – one to develop standards for iceberg hazard depiction and a parallel one for sea ice pressure. At time of writing in 2024, the work of these teams is continuing involving the science community and mariners.

5.1.5 Sea ice climate product standards

The role of climatological sea ice products has gained increased prominence with the Polar Code requirement for voyage-specific risk assessment. The IICWG recognized that there is a wide variation in the capacities of ice services to provide climate products and in the types of ice climate information made available. In 2023, a task team was created to develop guidance for the harmonization and standardization of sea ice climate products. This work is expected to take several years.

5.2 Ice service cooperation and collaboration

Cooperation and collaboration among the ice services is at the very heart of the IICWG's reason for being. Every ice service faces financial, people, and time constraints. From the beginning, the IICWG participants recognized the benefits that could be achieved by working together to eliminate duplication and optimize their collective efforts (Figure 4). Collaboration at the operational level is not an easy task in a multi-national environment where every organization has its own policies, procedures, technology, and products, not to mention different languages and corporate cultures. While fundamentally similar at a high level, myriad small differences manifest themselves at the working level. Over the course of 25 years, the IICWG has made considerable progress towards interoperability on several fronts.

FIGURE 4
IICWG ice services actively work together and with stakeholders.

5.2.1 Arctic METAREA/NAVAREA coordination

In 2010, the WMO and IMO announced the creation of five new METAREAs/NAVAREAs in the Arctic. The IICWG immediately recognized that there was a need for coordination of ice information at the boundaries between METAREAs served by different ice services (Figure 5). Over the next few years, the IICWG worked with the ETSI to implement a system to maintain a consistent ice edge description around the Arctic Ocean so that ships travelling across multiple METAREAs would see a continuity of information.

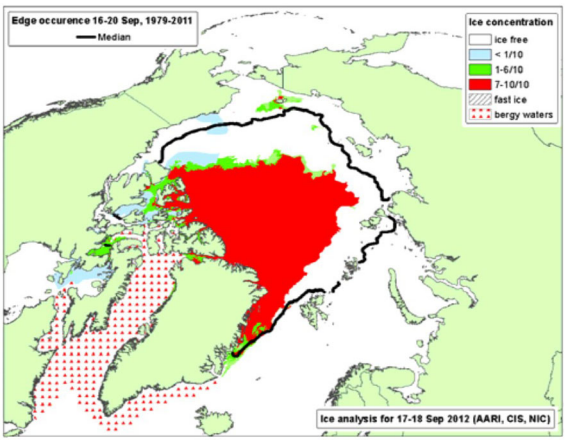

FIGURE 5
Ice Analysis for 17-18 September 2012. Prepared by AARI based on U.S., Canadian and Russian ice charts. Reproduced with permission from IICWG-XIII Meeting Report, https://nsidc.org/iicwg/iicwg-meetings.

5.2.2 Joint production of ice charts

In 2011, the U.S. National Ice Center and Russia's Arctic and Antarctic Research Institute demonstrated capabilities to produce global ice charts based on an integration of charts from different services. Over the next several years, this capability was gradually operationalized so that, since 2015, ice charts around Antarctica have been produced jointly by the U.S., Russia, and Norway with Argentina and Chile contributing complementary regional charts.

In an initiative pre-dating the IICWG, the Canadian ice service and the U.S. National Ice Center jointly produced charts for the shared boundary waters of the Great Lakes. Seeing the advantages this affords both services, the Finnish and Swedish ice services began jointly producing Baltic Sea ice charts in 2017.

The Canadian ice service and the International Ice Patrol have developed a closely integrated iceberg monitoring and modelling system for their shared areas of responsibility in the North Atlantic. The Greenland ice service subsequently joined the collaboration to produce integrated iceberg distribution charts for the North Atlantic.

These initiatives have allowed ice services to concentrate on their local areas of responsibility. Avoiding duplication of effort allows all to devote their resources to providing better ice information services to mariners world-wide. It also provides redundancy of capabilities so that, if one of the partners suffers a system interruption, the others can take over to ensure continued distribution of vital marine safety products. This backup capability has been exercised several times in recent years.

5.2.3 Automation in ice service operations

As science and technology-based organizations, ice services have always been near the forefront of innovation. Automated processes have been integrated into ice service operations for decades and the IICWG has served to spread the experiences throughout the community. As this paper is being written, applications of artificial intelligence are leaping forward in every domain, ice analysis and forecasting being no exception. The IICWG members share knowledge about developments in Artificial Intelligence (AI) applications for satellite image analysis, sea ice and iceberg forecasts in the short- and long-term, ice hazard warnings and risk assessment, and others. The most important current discussions within the IICWG are about how various ice services are integrating automated processes into their operation and about how the human-machine mix will evolve.

5.3 Increasing the availability of ice information globally

The IICWG has strived to increase the availability of quality ice information to mariners in all the polar and sub-polar seas. In some cases, the information is produced but not easily accessible. In other cases, completely new products and services must be developed. Significant progress has been made in twenty-five years, but it is a continuing task to remain abreast of advancing technology and expanding areas and seasons of marine activity in the vicinity of ice.

5.3.1 Iceberg information in Europe

At the first meeting in 1999, a concern was raised about the availability of iceberg information for the North Atlantic. Trans-Atlantic ships faithfully use the International Ice Patrol (IIP) "Limit of All Known Ice" to determine their course across the ocean (Figure 6). The Canadian ice service produces similar charts for waters north of the IIP area of responsibility. While iceberg charts were broadcast daily from North America, they could not be reliably received by ships leaving Europe until they were midway across the Atlantic – after they had already set their great circle sailing route. Since the 1970's, the German ice service had prepared hand-drawn iceberg charts 2-3 times a week, based on the daily IIP reports received via Global Telecommunications System. The charts were transmitted within the regular Marine Radiofacsimile Broadcast Service of the German Weather Service. Vessels were able to receive the iceberg information before setting out.

As a result of the discussion at the IICWG, arrangements were made for the IIP and the Canadian ice service to send their iceberg charts via modern communication directly to the German Weather Service for retransmission from the European side of the North Atlantic.

Prior to 2005, the iceberg charts drawn by Canada and the IIP extended only as far north as southern Labrador. In that year, the Greenland ice service, joined to extend the charts to the bergy waters around the southern tip of Greenland.

5.3.2 Ice logistics portal

As an International Polar Year (IPY) project, the IICWG in conjunction with JCOMM, implemented the Ice Logistics Portal (JCOMM-IICWG, 2018) – so named because, while the IPY was focused on scientific research, ice information was essential for planning logistics for field research campaigns. The Ice Logistics Portal provided a convenient single point of access to all the ice charts produced for every region of the globe. Individual ice services submit their charts in SIGRID-3 format to the portal which provides a simple user interface.

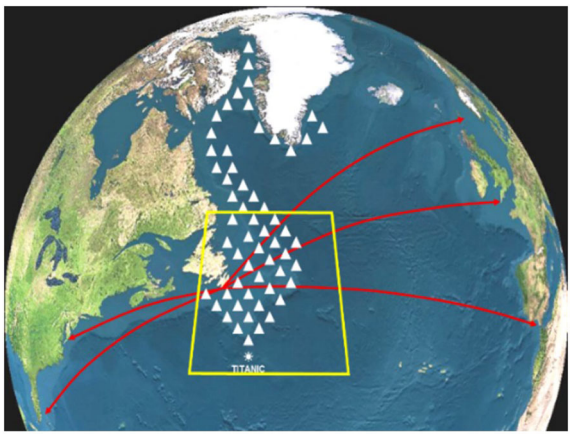

FIGURE 6
International ice patrol area of operations. Reproduced with permission from Michael Hicks, courtesy of International Ice Patrol.

Since 2018, the Ice Logistics Portal has featured prominently on the website of the Arctic Shipping Best Practices Information Forum, an initiative of the Arctic Council to aid in the implementation of the Polar Code. In 2022, discussions were initiated with PolarView aimed at integrating the Ice Logistics Portal with the PolarView portal. PolarView is a private company that operates a web portal delivering (mainly) satellite images of the Arctic and Antarctic sea ice and iceberg areas in near real-time. Thanks to European Commission and European Space Agency support, this service is free of charge to mariners and other users. It has become an extremely important resource for ice navigators. It is widely used to access satellite observations of ice-covered waters. Having ice charts available concurrently with satellite images will help mariners better interpret satellite imagery of ice and provide the greatest detail available for ice navigation.

5.3.3 Ice information for the Southern Ocean

Following earlier discussions about the lack of ice information for the Southern Ocean, the IICWG co-chairs wrote to the JCOMM in 2012 proposing that the Arctic METAREA ice information guidelines for the Global Maritime Distress and Safety System (GMDSS) and SafetyNet Marine Safety Information be implemented for the Southern Ocean. It took only three years, with assistance from the IICWG ice services, for the Argentine Navy Hydrographic Service to implement a permanent operational service issuing daily ice charts for its METAREA VI in 2015. Three years later, Chile began issuing regular ice charts for its METAREA XV.

The first two decades of the 2000's witnessed an increase in the breakup of Antarctic ice shelves which, together with a recent decrease in the amount of protective sea ice, led to a greater number of icebergs drifting further north than usual and into global shipping lanes. Icebergs represent the greatest hazard to shipping in the Southern Ocean. In 2018, an IICWG Task Team was formed to consider what iceberg information could be provided to improve marine safety. Over the next few years, the International Ice Patrol iceberg drift and deterioration model was transferred to Argentina's Naval Hydrographic Service for evaluation and adaptation to Antarctic waters. In 2022, Argentina started issuing iceberg density charts in the format recommended for standardization of iceberg hazard warnings that is under development.

In 2020, another IICWG Task Team was created to investigate the feasibility of implementing a hemispheric floating ice edge – the Southern Ocean Limit Of Known Ice (SOLOKI) – that would be maintained jointly by the five countries with METAREA responsibilities in the Southern Ocean (Figure 7). This task has proved daunting, requiring large quantities of satellite data from several space agencies, automated iceberg detection in the data, and modelling of iceberg drift and deterioration between observations. At time of writing in 2024, the work of this Task Team is continuing.

5.3.4 Ice information for Electronic Navigation Charts

The notion that ice information should become compatible with Electronic Navigation Charts (ENCs) and Electronic Chart Display and Information Systems (ECDIS) was raised at the very first IICWG meeting. It was obvious to all that ENCs represented the future of marine navigation and, since floating ice presents a major navigation hazard in the polar and sub-polar seas, the information traditionally portrayed in ice charts should be available to mariners' ENC systems.

FIGURE 7
The participants in the IICWG toured the Argentine icebreaker A.R.A. Almirante Irizar. Reproduced with permission from IICWG, John Falkingham, IICWG-V Meeting Report, https://nsidc.org/iicwg/iicwg-meetings.

By the meeting in 2006, a Catalogue of Ice Objects had been prepared and subjected to critical review. The Catalogue describes, in rigorous detail, the ice features that can be displayed on an ENC together with their attributes. It represented the first major step towards the ability to provide ice information compatible with Electronic Navigation Charts (ENCs). This Catalogue was given to the Expert Team on Sea Ice for approval as the formal standard for exchanging ice information in a format compatible with ENCs. The ETSI had been denoted the "authority for ice information in ENCs" by the International Hydrographic Organization (IHO). ETSI approved the initial version of the Ice Objects Catalogue in March 2007, and it was subsequently adopted by the IHO as part of the S-57 Standard for the exchange of digital hydrographic data. In 2012, the German ice service, under the leadership of Jürgen Holfort, developed software to convert SIGRID-3 ice chart data to S-57 format for direct ingest into ENCs. The software was given freely to all IICWG ice services.

Over this same time, the IHO was recognizing that the S-57 standard was inadequate to cope with an expanding volume and variety of data and began working on the new S-100 framework for hydrographic standards. The IICWG was at the forefront of this work. The S-411 Standard for Ice Information (Benke, 2014), compatible within the S-100 framework, was adopted by the IHO in 2014, four years before the S-100 framework itself was approved. Software to convert SIGRID-3 to S-411 was shared freely with all ice services. By 2015, most ice charts were available in S-411 format from the Ice Logistics Portal.

The IICWG had, from time to time, discussed the desirability, from the mariner's standpoint, of integrating ice information with weather, wave, and current information. A panel of experts at the 2020 meeting emphasized the idea that ice should not be treated

separately from weather and wave information. The IHO also recognized this and allocated the standards S-412, S-413, and S-414 for weather and wave information (IHO, 2025). At the IICWG meeting in 2023, a session devoted to this topic recognized that the S-411 standard itself needed updating and that harmonization, if not direct integration, with weather and wave standards would be essential. With the termination of the JCOMM and ETSI, the WMO Expert Team on Maritime Safety (ET-MS) has assumed authority for S-411. The close working relationship that the IICWG had enjoyed with the ETSI was carried over into the ET-MS. The IICWG is deeply involved in the re-development of the standards for ice, weather, and wave information for ENCs.

5.4 Space agency engagement

Earth observation data from satellites is critical to the monitoring activities of all ice services, and so it is not surprising that the IICWG meetings included sessions on satellite missions as early as its second meeting. At that time, Synthetic Aperture Radar (SAR) data was used sparingly by most services because of its high cost. The single exception was the Canadian ice service which had access to large quantities of SAR data from the Canadian government RADARSAT program. Much discussion took place concerning the possibility of reducing the cost through bulk purchases and shared access to data. About the same time, the European Space Agency (ESA), in its planning for Envisat, was heading towards a commercialization policy for its new Envisat SAR data. This would have been financially detrimental to the ice services as public services.

The IICWG invited Mark Doherty, Director of Earth Observation at the European Space Agency (ESA), to its 5th meeting in Hamburg in April 2004 to present ESA's views and become better informed on those of the ice services, the largest single group of users of satellite radar data. As a result of this discussion, the IICWG prepared a document that outlined the socio-economic benefits of freely available ice information as well as the specific requirements of the ice services for Earth observation data. The "*Ice Information Services: Socio-Economic Benefits and Earth Observation Requirements*" proved to be a valuable tool in discussions with several space agencies (Figure 8). It was updated in 2007 (Group on Earth Observations, 2007). Eventually, ESA adopted a policy of free and open access to most of its Earth observation data, a policy that the IICWG's advocacy certainly helped to promote and that spurred other agencies to follow suit.

Over the following years, annual meetings invariably included a session where space agencies, and more recently, private satellite data providers, could advise of future missions and receive feedback from the ice services. IICWG spokespersons were regularly invited to space agency planning sessions. The agencies appreciated the fact that the IICWG represented the global ice information services and were able, after internal discussion and debate, to bring forward comprehensive and coherent requirements for ice observations. In 2014, at the request of the Canadian Space Agency, John Falkingham, as IICWG Secretariat, authored *Global Satellite Observation Requirements for Floating Ice* (Falkingham, 2014),

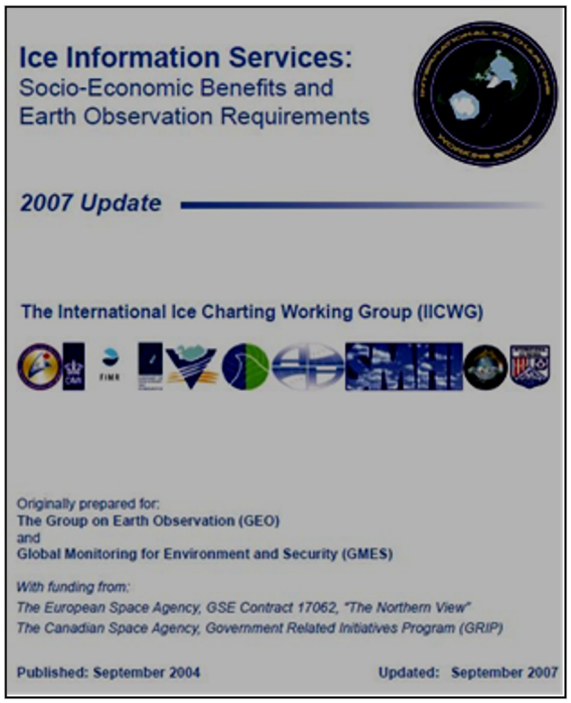

FIGURE 8
Socio-economic benefits and earth observation requirements. Reproduced with permission from Group on Earth Observations (2007).

based on significant input from all the IICWG participants. In 2015, at ESA's invitation, the IICWG developed an updated "statement of requirements for ice observations" for ESA's 5th Earth Observations Programme.

In 2018, the IICWG advocated for both the "Radar Observing System for Europe in L-band (ROSE-L)" and the "Copernicus Imaging Microwave Radiometer (CIMR)" missions, both of which were subsequently approved. In fact, over the ensuing few years, the IICWG was instrumental in providing operational assessments of L-Band SAR data for ice and iceberg observation. Wolfgang Dierking, former chair of the IICWG Research Committee, directed the ESA project "Use of L- and C-band SAR Satellites for Sea Ice Monitoring (LC-ICE)." In addition to numerical simulations of L-Band response to sea ice and icebergs, the ice services of Norway, Greenland, Canada, Argentina, and the International Ice Patrol, conducted real-world assessments of L-band images of ice and icebergs. ROSE-L was subsequently approved by ESA for a future mission and the radar instrument is currently undergoing testing.

The Argentina Space Agency (CONAE) provided L-Band SAR data from its new SAOCOM mission for the LC-ICE project (Figure 9). That grew into the operational use of SAOCOM for monitoring sea ice and icebergs in the Southern Ocean.

In 2022, one of the two ESA Sentinel-1 satellites failed in orbit, severely reducing the amount of SAR data available, particularly impacting ice monitoring in Antarctic waters. In the spirit of collaboration that the IICWG has fostered, the Canadian ice service asked the Canadian Space Agency to alter the RADARSAT Constellation Mission (RCM) mission profile to

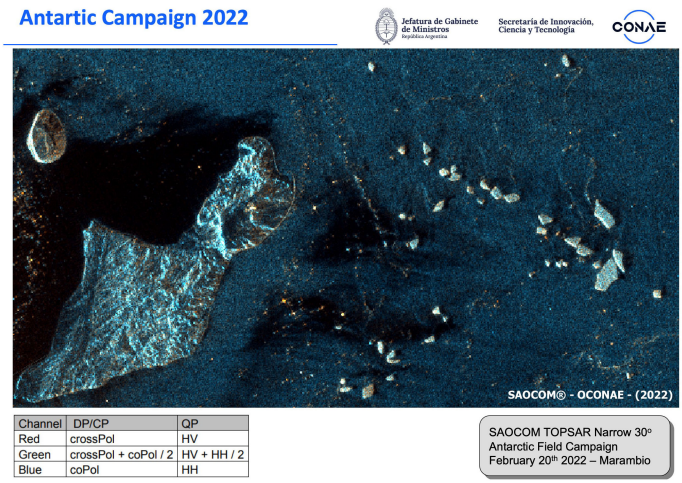

FIGURE 9
SAOCOM Imagery provided by CONAE. Source: Mario Camuyrano of CONAE. Permission from the Argentine Space Agency CONAE.

provide RCM SAR data to the Argentine ice service. It took a bit of time to accomplish, but RCM data eventually filled some critical holes in the observation gap. Without the IICWG, it is virtually certain that the Argentine ice service would not have even known that the RCM could help, much less been able to achieve it. In fact, RCM data was eventually made available to all ice services via the PolarView portal.

The continuing dialogue the IICWG has had with the space agencies throughout its history has proven greatly beneficial for ice monitoring and, by extension, for the safety of mariners in ice laden waters. The facts that there are now commitments to long-term, stable satellite programs for ice monitoring and a culture of free and open data exchange are due, in no small way, to the continuing efforts of the IICWG.

5.5 Engagement with mariners

The main raison d'être of the IICWG is to enhance the safety of marine operations in areas affected by floating ice. The annual meetings have regularly included sessions to interact with mariners to understand, not just their stated needs, but how they actually use ice information in their operations (Figure 10). Mariners have been regular participants in the IICWG meetings. Through presentations, expert panel discussions, small group breakout sessions, and general open discussion, ice services have learned in detail what mariners need in terms of ice information and how it is used. At the same time, mariners have gained a better appreciation for what is possible and how they can better interpret the information they receive.

5.5.1 Mariner training

At the meeting in 2011, David Jackson and Jürgen Holfort were nominated to lead a correspondence group to liaise with the International Maritime Organization (IMO) and the Nautical Institute about mariner training for ice information. The IMO was preparing to introduce the mandatory Polar Code with requirements for knowledge of ice and ice information services. The Nautical Institute, London (UK), representing over 7,000 mariners, was advocating for standardized training and certification in its Ice Navigator Project. Over the next couple of years, a curriculum for an ice information course was developed based on ice knowledge requirements developed by the IICWG. While not all the IICWG recommendations were adopted by the IMO, the major elements are embodied in the requirements for the Polar Code Basic and Advanced Polar Waters Training certificates.

The IICWG meeting in 2015 featured a session on "teaching sea ice and icebergs to mariners" initiated largely in response to the new Polar Code requirements for ice navigator training and certification (Figure 11). In breakout sessions with invited experts, the participants noted many opportunities for the ice services to help improve the training for ice navigators. A key recommendation was that this training should be done through a Maritime Training

FIGURE 10
Aboard icelandic coast guard vessel in 2013.

FIGURE 11
Ice expert giving ice information instruction to mariners. Photo by Bjørn Kay, SIMAC.

Institute with teachers with hands-on experience to ensure that it is compatible with seafarers' certification requirements.

In 2018, representatives from three major maritime training institutes were invited to address the annual meeting and participate in a panel discussion that identified a number of deficiencies and opportunities for the ice services to improve how mariners are trained in the use of ice information. It became clear the maritime training institutes would appreciate closer ties to the ice services. It was equally clear that, because mariners must regularly re-certify their licenses, the connection between mariners and the training institutes lasts throughout their careers – a connection that ice services could benefit from. A follow-on survey of maritime training institutes identified challenges and areas for continued/focused/enhanced collaboration between ice services and maritime training centres.

In 2020, an IICWG task team under the leadership of Keld Qvistgaard, conducted the most extensive survey of polar mariners ever done. Ninety-five responses were received, the majority of which were from ship captains or crew with experience operating in ice in both Polar Regions with a wide range of vessels. Valuable information was received that the IICWG is using to develop better training tools with the maritime training centres. The survey also generated several ideas for pilot projects to explore new ice information products and services.

5.6 Arctic Marine Shipping Assessment

In the face of dramatically decreasing sea ice extent in the Arctic, the Arctic Council initiated the Arctic Marine Shipping Assessment (AMSA) (Arctic Council - PAME, 2009) to conduct a comprehensive study of current and future shipping activity in the Arctic. Lawson Brigham, the lead author for the AMSA, briefed the IICWG meeting in 2006 about the study and solicited input from the participants. John Falkingham subsequently agreed to be a lead author on the Marine Infrastructure chapter. Over the next three years, Mr. Falkingham sought the assistance of IICWG members who made significant contributions, reviewed numerous drafts, and ultimately approved the sections on ice information services that appear in the report. The AMSA was published in 2009 and has been through several updates and revisions over the ensuing years. A key recommendation of the original report was that states "support the updating and the mandatory application of … the Guidelines for Ships Operating in Arctic Ice-Covered Waters" – the forerunner of the Polar Code.

5.7 IMO polar code

IICWG participation in the development and implementation of the Polar Code included, not only ice navigator training requirements and the Arctic Council Best Practices Forum as mentioned earlier but also work on risk assessment. The Polar Code requires vessels operating in and near ice to conduct voyage-specific risk assessment. One tool used by mariners is POLARIS (Bond, 2022), a simple "go/no-go" indication based on ice conditions and ice class related vessel type (Figure 12). IICWG encouraged all ice services to include the stage of ice development (ice thickness) on all ice charts, a key input for POLARIS. Some ice services experimented with prototype products depicting POLARIS Risk Indicators directly and the IICWG considered whether product standards were required. However, at the meeting in 2023, the ice services came to a collective decision that national ice services do not necessarily need to produce POLARIS calculations, but they do need to provide data in flexible, digital formats for others to translate the information into POLARIS.

Engagement with mariners led to discussions on conservatism in the charts produced by ice services that could lead to more restrictive POLARIS risk assessments than necessary. It was understood that this is related to the resolution of ice charts, covering broad areas with the observed or expected ice conditions. It may be one reason that, according to a 2022 survey, POLARIS was not being widely used by ice navigators. The IICWG continues to work with the maritime community as the Polar Code gains prominence.

While POLARIS was an easy solution for the risk assessment requirement, the IICWG recognized that, since it was developed in Canada based on Arctic ice conditions, it may not be applicable to the Antarctic. Projects were proposed to investigate but, to date, resources have not been found to conduct the necessary ship tests. The IICWG has asked the International Association of Antarctic Tour Operators (IAATO) to encourage their members to provide ice observations that would help with this initiative.

5.8 Emergency response

On occasion, vessels become trapped or damaged in sea ice precipitating action by emergency response organizations to assist the vessel, evacuate personnel, or contain potential oil pollution

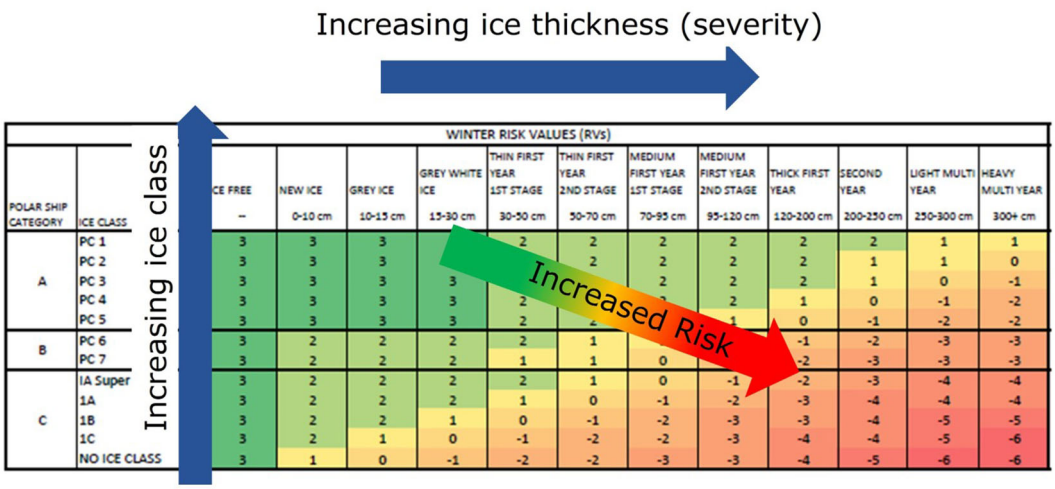

WINTER RISK VALUES (RVs)

POLAR SHIP CATEGORY	ICE CLASS	ICE FREE –	NEW ICE 0-10 cm	GREY ICE 10-15 cm	GREY WHITE ICE 15-30 cm	THIN FIRST YEAR 1ST STAGE 30-50 cm	THIN FIRST YEAR 2ND STAGE 50-70 cm	MEDIUM FIRST YEAR 1ST STAGE 70-95 cm	MEDIUM FIRST YEAR 2ND STAGE 95-120 cm	THICK FIRST YEAR 120-200 cm	SECOND YEAR 200-250 cm	LIGHT MULTI YEAR 250-300 cm	HEAVY MULTI YEAR 300+ cm
A	PC 1	3	3	3		2	2	2	2	2	2	1	1
	PC 2	3	3	3			2	2	2	2	1	1	0
	PC 3	3	3	3	3			2	2	2	1	0	-1
	PC 4	3	3	3	3	2			2	1	0	-1	-2
	PC 5	3	3	3	3	2			1	0	-1	-2	-2
B	PC 6	3	2	2	2	2	1			-1	-2	-3	-3
	PC 7	3	2	2	2	1	1	0		-2	-3	-3	-3
C	IA Super	3	2	2	2	2	1	0	-1	-2	-3	-4	-4
	1A	3	2	2	2	1	0	-1	-2	-3	-4	-4	-4
	1B	3	2	2	1	0	-1	-2	-3	-3	-4	-5	-5
	1C	3	2	1	0	-1	-2	-2	-3	-4	-4	-5	-6
	NO ICE CLASS	3	1	0	-1	-2	-2	-3	-3	-4	-5	-6	-6

FIGURE 12
Polaris risk assessment table. Reproduced with permission from James Bond, courtesy of the American Bureau of Shipping.

(Figure 13). These organizations, typically Coast Guards, need ice information to effectively plan and manage the response. An informal survey of ice services revealed an inconsistent mix of protocols and points of contact between emergency responders and ice service, often relying on personal contacts and informal knowledge. Following a session with the Icelandic Coast Guard at the meeting in 2013, the IICWG ice services agreed to several actions to improve effectiveness, including publication of emergency contact information on the IICWG website, agreement by the U.S. National Ice Center to be a contact point for emergency ice information world-wide, with direct contact numbers for the other ice services. In 2014, the IICWG requested and received clarification on how the International Charter for Space and Major Emergencies could be activated for sea ice emergencies.

Oil response organizations were invited to the 2015 meeting to discuss how the ice services could best inform an incident response. The following year, a table-top exercise simulating a major oil spill in Arctic waters was held with ice services.

5.9 Ice analyst/forecaster training

In the Terms of Reference, training of ice analysts and forecasters was identified as a key activity of the IICWG. The Group recognized that, despite regional differences, there was much commonality between the ice services with respect to the production of ice information. Operational staff in all the services do very much the same work and need essentially the same training. The exchange of training information, practices, and materials has been a regular part of IICWG activities.

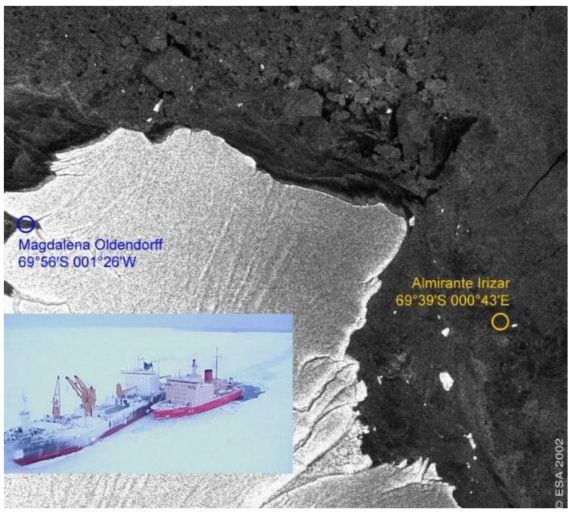

FIGURE 13
ENVISAT ASAR image (section) of 31-07-2002 used for rescue operation for M/V "Magdalena Oldendorff" ©ESA/BSH. Reproduced with permission from IICWG, Klaus Strübing, IICWG XXV Meeting Report, https://nsidc.org/iicwg/iicwg-meetings.

FIGURE 14
IICWG participants share time on a glacier in Iceland in 2013. Photo by IICWG.

The first Ice Analysts' Workshop convened at the German ice service in Rostock in June 2008 to bring working ice analysts together to share methods and best practices through hands-on exercises. Since then, six workshops have been held at six different ice services. The workshops have been extremely successful in promulgating best practices among the operational ice services, introducing ice analysts to new tools and techniques, and devising effective solutions to operational problems.

IICWG meetings originally included a "science day" to give an opportunity for ice forecasters and ice scientists to explore new ideas and developments. It soon became clear that one day was not sufficient for meaningful dialogue and the IICWG established the Sea Ice Data Assimilation and Modelling Working Group in 2006. To date, the Working Group has held 11 workshops to share developments on sea ice modelling and data assimilation – key aspects in forecasting ice conditions.

In 2013, a list of common training needs and tools was compiled. The list has grown with all ice services contributing materials and tools to assist with the training of ice analysts and forecasters. A task team was formed in 2019 to develop competency standards for ice analysts and forecasters as a means of ensuring a standard of quality of products and services offered by the ice services. The competency standards were approved by the WMO in 2023 (WMO, 2023).

5.10 The "soft" successes

Along with all the tangible accomplishments of the IICWG, the value of getting to know one another on a personal level, as well as on a corporate level, cannot be under-estimated. It has resulted in rapid, practical solutions to problems. Barriers of the unknown have been broken down so that ice service staff are less reticent to seek information or advice from their foreign counterparts. It is much easier to ask for help from someone you've shared a pint with or slid down a glacier slope beside (Figure 14). It is easier to refer clients to other ice services when they understand how those services work and what they are capable of. The safety of marine operations in the vicinity of ice has increased and overall service to the global shipping community has improved due to the spirit of collaboration that has been developed within the IICWG.

6 Conclusion

Over twenty-five years, the IICWG has brought the national ice services together with their clients and partners in a growing bond of cooperation and collaboration. This paper has attempted to trace the path that the Group has travelled and chronicle its achievements. While much has been accomplished, there are still many challenges to be met, and the future will undoubtedly reveal many more. Building on the solid foundation that has been established, the IICWG is well positioned to address these challenges with solutions that are both innovative and pragmatic.

Bookending the first quarter century, the 25th annual meeting allocated some time to take stock of its achievements, to review and update its governance, but most importantly, to look to the future – to how science and technology advances can be employed to meet the evolving needs of mariners in a changing ice environment. In her closing address, Naval Postgraduate School President Vice Admiral Ann Rondeau, observed that: "*The science by itself is extraordinary, but it needs to be transferred and applied to operations and actions.*" (IICWG, 2024) - precisely what the IICWG has been advocating and facilitating for 25 years.

As long as ice floats in the ocean, there will be a need for ice information and a role for the International Ice Charting Working Group to bring the information providers together in the interest of safety in the icy seas.

Author's note

The national ice services that participate in the IICWG fall within a variety of organizations in their respective countries' structures. Some are a branch of the Navy or Coast Guard. Others fall within civilian environmental, meteorological, oceanographic, or transportation departments. Only a few, such as the Greenland Ice Service and the Canadian Ice Service (since re-named), actually have "Ice Service" in their formal name. For the sake of brevity and to avoid confusion, I have adopted, throughout this document, the term "<country> ice service" as a generic reference. For example, the "Argentina ice service" refers to the section of the Argentine Naval Hydrographic Service (Servicio de Hidrografía Naval) that provides ice information services. As an exception, I keep the title "U.S. National Ice Center" to distinguish it from the National Weather Service's Alaska Sea Ice Program. I refer to the International Ice Patrol and British Antarctic Survey by their formal names. More information on the organizational structure of the ice services can be found on the IICWG web page (International Ice Charting Working Group).

I have not included specific references. Generally, the information is documented in the reports of the annual meetings of the IICWG (IICWG, n.d.). In addition, I have relied on my own recollections from fourteen years as secretariat.

Ethics Statement

Written informed consent was obtained from the individual(s) for the publication of any identifiable images or data included in this article.

Author contributions

JF: Writing – original draft, Writing – review & editing.

Funding

The author(s) declare that financial support was received for the research and/or publication of this article.

Acknowledgments

Many people have contributed to this paper and to the successes of the IICWG over the past 25 years. Some have passed on. Others have retired or moved to other challenges. Limitations of space and memory will not allow me to name them all. I would like to thank Klaus Strübing and Nick Hughes for their review and valuable additions to the manuscript. The author wishes to thank WMO's Global Cryosphere Watch for financial support to publish this paper.

Conflict of interest

The authors declares that the research was conducted in the absence of any commercial or financial relationships that could be construed as a potential conflict of interest.

Generative AI statement

The author(s) declare that no Generative AI was used in the creation of this manuscript.

Publisher's note

All claims expressed in this article are solely those of the authors and do not necessarily represent those of their affiliated organizations, or those of the publisher, the editors and the reviewers. Any product that may be evaluated in this article, or claim that may be made by its manufacturer, is not guaranteed or endorsed by the publisher.

Supplementary material

The Supplementary Material for this article can be found online at: https://www.frontiersin.org/articles/10.3389/fmars.2025.1563900/full#supplementary-material

References

Arctic Council - PAME. (2009). *Arctic Marine Shipping Assessment 2009 Report* (Akureyri, Iceland: Arctic Council - Protection of the Arctic Marine Environment Working Group). Available at: https://www.pame.is/ourwork/arctic-shipping/previous-shipping-projects/arctic-marine-shipping-assessment/ (Accessed March 15, 2025).

Benke, A. (2014). *Ice Information Product Specfication*. (Retrieved from Baltic Sea Ice Service). Available at: https://www.bsis-ice.de/S411/Docs/S-411_Specification_1_0_0_18032014.pdf (Accessed March 15, 2025).

Bond, J. (2022). *IMO Polaris Update: Current Usage and Status* (London, U.K.: International Maritime Organization). Available at: https://wwwcdn.imo.org/localresources/en/About/Events/Documents/Polar%20Maritime%20Seminar%202022%20presentations/Day%201/10_James_Bond-IMO%20POLARIS%20Update%20%20Current%20Usage%20and%20Status.pdf (Accessed March 15, 2025).

Falkingham, J. C. (2014). *Global Satellite Observation Requirements for Floating Ice - Focusing on Synthetic Aperture Radar (Global Cryosphere Watch)* (Geneva: WMO Polar Space Task Group). Available at: https://wmoomm.sharepoint.com/sites/wmocpdb/eve_activityarea/Forms/AllItems.aspx?id=%2Fsites%2Fwmocpdb%2Feve%5Factivityarea%2FWMO%20Space%20Programme%20%28WSP%29%2F2%2E%20Meetings%2FPSTG%2FPSTG%2D4%2FPSTG%2D4%5FDoc%5F08%2D04%5FGlobSatObsReq%2DFloatingIce%2Epdf&parent=%2Fsites%2Fwmocpdb%2Feve%5Factivityarea%2FWMO%20Space%20Programme%20%28WSP%29%2F2%2E%20Meetings%2FPSTG%2FPSTG%2D4&p=true&ga=1 (Accessed March 15, 2025).

Group on Earth Observations. (2007). *Ice Information Services: Socio-Economic Benefits and Earth Observations Requirements* (Boulder, Colorado: International Ice Charting Working Group). Available at: https://o365coloradoedu.sharepoint.com/sites/NSIDC-MT-IICWG/Shared%20Documents/Forms/AllItems.aspx?id=%2Fsites%2FNSIDC%2DMT%2DIICWG%2FShared%20Documents%2FGeneral%2FIICWG%2DBusiness%2FIICWG%5FSE%5F2007%5FUpdate%5FFinal%5F%2Epdf&parent=%2Fsites%2FNSIDC%2DM (Accessed March 15, 2025).

IHO. (2025) *International Hydrographic Organization S-100 based Product Specifications WMO S-411 to S-420*. Available online at: https://iho.int/en/wmo-s-411-to-s-420 (Accessed April 21, 2025).

IICWG. (n.d). *IICWG Meetings* (Boulder, Colorado: International Ice Charting Working Group). Available at: https://nsidc.org/noaa/iicwg/iicwg-meetings (Accessed March 15, 2025).

IICWG. (2016). *IICWG Charter* (Boulder, Colorado: International Ice Charting Working Group). Available at: https://nsidc.org/noaa/iicwg#anchor-iicwg-charter (Accessed March 15, 2025).

IICWG. (2024). *Excutive Summary Report - 25th Meeting of the International Ice Charting Working Group* (IICWG, Boulder, Colorado: International Ice Charting Working Group). Available at: https://nsidc.org/iicwg/iicwg-meetings (Accessed March 15, 2025).

JCOMM. (2023). *Overview Joint WMO/IOC Technical Commission for Oceanography and Marine Meteorology (JCOMM)* (Geneva: WMO). Available at: https://community.wmo.int/en/activity-areas/Marine/JCOMM/Overview#Programme-Areas (Accessed March 15, 2025).

JCOMM Expert Team on Sea Ice. (2004). *Ice Chart Colour Code Standard - WMO/TD-No.1215* (Geneva: WMO). Available at: https://library.wmo.int/viewer/37175/download?file=wmo-td_1215_en.pdf&type=pdf&navigator=1 (Accessed March 15, 2025).

JCOMM Expert Team on Sea Ice. (2004 & 2010). *SIGRID-3: A Vector Archive Format for Sea Ice Charts* (Geneva: WMO). Available at: https://library.wmo.int/viewer/37171/download?file=wmo-td_1214_2010.pdf&type=pdf&navigator=1 (Accessed March 15, 2025).

JCOMM-IICWG. (2018). *Ice Logistics Portal*. (Cambridge: Polar View). Available online at: https://www.icelogistics.info/ (Accessed March 15, 2025).

WMO. (2023). Ice Forecasting Competency Framework (WMO Executive Council 76 - Record of Decisions) (Geneva: WMO). Available at: https://meetings.wmo.int/EC-76/_layouts/15/WopiFrame.aspx?sourcedoc={6b6e357a-5c57-499d-9d44-94914fc441d8}&action=default (Accessed March 15, 2025).

frontiers | Frontiers in Marine Science

TYPE Original Research
PUBLISHED 07 July 2025
DOI 10.3389/fmars.2025.1588769

OPEN ACCESS

EDITED BY
Joey Voermans,
The University of Melbourne, Australia

REVIEWED BY
Dany Dumont,
Université du Québec à Rimouski, Canada
Ayumi Fujisaki-Manome,
University of Michigan, United States

*CORRESPONDENCE
Keguang Wang
keguang.wang@met.no

RECEIVED 06 March 2025
ACCEPTED 10 June 2025
PUBLISHED 07 July 2025

CITATION
Wang K, Wang C, Hughes N and Ali A (2025) Improving short-term forecasts of sea ice edge and marginal ice zone around Svalbard. *Front. Mar. Sci.* 12:1588769. doi: 10.3389/fmars.2025.1588769

Improving short-term forecasts of sea ice edge and marginal ice zone around Svalbard

Keguang Wang[1]*, Caixin Wang[1], Nick Hughes[2] and Alfatih Ali[3]

[1]Department of Research and Development, Norwegian Meteorological Institute, Oslo, Norway,
[2]Department of Research and Development, Norwegian Meteorological Institute, Tromsø, Norway,
[3]Department of Research and Development, Norwegian Meteorological Institute, Bergen, Norway

Sea ice is a major threat to marine operations around Svalbard, and accurate short-term (1–5 days) forecasts of sea ice edge (SIE) and marginal ice zone (MIZ) are crucial for safe marine operations. In this paper, we investigate the effects of assimilating the AMSR2 sea ice concentration (SIC), the Norwegian sea ice chart, and the OSTIA sea surface temperature (SST) on the short-term forecasts of SIE and MIZ around Svalbard. The used model, Barents-LAON, is based on the coupled ROMS-CICE model with the Local Analytical Optimal Nudging (LAON) for data assimilation. The assimilation effects are evaluated through seven model experiments, from Free run to the full assimilation of OSTIA SST, AMSR2 SIC, and ice chart. The results show that the Free run of Barents-LAON contains a large cold bias, which significantly overestimates the sea ice extent and underestimates the SST. Assimilation of SST mildly improves the analyses of SIE and MIZ, and additional assimilations of AMSR2 SIC and ice chart considerably improve the analyses and forecasts. We show that 1–3 days of forecasts of SIE and MIZ with assimilations of both SIC and SST outperform the CMEMS operational forecasts TOPAZ5 and neXtSIM, the US Navy GOFS3.1 system, and the Norwegian Meteorological Institute's Barents-EPS. The assimilation of both ice chart and OSTIA SST is shown to have the largest improvement for MIZ analysis and forecasts. All the Barents-LAON short-term SIE forecasts with assimilations of SIC and SST outperform the sea ice chart persistence forecasts after the first day. However, all the MIZ forecasts, regardless of using the operational models or the current model experiments, are shown to have lower skills than the sea ice chart persistence. This suggests two possible defects: 1) the present AMSR2 SIC is not sufficiently accurate for separating MIZ from dense pack ice, and 2) some important physical processes may be lacking for the transformation between dense pack ice and MIZ in the present coupled ocean and sea ice models.

KEYWORDS

short-term forecast, AMSR2 sea ice concentration, sea ice chart, OSTIA sea surface temperature, local analytical optimal nudging, sea ice edge, marginal ice zone

1 Introduction

Svalbard is the northernmost territory of Norway, composed of an archipelago in the Arctic Ocean about midway between mainland Norway and the North Pole. Compared to other areas at similar latitudes, the climate on Svalbard and the surrounding seas is considerably milder, wetter, and cloudier, due mainly to the atmospheric heat and moisture transport associated with the warm West Spitsbergen Current (AMAP, 2017). As a result, Svalbard waters have long been an area of high-level maritime activities from a pan-Arctic perspective (Olsen et al., 2020). Along with the reducing Arctic sea ice, there is a continuous growth in marine activities such as shipping, fisheries, tourism, and oil and gas exploration around Svalbard (AMAP, 2017; Olsen et al., 2020), with remarkable increases in the operational seasons and navigational areas (Stocker et al., 2020).

Sea ice is a major threat to ships and offshore operations around Svalbard. In general, operations in sea ice would require ice-strengthened vessels or icebreakers with a sufficient ice class. Offshore platforms, harbors, and coastal loading terminals would also require much stronger construction than those in ice-free waters. However, most ships and fishing vessels are not well ice-strengthened; therefore, they must be run in a confined area for safety purposes. In such a case, it is critically important to frequently monitor and accurately predict the sea ice conditions to assist safe marine operations. Accurate short-term (1–5 days) forecasts of sea ice edge (SIE) and marginal ice zone (MIZ) are of particular importance for supporting such marine operations around Svalbard.

SIE is the demarcation between open sea and sea ice of any kind (WMO, 2014). It can generally be separated into two types: compacted and diffuse. The compacted SIE refers to the close and clear-cut SIE, which is compacted commonly by winds/currents and occasionally by waves. The diffuse SIE refers to the poorly defined SIE, which has an area of dispersed ice. In practical usages, SIE is often defined as the demarcation where sea ice concentration (SIC) equals 0.15 in the passive microwave radiometer (PMR) sea ice mapping and climate modeling communities. By contrast, it is often defined as the demarcation where SIC = 0.1 in the operational ice charting community, such as the Norwegian Meteorological Institute ice chart (https://cryo.met.no) and US National Ice Center (NIC) ice chart (https://usicecenter.gov/Products). To our knowledge, there have been no intercomparison studies for these two SIE definitions. Basically, the ice chart combines a large number of satellite observations, so it generally provides a more accurate description of the SIE. By contrast, the PMR tends to underestimate the SIC in low SIC areas (Cavalieri, 1994; Breivik et al., 2009; Kern et al., 2019; Wang et al., 2024). As a result, the SIE in the ice chart generally defines a larger sea ice extent than in the PMR observations, when they use the same SIC of 0.1 for demarcation. Using a higher SIC (0.15) in the PMR observations tends to provide a SIE even more inside into the sea ice area compared with using SIC = 0.1. Therefore, except for compacted SIE, the SIE in the sea ice chart generally defines a larger sea ice extent than that in the PMR observations. In the current study, we have used SIC = 0.1 as the demarcation for model SIE, which agrees with the ice charting practice. Wang et al. (2023) argue that choosing SIC = 0.1 as the demarcation for SIE has several benefits. Most importantly, it has a clear physical representation that distinguishes open water (SIC < 1/10) and very open drift ice (SIC in 1–3/10), as defined in WMO (2014). In addition, it provides a consistent definition for the joint sea ice modeling and charting community. Here, we also use SIC = 0.1 as the demarcation for SIE.

According to WMO (2014), MIZ is defined as the region of an ice cover affected by waves and swell penetrating into the ice from the open ocean. Typical MIZ conditions are found along the southern edges of the ice pack in the Bering Sea, Greenland Sea, and Barents Sea, in the Baffin Bay, and along the complete northern edge of the Antarctic ice cover (Røed and O'Brien, 1983). MIZ is a dynamic zone under strong interactions between the atmosphere, ocean, sea ice, and waves, frequently with strong atmosphere-ice-ocean activities such as rapid sea ice freezing/melting (Josberger, 1983; Tucker et al., 1991), mesoscale ocean and atmosphere eddies (Johannessen et al., 1987; Inoue and Hori, 2011), turbulence (Padman and Dillon, 1991; Sunfjord et al., 2007), and ocean upwelling and downwelling (Røed and O'Brien, 1983; Häkkinen, 1986), therefore playing a critical role in the polar climate system. Due to the relatively low SIC and SIT, the MIZ is also an area much more navigable than the inner dense pack ice (Stephenson et al., 2011). Ocean waves and swell are the primary source of energy for ice breakup in the MIZ and are, therefore, the main driver determining its properties and extent (Squire et al., 1995; Squire, 2007; Dumont et al., 2011). The relatively small ice floes in the MIZ influence the mechanical properties of the ice and, thus, its response to winds and ocean waves and currents (Shen et al., 1987; Feltham, 2005). These small ice floes have a significant effect on the summer sea ice melting due to the increased lateral perimeters compared to large ice floes over the same area (Steele, 1992).

Due to the complicated interactions between atmosphere, ocean, sea ice, and waves, accurate modeling of MIZ is still one of the most challenging tasks in the sea ice research, particularly the MIZ dynamics (Bennetts et al., 2022; Dumont, 2022). In order to quantify the MIZ, Wang et al. (2024) separate the MIZ as traditional MIZ and dynamical MIZ. The traditional MIZ is defined solely on the basis of the SIC, commonly being [0.1–0.8]. By contrast, the dynamical MIZ can be parameterized through a combination of SIC and SIT. Although not adequate for describing the MIZ dynamics, the traditional MIZ has been applied in a large number of MIZ-related problems, such as sea ice charting (e.g., the NIC ice chart), satellite observations (e.g., Strong, 2012; Liu et al., 2019), primary productions (e.g., Barber et al., 2015), marine ecosystems (e.g., Wassmann, 2011; Arrigo, 2014), and ship navigation (e.g., Palma et al., 2019). Because the dynamical MIZ has not been systematically observed and its theory is still under development, in this study, we only consider the modeling of the traditional MIZ, which has been available in operational ice services for decades.

Sea ice around Svalbard, particularly in the Fram Strait and Barents Sea, is strongly affected by the atmosphere circulation (Vinje, 2001; Maslanik et al., 2012), and the northward Atlantic warm water (Sandø et al., 2010; Smedsrud et al., 2013).

Consequently, the sea ice conditions in this area are often under rapid and complex changes, resulting in extra challenges in accurate predictions of SIE and MIZ. Several operational sea ice forecast models have been monitored in the Norwegian Meteorological Institute with a focus on the evaluation of the forecast skills. These model systems include TOPAZ4 (Sakov et al., 2012) and its successor TOPAZ5 (now operational) and neXtSIM (Williams et al., 2021) at the EU Copernicus Marine Environmental Monitoring Service (CMEMS), the Global Ocean Forecasting System (GOFS 3.1) at the US Naval Research Lab (Posey et al., 2015), and the Barents-2.5km Ensemble Prediction System (Barents-EPS) at the Norwegian Meteorological Institute (Röhrs et al., 2023). It is often seen that the first 2 days of forecasts of these operational models have larger integrated ice edge error (IIEE) than persistence forecast.

The discrepancy between the modeled and observed SIE and MIZ has long been noticed in the operational sea ice forecasts and climate simulations. It is suspected that the insufficient representation of the MIZ processes, particularly the wave-ice interaction, may be the main reason for the low prediction capabilities of the sea ice models (Kohout et al., 2014; Dumont, 2022). In this study, we show that lack of accurate sea ice observations may be another important reason, since the widely used PMR generally has a poor capability in capturing low SIC (Cavalieri, 1994; Breivik et al., 2009; Kern et al., 2019; Wang et al., 2024). Assimilation of such biased observations would, therefore, also induce similar biases. In fact, a close inspection of the operational forecasts indicates that the IIEE is already large in the first day forecast, whereas the increase in the IIEE remains relatively small in the later days. This suggests that the main IIEE of the operational forecasts is in the initial condition, resulting from the data assimilation of PMR observations.

The main purpose of this study is to investigate whether and to what extent the assimilation of AMSR2 SIC and ice chart can improve the short-term forecasts of SIE and MIZ. Using the Local Analytical Optimal Nudging (LAON) method, Wang et al. (2023) assimilated the high-resolution AMSR2 SIC in a pan-Arctic coupled ocean and sea ice model (HYCOM-CICE). It is found that the LAON assimilation can significantly improve the simulated SIC and produce significantly more accurate SIE and MIZ than the CMEMS analyses TOPAZ4 and neXtSIM, as well as the PMR satellite observations AMSR2 SIC. In this study, we apply the LAON method in a regional coupled ocean and sea ice model (Barents-LAON) for the assimilation of AMSR2 SIC and sea ice chart. Due to the large systematic bias of the model system, we here also assimilate SST to avoid large bias of the simulated sea ice cover.

The present study is organized as follows. In section 2, we describe the regional coupled ocean and sea ice model system Barents-LAON. Section 3 introduces the observed SIC for assimilation and evaluation, as well as four SIC products from operational forecast models. Section 4 describes the evaluation metrics. In Section 5, we perform 5-day forecast experiments to evaluate the effects of assimilating AMSR2 SIC, sea ice chart, and OSTIA SST on the forecasts of SIE and MIZ. The results are compared with TOPAZ5, neXtSIM, GOFS 3.1, and Barents-EPS. The discussion and conclusions are given in Section 6.

2 Model and data assimilation

Barents-LAON is based on the METROMS COIN model (Wang, 2025), which is an independent branch of the METROMS model system (Kristensen et al., 2017). LAON is the optimal version of the Combined Optimal Interpolation and Nudging (COIN; Wang et al., 2013) method for data assimilation (Wang et al., 2023). METROMS is a coupled ocean and sea ice model based on the coupled Regional Ocean Modeling System (ROMS, version 3.7) and the Los Alamos sea ice model (CICE, version 5.1.2). The Barents-LAON model domain is the same as the Barents-2.5km, being a horizontal grid with a resolution of 2.5 km for the Barents Sea and Svalbard areas (Röhrs et al., 2023; also see Figure 1). The METROMS model physics has been well described in the previous studies (Duarte et al., 2022; Röhrs et al., 2023), and the LAON sea ice data assimilation system has been presented in the coupled HYCOM-CICE model (Wang et al., 2023). In this study, we extend the LAON method also for SST assimilation and implemented in the Barents-LAON system. The model components and data assimilation are briefly described below.

2.1 Ocean model

ROMS is a free-surface, terrain-following, primitive equations ocean model (Shchepetkin and McWilliams, 2005). It solves the Boussinesq primitive equations, with the basic state variables being temperature, salinity, surface elevation, and horizontal current velocities. The model setup includes a second order turbulence closure scheme with turbulent kinetic energy and a generic length scale as state variables (Warner et al., 2005). In the vertical, 42 layers are used with an increasing vertical resolution from 1.2 m to 0.2 m in the top 100 m. It uses split explicit time stepping for solving slow baroclinic modes separately from fast barotropic modes, with the time steps being 90 and 3 s, respectively. Momentum and tracers are advected using a third-order upwind scheme in the horizontal and a fourth-order centered scheme in the vertical. Turbulent kinetic energy and length scale are advected vertically and horizontally using a fourth-order centered scheme. Tracers are mixed along surfaces of constant geopotential, whereas momentum is mixed along the bottom topography following coordinate surfaces. The model uses the same configuration as in the work of Röhrs et al. (2023).

2.2 Sea ice model

CICE is a dynamic and thermodynamic, multiple ice-thickness category sea ice model (Hunke et al., 2015). In each computational cell, sea ice conditions, such as ice concentration and thickness, are described by the sub-grid scale distributions on the basis of the ice

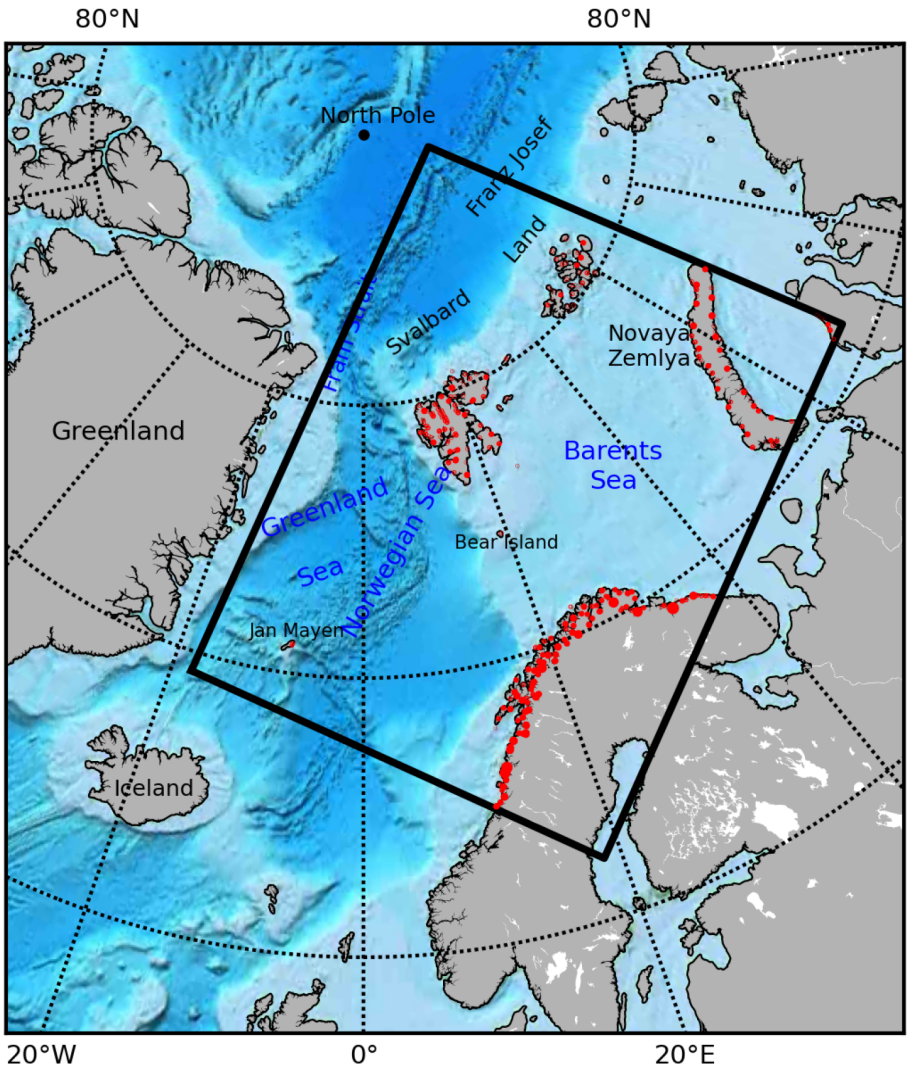

FIGURE 1
Barents-2.5km model domain shown by the thick rectangle. The red dots show the annual mean fluxes of the rivers (in total, 318), with the maximum of about 292.5 m^3 s^{-1}.

thickness distribution (ITD) theory (Thorndike et al., 1975). Evolution of the ice conditions is solved by splitting it into three pieces, namely, a horizontal two-dimensional (2D) transport, a vertical one-dimensional (1D) transport in the thickness space, and a redistribution of the ice in the thickness space through a ridging model. In our simulations, the original five category ITD (*kcatbound* = 0) is selected to describe the ice conditions, and the vertical snow and ice are resolved with seven ice layers and one snow layer for each ice thickness category.

The ice velocity is calculated from the sea ice momentum equation that account for air and water drags, Coriolis force, sea surface tilt, and the divergence of internal ice stress. In this study, the internal stress is calculated on the basis of the elastic-viscous-plastic (EVP) rheology (Hunke et al., 2015), using the revised EVP approach (Bouillon et al., 2013). The ice strength is reformulated according to Rothrock (1975). The sea ice advection is calculated using the incremental remapping scheme (Lipscomb and Hunke, 2004). The subgrid sea ice deformation and the redistribution of various ice categories follow Rothrock (1975), with a modified expression for the participation function (Lipscomb et al., 2007).

The sea ice thermodynamic growth rate is determined by solving the 1D vertical heat balance equations for each ice thickness category and snow, using the mushy-layer scheme that also accounts for the evolution of sea ice salinity (Turner et al., 2013). The upper snow/ice boundary (i.e., ice or snow surface) is assumed to be balanced under shortwave and longwave radiations and sensible, latent, and conductive heat fluxes when the surface temperature is below freezing. When the surface is warmed up to the melting temperature, it is held at the melting temperature and the extra heat is used to melt the snow/ice surface. The bottom sea ice boundary is assumed to be at dynamic balance, growing or melting due to the heat budget between ice conductive heat flux and the under-ice oceanic heat flux. The lateral melting is calculated using the default parameterization in CICE with a constant effective

ice floe diameter of 300 m (Maykut and Perovich, 1987). The melt pond is assumed to occur only on level ice, following the LEVEL-ICE melt pond parameterization (Hunke et al., 2013).

2.3 Ocean-sea ice coupling

The ROMS-CICE coupling utilizes the Model Coupling Toolkit (MCT; Larson et al., 2005) for intermodel exchange of state variables and fluxes (Duarte et al., 2022; Röhrs et al., 2023). The surface fluxes of heat, mass, and momentum are designed to be calculated in the component with most information about the surface using required information from the other components. The coupling employs the principle of "levitated" ice, so there is no actual exchange of mass between the ocean and the ice. Freshwater and salt fluxes from the ice model are converted to a virtual salt flux before they are used in the ocean model. In this "massless" state, the ice does not displace water (e.g., water flows do not see under-ice morphology such as keels), and it is only seen by the ocean as a source of surface fluxes responding to the present ocean state. The ice and ocean models are run concurrently, with exchange of information every baroclinic ocean time step (90s). The information used by each model is, therefore, of little time lag compared with its own state.

2.4 Atmospheric forcing and model boundary conditions

The atmospheric forcing is the surface fields from the operational analysis of the Integrated Forecast System (IFS) at European Centre for Medium Weather Forecasts (ECMWF), including wind speed, air temperature, humidity, rain fall, and cloud cover. These forcing fields have a horizontal resolution of 0.1° and temporal resolution of 6 h. They are used to calculate surface fluxes as the ocean upper boundary conditions in ROMS and to calculate surface stress, heat fluxes, and snow aggregation on the ice cover in CICE.

The model boundary conditions are provided by the newly operationalized TOPAZ5 (CMEMS, 2024a). It provides daily averages of temperature, salinity, sea surface elevation, and ocean current velocities for the ocean component, and daily averages of sea ice fraction, sea ice thickness, first year ice age, snow depth, and ice velocity for the sea ice component. In ROMS, a sponge zone with up to 10-fold increased horizontal tracer diffusivity and viscosity is implemented within 30 grid points from the boundary. Nudging of passive tracers toward the boundary fields from TOPAZ5 is imposed within the sponge zone. 2D momentum anomalies are radiated out of the model domain using the tangential phase speed of the barotropic signal.

Point sources for river influx are specified along the coasts in the model domain which include locations, daily values for temperature, salinity, and flux. The red dots show the annual mean fluxes of the 318 rivers (Figure 1), with a maximum of about 292.5 m^3 s^{-1}. Climatological values for rivers on the Svalbard archipelago are used, whereas river data on mainland Norway originates from daily estimates provided by the Norwegian Water Resources and Energy Directorate. Tidal forcing is provided as amplitudes and phases of the 10 major tidal constituents in the model domain, obtained from the TPXO global inverse barotropic model (Egbert and Erofeeva, 2002) and imposed on velocities and free surface elevation. The tidal signal is also added to velocities and surface elevation during the processing of boundary data.

2.5 LAON data assimilation

The LOAN data assimilation system is designed to nudge the model results to the optimal estimate such that (Wang et al., 2023)

$$\frac{\partial X}{\partial t} = F(X,t) + \frac{K}{\Delta T}[X_{obs} - X] \tag{1}$$

where X denotes any concerned variables to be assimilated, X_{obs} is the corresponding observations, ΔT is the observation time step, $F(X, t)$ denotes the processes related to the model free run, and K is the Kalman gain, which, in the local situation, becomes

$$K = \frac{\sigma_{mod}^2}{\sigma_{mod}^2 + \sigma_{obs}^2} \tag{2}$$

where $\sigma_{obs}$is the observation standard deviation (SD), and σ_{mod} is the model SD approximated by the absolute difference between model and observation values (Wang et al., 2013, 2023; Fritzner et al., 2018)

$$\sigma_{mod} = |X_{mod} - X_{obs}| \tag{3}$$

From Equations 1–3, the LAON assimilation of SST can be simply implemented following Wang et al. (2023)

$$SST_j = SST_{j-1} + \frac{\Delta t}{\Delta T} K(SST_{obs} - SST_{j-1}) \tag{4}$$

where SST and SST_{obs} are the model SST and observed SST, and subscript $j = 1, 2, 3,\ldots, N$, in which $N = \Delta T/\Delta t$ is ratio of observation time step ΔT to the model time step Δt (Wang et al., 2023). For the multi-category CICE model, we apply a same formulation as in Wang et al. (2023). When the total model SIC a_{ice} is greater than 0, a proportional formulation is applied to update all the ice categories such that

$$a_{n,j} = a_{n,j-1}(1 + \gamma) \tag{5}$$

$$v_{n,j} = v_{n,j-1}(1 + \gamma) \tag{6}$$

$$v_{sn,j} = v_{sn,j-1}(1 + \gamma) \tag{7}$$

where v_n and v_{sn} are ice and snow volumes for the nth ice category, and the rate of incremental innovation $\gamma$is (Wang et al., 2023)

$$\gamma = K\frac{\Delta t}{\Delta T}\left[\frac{a_{obs}}{max(a_{ice}, 0.1)} - 1\right] \tag{8}$$

where a_{obs} and a_{ice} are the observed and model total SIC. The function max in Equation 8 is used to avoid huge values when $a_{obs}/a_{ice} \gg 1$. When $a_{ice} = 0$ and $a_{obs} > 0$, we assume that new model sea ice will form with the sea ice thickness as follows (Fritzner et al., 2018; Wang et al., 2023, 2024)

$$h_{new} = 0.02e^{2.8767a_{obs}} \quad (9)$$

In addition to the new model ice thickness (Equation 9), we set the new snow volume as 0.1 of the ice volume, sea ice salinity as 5 psu, and sea ice temperature at the freezing temperature with the corresponding entropy.

2.6 Model experiments

We performed seven experiments to investigate the effects of data assimilation on the analyses and forecasts of SIE and MIZ. Table 1 shows the experiments with varying assimilations of SST and SIC for the period from 1 January to 30 April 2024. Free run assimilates no data, DA-SST assimilates the OSTIA SST only, DA-SIC assimilates the AMSR2 SIC only, and DA-Both0 assimilates the AMSR2 SIC and OSTIA SST. DA-Both1 and DA-Both2 are both designed to assimilate the merged SIC and OSTIA SST, but with different treatments when sea ice charts are not available. In DA-Both1, no SIC assimilation is performed when ice chart is unavailable, whereas DA-Both2 assimilates the AMSR2 SIC instead when no ice chart is available. DA-Both3 also assimilates both SST and SIC but assimilates the ice chart only when it is available and assimilate AMSR2 SIC when the ice chart is unavailable. The reason for the experiments DA-Both1, DA-Both2, and DA-Both3 is that the ice chart is unavailable during weekends and holidays. By performing these experiments, we hope to identify a best approach to predicting the SIE and MIZ in such an imperfect conditions.

We note here that only five experiments were performed to investigate the effects of assimilation on the short-term forecasts (Table 1), with daily 5-day forecasts for the period from 2 January to 24 April 2024. The Free run and DA-SST contain very large biases. Their forecasts are generally of very limited values to real sea ice predictions, so are not performed.

The model initial fields, boundary conditions, and atmosphere forcing are the same for all the seven experiments. The initial fields are interpolated from the operational analyses of TOPAZ5 at 0 o'clock on 1 January 2024. The boundary conditions are daily mean fields interpolated from the TOPAZ5 analyses, and the atmosphere forcing fields are the 6-h operational analyses from the ECMWF, both from 1 January to 30 April 2024. Both SIC and SST observations are daily fields. For model analysis, each observation is considered as unchanged [see (Equations 4-7)] on the day and continuously assimilated into the model using the LAON method, from 0 o'clock to the last time step before the next day. After a full-day assimilation each day, a new restart file is generated for model forecasts at 0 o'clock of the next day. The forecast starts from 0 o'clock on the next day, and no observations are assimilated during the 120 h forecast period.

3 Data

We use three observed SIC products and four modeled SIC products in this study. The observations include AMSR2 SIC from the University of Bremen, sea ice chart from the Ice Service of the Norwegian Meteorological Institute (NIS) and the merged SIC from an optimal combination of the AMSR2 SIC and NIS ice chart. The modeled SIC products are from TOPAZ5, NeXtSIM, GOFS3.1, and Barents-EPS. All the data were interpolated to the model grid using the nearest neighbor interpolation.

3.1 Observed SIC

3.1.1 AMSR2 SIC

The AMSR2 microwave radiometer onboard the GCOM-W1 satellite measures the microwave emission from the Earth, at a nominal incident angle of 55° and a swath width of 1,450 km. The AMSR2 SIC dataset that we used here is the version 5.4 with a grid resolution of 3.125 km, which utilizes the highest spatially resolving AMSR2 channels at 89 GHz (Melsheimer, 2019). It uses the same ARTIST sea ice (ASI) algorithm as it was developed for the AMSR-E 89-GHz channel (Spreen et al., 2008). It has a higher spatial resolution than most other AMSR2 SIC datasets although the atmospheric influence can be higher. The uncertainty is calculated following the same procedure in Spreen et al. (2008), where the overall error sums from three sources: the radiometric error from the bright temperature, the variability of the tie points, and the atmospheric opacity. The uncertainty is expressed in terms of standard deviation (SD).

3.1.2 NIS ice chart

The ice chart is produced on the basis of manual interpretation of satellite data and other observations such as coastal station and ship reports (Copeland et al., 2024). The ice charting employs a variety of satellite observations to obtain a more realistic SIE and MIZ, and these have evolved since ice charting began in 1967 to include higher spatial resolution and all-weather capable sensors over the years. The main satellite data used are the weather independent Synthetic Aperture Radar (SAR) data from Sentinel-1, RADARSAT-2, and RADARSAT Constellation Mission (RCM). The analyst also uses visual and infrared data from METOP and NOAA Advanced Very High Resolution Radiometer (AVHRR), NOAA Visible Infrared Imaging Radiometer Suite (VIIRS), and Sentinel-3 Ocean and Land Colour Instrument (OLCI) and Sea and Land Surface Temperature Radiometer (SLSTR) in cloud-free conditions. These satellites provide coverage of the charting area several times a day and allow the ice chart to be produced in a scale-free vectorized format, with a nominal resolution of less than 400 m. A rasterized NetCDF-format is produced for Copernicus Marine Service with a resampling to 1-km grid spacing (Dinessen and Hackett, 2018). The NIS ice chart includes seven ice concentration categories following the WMO sea ice nomenclature (WMO, 2014): fast ice (SIC = 10/10), very close drift ice (9–10/10), close drift ice

TABLE 1 Data assimilation (DA) experiments together with the applied observations.

Experiment	SST DA	SIC DA	Forecast
Free run	No	No	No
DA-SST	Yes	No	No
DA-SIC	No	AMSR2 SIC	Yes
DA-Both0	Yes	AMSR2 SIC	Yes
DA-Both1	Yes	Merged SIC on working days, no SIC assimilation otherwise	Yes
DA-Both2	Yes	Merged SIC on working days, AMSR2 SIC otherwise	Yes
DA-Both3	Yes	ice chart on working days, AMSR2 SIC otherwise	Yes

SST here represents the OSTIA SST data. The fourth column indicates whether the forecast experiments are performed.

(7–8/10), open drift ice (4–6/10), very open drift ice (1–3/10), open water (<1/10), and ice free (0). For practical use, a mean value is applied to denote the different ice categories in the ice chart. The uncertainty is approximated as the half of the range of the corresponding ice category, except being 0.01 for the fast ice.

3.1.3 Merged SIC

According to Wang et al. (2020), assimilating merged multisensor observations is equivalent to assimilating all the observations concurrently. Therefore, the effect of assimilating both AMSR2 SIC and sea ice chart can be investigated using the merged AMSR2-ice chart data. In this study, we use the merged SIC from multisensor optimal merging of AMSR2 SIC and NIS ice chart (Wang et al., 2024). The AMSR2 SIC is the same as in 3.1.1, and the NIS ice chart the same as 3.1.2. The merged SIC effectively mitigated the original shortcomings in both the AMSR2 SIC and the NIS ice chart (Wang et al., 2024). Because the NIS ice chart is only available during the working days, the merged SIC on weekends and holidays is the same as the AMSR2 SIC.

3.2 Modeled SIC

3.2.1 TOPAZ5 SIC

The TOPAZ5 SIC is obtained from the CMEMS operational product (CMEMS, 2024a, accessed in April 2024), which is a nominal product of the CMEMS Arctic Monitoring and Forecasting Center (MFC) for ocean physics (Hackett et al., 2023). It is produced by the newly operationalized TOPAZ5 Arctic Ocean and sea ice prediction system, using the version 2.2.98 of HYCOM ocean model (Bleck, 2002) coupled to the CICE 5.1.2 (Hunke et al., 2015), with the deterministic ensemble Kalman filter (DEnKF; Sakov and Oke, 2008) for data assimilation. The model domain covers the North Atlantic and Arctic basins with a grid spacing of approximately 6–8 km. The model is run daily to provide 10 days of forecast (average of 10 members) of the three-dimensional (3D) physical ocean and sea ice variables. The data assimilation is performed weekly to provide 7 days analysis (ensemble average), in which a 100-member DEnKF is used to assimilate SIC, SIT, sea ice drift, SST, sea level anomaly and *in situ* temperature/salinity (T/S) profiles (Hackett et al., 2023). TOPAZ5 runs once a day at the Norwegian Meteorological Institute. The forecast and analysis are then interpolated and disseminated to a 6-km grid using the polar stereographic projection. The disseminated product is available as hourly surface fields, daily and 6-h averaged 3D fields.

3.2.2 neXtSIM SIC

The neXtSIM SIC is from the CMEMS operational product (CMEMS, 2024b, accessed in May 2024). It is an hourly product produced by the Arctic MFC through the neXtSIM sea ice prediction system (Hackett et al., 2023). The neXtSIM is a stand-alone sea ice model using the Brittle-Bingham-Maxwell sea ice rheology (Rampal et al., 2019; Williams et al., 2021), on an adaptive triangular mesh of 10-km average cell length. The model is forced with surface atmosphere fields from the ECMWF and ocean fields from TOPAZ5. It runs daily, assimilating manual ice charts, SIT from CS2SMOS in winter and providing 9-day forecasts (CMEMS, 2024b). The output variables are SIC, SIT, ice drift velocity, snow depths, sea ice type, sea ice age, ridge volume fraction, and albedo, provided at hourly frequency. The adaptive Lagrangian mesh is interpolated for convenience on a 3-km resolution regular grid in a polar stereographic projection.

3.2.3 GOFS 3.1 SIC

The GOFS3.1 SIC is from https://www.hycom.org/dataserver, with the forecasts downloaded once they became available. The GOFS 3.1 is based on the HYCOM version 2.2.99 (Metzger et al., 2017), coupled to the CICE version 4.0 (Hunke and Lipscomb, 2008). The model uses a tripole global grid (grid resolution about 9 km at equator, 7 km at mid-latitude, and 3.5 km at the North Pole). The atmospheric forcing is from the Navy Global Environmental Model (NAVGEM) at Fleet Numerical Meteorology and Oceanography Center (Hogan et al., 2014). The system uses the Navy Coupled Ocean Data Assimilation (NCODA) system (Cummings and Smedstad, 2013) for data assimilation, which is based on a 3D variational scheme and assimilates available satellite and *in situ* observations. The assimilated ocean variables are SST, SSH anomaly, and T/S profiles. For sea ice assimilation, the AMSR2 SIC is firstly merged with the semi-automated analysis from Interactive Multisensor Snow and Ice Mapping System (IMS) produced by the U.S. National Ice Center, which is then assimilated into CICE for operational forecast (Posey et al., 2015). The output variables include 3D ocean temperature; salinity and velocity; surface mixed layer and location of mesoscale features; and ice concentration, thickness, and drift.

3.2.4 Barents-EPS SIC

The Barents-EPS SIC is obtained from https://thredds.met.no/thredds/fou-hi/barents_eps.html (accessed in May 2024). It is produced in the Norwegian Meteorological Institute using the operational coupled ocean and sea ice ensemble prediction model

Barents-2.5km v.20 (Röhrs et al., 2023). The model uses the same coupled ROMS-CICE model and configuration as in this study, but using the DEnKF (Sakov and Oke, 2008; Fritzner et al., 2019; Röhrs et al., 2023) for data assimilation. The assimilated variables include SIC, SST, and *in situ* T/S profiles. The model runs four times per day to provide 96 h of hourly ensemble mean and SD for SIC, SIT, ice velocity, SST, SSS, surface current velocity, and elevation.

4 Evaluation metrics

We use IIEE (Goessling et al., 2016) to evaluate the modeling skill for SIE and use integrated MIZ error (IME; Wang et al., 2023) to evaluate the modeling skill for MIZ. To be consistent with the NIS ice chart, we here use SIC = 0.1 as the demarcation for SIE and 0.85 as the demarcation between MIZ and dense pack ice. The prediction skills for SIE and MIZ are evaluated against the sea ice chart persistence. These metrics are briefly described below.

4.1 IIEE and IME

The IIEE is determined following Goessling et al. (2016)

$$IIEE = \int_A \max(c_f - c_t, 0)dA + \int_A \max(c_t - c_f, 0)dA \quad , \qquad (10)$$

where A denotes the whole model domain, the subscripts f and t denote the forecast and the truth (here, we use the NIS ice chart as an approximate). The variable $c = 1$ where SIC $a \geq 0.1$ and $c = 0$ elsewhere. The first term on the right side of (Equation 10) denotes the overestimate, and the second term denotes the underestimate.

Similar to the formulation for the IIEE, the IME is defined as follows (Wang et al., 2023)

$$IME = \int_A \max(c_f - c_t, 0)dA + \int_A \max(c_t - c_f, 0)dA \quad . \qquad (11)$$

The only difference between Equations 10, 11 is the definition of the variable c. For the IME, $c = 1$ where SIC $\in$ [0.1, 0.85], and $c = 0$ elsewhere.

4.2 Prediction skill of SIE and MIZ

We define the following metrics to evaluate the prediction skill for SIE,

$$S_{SIE} = 1 - \frac{IIEE_m}{IIEE_r} \quad , \qquad (12)$$

where the subscripts m and r denote the concerned model and reference, respectively. Similarly, we define the prediction skill for MIZ

$$S_{MIZ} = 1 - \frac{IME_m}{IME_r} \quad . \qquad (13)$$

Equations 12, 13 provide a simple description of the prediction skills for the concerned model against the reference. It is seen that the skills would be positive when the modeled IIEE or IME is smaller than the reference, and vice versa. When the model predicts the same IIEE or IME as the reference, the skill would be 0. When the model perfectly predicts the SIE or MIZ, the modeled IIEE or IME would be 0, and the skill would be 1.

5 Results

5.1 Effects of assimilation on the analyses of SIE and MIZ

5.1.1 Daily SIC spatial distribution

Figure 2 compares the observed and modeled SIC on 19 February 2024. For the purpose of evaluating the analyses of SIE and MIZ, we have separated the whole ice cover into dense pack ice (SIC > 0.85) and MIZ (SIC $\in$ [0.1,0.85]), with the rest as open water (SIC < 0.1). As pointed out in previous studies (Cavalieri, 1994; Kern et al., 2019; Wang et al., 2024), the PMR tends to underestimate low SIC area. This can also be seen when compared to the ice chart Figure 2a vs. Figure 2b), particularly where the AMSR2 MIZs are narrower.

The Free run indicates that the model system without data assimilation tends to significantly overestimate the sea ice cover (Figures 2c vs. 2b). This is particularly pronounced in the Greenland Sea. Assimilation of the OSTIA SST slightly reduces the large bias in the Greenland and Barents seas (Figures 2d vs. Figure 2b), but the overestimated sea ice cover in the Greenland Sea is still remarkable. By contrast, assimilation of SIC is able to substantially improve the simulation of the ice field. Even the assimilation of AMSR2 SIC alone can considerably improve the sea ice cover, although the MIZ is considerably overestimated in the northeastern Barents Sea (Figure 2e vs. Figure 2b). Additional assimilation of the OSTIA SST further improves the analyses of the SIE and MIZ (cf. Panels e and f with b in Figure 2). It is seen that the assimilation of AMSR2 SIC and OSTIA SST (Figure 2f) produces closer sea ice coverage to the ice chart (Figure 2b) than the AMSR2 observation (Figure 2a).

Figures 2g, h show the sea ice distribution using the assimilation of both merged SIC and OSTIA SST. Although both DA-Both1 and DA-Both2 assimilate the same merged SIC on 19 February 2024 (working day), there are still some noticeable differences in these two analyses, e.g., the MIZs in the Greenland Sea and west coast of Novaya Zemlya. When comparing these two experiments with DA-Both0 (Figure 2f), there are marked differences in the MIZs, e.g., in the Greenland Sea and west coast of Novaya Zemlya (cf. Panels f, g, d with b in Figure 2). In this case, DA-Both1 tends to be noticeably closer to the NIS ice chart (Figure 2g vs. Figure 2b). DA-Both3 also assimilates both OSTIA SST and SIC, using pure ice chart for the working days and AMSR2 SIC for the rest days. It provides a SIC analysis very close to DA-Both1 and DA-Both2 (cf. Figures 2g–i).

As a comparison, we also present the SIC analyses from the four operational products, namely, Barents-EPS, TOPAZ5, neXtSIM, and GOFS 3.1 (Figures 2j–m). In general, Barents-EPS overestimates the ice extent in the Greenland Sea, particularly overestimating the area of dense pack ice. TOPAZ5 generally has

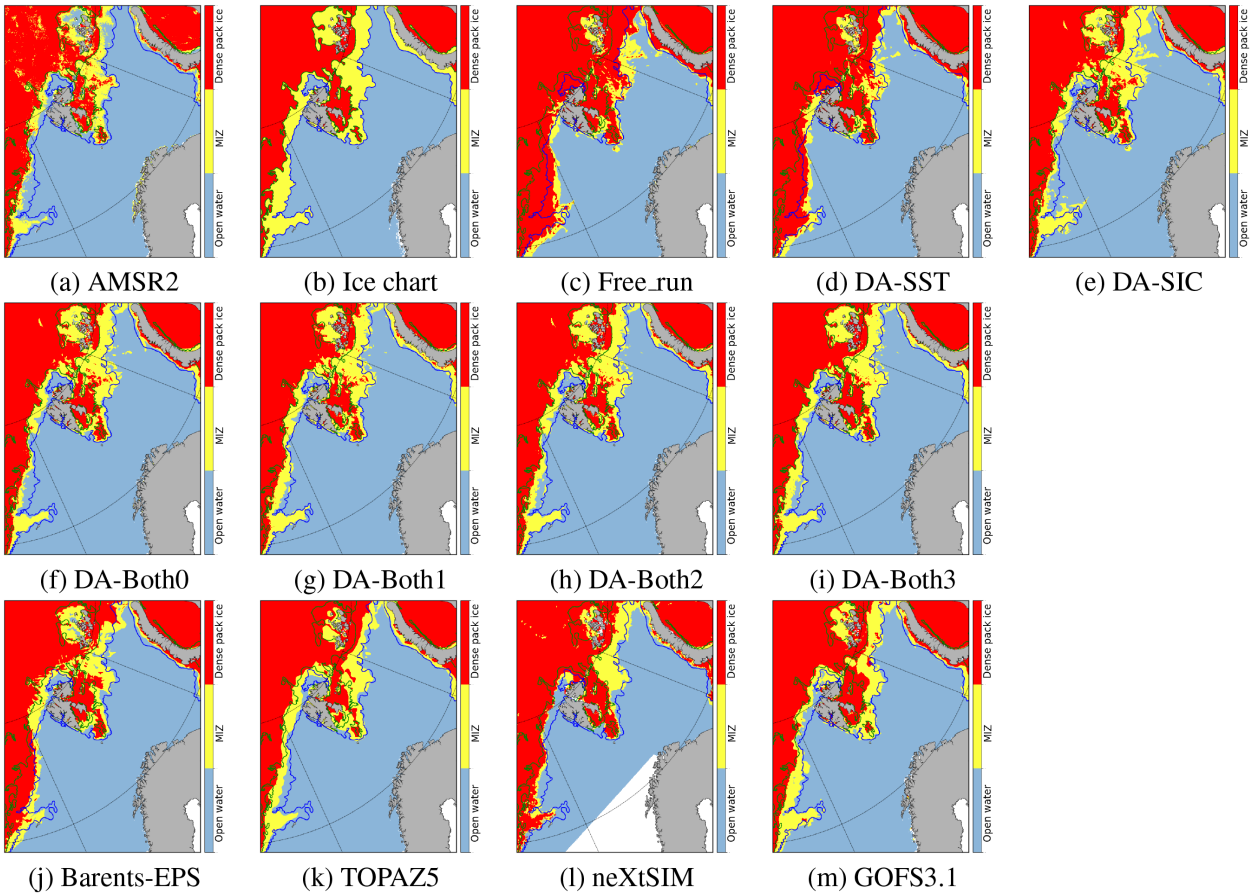

FIGURE 2
SIC observations **(a, b)** and analyses **(c–m)** on 19 February 2024, with the ice cover separated into dense pack ice (red), MIZ (yellow), and open water (light blue). The blue lines show the SIE of the ice chart, and the green lines show the demarcation between MIZ and dense pack ice of the ice chart. Here, DA denotes data assimilation. The experiments are referred to Table 1.

a much closer agreement with the ice chart, although it tends to overestimate the SIC in the northeastern Barents Sea. NeXtSIM tends to overestimate the SIC in the Greenland Sea and underestimate the MIZ there. GOFS3.1 generally gives an good analysis of the SIC, particularly in the Greenland Sea, although some underestimates occurs in the MIZ in the Barents Sea. This is partly due to the fact that GOFS3.1 assimilates the National Ice Center ice chart (Posey et al., 2015), whereas TOPAZ5 and Barents-EPS do not.

This daily distribution only provides one-case results. Further assessment of the model analyses is performed in Section 5.1.3, using IIEE and IME for the whole 4-month period—1 January to 30 April 2024.

5.1.2 Daily SST

Daily SST biases from the different experiments are shown in Figure 3, together with the daily ensemble mean SST bias from Barents-EPS (Figure 3a). These SST biases are evaluated against the daily OSTIA SST (CMEMS, 2024c). Except for the SST near the southern boundary and west of Svalbard, the Barents-EPS provides an analysis very close to the observation, with the mean bias of −0.01°C and SD of 0.40°C.

The Free run has a considerable cold bias in much of the Norwegian Sea and Greenland Sea (Figure 3b). The underestimate of the SST in the Greenland Sea is mainly due to the overestimated sea ice cover, under which the SST is maintained close to the freezing point. The underestimate of the SST in the Norwegian Sea is most likely due to the underestimate of the warm current from the south, as seen from the overall spatial pattern of the underestimated SST. Assimilation of the AMSR2 SIC significantly mitigates the underestimated SST in the Greenland Sea (Figure 3b vs. Figure 3c). However, there is almost no improvement in the ice-free Norwegian Sea. Both Free run and DA-SIC have large mean bias, being −0.33°C and −0.27°C, respectively.

Assimilation of SST significantly improves the simulated SST (Figure 3d). Over much of the Norwegian Sea and Greenland Sea, the large underestimation of the SST has been remarkably mitigated. However, there is still a mean bias of −0.22°C over the whole Barents region. In particular, the large cold SST bias remains north of Svalbard, due to the overestimated sea ice cover.

There is little difference in the SST when both SIC and SST are assimilated (Figures 3e–h). Compared with the assimilations of SIC alone (Figure 3c) and SST alone (Figure 3d), most of the large biases have been mitigated, except for the small areas along the west coast

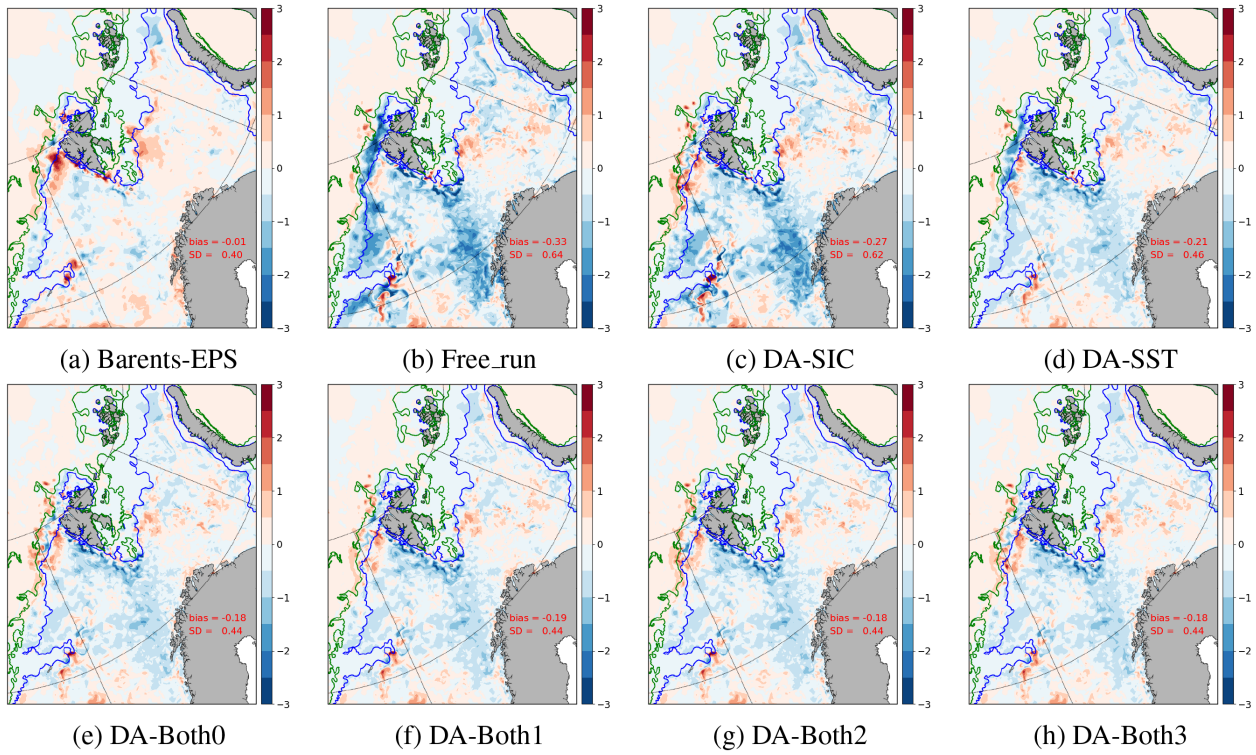

FIGURE 3
SST biases (°C) on 19 February 2024 from Barents-EPS **(a)** and the experiments **(b–h)**. The blue lines show the SIE of the ice chart, and the green lines show the demarcation between MIZ and dense pack ice of the ice chart. Here DA denotes data assimilation. The experiments are referred to Table 1.

of Svalbard. It is noteworthy that the mean biases in these experiments are still about −0.18°C (Figures 3e–h). This indicates that the SST assimilation is still not optimal. Further investigations are needed to improve the SST analysis.

5.1.3 IIEE and IME

Figure 4 shows the IIEE and IME from 1 January to 30 April 2024 for all the model runs, the AMSR2 observations, and the four operational analyses (Barents-EPS, TOPAZ5, neXtSIM, and GOF3.1). All the IIEE and IME are calculated against the sea ice charts. The discontinuities in the IIEE and IME are due to the missing sea ice charts on weekends and holidays. It is seen that, in the whole simulation period, the Free run has very large IIEE (Figure 4a), largely over 4×10^5 km² after 1 February, indicating a large bias in the model system. Compared with the Free run, the assimilation of the OSTIA SST (DA-SST) has a mild correction in the SIE, with the IIEE generally about 2×10^5 km² after 1 February. Compared with the other model analyses, these two runs are significantly larger, being about three and two times of the other IIEEs (see the legend in Figure 4a). The relatively large IIEE of DA-SST is mainly due to the characteristics of the LAON assimilation, which only nudges the SST to the optimal estimate but without direct modification of the sea ice cover during the assimilation. Due to the systematic cold biases in both of the sea ice and ocean model components, the sea ice coverage would still be notably overestimated when only SST is assimilated, resulting in large IIEE. At the same time, the updated SST near the SIE would also be modified by the overestimated sea ice cover, resulting in underestimated SST and improved sea ice extent through sea ice melting. Such a change in the SST can be seen in the northern coast of Svalbard in Figure 3d.

The AMSR2 observation provides a consistent reference for the present study to the earlier study in Wang et al. (2023), although for different sea areas. It is seen that TOPAZ5 IIEE has a smaller mean than the AMSR2 IIEE (see legend in Figure 4a). This is different from the TOPAZ4 IIEE, which is considerably larger than the AMSR2 IIEE (Wang et al., 2023), indicating a significant improvement in the model development of the TOPAZ system. Barents-EPS and neXtSIM generally produce similar large IIEE. GOFS3.1 produces a similar IIEE to TOPAZ5, both smaller than Barents-EPS and neXtSIM.

Due to the large bias in the model system, the assimilation of AMSR2 SIC alone (DA-SIC) tends to have large IIEE in the analysis (Figure 4a). Contrast to the results in the NorHAPS (Wang et al., 2023), DA-SIC IIEE is larger than the AMSR2 IIEE. It is also larger than those of TOPAZ5 and GOFS3.1 but still smaller than those of Barents-EPS and neXtSIM (Figure 4a). With the additional assimilation of the OSTIA SST (DA-Both0), the model produces smaller IIEE than all the other operational analyses. Further assimilation of the merged SIC provides further improvements, with the mean IIEE down to about 0.65×10^5 km² (DA-Both1 and DA-Both2). There remains of little difference in the modeled IIEEs between DA-Both1 and DA-Both2, partly due to the fact that the evaluations are only based on the days when sea ice charts are

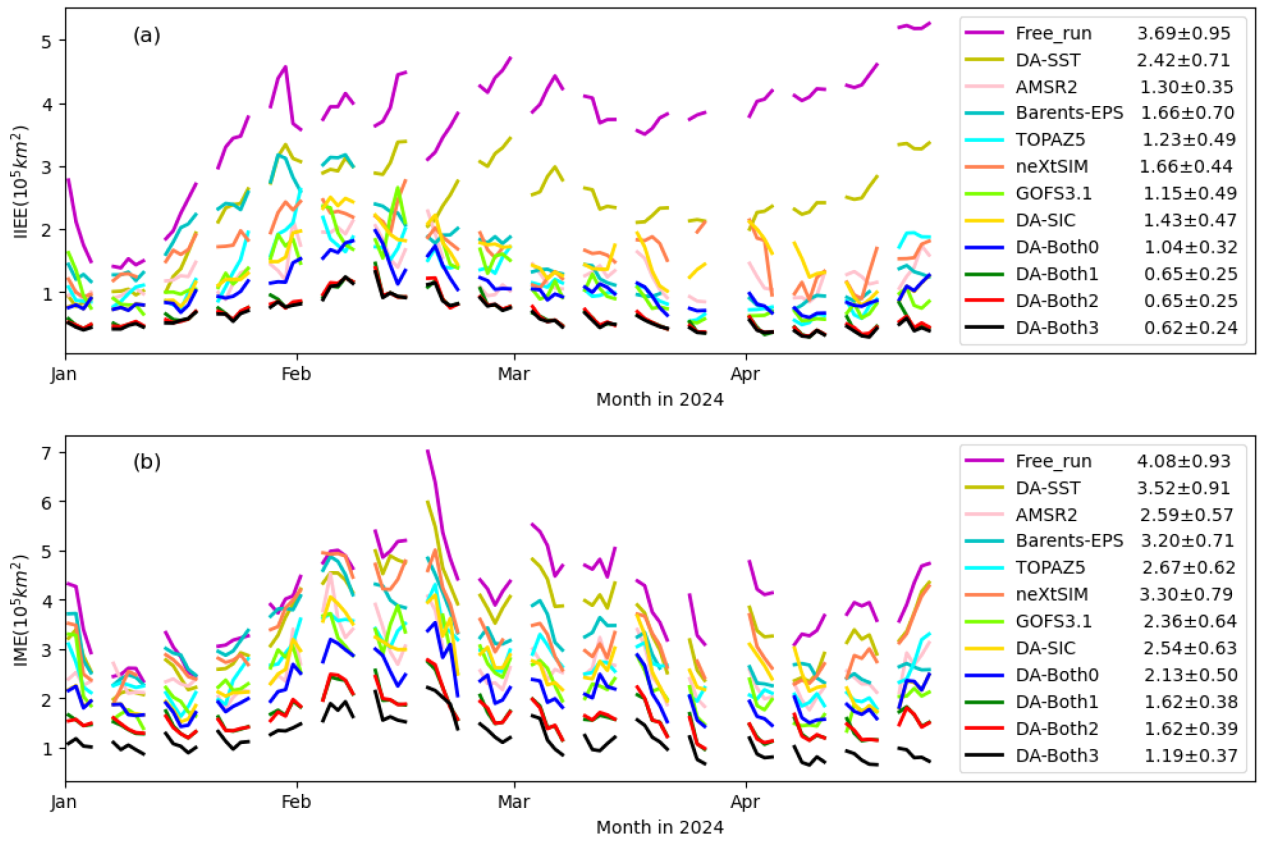

FIGURE 4
Time series of the integrated ice edge error (IIEE) and integrated marginal ice zone error (IME) for different products from 1 January to 30 April 2024: **(a)** IIEE and **(b)** IME. The numbers in the legends show the mean ± standard deviation of the corresponding IIEE and IME. The experiments are described in Table 1.

available. DA-Both3 produces slightly lower IIEE than DA-Both1 and DA-Both2, indicating a slight advantage for SIE analysis.

Similar to the results in Wang et al. (2023), the IME is about twice of the IIEE for most analyses, suggesting about half of the IME is due to the misclassifications between MIZ and dense pack ice. In the present case, the Free run IME is very close to its IIEE (Figure 4), particularly after 1 February. This exceptional result can be well explained by Figure 2, where the Free run significantly overestimated the sea ice cover. In such a case, the open water and MIZ (Figure 2b) is largely modeled as dense pack ice in the Free run, thereby generating similar values of IME and IIEE (Figure 4). For the four operational analyses, only GOFS3.1 has lower IME than the AMSR2 observation. The assimilation of AMSR2 SIC alone produces slightly smaller IME than the AMSR2 observation but larger than that of GOFS3.1. The assimilations of both SIC and SST (DA-Both0, DA-Both1, DA-Both2, and DA-Both3) all produce lower IME than GOFS3.1. Both DA-Both1 and DA-Both2 produce considerably lower IME than DA-Both0 (Figure 4b), but there is generally little difference in the simulated SIE and MIZ between DA-Both1 and DA-Both2. It is noteworthy that DA-Both3 produces a considerably better MIZ analysis than DA-Both1 and DA-Both2, appearing to be the best option for the MIZ analysis. This tends to suggest that the present AMSR2 SIC is not very accurate for separating MIZ from dense pack ice.

5.2 Effects of assimilation on the forecasts of SIE and MIZ

5.2.1 Effect on SIE forecast

Figure 5 shows the prediction skills of the five experiments (DA-SIC, DA-Both0, DA-Both1, DA-Both2, and DA-Both3) and the four operational forecasts (Barents-EPS, TOPAZ5, neXtSIM, and GOFS3.1), evaluated against the persistence forecast of the sea ice chart using (Equations 12, 13). As noted in Section 4.2, positive skill indicates that the model prediction skill is higher than the referenced sea ice chart persistence, and vice versa. It is seen that all the mean prediction skills for the 1-day SIE forecast are low than 0 (see legend in Figure 5a), indicating these models are still less skillful in predicting the SIE than the sea ice chart produced one day before. For longer days of forecast, all the experiments using both SIC and SST assimilations have higher skills than the sea ice chart persistence (panels b–e in Figure 5). By contrast, the assimilation of SIC alone (DA-SIC) always shows notably negative skills. This indicates that a noticeable portion of the prediction skill is from the improved initial fields due to the addition of SST assimilation (see DA-SIC vs. DA-Both0 in Figure 4a). The initial fields without SST assimilation have a cold bias in the SST field, which enhances the freezing of open water near the SIE. The additional assimilation of SST significantly suppresses the SST underestimate and therefore

10.3389/fmars.2025.1588769

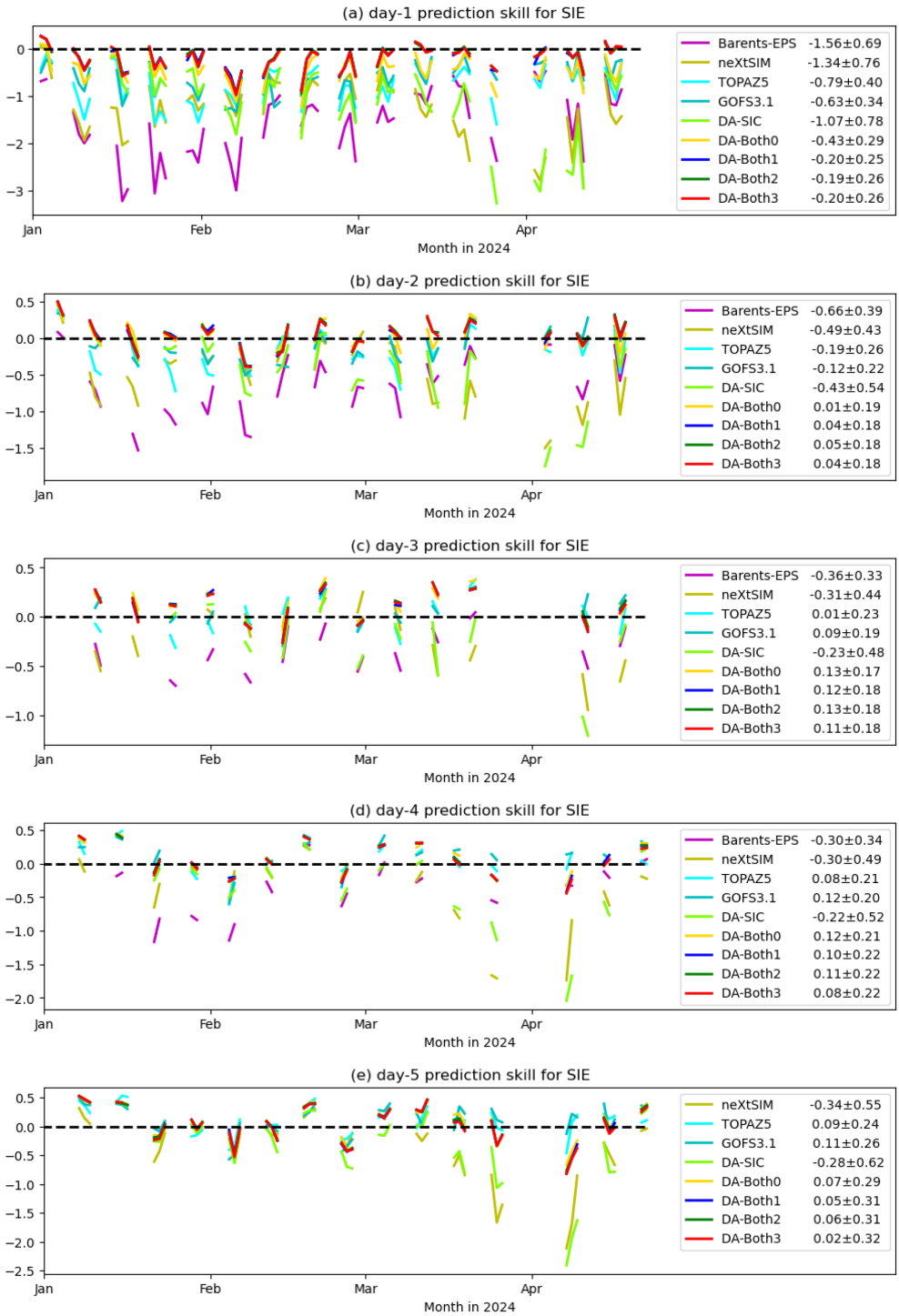

FIGURE 5
Prediction skills of the forecast SIE evaluated against the persistence forecast of sea ice chart, from 1 day to 5 days **(a–e)**. The experiments are referred to Table 1. It is noted that Barents-EPS only provides 4 days of forecast.

mitigates the overestimate of the sea ice cover from excessive freezing.

It is noted that the seasonal simulation with only SST assimilation has quite high errors in the IIEE (DA-SST in Figure 4a). This is partly due to the characteristics of the LAON assimilation. In the situation of assimilating the SST alone, it only modifies the SST field but does not directly modify the sea ice cover. In such a case, the overestimated sea ice cover is only adjusted through the model physics. When the cold bias in the sea ice model component is large, the overestimate of the simulated sea ice cover tends to substantially remain, thereby resulting in a large bias in the simulated SIE. On the whole, the large IIEE in DA-SST is due to the

model bias in the sea ice model component, whereas the improvement in the simulated SIE with additional SST assimilation is due to the overall improved initial ocean and sea ice conditions.

The experiments performed here assimilate SIC and SST using the LAON method. These two assimilated data are generally less than those used in the operational products that commonly include SIT, sea ice velocity, and SSS. Similar to the assimilation results in Wang et al. (2023), the LAON assimilation exhibits higher SIE prediction skills compared with the assimilations using EnKF (TOPAZ5 and BarentEPS), 3D variational (GOFS 3.1), and nudging (neXtSIM). There are generally little differences in the forecast IIEEs between DA-Both1, DA-Both2, and DA-Both3 (Figure 5). Due to the large systematic bias in the METROMS Barents-2.5km model (see the Free run in Figure 4), the effect of LAON data assimilation starts to diminish from 5-day forecast, and the prediction skills start to decrease accordingly (Figure 5). While still positive, the prediction skills of these experiments are surpassed by the operational forecasts of TOPAZ5 and GOFS3.1. TOPAZ5 and GOFS 3.1 become more skillful than the sea ice chart persistence after 3-day forecast (panels c–e in Figure 5), whereas Barents-EPS and neXtSIM remain to be negative prediction skills for all the 5 days (Figure 5).

5.2.2 Effects on MIZ forecast

Figure 6 illustrates the prediction skills for MIZ from 1 to 5 days of forecasts. On the whole, the LAON assimilations of both ice chart and SST (DA-Both1, DA-Both2, and DA-Both3) show remarkably higher skills than the other products, particularly for the 1–3 days of forecasts (see the mean skills in the legends). It is of negligible difference whether to assimilate the AMSR2 SIC during the weekends or holidays, as shown by the prediction skills between DA-Both1 and DA-Both2. DA-Both2 is slightly better in SIE forecast (Figure 5), whereas DA-Both1 is slightly better in MIZ forecast (Figure 6). DA-Both3 has the highest prediction skills for MIZ in the first two days (Figure 6). This suggests that the AMSR2 SIC is not as accurate as the ice chart for separating the MIZ from dense pack ice.

DA-Both0 does not assimilate the sea ice chart, but it also shows comparable prediction skills to those assimilating the ice chart, except for the first day. This is partly due to the biases in the AMSR2 SIC observation and the model system. The AMSR2 SIC generally provides an underestimated sea ice extent, whereas the model system tends to provide an overestimate of the sea ice extent during the winter season. On the whole, the excessive growth of the model sea ice counteracts the initially underestimated sea ice cover with AMSR2 SIC assimilation, thus improving the prediction skill in the later days. This can be clearly seen in both Figures 5 and 6, where DA-Both0 has lower prediction skills than DA-Both1, DA-Both2 and DA-Both3 in the first 2 or 3 days but becomes to have higher or comparable prediction skills in the later days. Assimilation of SIC alone (DA-SIC) generally produces low prediction skills for MIZ forecasts. This indicates that additional assimilation of SST can significantly improve the forecast of MIZ when the model is highly biased, similar to the SIE forecasts (Section 5.2.1).

It is noteworthy that the mean prediction skills for MIZ are all negative for all the models and experiments from 1 to 5 days (Figure 6). This indicates that the model predictions are not yet sufficiently mature for skillful MIZ forecasts. Nevertheless, the LAON assimilation of the SIC and SST illustrates close prediction skills to the sea ice chart persistence forecasts, particularly for 3–5 days (Figure 6c–e). Considering the bias in the SST field (Section 5.1.2), improving the data assimilation may still be a feasible way to further improve the MIZ forecast.

6 Concluding remarks

Sea ice is a major threat to the marine operations around Svalbard. Accurate forecasts of SIE and MIZ are crucial but remain extremely challenging. A large number of efforts have been made in recent years to improve the mechanisms on the interactions among the atmosphere, ocean, sea ice, and waves (see overviews in Bennetts et al., 2022; Dumont, 2022). How these new understandings and developments can improve the forecasts of SIE and MIZ remains to be further verified, particularly for short-term operational forecasts.

In this study, by using a coupled ocean and sea ice model (METROMS) with the LAON data assimilation in a regional configuration (Barents-LAON), we demonstrate that the LAON is an effective method for data assimilation. Despite the large biases in the model system, the Barents-LAON with both SIC and SST assimilations can provide better analyses and better 1–3 days of forecasts of SIE and MIZ (Figures 4–6) than all the operational products (TOPAZ5, neXtSIM, GOFS3.1, and Barents-EPS). Although the assimilation of SST alone generally has a limited contribution to the improvements of SIE and MIZ analyses (Figure 4), the SST assimilation does have a notable contribution to the improvements of SIE and MIZ forecasts when it is performed together with the SIC assimilation (DA-SIC vs. DA-Both0 in Figures 5, 6). This change is due to the overall improvements in the initial ocean and sea ice conditions with SIC and SST assimilations.

The model experiments show that the differences in the prediction skills for SIE and MIZ are generally small between DA-Both1 and DA-Both2. This suggests that it is not very critical whether or not to assimilate the AMSR2 SIC on weekends and holidays, when the sea ice chart has been assimilated on working days. Additional assimilation of the AMSR2 SIC on weekend and holidays (DA-Both2) has slightly higher prediction skill for SIE forecasts (Figure 5), whereas no such assimilation (DA-Both1) appears to have slightly higher prediction skill for MIZ forecasts (Figure 6). However, more studies are needed to truly confirm this conclusion.

Assimilation of sea ice chart can significantly improve the analysis and short-term forecasts of SIE and MIZ. Compared with the assimilation of AMSR2 SIC and SST (DA-Both0), all the experiments with the assimilation of sea ice chart (DA-Both1, DA-Both2, and DA-Both3) show significantly lower IIEE and IME (Figure 4). In particular, DA-Both3 emerges to produce significantly better analyses (Figure 4) and 1–2 days of forecasts for MIZ compared with DA-Both1 and DA-Both2 (Figure 6), although they tend to

10.3389/fmars.2025.1588769

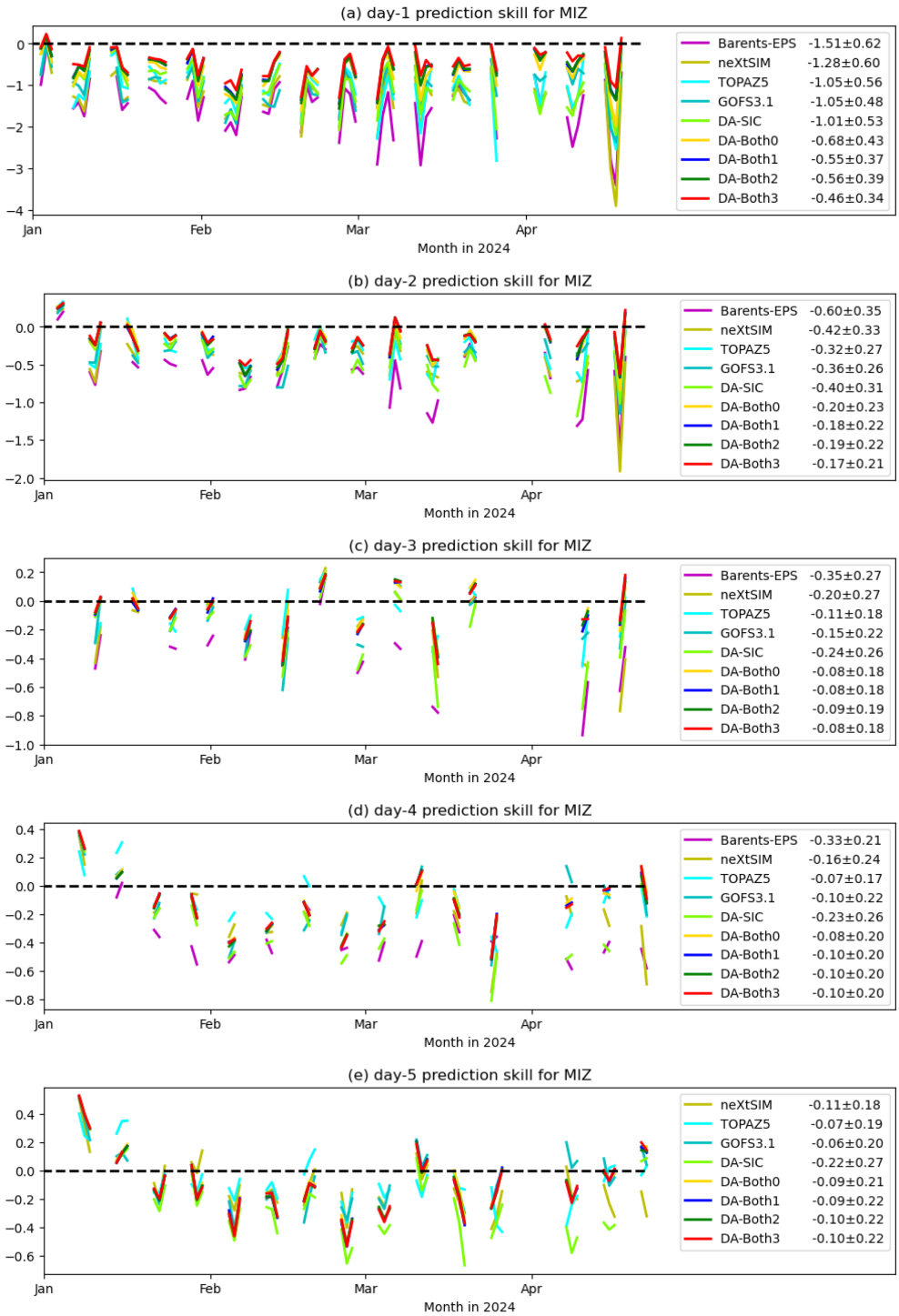

FIGURE 6
Prediction skills of the forecast MIZ evaluated against the persistence forecast of sea ice chart, from 1 to 5 days **(a–e)**. The experiments are referred to Table 1. It is noted that Barents-EPS only provides 4 days of forecast.

provide similar analyses and forecasts for SIE (Figures 4, 5). This indicates that the additional assimilation of the AMSR2 SIC tends to degrade the analyses and forecasts of MIZ when the ice chart has already been assimilated. This implies that the present AMSR2 SIC is not sufficiently accurate for distinguishing the MIZ from dense pack ice.

The present prediction skills for SIE and MIZ differ considerably. The Barents-LAON with assimilations of both SIC and SST (DA-Both0, DA-Both1, DA-Both2, and DA-Both3) all outperform the sea ice chart persistence for SIE forecasts except for the first day (Figure 5). However, the mean prediction skills for MIZ are still lower than the sea ice chart persistence (Figure 6), in all the experiments and all the operational

forecasts. This suggests that some important physical processes connected with the MIZ evolution may be not adequately described in the present coupled ocean and sea ice models, such as those related to waves. Such missing processes are particularly important for the regions of large transformation between MIZ and dense pack ice, as the Barents-LAON model does provide rather high prediction skills for SIE forecasts. The large model bias may be another factor leading to the unsatisfactory MIZ forecasts. Further improvements are needed for the present Barents-LAON to fully outperform the sea ice chart persistence for short-term SIE and MIZ forecasts.

The prediction skills for SIE and MIZ can be further improved, which is planned to be done in the near future. Firstly, the model system needs to be optimized. This is essential and actually a notable portion of the deterioration of the prediction skill is from the systematic model bias. As shown in Section 5, both of the ocean and sea ice model components have cold biases. Such model biases are highly likely related to the overestimated sea ice drift (Röhrs et al., 2023) and to the underestimated warm North Atlantic Current in the Norwegian Sea as seen in this study. These biases can be greatly mitigated through optimization of model parameters, for example using Green's functions (Menemenlis et al., 2005) or machine learning (Kutz, 2023). Secondly, the assimilation of the SST may be refined. The present configuration for the assimilations of both SIC and SST still has a noticeable mean bias in the SST field, for example, about −0.18°C on 19 February 2024 (Figure 3). This bias tends to increase with time, which can deteriorate the analyses and forecasts of SIE and MIZ. A better assimilation can mitigate the overall SST bias, thus improving the forecasts of SIE and MIZ. Thirdly, using instantaneous SIC observations instead of the daily mean observations for data assimilation may also improve the analyses and forecasts, as shown using the EnKF (Durán Moro et al., 2024). Finally, coupling the model system with a wave model may further improve the MIZ, particularly for the demarcation between the MIZ and dense pack ice, as the wave-ice interactions influence both physical/dynamical and thermodynamical processes in the MIZ.

Data availability statement

The raw data supporting the conclusions of this article will be made available by the authors, without undue reservation.

Author contributions

KW: Conceptualization, Data curation, Formal analysis, Funding acquisition, Investigation, Methodology, Project administration, Resources, Software, Validation, Visualization, Writing – original draft, Writing – review & editing. CW: Formal analysis, Investigation, Validation, Writing – review & editing. NH: Data curation, Investigation, Validation, Writing – review & editing. AA: Data curation, Investigation, Validation, Writing – review & editing.

Funding

The author(s) declare that financial support was received for the research and/or publication of this article. This study was supported by the Nordic Council of Ministers through project NOCOS DT (grant no. 102642), the Norwegian Research Council through project 4SICE (grant no. 328886), and the Norwegian FRAM Flagship program through project SUDARCO (grant no. 551323).

Acknowledgments

The authors are grateful to Gunnar Spreen in the University of Bremen for the discussion about the AMSR2 SIC. The constructive comments from the two reviewers are gratefully acknowledged.

Conflict of interest

The authors declare that the research was conducted in the absence of any commercial or financial relationships that could be construed as a potential conflict of interest.

Generative AI statement

The author(s) declare that no Generative AI was used in the creation of this manuscript.

Publisher's note

References

AMAP (2017). *Adaptation actions for a changing arctic (AACA) - barents area overview report, arctic monitoring and assessment programme (AMAP)* (Oslo, Norway: AMAP).

Arrigo, K. R. (2014). Sea ice ecosystems. *Annu. Rev. Mar. Sci.* 6, 439–467. doi: 10.1146/annurev-marine-010213-135103

Barber, D., Hop, H., Mundy, C., B., E., Dmitrenko, I., Tremblay, J., et al. (2015). Selected physical, biological and biogeochemical implications of a rapidly changing arctic marginal ice zone. *Prog. Oceanogr.* 139, 122–150. doi: 10.1016/j.pocean.2015.09.003

Bennetts, L., Bitz, C., Feltham, D. L., Kohout, A. L., and Meylan, M. H. (2022). Theory, modelling and observations ofmarginal ice zone dynamics:

multidisciplinaryperspectives and outlooks. *Phil.Trans.R.Soc.* 380, 20210265. doi: 10.1098/rsta.2021.0265

Bleck, R. (2002). An oceanic general circulation model framed in hybrid isopycnic-cartesian coordinates. *Ocean Model.* 37, 55–88. doi: 10.1016/S1463-5003(01)00012-9

Bouillon, S., Fichefet, T., Legat, V., and Madec, G. (2013). The elastic-viscous-plastic method revisited. *Ocean Model.* 71, 1–12. doi: 10.1016/j.ocemod.2013.05.013

Breivik, L., Carrieres, T., and Eastwood, S. (2009). *Remote sensing of sea ice* (Venice, Italy: ESA Publication WPP-306). doi: 10.5270/OceanObs09.cwp.11

Cavalieri, D. J. (1994). A microwave technique for mapping thin sea ice. *J. Geophys. Res.* 99, 12561–12572. doi: 10.1029/94JC00707

CMEMS (2024a). *Arctic ocean physics analysis and forecast, marine data store (mds).* doi: 10.48670/moi-00001

CMEMS (2024b). *Arctic ocean sea ice analysis and forecast, marine data store (mds).* doi: 10.48670/moi-00004

CMEMS (2024c). *Global ocean ostia sea surface temperature and sea ice analysis, marine data store (mds).* doi: 10.48670/moi-00165

Copeland, W., Wagner, P., Hughes, N., Everett, A., and Robertsen, T. (2024). The met Norway ice service: a comprehensive review of the historical and future evolution, ice chart creation, and end user interaction within metarea xix. *Front. Mar. Sci.* 11. doi: 10.3389/fmars.2024.1400479

Cummings, J., and Smedstad, O. (2013). "Variational data assimilation for the global ocean," in *Data assimilation for atmospheric, oceanic and hydrologic applications (Vol. II)*. Eds. S. Park and L. Xu (Springer-Verlag, Berlin, Heidelberg). doi: 10.1007/978-3-642-35088-713

Dinessen, F., and Hackett, B. (2018). *Product user manual for regional high resolution sea ice charts Svalbard region* (Toulouse, France: Copernicus Marine Service).

Duarte, P., Brændshøi, J., Shcherbin, D., Barras, P., Albretsen, J., Gusdal, Y., et al. (2022). Implementation and evaluation of open boundary conditions for sea ice in a regional coupled ocean (roms) and sea ice (cice) modeling system. *Geosci. Model. Dev.* 15, 4373–4392. doi: 10.5194/gmd-15-4373-2022

Dumont, D. (2022). Marginal ice zone dynamics: history, definitions and research perspectives. *Phil. Trans. R. Soc A* 380. doi: 10.1098/rsta.2021.0253

Dumont, D., Kohout, A., and Bertino, L. (2011). A wave-based model for the marginal ice zone including a floe breaking parameterization. *J. Geophys. Res.-Oceans* 116. doi: 10.1029/2010JC006682

Durán Moro, M., Sperrevik, A. K., Lavergne, T., Bertino, L., Gusdal, Y., Iversen, S. C., et al. (2024). Assimilation of satellite swaths versus daily means of sea ice concentration in a regional coupled ocean–sea ice model. *Cryoshpere* 18, 1597–1619. doi: 10.5194/tc-18-1597-2024

Egbert, G. D., and Erofeeva, S. Y. (2002). Efficient inverse modeling of barotropic ocean tides. *Atmos. Ocean. Tech.* 19, 183-204. doi: 10.1175/1520-0426(2002)019<0183:EIMOBO>2.0.CO;2

Feltham, D. L. (2005). Granular flow in the marginal ice zone. *Phil. Trans. R. Soc A* 363, 1677–1700. doi: 10.1098/rsta.2005.1601

Fritzner, S., Graversen, R., Christensen, K. H., Rostosky, P., and Wang, K. (2019). Impact of assimilating sea ice concentration, sea ice thickness and snow depth in a coupled ocean-sea ice modelling system. *Cryosphere* 13, 491–509. doi: 10.5194/tc-13-491-2019

Fritzner, S., Graversen, R., Wang, K., and Christensen, K. (2018). Comparison between a multi-variate nudging method and the ensemble kalman filter for sea-ice data assimilation. *J. Glaciol.* 64, 387–396. doi: 10.1017/jog.2018.33

Goessling, H. F., Tietsche, S., Day, J. J., Hawkins, E., and Jung, T. (2016). Predictability of the arctic sea ice edge. *Geophys. Res. Lett.* 43, 1642–1650. doi: 10.1002/2015GL067232

Hackett, B., Bertino, L., Ali, A., Burud, A., Williams, T., Xie, J., et al. (2023). *PRODUCT USER MANUAL for arctic ocean physical and BGC analysis and forecasting products, issue: 5.17* (Toulouse, France: Copernicus Marine Service).

Häkkinen, S. (1986). Coupled ice-ocean dynamics in the marginal ice zones: Upwelling/downwelling and eddy generation. *J. Geophys. Res.* 91, 819–832. doi: 10.1029/JC091iC01p00819

Hogan, T. F., Liu, M., Ridout, J. A., Peng, M. S., Whitcomb, T. R., Ruston, B. C., et al. (2014). The navy glabal environmental model. *Oceanography* 27, 116–125. doi: 10.5670/oceanog.2014.66

Hunke, E., Hebert, D., and Lecomte, O. (2013). Level-ice melt ponds in the los alamos sea ice model, cice. *Ocean Mod.* 71, 26–42. doi: 10.1016/j.ocemod.2012.11.008

Hunke, E., and Lipscomb, W. (2008). *CICE: The Los Alamos sea ice model, documentation and software user's manual, version 4.0. Tech. Rep. LA-CC-06-012* (Los Alamos, NM: LA-CC-06–012 Los Alamos National Laboratory).

Hunke, E., Lipscomb, W., Turner, A., Jeffery, N., and Elliott, S. (2015). CICE: the los alamos sea ice model documentation and software user's manual, version 5.1 *(LA-CC-06-012)*. Los Alamos, US.

Inoue, J., and Hori, M. E. (2011). Arctic cyclogenesis at the marginal ice zone: A contributory mechanism for the temperature amplification? *Geophys. Res. Lett.* 38. doi: 10.1029/2011GL047696

Johannessen, J. A., Johannessen, O. M., Svendsen, E., Shuchman, R., Manley, T., Campbell, W. J., et al. (1987). Mesoscale eddies in the fram strait marginal ice zone during the 1983 and 1984 marginal ice zone experiments. *J. Geophys. Res.-Oceans* 92, 6754–6772. doi: 10.1029/JC092iC07p06754

Josberger, E. G. (1983). Sea ice melting in the marginal ice zone. *J. Geophys. Res.-Oceans* 88, 2841–2844. doi: 10.1029/JC088iC05p02841

Kern, S., Lavergne, T., Notz, D., Pedersen, L., Tonboe, R., Saldo, R., et al. (2019). Satellite passive microwave sea-ice concentration data set intercomparison: closed ice and ship-based observations. *Cryosphere* 13, 3261–3307. doi: 10.5194/tc-13-3261-2019

Kohout, A. L., Williams, M. J. M., Dean, S. M., and Meylan, M. H. (2014). Storm-induced sea-ice breakup and the implications for ice extent. *Nature* 509, 604–607. doi: 10.1038/nature13262

Kristensen, N., Debernard, J., Maartensson, K., Wang, S., and Hedstrom, K. (2017). *metno/metroms: Version 0.3 - before merge (v0.3)*. Geneva, Switzerland. doi: 10.5281/zenodo.1046114

Kutz, J. N. (2023). Machine learning for parameter estimation. *PNAS* 120. doi: 10.1073/pnas.2300990120

Larson, J., Jacob, R., and Ong, E. (2005). The model coupling toolkit: A new fortran90 toolkit for building multiphysics parallel coupled models. *he Int. J. High Perform. C.* 19, 277–292. doi: 10.1177/1094342005056115

Lipscomb, W., and Hunke, E. (2004). Modeling sea ice transport using incremental remapping. *Mon. Wea. Rev.* 132, 1341–1354. doi: 10.1175/1520-0493(2004)132<1341:MSITUI>2.0.CO;2

Lipscomb, W., Hunke, E., Maslowski, W., and Jakacki, J. (2007). Improving ridging schemes for high-resolution sea ice models. *J. Geophy. Res.-Ocean* 112, C03S91. doi: 10.1029/2005JC003355

Liu, J., Scott, K. A., and Fieguth, P. W. (2019). Detection of marginal ice zone in synthetic aperture radar imagery using curvelet-based features: a case study on the canadian east coast. *J. Appl. Remote Sens.* 13, 1–14. doi: 10.1117/1.JRS.13.014505

Maslanik, J., Drobot, S., Fowler, C., Emery, W., and Barry, R. (2012). On the arctic climate paradox and the continuing role of atmospheric circulation in affecting sea ice conditions. *Geophys. Res. Lett.* 34, 1501–1515. doi: 10.1029/2006GL028269

Maykut, G. A., and Perovich, D. K. (1987). The role of shortwave radiation in the summer decay of a sea ice cover. *J. Geophy. Res.* 92, 7032–7044. doi: 10.1029/JC092iC07p07032

Melsheimer, C. (2019). *ASI version 5 sea ice concentration user guide, version V0.92* (Bremen, Germany: Unversity of Bremen).

Menemenlis, D., Fukumori, I., and Lee, T. (2005). Using green's functions to calibrate an ocean general circulation model. *Monthly Weather Reviewer* 133, 1224–1240. doi: 10.1175/MWR2912.1

Metzger, E. J., Helber, R. W., Hogan, P. J., Posey, P., Thoppil, P., Townsend, T., et al. (2017). *Global ocean forecast system 3.1 validation testing, NRL/MR/7320-17-9722* (Stennis Space Center, MS: Naval Research Laboratory).

Olsen, J., Hovelsrud, G., and Kaltenborn, (2020). *Increasing shipping in the arctic and local communities' Engagement: A case from longyearbyen on svalbard* (New York, US: Springer). doi: 10.1007/978-3-030-28404-614

Padman, L., and Dillon, T. M. (1991). Turbulent mixing near the yermak plateau during the coordinated eastern arctic experiment. *J. Geophys. Res.* 96, 4769–4782. doi: 10.1029/90JC02260

Palma, D., Varnajot, A., Dalen, K., Basaran, I. K., Brunette, C., Bystrowska, M., et al. (2019). Cruising the marginal ice zone: climate change and arctic tourism. *Polar Geogr.* doi: 10.1080/1088937X.2019.1648585

Posey, P. G., Metzger, E. J., Wallcraft, A. J., Hebert, D. A., Allard, R. A., Smedstad, O. M., et al. (2015). Improving arctic sea ice edge forecasts by assimilating high horizontal resolution sea ice concentration data into the us navy's ice forecast systems. *Cryosphere* 9, 1735–1745. doi: 10.5194/tc-9-1735-2015

Rampal, P., Dansereau, V., Olason, E., Bouillon, S., Williams, T., Korosov, A., et al. (2019). On the multi-fractal scaling properties of sea ice deformation. *Cryosphere* 13, 2457—2474. doi: 10.5194/tc-13-2457-2019

Røed, L. P., and O'Brien, (1983). A coupled ice-ocean model of upwelling in the marginal ice zone. *J. Geophys. Res.* 88, 2863–2872. doi: 10.1029/JC088iC05p02863

Röhrs, J., Gusdal, Y., Rikardsen, E., Duran Moro, M., Brændshøi, J., Kristensen, N. M., et al. (2023). Barents-2.5km v2.0: An operational data-assimilative coupled ocean and sea ice ensemble prediction model for the barents sea and svalbard. *Geosci. Model. Dev.* 16, 5401–5426. doi: 10.5194/gmd-16-5401-2023

Rothrock, D. (1975). The energetics of the plastic deformation of pack ice by ridging. *J. Geophys. Res. Oceans* 80, 4514–4519. doi: 10.1029/JC080i033p04514

Sakov, P., Counillon, F., Bertino, L., Lisæter, K. A., Oke, P. R., and Korablev, A. (2012). Topaz4: an ocean-sea ice data assimilation system for the north atlantic and arctic. *Ocean Sci.* 8, 633-656. doi: 10.5194/os-8-633-2012

Sakov, P., and Oke, P. (2008). A deterministic formulation of the ensemble kalman filter: an alternative to ensemble square root filters. *Tellus* 60A, 361–371. doi: 10.1111/j.1600-0870.2007.00299.x

Sandø, A., Nilsen, J., Gao, Y., and Lohmann, K. (2010). Importance of heat transport and local air-sea heat fluxes for barents sea climate variability. *J. Geophys. Res. - Oceans* 115, C07013. doi: 10.1029/2009JC005884

Shchepetkin, A. F., and McWilliams, J. C. (2005). The regional ocean modeling system: A split-explicit, free-surface, topography following coordinates ocean model. *Ocean Model.* 9, 347–404. doi: 10.1016/j.ocemod.2004.08.002

Shen, H. H., Hiber, W. D., and Lepparanta, M. (1987). The role of floe collisions in sea ice rheology. *J. Geophys. Res.-Oceans* 92, 7085–7096. doi: 10.1029/JC092iC07p07085

Smedsrud, L., Esau, I., Ingvaldsen, R., Eldevik, T., Haugan, P., Li, C., et al. (2013). The role of the barents sea in the arctic climate system. *Rev. Geophys.* 51, 415–449. doi: 10.1002/rog.20017

Spreen, G., Kaleschke, L., and Heygster, G. (2008). Sea ice remote sensing using amsr-e 89-ghz channels. *J. Geophys. Res. Oceans* 113, C02S03. doi: 10.1029/2005jc003384

Squire, V. A. (2007). Of ocean waves and sea-ice revisited. *Cold Regions Sci. Tech.* 49, 110–133. doi: 10.1016/j.coldregions.2007.04.007

Squire, V. A., Dugan, J. P., Wadhams, P., RotTier, P. J., and Liu, A. K. (1995). Of ocean waves and sea-ice. *Annu. Rev. Fluid Mechanics* 27, 115–168. doi: 10.1146/annurev.fl.27.010195.000555

Steele, M. (1992). Sea ice melting and floe geometry in a simple ice-ocean model. *J. Geophys. Res.-Oceans* 97, 17729–17738. doi: 10.1029/92JC01755

Stephenson, S. R., Smith, L. C., and Agnew, J. A. (2011). Divergent long-term trajectories of human access to the arctic. *Nat. Climate Change* 1, 156–160. doi: 10.1038/nclimate1120

Stocker, A., Renner, A., and Knol-Kauffman, M. (2020). Sea ice variability and maritime activity around svalbard in the period 2012–2019. *Sci. Rep.* 10, 17043. doi: 10.1038/s41598-020-74064-2

Strong, C. (2012). Atmospheric influence on arctic marginal ice zone position and width in the atlantic sector, february–april 1979–2010. *Clim. Dyn.* 39, 3091–3102. doi: 10.1007/s00382-012-1356-6

Sunfjord, A., Fer, Y., Kasajima, I., and Svendsen, H. (2007). Observations of turbulent mixing and hydrography in the marginal ice zone of the barents sea. *J. Geophys. Res.-Oceans* 112. doi: 10.1029/2006JC003524

Thorndike, A., Rothrock, D., Maykut, G., and Colony, R. (1975). The thickness distribution of sea ice. *J. Geophys. Res.* 80, 4501—4513. doi: 10.1029/JC080i033p04501

Tucker, W. B., Grenfell, T. C., Onstott, R. G., Perovich, D. K., Gow, A. J., Shuchman, R. A., et al. (1991). Microwave and physical properties of sea ice in the winter marginal ice zone. *J. Geophys. Res.* 96, 4573–4587. doi: 10.1002/jgrc.20171

Turner, A. K., Hunke, E. C., and Bitz, C. M. (2013). Two modes of sea-ice gravity drainage: A parameterization for large-scale modeling. *J. Geophys. Res. Oceans* 118, 2279–2294. doi: 10.1002/jgrc.20171

Vinje, T. (2001). Fram strait ice flux and atmospheric circulation: 1950-2000. *J. Clim.* 14, 3508–3517. doi: 10.1175/1520-0442(2001)014<3508:FSIFAA>2.0.CO;2

Wang, K. (2025). *metroms coin v2.0: Coupled ROMS-CICE with COIN/LAON data assimilation for SIC and SST*. Geneva, Switzerland. doi: 10.5281/zenodo.15433887

Wang, K., Ali, A., and Wang, C. (2023). Local analytical optimal nudging for assimilating amsr2 sea ice concentration in a high-resolution pan-arctic coupled ocean (hycom 2.2.98) and sea ice (cice 5.1.2) model. *Cryosphere.* 17, 4487–4510. doi: 10.5194/tc-17-4487-2023

Wang, K., Debernard, J., Sperrevik, A. K., Isachsen, P. E., and Lavergne, T. (2013). A combined optimal interpolation and nudging scheme to assimilate osisaf sea-ice concentration into roms. *Ann. Glaciology* 64, 8–12. doi: 10.3189/2013aog62a138

Wang, K., Lavergne, T., and Dinessen, F. (2020). Multisensor data merging of sea ice concentration and thickness. *Adv. Polar Sci.* 31, 1–13. doi: 10.3189/2013aog62a138

Wang, K., Wang, C., Dinessen, F., Spreen, G., Ricker, R., and Tian-Kunze, X. (2024). Multisensor data fusion of operational sea ice observations. *Front. Mar. Sci.* 11. doi: 10.3389/fmars.2024.1366002

Warner, J. C., Sherwood, C. R., Arango, H. G., and Signell, R. P. (2005). Performance of four turbulence closure models implemented using a generic length scale method. *Ocean Model.* 8, 81–113. doi: 10.1016/j.ocemod.2003.12.003

Wassmann, P. (2011). Arctic marine ecosystems in an era of rapid climate change. *Prog. Oceanography* 90, 1–17. doi: 10.1016/j.pocean.2011.02.002

Williams, T., Korosov, A., Rampal, P., and Ólason, E. (2021). Presentation and evaluation of the arctic sea ice forecasting system nextsim-f. *Cryosphere* 15, 3207–3227. doi: 10.5194/tc-15-3207-2021

WMO (2014). SEA ICE NOMENCLATURE. *No. 259* (Geneva, Switzerland: WMO).

frontiers | Frontiers in Marine Science

TYPE Review
PUBLISHED 08 October 2025
DOI 10.3389/fmars.2025.1561461

OPEN ACCESS

EDITED BY
Ludovic Brucker,
NOAA NESDIS Center for Satellite Applications and Research, United States

REVIEWED BY
Lynn Pogson,
Environment and Climate Change Canada, Canada
Laurence Connor,
Center for Satellite Applications and Research (NOAA), United States

*CORRESPONDENCE
Patrick B. Eriksson
patrick.eriksson@fmi.fi

RECEIVED 15 January 2025
ACCEPTED 05 September 2025
PUBLISHED 08 October 2025

CITATION
Eriksson PB, Vainio J, Tollman N, Jokiniemi A, Arola A, Mäkynen M, Karvonen J and Kangas A (2025) The Finnish Ice Service, its sea-ice monitoring of the Baltic Sea and operational concept.
Front. Mar. Sci. 12:1561461.
doi: 10.3389/fmars.2025.1561461

The Finnish Ice Service, its sea-ice monitoring of the Baltic Sea and operational concept

Patrick B. Eriksson[1]*, Jouni Vainio[1], Niko Tollman[1], Anni Jokiniemi[1], Aleksi Arola[1], Marko Mäkynen[2], Juha Karvonen[2] and Antti Kangas[3]

[1]Oceanographical Services, Ice Service, Finnish Meteorological Institute, Helsinki, Finland, [2]Marine Research, Sea Ice and Remote Sensing, Finnish Meteorological Institute, Helsinki, Finland, [3]Customer Services, Safety, Finnish Meteorological Institute, Helsinki, Finland

The Finnish Ice Service is part of the Finnish Meteorological Institute (FMI). Based on the mandate in the Finnish legislation, it provides information on the ice conditions in the Baltic Sea. This paper introduces the methods used by the Finnish Ice Service, data sources, products, services, datasets, and supporting Baltic Sea ice remote sensing and geophysics research conducted at FMI. The predecessor of the Finnish Ice Service started its operational ice charting in 1915 to provide ice information for the winter navigation. To this day, the main users still are the winter navigation authorities, including the icebreaker fleet and management, as well as the shipping community, scientists and general public. The focus area is the Baltic Sea. Typically, the service operates from mid-October to the end of May, providing up-to-date sea-ice information in several products and formats. The prevailing ice situation is described in ice charts, ice reports and ice codes, which are based on a range of different observation sources like satellite images, predominantly from synthetic aperture radars, and surface observations from both icebreakers and coastal observers. The Finnish Ice Service has long sea ice observation timeseries and archives of manually analysed ice charts. To help users and customers optimize their operations in ice infested waters, the Finnish Ice Service provides numerical and manual sea ice forecasts with various forecast lengths. The Finnish Ice Service processes and disseminates satellite data and also provides advisory and consultant services to users. As FMI is committed to the open data policy, the main ice service products are provided free of charge. A number of products are also available through the Copernicus Marine Service (CMS).

KEYWORDS

sea ice, ice service, remote sensing, ice chart, Baltic Sea

1 Introduction

Sea ice has always been intriguing and interesting for a lot of people and for many reasons. To know its structure and physics are scientifically important, but it also has a major effect on the transport at sea. In the seasonally ice-covered sea areas, like the Baltic Sea, the ice conditions must be taken into account in shipping and other travelling (Figure 1). Understanding sea ice and its behaviour, and translating that understanding into supportive services for shipping, was early identified as a key topic for the countries on both sides of the northern Baltic Sea (WNRB, 1972). Continuous shipping also during wintertime has been considered a vital component for maintaining a competitive national economy (MINTC, 2014). The Finnish Ice Service has been established to support and facilitate this wintertime activity.

1.1 History of the Finnish Ice Service

The Baltic Sea has always been an important sailing route and in the 19th century there was a rising interest in extending the navigational season also during winter. For this purpose, many different ways of observing and exchanging information on ice conditions were created. In 1846, the Finnish Society of Sciences and Letters began to collect ice observations from the coastal sea areas. Since then, the work has increasingly been carried out to favour economic interests. In 1890, Finland got its first icebreaker called 'Murtaja' (Ramsay, 1949).

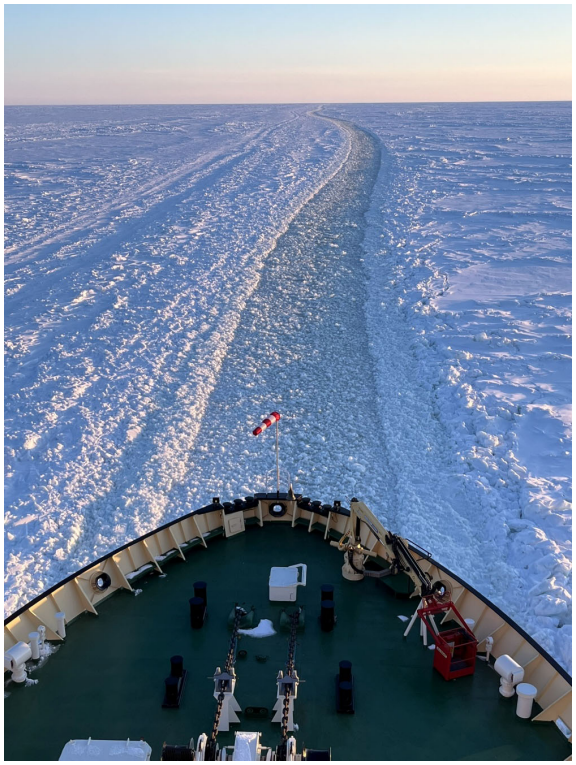

FIGURE 1
Sea ice field and ship track in the Bay of Bothnia as seen from the bridge of the Finnish icebreaker Urho (photo: Jarkko Toivola).

At the very end of the 19th century, the ice observation network was made operational. Ice charts were drawn at eight lighthouses along the Finnish coast. The work was supervised by the Finnish Society of Sciences and Letters. However, the data was collected with a delay. The World War I changed the situation. The Russian Imperial Navy quickly needed reliable ice data for its strategic planning and merchant ships also needed better and more real-time sea ice information. The Imperial Navy ordered the Finnish Society of Science and Letters to make real-time ice charts. The Finnish Society of Science and Letters began to renew its observation routines, and since March 1915, ice charts were drawn weekly (Granqvist, 1926).

The Finnish Institute of Marine Research (FIMR) began its operation on the 1st of January 1919 with the task of studying and monitoring the sea areas around Finland. At the same time, the existing ice monitoring duties were transferred to FIMR, where the ice service now was an essential part of the institute's functions. The first ice chart published by the institute was on the 17th January 1919 (Witting, 1920). The Finnish Ice Service was part of FIMR until it was disbanded 31.12.2008. Since then, the Finnish Ice Service, along with ice research and physical oceanography, has been part of FMI. Today the Ice Service is part of FMI's operational duty functions. The Institute's main duties are to observe and research the atmosphere, near space, and the seas, and to provide information and services for public safety, businesses, and citizens.

An in-depth historical review of the Ice Service's first 75 years has been published by Seinä et al. (1997).

1.2 The Baltic Sea

The Baltic Sea is a semi-enclosed brackish sea water basin in Northern Europe. The ice cover in the Baltic Sea usually begins to form in November and has its largest extent between January and March (Leppäranta, 1984). The normal ice break-up starts in April and the ice melts completely by the beginning of June. The maximum annual extent of ice cover in the Baltic Sea has varied from 37–000 km² to 420–000 km² (which is the whole Baltic Sea coverage). As longest, the ice season may be up to 220 days in the northern Bay of Bothnia. Figure 2 shows time series of maximum ice extent in 1971-2024.

The ice in the Baltic Sea occurs as landfast ice and drift ice. Landfast ice occurs in the coastal and archipelago areas. Drift ice has a dynamic nature due to forcing by winds and currents. The motion of drift ice results in an uneven and broken ice field with distinct floes up to several kilometres in diameter, leads and cracks, brash ice barriers, rafted ice and ice ridges. In the Bay of Bothnia, the annual maximum level ice thickness is typically 0.65–0.80 m, and it reaches 0.3–0.5 m even in mild winters (Seinä and Peltola, 1991; Vihma and Haapala, 2009). The measured all time maximum is around 1.2 m. In the Southern Baltic Sea, the coastal areas of Germany and Poland and the Danish Straits, the annual maximum level ice thickness seldom exceeds 0.5 m (Leppäranta and Hakala, 1992). The

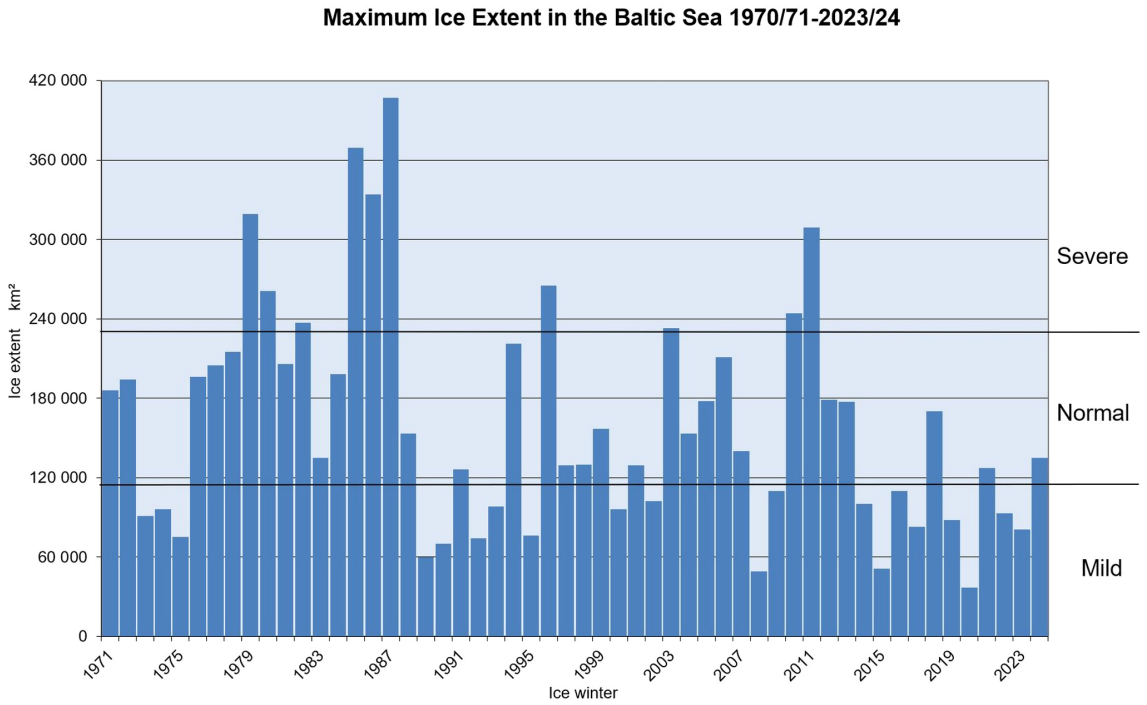

FIGURE 2
Maximum ice extent of the Baltic Sea 1970/71 - 2023/24, including the ice winter severeness limits.

thickness of ice ridges, calculated as the sail height plus keel depth, is typically 5 to 15 m (Leppäranta and Hakala, 1992). The salinity of the Baltic Sea ice is typically from 0.2 to 2‰ depending on the location, time and weather (Hallikainen, 1992).

1.3 Finnish Ice Service today

The Finnish Ice Service operates at the FMI under the Ministry of Transport and Communications, alongside other maritime agencies. The service is part of the Oceanographic Services group, within the Weather and Safety Centre, working side by side with the operational weather forecasters, see Figure 3. The Ice Service staff currently consists of six junior and senior sea ice analysts, located in the FMI main office in Helsinki.

Nowadays approximately 95% of Finland's international trade is transported by sea (Tulli, 2024). Finland and Estonia are the only countries in the world where all mainland harbours freeze during normal winters. Operating effectively and safely in ice conditions is crucial for year-round commercial shipping and supply security.

Still today, the main purpose of the Ice Service is to provide ice information for the support of winter navigation. Wintertime ship navigation and icebreaker operations in the Baltic Sea rely heavily on this information, provided by national Ice Services. The other users are researchers and citizens interested in ice conditions. The most important source of sea ice information is provided by satellite images. Other sources include sea ice model data and *in-situ* observations. The most important sea ice parameters comprise the location of the sea ice edge, sea ice and snow thickness, degree of deformation and ice concentration (Berglund and Eriksson, 2015).

The daily ice chart is the main product of the Ice Service, but the work consists of several other duties too. The Finnish Ice Service provides ice information as text and in numeral formats, makes ice forecasts, gives consultancy services and answers questions from the public and media.

The Finnish Ice Service is closely co-operating with the Ice Service at the Swedish Meteorological and Hydrographical Institute (SMHI). Since the winter 2017/18 the ice chart has been produced together, on a week-to-week basis.

The Finnish Ice Service is part of the international network of ice experts and the ice expert community of the Baltic Sea. It is a founding member of the International Ice Charting Working Group (IICWG) and the Baltic Sea Ice Meeting (BSIM) and an active member of the World Meteorological Organization (WMO).

2 Operational service

2.1 Description of the operational routines

The Finnish Ice Service starts operation in early October by monitoring the cooling of the sea surface water. Charts with analysed SST's are produced bi-weekly, on Mondays and Thursdays. The start date has varied on the course of time, but in recent years it has been fixed to the start in mid-October. When the freezing starts and ice conditions become more challenging for the maritime traffic, the Finnish Transport Infrastructure Agency

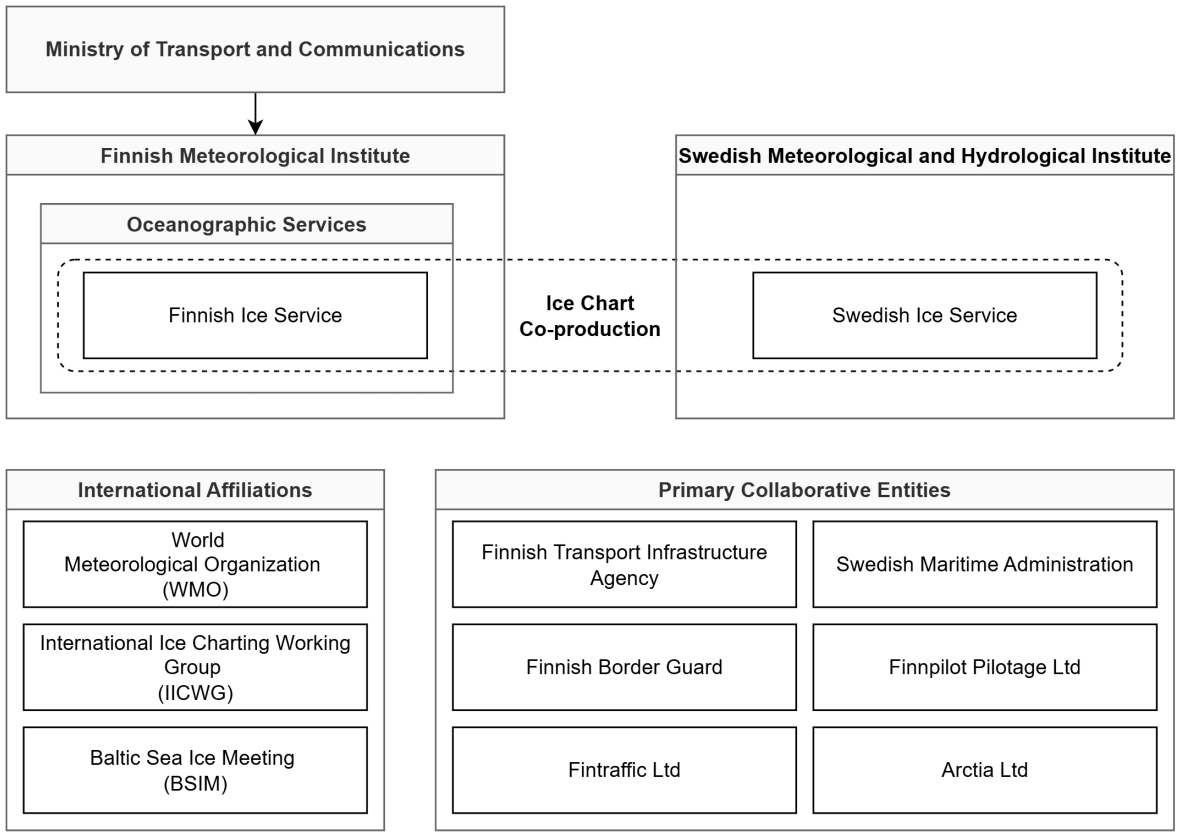

FIGURE 3
Organizational chart of the Finnish Ice Service and its most important connections.

(FTIA) or the Swedish Maritime Administration (SMA) sends out their first icebreakers and issue national assistance restrictions for the ships. That triggers daily production of the ice charts, ice reports and ice codes along with the other ice service products and services, see Figure 4 for operational workflow. Typically, this happens in mid-December but may vary between late November and early January. During normal operation in mid-winter, ice charts are published daily seven days a week until the ice melt-up. The ice service is continued until the sea ice has practically melted from the northern Baltic Sea, typically mid-May [varying from early May to early June (FMI, 2025)]. The typical operation day starts when the ice analyst checks the weather observations and forecasts, the previous day's ice conditions and the icebreaker and administration messages and announcements. Then the ice analyst goes through all available satellite images, which serve as a backbone for the sea-ice charting. The Synthetic Aperture Radar satellites (SAR), which are the main source of spatial information, are in a sun-synchronous polar orbit, meaning the acquisition happens early morning and early evening. The downlinking and processing take from 30 minutes up to a few hours, and images are available for the analyst in the morning, well before noon. Analysis of the ice situation is typically based on morning SAR images, but in lack of such, the previous evening's SAR images or optical satellite images are used. The darkness and cloudiness frequently prohibit the use of optical satellites until March. The ice report is written before noon, and the assisting ice analyst translates it to Swedish and English and publishes it around noon. After this the ice chart is finalized. The ice chart contains information from the icebreaking administrations in both Finland and Sweden and is added to the chart along any additional comments from the stand-by institute. The ice chart is published in the afternoon around 2 pm. At the end of the day, the ice codes are generated and published.

At present, three ice experts are responsible for the ice information production. The duty work is conducted during office hours, also including weekends. In addition to the operational duties, the ice experts are responsible for various support tasks. These include ordering satellite images, managing the ice observation network and numerical processing of observation data, to mention a few. Since the operational duty is limited to office hours, it may not be possible to get answers to questions about satellite imagery on weekends or in the evenings. However, inquiries about the ice situation on weekends and often also in the evenings are answered, as the on-call phone is forwarded to the mobile phone of the ice expert on duty. The on-duty ice expert also responds to inquiries from the media.

The co-production with the Swedish Ice Service runs on a week-to-week basis, where one of the ice services is doing the analysis from Tuesday to Monday, and the other is in stand-by. Other products and services than ice charts are produced separately at each institute. Thus, when the FMI Ice Service is in standby mode, the SMHI Ice Service

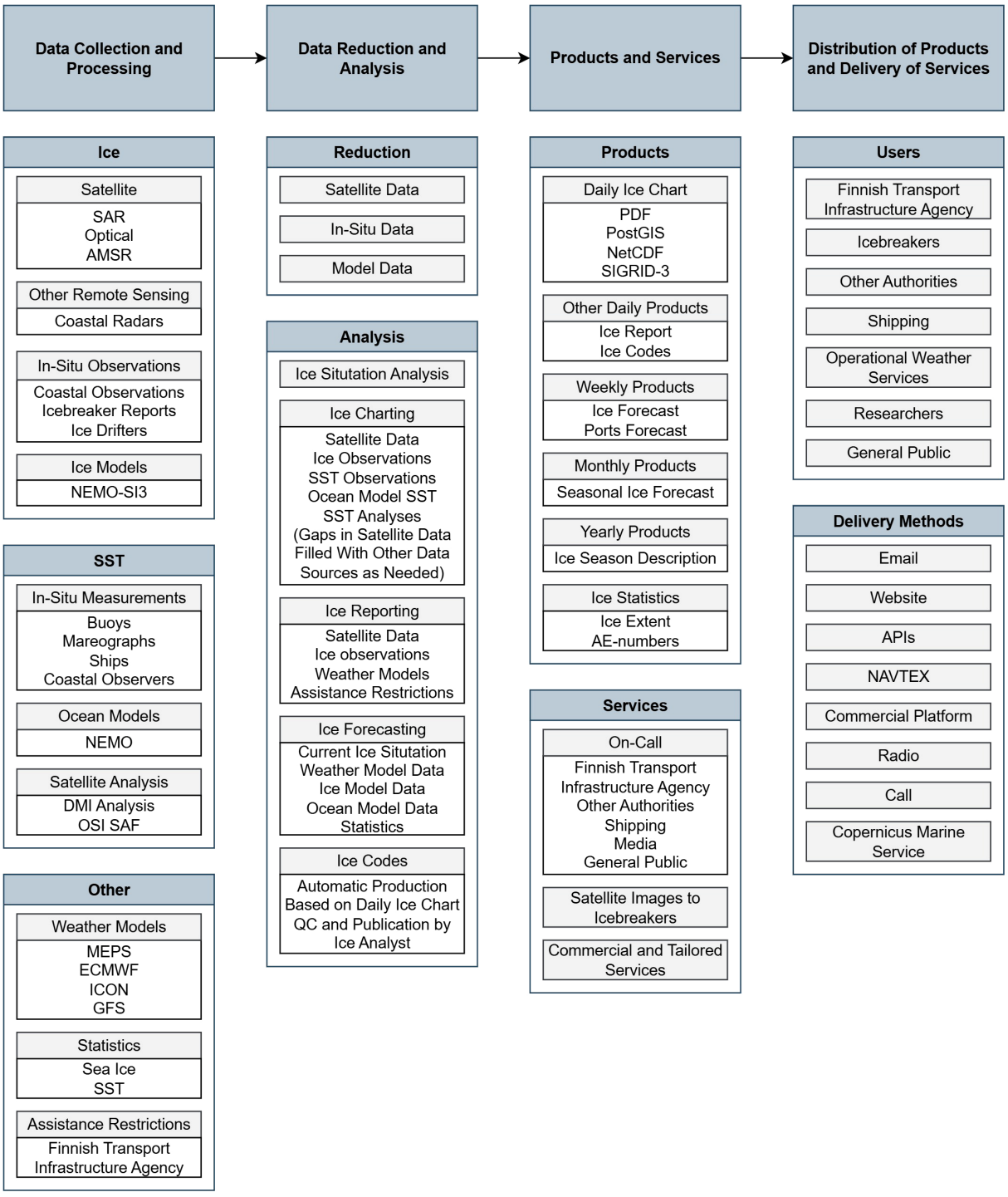

FIGURE 4
Operational workflow at the Finnish Ice Service.

performs the actual ice charting, but a certain review of the ice condition is anyhow done at FMI in order to be able to issue ice reports and codes and serve any customers, the media or other users.

For the ice charting, commonly available GIS software are used. At the moment of writing, FMI is using ArcGIS10 with in-house developed plug-ins, co-developed with the SMHI ice service. FMI uses its own ice service tools and software, dedicated for generating and publishing ice reports and ice codes. The data formats are commonly used standard formats, such as pdf's, shapefiles, png's or plain text.

2.2 Winter navigation authorities

The operational winter navigation function can be seen as a consortium of the units of the different authorities that manage ice navigation to Finnish ports. The winter navigation is managed by the Finnish Traffic Infrastructure Agency and supported by the relevant actors at Fintraffic VTS (Vessel Traffic Service), the Border Guard, the pilotage company FINNPILOT and the FMI Ice Service. One of the most important elements of the winter navigation is the assistance provided by icebreakers and the associated assistance restriction system. The Ice Service contributes to the dissemination of this navigational information by including the restriction information in both the ice chart and the ice reports.

The Ice Service works closely with the icebreaking operation, and the on-duty ice analyst closely monitors the reports and ice observations from the icebreakers and pilots, using these to describe the ice situation. From icebreaker reports, it is possible to interpret many other details about the ice conditions than just specific ice observation information. For example, the trafficability and difficulty in a sea area can be interpreted if an icebreaker reports the need for towing vessels, which types of vessels manage without assistance and which not, or where vessels get stuck in the ice. Additional aid to the ice analysis can be retrieved from the icebreakers' observations of the ice drift.

2.3 IBNet

The icebreaking operation uses an online information system called IBNet. It is jointly developed and operated by the Finnish Transport Infrastructure Agency and the Swedish Maritime Administration for coordination of the joint icebreaking operations by the two neighbouring countries. IBNet contains information about the weather, ice and traffic situation, and transmits the information between the different connected units (icebreakers, coordination centres, VTS etc.) (BIM, 2020). The Ice Services in both Finland and Sweden have access to the system in order to share information with the icebreaking parties.

In IBNet, the icebreakers report on the prevailing ice conditions in their respective operation areas. This reporting is done on a regular basis with several reports per day. The reporting form contains predefined fields for the most important sea ice parameters: ice concentration, thickness, degree of deformation, ice pressure, drift direction and speed, weather and a free text field for additional ice information.

FMI can also be considered a content producer for IBNet. The satellite data processed by FMI are uploaded to its data interface (WMS server), from where the IBNet server extracts them in an agreed format in near-real-time. Also weather observations, weather and ice forecasts and water level observations are visualized in IBNet. In the map user interface of IBNet, the icebreaking personnel can visualize all metocean products, including satellite imagery, in one view together with essential traffic and maritime information (AIS targets and tracks, fairway information etc.). The information provided by FMI via IBNet also serves pilots and VTS centres.

2.4 Commercial and tailored services

In addition to the daily ice monitoring, the FMI Ice Service also provides customized services like briefings, and special operational services. The Ice Service offers tailored products like weather and ice case studies, official statements and statistical ice studies and reports. The clients for these products are often entities involved in navigation, offshore construction or coastal engineering.

As the FMI operates a separate Customer Services unit, the Ice Service naturally works in close cooperation with the maritime sector of that unit, providing content and expertise to their services.

3 Input data sources

Like most ice services in the world, the FMI Ice Service also collects data from all available sources and compiles it in a number of different outputs, in particular in the form of an ice chart in vectorized form (polygons with several parameters) (WMO, 2021). The analysis is almost entirely based on manual interpretation made by ice analysis experts. The most important ice information sources are 1) satellite images, 2) icebreaker observations, 3) manual observations from coastal stations, 4) ice drifters and 5) numerical prediction models, in order of importance. The output formats are printable charts (PDF), NetCDF grids and the Shape-like SIGRID-3 format (although still in Beta phase).

3.1 Ice thickness and sea surface temperature observations

FMI has around 20 ice observation stations along the Finnish coast where fast ice thickness is measured manually by drilling a hole through the ice, see Figure 5 Observers are typically local people like fishermen, ice skaters, or border guards. If the ice situation doesn't allow an observer to go on the ice, ice thickness can be visually estimated. The snow depth on ice is also measured. Measurements are done once a week and delivered to the Ice Service using an electronic form. The oldest observations were done in 1897. Most of the old observations are in paper form. Since 2016, observations have been collected in digital form. In addition to FMI's own observation network, ice observations are obtained directly from icebreakers, as described above.

Sea Surface Temperature (SST) is measured by water level measurement stations, wave and temperature buoys, and fixed stations. In total, FMI has around 30 temperature measurement sites. The vast majority of buoys are lifted up for the winter. In addition, SST information is obtained from a few merchant ships travelling in the Baltic Sea with a Ferry Box or hull thermometer installed. Not all SST observations are obtained in real-time. The ice

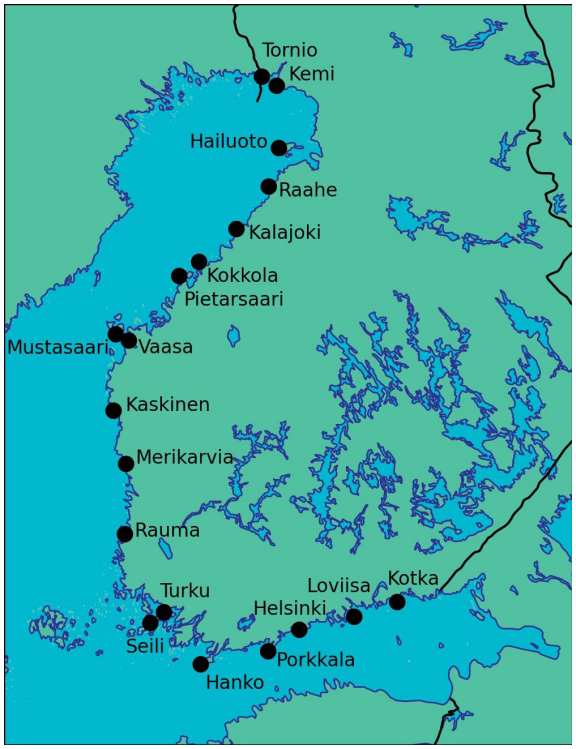

FIGURE 5
Locations of the FMI coastal ice observation stations active in the recent years. In some locations there are multiple measurement stations close by.

analysis takes into account up to two days old temperature observations. In addition to surface observations, temperature information is also collected from satellite analysis products, like OSI SAF products offered by Eumetsat, and from numerical oceanographic models.

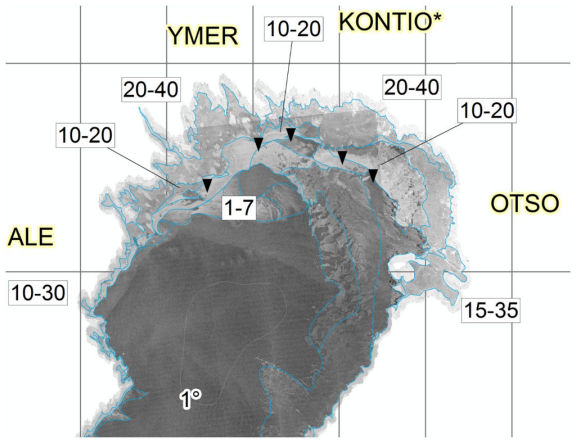

FIGURE 6
A Sentinel-1 SAR satellite image over the Northern Bay of Bothnia as viewed in the ice charting tool Vanadis, with the ice analyst's division of the sea ice into polygons.

3.2 Satellite data

Remote sea-ice monitoring was done by means of aerial reconnaissance from 1934 through an agreement with the Navy and the Coast Guard. In the 1940's, aerial reconnaissance was already a regular help for the ice monitoring and for the winter navigation. Later, the airplanes were replaced by helicopters operated from icebreakers. With the introduction of satellite imaging in the late 1960's, the importance of EO data gradually increased. The first test images became available for ice monitoring in 1967 (Grönvall, 1984). The following winter, the Ice Service received images already a couple of hours after acquisition. In the beginning of the 21st century, aerial reconnaissance practically phased out as increasingly frequent acquisition of SAR imagery became routine.

By cloudy weather the Ice Service relies almost entirely on SAR acquisitions conducted the same morning. And in fact, this is the case during most of the first half of the winter. The use of optical imagery increases from March with more daylight and clearer skies.

3.2.1 SAR images

The use of spaceborne SAR started in 1992 with ERS-1 SAR, first in experimental mode and operationally in 1994 (Seinä et al., 1997). The major advantages of SAR images compared to optical images are their independence on the amount of daylight and cloud cover, and better information content on sea ice cover, notably degree of ice deformation can be interpreted from the SAR images. The spatial resolution of ERS-1 SAR in operational use was 100 m and the image size 100 by 100 km. The small image size was the major drawback of the ERS-1 images; one image did not even cover the Bay of Bothnia. In 1998 RADARSAT-1 ScanSAR Narrow images (width 300 km) replaced ERS-1/2 SAR images and in 2003 ScanSAR Wide images were used for the first time. The RADARSAT-1 ScanSAR Wide images also had a resolution of 100 m in operational use, but their image size was around 500 by 500 km and, thus, one image covered e.g. the whole Bay of Bothnia or Gulf of Finland. Currently, the SAR imagery used are mainly acquired by Sentinel-1 in Extra-Wide Swath (EW, width 410 km) and Interferometric Wide Swath (IW, 250 km width) modes and by RADARSAT-2 and Radarsat Constellation Mission (RCM, a Canadian three SAR satellite constellation) in ScanSAR mode. The SAR imagery is received through licenced services from CMS. These all operate at C-band (wavelength about 5 cm). Additionally, a valuable set of X-band (wavelength about 3 cm) SAR data from COSMO-SkyMed, TerraSAR-X and Hisdesat PAZ completes the selection. Figure 6 shows a SAR satellite image viewed in the ice charting tool Vanadis.

3.2.2 Optical and Infrared sensors

When a satellite orbit passes over the Baltic Sea, a medium resolution (250 to 1000 m) spectrometer imagery usually cover the whole Baltic Sea. Unfortunately, the use of optical and thermal infrared imagery is heavily restricted by cloud cover, and optical imagery also by the short days during the early and mid-winter. The benefit of using optical imagery increases from March with more

daylight and clearer skies. In cases when satellites operated in the optical bands offer a clear view of the ice situation, it often makes distinction between ice and open water remarkably easier than can be done from SAR imagery. This benefit is further accentuated during the melt period, since wet snow on ice or wet ice surface attenuate the SAR backscattering from sea ice, resulting to reduced contrast in the SAR imagery (Howell et al., 2018; Mahmud et al., 2020).

3.2.3 Satellite data transmission and preprocessing

The satellite data are ordered in advance by the FMI ice analysts using a dedicated online ordering system. The satellite data are received at the Sodankylä ground station located in northern Finland. ESA Sentinel data are available in near-real-time (NRT) though the Copernicus data hubs with their user interface and also through ftp. The data from the other satellites are available from ftp sites provided by the satellite operators or ESA. The data are transmitted to ftp by frequently polling the ftp sites and retrieving the new data as soon it is detected by the polling script. After data transmission, the data are georectified to Mercator projection with a center latitude of 61 2/3 degrees. This projection is similar to the one used in the Baltic Sea nautical charts. After the georectified SAR images are calibrated, an incidence angle correction is applied to them and also thermal noise reduction is performed. Finally, a land mask is applied to remove the unnecessary land areas, thus enabling reduction of data size. The images are then provided in GeoTIFF format for the ice services and for the automated algorithms applied in CMS. The data are also stored for further use in research.

4 Products and services

4.1 Ice chart

The primary product of the sea-ice monitoring is the ice chart. The daily ice charting is done by one sea ice analyst. The analysis is finished slightly after noon, by when most satellite images from that same morning can be utilized. As the whole charted area rarely is fully covered by imagery every morning, images can be ordered to cover the operationally most important areas almost daily (where the navigation in ice is the most intense). Occasionally, the ice analysis is also based on evening passes from the day before. The aim is that the date of the chart ultimately corresponds to imagery from the same morning. Used imagery are mainly dusk-pass SAR but also optical imagery from before noon (MODIS, VIIRS, Sentinel-2). Additionally, satellite image information, which always represents a specific time in the past, can be altered with observations from icebreakers, coastal radars and drift buoys. The final ice analysis thus depends on all the used data, on the prevailing weather and the interpretation of the ice analyst.

The ice chart is compiled in vector form, consisting of polygons to which the ice analyst applies one parameter value to represent the general ice features of the defined area as accurately and consistently as possible. The polygon division is chosen to collect the same type of ice as comprehensively as possible. Thus, the ice charts cannot indicate exact values for every location, but the used ground truth is rather echoed as a general representation and distribution for the defined polygons. This does create some uncertainty when estimating specific local conditions and this feature needs to be taken into account by the user. The discretized nature of the ice chart is visually easy to interpret, but when used for, say, satellite image or sea-ice model validation, the characteristics of the data needs to be understood.

The manually analysed ice chart is based on the following information sources:

1. Satellite images.
2. Icebreaker observations.
3. Manual observations from coastal stations.
4. Ice drifters.
5. Numerical prediction models.
6. Coastal radars.

As almost all source data used in the ice charting include higher degrees of detail than can be expressed in the ice chart analysis, certain aspects need to be considered by the users. First of all, the representation of the ice situation is relative to the scale of the entire Baltic Sea, fitted to one A3 page. Secondly, focus is given to areas where vessel traffic is hampered by ice and where icebreaker assistance is needed. The main purpose of the ice chart, namely, to give the shipping sector and ice navigation a general view of the ice resistance in each zone. The high resolution of satellite image bitmaps is difficult to match with the highly discrete form of the ice chart, in which we may choose to include vast areas in one polygon based on some chosen feature. This could be high concentration combined with a fairly similar level-ice thickness, thus possibly neglecting a high variation in ice deformation, even if it can be identified in SAR texture. In the PDF ice chart, deformed ice therefore is indicated by symbols for ridged ice, rafted ice and brash ice barriers.

4.2 Ice chart parameters

4.2.1 Ice type

The ice type definitions used in the ice charts have slightly evolved over the course of time. There have been variations in the way ice type and the concentration have been defined. The harmonized standard of today is the WMO Sea-Ice Nomenclature (WMO, 2014a) and the ice types used in the Finnish-Swedish Baltic Sea ice chart are shown in Figure 7.

4.2.2 Concentration

The concentration indicates the fraction of the sea surface in tenths, where 0/10 means ice-free and 10/10 full ice coverage. The ice type and concentration are partly linked to each other, as most of them include a concentration value or interval.

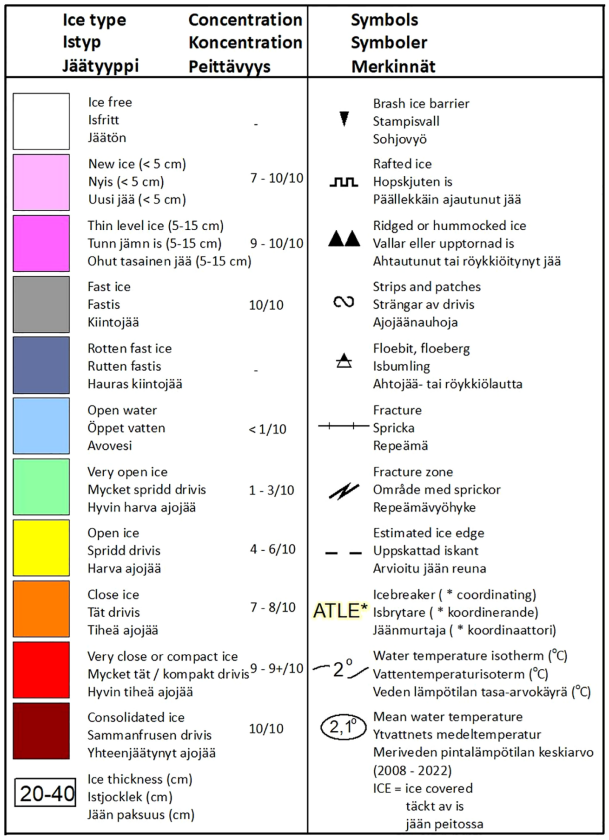

FIGURE 7
Legend of the ice chart explaining the meaning of colours, symbols, annotations and text used.

4.2.3 Ice thickness

The given ice thickness describes the thickness of level ice, meaning that all forms of deformed ice are excluded from the thickness values. This also means that the thickness reading, at least in principle, should correspond to the thickness of thermally grown ice. This has been the leading principle throughout the history of ice charting. In the ice charting tool, ice thickness has three input categories: minimum, mean and maximum ice thickness. These make it possible to indicate what stages of development are included within the area and thus define a rough thickness distribution for the given polygon. In the PDF chart's ice thickness annotations, however, only the minimum and maximum are indicated as a total interval.

- The minimum thickness indicates the youngest form of ice.
- The mean thickness is intended to describe the typical, or most common, occurring ice thickness. This value would therefore rather indicate the mode in a thickness distribution.
- The maximum thickness indicates the highest stage of development.

The thickness readings have occasionally been compared to electromagnetic (EM) ice thickness measurements performed and the mode of the observed thickness histograms have matched fairly well with the ice chart readings.

Observations of drift ice are almost entirely based on icebreaker observations, and the icebreaker crews have the best experience for assessing the different features of the ice, like how to determine ice thickness and concentration. The ice analyst on duty nevertheless performs a quality check on the incoming icebreaker observations.

Maps digitised from archived old paper ice charts no longer contain original observations, so the average thickness has been set to the average of the minimum and maximum, but rounded to an accuracy of 5 cm, and up rather than down.

4.2.4 Ice deformation

The forms of deformed ice indicated in the ice charts are ridged ice (Figure 8), rafted ice and brash ice. One polygon parameter used in the Finnish-Swedish ice chart is the Degree of Deformation (DoD). It's a numeral on a six-digit scale (0: undeformed, 1: rafted ice, 2: slightly ridged ice, 3: moderately ridged ice, 4: heavily ridged ice, 5: brash (typically indicating a compacted ice edge zone of brash ice, connected to the brash ice barrier symbol).

The ice analyst determines the degree of deformation (DoD) both from satellite imagery and based on observation reports from the icebreaker fleet. The icebreaker observations are considered as more reliable ground truth and are therefore the primarily reference when setting the DoD value. The satellite imagery, on the other hand, indicates the aerial distribution of the deformation zones.

As all parameters applied to one polygon, the DoD gives only one numeral for the whole polygon area. Consequently, it is a poor indicator of ice ridge distribution and can only give a flattened average of the deformation rate in the specific polygon.

Also, the scale of DoD is highly practical and simplified, based on how the deformed ice affects icebreaking operations and navigation in ice. Therefore, the categories are non-physical, applied by empirical judgment as reported by icebreaker bridge officers and the ice analyst, and have to be treated accordingly.

4.2.5 Sea surface temperature

The Sea Surface Temperature (SST) is drawn in the ice-free regions of the ice chart. Isoterms with one-degree intervals are drawn based on *in-situ* observations from buoys, coastal stations and vessels. Also, satellite-based analysis products and numerical oceanographic models are used.

The SST as part of the operational ice chart is an important parameter for the users as it indicates the cooling of the surface water, and that way anticipates the onset of freezing. In the ice chart, also statistical means of the SST are shown for selected locations, which tells how the season is progressing in a climatological reference.

4.3 Output and distribution

The main issuing format is the visual chart, published on the FMI website and distributed by e-mail and other web applications (Figure 9). All the coding of the chart follows the guidelines of the

FIGURE 8
Ridged drift ice field in the northern Bay of Bothnia (photo: Patrick Eriksson).

WMO sea ice nomenclature, and specifically the one assigned to Baltic Sea conditions (WMO, 2014b). The ice information is depicted by the parameters and symbols presented below.

The output formats of the ice chart are printable charts, NetCDF grids and the Shape-like SIGRID-3 format (although currently still in Beta phase). Today the printable chart is in PDF format as colour and black-and-white versions.

As the ice charting tool makes it possible to store more parameters to the polygons than are shown in the PDF chart, these parameters can be included in numerical output formats like grid files or digital vector formats. Possible parameters in the numerical outputs are:

- Ice type.
- Ice concentration.
- Level ice thickness (minimum, mean, maximum).
- Degree of deformation.
- Sea surface temperature.

4.4 Ice codes

Publishing of the ice codes in Finland began in 1921. The ice codes contain information of the sea ice conditions along the Finnish fairways and adjacent sea areas in a very condensed form. Initially each individual code consisted of only two digits describing the ice conditions, but over the years they have gone through a few steps of changes before the Baltic Sea ice code, currently in use, was adapted in 1981 (SMHI, 1981).

The ice codes are series of character strings containing an area definition, followed by four digits describing the ice conditions. The first of these four digits describes the amount and arrangement of ice, the second digit the stage of development, the third digit the topography or form of ice, and the last digit the navigation conditions in ice.

For example, the code BB1–8376 means that on the fairway from Oulu harbours to Kattilankalla (BB1) there is fast ice (8) of 15–30 cm thickness (3) with hummocks or ridges (7) and a specific ice class and size is required of a vessel to be allowed icebreaker assistance (6).

Ice code production for the winter starts with the setting of first assistance restrictions to Finnish ports by the winter navigation authorities, coinciding with the start of daily ice charting and the start of ice reports. They are distributed using the GTS network (Global Telecommunication System) as NAVTEX messages and shared with all the other ice services around the Baltic Sea, as agreed by the Baltic Sea Ice Meeting. As the ice code format is uniform within the Baltic Sea ice service community, its compressed and easily interpreted nature has been used as a practical source of information, giving a comprehensive picture of the whole sea area in daily time steps. Based on this, the ice codes are used for statistical analyses, like the ones compiled on the Baltic Sea Ice Services' web page (BSIS, 2025).

4.5 Ice report

Finnish ice reports have been read on the radio since the 7th of January 1927. Today, the ice report is a literal description of the ice conditions relevant for the traffic to the Finnish ports, followed by information from the winter navigation authorities. It is published daily during the winter navigation season. The first reports are issued when the winter navigation authorities set the first assistance restrictions for the season and the last when the last ice chart is published.

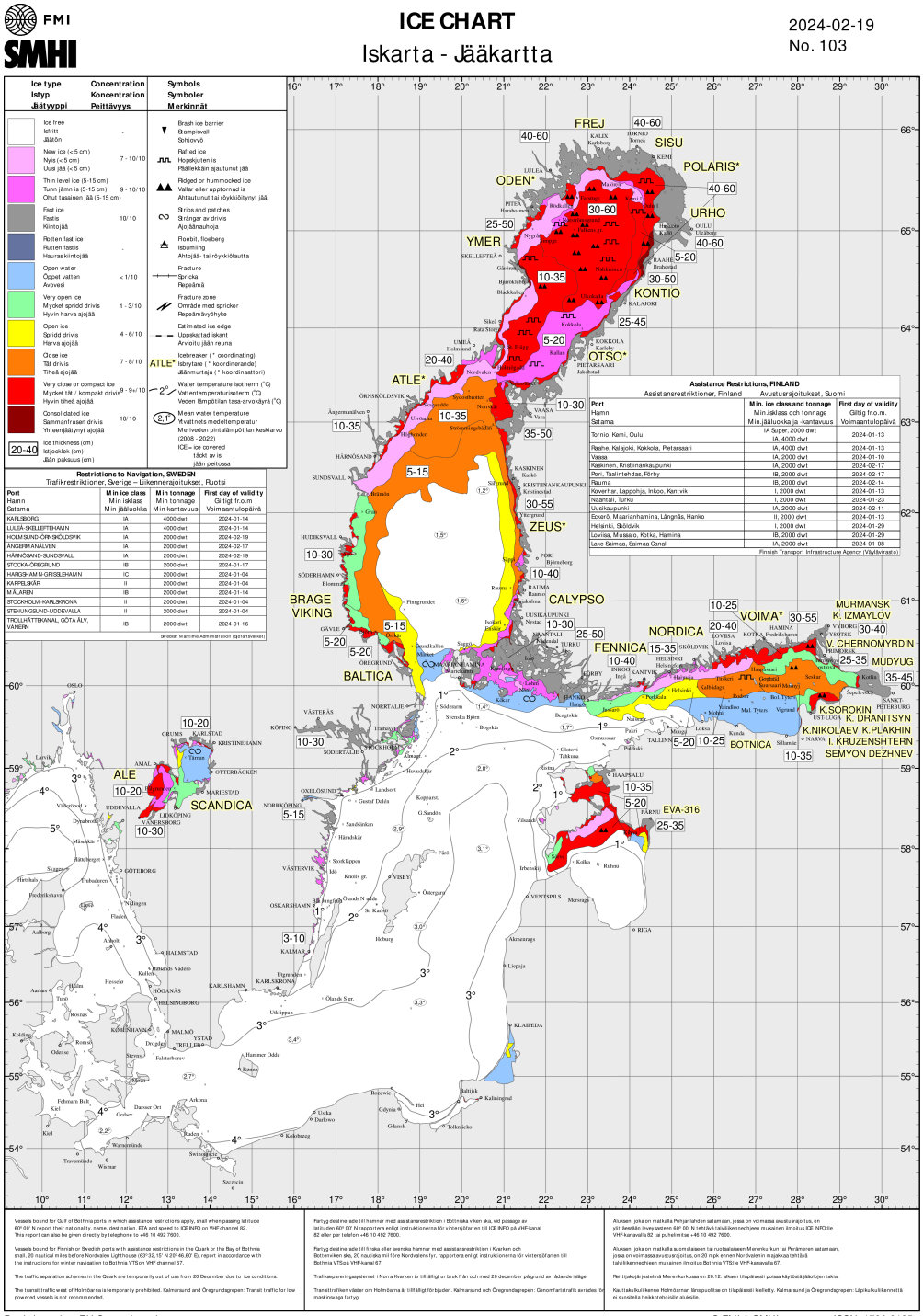

FIGURE 9
The Finnish-Swedish ice chart of 19th February 2024. On the back page there is more traffic information for navigation.

The ice report consists of two parts. The first part describes the ice situation in the whole Baltic Sea, with an emphasis on the Finnish sea areas and the Lake Saimaa and Saimaa Canal route during its winter navigation season. The ice report focuses on the ice conditions along fairway areas, describing the type of ice, its thickness and deformation stage. Features with importance to navigation, such as brash ice barriers, ice pressure areas, cracks and leads, are also described. There is an endeavour to keep the ice report relatively short, but at the same time it must contain all the required and critical information.

The data sources for the ice report are the same as for the ice chart, but the report is published earlier than the chart, around noon.

The second part of the ice report contains information from the winter navigation authorities. The operating icebreakers are listed along with their operation locations. The current assistance restrictions to Finnish ports are given, as well as coming changes to these. Other announcements from the winter navigation authorities concerning winter navigation are also mentioned, like reporting rules and possible exceptions to navigation directives caused by the ice conditions.

The ice report is written in Finnish, Swedish and English. The text is published on the FMI website and distributed via e-mail. The Finnish Broadcasting Company (YLE) reads the report in Finnish and Swedish on its radio channels and the Maritime safety radio, Turku Radio, reads it in English.

4.6 Ice forecasts

The Ice Service produces a 10-day ice condition development forecast for the Finnish Transport Infrastructure Agency once a week. The forecast describes the daily development of ice conditions in Finnish sea areas, including ice movement, thickness growth, and deformation. Also zones of anticipated ice pressure are mentioned, to the extent it can be evaluated based on both icebreaker observations and sea-ice models. The forecast is based on the initial conditions and the wind and temperature forecasts for the coming days. A numerical sea-ice forecast model is utilized for the first few days. The ice model used is the NEMO-SI3. Icebreaking operations use the forecast for planning winter navigation and the vessel assistance activity. Additionally, a weekly ice thickness forecast for Finnish ports is made for the Finnish Transport Infrastructure Agency. Ice thickness growth is predicted using the formula defined by HELCOM (HELCOM, 2004) and is based on the cumulative freezing degree days. The initial ice thickness in the forecast is obtained from ice observations. If no ice observation is available, a calculated value is used as the initial ice thickness. The nearest weather observation station and temperature forecast are used for calculating the freezing degree days.

In the monthly seasonal forecast SEASON (Seasonal Forecast), the extent and thickness of ice in the Baltic Sea, as well as the number of icebreakers required, are predicted on a monthly basis. The forecast utilizes the prevailing ice conditions and sea temperature at the initial situation, comparing them to similar situations in previous winters. Based on data from past winters, it is possible to estimate how the ice conditions will develop if the weather is predicted to follow the observed weather of those winters. The weather forecast primarily uses long-term forecasts from ECMWF. Due to uncertainties in the weather forecasts, the seasonal ice forecast relies heavily on the professional experience of ice experts.

4.7 Ice season descriptions and maximum ice chart

Each year, after the season ends, the Ice Service writes a description of the past ice season. These descriptions have been made since season 1913/1914 (Granqvist, 1921), and since the season of 1995/1996, the reports have been published on the institute's website in Finnish, Swedish, and English. Currently, the description is a verbal summary of the evolution of ice conditions during the winter, and it includes information on ice thickness and a climatic comparison of the length of the ice season. The description also includes the maximum ice extent in the Baltic Sea and the date of this maximum. In the calculation, areas with at least 1/10 ice coverage are considered ice-covered.

Along with the ice season description, a chart of the maximum ice extent is also published on the website, see example in Figure 10. Compared to the regular ice chart, this chart includes additional information on icebreaking activities and assistance restrictions in Finland and Sweden. Nowadays, ice areas in the maximum ice chart are not drawn separately afterward; instead, the operational ice chart published on that day is used.

4.8 Data and product storages and archives

The ice service archives its operational products and part of the data used in their production. The latest ice chart is available in PDF format at FMI web pages and archived ice charts can be delivered at request. Ice charts in PDF format are available from ice season 2001. The ice analysis resulting in the printable ice chart is stored in PostGIS databases and used in production of gridded and vector format datasets. Digitized ice chart data is available weekly from 1980.

The gridded ice chart data is produced in NetCDF format in ¼ nautical mile nominal resolution. It contains eight parameters: land-sea mask, ice type, total ice concentration, minimum ice thickness, average ice thickness, maximum ice thickness, sea ice degree of deformation and sea surface temperature. The data is compatible with JCOMM Electronic Chart Systems Ice Objects Catalogue (JCOMM. Joint Technical Commission for Oceanography and Marine Meteorology (JCOMM) and Expert Team on Sea Ice, 2014). Currently ice chart data in NetCDF format is available daily from 2007 and weekly from 1980. Occasionally, there are short gaps in the NetCDF data series, since on some dates the ice chart hasn't been produced due to national public holidays and weekends near the very end of the season. Additionally, there is a gridded CMS product (004) with ice concentration and average ice thickness data in 1 km nominal resolution.

The vector ice chart data is produced in a shapefile format called SIGRID-3 (WMO, 2010). The SIGRID-3 files contain most of the data included in the ice analysis, except for the ice type, which is not recognized by the SIGRID-3 standard. Daily production of SIGRID-3 began at the start of ice season 2019.

Published ice reports and ice codes are archived by the ice service. In digital format they're available from ice season 2011 and can be delivered at request.

The coastal ice thickness observations submitted via electronic form are available through FMI open data from 2016. The

measurements from ice season 1991 onwards are stored in digital format, while older coastal ice observations are currently archived in original measurement forms on paper and available in ice season publications by the Finnish Institute of Marine Research.

Satellite images used in the ice analysis and sea ice forecasts produced for the winter navigation authorities are archived, but not available to the public. When there are multiple satellite images available for the same sea area during the analysis, only the most suitable image is

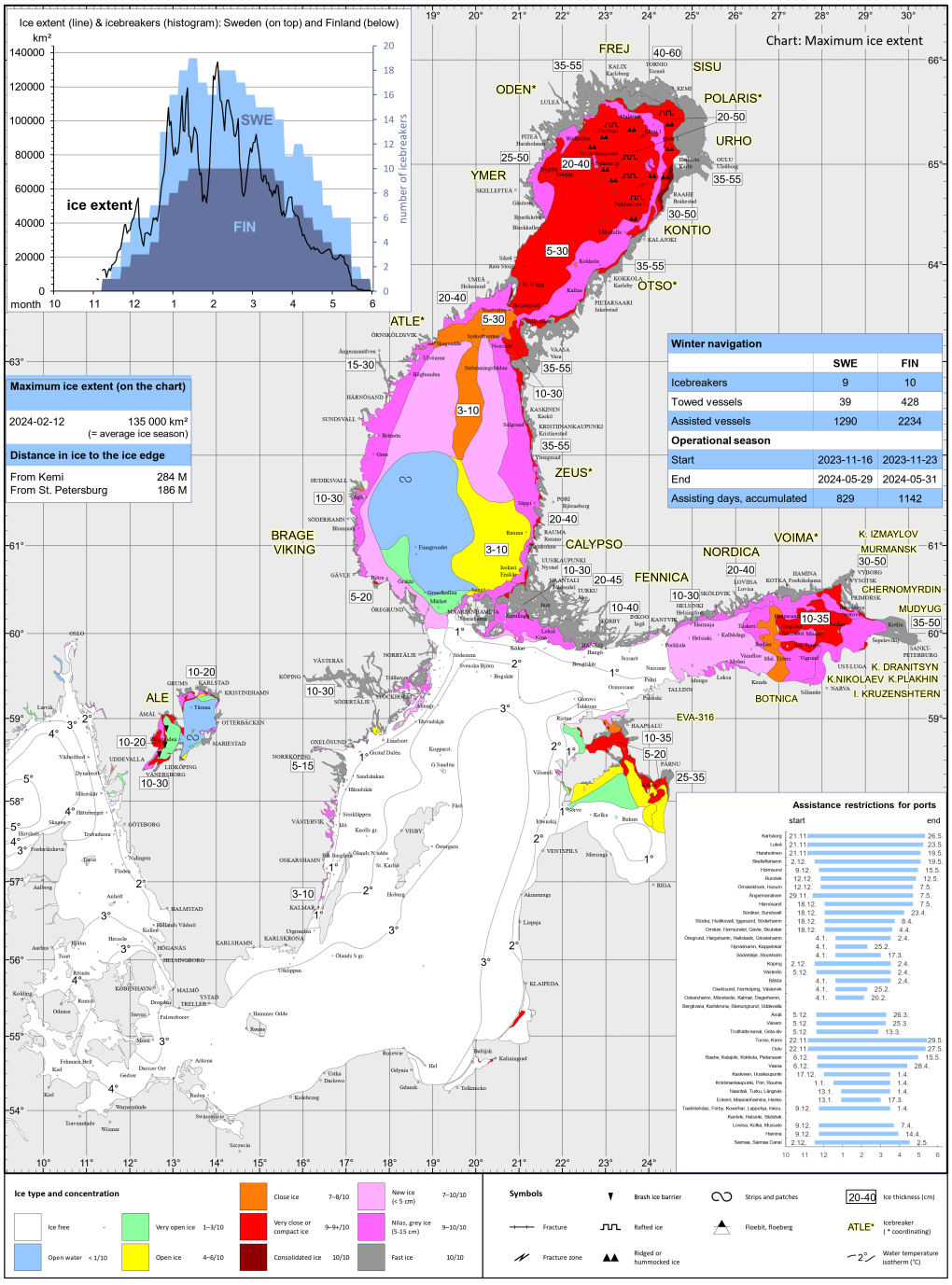

FIGURE 10
The maximum ice chart of season 2023/2024. Since 2018 the product has also included data of the winter navigation of the season, like how much assistance was done.

archived. Images not containing any ice are not archived, even when used in the analysis to see if there is any ice in the area.

4.9 Copernicus marine service and its relation to the ice service

The Copernicus Marine Service (CMS, https://marine.copernicus.eu) is the marine component of the EC Copernicus programme, and forms one of the six key thematic components of Copernicus. Copernicus Marine is devoted to the monitoring of the ocean worldwide, with a focus on satellite-derived data but also with *in situ* (measurements made on site) thematic assembly centres (TAC's) along with model-based products, and offers free access to a catalogue of about 200 standardized and quality-controlled products describing the physical, sea ice and biogeochemical features of European seas and the Global Ocean.

The CMS sea ice TAC (SITAC) is coordinated by Met Norway and the SITAC Baltic Sea production unit is at FMI. CMS provides NRT satellite imagery from ESA's Sentinels and also so-called Copernicus Contributing Missions (CCM) data for use in ice charting and automated sea ice products. FMI receives CCM data from RADARSAT-2, Radarsat Constellation Mission (RCM), TerraSAR-X, COSMO-SkyMed and PAZ. Also some other SAR instruments, such as ICEYE have been in operational test use.

The CMS is in close connection with the FMI Ice Service. The SAR data for the ice charting is received in near-real-time (NRT) through CMS and data derived from the FMI ice charts are provided to CMS SITAC. CMS enables that the data from the ESA Sentinels are available with minimal time gap from the data acquisition and also the coordinated availability of CCM data. Further, the access to CCM data makes it possible to fill acquisition gaps caused by the fixed predefined data acquisition plans of Sentinel-1 and RADARSAT-2.

The CMS SITAC Baltic Sea production unit at FMI has two major product groups: SEAICE_BAL_SEAICE_L4_NRT_OBSERVATIONS_011_004 (in the following shortly 004) and SEAICE_BAL_SEAICE_L4_NRT_OBSERVATIONS_011_011 (011). The 004 data sets are directly based on digitized FMI ice charts and 011 data sets are automated products based on the EO data. The area covered by the SITAC products is the whole Baltic Sea.

The gridded CMS ice analysis (004) products in CMS are sea ice concentration (SIC) and average sea ice thickness (SIT). These products are both given in a 1 km nominal resolution corresponding to that of the FMI ice chart. These CMS products are provided daily after completion of the daily ice chart.

The 011 products are mainly based on C-band SAR imagery from Sentinel-1, RADARSAT-2 and RCM. X-band SAR data from TSX, CSK and PAZ are used for SIT products only. The CMS 011 datasets currently include SIT., SIC and sea ice drift (SID), as well as sea ice extent (SIE) derived directly from SIC. The products are produced after reception of a SAR image and a SIT mosaic product is updated twice daily if new SAR data are available. The SID dataset is updated each time when overlapping SAR data with a time difference less than three days are available.

The CMS SITAC algorithms for the SIT estimation are described in more detail in (Karvonen et al., 2003, 2008; Karvonen and Cheng, 2024), the ice drift estimation method in (Karvonen, 2012b) and the SIC estimation algorithm in (Karvonen, 2017).

Starting from the beginning of the Baltic ice season 2020–2021 also another 011 dataset of SIT is provided as part of CMS. These data are similar to the abovementioned 011 SIT, except that they are computed from the Sentinel-1 IW mode (VV/VH) data.

The CMS products are evaluated after each season w.r.t. reference data sets. These data sets include SIT observations from Finnish and Swedish icebreakers, coastal SIT measurements, SIC based on microwave radiometer data from Universities of Hamburg and Bremen, and buoy measurements of the ice drift. The evaluation results are published in the annual CMS data quality reports, issued after each Baltic Sea winter season.

5 Sea ice research

Studies related to the Baltic Sea ice have been conducted over 100 years, first motivated by the development of winter navigation and later including geophysical studies on the Baltic Sea ice properties and climatology. Since the 1950's, studies have focused on large scale problems, such as sea ice climatology and dynamics, sea ice thermodynamics, sea ice ecology, thickness distributions of level ice and deformed ice, ice ridge statistics (e.g. ridge density), mechanical properties of sea ice (e.g. shear strength of ridges), and on sea ice properties particularly relevant for microwave remote sensing (e.g. surface roughness). Sea ice remote sensing studies started in mid 1970s and intensified in late 1980s and 1990s for the usage of SAR imagery in operational sea ice monitoring.

Theoretical geophysical modelling of sea ice has included the following topics: 1) Seasonal sea ice climate, e.g (Haapala, 2000), 2) Sea ice dynamics, e.g (Zhang, 2000), and 3) Sea ice thermodynamics and air-ice interaction, e.g (Cheng, 2002). These studies are mainly focused on the numerical model constructions, validations, and to better reproduce sea ice physics with numerical modelling on the basis of seasonal and synoptic time scales. In general, the large-scale ice conditions, like ice extent, in the Baltic Sea are well known, but little is still known about the small-scale properties of the ice, the processes during initial ice formation, and the temporal development of the ice properties (Granskog, 2004). The main reason for this is the need of time consuming and expensive logistical efforts for studying sea ice processes in harsh field conditions.

5.1 Remote sensing of the Baltic Sea ice

There is a long history of Baltic Sea ice remote sensing and geophysics research conducted at FIMR and later at FMI for development of operational FIS services and products. Remote sensing research since late 1980's has been heavily focused on the usage of the SAR imagery for automatic retrieval of various sea ice parameters, like ice types, degree of deformation, and sea ice concentration. FIS has used SAR imagery since 1992 with the availability of ERS-1 SAR.

Investigations on the feasibility of microwave remote sensing for the Baltic Sea ice monitoring started in 1975 (Hallikainen, 1992). The first research campaign was Sea Ice-75 organized jointly by Finland and Sweden. In this campaign first airborne radar (10 GHz side-looking airborne radar (SLAR)) and radiometer (0.6 and 5 GHz) measurements were conducted. It was followed in 1987 by the Bothnian Experiment in Preparation of ERS-1 (BEPERS-87) pilot study (Leppäranta and Hakala, 1992). This study included the first airborne SAR measurements over the Baltic Sea ice with a French X-band SAR. BEPERS-88 study included first airborne C-band SAR measurements conducted by Canada Centre for Remote Sensing (CCRS), and first C- and X-band helicopter-borne scatterometer measurements conducted by Laboratory of Space Technology of Helsinki University of Technology (Leppäranta and Thompson, 1989). In the late 1980's the research work intensified for studying the use of the ERS-1 SAR images for the Baltic Sea ice monitoring. First ERS-1 images, and also, the first spaceborne SAR images over the Baltic Sea ice, were acquired in the winter 1992. In general, remote sensing research has been heavily focused on the usage of the SAR imagery for automatic retrieval of various sea ice parameters, like degree of deformation, Optical and TIR imagery has been used only for development and validation of SAR based sea ice products.

Utilization of spaceborne microwave radiometer data for the Baltic Sea ice monitoring has not been studied much. The main reason for this is the coarse resolution of the radiometer data, e.g. in the current AMSR2 radiometer data the resolution is from 35 by 62 km (6.9 GHz channel) to 3 by 5 km (89 GHz channel) (Maeda et al., 2016), compared to area of the Baltic Sea and its typically rugged coastline with many islands (land contamination of measured ocean/sea ice brightness temperatures). Few studies have been conducted for the sea ice concentration estimation (Hallikainen and Mikkonen, 1986; Grandell et al., 1996).

Research work on the usage of laser and radar altimeters for retrieving Baltic Sea ice properties has also been limited as they have little usage in the operational monitoring due to spatial and temporal sparseness of the altimeter ground tracks. Estimation of degree of ice ridging has been demonstrated (Fredensborg Hansen et al., 2021). Uncertainties in sea ice thickness estimation with Cryosat-2 radar altimeter rise asymptotically towards thinner ice less than 1 m thick (Ricker et al., 2017). As level sea ice in the Baltic Sea is generally less than 1 m thick, the radar altimeter based ice thickness estimation can be considered mostly useless in the Baltic Sea. In the Arctic, the Cryosat-2 observations have been successfully merged with SMOS microwave radiometer observations, but in the Baltic SMOS observations are likely to suffer from land contamination (Li et al. 2017; Maaß et al., 2015).

In the following is a list of the Baltic Sea ice properties which can be estimated using SAR data alone or together with other data. Methods for the sea ice property estimations are also shortly described. This list is mainly based on studies with the C-band dual-polarized SAR data which is the main operational satellite data used by the Finnish Ice Service. Only some of the methods are used for operational sea ice products.

- Sea ice extent and concentration: with SAR data only (Karvonen et al., 2005; Karvonen, 2012a; Karvonen, 2014), and combination of SAR and microwave radiometer data.
- Sea ice thickness based on combination of ice chart SIT data and SAR image statistical analysis (Karvonen et al., 2003, 2004; Similä et al., 2005), or empirical relationship between ice freeboard derived from airborne laser altimeter data and SAR backscatter (Similä et al., 2010).
- Sea ice types (Karvonen, 2004) based on statistical SAR image segmentation and texture feature classification.
- Sea ice drift/dynamics based on time series of SAR images (Karvonen, 2012).
- Land fast ice extent based on time series of SAR images (Karvonen, 2018).
- Degree of deformation (Gegiuc et al., 2018) based on statistical SAR image segmentation and texture feature classification.
- Estimation of ice-going ship speed by Random forest regression between local statistical SAR features and AIS data (Similä and Lensu, 2018).

Few case studies have utilized SAR interferometry for estimation of small horizontal deformations in level ice or displacements of level ice, e.g (Dammert et al., 1998,; Marbouti et al., 2017). As Sentinel-1 has long temporal baseline SAR interferometry, it only can be applied over fast ice, and snow and sea ice conditions should not change much between acquisitions in order to have high coherence. Polarimetric SAR remote sensing of the Baltic Sea ice is still in infancy, mainly due to the very limited amount of data available so far. Likewise, multifrequency SAR approaches have not been used much due to limited availability of co-incident SAR data.

In many SAR algorithms for retrieval of sea ice properties, FMI ice charts and their concentration and degree of ice ridging fields, have been used as training data.

Machine-learning methods and neural networks have traditionally played a major role in the sea ice analysis algorithms that are based on EO data, and the development in this sector has proven to be ongoing. For instance, models for sea ice concentration estimation and degree of deformation using a modified U-net (Ronneberger et al., 2015) neural network with hyper-parameter optimization are under development and currently in test phase at FMI. These methods will be applied in the operational Copernicus Marine Service sea ice products in the near future. According to the preliminary tests, these new methods will improve the estimation and classification accuracy by a few percentage points.

The above-mentioned sea ice research activities at FMI, and formerly at FIMR, emphasize the fact that the research part is an integral part of the operational Ice Service and its capabilities.

The research projects in Finland on the development of operational sea ice classification algorithms for spaceborne SAR data have also included following tasks: (1) basic research in backscatter signatures of sea ice, e.g. statistics for various ice types and effect of snow wetness in the statistics, e.g (Mäkynen and Hallikainen, 2004: Mäkynen, 2007), (2) theoretical modelling of backscatter signatures, e.g (Manninen, 1992; 1996a; 1996b), (3) field

campaigns to gather ground truth data and radar data with airborne, coastal and shipborne radars, (4) development of end-user software for interpretation and use of the sea ice products, and (5) various issues of data delivery to end-users at ships, e.g (Karvonen and Simila, 2002). Tasks (1)-(3) support the development and validation of the SAR classification algorithms.

6 Future outlook

In this paper, the concept of ice monitoring at the Finnish Ice Service, and its focus on the winter navigation needs, has been presented. The over 100 years of ice monitoring and ice charting has always responded to the specific evolution in shipping in ice and to the technological advances in all related fields. The future evolvement is not that easy to foresee, but the sea ice services will nevertheless continue to adapt to the circumstances ahead.

Climate change has for some time already appeared as one constraint to the development of the ice service. But even if the average winters aren't as long as they used to be, harsh winters are still to occur and difficult navigational conditions still will cause trouble, especially in the northernmost basins of the Baltic Sea. Milder winters result in more mobile ice, which even causes new obstacles at sea. Formation of difficult brash ice zones seems to have increased. Phenomena like these may demand new ways of describing the ice conditions and the forecasting and information flow needs to be able to respond to the ever-tighter requirements.

As the amount of available satellite imagery is increasing and, simultaneously, the demand for higher levels of detail in the service products, the manual analysis process used during the past few decades is facing new challenges. In the near future, new automated or semi-automated methods have to be developed in order to handle the growing amounts of data.

One thing is still clear, however. The need for safe and efficient ice navigation will not disappear any time soon, and ice services will still be needed, in one form or another.

Author contributions

PE: Conceptualization, Investigation, Project administration, Supervision, Writing – original draft, Writing – review & editing. JV: Writing – original draft, Writing – review & editing. NT: Writing – original draft, Writing – review & editing. AJ: Writing – original draft, Writing – review & editing. AA: Writing – original draft, Writing – review & editing. MM: Writing – original draft, Writing – review & editing. JK: Writing – original draft, Writing – review & editing. AK: Conceptualization, Project administration, Writing – original draft, Writing – review & editing.

Funding

The author(s) declare that no financial support was received for the research and/or publication of this article.

Conflict of interest

The authors declare that the research was conducted in the absence of any commercial or financial relationships that could be construed as a potential conflict of interest.

Generative AI statement

The author(s) declare that no Generative AI was used in the creation of this manuscript.

Any alternative text (alt text) provided alongside figures in this article has been generated by Frontiers with the support of artificial intelligence and reasonable efforts have been made to ensure accuracy, including review by the authors wherever possible. If you identify any issues, please contact us.

Publisher's note

References

Berglund, R., and Eriksson, P. B. (2015). "National ice service operations and products around the world," in H. Shen (Ed.), *Cold Regions Science and Marine Technology*, vol. 2, pp. 1–20. EOLSS Publishers. Available online at: https://www.eolss.net/ebooklib/bookinfo/cold-regions-science-marine-technology.aspx (Accessed September 23, 2025)

BIM (2020). Baltic Sea Icebreaking Report 2019-2020. Baltic Icebreaking Management. Available online at: https://www.baltice.org/api/media/get?folder=icebreaking_reports&file=BIM%20Report%202019-2020.pdf (Accessed August 14, 2025).

BSIS (2025). Sea ice statistics Baltic. Available online at: https://www.bsis-ice.de/statistik/Stationindex.html (Accessed August 14, 2025).

Cheng, B. (2002). *On the modelling of sea ice thermodynamics and air-ice coupling in the Bohai Sea and the Baltic Sea* (Finland: Finnish Institute of Marine Research – Contributions).

Dammert, P. B. G., Leppäranta, M., and Askne, J. (1998). SAR interferometry over Baltic Sea ice. *Int. J. Remote Sens.* 19, 3019–3037. doi: 10.1080/014311698214163

FMI (2025). Sea Ice statistics. Available online at: https://en.ilmatieteenlaitos.fi/icestatistics (Accessed January 7, 2025).

Fredensborg Hansen, R. M., Rinne, E., Farrell, S. L., and Skourup, H. (2021). Estimation of degree of sea ice ridging in the Bay of Bothnia based on geolocated photon heights from ICESat-2. *Cryosphere* 15, 2511–2529. doi: 10.5194/tc-15-2511-2021

Gegiuc, A., Simila, M., Karvonen, J., Lensu, M., Mäkynen, M., and Vainio, J. (2018). Estimation of degree of sea ice ridging based on dual-polarized C-band SAR data. *Cryosphere* 12, 343–364. doi: 10.5194/tc-12-343-2018

Grandell, J., Johannessen, J. A., and Hallikainen, M. (1996). Comparison of ERS-1 AMI wind scatterometer and SSM/I sea ice detection in the Baltic Sea. *Photogrammetric J. Finland* 15, 6–23. Available at: https://hdl.handle.net/10013/epic.21482 (Accessed September 23, 2025).

Granqvist, G. (1921). *Jäät vuonna 1913–14 Suomen rannikolla. Merentutkimuslaitoksen julkaisu N:o 3* Helsinki: Valtioneuvoston kirjapaino. Available at: http://hdl.handle.net/10138/158441 (Accessed September 23, 2025).

Granqvist, G. (1926). *Yleiskatsaus talven 1914–15 jääsuhteisiin. Merentutkimuslaitoksen julkaisu N:o 37* Helsinki: Valtioneuvoston kirjapaino. Available online at: http://hdl.handle.net/10138/158829 (Accessed September 23, 2025).

Granskog, M. (2004). *Investigations into the physical and chemical properties of Baltic Sea ice*. Division of Geophysics, Department of Physical Sciences, University of Helsinki, Helsinki.

Grönvall, H. (1984). Jäätilanne ja pintaveden lämpötila merialueilla. In: M. Punkari (ed.) *Suomi avaruudesta. Tähtitieteellinen yhdistys Ursa, Julkaisu 24*. Vaasa: Tähtitieteellinen yhdistys Ursa, pp. 152–157.

Haapala, J. (2000). *Modelling of the seasonal ice cover of the Baltic Sea*. Department of Geophysics, University of Helsinki, Helsinki.

Hallikainen, M. (1992). "Microwave remote sensing of low-salinity sea ice," in *Sea Ice*, vol. 68. (American Geophysical Union (AGU, Washington, DC, USA), 361–373.

Hallikainen, M., and Mikkonen, P.-V. (1986). Sea ice studies in the Baltic Sea using satellite microwave radiometer data. In: *Proceedings of IGARSS'86, Zurich, Switzerland*, pp. 1089–1094. New York: IEEE.

HELCOM (2004). *Helcom recommendation 25/7, Safety of winter navigation in the Baltic Sea Area* (Helsinki: Baltic Marine Environm. Prot. Comm.).

Howell, S. E. L., Komarov, A. S., Dabboor, M., Montpetit, B., Brady, M., Scharien, R. K., et al. (2018). Comparing L- and C-band synthetic aperture radar estimates of sea ice motion over different ice regimes. *Remote Sens. Environ.* 204, 380–391. doi: 10.1016/j.rse.2017.10.017

JCOMM. Joint Technical Commission for Oceanography and Marine Meteorology (JCOMM) and Expert Team on Sea Ice (2014). Electronic Chart Systems Ice Objects Catalogue, Version 5.2. Available online at: https://community.wmo.int/activity-areas/Marine/Pubs/SeaIce (Accessed September 23, 2025).

Karvonen, J. (2004). Baltic sea ice SAR segmentation and classification using modified pulse-coupled neural networks. *IEEE Trans. Geosci. Remote Sens.* 42, 1566–1574. doi: 10.1109/TGRS.2004.828179

Karvonen, J. (2012a). Baltic sea ice concentration estimation based on C-band HH-polarized SAR data. *IEEE J. Selected Topics Appl. Earth Observations Remote Sens.* 5, 1874–1884. doi: 10.1109/JSTARS.2012.2209199

Karvonen, J. (2012b). Operational SAR-based sea ice drift monitoring over the Baltic Sea. *Ocean Sci.* 8, 473–483. doi: 10.5194/os-8-473-2012

Karvonen, J. (2014). Baltic sea ice concentration estimation based on C-band dual-polarized SAR data. *IEEE Trans.on Geosci. Remote Sens.* 52, 5558–5566. doi: 10.1109/TGRS.2013.2290331

Karvonen, J. (2017). Baltic sea ice concentration estimation using SENTINEL-1 SAR and AMSR2 microwave radiometer data. *IEEE Trans. Geosci. Remote Sens.* 55, 2871–2883. doi: 10.1109/TGRS.2017.2655567

Karvonen, J. (2018). Estimation of Arctic land-fast ice cover based on dual-polarized Sentinel-1 SAR imagery. *Cryosphere* 12, 2595–2607. doi: 10.5194/tc-12-2595-2018

Karvonen, J. A., and Cheng, B. (2024). Baltic sea ice thickness estimation based on X-band SAR data and background information. *Ann. Glaciology* 65, e23. doi: 10.1017/aog.2024.24

Karvonen, J., Cheng, B., and Similä, M. (2008). Ice thickness charts produced by C-band SAR imagery and HIGHTSI thermodynamic ice model. In *Proceedings of the Sixth Workshop on Baltic Sea Ice Climate, Lammi Biological Station, Finland, 25–28 August 2008. Report Series in Geophysics No. 61, University of Helsinki*, pp. 71–81.

Karvonen, J., and Similä, M. (2002). A wavelet transform coder supporting browsing and transmission of sea ice SAR imagery. *IEEE Tansactions Geosci. Remote Sens.* 40, 2464–2485. doi: 10.1109/TGRS.2002.805068

Karvonen, J., Similä, M., Haapala, J., Haas, C., and Mäkynen, M. (2004). Comparison of SAR data and operational sea ice products to EM ice thickness measurements in the Baltic Sea. In *Proceedings of the IEEE International Geoscience and Remote Sensing Symposium (IGARSS'04)*, Anchorage, Alaska, pp. 3021–3024. Available at: https://hdl.handle.net/10013/epic.21482 (Accessed September 23, 2025).

Karvonen, J., Similä, M., and Heiler, I. (2003). Ice thickness estimation using SAR data and ice thickness history. *Proc. IEEE Int. Geosci. Remote Sens. Symposium 2003 (IGARSS'03)*, Toulouse, France, Vol. 1, pp. 74–76. doi: 10.1109/IGARSS.2003.1293683

Karvonen, J., Similä, M., and Mäkynen, M. (2005). Open water detection from baltic sea ice radarsat-1 SAR imagery. *IEEE Geosci. Remote Sens. Lett.* 2, 275–279. doi: 10.1109/LGRS.2005.847930

Leppäranta, M. (1984). *Jääpeite. Teoksessa Voipio, Aarno ja Leinonen, Matti (toim.)* (Kirjayhtymä, Rauma: Itämeri).

Leppäranta, M., and Hakala, R. (1992). The structure and strength of first-year ice ridges in the Baltic Sea. *Cold Reg. Sci. Technol.* 20, 295–311. doi: 10.1016/0165-232X(92)90036-T

Leppäranta, M., and Thompson, T. (1989). BEPERS-88 sea ice remote sensing with synthetic aperture radar in the Baltic Sea. *Eos* 70, 698–699, 708-709. doi: 10.1029/89EO00216

Li, Y., Li, Q., and Hailiang, L. (2017). Land contamination analysis of SMOS brightness temperature error near coastal areas. *IEEE Geosci. Remote Sens. Letters.* 14, 1–5. doi: 10.1109/LGRS.2016.2637440

Maaß, N., Kaleschke, L., Tian-Kunze, X., Mäkynen, M., Drusch, M., Krumpen, T., et al. (2015). Validation of SMOS sea ice thickness retrieval in the northern Baltic Sea. *Tellus A.* 67, 24617. doi: 10.3402/tellusa.v67.24617

Maeda, T., Taniguchi, Y., and Imaoka, K. (2016). GCOM-W1 AMSR2 level 1R product: Dataset of brightness temperature modified using the antenna pattern matching technique. *IEEE Trans. Geosci. Remote Sens.* 54, 770–782. doi: 10.1109/TGRS.2015.2465170

Mahmud, M. S., Nandan, V., Howell, S. E. L., Geldsetzer, T., and Yackel, J. (2020). Seasonal evolution of L-band SAR backscatter over landfast Arctic sea ice. *Remote Sens. Environ.* 251, 112049. doi: 10.1016/j.rse.2020.112049

Mäkynen, M. (2007). *Investigation of the Microwave Signatures of the Baltic Sea Ice, Thesis for the degree of Doctor of Science in Technology, Laboratory of Space Technology* Vol. 69 (Espoo, Finland: Helsinki University of Technology).

Mäkynen, M., and Hallikainen, M. (2004). Investigation of C- and X-band backscattering signatures of the Baltic Sea ice. *Int. J. Remote Sens.* 25, 2061–2086. doi: 10.1080/01431160310001647697

Manninen, T. (1992). Effects of ice ridge properties on calculated surface backscattering in BEPERS-88. *Int. J. Remote Sens.* 13, 2467–2487. doi: 10.1080/01431169208904282

Manninen, T. (1996a). *Microwave surface backscattering and surface roughness of Baltic Sea ice* (Helsinki, Finland: Finnish Marine Research Institute).

Manninen, T. (1996b). Surface morphology and backscattering of ice-ridge sails in the Baltic Sea. *J. Glaciology* 42, 141–156. doi: 10.3189/S0022143000030604

Marbouti, M., Praks, J., Antropov, O., Rinne, E., and Leppäranta, M. (2017). A study of landfast ice with sentinel-1 repeat-pass interferometry over the baltic sea. *Remote Sensing.* 9, 833. doi: 10.3390/rs9080833

MINTC (2014). *Finland's maritime strategy 2014–2022*. Publications of the Ministry of Transport and Communications, Helsinki.

Ramsay, H. (1949). *Jääsaarron murtajat*. (Helsinki: WSOY), 475.

Ricker, R., Hendricks, S., Kaleschke, L., Tian-Kunze, X., King, J., and Haas, C. (2017). A weekly Arctic sea-ice thickness data record from merged CryoSat-2 and SMOS satellite data. *Cryosphere* 11, 1607–1623. doi: 10.5194/tc-11-1607-2017

Ronneberger, O., Fischer, P., and Brox, T. (2015). "U-Net: Convolutional Networks for Biomedical Image Segmentation," in *Medical Image Computing and Computer-Assisted Intervention – MICCAI 2015. MICCAI 2015. Lecture Notes in Computer Science ()*, vol. 9351 . Eds. N. Navab, J. Hornegger, W. Wells and A. Frangi (Springer, Cham). doi: 10.1007/978-3-319-24574-4_28

Seinä, A., Palosuo, E., and Grönvall, H. (1997). *Merentutkimuslaitoksen Jääpalvelu 1919-1994* (MERI Report Series of the Finnish Institute of Marine Research No. 32). Finnish Institute of Marine Research, Helsinki, Finland. Available online at: http://hdl.handle.net/10138/157935 (Accessed September 23, 2025).

Seinä, A., and Peltola, J. (1991). *Duration of Ice Season and Statistics of Fast Ice Thickness along the Finnish Coast 1961–1990; Finnish Marine Research Report No. 258* (Helsinki, Finland: Finnish Institute of Marine Research), 1–46.

Similä, M., Karvonen, J., Hallikainen, M., and Haas, C. (2005). On SAR-based statistical ice thickness estimation in the baltic sea. *Proc. Int. Geosci. Remote Sens. Symposium 2005 (IGARSS'05)*, 4030–4032. doi: 10.1109/IGARSS.2005.1525798

Similä, M., and Lensu, M. (2018). Estimating the speed of ice-going ships by integrating SAR imagery and ship data from an automatic identification system. *Remote Sens* 10, 1132. doi: 10.3390/rs10071132

Similä, M., Mäkynen, M., and Heiler, I. (2010). Comparison between C band synthetic aperture radar and 3-D laser scanner statistics for the Baltic Sea ice. *J. Geophysical Research Oceans* 115, C10056. doi: 10.1029/2009JC005970

SMHI (1981). *The Baltic Sea Ice Code. Description with illustrations of the code valid from October 1981*. Swedish Meteorological and Hydrological Institute, Norrköping, Sweden.

Tulli (2024). Ulkomaankaupan kuljetukset vuonna 2023. Available online at: https://tilastot.tulli.fi/-/ulkomaankaupan-kuljetukset-vuonna-2023 (Accessed January 7, 2025).

Vihma, T., and Haapala, J. (2009). Geophysics of sea ice in the Baltic Sea: A review. *Prog. Oceanogr.* 80, 129–148. doi: 10.1016/j.pocean.2009.02.002

Witting, R. (1920). *Merentutkimuslaitoksen toiminta vuonna 1919. Merentutkimuslaitoksen julkaisu / Havsforskningsinstitutets skrifter N:o 1*. Helsinki: Valtioneuvoston kirjapaino.

WMO (2010). SIGRID-3: a vector archive format for sea ice charts. Available online at: https://library.wmo.int/idurl/4/37171 (Accessed September 23, 2025).

WMO (2014a). Sea-Ice Nomenclature: WMO-No. 259. Available online at: https://library.wmo.int/idurl/4/41953 (Accessed October 1, 2025).

WMO (2014b). *Ice Chart Colour Code Standard, World Meteorological Organization* (Geneva: World Meteorological Organization). Available online at: https://library.wmo.int/idurl/4/37175 (Accessed September 23, 2025).

WMO (2021). *Sea-ice Information and Services (WMO-No. 574)*. Geneva: World Meteorological Organization.

WNRB (1972). "Havsiskonferens," in *Meeting report of the first Winter Navigation Research Board meeting*. Stockholm, Sweden: Sjöfartsverkets tryckeri. Available online at: https://www.traficom.fi/sites/default/files/10680-No_1_Haviskonferens.pdf (Accessed September 23, 2025).

Zhang, Z. (2000). *On modelling ice dynamics of semi-enclosed seasonally ice-covered seas*. Department of Geophysics, University of Helsinki, Helsinki.

Frontiers in Marine Science

Explores ocean-based solutions for emerging global challenges

The third most-cited marine and freshwater biology journal, advancing our understanding of marine systems and addressing global challenges including overfishing, pollution, and climate change.

Discover the latest Research Topics

See more →

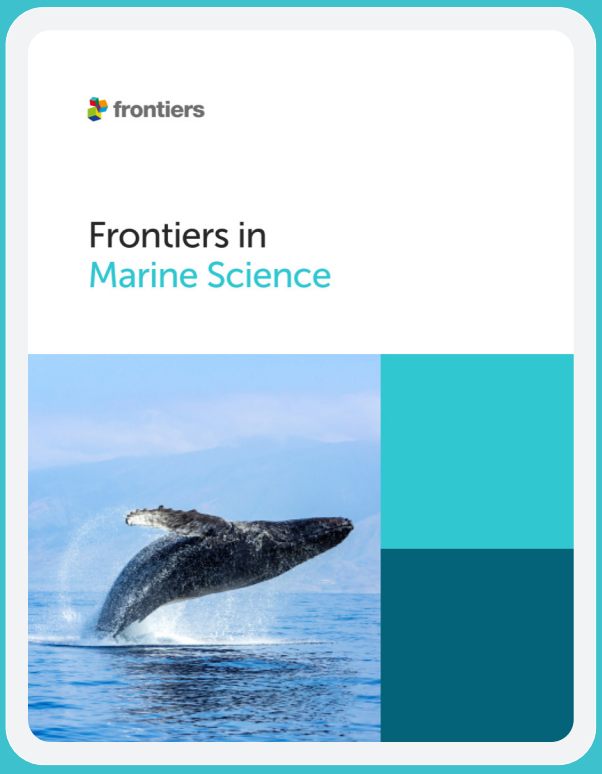

Frontiers

Avenue du Tribunal-Fédéral 34
1005 Lausanne, Switzerland
frontiersin.org

Contact us

+41 (0)21 510 17 00
frontiersin.org/about/contact